AtkinsRéalis

Final Report

Yukon Energy Corporation

September 26, 2024

AtkinsRéalis Ref: 697897-4HER-0001-02

LEWES BOAT LOCK REPLACEMENT – HYDROTECHNICAL STUDY

Signature Page

Prepared By:

Michel Dang, P. Eng.

Hydraulic and Hydrology Engineer
Waterpower & Dams Practice
Engineering Services Canada

Razieh Anari

Razieh Anari, PhD.

Hydraulic and Hydrology Specialist

Waterpower & Dams Practice
Engineering Services Canada

Reviewed By:

Francis Lepage, P. Eng.

Hydraulic and Hydrology Engineer
Waterpower & Dams Practice
Engineering Services Canada

Approved By:

Mahar Suleyman, P.Eng.

Project Manager

Project Delivery
Engineering Services Canada

Notice

This document and its contents have been prepared and are intended solely as information for Yukon Energy Corporation and use in relation to the Lewes Boat Lock replacement project.

AtkinsRéalis assumes no responsibility to any other party in respect of or arising out of or in connection with this document and/or its contents.

Contents

In Text Figures

In-Text Tables

1. Introduction

The Lewes Control Structure (LCS), located approximately 40 km southeast of the City of Whitehorse along the Yukon River, was built in 1976 to replace an older structure. The LCS features a 9-meter-long steel cantilever and sheet pile structure, equipped with 30 gates and a wooden fish ladder. Adjacent to the LCS's eastern bank lies a boat lock, facilitating public passage to small watercraft navigating along the Yukon River.

The LCS serves to regulate the flows out of the Marsh Lake to increase the water available for winter generation at the Whitehorse Generating Station. Governed by water license HY99-010, the LCS operates between summer and winter modes where all 30 gates are open from May 15 to August 15 each year, while for the rest of the year most of the gates are closed and with a few operated to maintain a minimum flow of 85 m^3/s in the Yukon River.

Following an opening the boat lock to mitigate the high-water level at Marsh Lake, resulting from an unprecedented flood event in summer 2021, the boat lock and its equipped gates were damaged, while the downstream shoreline was progressively eroded by the high flows. In response to these challenges, YEC opted to replace the boat lock, also including a modification of LCS. In particular, YEC intends to add two (2) new gates and to equip the lock with removable gates with the aim of increasing the capacity of the structure during flooding period,

YEC retained the service of AtkinsRéalis to carry out the design of components of the Lewes Dam Control Structure. The purpose of this study is to determine Inflow Design Flow and to assess the impact of additional gates and various modification scenarios of the structure on the LCS's hydraulic performance. The study area location depicted in Figure 1-1 and a rendering of the proposed boat lock replacement is shown in Figure 1-2.

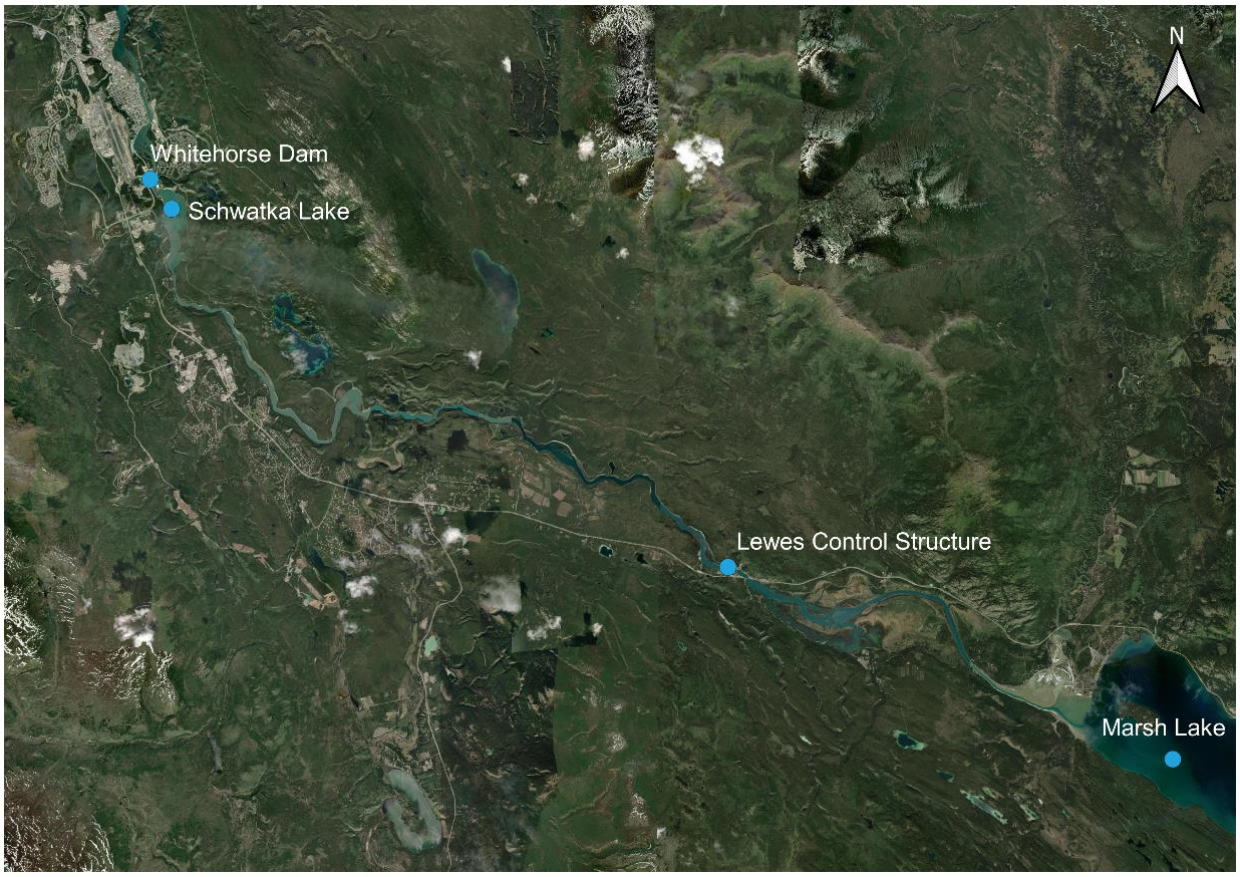

Figure 1-1 Project Site Location

Figure 1-2 Rendering of Proposed Boat Lock Replacement – Lewes Control Structure

1.1 Scope of Work

The objectives of the hydrotechnical study are described below:

- Determination of the return period of the 2021 peak flow.
- Determination of the design flood (1;100-year flood) under future climate using a various climate change scenarios.
- Revision and re-calibration of the 1D hydraulic model. Assessment of the validity of existing one-dimensional hydraulic model of the Yukon River, between Whitehorse Dam and Marsh Lake
- 3D modelling of various proposed geometries to determine the flow pattern and the impact on the structure capacity.
- Determination of the impact of various proposed geometries on the river reach capacity and on potential flood levels in Marsh Lake,

2. Site Geometry Data

2.1 Lewes Control Structure Dimensions

The dimensions and sill elevations of the control structure were extracted from various documents, including the original drawings provided by YEC and the owner's requirement and conceptual drawings prepared by Stantec for YEC. The schematic of control structure is presented in Figure 2-1.

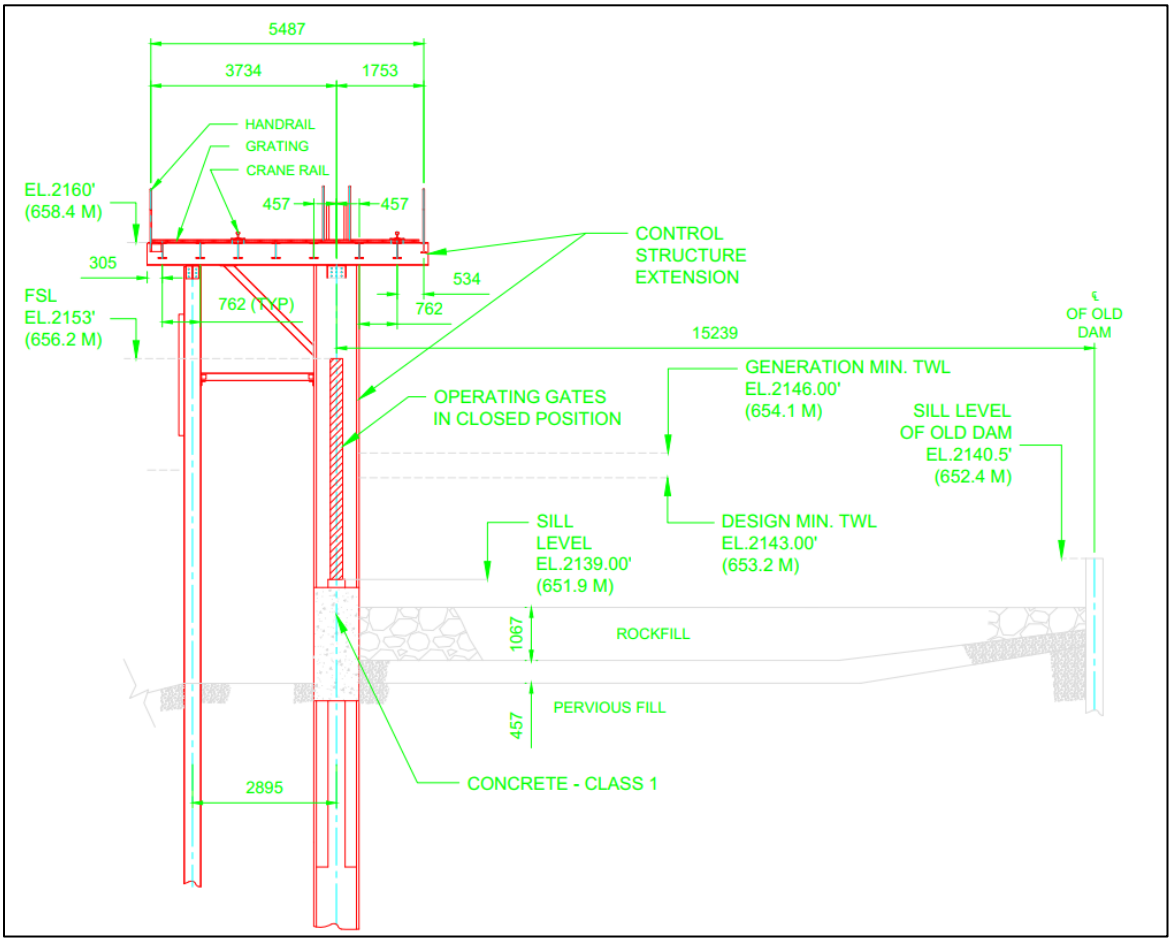

Figure 2-1 Cross Section View of Lewes Control Structure and Old Dam Sill (Conceptual Drawings – Stantec)

Unless specified otherwise, elevation data presented in this report is provided in the Canadian Geodetic Vertical Datum of 1928 (CGVD28).

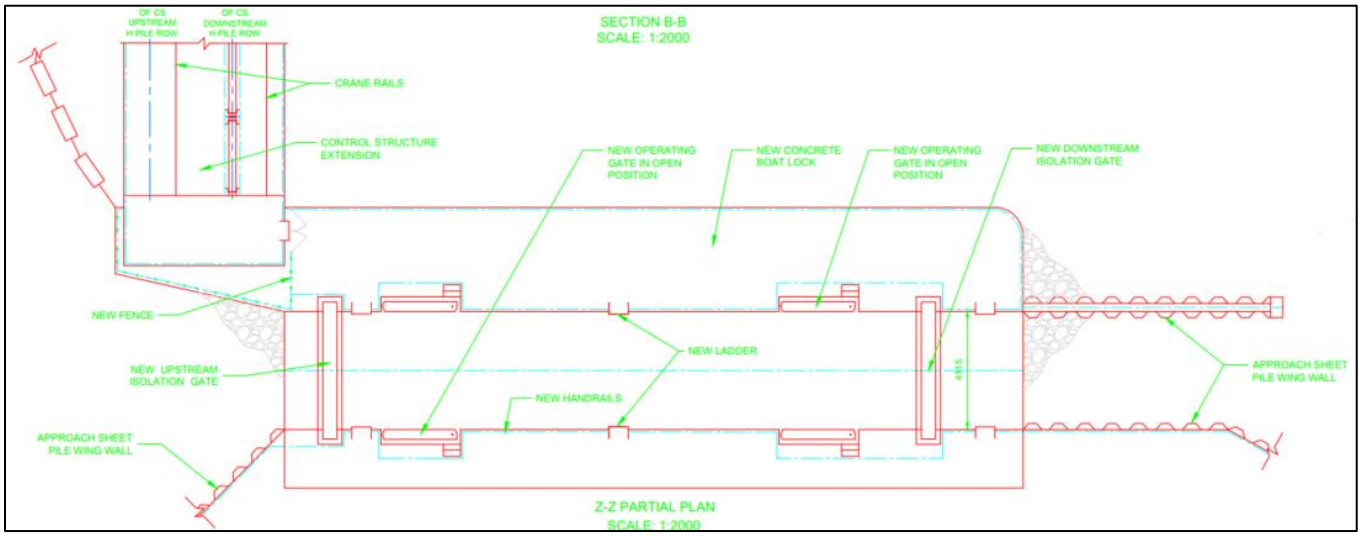

Figure 2-2 Boat Lock Replacement

2.2 Terrain Model

For the three-dimensional simulations, a digital elevation model (DEM) was developed using topographic data (LiDAR) and bathymetry data surveyed in 2023 by Underhill Geomatic. This survey was conduction using a single-beam sonar and encompassed a zone spanning 250 meters upstream and 250 meters downstream of the Lewes control structure. The LiDAR data collected in 2023 was processed into a DEM with 1 m resolution, which was subsequently integrated into the three-dimensional model. Figure 2-3 shows the developed DEM and the surveyed bathymetric points for the project area.

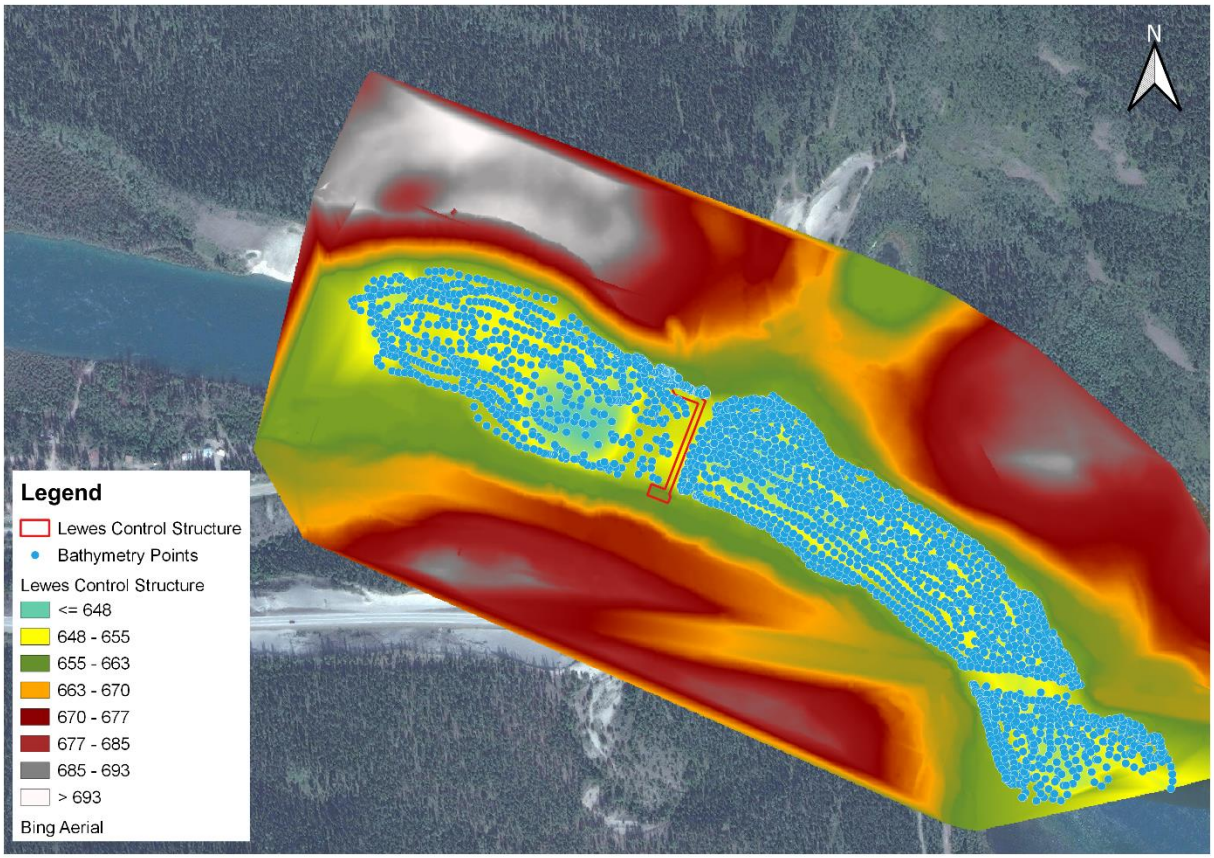

Figure 2-3 Digital Elevation Model (DEM) of Study Area

3. Design flood

3.1 Present Climate Frequency Analysis

In the summer of 2021, the Yukon River experienced an unprecedented flood event. YEC sought to determine the return period of this flood.

For this purpose, YEC provided a detailed flow rate calculated at Whitehorse hydropower plant from 2004 to 2023. This flow series was compared with the flow data obtained from Environment Canada at the hydrometric station Yukon River at Whitehorse (09AB001) from 1943 to 2023. A single set of annual maximum flow rate, covering from 1944 to 2023 (80 years), was established by combining the two sets of data for flood frequency analysis. The flow of the year 1943 was excluded from the sample since only 92/365 days were available. To assess the 2021 flood, the frequency analysis was performed for two sets of data: one from 1944 to 2020 (excluding 2021 flood and later) and another covering entire range from 1944 to 2023.

An in-house tool developed using the R language and based the HYFRAN package methodology was used to analyze the samples of the annual maximum discharge. Three statistical tests, including the Wald-Wolfowitz test of independence, Kendall's stationarity test, and the Wilcoxon homogeneity test were applied to the samples. Only samples passing these tests for a level of significance of 5% and 1% were considered for further adjustment.

Probability distributions were selected for each data set using the Bayesian Information Criterion (BIC) and a visualization of the fit between the sample and the adjusted distribution. The BIC is a mathematical criterion that gauges the goodness of fit of a model to observations, with lower BIC values indicating a better fit. Based on these criteria, the log-normal distribution is chosen for both data set.

The frequency analysis results, presented in Figure 3-1, indicated that the 2021 flood was a significant outlier, with a return period estimated as 1 in 500-year event for the dataset from 1944 to 2020. Meanwhile the 2021 flood is considered as a 1 in 200-year event for the dataset from 1944 to 2023, as shown in Figure 3-2.

Therefore, the 2021 peak discharge of 723 m^3/s exceeds the safety flood requirement of a 1:100-year based on the dam classification, when considering present-day climate.

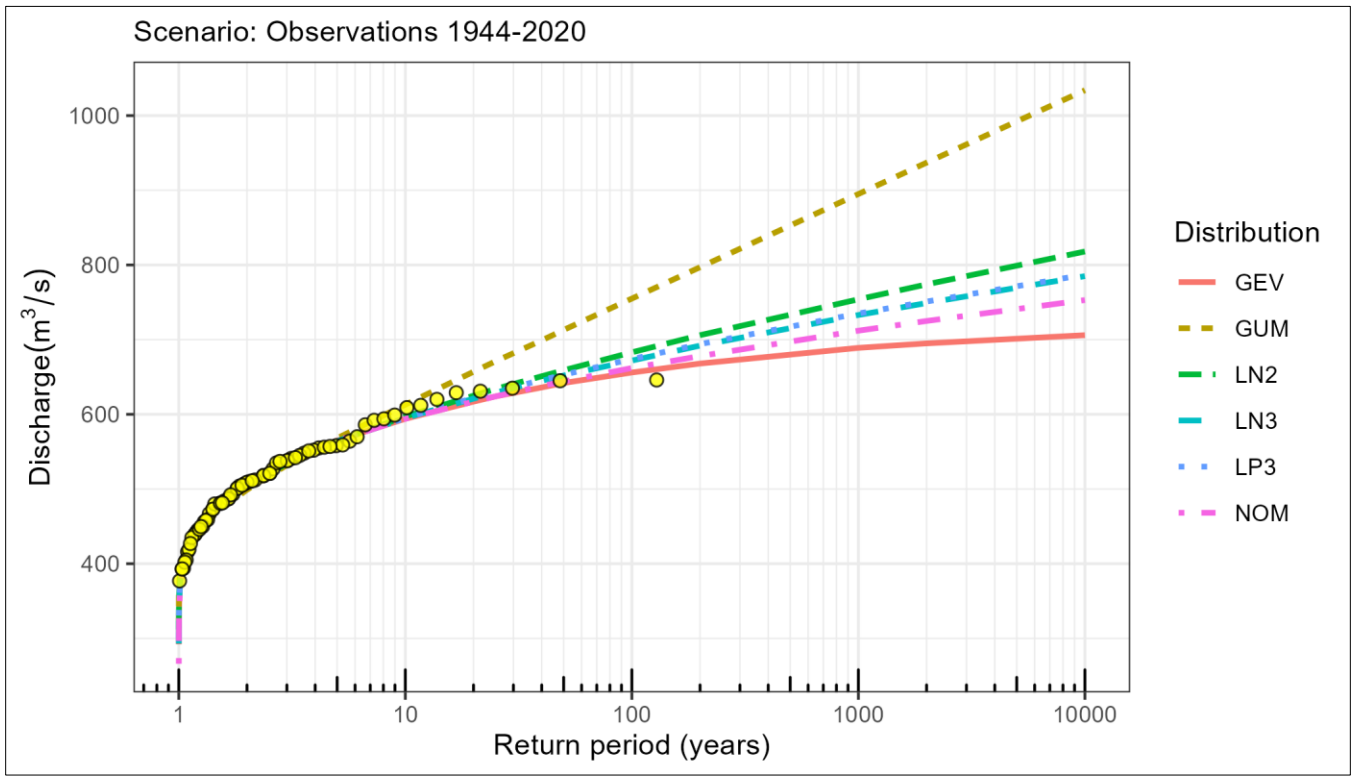

Figure 3-1 Peak Flow Statistical Analysis Results for 1944-2020 Series

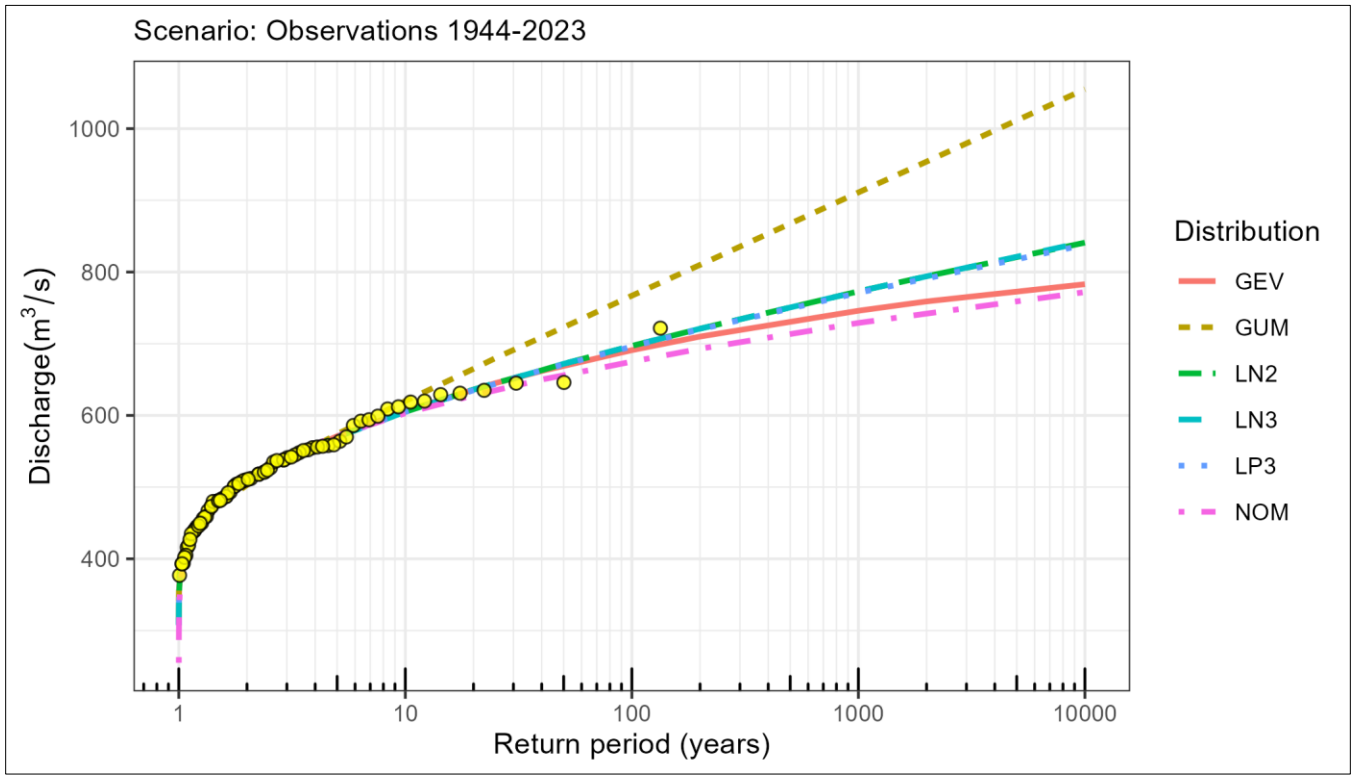

Figure 3-2 Peak Flow Statistical Analysis Results for 1944-2023 Series

3.2 Future Climate Frequency Analysis

Following YEC's request, additional analysis was performed to determine if the 2021 peak discharge exceeds the 1:100-year frequency flood discharge for a future climate scenario, i.e., under the influence of climate change.

3.2.1 Dataset

To perform the future climate analysis, AtkinsRéalis was provided by YEC with adjusted daily inflow series for Marsh Lake, based on several climate change scenarios (INRS-ETE, 2020) (see Appendix A). The series are based on 1981 to 2018 observations and cover two horizons, 2010-2040 and 2041-2070. Three scenarios of Representative Concentration Pathways (RCPs) were provided, namely RCP 2.6, RCP 4.5 and RCP 8.5. RCPs are scenarios describing the future radiation forcing, which is the heat the lower atmosphere will retain under the effect of greenhouse gases. Each scenario represents a range of outcomes of emission mitigation efforts.

Only the RCP 8.5 scenario was considered in the present study. The RCP 8.5 scenario is the most conservative and represents a baseline emission scenario with no or little success in greenhouse gas emission mitigation. Climate research shows that emissions in the last decade have been closely aligned with the RCP 8.5 scenario. Series were provided for different climate models.

Series were provided for 10 different climate scenarios, listed in Table 3-1 and presented in the climate report (INRS-ETE, 2020). The future climate series are based on a forecasting method using Ensemble Streamflow Forecast (ESP) schemes, which use randomly selected historical sequences of climate data. The methodology is described in detail in the report (INRS-ETE, 2020).

3.2.2 Frequency Analysis of Peak Discharge and Volume

All 2010-2040 and 2041-2070 RCP 8.5 series were analyzed using the following methodology:

- The projected inflows during the time span from the 120th day (commencement of the rising limb of the hydrograph) to the 365th day of each year are employed to compute the volume associated with each scenario.
- Both the inflow data and the calculated volumes are subjected to statistical analysis utilizing the R programming language and employing the methodology outlined in the HYFRAN package. This analysis aims to ascertain the peak inflow and volume corresponding to a 100-year return period.

Table 3-1 illustrates the scenarios alongside the estimated peak inflow and flood volume corresponding to a 100-year return period under climate change forecasting scenarios.

The median peak discharge and peak volume obtained for every climate model was calculated. The series providing results closest to the highest median between the two horizons, namely miroc5_rcp85 for 2041-2070, was selected for the future climate forecast. The use of the median climate model is deemed a reasonable assumption, since the most conservative RCP scenario is used.

Figures 3-3 and 3-4 shows the series and the adjusted distributions for the miroc5_rcp85 scenario.

Table 3-1 Statistical Analysis Results of Peak Inflow and Flood Volume for Future Climate Scenarios

Scenario	1;100-year Peak Inflow (m^3/s)	Probability Distribution	1;100-year Flood Volume ($10^6 m^3$)	Probability Distribution
Observed	1,288	Gumbel	9324	Normal
2010-2040 period				
access1-0_rcp85	1,467	Gumbel	10,595	Normal
canesm2_rcp85	1,582	Lognormal	11,982	Normal
ccsm4_rcp85	1,453	Gumbel	12,123	Normal
cnrm-cm5_rcp85	1,292	Lognormal	10,022	GEV
csiro-mk3-6-0_rcp85	1,355	Log.Normal.3P	10,156	Normal
gfdl_esm2g_rcp85	1,386	Lognormal	10,261	GEV
inmcm4_rcp85	1,446	Lognormal	10,784	Lognormal
miroc5_rcp85	1,521	Lognormal	11,446	Normal
mpi-esm-lr_rcp85	1,718	Lognormal	12,240	Lognormal
mri-cgcm3_rcp85	1,070	Normal	10,511	Normal
2041-2070 period				
access1-0_rcp85	1,471	Normal	10,717	Log.Normal.3P
canesm2_rcp85	1,999	Lognormal	11,364	Normal
ccsm4_rcp85	1,674	Normal	11,568	Normal
cnrm-cm5_rcp85	1,132	Normal	8,945	GEV
csiro-mk3-6-0_rcp85	1,941	Gumbel	11,209	Normal
gfdl_esm2g_rcp85	1,533	Lognormal	10,661	Lognormal
inmcm4_rcp85	1,514	Gumbel	10,877	Lognormal
miroc5_rcp85	1,550	Log.Normal.3P	11,270	Lognormal
qpi-esm-lr_rcp85	2,390	Gumbel	12,725	Lognormal
mri-cgcm3_rcp85	1,619	Gumbel	10,039	Lognormal
Median of 2010-2040 period	1,449		10,690	
Median of 2041-2070 period	1,585		11,043	

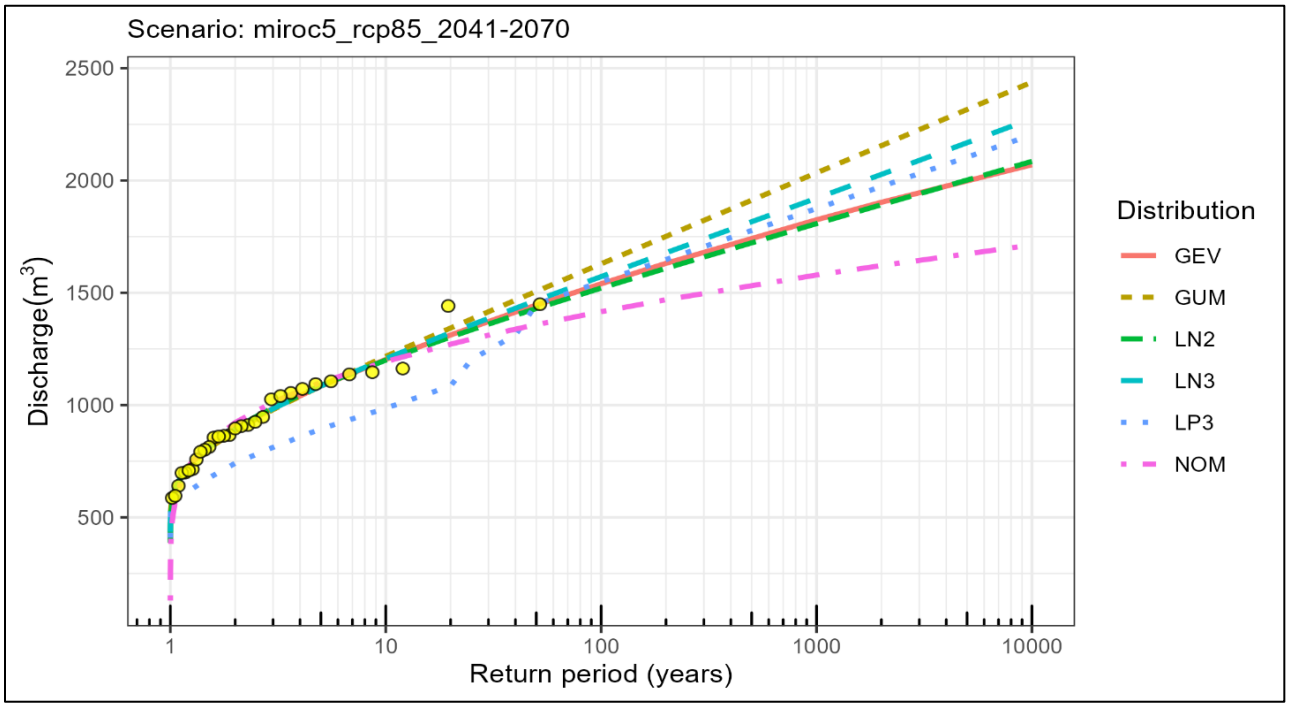

Figure 3-3 Statistical Analysis – Miroc5_rcp85 – 2041-2070 period – Peak Inflow

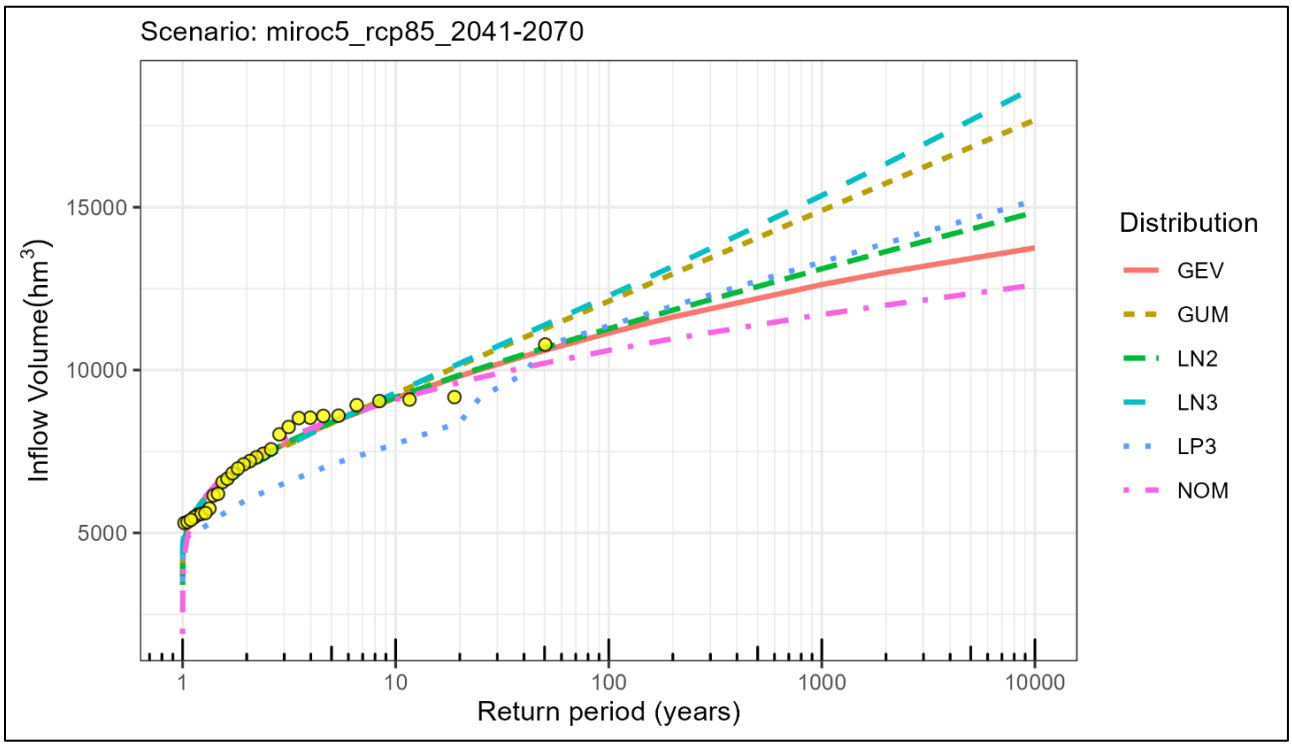

Figure 3-4 Statistical Analysis – Miroc5_rcp85 – 2041-2070 period – Flood Volume

3.2.3 Flood Hydrograph

A flood hydrograph was built to match the 1:100-year peak inflow and flood volume obtained from the statistical analysis of the median scenario for the 2041-2070 period (miroc5_rcp85). The shape of the hydrograph was based on the most severe flood within the forecasted inflows (year 2032), with adjustment made to match the 1:100-year peak flow and flood volume. The use of one of the forecasted flood hydrographs was deemed more appropriate than the use of an observed flood event, as climate change will impact the timing and severity of future flood events.

The resulting hydrograph is shown in Figure 3-5.

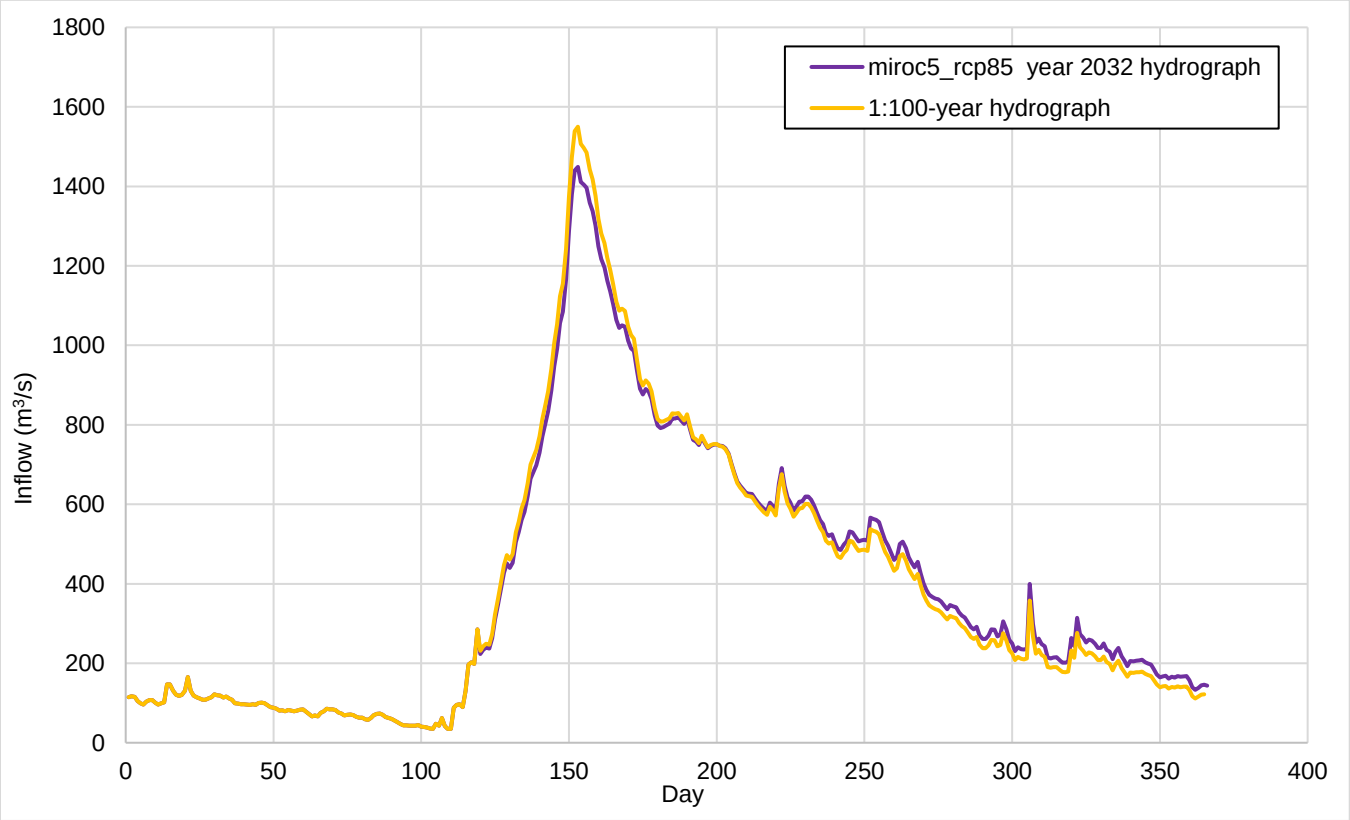

Figure 3-5 Future Climate 1:100-year Inflow Hydrograph Based on miroc5_rcp85 series.

3.2.4 Flood Routing

In order to determine the discharge at the Lewes Control Structure, the inflow hydrograph must be routed through Marsh Lake.

A spreadsheet-based routing model of Marsh Lake was built. The lake storage curve was extracted from the Digital Elevation Model (DEM) obtained from the Canadian Digital Elevation Model (CDEM) website.

The rating curve for the Marsh Lake outflow was established using 1D modelling results. The 1D model is presented in detail in Section 4.0. The curve extracted from the model was used instead of a linear regression, because it allowed for a better comparison of the impact of different geometries of the Lewes Structure (see Section 6.0).

The flood routing was modelled while considering 30 open gates at the Lewes Control structure. The rating curves extracted from the 1D model are presented in Figure 3-6, along observed data from 2004 to 2018, for months where the gates of the Lewes Control Structure are open (May to August). While a poorer fit is obtained for Marsh Lake elevation ranging from 654 to 656 m (see discussion section 4.3.2), the rating curves are sufficiently accurate to allow for an adequate estimate of the peak outflow at Marsh Lake (see below the routing model validation results).

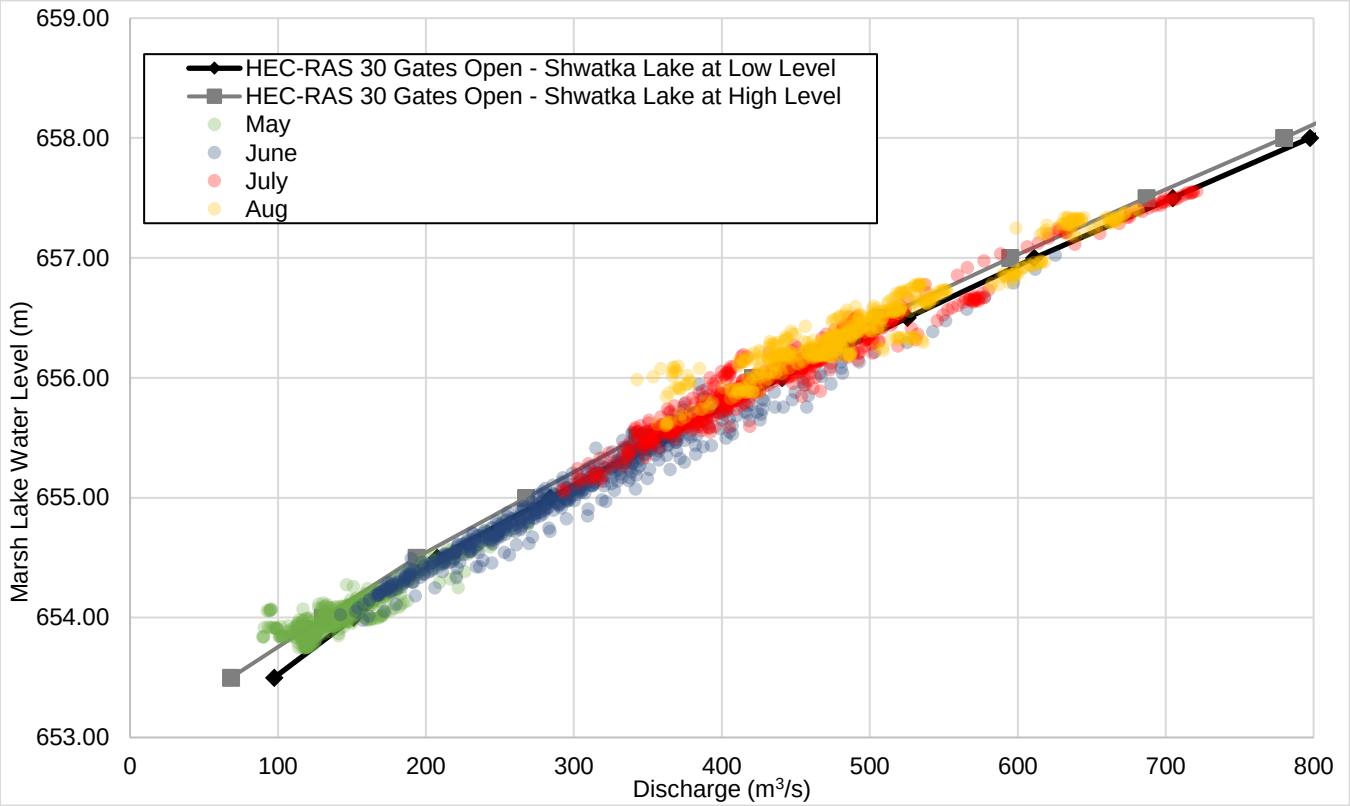

Figure 3-6 Rating Curve from HEC-Ras Model and Historical Data from 2004 to 2018

The Excel routing model was validated using recorded inflow hydrographs and water level for various years. Results were compared with the water levels observed at Marsh Lake (station 09AB004) and the outflow of the Yukon River at Whitehorse (station 09AB001).

Routing results for the 2007 flood, the most severe on record between 2004 and 2018, are shown in figures 3-7 and 3-8. The routing model successfully represents the maximum level in Marsh Lake, while the peak discharge is slightly overestimated (+3.5%).

It should be noted that observed and modelled levels diverge in mid-October (day 289) since the gate operation conducted in 2007 (closing of 10 gates) is not represented in the routing model. The routing model only modelled the full opening of the structure gates since the objective is the characterization of the impact of severe flood events.

Routing of the 1:100-year flood was performed using the curve corresponding to 30 open gates, with a low level in Schwatka Lake. Historical data shows that these are valid hypothesis of potential operation during a severe flood.

Routing results are shown in Figure 3-9. The peak discharge out of Marsh Lake is 844 m^3/s, a 17% increase in comparison with the peak 2021 discharge of 727 m^3/s.

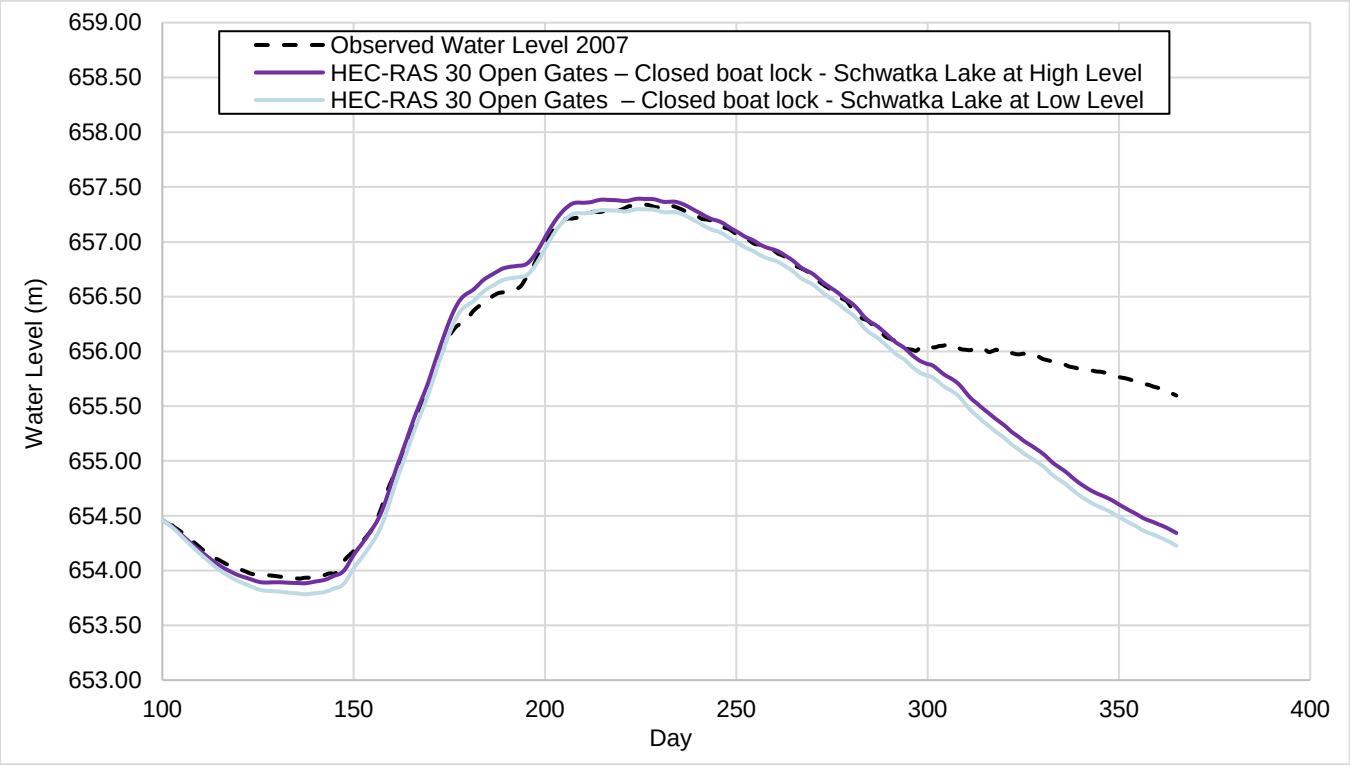

Figure 3-7 Routing Model Validation – Routed Water Levels for the 2007 Flood

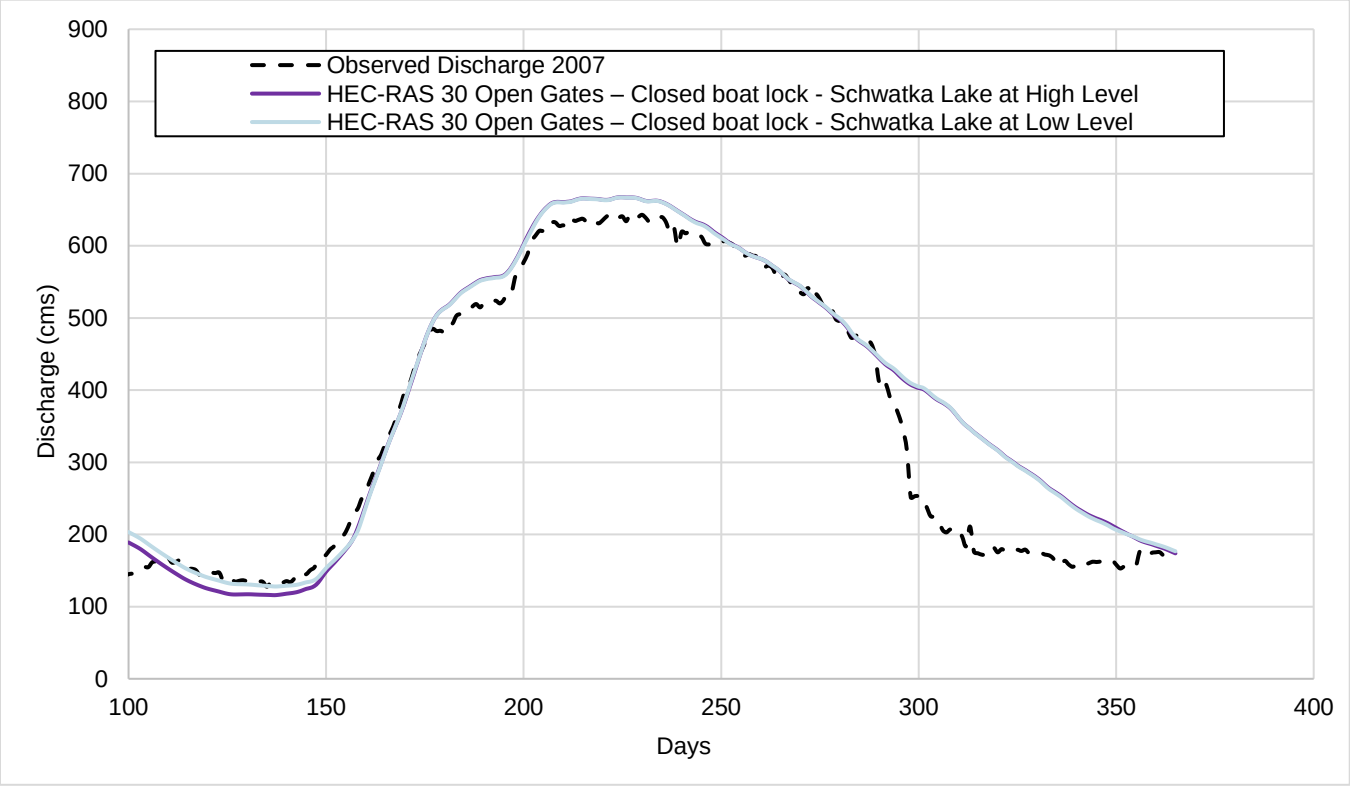

Figure 3-8 Routing Model Validation – Routed Discharges for the 2007 Flood

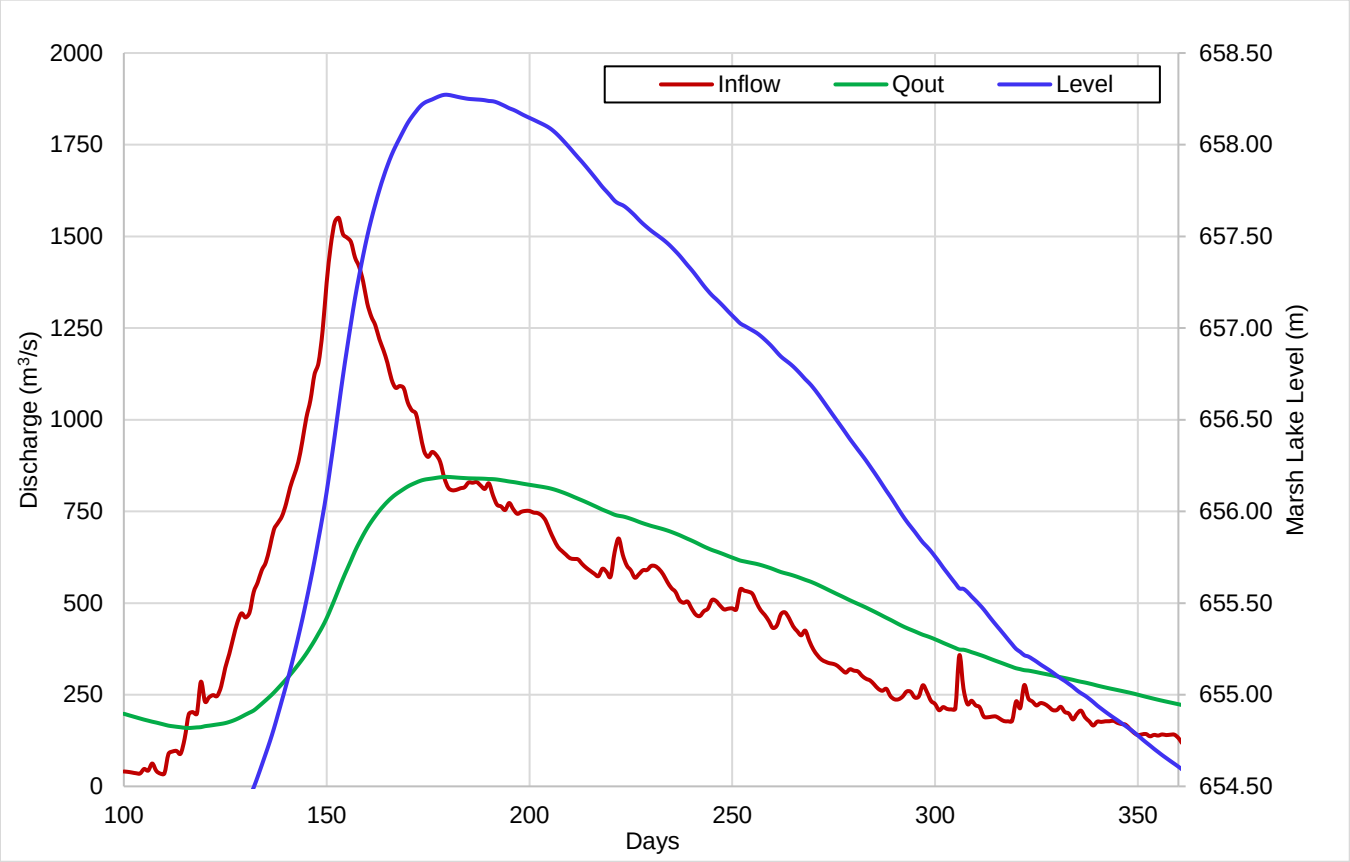

Figure 3-9 Future Climate 1:100-year Flood Routing in Marsh Lake

3.3 Summary

Statistical analysis showed that the 2021 peak discharge is more conservative than the prescribed design flood event for the Lewes Control Structure under present climate since the discharge is above the 1:100-year estimation.

However, a higher flow of 844 m^3/s, corresponding to the peak discharge out of Marsh Lake, should be used as the 1:100-year flow if considering future climate estimates.

4. 1D Hydraulic Model

4.1 Modifications to the Existing Model

The software HEC-RAS (version 6.3.1), developed by the US (United States) Army Corps of Engineer (HEC-RAS 2022), is a computer application designated to simulate the hydraulics of water flow through natural rivers, and it is widely used to assess the flood routing. For this study, the one-dimensional HEC-RAS model developed by KGS Group was used. This model spans from Marsh Lake to the Forebay of Schwatka Lake, in which the Lewes control structure and the old dam sill are integrated. Various parameters in the original KGS hydraulic model were adjusted based on available data, as summarized in Table 4-1.

Table 4-1 Parameters in hydraulic model KGS vs AtkinsRéalis

Parameters	KGS model (2010)	AtkinsRéalis model (2024)
Gate width of LCS (m)	1.9	2.5
LCS Sill elevation (m)	652.13	651.97
Old dam downstream sill elevation (m)	652.6	652.40

KGS initially modelled LCS using a smaller gate bay width of 1.9 m compared to the existing structure width of 2.5 m, possibly to account for contraction losses. However, AtkinsRéalis believes that this approach may not be optimal for model calibration, as the difference in width might have an outsized impact on results for flood events of different magnitudes compared to those used during the calibration stage. Consequently, the model was re-calibrated using peak discharge and the surveyed water profile during 2005 flood event. It should be noted that the cross-sections geometry of the KGS model was not modified, with the exception of the proximity of the control structure, where the 2023 survey bathymetry was used (see section 2.2). The remaining cross-sections are therefore based on the bathymetry surveyed in 2005 and 2008, as referenced in KGS report (KGS, 2010). The details of this calibration are provided in the following sections.

Furthermore, the upstream section of the model was also recalibrated to align with the measured peak level in Marsh Lake in 2021. The downstream section of the 1D model, beyond the LCS, was left unchanged. Finally, the calibration process was revisited to use an unsteady flow regime and enhance accuracy near the rapids.

Finally, the discharge coefficients used in the 1D model were adjusted based on the results obtained from FLOW-3D simulations (see sections 5 and 6).

4.2 Boundary Conditions

The flow rate or stage at Marsh Lake is specified as the boundary condition at the upstream limit of the model, while the stage (water level) at forebay of Schwatka Lake is applied as the boundary condition at the downstream limit of the model.

4.3 HEC-RAS 1D Calibration and Validation

4.3.1 Model Calibration

The model was re-calibrated to match a water surface profile surveyed by Underhill Geomatics Ltd on July 8, 2005. The estimated flow for the date of water surface profile survey in 2005 was 435 m^3/s. original calibration results from KGS and the reviewed calibration results are shown in figures 4-1 and 4-2, respectively.

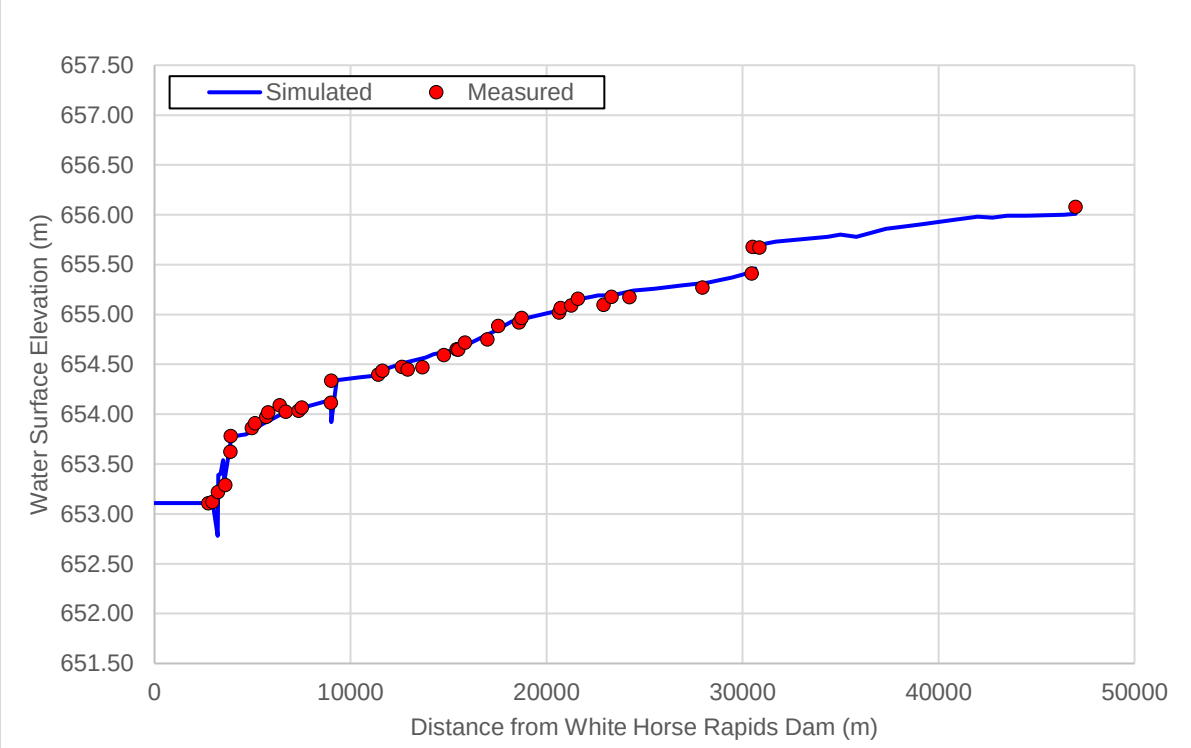

Figure 4-1 Original KGS 2005 Flood Calibration Results

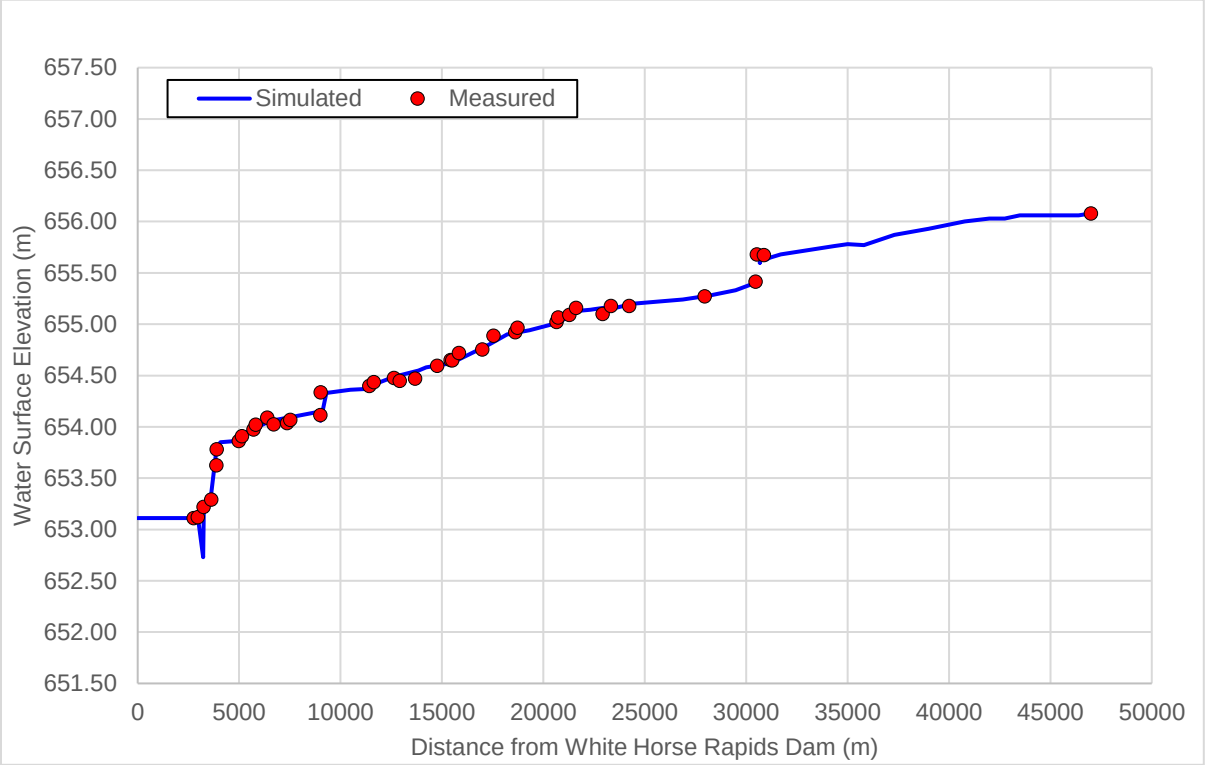

Figure 4-2 Reviewed 2005 Flood Calibration Results

4.3.2 Model Validation

The model was further validated using the peak flows and observed elevation of Marsh Lake recorded during various flood events, including the years 2007, 2021, and 2022. The result of this validation is summarized in Table 4-2.

Table 4-2 Calibration Results of HEC-RAS 1D for Different Floods

Flood Event (Year)	Recorded Yukon River Flows (m^3/s)	Observed Elevation Marsh Lake (m)	Modeled Elevation Marsh Lake (m)	Difference (m)
2021*	723	657.56	657.58	+0.02
2022	629	656.98	657.10	+0.12
2007	645	657.34	657.19	-0.15

***Note:** Boat lock was open during the 2021 flood peak

In 2022 and 2023, all gates of LCS were opened prior to the freshet, which allow for the establishment of a discharge/lake level relationship from the data collected at the plant and the water level measured at Marsh Lake. This relationship will be used to validate the HEC-RAS 1D model.

Recorded levels in the Forebay of Schwatka Lake and Marsh Lake and recorded average daily discharge from 2022 and 2023, were used to construct a rating curve for both high and low levels of Schwatka Lake. Comparisons between the results of the HEC-RAS 1D model and the established rating curve are presented in Figure 4-3 (for high levels of Marsh Lake) and Figure 4-4 (for low levels of Marsh Lake).

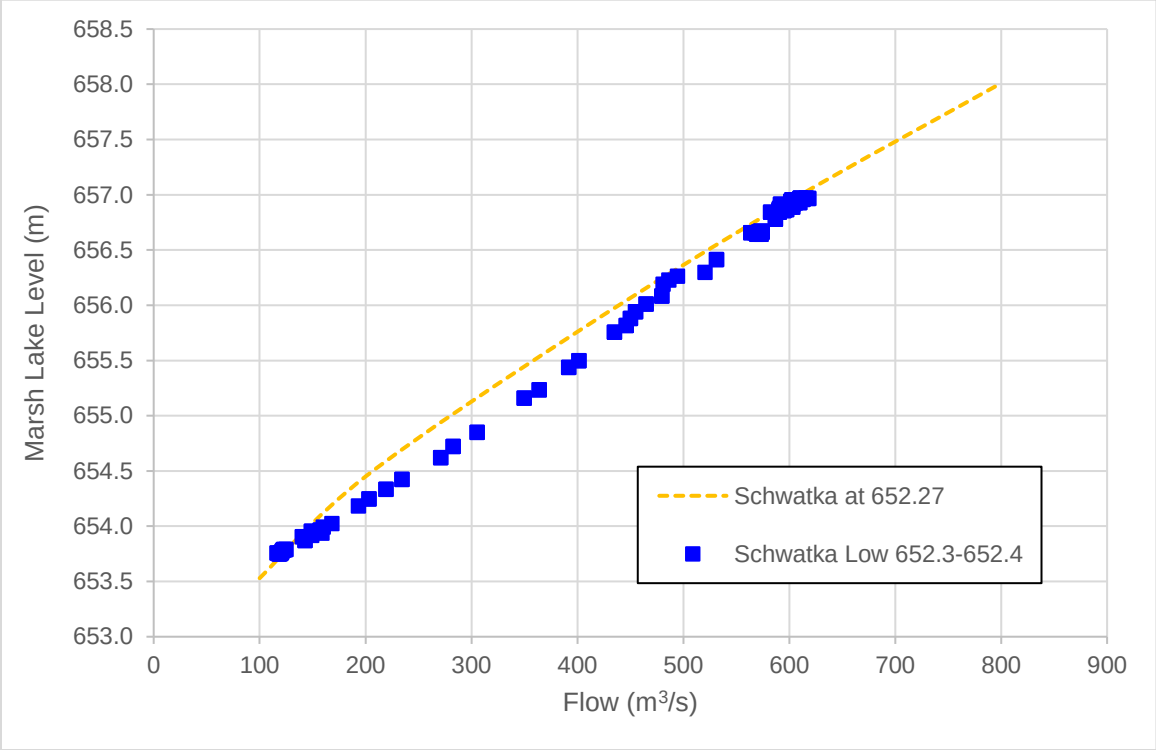

Figure 4-3 Validation of 1D Model Results for Low Schwatka Lake Levels

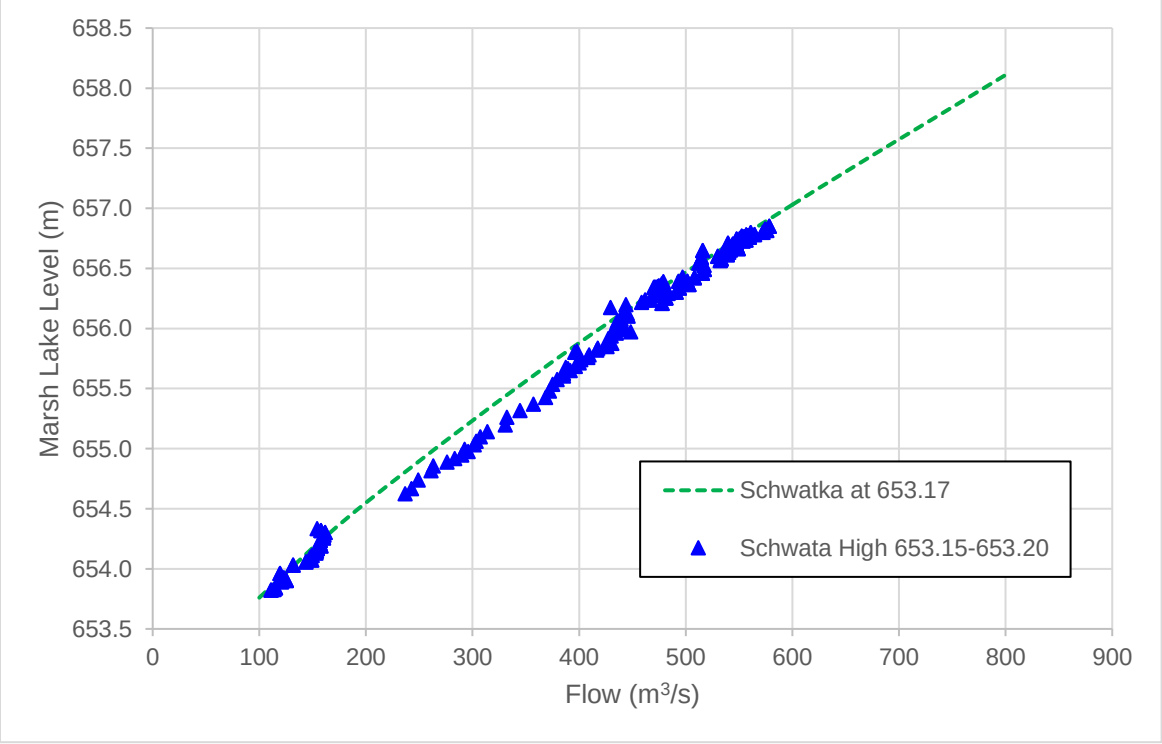

Figure 4-4 Validation of 1D Model Results for Low Schwatka Lake Levels

The results indicate that the models demonstrate a good performance for high Marsh Lake levels (above 656 m). This was as expected since it was calibrated for flood events. Additionally, the results are satisfactory at low levels, around 654 m. However, more significant discrepancies were observed for Marsh Lake elevations between these levels, particularly at low Schwatka Lake levels. However, these differences are deemed acceptable, for the following reasons:

1. Many of these points were measured during the initial stages of the freshet when the Marsh Lake levels are rising. Consequently, the system is not yet stable during these points, and the discrepancies may be attributed to limitations associated with the daily averages utilized in the analysis.
2. The routing model built using the 1D model results was able to properly represent the routing of historical events (see section 3.2).
3. Despite uncertainties regarding the existing capacity at certain lake elevations, we believe that the model remains suitable for determining the relative impact of proposed gates on the hydraulic capacity of LCS.

5. 3D Hydraulic Model

5.1 Objectives

A Computational Fluid Dynamics (CFD) of 3D hydraulic model of the Lewes Control Structure was built using the FLOW-3D software.

FLOW-3D solves the full three-dimensional free surface governing equations of flow, taking into account turbulence effects. This enables more accurate modelling of (1) the submerged weir flow, (2) the interaction between different spill structures (such as the old dam versus Lewes in this study), and (3) the impact of the steel cantilever contraction on the hydraulic capacity.

These advanced capabilities of FLOW-3D provide a valuable methodology for the present study, which involves a combination of 1D and 3D modelling. Specifically, 3D CFD model will be employed to simulate detailed flow characteristics in the vicinity of the Lewes structure, while a 1D model used to characterize the large-scale water flow system from Marsh Lake to Schwatka Lake. In this methodology, the discharge coefficient used in 1D model will be adjusted based on the results obtained from 3D modelling.

5.2 Model

The spatial domain of the current study encompassed a section of the Yukon River extending 200 m upstream and 200 m downstream relative to the LCS. The Cartesian structured mesh was employed with different mesh sizes. A fine mesh with a resolution of 0.25 m was used in the vicinity of Lewes structure to accurately capture the length scale of the steel cantilevers, while a coarser mesh with a resolution of 1 m is used for the upstream and downstream zones of the structure. A transitional medium-sized mesh block with a resolution of 0.5 m was used between these mesh blocks. The schematic of 3D modelling approach is presented in Figure 5-1.

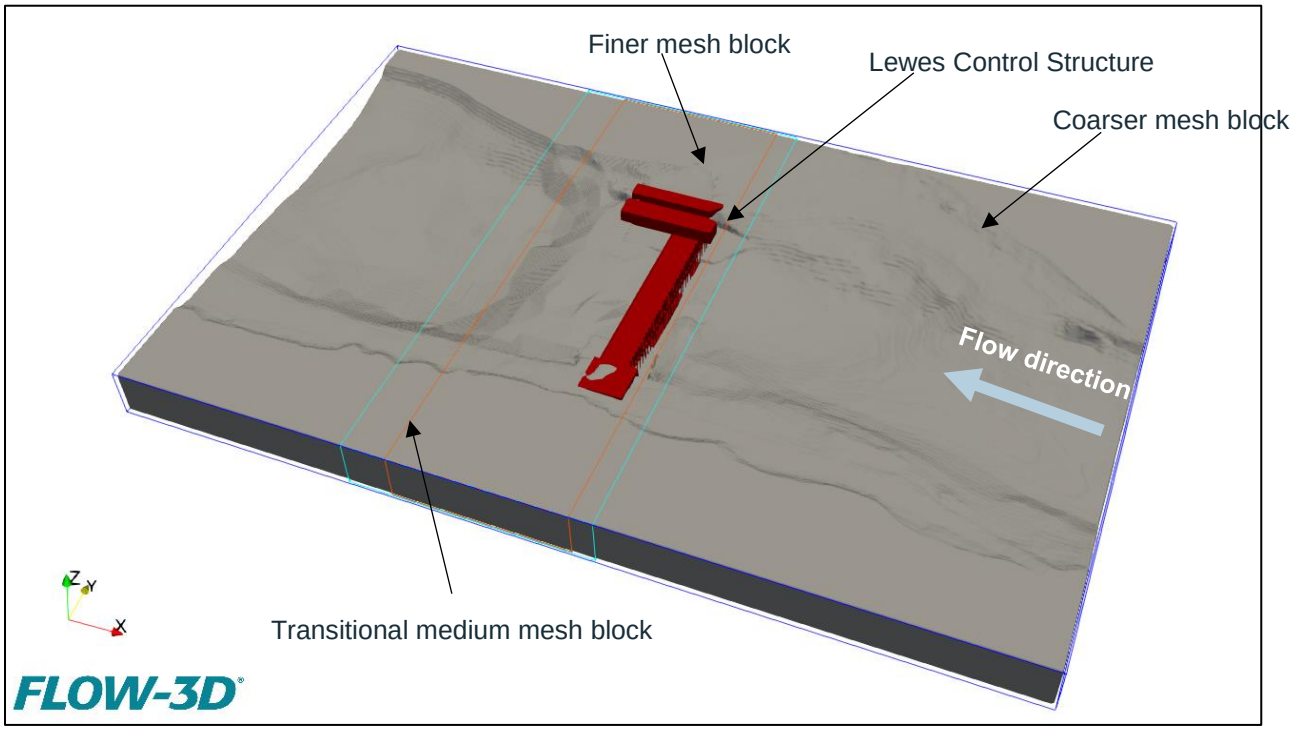

Figure 5-1 FLOW-3D Modelling Schematic

Boundary condition for the fluid (water) within the computational domain were set with a specified flow rate at the inlet, and a fixed tailwater elevation at the outlet. The level at the downstream boundary were determined for each of the modeled flow rate using the 1D model.

The simulations were terminated either after a simulation time of 500 seconds or upon reaching a steady-state condition. Several flow quantities were monitored to assess the steady state termination conditions, including (1) total mass of water, (2) average kinetic energy, (3) flow rate thorough the structure, and (4) pressure at monitoring points. A simulation is considered stable when the difference of monitored quantities between two consecutive time steps was less than 0.01 %.

5.3 Scenarios

Four geometries were modelled, each for the two flow scenarios presented in section 3. The geometries are presented in Table 5-1. Note than additional geometries, corresponding to a partial removal of the older structures located downstream of LCS, are discussed in detail in a different section of the present report (see Section 5.6).

Table 5-1 Modelled Geometries

Geometry	Description	Notes
1	30 open gates and closed boat lock gates	Baseline scenario corresponding to the existing structure geometry if the boat lock is rehabilitated without removable lock gates. Corresponds to the flood condition for most recorded years.
2	30 open gates and opened boat lock gates	Existing spillway structure with removable lock gates. Comparison with geometry 1 will isolate the effect of removable lock gates. Also corresponds to the 2021 flood conditions, where the lock gates were opened.
3	32 open gates and opened boat lock gates	Structure with 2 additional gates, corresponding to the preliminary design proposed by KGS. Comparison with geometry 2 will isolate the effect of adding two gates.
4	Lewes Control Structure	Steel cantilevers LCS and the attached boat lock are completely removed down to the sill elevation, but the left abutment is still in place.

5.4 3D Modelling Results – 2021 Peak Flow

This section presents the 3D modelling results for the four aforementioned geometries, under the 2021 peak discharge (723 m^3/s). Figures 5-2 to 5-5 show the modelled velocities. Water surface elevations are detailed in Table 5-3. Modelled longitudinal water surface profiles of the middle of the river is presented in figures 5-6 and 5-7.

Generally, the modelled geometry has little impact on the upstream level. This is due to the high downstream level, which controls the capacity at the structure. For instance, opening the lock lowers the level 200 m upstream of the structure by about 1 cm, while adding two gates has a 2 cm impact. Even the complete removal of the structure has quite a limited impact of 4 cm.

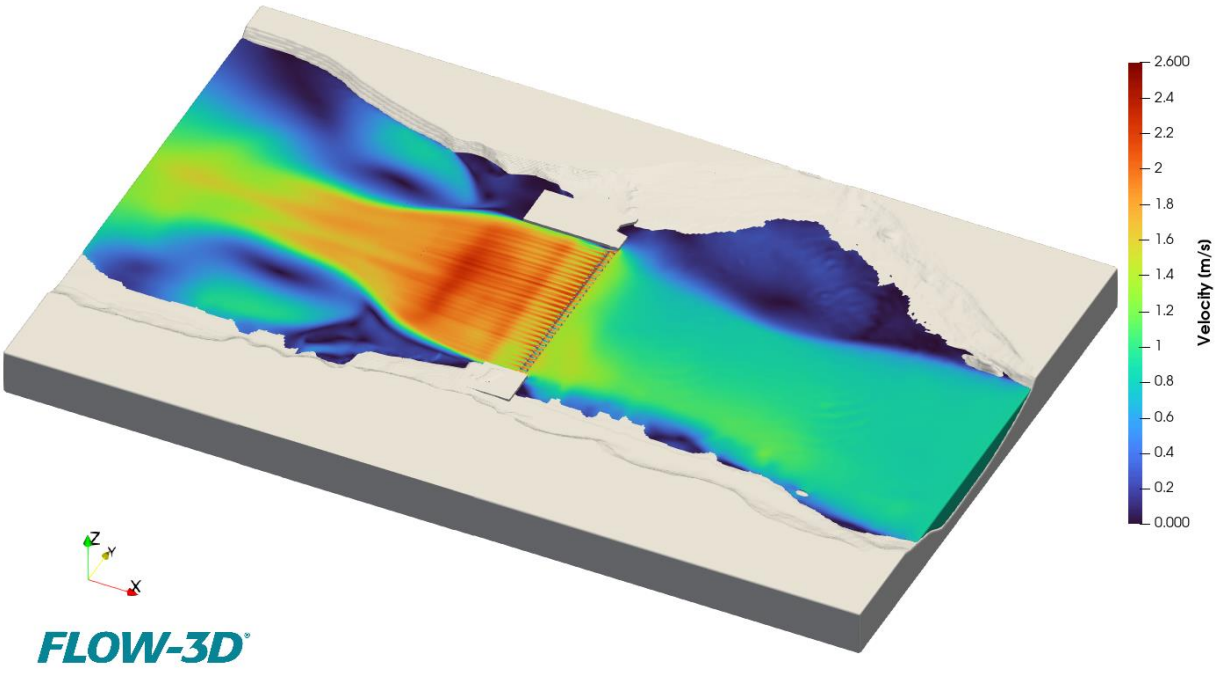

Figure 5-2 FLOW-3D Results – 723 m^3/s – LCS with 30 gates – Closed Boat Lock (Geometry 1)

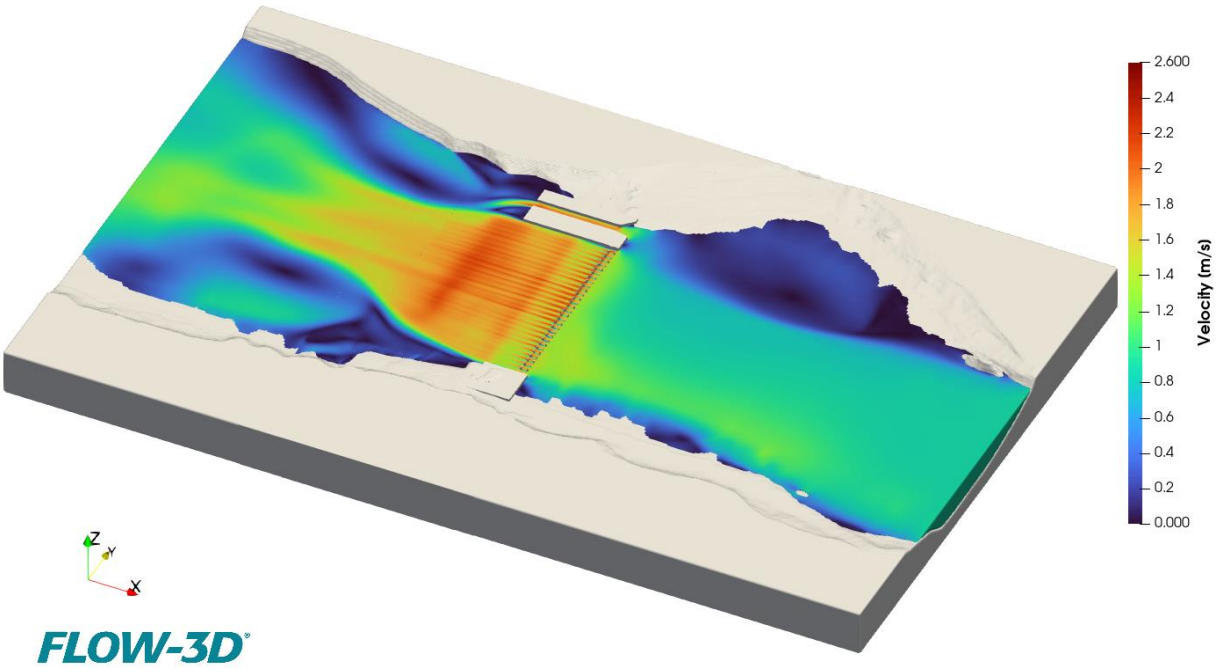

Figure 5-3 FLOW-3D Results – 723 m^3/s – LCS with 30 gates – Opened Boat Lock (Geometry 2)

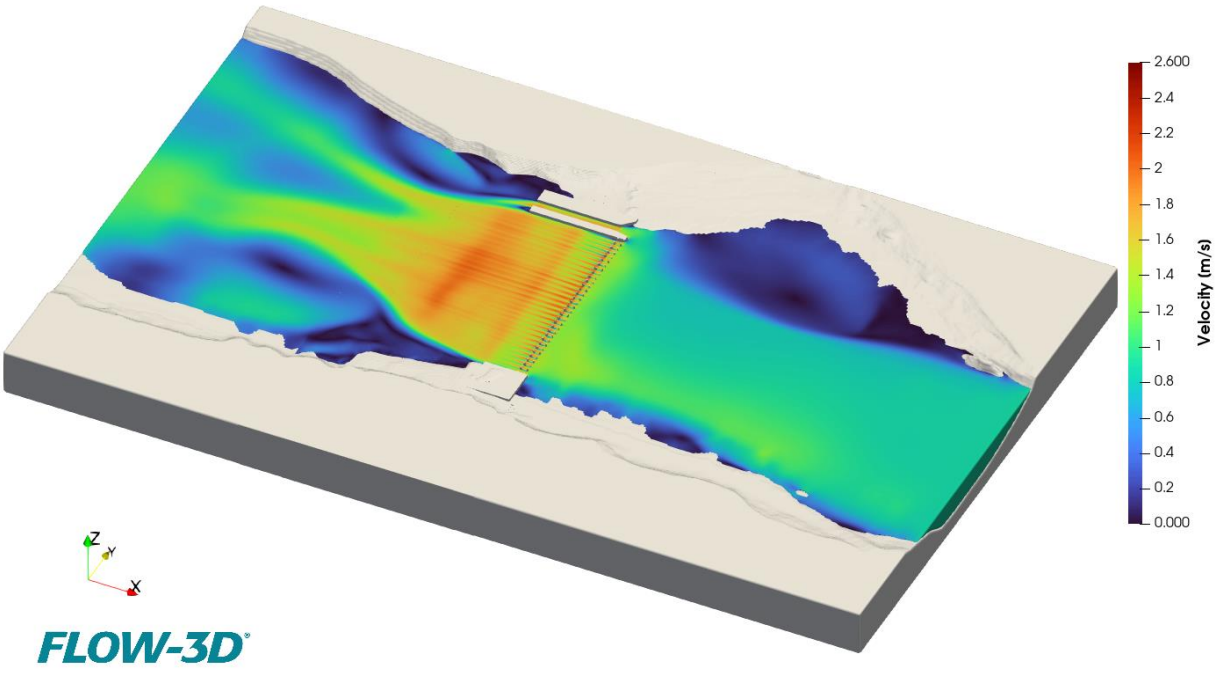

Figure 5-4 FLOW-3D Results – 723 m^3/s – LCS with 32 gates – Opened Boat Lock (Geometry 3)

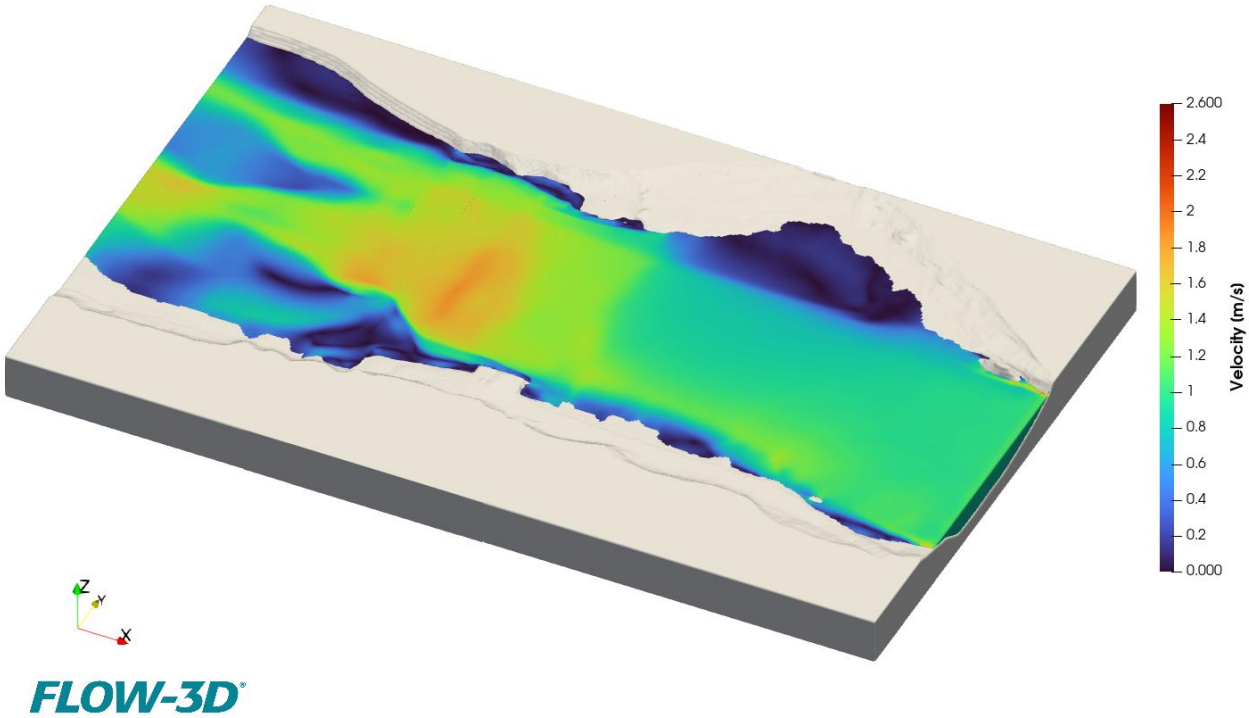

Figure 5-5 FLOW-3D Results – 723 m^3/s – LCS and Lock Removed (Geometry 4)

Table 5-2 Flow 3D Modelling Results – 2021 Peak Discharge (723 m^3/s)

Location	Modelled Geometry			
	Water Surface Elevation – 30 gates – Closed Lock (m)	Water Surface Elevation – 30 gates – Open Lock (m)	Water Surface Elevation – 32 gates – Open Lock (m)	Water Surface Elevation – LCS Removed at Sill Elevation (m)
200 m downstream of LCS	656.82	656.82	656.82	656.82
100 m downstream of LCS	656.79	656.79	656.79	656.79
100 m upstream of LCS	657.00	656.99	656.97	656.94
200 m upstream of LCS	657.02	657.00	656.99	656.95

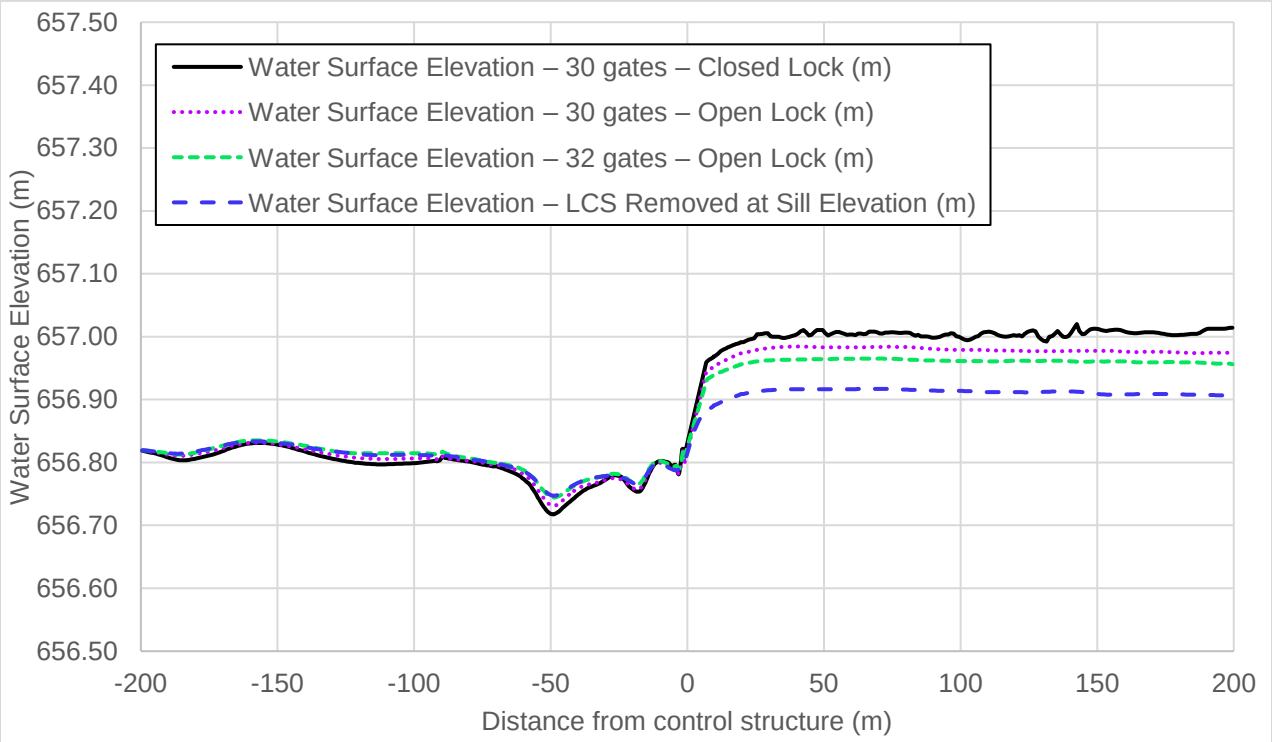

Figure 5-6 Flow 3D Modelling Results – 2021 Peak Discharge (723 m^3/s) – Water Surface Profile without Terrain Profile

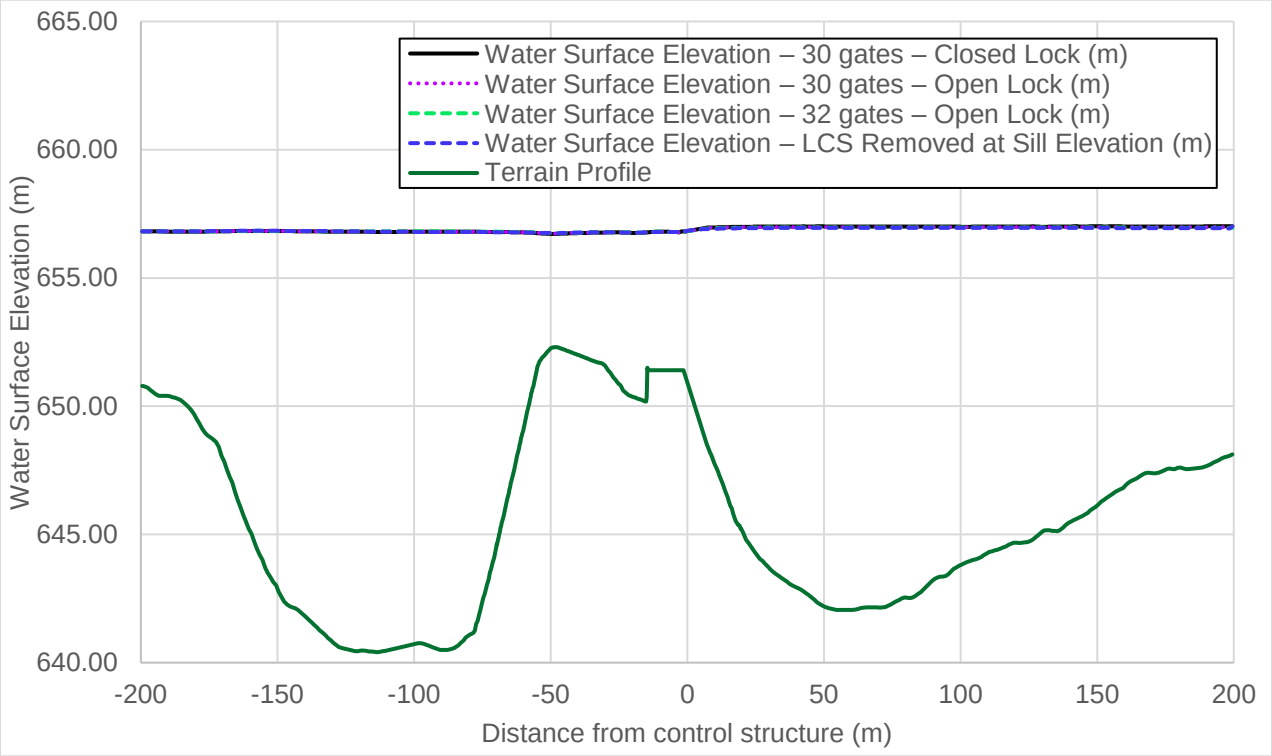

Figure 5-7 Flow 3D Modelling Results – 2021 Peak Discharge (723 m3/s) – Water Surface Profile with Terrain Profile

5.5 3D Modelling Results – 1:100-year Discharge for Future Climate

This section presents the 3D modelling results for the four geometries under the future climate 1:100-year peak discharge (844 m^3/s). Figures 5-8 to 5-11 show the modelled velocities. Water surface elevations are detailed in Table 5-3. Modelled longitudinal water surface profiles of the middle of the river is presented in figures 5-12 and 5-13.

Under a 844 m^3/s discharge, the water level reaches the bottom of the gates in their fully opened position (657.15 m), for all modelled geometries. However, the control structure deck is not submerged. It should be noted that this can be prevented by the complete removal of the gates, as it was done during the 2021 flood. The complete removal was not modelled, as it is considered that it would have an insignificant impact on the relative discharge capacities of the modelled geometries.

Generally, the modelled geometry has little impact on the upstream level. This is due to the high downstream level, which controls the capacity at the structure. For instance, opening the lock lowers the level 200 m upstream of the structure by about 2 cm, while adding two gates has a 3 cm impact.

However, the complete removal of the structure has a more significant impact of 12 cm at the 200 m upstream of Lewes structure.

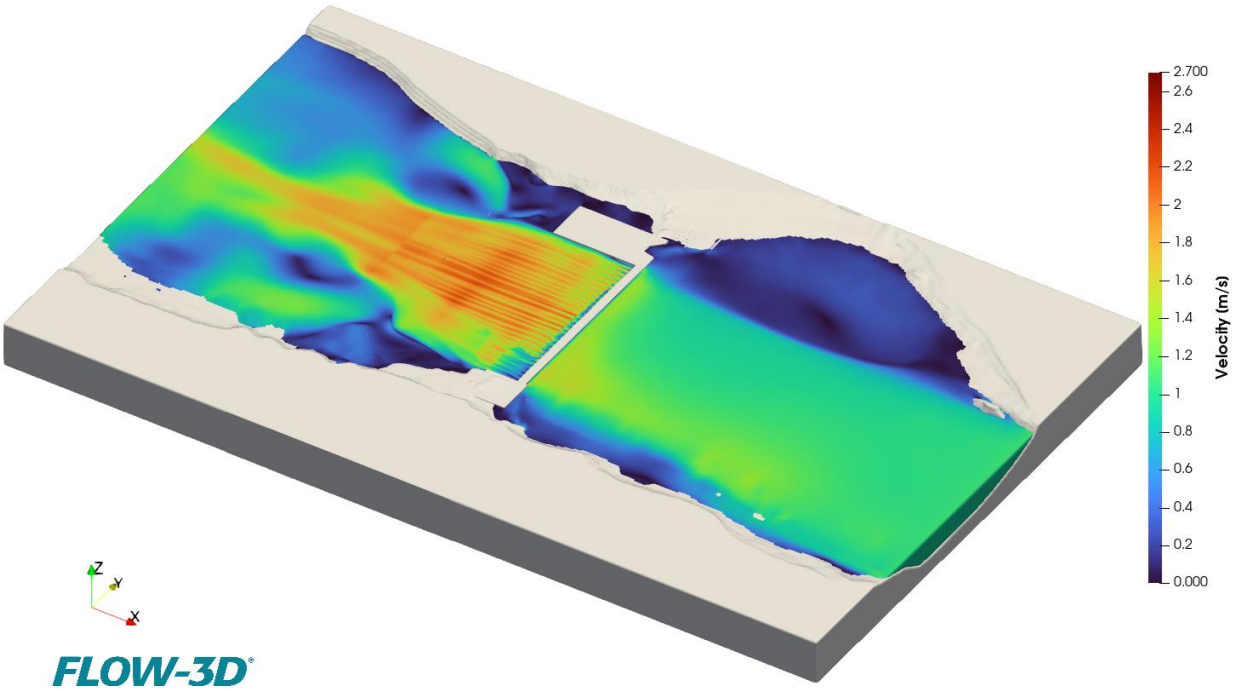

Figure 5-8 FLOW-3D Results – 844 m^3/s – LCS with 30 gates – Closed Boat Lock (Geometry 1)

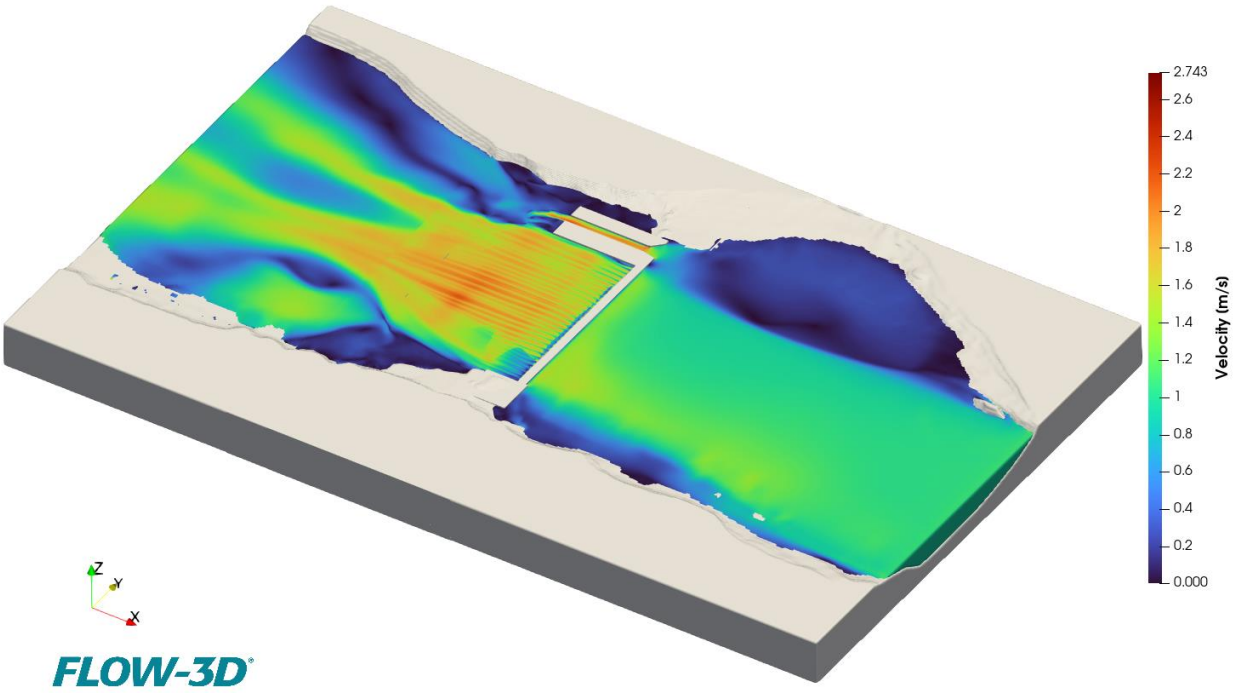

Figure 5-9 FLOW-3D Results – 844 m^3/s – LCS with 30 gates – Opened Boat Lock (Geometry 2)

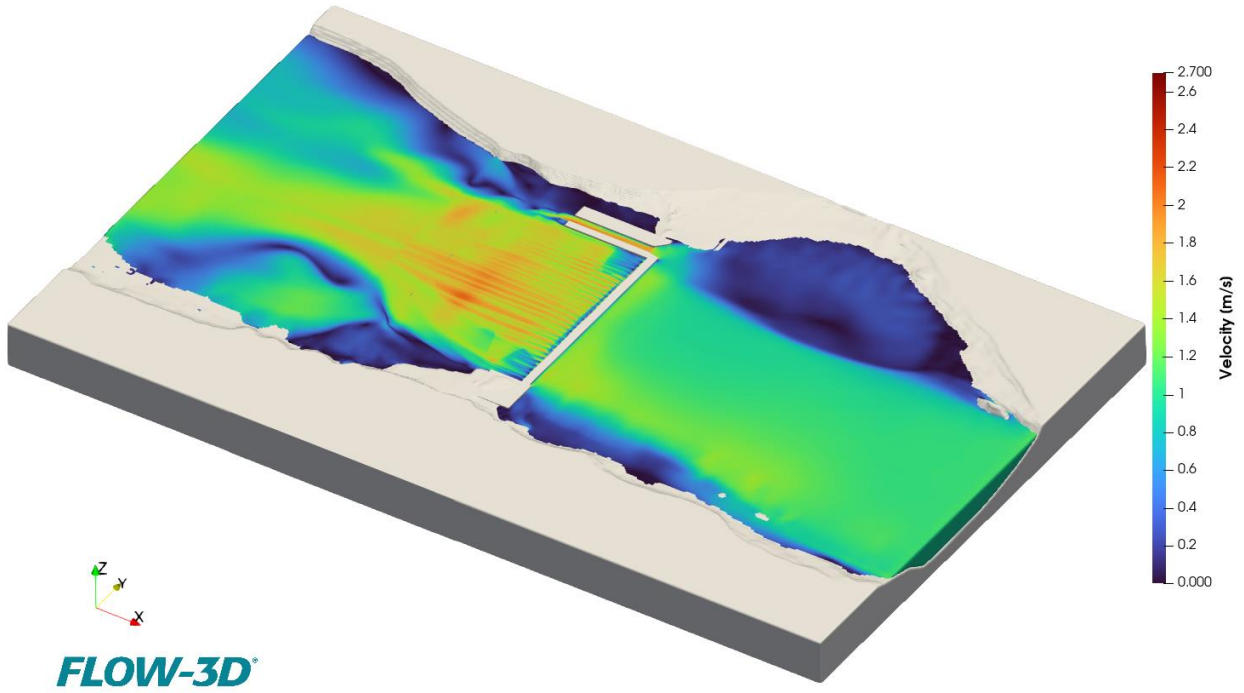

Figure 5-10 FLOW-3D Results – 844 m^3/s – LCS with 32 gates – Opened Boat Lock (Geometry 3)

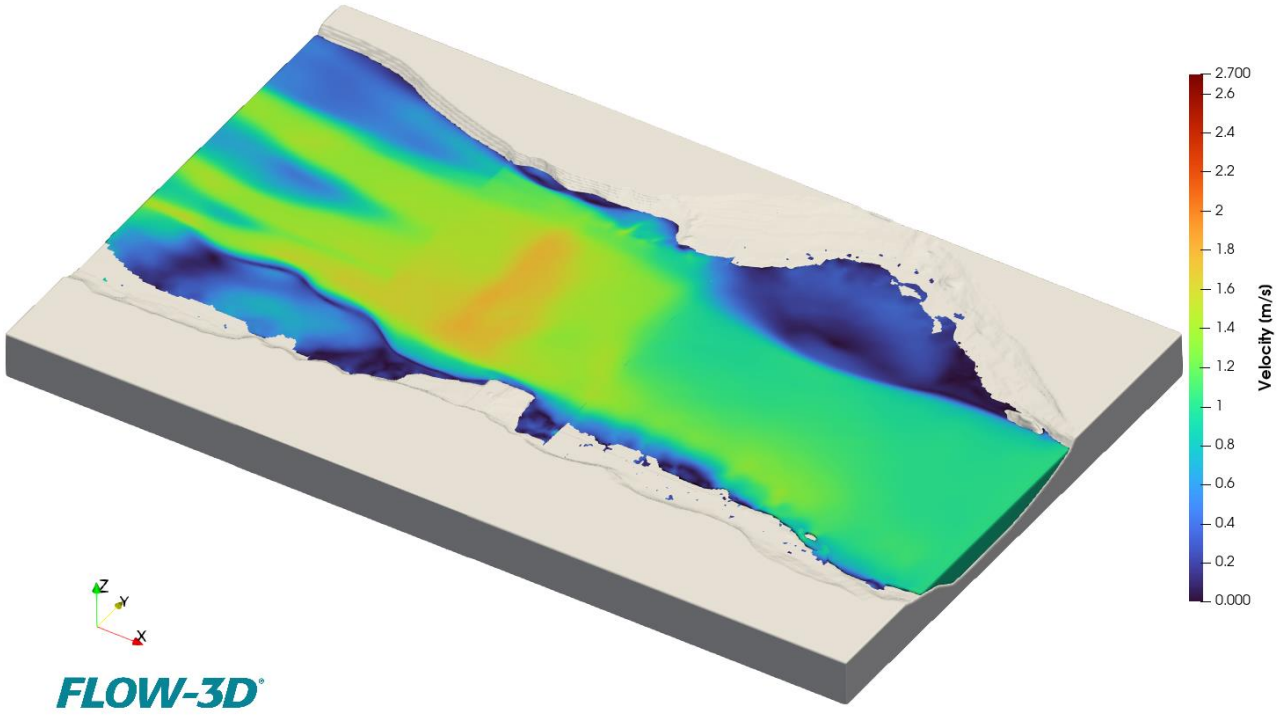

Figure 5-11 FLOW-3D Results – 844 m^3/s – LCS and Lock Removed (Geometry 4)

Table 5-3 Flow 3D Modelling Results – 1:100-year Discharge for Future Climate (844 m^3/s)

Location	Modelled Geometry			
	Water Surface Elevation – 30 gates – Closed Lock (m)	Water Surface Elevation – 30 gates – Opened Lock (m)	Water Surface Elevation – 32 gates – Opened Lock (m)	Water Surface Elevation – LCS Removed at Sill Elevation (m)
200 m downstream of LCS	657.40	657.40	657.40	657.40
100 m downstream of LCS	657.37	657.37	657.37	657.35
100 m upstream of LCS	657.60	657.58	657.55	657.45
200 m upstream of LCS	657.62	657.60	657.57	657.49

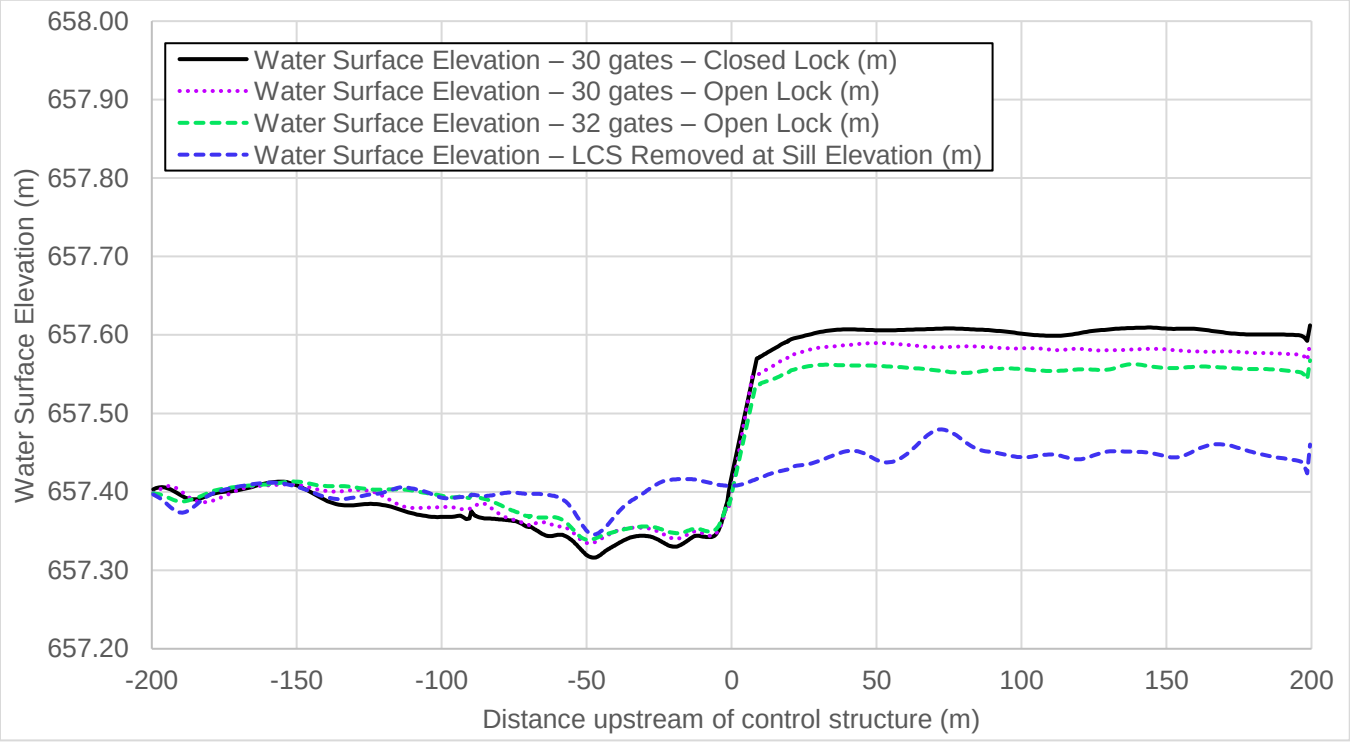

Figure 5-12 Flow 3D Modelling Results – 1:100-year Discharge for Future Climate (844 m^3/s) – Water Surface Profile without Terrain Profile

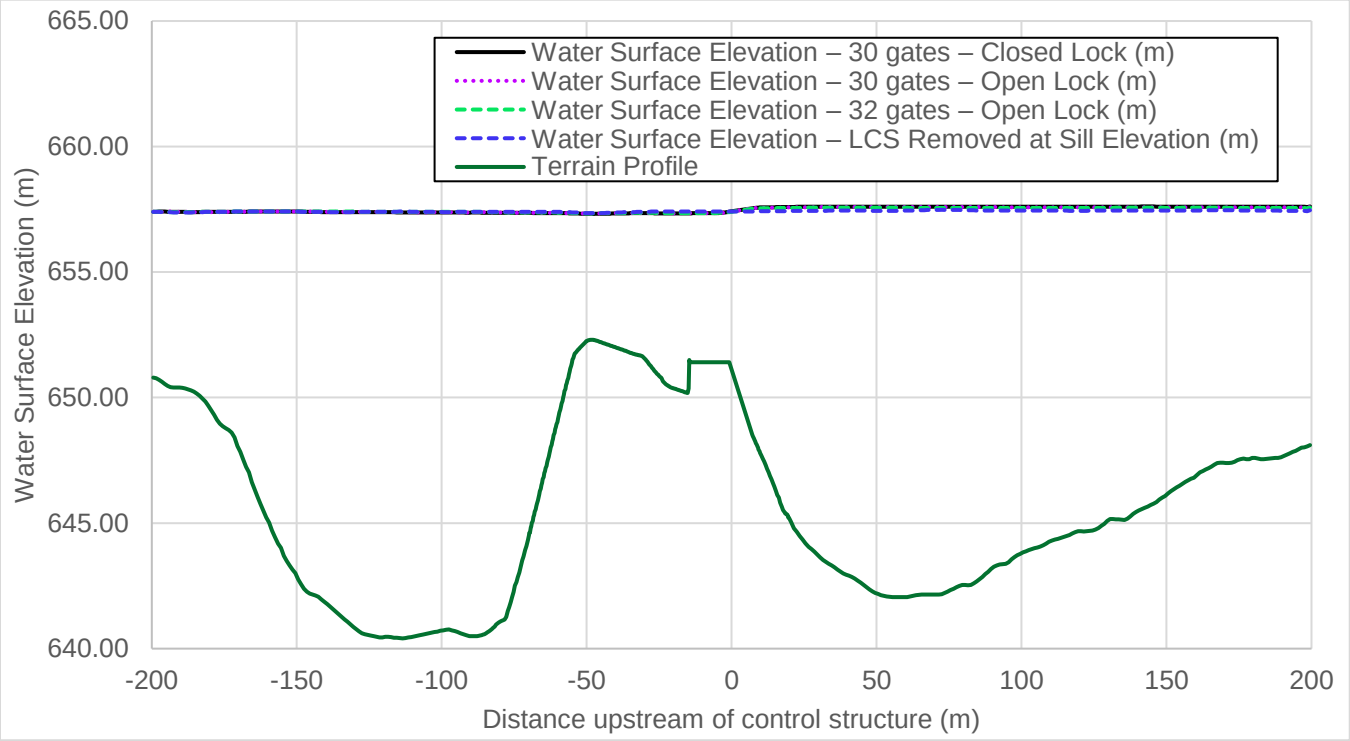

Figure 5-13 Flow 3D Modelling Results – 1:100-year Discharge for Future Climate (844 m^3/s) – Water Surface Profile with Terrain Profile

5.6 Partial Removal of the Old Dam

Following YEC's request, an additional scenario was modelled to study the impact of partially removing the remains of the old dam located downstream of the structure. The old structure is located just under the surface, as shown in Figure 5-14.

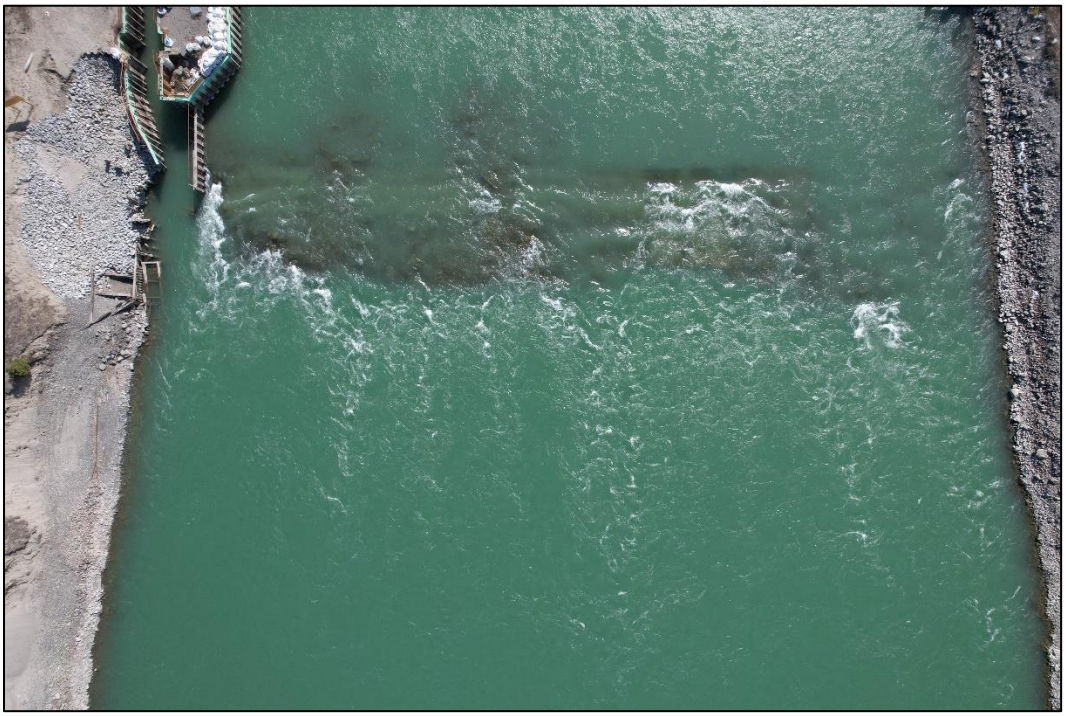

Figure 5-14 Remains of the Old Dam Downstream of LCS

The terrain downstream was excavated to an elevation of 650 m, as depicted in Figure 5-15. This elevation was selected as it corresponds to another high section of the riverbed, located about 150 m further downstream. In addition, there are doubts about the feasibility of deeper excavation at this location.

The FLOW-3D results are illustrated in Figure 5-16 and Figure 5-17, for the 2021 peak flow and for future climate scenarios, respectively. A comparison of the modelled longitudinal water surface profiles with and without the excavation under the 844 m^3/s discharge is shown in figures 5-18 and 5-19.

Results reveal that partial removal of the old dam had no impact on the water level within the first 200 m upstream of the Lewes Control Structure, and consequently, would have an insignificant impact on the reach capacity and on flood levels upstream of LCS. This can be explained by the fact that the area located directly downstream of the structure is submerged by approximately 4 to 5 m during extreme floods. Under high flow, water levels are this location are dictated by other hydraulic controls located further downstream.

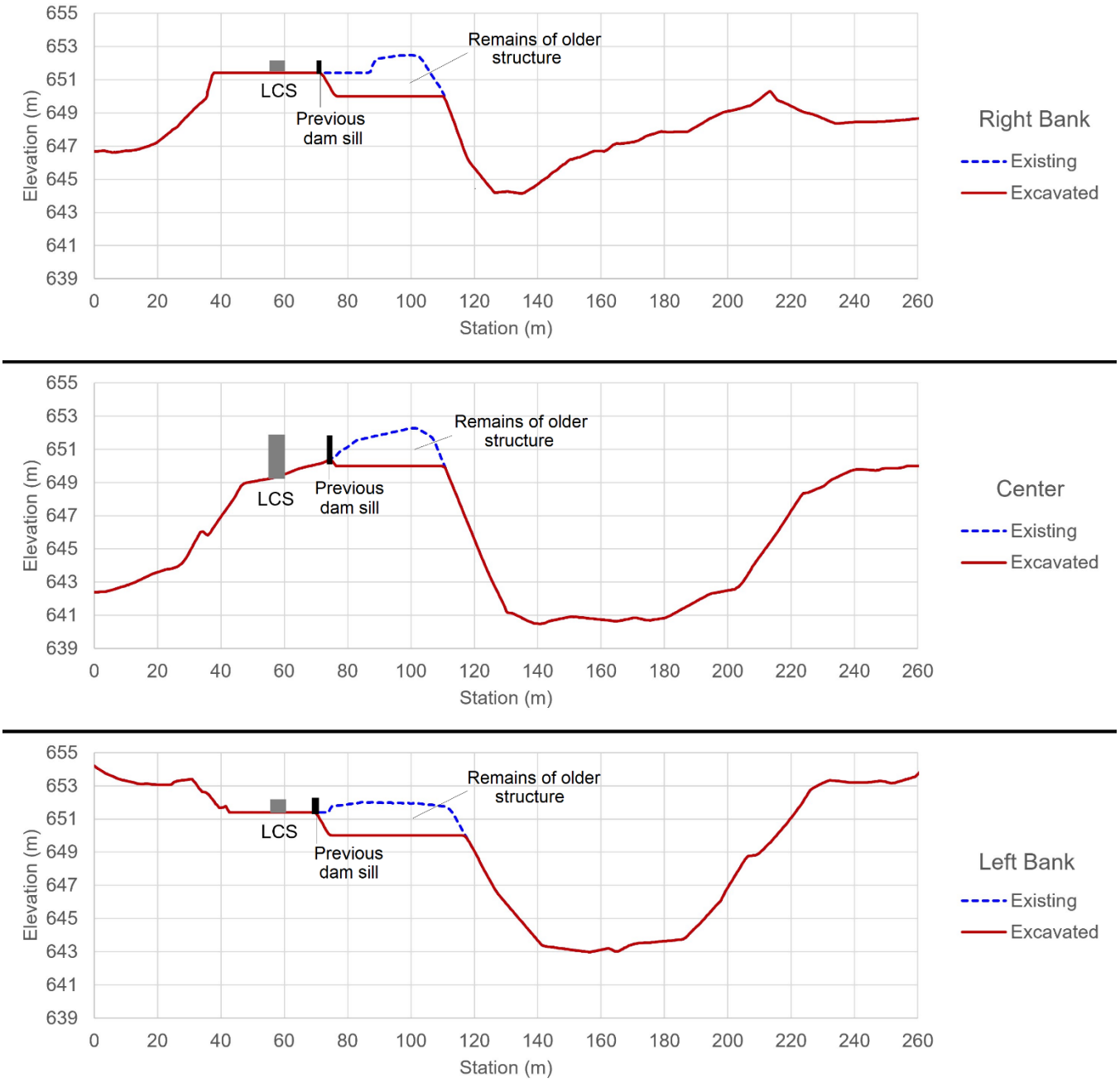

Figure 5-15 Existing and Excavated Terrain Profile on Right Bank, Centre, and Left Bank

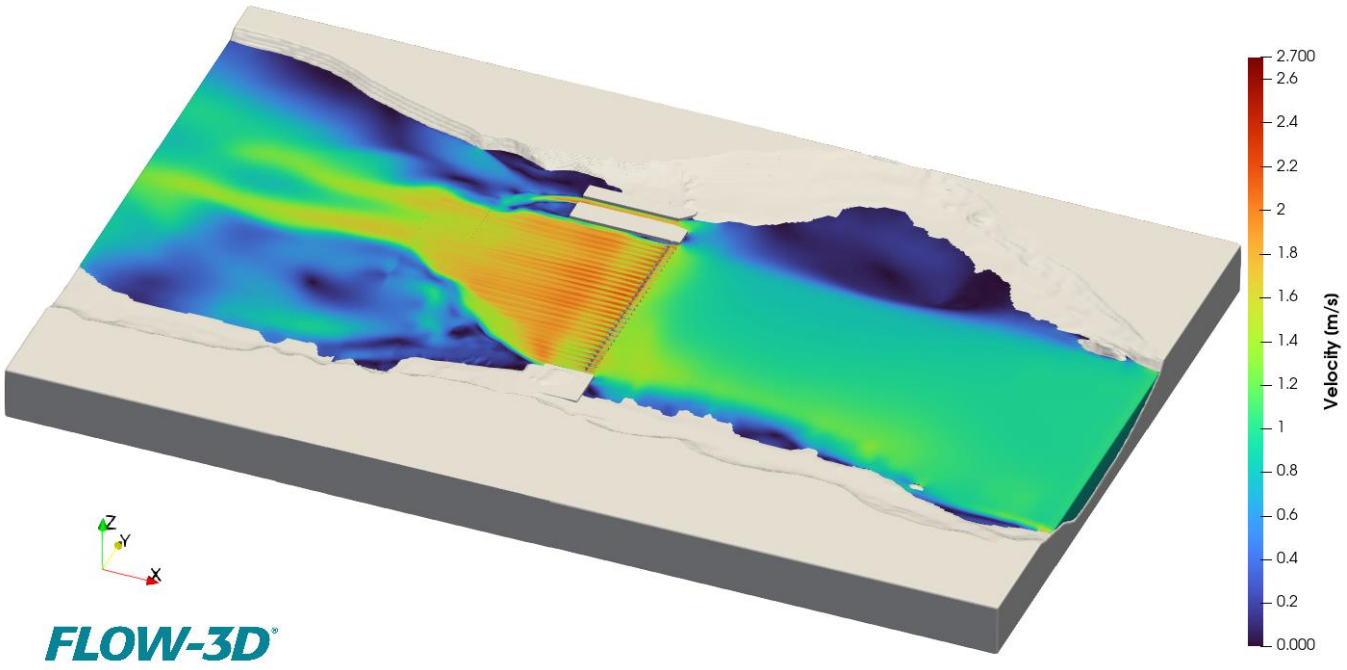

Figure 5-16 FLOW-3D Results – 723 m^3/s – LCS 30 gates – Opened Boat Lock – Excavated Downstream

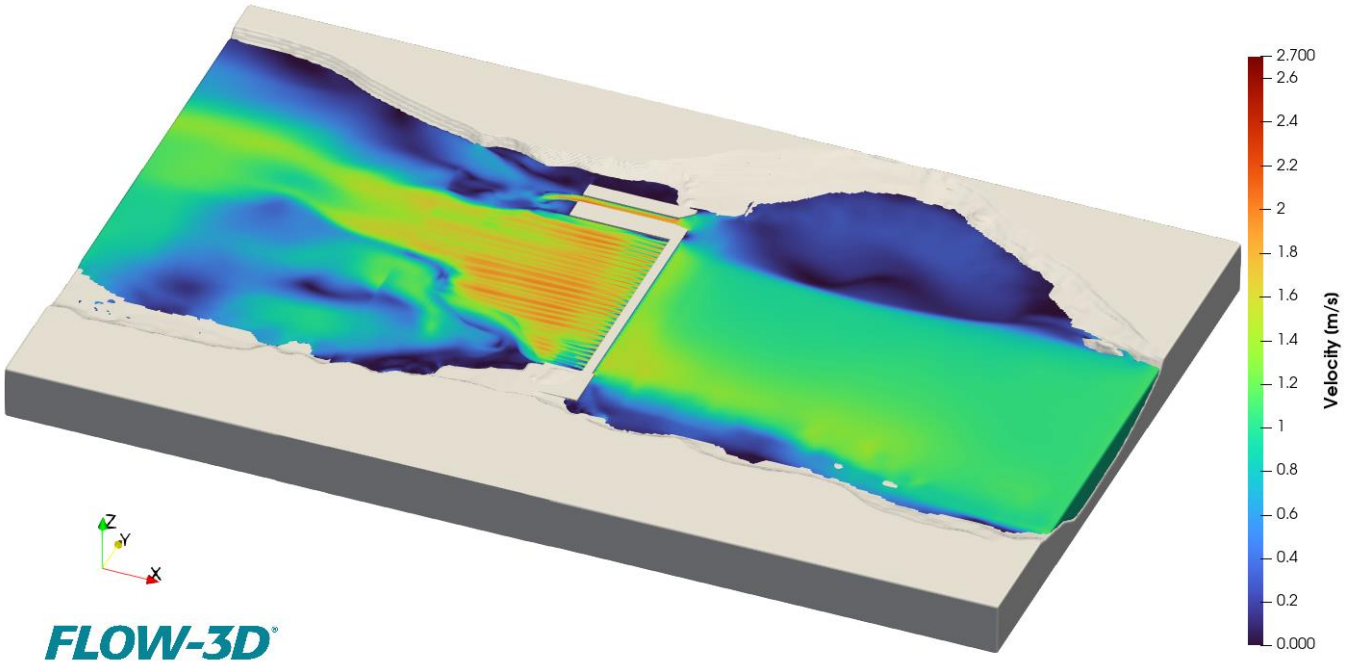

Figure 5-17 FLOW-3D Results – 844 m3/s – LCS 30 gates – Opened Boat Lock – Excavated Downstream

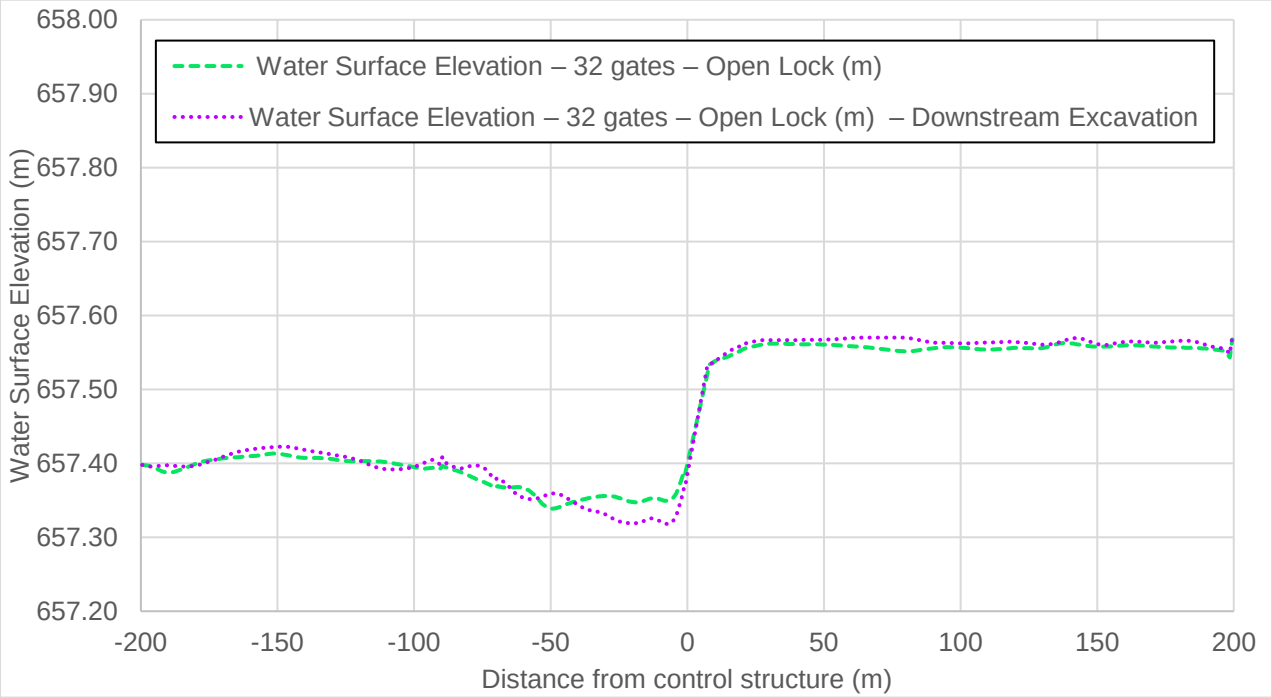

Figure 5-18 Flow 3D Modelling Results – Impact of Downstream Excavation – 1:100-year Discharge for Future Climate (844 m^3/s) – Water Surface Profile without Terrain Profile

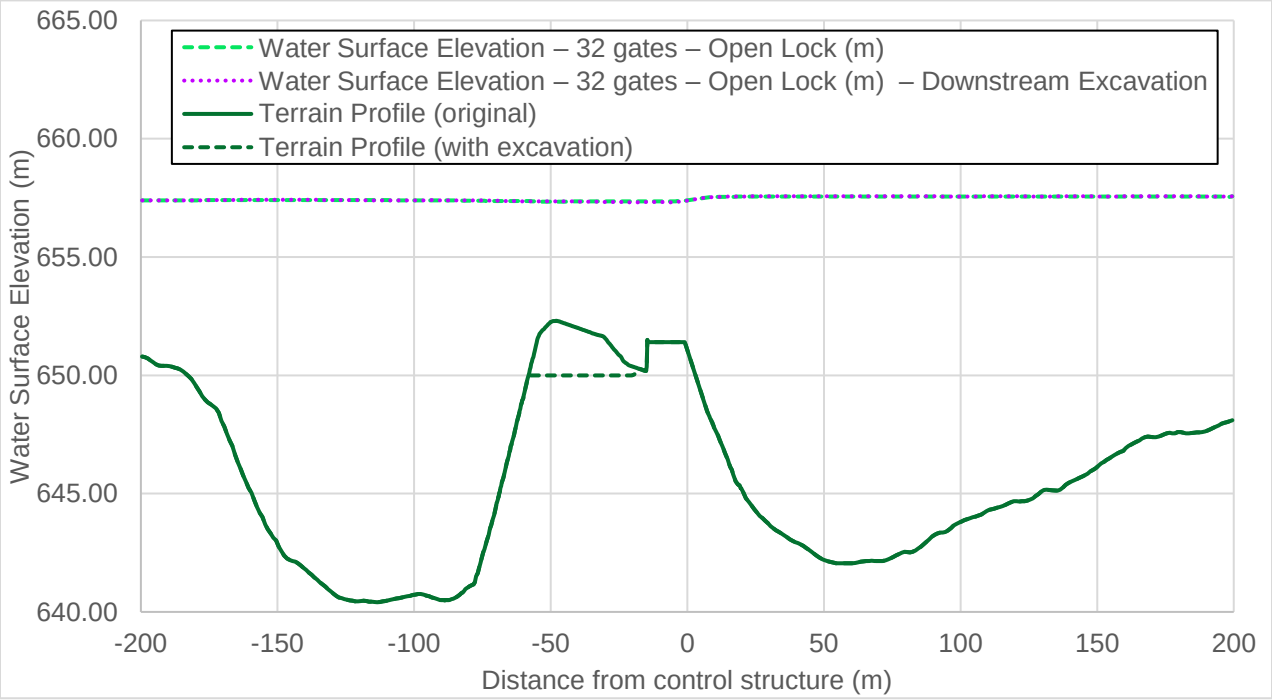

Figure 5-19 Flow 3D Modelling Results – Impact of Downstream Excavation – 1:100-year Discharge for Future Climate (844 m^3/s) – Water Surface Profile without Terrain Profile

6. Upstream Impact of Studied Geometries

The 3D modelling results were used to validate and calibrate the head losses at the Control Structure modelled in the 1D model. The 1D model was subsequently used to determine the impact of the different geometries on the capacity of the reach and the potential flood levels in Marsh Lake.

It was generally expected that the studied modifications to the geometry would have very limited impact on both the reach capacity and the Marsh Lake flood levels. This is due to the hydraulic controls located downstream of LCS:

1. A narrow water passage known as Miles Canyon is located approximately 3.5 km upstream of the Whitehorse Generating Station. Here, the riverbed abruptly rises, and the width of the river is less than 30 m A previous study conducted by Acres International concluded that during high flows, the flow through Miles Canyon would be nearly critical, effectively acting as a control for upstream levels independent of the water levels at Schwatka Lake (KGS 2010). The impact on the canyon can clearly be seen on the water profile under high flow presented in figure 6-4.

2. Approximately 9 km from the Whitehorse Generating Station, near the area known as McCrae, a set of rapids serves as an additional hydraulic control on upstream river levels. The rapids still create a partial control under high flow, as shown in figure 6-4.

The high downstream level creates significant submergence of flow at the LCS and consequently limits the hydraulic capacity of the structure under severe flood events.

It should be noted that the additional geometry detailed in Section 5.6 for a partial removal of the old structure located downstream of LCS was not included in the 1D analysis. The 1D model calibration only relied on a single location of water measures directly downstream of the structure. Therefore, it is not possible to know if the head losses directly caused by the old structure are well represented in the 1D model, or if they are represented in aggregate with other losses along the reach between the two control points. It is not possible to model with confidence the impact of this alternative geometry using the 1D model.

6.1 Impact on River Reach Capacity

The HEC-RAS scenarios were modelled with discharges as input and Marsh Lake Level as the resulting output. Consequently, results were re-interpolated to provide discharges for specific Marsh Lake levels. Table 6-1 to 6-4 show the impact of the different studied geometry on the overall river each capacity, for given Schawtka and Marsh Lake levels. Results show that the modifications to the structure geometry have limited impact on the capacity of the river reach, due to the presence of other hydraulic controls, as discussed above.

Table 6-1 Impact of Open Boat Lock Gate (or Removable Gate) on the River Capacity Downstream of Marsh Lake

	Schwatka Lake at Low Level – 652.33 m			Schwatka Lake at High Level – 653.17 m		
Marsh Lake Level (m)	Discharge 30 gates – Closed Lock (m^3/s)	Discharge 30 gates – Opened Lock (m^3/s)	Capacity increase (m^3/s)	Discharge 30 gates – Closed Lock (m^3/s)	Discharge 30 gates – Opened Lock (m^3/s)	Capacity increase (m^3/s)
653.50	97.5	98.3	0.8	68.3	68.3	**0.0**
654.00	151.1	152.2	1.1	130.4	130.8	0.4
654.50	207.6	209.2	1.5	193.7	194.9	1.2
655.00	284.0	285.5	1.5	267.7	269.2	1.5
655.50	360.3	361.8	1.5	342.9	344.4	1.5
656.00	440.7	442.7	2.1	420.9	422.8	1.9
656.50	525.4	528.2	2.8	507.8	510.5	2.7
657.00	611.2	615.0	3.7	594.8	598.2	3.5
657.50	704.7	708.4	3.7	687.0	691.6	4.6
658.00	797.5	802.2	4.6	780.0	784.7	4.6
658.50	882.8	889.5	6.6	868.0	874.3	6.3

Table 6-2 Impact of Two Additional Gates on the River Capacity Downstream of Marsh Lake

	Schwatka Lake at Low Level – 652.33 m			Schwatka Lake at High Level – 653.17 m		
Marsh Lake Level (m)	Discharge 30 gates (m^3/s)	Discharge 32 gates (m^3/s)	Capacity increase (m^3/s)	Discharge 30 gates (m^3/s)	Discharge 32 gates (m^3/s)	Capacity increase (m^3/s)
653.50	97.5	98.3	0.8	68.3	68.7	0.5
654.00	151.1	152.2	1.1	130.4	131.6	1.3
654.50	207.6	209.2	1.5	193.7	194.9	1.3
655.00	284.0	285.5	1.5	267.7	269.7	2.0
655.50	360.3	361.8	1.5	342.9	345.5	2.6
656.00	440.7	442.7	2.1	420.9	424.3	3.5
656.50	525.4	528.2	2.8	507.8	511.3	3.5
657.00	611.2	615.1	3.9	594.8	598.3	3.5
657.50	704.7	709.4	4.8	687.0	691.6	4.6
658.00	797.5	803.0	5.4	780.0	785.4	5.4
658.50	882.8	890.7	7.8	868.0	875.5	7.5

Table 6-3 Impact of Two Additional Gates and Opened Boat Lock Gate on the River Capacity Downstream of Marsh Lake

	Schwatka Lake at Low Level – 652.33 m			Schwatka Lake at High Level – 653.17 m		
Marsh Lake Level (m)	Discharge 30 gates – Closed Lock (m^3/s)	Discharge 32 gates – Opened Lock (m^3/s)	Capacity increase (m^3/s)	Discharge 30 gates – Closed Lock (m^3/s)	Discharge 32 gates – Opened Lock (m^3/s)	Capacity increase (m^3/s)
653.50	97.5	99.2	1.7	68.3	68.7	0.5
654.00	151.1	153.3	2.2	130.4	131.6	1.3
654.50	207.6	210.8	3.1	193.7	194.9	1.3
655.00	284.0	287.7	3.7	267.7	270.2	2.6
655.50	360.3	364.6	4.3	342.9	346.6	3.7
656.00	440.7	446.2	5.5	420.9	426.1	5.2
656.50	525.4	531.6	6.2	507.8	513.0	5.2
657.00	611.2	618.9	7.7	594.8	600.0	5.2
657.50	704.7	713.2	8.5	687.0	694.3	7.3
658.00	797.5	807.0	9.5	780.0	789.5	9.5
658.50	882.8	895.7	12.9	868.0	880.2	12.2

Table 6-4 Impact of Removing LCS to Sill Level on the River Capacity Downstream of Marsh Lake

	Schwatka Lake at Low Level – 652.33 m			Schwatka Lake at High Level – 653.17 m		
Marsh Lake Level (m)	Discharge 30 gates (m^3/s)	Discharge LCS removed (m^3/s)	Capacity increase (m^3/s)	Discharge 30 gates (m^3/s)	Discharge LCS removed (m^3/s)	Capacity increase (m^3/s)
653.50	97.5	102.2	4.7	68.3	70.0	1.7
654.00	151.1	155.9	4.8	130.4	133.8	3.4
654.50	207.6	214.1	6.4	193.7	198.7	5.0
655.00	284.0	292.2	8.2	267.7	275.4	7.7
655.50	360.3	370.3	10.0	342.9	352.3	9.5
656.00	440.7	453.4	12.8	420.9	433.3	12.5
656.50	525.4	539.7	14.2	507.8	521.1	13.2
657.00	611.2	629.1	17.9	594.8	609.8	15.0
657.50	704.7	726.2	21.5	687.0	707.8	20.8
658.00	797.5	824.3	26.8	780.0	806.7	26.7
658.50	882.8	926.6	43.8	868.0	911.0	42.9

6.2 Impact on Marsh Lake Flood Levels

The 1D model results and the spread sheet-based routing model were used to determine the impact of the studied geometries on maximum flood levels in Marsh Lake.

All scenarios were routed using the capacity curves presented in section 6.1, for a low Schwatka Lake level. Initial conditions correspond to the April 9th (100th day of the year) conditions right before the 2021 flood, with an initial Marsh Lake Elevation of 654.42 m,

The 2021 flood hydrograph was first reconstructed using the measured outflows provided by YEC, the measured lake levels in Marsh Lake and the storage curved developed for the routing model. The resulting inflow hydrograph was then routed through Marsh Lake for different rating curves, corresponding to the studied geometries. The results are presented in Table 6-5.

The obtained maximum level for geometry 2 (30 gates + open lock) is 8 cm higher than the maximum level measured in 2021 for a similar configuration at LCS, an acceptable difference considering the uncertainties related to both the routing and the hydraulic models. Results show that the opening of the lock has very limited impact on the peak Marsh Lake level (-0.01 m). The addition of two gates also has very limited impact (-0.02 m), and so does a removal of the structure at sill elevation (-0.06 m). These results show that the Lewes Control Structure has little impact on the Marsh Lake flood levels, due to the presence of the hydraulic control on the river reach (See section 6.0).

Table 6-5 Impact of Studied Geometries on Flood Levels in Marsh Lake – 2021 Flood

Results	Modelled Geometry			
	30 gates – Closed Lock (Geometry 1)	30 gates – Open Lock (Geometry 2)	32 gates – Open Lock (Geometry 3)	LCS Removed (Geometry 4)
Peak Marsh Lake Level (m)	657.65	657.64	657.63	657.59
Difference with base Case (geometry 1)	N/A	-0.01	-0.02	-0.06

The 1:100-year hydrograph for future climate was also routed through Marsh Lake, and results are presented in Table 6-6. The impact of the studied geometries is similarly limited.

Table 6-6 Impact of Studied Geometries on Flood Levels in Marsh Lake for Future Climate – 1:100-year Future Climate Flood

Results	Modelled Geometry			
	30 gates – Closed Lock (Geometry 1)	30 gates – Open Lock (Geometry 2)	32 gates – Open Lock (Geometry 3)	LCS Removed (Geometry 4)
Peak Marsh Lake Level (m)	658.27	658.26	658.24	658.18
Difference with base Case (geometry 1)	N/A	-0.01	-0.03	-0.09

An example of the graphical routing results is presented in figures 6-1 and 6-2, showing a comparison between Marsh Lake Level and outflows obtained for geometries 1 and 4 under the 1:100-year Future Climate Flood.

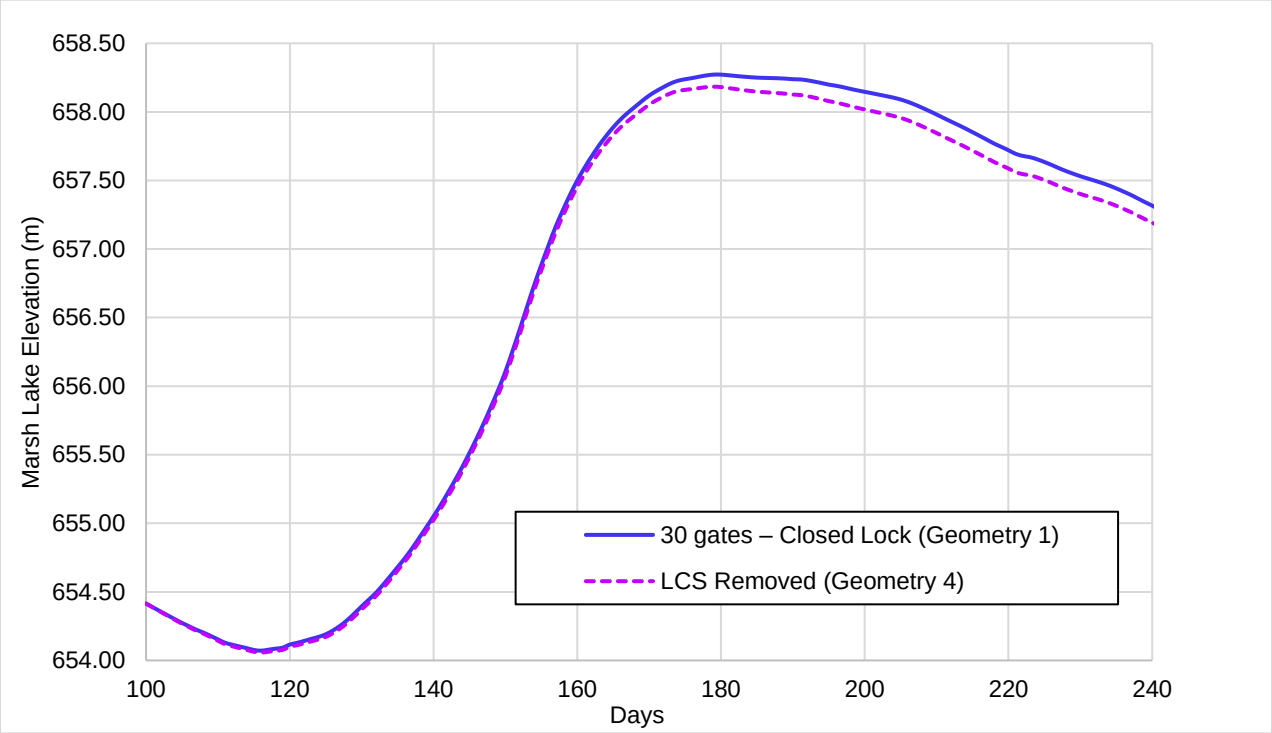

Figure 6-1 Comparison of 1:100-year Future Climate Flood Routing Results – Geometries 1 & 4 – Marsh Lake Elevation

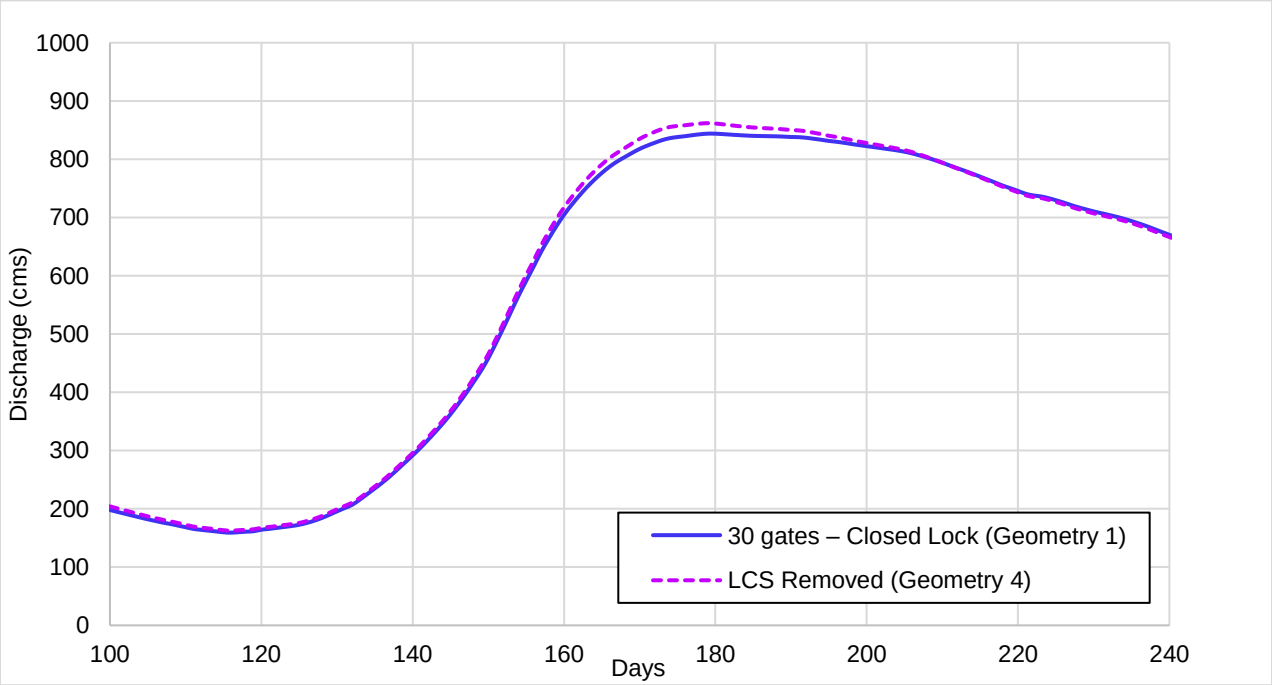

Figure 6-2 Comparison of 1:100-year Future Climate Flood Routing Results – Geometries 1 & 4 – Marsh Lake Outflow

6.3 Effect of Lowering Schwatka Lake on Marsh Lake

YEC also is interested in the effect of lowering Schwatka Lake elevation on the regulation of Marsh Lake elevation during the flooding periods. Results shown in Figure 6-3 indicate that a 0.9 m difference in water elevation at Schwatka Lake translates to a 0.10 m difference on the Marsh Lake level at equilibrium under high flow (800 m^3/s).

Figure 6-4 shows a comparison of the modelled profiles for an 800 m^3/s discharge with low and high Schwatka lake Levels. The profile shows the outsize impact of Miles Canyon on levels downstream of Lewes Control Structure.

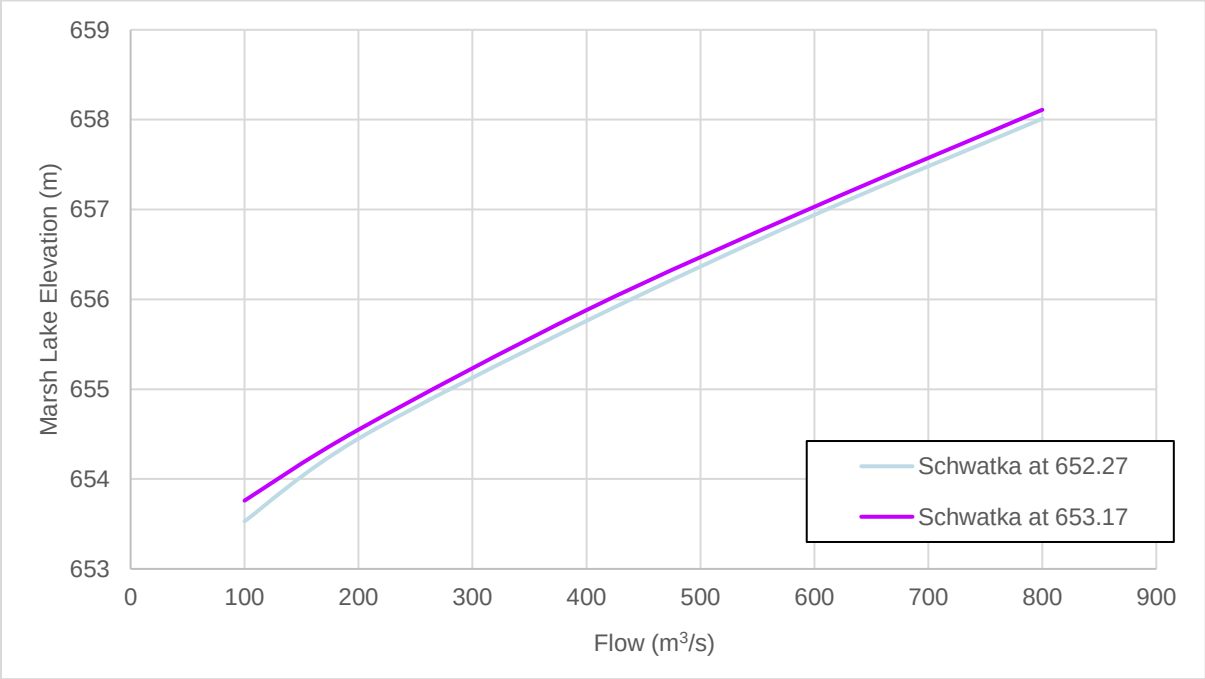

Figure 6-3 Effect of Lowering Schwatka Lake Level on Marsh Lake Elevation at Equilibrium

Table 6-7 shows the impact of lowering Schwatka Lake during the complete flood season, from the beginning of April, on flood routing results. The 0.9 m water level difference in Schwatka Lake leads to a 0.10 m difference on the maximum modelled Marsh Lake level under the 2021 flood, and a 0.08 m difference under the 1:100-year future climate flood. The impact on the maximum discharge is negligible.

Table 6-7 Impact of Schwatka Lake Level on Flood Levels in Marsh Lake for Geometry 1 (30 gates – Closed Lock)

Level in Schwatka Lake from April 10th and Beyond	Maximum Marsh Lake Level (m)	
	2021 Flood	100-year Future Climate Flood
Schwatka Lake at 653.17 m	657.75	658.35
Schwatka Lake at 652.27 m	657.65	658.27
Difference (m)	0.10	0.08

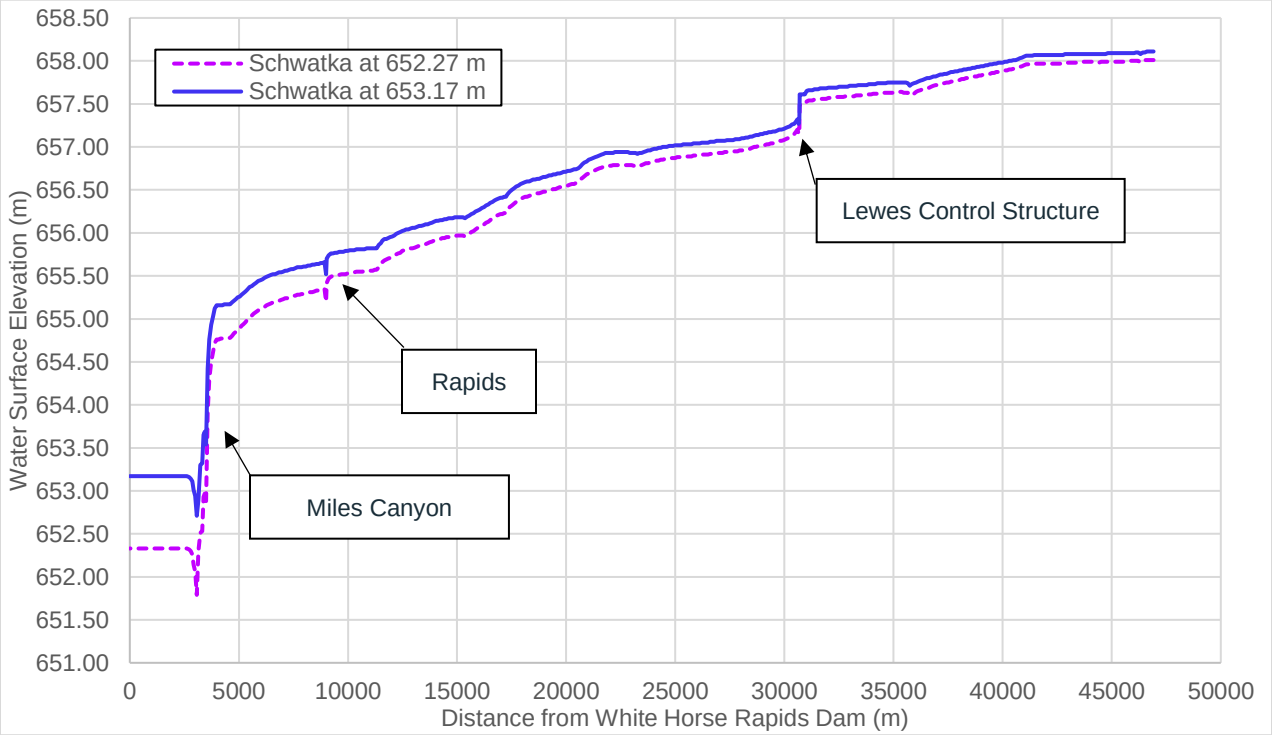

Figure 6-4 Effect of Lowering Schwatka Lake Elevation on the Water Surface Elevation Profile in the River under an 800 m^3/s discharge

It should be noted that while the lowering of Schwatka Lake level can have a small impact on the Marsh Lake levels when maintained over a complete season, such operation offers too little of a capacity gain to significantly impact Marsh Lake on a short time frame.

As an example, let.s consider a sudden lowering of the Schwatka Lake from 653.17 m to 652.27 m when Marsh Lake is at equilibrium at its full supply level (656.23 m). Assuming fixed inflows, it would take more than 3 months for Marsh Lake to reach a new equilibrium (656.12 m).

As shown by this example, the lowering of Schwatka Lake level does not provide sufficient additional capacity to allow for short term flooding mitigation.

7. CONCLUSIONS

Statistical Analysis results showed that the 2021 peak flow at Lewes Control Structure (723 m^3/s) corresponds to a 1:200-year event. This result is coherent with the statistical analysis by Morrison Hershfield (2022), performed on the Marsh Lake water-level data from 1985 to 2021 (36 years). In that study, the 2021 flood is considered a 1 in 160-year event. Therefore, the 2021 peak flow value exceeds the 1:100-year return period associated with the dam classification.

Further analysis was done to determine the 1:100-year peak flow for future climate, taking into account the impact of climate change. Statistical and flood routing analysis using a future climate flow series established using a RCP 8.5 climate scenario provided a peak discharge of 844 m^3/s. It should be noted that, under this discharge, the bottom of the lifted gates at the control structure is submerged, although the deck is not. It is, however, possible to fully remove the gate using a crane during a severe flood event, as it was done in 2021.

1D and 3D modelling results show that the proposed modifications to the existing structure (addition of two spillway gates and use of removable lock gates) would have very little impact on the river reach capacity and on flood levels in Marsh Lake. For instance, the combined effect of these two modifications would lead to a difference in flood levels in Marsh Lake of 0.02 m under the 2021 peak flow, and 0.03 m under the 1:100-year future climate scenario. In fact, even the removal of the Lewes Control Structure and the boat lock down to the sill elevation would have very limited impact, due to the presence of other hydraulic controls located further downstream.

Considering the uncertainties related to the input data, the modelling hypothesis and the models themselves, it is the opinion of the modellers that the aforementioned differences of 0.02 and 0.03 m should be considered insignificant.

Finally, an analysis of the impact of lowering Schwatka Lake on the flood levels in Marsh Lake showed that such operation can have a limited impact on peak flood levels (±10 cm) if it is sustained during the complete flood season. However, the lowering of Schwatka Lake level does not provide sufficient additional capacity to allow for short term flooding mitigation.

8. REFERENCES

1. FLOW-3D® Version 2023R1 User's Manual (2023). FLOW-3D [Computer software]. Santa Fe, NM: Flow Science, Inc. https://www.flow3d.com

2. HEC-RAS (2021). HEC-RAS (version 6.0). River Analysis System. User's Manual. Hydrologic Engineering Center. U.S (United States). Army Corps of Engineers. Davis, CA. 2021.

3. INRS-ETE (2020). A Distributed Hydrological Modelling System to Support Hydroelectric Production in Northern Environments under Current and Changing Climate Conditions. Centre Eau Terre Environnement. Report No- R1926 – Final. August 2020.

4. Institut national de la recherche scientifique

5. KGS (2010). Hydraulic Modelling of Yukon River – Marsh Lake to Schwatka Lake, Final report 2010, KGS Group, Winnipeg, Manitoba.

6. Morrison Hershfield (2022). Updated flood frequency analysis for Southern Lakes. Memorandum submitted to Yukon Government Department of Environment Water Resources Branch on13 January 2022

7. Stantec (2023). Lewes Control Structure – Boat Lock Replacement – Owners Requirements, Prepared for Yukon Energy Corporation by Stantec, April 16, 2023.

8. YEC, Original Drawings of Lewes Structure, Yukon Energy Corporation.

APPENDIX A: CLIMATE REPORT

AtkinsRéalis

AtkinsRéalis
Choose an item.

atkinsrealis.com

A Distributed Hydrological Modelling System to Support Hydroelectric Production in Northern Environments under Current and Changing Climate Conditions

Final Report presented to:

Yukon Energy
#2 Miles Canyon Road
Box 5920
Whitehorse YT Y1A 6S7

Alain N. Rousseau, P.Eng., Ph.D.
Stéphane Savary, Jr Eng. (E.I.T.), M.Sc.
Sébastien Tremblay
Laurie Caillouet, Ph.D.
Cheick Doumbia
Julien Augas
Etienne Foulon, Jr Eng. (E.I.T.), Ph.D.
Kian Abbasnezhadi, Jr Eng. (E.I.T.), Ph.D.

Centre Eau Terre Environnement
Institut national de la recherche scientifique (INRS-ETE)
490, rue de la Couronne, Québec (QC), G1K 9A9

Report No- R1926 - Final

August 2020

Project team

Lead authors

Alain N. Rousseau	Institut national de la recherche scientifique Eau Terre et Environnement
Stéphane Savary	Institut national de la recherche scientifique Eau Terre et Environnement
Sébastien Tremblay	Institut national de la recherche scientifique Eau Terre et Environnement
Laurie Caillouet	Institut national de la recherche scientifique Eau Terre et Environnement
Julien Augas	Institut national de la recherche scientifique Eau Terre et Environnement
Cheick Doumbia	Institut national de la recherche scientifique Eau Terre et Environnement
Étienne Foulon	Institut national de la recherche scientifique Eau Terre et Environnement
Kian Abbasnezhadi	Institut national de la recherche scientifique Eau Terre et Environnement

Contributors

Jos Samuel	Yukon University Research Centre, Yukon University
Brian Horton	Yukon University Research Centre, Yukon University
Maciej Stetkiewicz	Yukon University Research Centre, Yukon University
Stephanie Saal	Yukon University Research Centre, Yukon University
Marc-André Lavigne	Yukon Energy Corporation
Ron Gee	Yukon Energy Corporation
Shannon Mallory	Yukon Energy Corporation
Stephanie Whitehead	Yukon Energy Corporation
Kevin Maxwell	Yukon Energy Corporation
Goran Sreckovic	Yukon Energy Corporation
Blaise Gauvin St-Denis	Ouranos
Diane Chaumont	Ouranos

Disclaimer

representation, express or implied, as to its accuracy or completeness. Any reliance you place upon the information contained here is your sole responsibility and strictly at your own risk. In no event will the INRS-ETE be liable for any loss or damage whatsoever, including without limitation, indirect or consequential loss or damage, arising from reliance upon the Information.

Acknowledgements

We gratefully acknowledge the financial support from the Natural Sciences and Engineering Research Council of Canada (NSERC) and Yukon Energy Corporation (YEC).

This project would also not have been possible without contributions from staff and students at the INRS-ETE namely: Pascal Castellazzi, Guillaume Talbot and Alexandre Alix.

The staff at YEC represents one of the driving forces behind this project, thus, we would like to acknowledge their strong contributions towards the achievement of the different project objectives (a.k.a., work packages).

We acknowledge the World Climate Research Programme's Working Group on Coupled Modelling, which is responsible for CMIP, and we thank the climate modeling groups (listed in Table 6.1 of this document) for producing and making available their model output. For CMIP, the U.S. Department of Energy's Program for Climate Model Diagnosis and Intercomparison provided coordinating support and led development of software infrastructure in partnership with the Global Organization for Earth System Science Portals. Also we are thankful to Ouranos for providing the CMIP5 climate changes scenarios.

Table of contents

List of Figures

List of Tables

Summary

The objective of this project was to implement a distributed hydrological modeling system on key watersheds where Yukon Energy produces electricity. The system will be used for hydrological forecasting (*i.e.*, inflows and stream flows) with different lead times (*e.g.*, 1-14 days, 12 months) to assist hydroelectric operations as well as seasonal and long-term planning. Long-term planning will use the modeling system to predict impacts of climate change on inflows and flow availability, timing and extreme events. The results will provide strategic information for the assessment of potential energy projects to supply Yukon with enough electricity to meet projected demands. Understanding climate change and associated effects will be useful to other processes such as relicensing activities. This report provides a description of the accomplishments of each work package (WP) conducted over the course of the entire project, that is nearly three and a half (3.5) years.

List of acronyms

ARD	Applied Research and Development
ACCESS	Australian Community Climate and Earth-System Simulator
BC	British Columbia
CanESM	Canadian Earth System Model
CanSIPS	Canadian Seasonal and Inter-annual Prediction System
CaPA	Canadian Precipitation Analysis
CGCM	Canadian General Circulation Model
CCSM	Community Climate System Model
CMIP5	Coupled Model Intercomparison Project Phase 5
CNRM-CM	Centre National de Recherches Météorologiques-Climate Model
CSIRO-MK	Commonwealth Scientific and Industrial Research Organisation Mark
CRD	Collaborative Research and Development
DA	Data Assimilation
DEM	Digital Elevation Model
ECCC	Environment and Climate Change Canada
EnKF	Ensemble Kalman Filter
ENSO	El Niño Southern Oscillation
ESP	Ensemble Streamflow Prediction
GDPS	Global Deterministic Prediction System
GEPS	Global Ensemble Prediction System
GFDL-ESM	Geophysical Fluid Dynamics Laboratory-Earth System Model
GIS	Geographic Information System
GLIMS	Global Land Ice Measurements from Space
GUI	Graphical user interface

HADGEM-CC	Hadley Global Environment Model – Carbon Cycle
HADGEM-ES	Hadley Global Environment Model – Earth System
HQP	Highly Qualified Personnel
INMCM	Institute for Numerical Mathematics Climate Model
INRS	Institut National de la Recherche Scientifique
IPCC	Intergovernmental Panel on Climate Change
MDDELCC	Ministère du Développement Durable, de l'Environnement et de la Lutte aux Changements Climatique
MICRO	Model for Interdisciplinary Research On Climate
MPI-ESM-LR	Max Planck Institute-Earth System Mode-Low Resolution
MRI-CGCM	Meteorological Research Institute Coupled General Circulation Model
NAEFS	North American Ensemble Forecast System
MSC	Meteorological Service of Canada
NSERC	Natural Sciences and Engineering Research Council of Canada
PCIC	Pacific Climate Impacts Consortium
PDO	Pacific Decadal Oscillation
RCPs	Representative Concentration Pathways
RDPS	Regional Deterministic Prediction System
RHHU	Relatively Homogenous Hydrologic Units
RFS	River Forecasting System
RSs	River Segments
SWE	Snow Water Equivalent
SVD	Singular Value Decomposition
SVM	Support Vector Machine
WP	Work package
YU	Yukon University
YEC	Yukon Energy Corporation

Context

In northern environments, limited hydro-meteorological networks and evolving climate conditions provide continuous challenges to water resource managers. YEC operates hydroelectric facilities under such conditions. For long-term resource planning exercises where capacity and predicted electrical load are analyzed to inform new projects, YEC does noes not currently factor in climate variability and change. Thus, there is a fundamental need to: (i) establish detailed knowledge of current and future hydro-meteorological conditions and (ii) assess the sensitivity of each hydroelectric facility to climate.

To address these issues, YEC has recruited a multidisciplinary team of hydrology and climate change experts to jointly undertake an applied research project under NSERC Applied Research and Development (ARD) and Collaborative Research and Development (CRD) Programs. This research team includes members from the Yukon University (YU) Research Centre, *Institut national de la recherche scientifique* (INRS, Quebec) and Ouranos (Consortium on regional climatology and adaptation to climate change, Quebec).

The team of experts has developed a hydrological modeling framework using existing data and providing context-specific studies and model advancements, tailored for northern environments, using a combination of field studies and cutting-edge data assimilation techniques. For YU, the primary focus was to develop an innovative data assimilation tool embedded into a hydrological forecasting system that YEC can use to perform accurate short-to-medium-term inflow and flow forecasting (daily and up to 1-year lead) and to optimize operational reservoir monitoring and management. Other tasks relate to providing support to the CRD project proposed by INRS (e.g., bias correction of weather forecast products; snow survey data). For INRS and with the collaboration of YU, the focus was on implementing a robust, distributed, hydrological modelling system for short-term (1-14 days) predictions (i.e., inflow and streamflow forecasting), seasonal projections (1-12 months) and long-term hydrological trends (30-year time periods, e.g., 2040-2070). YU has used the forecasting framework to develop the aforementioned data assimilation tool. INRS has provided training to YEC professionals (operation of the inflow and streamflow forecasting system) and highly qualified personnel (HQP) to conduct research in northern hydrology and build the professional and technological capacities of YEC.

1. Introduction

Inflow and streamflow forecasts have proven to be of value for the operations of hydropower systems in Canada. Forecasts are often used with the dual purpose of maximizing energy production while providing flood control. For example, Hydro-Quebec and BC Hydro use forecasts to optimize hydropower system operations (Schaffer and Shawwash, 2014; Gignac et al., 2014; Martin et al., 2014) while Rio-Tinto Alcan operates hydroelectric plants to supply energy to aluminum smelters in Quebec and British-Columbia (Larouche et al., 2014). Both utility companies operate plants in northern environments where snowmelt represents a major hydrologic process. Meanwhile, the Quebec Ministry of Sustainable Development, Environment and Climate Change (MDDELCC) uses inflow forecasts to manage a considerable number of dams affected by significant spring freshets, several of them requiring real-time management (Turcotte and Lafleur, 2014). Uncertainty associated with the monitoring of snow water equivalent (SWE) and spatial distribution of snowpack adds complexity to forecasting the timing and volume of the spring freshet. YEC faces equivalent challenges in the operation of three hydroelectric dams, the Whitehorse, Aishihik and Mayo Facilities. The impacts of climate change on watershed hydrology, glacier dynamics and permafrost provide additional uncertainty when there is a need to asses long-term hydrological trends (30-year time periods, e.g., 2040-2070). YEC has recognised the need to account for climate change in the planning, management and relicensing (25-year license) of hydroelectric reservoirs. For YEC, there is also a need for basic short-term as well as mid-term seasonal forecasts. This latest requirement is in line with the need to support water resource managers with environmental predictions with forecast ranges from 2 weeks to 12 months (National Academies of Sciences, Engineering and Medicine, 2016).

Hydrological forecasting requires the use of weather forecasts as inputs to a hydrological modelling system. For short-term forecasts, data assimilation techniques based on post-processing of model outputs or adjusting model inputs, state variables or parameters, are generally used to improve forecasts. For short lead times, weather forecasts are usually deterministic, while they are probabilistic (i.e., ensemble forecasts) for longer lead times (e.g., Thirel et al., 2008). Sene (2010) reports knowledge of correlations between large-scale atmosphere and oceanic structures (e.g., Pacific Decadal Oscillation, PDO, El Niño Southern Oscillation, ENSO) may be useful for long-term forecasts. Furthermore, demand

forecasts for energy supply along with reservoir/lake level constraints and/or downstream flow regulations, may then be used as inputs to an existing reservoir management model.

The overarching goal of this project was to implement a distributed hydrological modelling system to support hydroelectric production in Yukon under current and changing climate conditions. Building from previous collaboration between YU and YEC, the project has increased the capacity for short and mid-term inflow forecasts for the Whitehorse (including Marsh Lake), Aishihik and Mayo Facilities and assess potential change in flow volume and extreme events due to climate change in terms of severity, timing and frequency. To achieve these goals, model advancements, tailored for northern environments, were either required (e.g., development of multi-layer snow and glacier models) or not deemed necessary (e.g., development of permafrost model), using a combination of field and theoretical studies. Environment and Climate Change Canada (ECCC) products (i.e., observed and weather forecasts, stream flows) and different sources of reanalysis data and climate projections supplied by Ouranos were used for calibration and operation of the hydrological modelling system. It also required the development of a methodology to link inland precipitation and temperature conditions to large-scale circulation indices using climate model data along with historical data.

This report presents the achievements of different work packages of the project under specific chapters, namely Chapter 2, implementation of a distributed hydrological modelling system for short and mid-term forecasts; Chapter 3, implementation of permafrost and multilayer snow modules; Chapter 4, development and/or adaption of a glacier module for the Upper Yukon River watershed; Chapter 5, development of a methodology to link regional precipitation and temperature with large-scale circulation indices; and Chapter 6, assessment of long-term changes in flow volume and timing, and extreme events due to climate change (i.e., hydroclimatic assessment). Each chapter includes the supporting literature, the proposed methodology and results.

Finally, throughout the project, the team responded to four special requests made by YEC which were beyond the scope of the project in is initial form, but worth investigating, namely to: (i) add the Upper Yukon River Watershed into the forecasting system; (ii) contribute to the strategic planning of meteorological and snow monitoring stations in Mayo; (iii) assess the contribution of snow to the simulated annual inflows to Aishihik Lake and Mayo Lake and (iv) develop a framework to define the

optimal number of precipitation stations in each watershed to increase the accuracy of simulated flows and inflows? Given the scientific relevancy of these requests, the outcomes of the first request are presented in this report in Chapters 2 and 6, the second investigation was concealed in a Technical Report (Rousseau and Savary, 2017) while those of the last two requests are introduced in Appendix I and II.

2. Distributed hydrological modelling and forecasting system

2.1. General methodology and supporting literature

Operational hydrological models for forecasting inflows, stream flows, and extreme flows (floods or droughts) are conceptual, distributed or data-driven models. For example, Sene (2010) reported that the BC Hydro River Forecasting System (RFS) relies on the semi-distributed UBC Watershed Model (Quick, 1995). Five-day inflow forecasts are issued for several reservoirs using a daily time step which can be switched to hourly when required. For operational purposes, BC Hydro uses lead times varying between two days and nearly 10 days. For longer lead times (*i.e.*, seasonal), BC Hydro uses an Ensemble Streamflow Prediction (ESP) framework based on weather forecasts or climate data (*i.e.*, historical). Such forecasts are very important, since the spring freshet represents a major portion of the annual water supply. Hence, for northern watersheds, assimilation of SWE becomes an essential key feature of any forecasting systems. Other deterministic models currently used by operators of hydroelectric facilities or river forecasting centres include: (i) the lumped models SAC-SMA (Finnerty et *al*., 1997; Burnash, 1995) coupled or not with SRM (Martinec, 1975; Abudu et *al*., 2012), SLURP (*e.g.*, Su et *al*., 2000) and HSAMI (Bisson and Roberge, 1983; Fortin 2000); (ii) the semi-distributed models HBV (Lindström et *al*., 1997, Sorman et *al*., 2009), HEC-HMS (Anderson et *al*., 2002), WATFLOOD (Kouwen et *al.*, 2005) and HYDROTEL (Fortin et *al.*, 2001; Turcotte et *al.*, 2003, 2007; Fossey et *al.*, 2015); and (iii) the distributed model HL-RDHM (Koren et *al*., 2004), to name a few.

This section presents the implementation of a forecasting system for short- and mid-term lead times using HYDROTEL as the core hydrological model. HYDROTEL developed at INRS, in collaboration with Hydro-Quebec, is supported by the project research group. HYDROTEL is currently used for inflow and hydrological forecasting of publicly-owned dams in Quebec (Turcotte et al., 2004). Since YEC did not have any experience in operating an inflow forecasting system, a multimodel approach (*e.g.*, Oudin et *al.*, 2006, Kayastha et *al.*, 2013, Sellier et *al.*, 2012) was beyond the scope of this project.

From a hydrological modelling perspective, the model simulates evapotranspiration, snow accumulation/melt, soil temperature/freezing depth, infiltration, recharge, surface flow, subsurface flow and channel routing; using an intra-daily (*i.e.*, 1, 3, 6, 12 hr) or a daily time step. Hydrometeorological

data include gridded or site-specific precipitation, maximum and minimum air temperatures; and for model calibration, stream flows, reconstructed reservoir inflows and any other relevant state variables (*e.g.*, SWE). The computational domain is made of interconnected river segments (RSs) and either three-soil-layer sub-watersheds or hillslopes, referred to as relatively homogeneous hydrological units (RHHUs). The latter units are defined using PHYSITEL, a specialized geographic information system (GIS) (Turcotte et *al.*, 2001; Rousseau et *al.*, 2011; Royer et *al*. 2006) for the determination of the complete drainage structure of a watershed using a Digital Elevation Model (DEM) and digitized river and lake networks. Additional characterization of the watershed by PHYSITEL requires integration of a classified land cover map, soil texture map based on percentage of sand, loam, and clay, along with corresponding hydrodynamic properties (Rawls and Brakensiek, 1989), and wetland attributes.

Implementation of HYDROTEL for short- and mid-term forecasts at YEC is being achieved by using a customized Graphical User Interface (GUI) developed at INRS. The system which is developed in collaboration by INRS and YU accomplishes the following tasks: (i) updating and formatting monitored water levels and flows and calculating recent reservoir inflows; (ii) downloading the North American Ensemble Forecast System (NAEFS) issued by the Meteorological Service of Canada (MSC) for the 1 to 14 days weather forecast; (iii) formatting and correcting of weather forecast data compatible with HYDROTEL; (iv) adjusting values of state variables (as initial conditions for forecast simulation) with data assimilation; (v) if data are available, data assimilation of SWE; (vi) using HYDROTEL to generate hydrological forecasts; and (vii) sharing of hydrological forecasts for the target lead time. Along the process NAEFS requires bias correction using tools developed by YU.

For longer lead times (*i.e.*, seasonal inflow forecasts; 1 to 12 months), an ESP framework based on weather forecasts is available. The current framework includes: ECCC's seasonal forecasting system CanSIPS (Canadian Seasonal and Inter-annual Prediction System, Merryfield et *al.*, 2011), which relies on the Canadian General Circulation Model (CGCM) producing forecasts for up to one year, performed every month (*i.e.*, 20 members, monthly mean for each member). It is noteworthy that beyond the first month, most seasonal weather forecasts have low skill scores for precipitation; that is why ensuing hydrological forecasts have limited reliability. For large northern watersheds, seasonal weather forecasts could be valuable for assessing the effect of a warming trend on snowpack and spring freshet dynamics.

Nevertheless, downscaling issues related to spatial and temporal resolutions associated with CanSIPS were dealt with and hence data were downscaled and disaggregated for the watersheds studied by YU which had experience in the subject matter.

Yukon Geomatics public portal, British Columbia (BC) geomatics portal and ECCC were the major spatial data providers for the development of the hydrological forecasting system. The required data include: physiographic information (30-m horizontal & 5-30-m vertical resolutions DEM), land cover (2005 MODIS and 2000 CIRCA Canadian Land Cover Classification 2005 MODIS and 2000 CIRCA Canadian Land Cover Classification and Alaska National Land Cover Database, 250-m to 30-m resolution), soil texture (Canadian soil texture map for percentage of sand, silt and clay (Szeto et *al.*, 2008)), weather and climate data. Due to a relicensing constraint (December 31, 2019), the Aishihik watershed was modelled first, followed by the Mayo watershed and the Upper Yukon River watershed including Marsh Lake as a sub-watershed. For model calibration, reanalysis data (precipitation and minimum and maximum temperature) available on a 10-km grid such as the Canadian Precipitation Analysis (CaPa) (Fortin et *al*., 2014, 2015) and ANUSPLIN (Hutchinson et *al.*, 2009), could also be of interest for further investigation. Several studies have relied upon reanalysis datasets in Northwestern Canada, for examples: (i) NCEP/NCAR (Kalnay et *al.*, 1996) have been used for studies in BC, southern Yukon, and Yukon River basin (Cannon and Whitfield, 2002; Pinard et *al.*, 2009 Rawlins et *al.*, 2006); (ii) NARR (Mesinger et *al.*, 2006) for glacier modeling in BC and Yukon River basin (Jarosch et *al.*, 2012; Ainslie and Jackson, 2010; Semmens et *al.*, 2013); and (iii) ERA-40 (Uppala et *al*., 2005) for several studies as well (Cassano and Cassano, 2010 Kerkhoven and Gan, 2011; Pointras et *al.*, 2011]. For this project, recent reanalysis datasets such as CFSR (Saha et *al.*, 2010), ERA-Interim (Dee et *al*., 2011), MERRA2 (Rienecker et *al*., 2011], JRA55 (Kobayashi et *al*. 2015) were considered, but did not prove to be of good quality enough in Yukon.

2.2. Integration of the studied watersheds into HYDROTEL

This section introduces: (i) the discretization of the Mayo, Aishihik and Upper Yukon Watersheds (including Marsh Lake sub-watershed) using PHYSITEL including presentation of the input data and construction of the ensuing database for the hydrological modelling; (ii) the importation of the database into HYDROTEL followed by model calibration, and (iii) the development of the inflow forecasting system.

2.2.1. Input data

Table 2.1 presents the information required for hydrological modelling of the study watersheds using the HYDROTEL/PHYSITEL modelling platform.

Table 2.1 Spatial data for watershed discretization using PHYSITEL

Input data	Available source
Digital elevation model (DEM)	Geomatics Yukon Natural Resource Canada
Stream and lake networks	Geomatics Yukon and DataBC geomatics portal
Land Cover	Natural Resources Canada Geomatics Yukon, United States Geological Survey
Soil Type (Texture)	Environment Canada Geomatics Yukon

Additional data required for hydrological modelling include: (i) meteorological data measured at different existing stations or reconstructed and distributed on grid; (ii) measured streamflow data at any location on the stream network or reconstructed reservoir inflows based on water level variation and known reservoir outflow or river flow. Other data source such as reanalysis data (precipitation and minimum and maximum temperature) CFSR (Saha et *al.*, 2010), ERA-Interim (Dee et *al*., 2011), MERRA2 (Rienecker et *al*., 2011], JRA55 (Kobayashi et *al*. 2015) were tested through the calibration process. Although other reanalysis data available such as CaPA (Fortin et *al*., 2014, 2015) and ANUSPLIN (Hutchinson et *al*., 2009) where not tested considering results for listed reanalysis data sets.

DEM

For all watersheds, the DEMs were created with 30-m resolution data sheets obtained from the Geomatics Yukon file transfer protocol (ftp) site (ftp.geomaticsyukon.ca/DEMs/) and Natural Resources Canada ftp site. In both cases, we used the ArcMap Mosaic tool to generate complete DEMs. Each data sheet was identified given coarse watershed limits available on the Geomatics Yukon site or roughly defined by INRS for the Upper Yukon River watershed. As a reminder, DEM data for Canada are commonly interpolated from the digital 1:50,000 Canadian National Topographic Database (NTDB Edition 2). The resulting DEMs will be introduced with the stream and lake network of each watershed.

Stream and lake networks

Each watershed stream and lake networks were extracted and built using the 1:50,000 watercourse and water body files available at the Geomatics Yukon and DataBC portal. The downloaded files were not fully readily compatible with HYDROTEL, thus, precise data processing steps were taken to create satisfying networks. The following steps were achieved using the Arc Map tool:

1. For all watersheds, only streams and lakes within watershed boundaries were selected and those remaining removed. It is noteworthy that the watershed limits were reassessed to make sure that all streams and lakes contributing to the watershed outlet were carefully identified.

2. All isolated lakes – those not having any connection to the river network - were identified and removed.

3. Since really small lakes can generate errors during the integration process, all lakes covering less than 0.0144km² were removed and replaced by small river segments.

4. Since lakes are delineated by water bodies (polygons), large streams depicted as waterbodies using left and right banks were replaced with a single centerline watercourse.

5. All stream segments were properly connected together and when required connected to a lake contour vertex (point that defined the lake contour).

6. Using the MapInfo software, the stream network and the lake network were merged to provide a unique network for subsequent importation in PHYSITEL except for the Upper Yukon River watershed where rivers and lakes were used separately in a newer version of PHYSITEL.

7. Use of PHYSITEL provided a mean to identify any remaining errors in each stream and lake networks. PHYSITEL highlighted lakes with multiple outlets or small rivers that were fully contained within one tile of the DEM. These errors were rectified using PHYSITEL to ensure that the stream and lake networks were fully compatible with HYDROTEL.

Figure 2.1 presents the DEM and the stream and lake networks of the Mayo, Aishihik and Upper Yukon watersheds. Note that DEMs cover larger areas than those of each watershed.

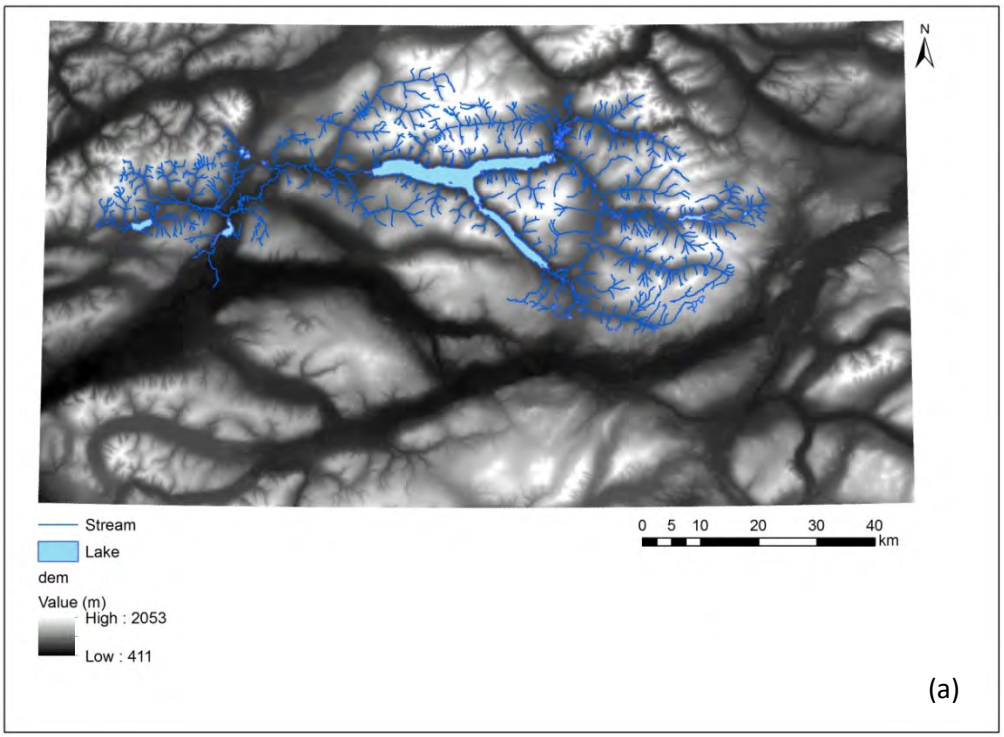

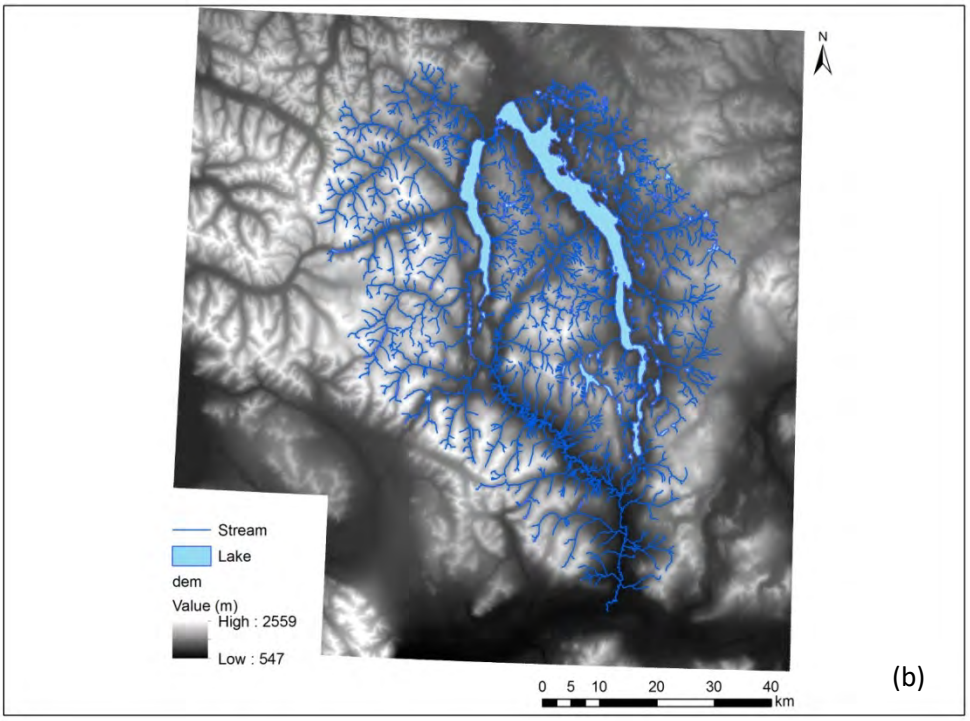

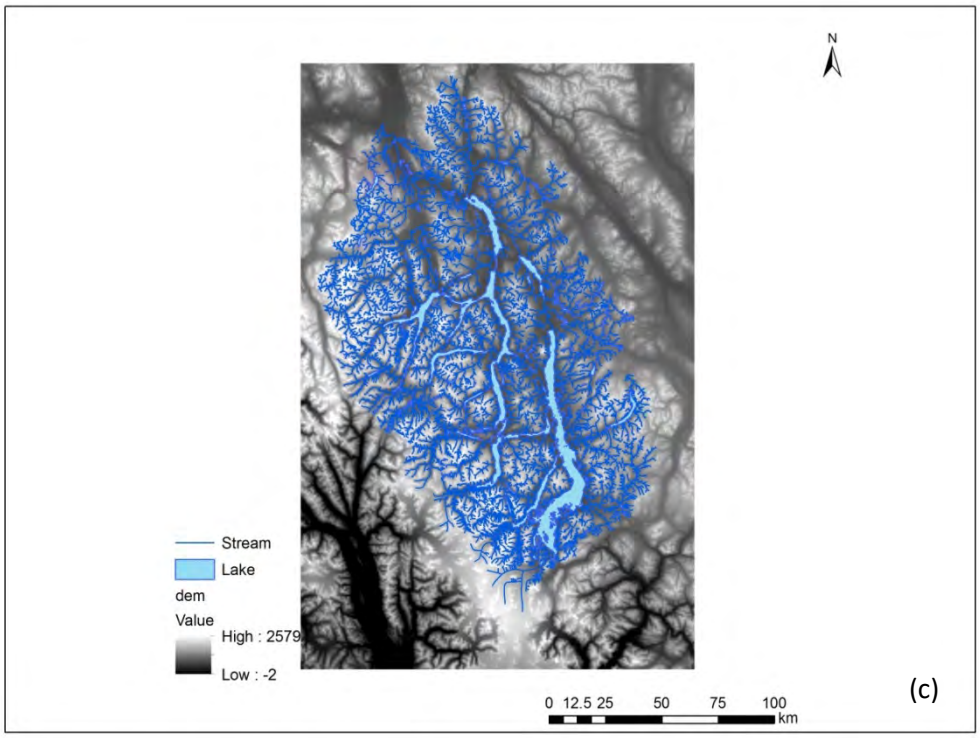

Figure 2.1 DEMs and stream and lake networks: (a) Mayo Watershed (b) Aishihik Watershed and (c) Upper Yukon River watershed.

Figure 2.1 illustrates that the corrected stream and lake network is dense and complex with a high level of details.

Land cover

Initially, we explored various sources of data that could be used to define the required land cover map. Two sets of existing data were selected based on their coverage and standardized format. We built an initial land cover map based on the MODIS Canadian land cover map. This classification, dating back to 2005, was performed by the Canadian Remote Sensing Center (Natural Resources Canada) using MODIS satellite images. To our knowledge, this classification is the most recent that entirely covers Canada. It has a 250-m horizontal resolution and includes 39 different land cover classes. From a hydrological modelling point of view, there are too many land cover classes. Thus, we reduced the number of classes to 7 for Aishihik and Mayo watersheds or 9 for the Upper Yukon River watershed. There is no need of having a large number of land cover classes as they will mostly end up having similar or identical parameter values. Table 2.1 presents the regrouped classes of the MODIS classification.

Second, we built a supplementary land cover map based on the Canadian 2000 CIRCA classification from Natural Resources Canada. This classification which covers the whole country was performed with Landsat images. When compared to the MODIS classification, the CIRCA classification has a better horizontal resolution (*i.e.*, 30 m) which incidentally matches the DEM resolution. It includes 43 different land cover classes. Again to ensure a certain agreement with the MODIS classification, we reduced the number of classes to 7 for Aishihik and Mayo watersheds or 9 for the Upper Yukon River watershed. Table 2.2 presents the regrouped classes for the CIRCA classification.

Table 2.2 Regrouped classes of the MODIS classification for the Mayo and Aishihik watersheds

MODIS classes	Regrouped classes
Temperate or subpolar needle-leaved evergreen closed tree canopy (1)	Evergreen Forest
Cold deciduous closed tree canopy (2)	Deciduous Forest
Mixed needle-leaved evergreen – cold deciduous closed tree canopy (3)	Mixed Forest
Mixed needle-leaved evergreen – cold deciduous closed young tree canopy (4)	Mixed Forest
Mixed cold deciduous – needle-leaved evergreen closed tree canopy (5)	Mixed Forest
Temperate or subpolar needle-leaved evergreen medium density, moss-shrub understory (6)	Evergreen Forest
Temperate or subpolar needle-leaved evergreen medium density, lichen-shrub understory (7)	Evergreen Forest
Temperate or subpolar needle-leaved evergreen low density, shrub-moss understory (8)	Evergreen Forest
Temperate or subpolar needle-leaved evergreen low density, lichen (rock) understory (9)	Evergreen Forest
Temperate or subpolar needle-leaved evergreen low density, poorly drained (10)	Evergreen Forest
Cold deciduous broad-leaved, low to medium density (11)	Deciduous Forest
Cold deciduous broad-leaved, medium density, young regenerating (12)	Deciduous Forest
Mixed needle-leaved evergreen – cold deciduous, low to medium density (13)	Mixed Forest
Mixed cold deciduous - needle-leaved evergreen, low to medium density (14)	Mixed Forest
Low regenerating young mixed cover (15)	Mixed Forest
High-low shrub dominated (16)	Shrub, Herb, lichen, bare soil, rock
Herb-shrub-bare cover (18)	Shrub, Herb, lichen, bare soil, rock
Wetlands (19)	Wetlands
Sparse needle-leaved evergreen, herb-shrub cover (20)	Shrub, Herb, lichen, bare soil, rock
Polar grassland, herb-shrub (21)	Shrub, Herb, lichen, bare soil, rock
Shrub-herb-lichen-bare (22)	Shrub, Herb, lichen, bare soil, rock
Herb-shrub poorly drained (23)	Shrub, Herb, lichen, bare soil, rock
Lichen-shrub-herb-bare soil (24)	Shrub, Herb, lichen, bare soil, rock
Low vegetation cover (25)	Shrub, Herb, lichen, bare soil, rock
High biomass cropland (27)	Shrub, Herb, lichen, bare soil, rock
Lichen barren (30)	Shrub, Herb, lichen, bare soil, rock
Lichen-spruce bog (32)	Wetlands
Rock outcrops (33)	Shrub, Herb, lichen, bare soil, rock
Recent burns (34)	Burns
Old burns (35)	Burns
Urban and Built-up (36)	Urban
Water bodies (37)	Water
Mixes of water and land (38)	Water
Snow / Ice (39)	Water / Snow/Ice (uYRW)

Table 2.3 Regrouped classes of the CIRCA classification for the Mayo and Aishihik Watersheds

CIRCA classes	Regrouped
Cloud(11)	No Data
Shadow (12)	No Data
Water (20)	Water
Snow/Ice (31)	Water / Snow/Ice (uYRW)
Rock/Rubble (32)	Shrub, Herb, lichen, bare soil, rock
Exposed land (33)	Shrub, Herb, lichen, bare soil, rock
Bryoids (40)	Shrub, Herb, lichen, bare soil, rock
Shrub tall (51)	Shrub, Herb, lichen, bare soil, rock
Shrub low (52)	Shrub, Herb, lichen, bare soil, rock
Wetland - Treed (81)	Wetlands
Wetland - Shrub (82)	Wetlands
Wetland - Herb (83)	Wetlands
Herb (100)	Shrub, Herb, lichen, bare soil, rock
Coniferous Dense (211)	Evergreen Forest
Coniferous Open (212)	Evergreen Forest
Coniferous Sparse (213)	Evergreen Forest
Broadleaf Dense (221)	Deciduous Forest
Broadleaf Open (222)	Deciduous Forest
Mixedwood Open (232)	Mixed Forest
Mixedwood Sparse (233)	Mixed Forest

Regarding the two available products, we decided to use the land cover map build from the CIRCA classification since the 30-m resolution of the latter corresponded to that of the DEMs. Furthermore, for both watersheds, the NoData of the CICRA classification were corrected using the more recent MODIS classification (2005 versus 2000). This correction affected more the Aishihik Watershed because of a larger non-classified area on the CIRCA classification. Figure 2.2 shows the resulting land cover maps of the Mayo, Aishihik and Upper Yukon Watersheds. Also, for all watersheds, the stream and lake networks were superimposed on the original classification in order to properly match the water routing and the land cover. Note also that the Alaska National Land Cover Database classification was included to have a complete coverage of the Upper Yukon River watershed. Moreover, this latter watershed included two additional classes, namely Urban and Snow/Ice due to the presence of denser urban areas and glaciers in the upstream portion of the watershed. Also the land cover map for the Upper Yukon River was recently updated to represent the glacier area based on the most recent GLIMS (Global Land Ice Measurements from Space) measurements.

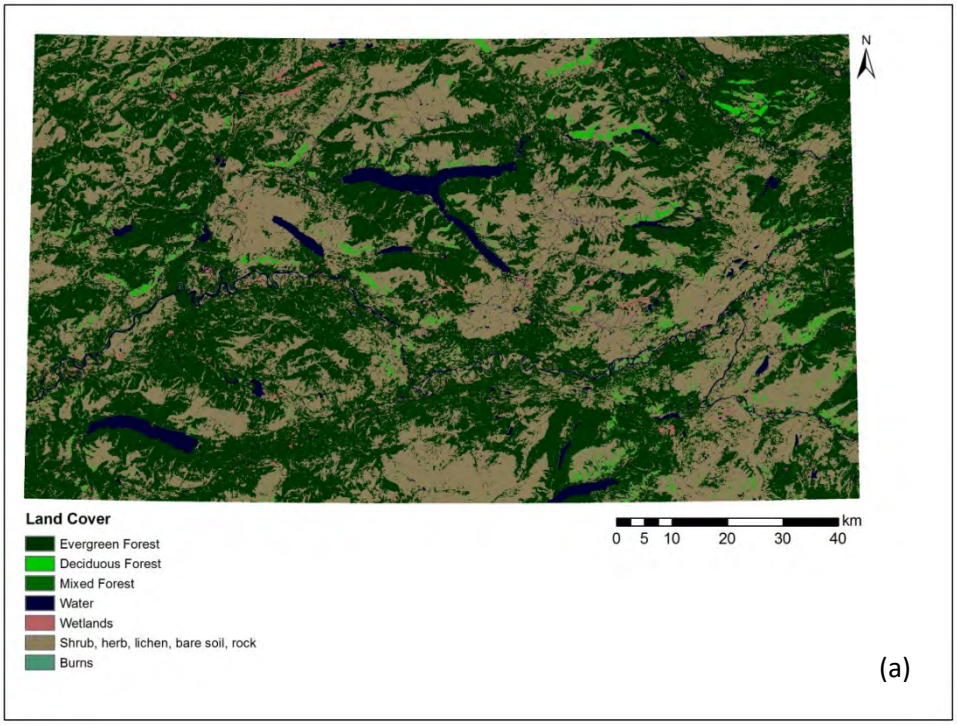
N
Land Cover
Evergreen Forest
Deciduous Forest
Mixed Forest
Water
Wetlands
Shrub, herb, lichen, bare soil, rock
Burns
km
0 5 10 20 30 40
(a)

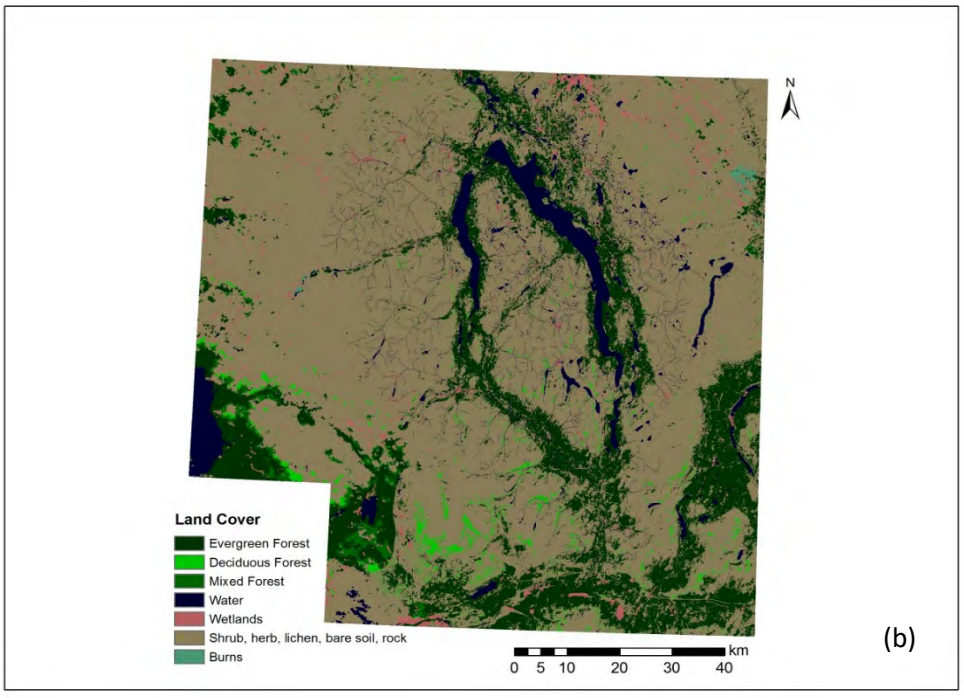
N
Land Cover
Evergreen Forest
Deciduous Forest
Mixed Forest
Water
Wetlands
Shrub, herb, lichen, bare soil, rock
Burns
km
0 5 10 20 30 40
(b)

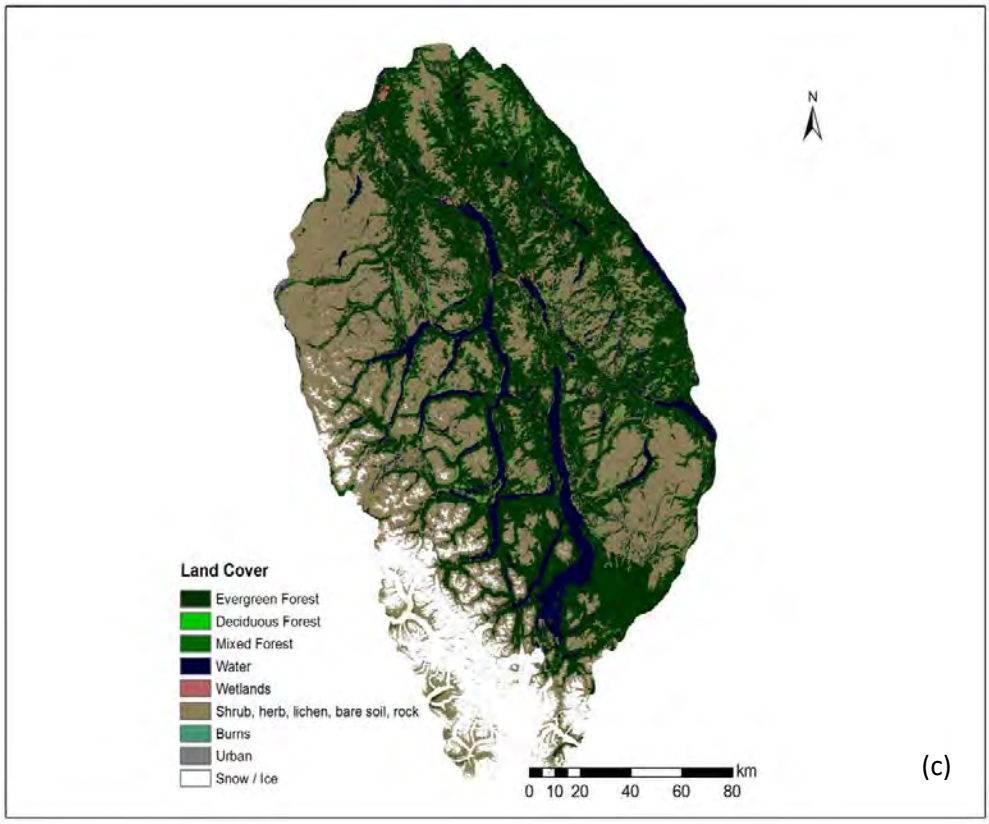

Figure 2.2 Land cover maps: (a) Mayo, (b) Aishihik and (c) Upper Yukon River Watersheds.

It can be mentioned that the Geomatics Yukon website offers other land cover products that focus mainly on forest resources. Namely, Vegetation and Vegetation Inventory products were not used to produce the land cover maps because they solely depict the presence or absence of forested areas and give information on tree species for the forest industry. From a hydrological modelling perspective, there is no need for a complete coverage of the area and the type of trees does not need to be as precise as that reported in the Vegetation Inventory. Indeed, ultimately the land cover classes will be regrouped in integrated classes with specific parameter values. At this point there was no need to use such products and improving the land cover map would not have guaranteed any improvement to the hydrological modelling.

Soil type

The Geomatics Yukon website currently offers limited information on soil texture. Bedrocks geology does not provide the needed information and the associated data only cover limited areas of the Mayo and Upper Yukon River Watershed; while there is no soil information for the Aishihik Watershed. That is why we have decided to look for other sources of information. Based on previous work performed in northern Quebec, there exists an alternative soil texture map covering Northern America at a 1-km resolution.

From a hydrological modelling perspective, HYDROTEL conceptualizes the soil profile as a series of different soil layers with constant hydrodynamics properties. When field measurements are unavailable, default values based on the work of Rawls and Brakensiek (1989) can be used, given basic soil texture information, namely percentages of sand, silt and clay.

The soil type maps developed for the Mayo, Aishihik and Upper Yukon River Watersheds are based on percentages of sand, silt and clay available for three soil layers. These maps were derived from the work of Szeto *et al*. (2008) and they are based on the Soil Landscape of Canada V.2.2. It is the same data that were used as input data to the Canadian Land Surface Scheme (CLASS) of the Canadian Regional Climate Model. It is noteworthy that these maps do not provide any information on non-mineral land cover such as water, outcrops, and organic soils, as they cannot be related to any soil texture composition. The soil type maps were derived as follows.

1. For each 1-km tile and soil horizon (0-10cm; 10-25cm; 25-375cm), the soil type was defined by percentages of sand, silt and clay based on the following soil texture triangle (Figure 2.3).

2. Development of a soil type map for the second soil layer (10-25cm). HYDROTEL allows for the use of a different soil type map for each soil layer required by the vertical water budget sub-model (BV3C). Given the coarse spatial resolution of the basic information, it was decided to use a unique soil type map valid for all three soil layers based on the information available for the second soil layer of the reference data. However, in the presence of a non-mineral soil type, the information available for layer one or layer three were used to substitute the non-mineral soil with the mineral soil information when available. Nonetheless, the resulting maps for all watersheds include non-mineral soils with default values for hydrodynamic properties.

3. The ensuing tiles of 1-km resolution were subdivided into 30-m tiles; that is the resolution of the DEMs.

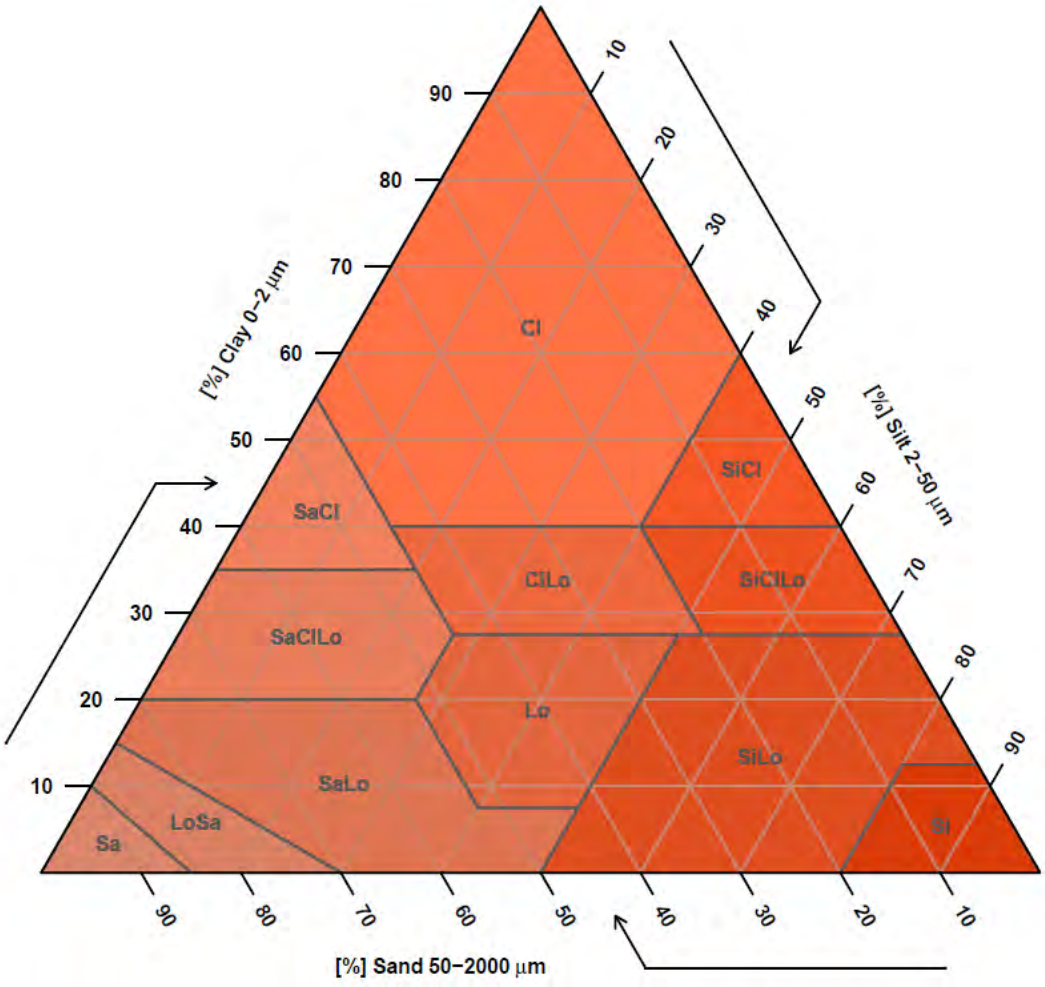

Figure 2.3 Soil texture triangle (Moeys, 2009).

Abbreviations used within the triangle are: Cl : clay, SiCl : silty-clay, SaCl : sandy-clay, SiClLo : silty-clay-loam, ClLo : clay-loam, SaClLo : sandy-clay-loam, SiLo : silty-loam, Lo : loam, SaLo : sandy-loam, Si : silt, LoSa : loamy-sand, Sa : sand.

Figure 2.4 introduces the resulting soil type maps for the Mayo, Aishihik and Upper Yukon River Watersheds.

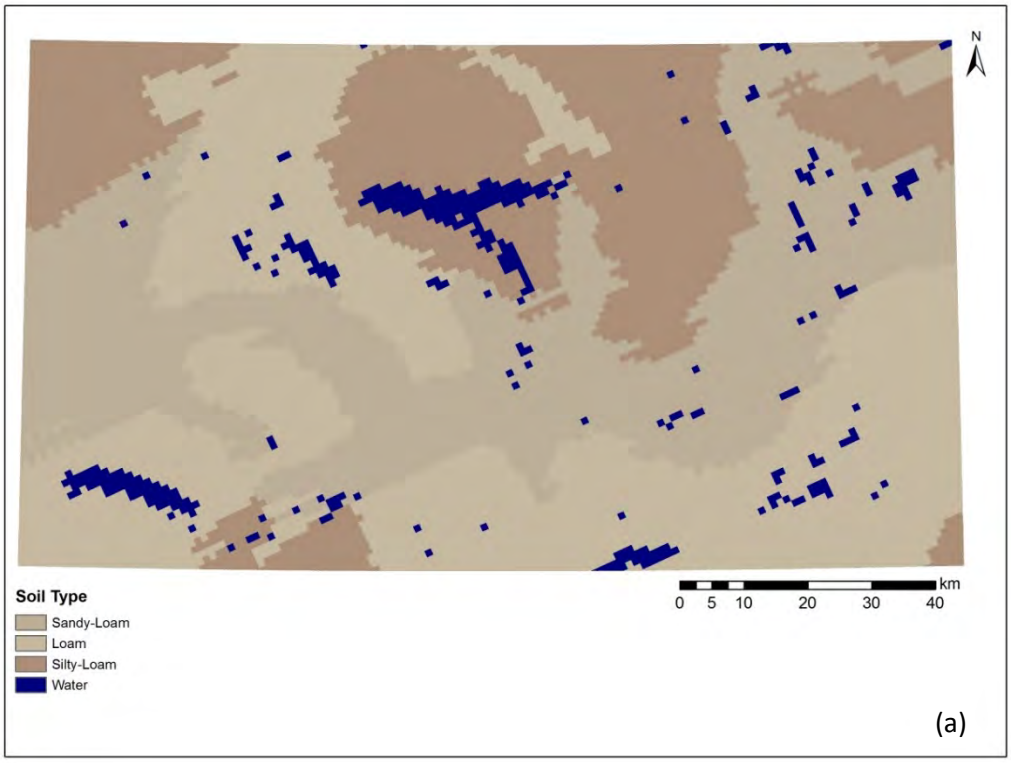
N
Soil Type
Sandy-Loam
Loam
Silty-Loam
Water
km
0 5 10 20 30 40
(a)

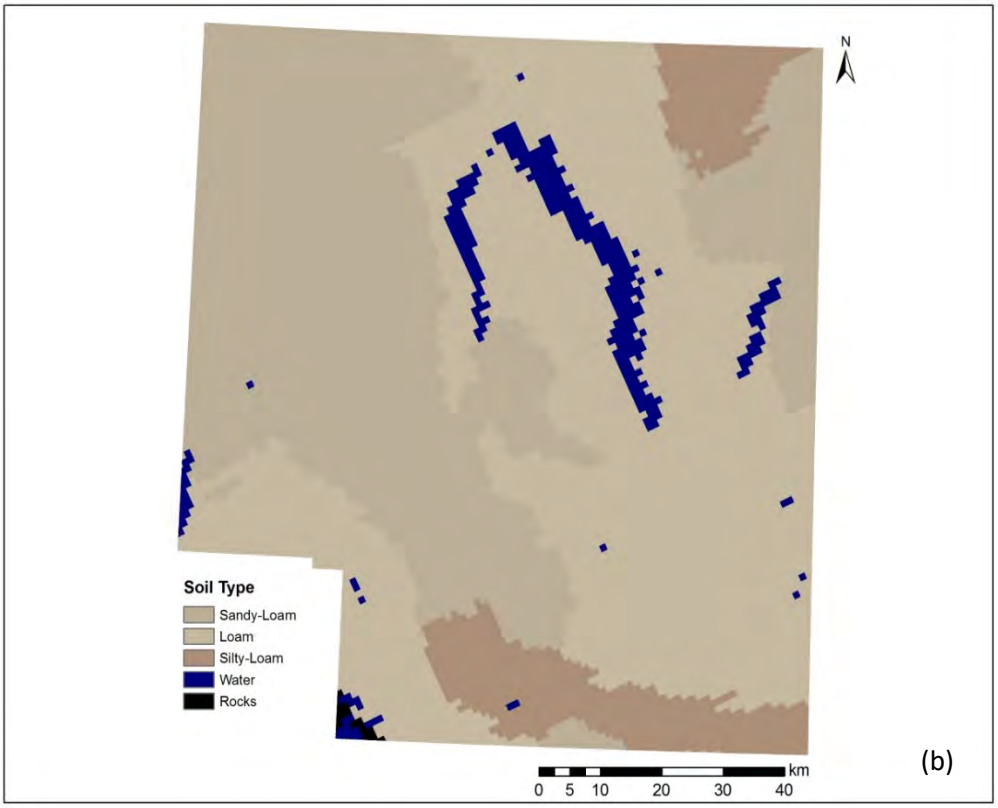
N
Soil Type
Sandy-Loam
Loam
Silty-Loam
Water
Rocks
km
0 5 10 20 30 40
(b)

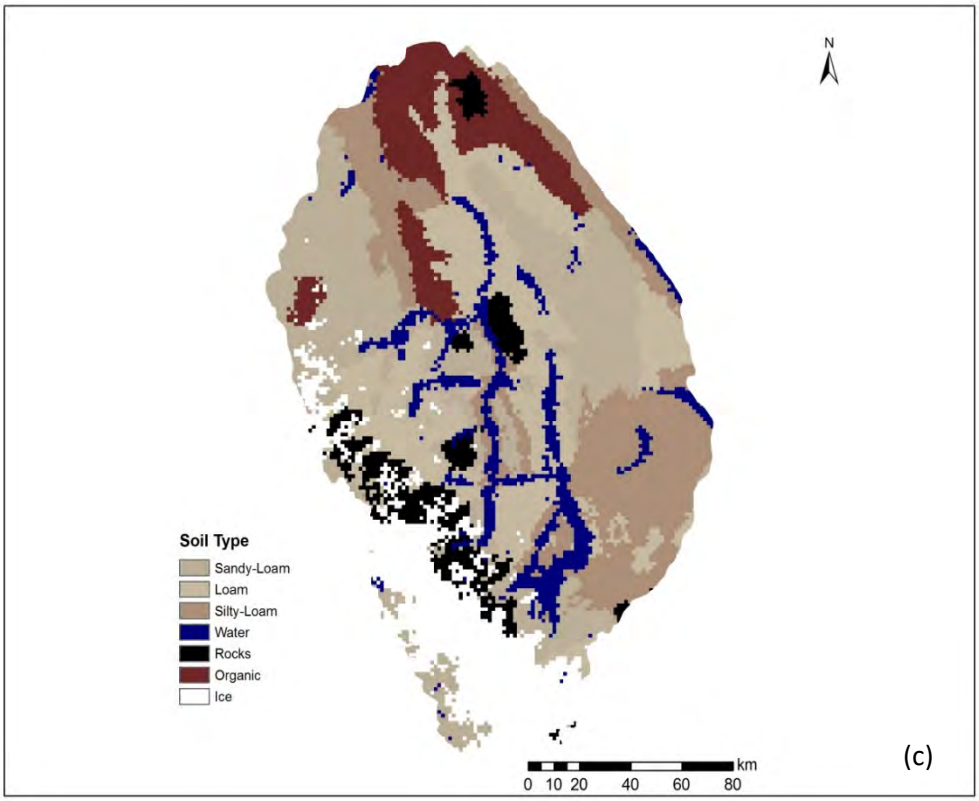

Figure 2.4 Soil type maps: of (a) Mayo, (b) Aishihik) and (c) Upper Yukon River Watersheds.

As mentioned earlier, there exists in PHYSITEL a table relating the soil textures of various soil types developed by Rawls and Brakensiek (1989). It is noteworthy that non-mineral textures can be added to the existing table. Using the soil type map, PHYSITEL determines the dominant soil type of each RHHU. Using the hydrodynamic soil properties look-up table, HYDROTEL estimates the ensuing properties for each RHHU. For mineral soils, the hydrodynamic properties correspond to the default values described in the Rawls and Brakensiek (1989). For non-mineral soils, the hydrodynamic properties have to be determined. Similarly to the works of Jutras et *al*. (2009), these properties for clay were assigned to the water, rocks, ice and outcrop classes. Then again, if required the user can further modify all hydrodynamic properties by simply editing the *proprietehydrolique.sol* file present in the physitel folder of any HYDROTEL project.

2.2.2. Watershed discretization using PHYSITEL

Using a DEM, a soil type map, a land cover map, and optionally a hydrographic network; PHYSITEL computes physiographic parameters for each RHHU. Namely, PHYSITEL determines the internal drainage structure (slopes and flow directions), watershed boundaries, sub-watershed and hillslope boundaries, and hydrographic network. For each RHHU, PHYSITEL calculates the topographic index distribution and characterizes the dominant soil type, and percentages of different land covers. Because of standard data formats and universal data types, output data can be used for a wide range of distributed hydrological models. What differentiates PHYSITEL from most GISs are the following characteristics: (i) use of the D8-LTD algorithm of Orlandini et *al*. (2003) to compute the flow matrix, (iii) access to editing tools to modify the flow matrix and correct the stream and lake network, and (iii) optional use of a hydrographic network to determine the internal drainage structure of a watershed.

PHYSITEL can be described as a step by step wizard that guides and helps the user to proceed to watershed discretization. Figure 2.5 summarizes the PHYSITEL input data and data processing.

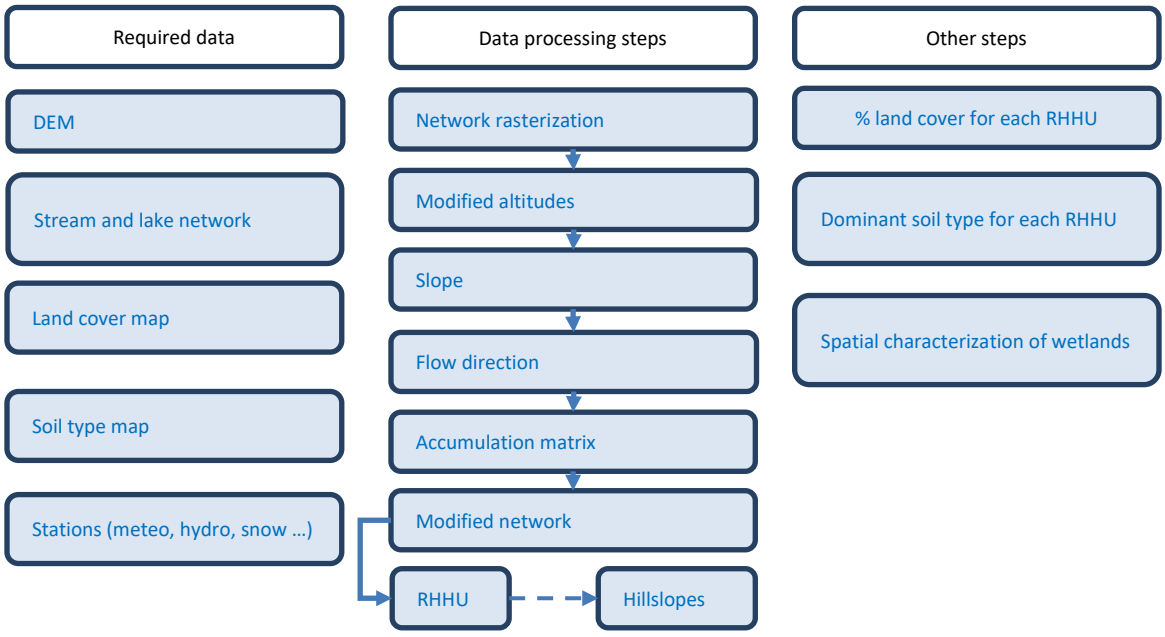

Figure 2.5 PHYSITEL – Input data and data processing.

The different steps of data processing can be described as follows:

1. After correcting the stream and lake network, the vector and polygon network is converted into a raster file.

2. The rasterized network is burned on the DEM to facilitate water routing to and through the network.

3. Using the DEM, PHYSITEL calculates the slope of each cell or tile based on the north-south and east-west transects of each cell.

4. Again for each cell composing the DEM, PHYSITEL calculates the flow direction matrix using the D8-LTD algorithm of Orlandini et al. (2003).

5. Based on the flow direction of each cell, PHYSITEL determines the flow accumulation matrix that is for each cell the number of upstream drained cell. For a given outlet, such matrix regroups all the drained upstream cells.

6. Depending on the complexity of the streams and lakes, PHYSITEL allows for the derivation of the hydrologic network using either one of the following options. First, the final network can be identical to the imported and rasterized network. Second, the user can specify a threshold that determines the inclusion or not of a cell into the final network based on the number of upstream drained cells.

7. PHYSITEL identifies the drained cells of each stream or lake to determine the RHHUs. PHYSITEL subdivides the RHHUs into hillslopes in order to have a better representation of the terrain mean slope and mean aspect.

8. Following the RHHU or hillslope delineation, PHYSITEL calculates the land cover percentages and dominant soil type of each RHHU.

For Mayo and Aishihik, a threshold of 5000 upstream drained cells was used; while a 30000 upstream drained cells threshold was set for the Upper Yukon River Watershed to produce a simplified hydrological network for each HYDROTEL project supporting the hydrological forecasting system. This way, a reduced number of streams and lakes will be supported by a more reasonable number of RHHUs.

Figures 2.6 and 2.7 present the final hydrographic networks and hillslope subdivisions for the Mayo, Aishihik and Upper Yukon River Watersheds.

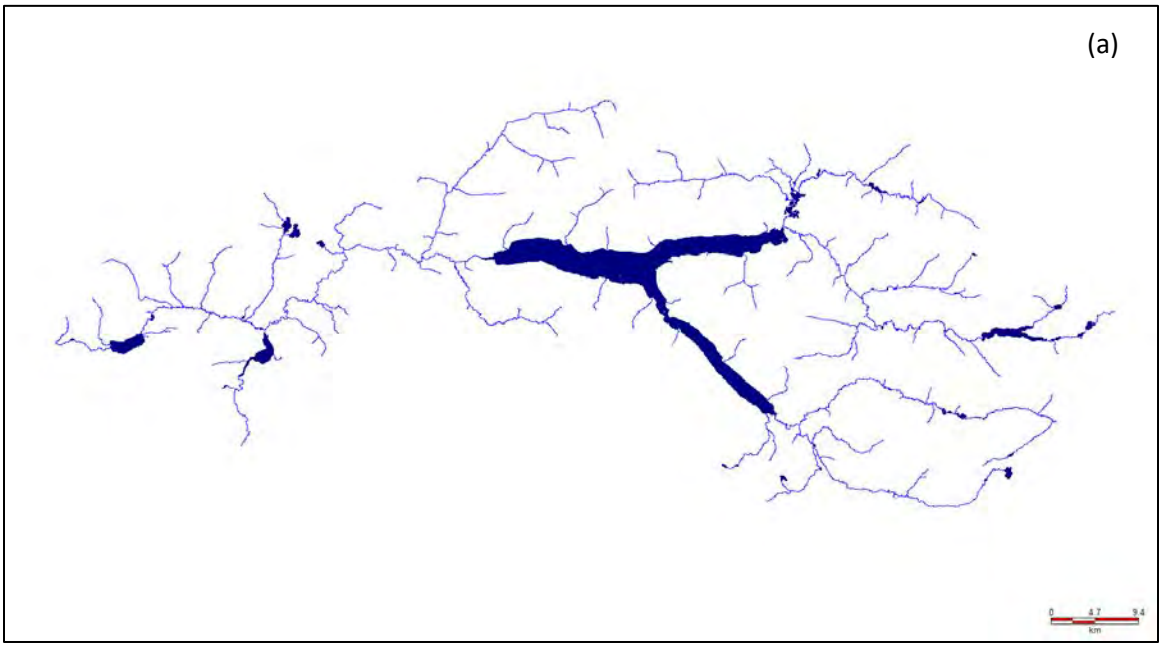

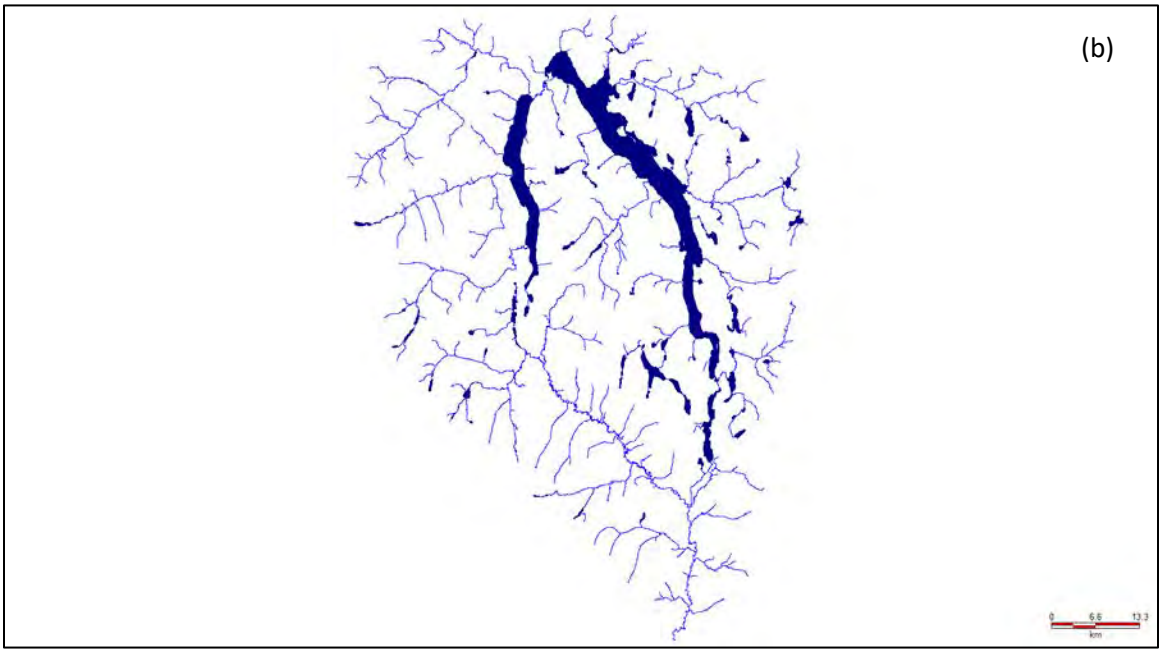

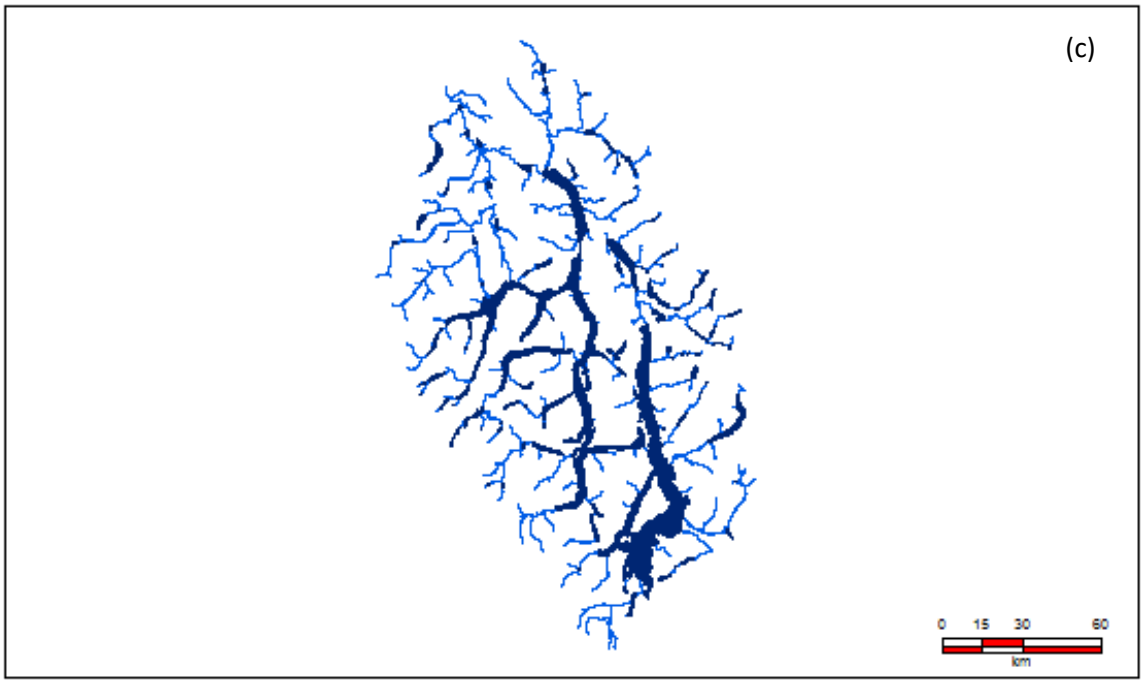

Figure 2.6 Modelled hydrological networks for: (a) Mayo, (b) Aishihik and (c) Upper Yukon River Watersheds.

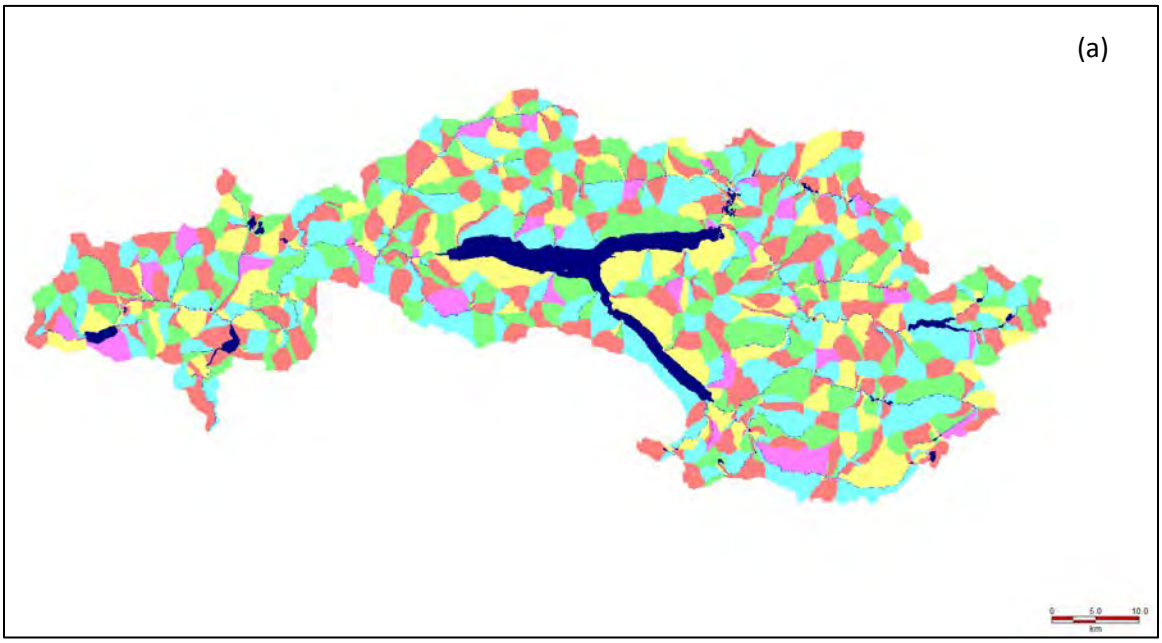

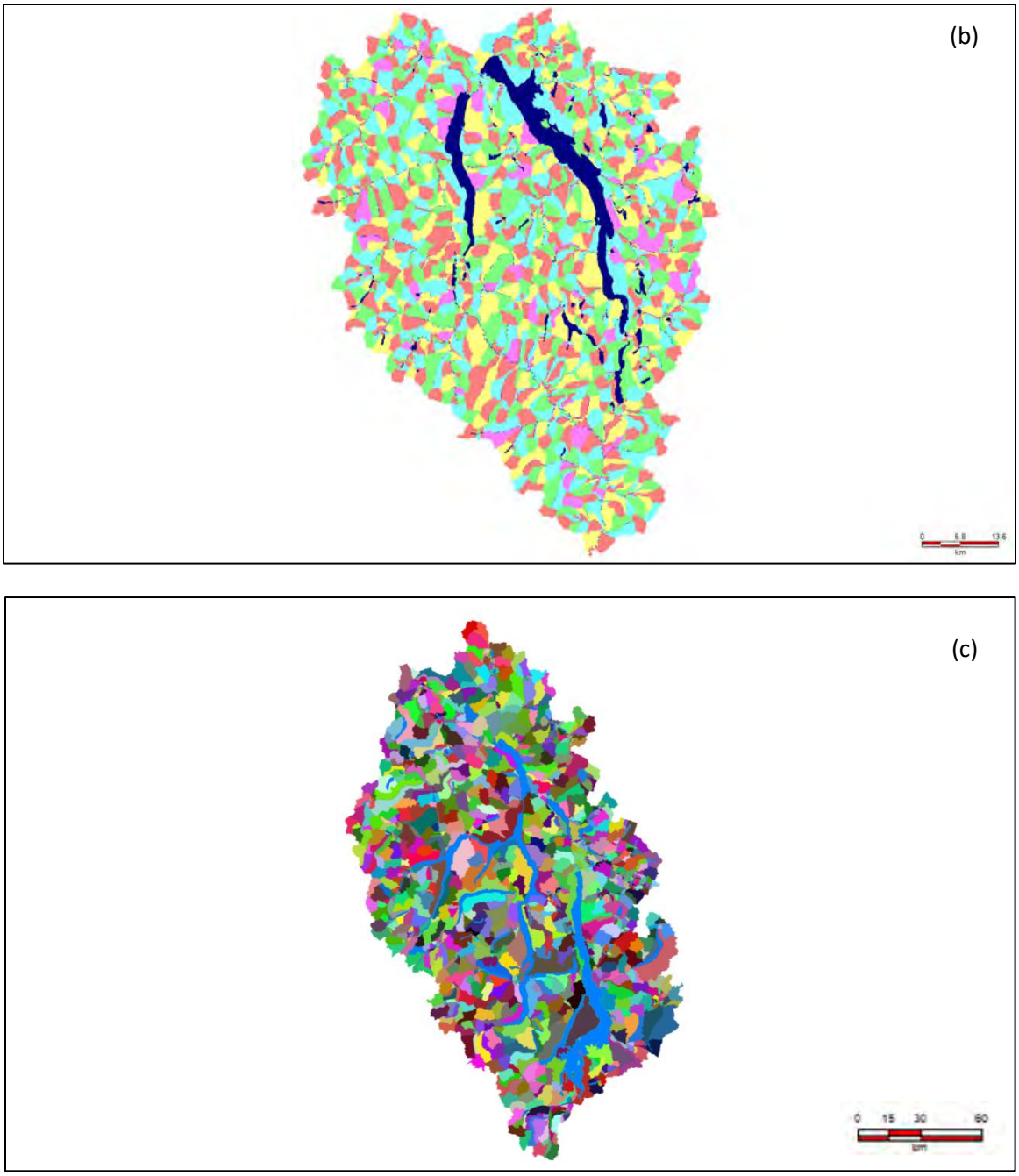

Figure 2.7 RHHU / Hillslope delineation of Mayo (a) Aishihik (b) and (c) Upper Yukon River Watersheds.

The distinctive color pattern for the Upper Yukon River Watershed relates to the use of a newer version of PHYSITEL to perform watershed discretization. This newer version allows for larger watershed to be discretized.

Table 2.4 summarizes the modelling characteristics of the discretized Mayo, Aishihik and Upper Yukon River Watersheds.

Table 2.4 Modelling characteristics of the discretized Mayo, Aishihik and Upper Yukon River Watersheds.

	Mayo	Aishihik	Upper Yukon River
Number of RHHUs (i.e., Hillslopes)	838	1737	1960
Mean RHHU area (km²)	3.19	2.63	10.39
Number of streams and lakes	311	668	702

The RHHU mean area for the Upper Yukon is larger than those for Mayo and Aishihik. The reason is simply related to the number of RRHUs that are used to represent a larger watershed. The number of RHHUs remains under 2000 in order to have an acceptable computational time for simulation and data assimilation for each watershed. It is noteworthy that the data assimilation scheme developed by YU limits the maximum number of RHHUs to 2000.

The final step corresponds to the identification of nearby meteorological stations owned by Environment and Climate Change Canada and to the downloading of historical and available data (temperature and precipitations).

2.2.3. HYDROTEL integration and hydrological simulation

Integration of the Mayo, Aishihik and Upper Yukon River Watersheds (including Marsh Lake sub-watershed) to HYDROTEL is supported by the different files created by PHYSITEL; while simulations are driven by hydrometeorological data. Model calibration requires observed stream flows or reconstructed reservoir/lake inflows and any other relevant state variables (*e.g.*, SWE). From a hydrological modelling perspective, HYDROTEL is a semi-distributed model; that is based on one-dimensional and two-dimensional governing equations. Given the available meteorological data for the studied watersheds, the model runs on a daily time step. The computational domain is made of interconnected river segments (RSs) and three-soil-layer hillslopes, referred to as relatively homogeneous hydrological units (RHHUs) as depicted previously.

Prior to any model simulations, there a need to build a satisfying hydrometeorological database with continuous meteorological data and relevant streamflow or reconstructed reservoir/lake inflows. Such data, especially available stream flows or reservoir/lake inflows can either be provided by YEC or downloaded from the Water Survey Canada website. Any additional meteorological data located within or near the studied watersheds would be welcome and could contribute to the quality of the hydrological simulations along the calibration procedure. This database also includes snow survey measurements (snow height and SWE) that can be assimilated during the production of the hydrological forecasts.

Figure 2.8 and Table 2.5 present the different hydrometeorological stations and snow survey sites for all three watersheds.

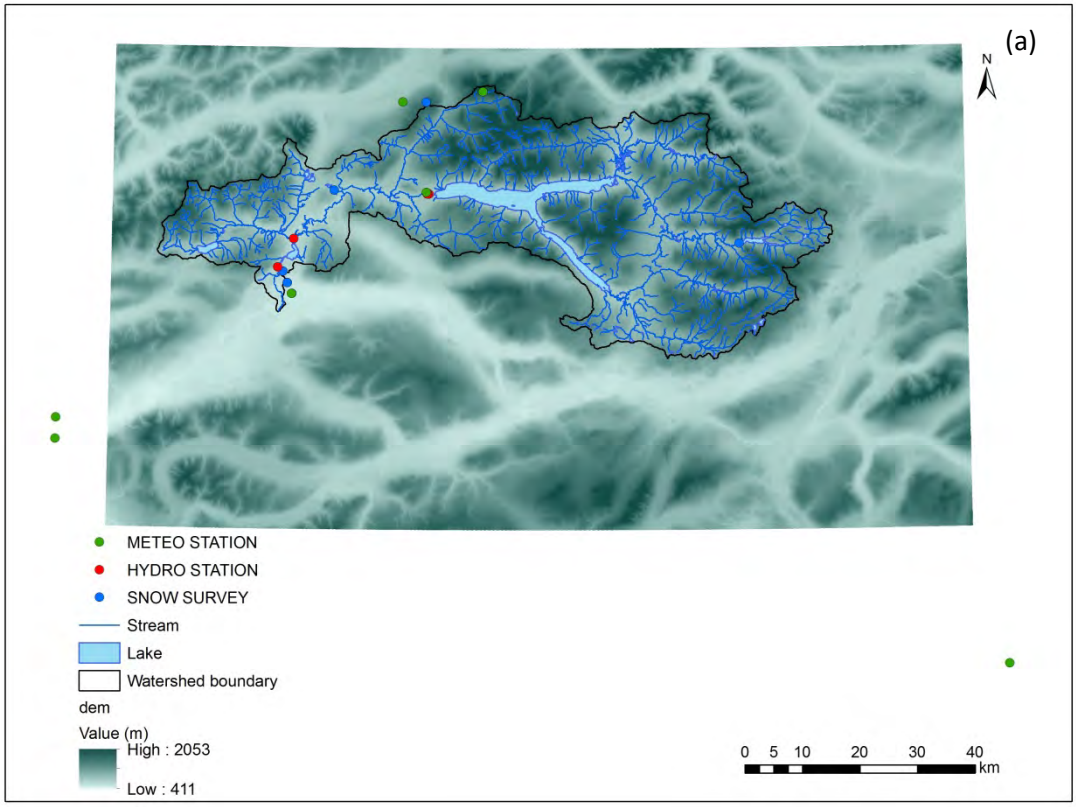

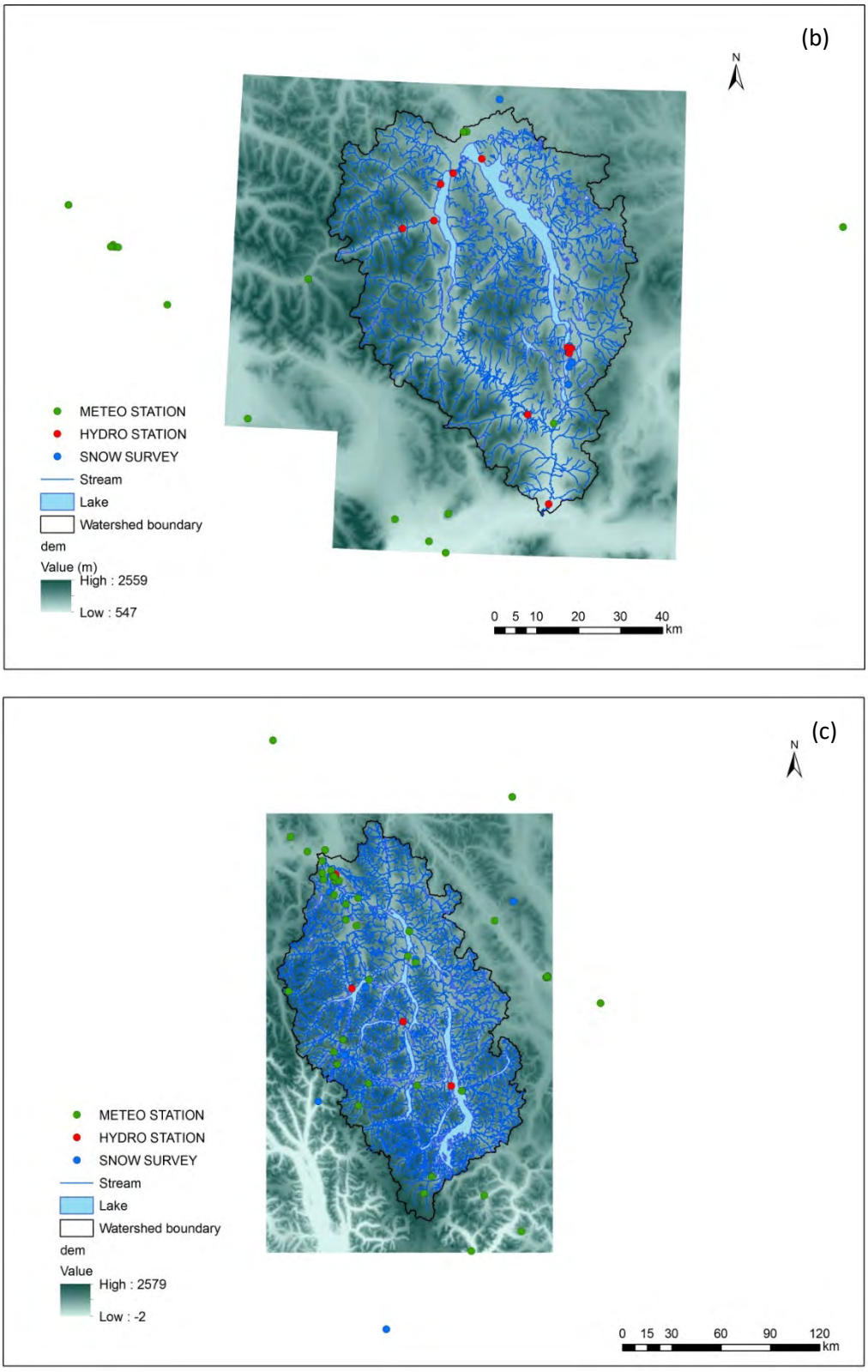

Figure 2.8 Meteorological and hydrometric stations and snow survey sites for Mayo (a) Aishihik (b) and (c) Upper Yukon River Watersheds.

Table 2.5 Meteorological stations of the Mayo, Aishihik and Upper Yukon River Watersheds.

Mayo

NAME OF THE STATION	PROVINCE	STATION #	DATA	START	END	TIME STEP	TYPE	DATA FROM
DRURY CREEK	YT	2100460	T. AND P.	1970	2009	DAILY	MANUAL	MSC
ELSA	YT	2100500	T. AND P.	1948	1989	DAILY	MANUAL	MSC
KENO HILL	YT	2100677	T. AND P.	1974	1982	DAILY	MANUAL	MSC
MAYO A	YT	2100700	T. AND P.	1924	2013	HOURLY AND DAILY	AUTO. AND MANUAL	MSC
MAYO A	YT	2100701	T. AND P.	2013	-	HOURLY AND DAILY	AUTO. AND MANUAL	MSC
MOOSE CREEK	YT	2100746	T. AND P.	1972	1975	DAILY	MANUAL	MSC
RUSSELL CREEK	YT	2100942	T. AND P.	1989	1993	DAILY	MANUAL	MSC
STEWART CROSSING	YT	2101030	T. AND P.	1953	2008	DAILY	MANUAL	MSC
STEWART CROSSING TOWER	YT	2101031	T. AND P.	1976	1976	DAILY	MANUAL	MSC
TWO PETE CREEK	YT	2101138	T. AND P.	1979	1984	DAILY	MANUAL	MSC
MAYOMET	YT	MAYOMET	T. AND P.	2017	-	HOURLY AND DAILY	AUTO. AND MANUAL	YEC-YNC

Aishihik

NAME OF THE STATION	PROVINCE	STATION #	DATA	START	END	TIME STEP	TYPE	DATA FROM
MULE CREEK	BC	1205248	T. AND P.	1970	1986	DAILY	MANUAL	MSC
WINDY CRAGGY	BC	120HRNP	T. AND P.	1987	1990	DAILY	MANUAL	MSC
AISHIHIK A	YT	2100100	T. AND P.	1943	1966	HOURLY AND DAILY	MANUAL	MSC
BLANCHARD RIVER	YT	2100163	T. AND P.	1986	2012	DAILY	AUTOMATIC	MSC
BRAEBURN	YT	2100167	T. AND P.	1974	1995	DAILY	MANUAL	MSC
BURWASH	YT	2100179	T. AND P.	1993	2004	HOURLY AND DAILY	AUTOMATIC	MSC
BURWASH A	YT	2100181	T. AND P.	2011	-	HOURLY AND DAILY	AUTO. AND MANUAL	MSC
BURWASH A	YT	2100182	T. AND P.	1966	2015	HOURLY AND DAILY	AUTOMATIC	MSC
BURWASH AIRPORT AUTO BC	YT	2100184	T. AND P.	2013	-	HOURLY AND DAILY	AUTOMATIC	MSC
CARMACKS	YT	2100300	T. AND P.	1963	2008	DAILY	MANUAL	MSC
CARMACKS CS	YT	2100301	T. AND P.	1999	-	HOURLY AND DAILY	AUTOMATIC	MSC
CARMACKS TOWER	YT	2100302	T. AND P.	1974	1976	DAILY	MANUAL	MSC
DESTRUCTION BAY	YT	2100418	T. AND P.	1975	1984	DAILY	MANUAL	MSC
DEZADEASH	YT	2100430	T. AND P.	1974	1986	DAILY	MANUAL	MSC
HAINES APPS #4	YT	2100627	T. AND P.	1969	1971	DAILY	MANUAL	MSC
HAINES JUNCTION	YT	2100630	T. AND P.	1944	-	HOURLY AND DAILY	AUTOMATIC	MSC
HAINES JUNCTION YTG	YT	2100631	T. AND P.	1985	2008	DAILY	MANUAL	MSC
KLUANE LAKE	YT	2100680	T. AND P.	1946	1983	DAILY	MANUAL	MSC
MINTO	YT	2100744	T. AND P.	1974	1974	DAILY	MANUAL	MSC
OTTER FALLS NCPC	YT	2100840	T. AND P.	1980	2015	DAILY	MANUAL	MSC
PAINT MOUNTAIN TOWER	YT	2100850	T. AND P.	1976	1976	DAILY	MANUAL	MSC

PELLY RANCH	YT	2100880	T. AND P.	1898	2015	DAILY	MANUAL	MSC
QUILL CREEK	YT	2100914	T. AND P.	1983	1985	DAILY	MANUAL	MSC
MIDWAY LODGE	YT	2100PLF	T. AND P.	1987	1988	DAILY	MANUAL	MSC
TAKHINI RIVER RANCH	YT	2101095	T. AND P.	1980	2015	DAILY	MANUAL	MSC
GLADSTONE MET STATION	YT	GLADMET	T. AND P.	2009	2012	HOURLY	AUTOMATIC	YEC
AISHIHIK MET STATION	YT	AISHMET	T. AND P.	2017	-		AUTOMATIC	YEC-YNC

Upper Yukon River

NAME OF THE STATION	PROVINCE	STATION #	DATA	START	END	TIME STEP	TYPE	DATA FROM
ATLIN	BC	1200560	T. AND P.	1899	-	DAILY	MANUAL	MSC
BENNET	BC	1200847	T. AND P.	1972	1974	DAILY	MANUAL	MSC
GRAHAM INLET	BC	1203255	T. AND P.	1973	2011	DAILY	MANUAL	MSC
LINDEMAN CITY	BC	1204632	T. AND P.	1968	1981	DAILY	MANUAL	MSC
NAKONAKE RIVER	BC	1205295	T. AND P.	1956	1956	DAILY	MANUAL	MSC
FRASER CAMP	BC	120C036	T. AND P.	1980	2008	DAILY	MANUAL	MSC
ANNIE LAKE ROBINSON	YT	2100115	T. AND P.	1976	2006	DAILY	MANUAL	MSC
BRAEBURN	YT	2100167	T. AND P.	1974	1995	DAILY	MANUAL	MSC
BRYN NYRDDIN FARM	YT	2100174	T. AND P.	1988	1996	DAILY	AUTOMATIC	MSC
CARCROSS	YT	2100200	T. AND P.	1907	2008	DAILY	MANUAL	MSC
FISH LAKE ROAD	YT	2100535	T. AND P.	1988	1989	DAILY	MANUAL	MSC
GOLDEN HORN	YT	2100615	T. AND P.	1989	1994	DAILY	MANUAL	MSC
HAECKEL HILL TOWER	YT	2100620	T. AND P.	1974	1976	DAILY	MANUAL	MSC
JOHNSONS CROSSING	YT	2100670	T. AND P.	1963	1995	DAILY	MANUAL	MSC
MARSH LAKE	YT	2100698	T. AND P.	1994	2002	DAILY	MANUAL	MSC
MAYO ROAD	YT	2100709	T. AND P.	1983	2016	DAILY	MANUAL	MSC
NEW IMPERIAL	YT	2100765	T. AND P.	1968	1969	DAILY	MANUAL	MSC
PORTER CREEK WAHL	YT	2100907	T. AND P.	1989	2005	DAILY	MANUAL	MSC
QUIET LAKE	YT	2100910	T. AND P.	1966	1992	DAILY	MANUAL	MSC
MACPHERSON	YT	2100FRN	T. AND P.	1984	1988	DAILY	MANUAL	MSC
TAGISH	YT	2101089	T. AND P.	1979	1984	DAILY	MANUAL	MSC
TAGISH TOWER	YT	2101093	T. AND P.	1976	1976	DAILY	MANUAL	MSC
TAKHINI RIVER RANCH	YT	2101095	T. AND P.	1980	2015	DAILY	MANUAL	MSC
TESLIN	YT	2101099	T. AND P.	1980	1984	DAILY	MANUAL	MSC
TESLIN A	YT	2101100	T. AND P.	1953	2014	HOURLY AND DAILY	AUTO. AND MANUAL	MSC
TESLIN A	YT	2101101	T. AND P.	2014	-	HOURLY AND DAILY	MANUAL	MSC
TESLIN (AUT)	YT	2101102	T. AND P.	1994	-	HOURLY AND DAILY	AUTOMATIC	MSC
WHITEHORSE	YT	2101290	T. AND P.	1900	1960	DAILY	MANUAL	MSC
WHITEHORSE A	YT	2101300	T. AND P.	1953	2012	HOURLY AND DAILY	AUTO. AND MANUAL	MSC
WHITEHORSE A	YT	2101303	T. AND P.	2012	-	HOURLY AND DAILY	AUTOMATIC	MSC
WHITEHORSE AUTO	YT	2101310	T. AND P.	2009	-	HOURLY AND DAILY	AUTOMATIC	MSC
WHITEHORSE RIVERDALE	YT	2101400	T. AND P.	1959	2012	DAILY	MANUAL	MSC

WHITEHORSE WSO	YT	2101415	T. AND P.	1996	1998	DAILY	MANUAL	MSC
WOLF CREEK	YT	2101600	T. AND P.	1969	1974	DAILY	MANUAL	MSC
WOLF CREEK	YT	2101601	T. AND P.	1985	1989	DAILY	MANUAL	MSC
PORTERS LANDING	BC	1206258	T. AND P.	1972	1972	DAILY	MANUAL	MSC
TULSEQUAH	BC	1208295	T. AND P.	1964	1966	DAILY	MANUAL	MSC
MORLEY RIVER	YT	2100750	T. AND P.	1984	1989	DAILY	MANUAL	MSC
FANTAIL LOWER	BC	FANTLOW	T. AND P.	2012	2017	HOURLY	AUTOMATIC	YRC-YEC
FANTAIL UPPER	BC	FANTUPP	T. AND P.	2012	2017	HOURLY	AUTOMATIC	YRC-YEC
LLEWELLYN LOWER	BC	LLEWLOW	T. AND P.	2013	-	HOURLY	AUTOMATIC	YRC-YEC
LLEWELLYN UPPER	BC	LLEWUPP	T. AND P.	2013	2016	HOURLY	AUTOMATIC	YRC-YEC
WHEATON	YT	WHEATON	T. AND P.	2014	-	HOURLY	AUTOMATIC	YRC-YEC

For the three studied watersheds, all meteorological stations own by Environment Canada or YEC with measurements from the 20th century and located within a 200-km radius are included in Table 2.5. For the forecasting system, only stations with current measurements are relevant for NAEFs or CanSIPS redistribution and correction. Also new or existing stations not related to Meteorological Service of Canada were added to the previous list. Note that for the Mayo, Aishihik, and Upper Yukon River Watersheds, there are 2, 5 and 7 operational stations, respectively, including recently added meteorological station in Aishihik and Mayo Watersheds. During the calibration process, specific stations were considered while limiting stations with measurements from 1981 to current days. This consideration prevents the use of older and closed stations for model calibration, since the forecasting system was developed using only operational stations for NAEFs development and stations with measurements form 1981 to current days for CanSIPS development. Note that the Upper Fantail station was removed from the Upper Yukon River Watershed and relocated within the boundaries of the Mayo Watershed which only had one operational meteorological station. It is noteworthy that operational stations can be located beyond watershed boundaries, but their monitored conditions may note represent those occurring within the watershed boundaries.

Table 2.6 Hydrometric stations of the Mayo, Aishihik and Upper Yukon River Watersheds.

Mayo

NAME OF THE STATION	PROVINCE	STATION #	DATA	START	END	OPERATION	TYPE	DATA FROM
MAYO LAKE NEAR THE OUTLET	YT	09DC005	WATER LEVEL	1979	-	CONTINUOUS	5 MINUTES	WSC
MAYO RIVER NEAR MAYO	YT	09DC001	FLOW	1945	1951	DISCONTINUOUS	DAILY	WSC
WAREHAM LAKE AT HEADGATE	YT	09DC004	WATER LEVEL	1979	2000	CONTINUOUS	DAILY	WSC
MAYO LAKE AT THE OUTLET	YT	YECMAYO	FLOW	1979	2019	CONTINUOUS	5 MINUTES	YEC
INFLOW TO MAYO LAKE	*YT*	*0000003*	*FLOW*	*1979*	*2019*	*CONTINUOUS*	*DAILY*	*YEC*

Aishihik

NAME OF THE STATION	PROVINCE	STATION #	DATA	START	END	OPERATION	TYPE	DATA FROM
AISHIHIK RIVER NEAR WHITEHORSE	YT	08AA001	FLOW	1950	1986	CONTINUOUS	DAILY	WSC
AISHIHIK LAKE NEAR WHITEHORSE	YT	08AA005	WATER LEVEL	1972	-	CONTINUOUS	5 MINUTES	WSC
AISHIHIK RIVER BELOW AISHIHIK LAKE	YT	08AA010	FLOW AND WATER LEVEL	1980	-	CONTINUOUS	5 MINUTES	WSC
GILTANA CREEK NEAR THE MOUTH	YT	08AA009	FLOW AND WATER LEVEL	1980	-	CONTINUOUS	5 MINUTES	WSC
SEKULMUN LAKE NEAR WHITEHORSE	YT	08AA007	WATER LEVEL	1980	-	CONTINUOUS	5 MINUTES	WSC
SEKULMUN RIVER AT OUTLET OF SEKULMUN LAKE	YT	08AA008	FLOW AND WATER LEVEL	1981	-	CONTINUOUS	5 MINUTES	WSC
WEST AISHIHIK RIVER NEAR THE MOUTH	YT	08AA011	FLOW	1995	2000	CONTINUOUS	DAILY	WSC
AISHIHIK LAKE NEAR AISHIHIK	YT	08AA012	WATER LEVEL	1995	2015	CONTINUOUS	5 MINUTES	WSC
ISAAC CREEK 1	YT	ISAAC01	FLOW	2009	2013	CONTINUOUS	5 MINUTES	YEC
ISAAC CREEK 2	YT	ISAAC02	FLOW	2009	2013	CONTINUOUS	5 MINUTES	YEC
INFLOW TO AISHIHIK LAKE	*YT*	*0000003*	*FLOW*	*1980*	*-*	*CONTINUOUS*	*DAILY*	*YEC*

Upper Yukon River

NAME OF THE STATION	PROVINCE	STATION #	DATA	START	END	OPERATION	TYPE	DATA FROM
YUKON RIVER AT WHITEHORSE	YT	09AB001	FLOW AND WATER LEVEL	1902	-	CONTINUOUS	5 MINUTES	WSC
ATLIN RIVER NEAR ATLIN	BC	09AA006	FLOW AND WATER LEVEL	1950	-	CONTINUOUS	5 MINUTES	WSC
WHEATON RIVER NEAR CARCROSS	YT	09AA012	FLOW AND WATER LEVEL	1955	-	CONTINUOUS	5 MINUTES	WSC
TUTSHI RIVER AT OUTLET OF TUTSHI LAKE	BC	09AA013	FLOW AND WATER LEVEL	1956	-	CONTINUOUS	5 MINUTES	WSC
INFOLW TO MARSH LAKE	*YT*	*0000003*	*FLOW*	*1980*	*-*	*CONTINUOUS*	*DAILY*	*YEC*

For the three watersheds, all the hydrometric stations that were operational at one time or actual times are listed in Table 2.6. It is noteworthy that stations that only monitored water levels cannot be used, since HYDROTEL does not simulate reservoir or lake levels. For the forecasting system, some stations will have no use (i.e., non-operational stations, water level stations, stations located downstream of relevant points). Also for Aishihik, ISAAC CREEK 1 and 2 were not used since they have limited measurements and are located upstream of the Sekulmun River station.

Table 2.7 Snow survey sites for the Mayo, Aishihik and Upper Yukon River Watersheds.

Mayo

NAME OF THE STATION	PROVINCE	COURSE ID #	DATA	START	END	OPERATION	TYPE	DATA FROM
CALUMET	YT	09DD-SC01	DEPTH / SWE	1975	-	UP TO 5 days / Year	MANUAL	Environment Yukon
EDWARDS LAKE	YT	09DD-SC02	DEPTH / SWE	1987	-	UP TO 5 days / Year	MANUAL	Environment Yukon
MAYO AIRPORT A	YT	09DC-SC01A	DEPTH / SWE	1968	-	UP TO 5 days / Year	MANUAL	Environment Yukon
MAYO AIRPORT B	YT	09DC-SC01B	DEPTH / SWE	1987	-	UP TO 5 days / Year	MANUAL	Environment Yukon
MAYO DAM	YT	MAYODAM	DEPTH / SWE	2018	2018	UP TO 5 days / Year	MANUAL	Yukon University
MAYO WARHAM	YT	MAYOWAR	DEPTH / SWE	2018	2018	UP TO 5 days / Year	MANUAL	Yukon University
WARHAM DAM	YT	WARHDAM	DEPTH / SWE	2018	2018	UP TO 5 days / Year	MANUAL	Yukon University

Aishihik

NAME OF THE STATION	PROVINCE	COURSE ID #	DATA	START	END	OPERATION	TYPE	DATA FROM
AISHIHIK LAKE	YT	08AA-SC03	DEPTH / SWE	1994	-	UP TO 5 days / Year	MANUAL	Environment Yukon
CANYON LAKE	YT	08AA-SC01	DEPTH / SWE	1975	-	UP TO 5 days / Year	MANUAL	Environment Yukon
MACINTOSH	YT	09CA-SC02	DEPTH / SWE	1976	-	UP TO 5 days / Year	MANUAL	Environment Yukon
AISHMET	YT	AISHMET	DEPTH / SWE	2017	2018	UP TO 5 days / Year	AUTOMATIC	Yukon University
AISRS01	YT	AISRS01	DEPTH / SWE	2017	2018	UP TO 5 days / Year	MANUAL	Yukon University
AISRS02	YT	AISRS02	DEPTH / SWE	2017	2018	UP TO 5 days / Year	MANUAL	Yukon University

Upper Yukon River

NAME OF THE STATION	PROVINCE	COURSE ID #	DATA	START	END	OPERATION	TYPE	DATA FROM
WHITEHORSE AIRPORT	YT	09AB-SC2	DEPTH / SWE	2006	-	UP TO 5 days / Year	MANUAL	Environment Yukon
MT. MCINTYRE (B)	YT	09AB-SC1B	DEPTH / SWE	2006	-	UP TO 5 days / Year	MANUAL	Environment Yukon

TAGISH	YT	09AA-SC1	DEPTH / SWE	2006	-	UP TO 5 days / Year	MANUAL	Environment Yukon
MONTANA MOUNTAIN	YT	09AA-SC2	DEPTH / SWE	2006	-	UP TO 5 days / Year	MANUAL	Environment Yukon
LOG CABIN (B.C.)	BC	09AA-SC3	DEPTH / SWE	2006	-	UP TO 5 days / Year	MANUAL	Environment Yukon
MOORE CREEK BRIDGE	AL	0034K02	DEPTH / SWE	2006	-	UP TO 5 days / Year	MANUAL	USDA NRCS
ATLIN (B.C.)	BC	09AA-SC4	DEPTH / SWE	2006	-	UP TO 5 days / Year	MANUAL	Environment Yukon
EAGLECREST	AL	0034J03	DEPTH / SWE	2006	-	UP TO 5 days / Year	MANUAL	USDA NRCS
MEADOW CREEK	YT	09AD-SC1	DEPTH / SWE	2006	-	UP TO 5 days / Year	MANUAL	Energy Mines and Ressources Yukon
FANTAIL LOWER	BC	FANTLOW	DEPTH / SWE	2012	2017	HOURLY	AUTOMATIC	Yukon University
FANTAIL UPPER	BC	FANTUPP	DEPTH / SWE	2012	2017	HOURLY	AUTOMATIC	Yukon University
LLEWELLYN LOWER	BC	LLEWLOW	DEPTH / SWE	2013	-	HOURLY	AUTOMATIC	Yukon University
LLEWELLYN UPPER	BC	LLEWUPP	DEPTH / SWE	2013	2016	HOURLY	AUTOMATIC	Yukon University
WHEATON	YT	WHEATON	DEPTH / SWE	2014	-	HOURLY	AUTOMATIC	Yukon University

Table 2.7 introduces the different snow courses for the three watersheds and those snow stations with snow height and snow SWE measurements. Note that the Upper Fantail station was removed from the Upper Yukon River Watershed and relocated within the Mayo Watershed. For the Upper Yukon River Watershed, snow courses prior to 2006 were not included in the database.

The resulting hydrometeorological database for the Mayo, Aishihik and Upper Yukon River Watersheds were then integrated into HYDROTEL. Figure 2.9 presents a screenshot of the three watersheds within the HYDROTEL graphical user interface while Figure 2.10 gives an example of the workspace window for the Aishihik Watershed. The portion of the Aishihik Watershed (displayed in beige) represents the simulated area and the grey portion the non-simulated area. It also shows the information menu on the right and the action menu at the top. Recently a new HYDROTEL project was created specifically for the Marsh Lake sub-watershed to perform specific calibration on this lake inflows and support the operation of the forecasting system for this lake as well. This new project was simply based on the Upper Yukon River watershed using Marsh Lake as the outlet. There is no need to represent Marsh Lake integration to HYDROTEL since it is simply a sub-watershed of the Upper Yukon River watershed.

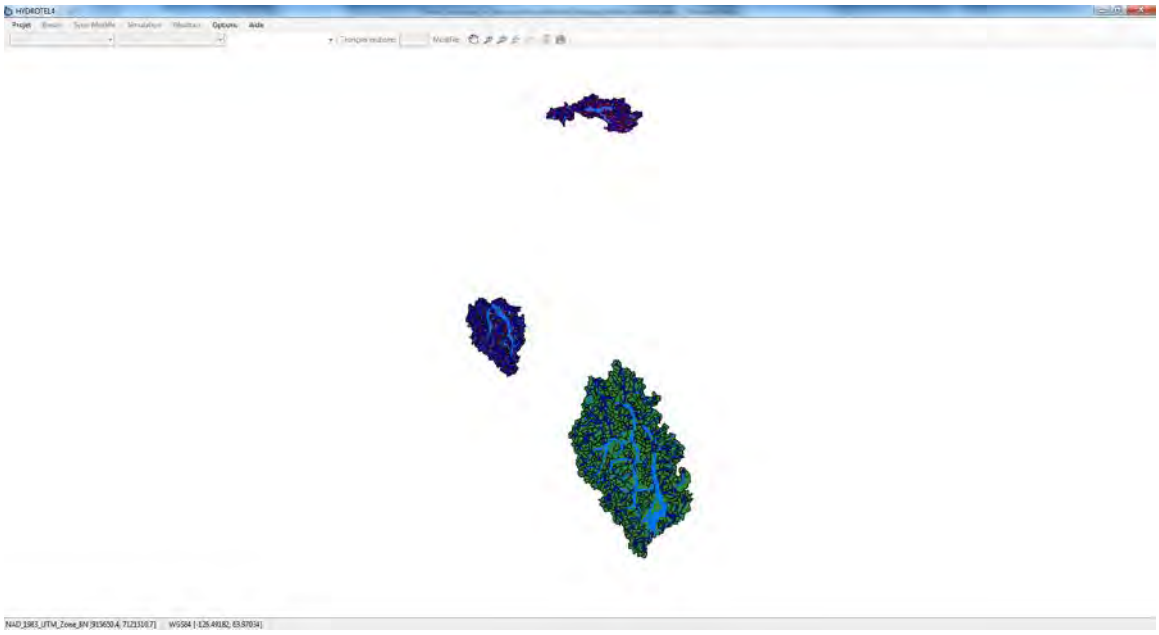

Figure 2.9 Mayo, Aishihik and Upper Yukon River Watersheds displayed using the HYDROTEL graphical user interface.

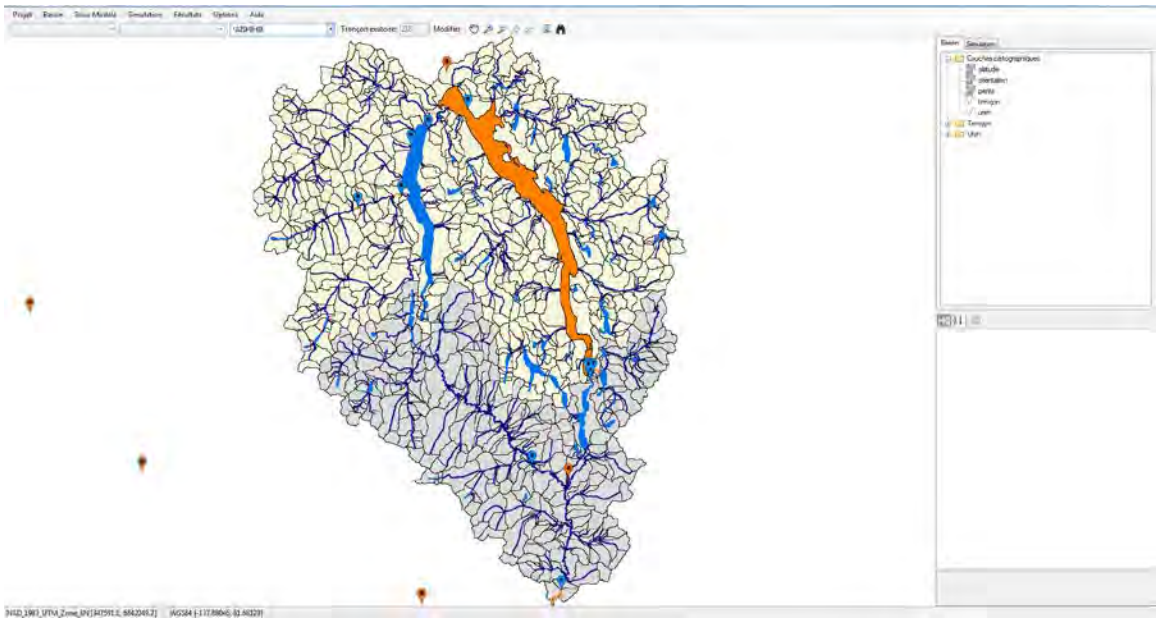

Figure 2.10 Example of workspace window of HYDROTEL.

HYDROTEL models the major physical processes of the water budget using sub-models that include different algorithms or simulation options. As shown in Table 2.8, each sub-model generally offers more than one simulation options.

Table 2.8 HYDROTEL sub-model and simulation Options

Water budget component (sub-model)		Simulation options	
1	Interpolation of meteorological data	1.1	Thiessen polygons
		1.2	**Weighted mean of nearest three stations**
2	Snow accumulation and melt	2.1	**Mixed (degree-day) energy-budget method *(optionally operating by 100-m altitude bands*)***
		2.2	*Multi-layer model operating by 100-m altitude bands**
3	Soil temperature and soil freezing	3.1	**Rankinen**
		3.2	Thorsen
4	Glacier dynamics	*4.1*	***Mixed (degree-day) energy-budget method operating by 100-m altitude bands****
5	Potential evapotranspiration	5.1	Thornthwaite
		5.2	Linacre
		5.3	Penman
		5.4	Priestley-Taylor
		5.5	Hydro-Québec
		5.6	**Penman-Monteith**
6	Vertical water budget	6.1	**BV3C**
		6.2	CEQUEAU (modified)
7	Overland water routing	7.1	**Kinematic wave equation**
8	Channel water routing	8.1	**Kinematic wave equation**
		8.2	Diffusive wave equation

* Model and simulation option developed as part of the current project.

In the above table, the bold face names represent the simulation option used for hydrological simulation.

Model calibration and results

Calibration of the model parameters was done by comparing simulated and measured stream flows or simulated and reconstructed reservoir/lake inflows or any relevant state variables (*e.g.*, SWE) for the 2010-2016 period for Aishihik and Mayo watersheds and the 2010-2017 for Upper Yukon watershed (including Marsh Lake Sub-watershed). The calibration involved adjusting the sub-model parameter values in order to corroborate as much as possible with stream flow measurements or lake inflows using an objective function. The result is an optimized set of parameter values that are identical for all RHHUs for the whole watershed (Mayo) or grouped RHHUs (Aishihik and Upper Yukon). This does not mean that everything is identical for each one of those units, as the hydraulic characteristics on each unit depend on soil type, which are different from unit to another, for instance.

Since model calibration for the Aishihik and Mayo Watersheds and Marsh Lake Sub-watershed relies heavily on the reconstructed reservoir/lake inflows, it seems important to describe the methodology and the equation currently used to determine them.

The general water budget equation for a reservoir or a lake can be expressed as follows:

$$\Delta V = IN + P - E - Q_{out} \quad (2.1)$$

Where:

ΔV = variation of lake or reservoir volume (*V*) between time (*j*-1) and (*j*) (m^3/s);

IN = sum of inflows from upstream rivers and surrounding hillslopes;

P = precipitation on the surface of the lake or reservoir;

E = evaporation from the surface of the lake or reservoir;

Q_{out} = sum of the entire lake or reservoir outflows.

For all lakes, that is Aishihik, Mayo and Marsh, P and E were not considered since they can be assumed to be similar over time. Only ΔV and Q_{out} need to be determined to estimate IN as the total inflow.

For all watersheds, we adopted a calculation procedure based on the three-day water level average, thus:

$$\Delta V = V_j - V_{j-1} \quad (2.2)$$

For Aishihik Lake the general volume calculation provided by YEC is as follows:

When L < 915

$$V = -38627.31L^6 + 678170.61L^5 - 3270008.00L^4 + 6352008.56L^3 - 3111511.38L^2 + 134383853.50L \quad (2.3)$$

When L >= 915

$$V = -50827494.83L^4 + 731085628.63L^3 - 3932429415.76L^2 + 9545583654.41L - 8448705648.59 \quad (2.4)$$

Where L represents the water level recorded at *Aishihik Lake near Whitehorse* hydrometric station (08AA005). Note that the record at the (08AA005) station must be cumulative using the reference level (911.565) in order to have the proper value for the volume calculation in Equations (2.3) and (2.4). The results of Equation (2.4) need to be multiplied by 3600 to get a daily volume.

For Mayo Lake the general volume calculation is as follows:

$$V = \frac{(L-660)}{0.00003814} * 3600 \quad (2.5)$$

Here L represents the water recorded at the *Mayo Lake near the outlet* hydrometric station (09DC005). Note that the record at the (09DC005) station must be cumulative using the reference water level (662.337) in order to have the proper value for the volume calculation in Equation (2.5).

For Marsh Lake the general volume calculation is as follows:

$$V = \frac{(L-652)}{0.00000648} * 3600 \quad (2.6)$$

Here L represents the water recorded at the *Marsh Lake near Whitehorse* hydrometric station (09AB004). Note that the record at the (09AB004) station must be cumulative using the reference water level (653.357) in order to have the proper value for the volume calculation in Equation (2.6).

To calculate volume variations based on the average water level of the last three days, L values in Equations (2.3) to (2.6) are calculated as follows:

$$L = \frac{L_j + L_{j-1} + L_{j-2}}{3} \quad (2.7)$$

Where:

L_j , L_{j-1} and L_{j-2} represent the daily mean water level at the reference hydrometric station for the current day (*j*), previous day (*j*-1) and previous two days (*j*-2).

Before determining the total inflow (IN) in Equation (2.1), the volume variation must be divided by 86400 s/day to get the flow units (m^3/s).

To determine Q_{out} for Aishihik Lake, we used the following equation:

$$Q_{out} = Q_{08AA010} - Q_{08AA009} \quad (2.8)$$

Where:

$Q_{08AA010}$= The average daily flow at the *Aishihik River below Aishihik Lake* hydrometric station (08AA010);

$Q_{08AA009}$= The average daily flow at the *Giltana Creek near the mouth* hydrometric station (08AA009).

To calculate the most accurate lake outflow, we need to subtract the Giltana Creek (08AA009) flow from the Aishihik River measurements since the (08AA010) hydrometric station is located downstream of both Aishihik Lake and Giltana Creek and is the nearest flow measurement downstream of the Lake.

To determine Q_{out} for Mayo Lake, we used the following equation:

$$Q_{out} = Q_{YECMAYO} \quad (2.9)$$

Where:

$Q_{YECMAYO}$= The average daily flow measurement made by YEC at the outlet of the Mayo Lake facility.

To determine Q_{out} for Marsh Lake, we used the following equation:

$$Q_{out} = Q_{09AB001} \quad (2.10)$$

Where:

$Q_{09AB001}$= The average daily flow at the Yukon River at Whitehorse hydrometric station (09AB001).

As the volume variation ΔV is calculated between the current day (*j*) and the previous day (*j*-1) the Q_{out} value in Equation (2.1) must be calculated as follows:

$$Q_{out} = \frac{Q_{out,j} + Q_{out,j-1}}{2} \quad (2.11)$$

Where $Q_{out,j}$ and $Q_{out,j-1}$ represent for all watersheds the outflow (Equations 2.8, 2.9 & 2.10) for the current day (*j*) and the previous day (*j*-1).

For Aishihik, a particular case must be addressed to ensure proper calculation of the total daily average inflow. Indeed, sometimes, measurements at the Giltana Creek hydrometric station (08AA009) are missing. Under such circumstances, a precise procedure was developed by YEC to correct flow measurements at the Aishihik River station (08AA010) and it can be accounted for using a specific equation.

When $Q_{08AA009}$ is missing, the correction applied to the $Q_{08AA010}$ measured flow is given by the general linear regression:

$$Q_{08AA010} = m_{(month)} Q_{08AA010} + b_{(month)} \quad (2.12)$$

Where $m_{(month)}$ and $b_{(month)}$ represent the slope and the intercept of the linear regression equation calculated for every month of the year. The monthly values of m and b are introduced in Table 2.9.

Table 2.9 Monthly values of slope and intercept of the linear regression equation to estimate flows at the Aishihik River station (08AA010) when measurements at the Giltana Creek hydrometric station (08AA009) are missing.

Month	m	b
1	0.996	-0.053
2	0.997	-0.046
3	0.999	-0.055
4	0.990	-0.102
5	0.869	-1.070
6	0.822	-0.576
7	0.980	-0.592
8	0.957	-0.193
9	0.959	-0.352
10	0.978	-0.416
11	0.995	-0.266
12	0.992	-0.093

It is important to highlight that for all watersheds, the estimated total inflows may result in a negative value. This is known as a false negative value because the water budget equation assumes a horizontal

surface. However, large Lakes act as large mechanical oscillator driven by wind forces, precipitations, ice, water management etc… Such conditions can result in errors in total inflow calculation; including excessive variations and negative values (Perreault et al., 1995). In the case of negative inflow values, it was decided to substitute the negative values by a nominal value for Mayo Lake and Marsh Lake. Also for Aishihik, it was also proposed to use the flow measurements at the *Sekulmun River at the outlet of the Sekulmun Lake* hydrometric station (08AA008) as an option to correct the negative values.

For Aishihik Lake:

When IN < 0.0 m³/s then $IN = Q_{08AA008}$

For Mayo Lake or Marsh Lakes:

When IN < 0.0m³/s then $IN = 0.01$

The nominal values for Mayo Lake or Marsh Lake correspond to the minimum positive inflow calculated for the entire historical period available.

Throughout the calibration procedure of HYDROTEL, model performance with respect to corroborating with measured flows or reconstructed inflows was evaluated using different criteria.

1. A visual inspection of the graphical representation of observed and simulated flows;

2. The Nash-Sutcliffe criterion calculated with the following equation:

$$NS = 1 - \frac{\sum_{i=1}^{n}(Q_{obs} - Q_{sim})^2}{\sum_{i=1}^{n}(Q_{obs} - Q_{obs,mean})^2} \quad (2.13)$$

Where Q_{obs} represents the observed flow or reconstructed inflow, Q_{sim} the simulated flow or inflow, $Q_{obs,mean}$ the mean observed flow or reconstructed inflow from day 1 to (*n*) number of days (daily time step).

The value of the criterion ranges from (-∞ to 1.0), where one (1) represents the optimum. This criterion evaluates the amplitude and the synchronism between observed and simulated flows or inflows. Generally, this criterion is highly influenced by the presence and representation of the peak freshet and that makes it less adapted for a long low flow period;

3. The observed and simulated annual runoff (water volume / watershed area) can be used to compare water volumes based on the following equation:

$$Runoff_{year} = \frac{\sum_{i=1}^{n}(Q\ x\ CONV)}{AREA} \quad (2.14)$$

Where $Runoff_{year}$ represents the annual runoff expressed in (mm), Q the observed or simulated flow or inflow (m^3/s), $AREA$ the drainage area upstream of the comparison site (km^2) and CONV a conversion factor to transform (in mm) the resulting annual runoff;

4. The PBIAS criterion (bias percentage) is calculated as follows:

$$PBIAS = \frac{\sum_{i=1}^{n}(Q_{sim}-Q_{obs})}{\sum_{i=1}^{n}Q_{obs}}\ x\ 100 \quad (2.15)$$

This criterion, expressed in (%), can be used to quantify the bias between simulated and observed values. The value of the criterion varies between (-∞ to +∞) where zero (0) is the optimum;

5. Root mean square error (RMSE) that can be calculated as follow:

$$RMSE = \sqrt{\frac{\sum_{i=1}^{n}(Q_{obs}-Q_{sim})^2}{n}} \quad (2.16)$$

The resulting value varies between (0 to +∞) where zero (0) is the optimum. This criterion, expressed in m^3/s for flows or inflows, assesses the general agreement between observed and simulated flows or inflows. Essentially it is influenced by the largest discrepancies.

Calibration of HYDROTEL was first performed on the Aishihik Watershed using flows measured at the *Sekulmun River at the outlet of the Sekulmun Lake* hydrometric station (08AA008) and reconstructed inflows for Aishihik Lake. The model was calibrated on the Mayo Watershed using the reconstructed inflows of Mayo Lake. Finally, a complete distributed calibration was performed for the Upper Yukon River Watershed using the flows recorded at the *Tutshi River at outlet of Tutshi Lake* hydrometric station (09AA013), the *Wheaton River near Carcross* hydrometric station (09AA012), the *Atlin River near Atlin* hydrometric station (09AA006), the *Yukon River at Whitehorse* hydrometric station (09AB001) and the reconstructed inflows of Marsh Lake. Note that at this stage of the project, we performed a spatial calibration on the Aishihik Watershed with specific model calibration parameters for the entire

Sekulmun River Watershed and another set of calibration parameter values for the remaining portion of the watershed. For Mayo Lake, we performed a global calibration with unique sets of model parameter values for each watershed. For the Upper Yukon River watershed we performed a spatial calibration with specific model calibration parameter values for the different sub-watersheds of the hydrometric stations. The calibrated parameter values related to the different sub-watersheds were used as baselines for the development of the data assimilation procedure developed by YU. The models and data assimilation scheme represent the core of the flow and inflow forecasting system.

Model calibration and development of the data assimilation procedure for the Aishihik watershed were based on the aforementioned methodology used to reconstruct inflows (*i.e.*, Aishihik Lake). An updated version of the water level/lake water volume relationship (Equations 2.3 and 2.4) was proposed in November 2017. Throughout the calibration process, the Sekulmun River flows were used as inflows for cases characterized by negative reconstructed inflows. As mentioned before, the maximum calibration period was from 01/01/2010 to 31/12/2018 based on available data and project progress. At the first stage of the project the calibration was performed manually and during the last year of the project the calibration was refined using an automatic calibration procedure through OSTRICH, an Optimization Software Toolkit for Research Involving Computational Heuristics. Figures 2.11, 2.12, 2.13 and Table 2.10 present the calibration results.

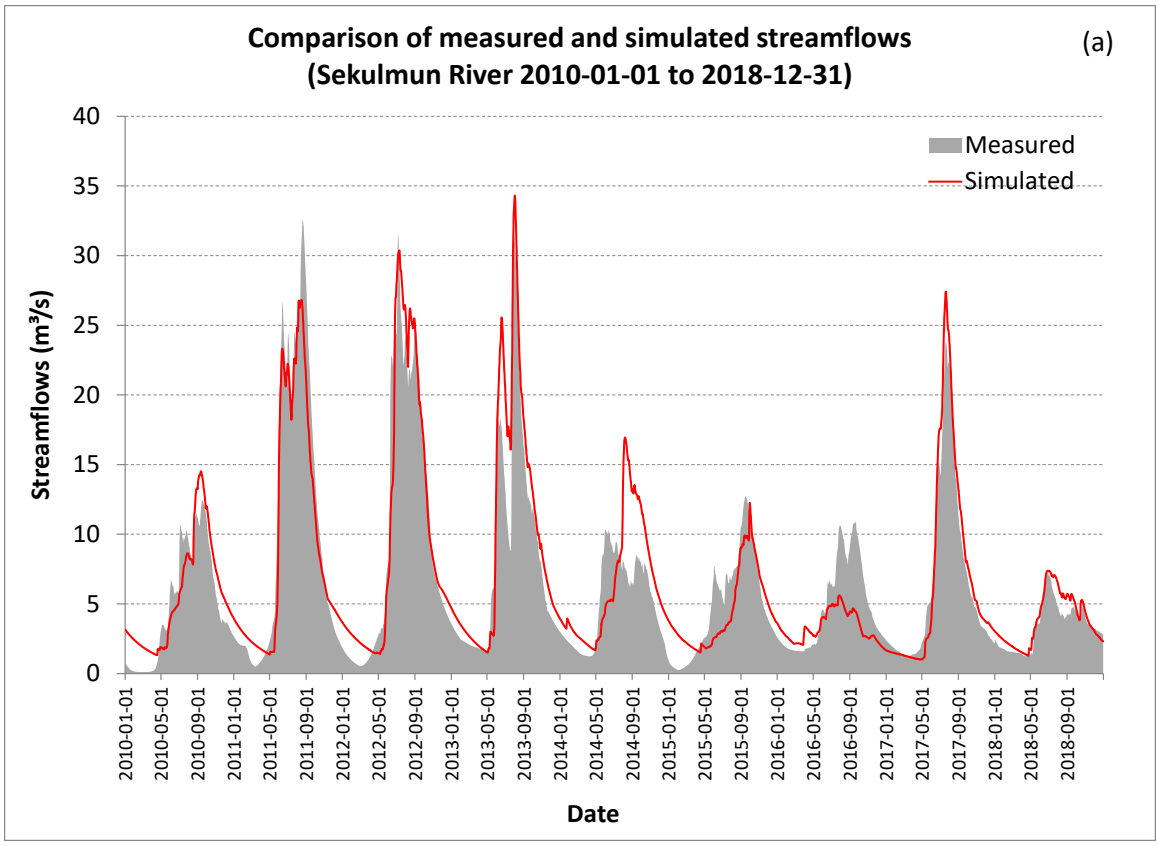
Comparison of measured and simulated streamflows
(Sekulmun River 2010-01-01 to 2018-12-31)
(a)
Measured
Simulated
Streamflows (m³/s)
0
5
10
15
20
25
30
35
40
2010-01-01
2010-05-01
2010-09-01
2011-01-01
2011-05-01
2011-09-01
2012-01-01
2012-05-01
2012-09-01
2013-01-01
2013-05-01
2013-09-01
2014-01-01
2014-05-01
2014-09-01
2015-01-01
2015-05-01
2015-09-01
2016-01-01
2016-05-01
2016-09-01
2017-01-01
2017-05-01
2017-09-01
2018-01-01
2018-05-01
2018-09-01
Date

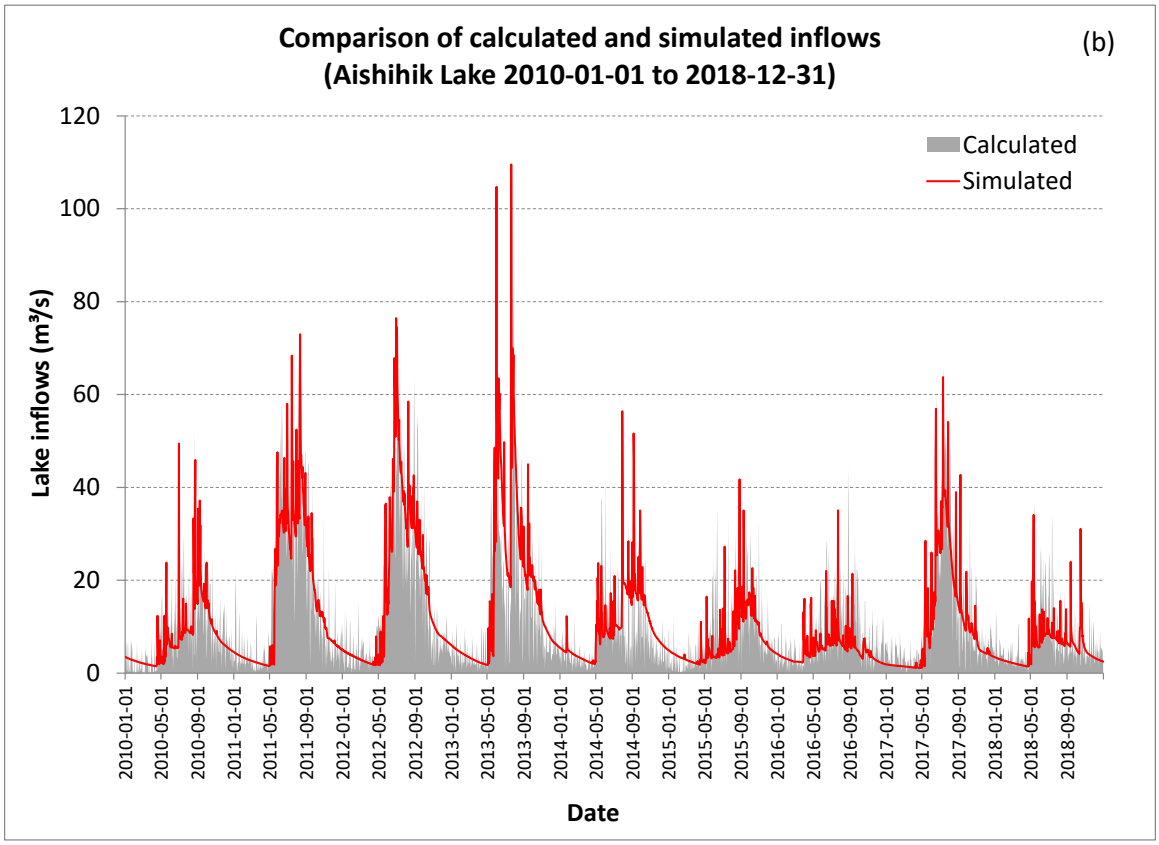
Comparison of calculated and simulated inflows
(Aishihik Lake 2010-01-01 to 2018-12-31)
(b)
Calculated
Simulated
Lake inflows (m³/s)
0
20
40
60
80
100
120
2010-01-01
2010-05-01
2010-09-01
2011-01-01
2011-05-01
2011-09-01
2012-01-01
2012-05-01
2012-09-01
2013-01-01
2013-05-01
2013-09-01
2014-01-01
2014-05-01
2014-09-01
2015-01-01
2015-05-01
2015-09-01
2016-01-01
2016-05-01
2016-09-01
2017-01-01
2017-05-01
2017-09-01
2018-01-01
2018-05-01
2018-09-01
Date

Figure 2.11 Graphical comparisons of measured flows or calculated inflows with simulated flows or inflows for: (a) Sekulmun River, (b) Aishihik Lake.

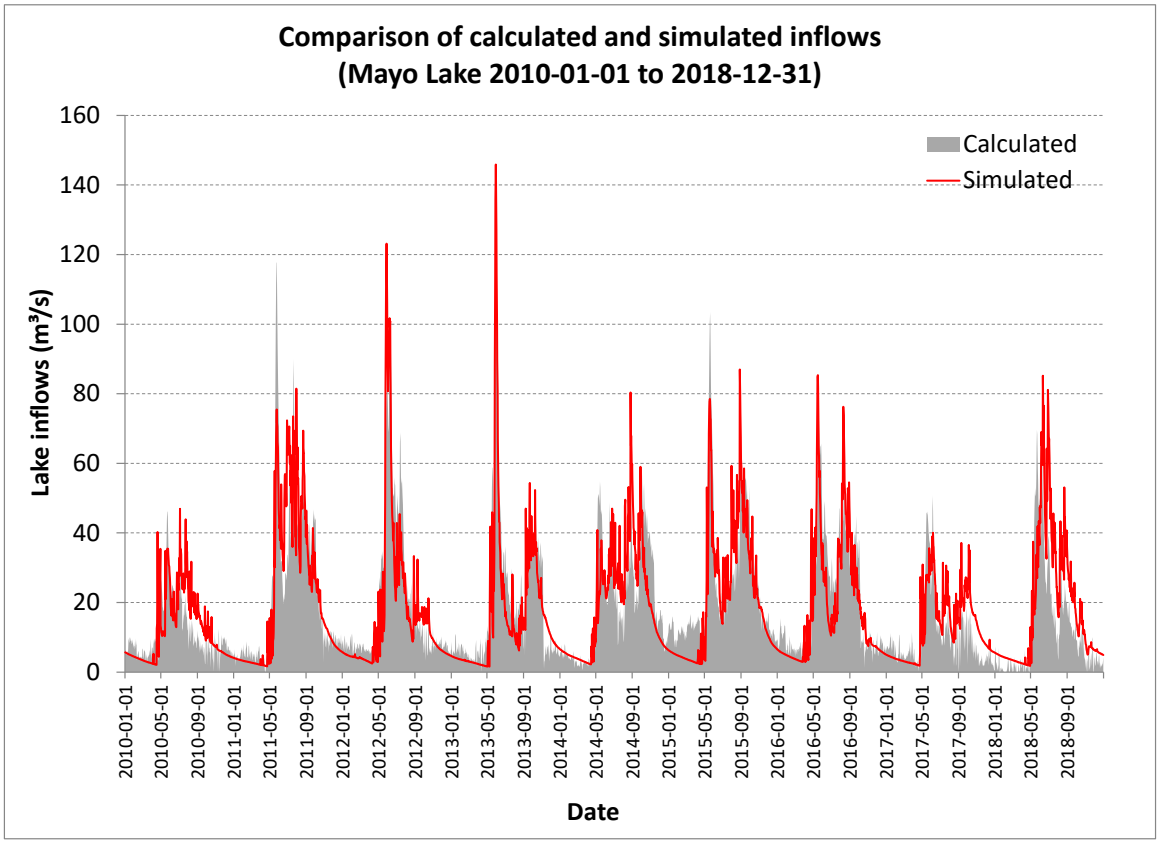

Figure 2.12 Graphical comparisons of calculated inflows with simulated inflows for Mayo Lake.

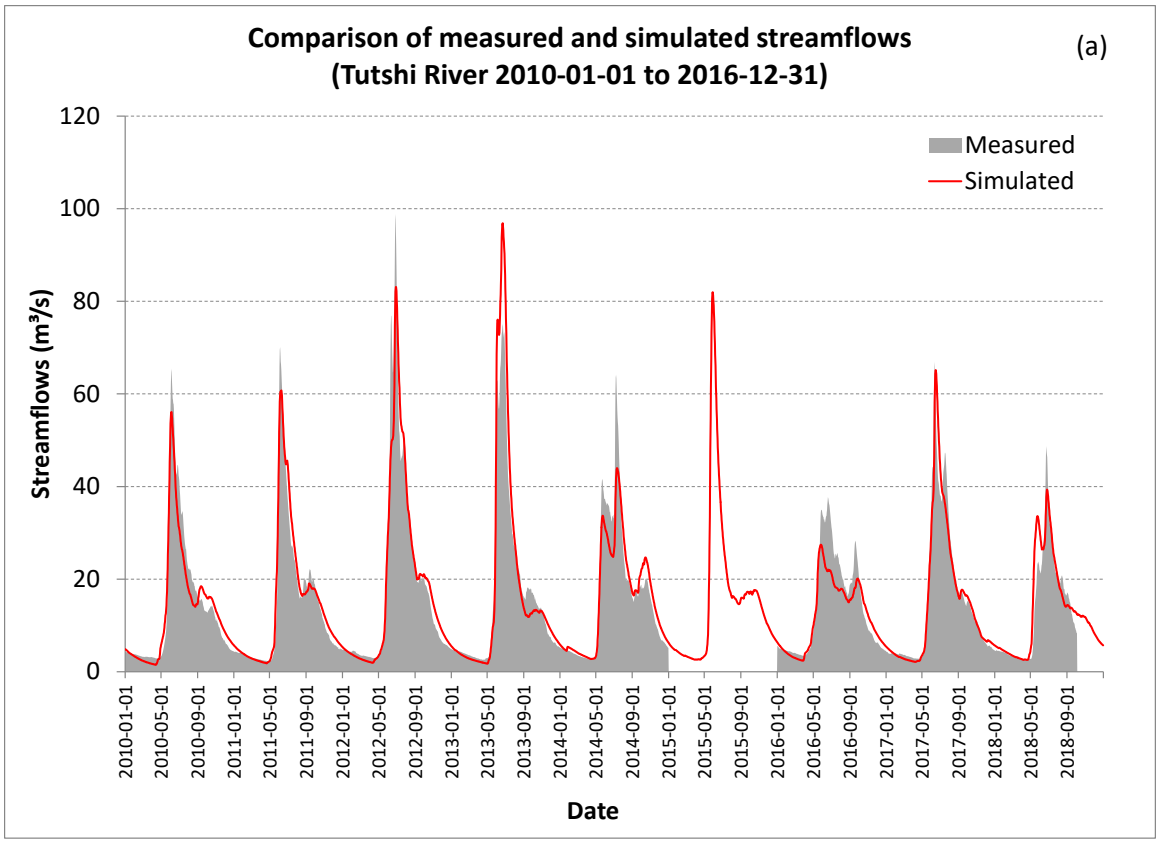
Comparison of measured and simulated streamflows
(Tutshi River 2010-01-01 to 2016-12-31)
(a)
Measured
Simulated
Streamflows (m³/s)
0
20
40
60
80
100
120
2010-01-01
2010-05-01
2010-09-01
2011-01-01
2011-05-01
2011-09-01
2012-01-01
2012-05-01
2012-09-01
2013-01-01
2013-05-01
2013-09-01
2014-01-01
2014-05-01
2014-09-01
2015-01-01
2015-05-01
2015-09-01
2016-01-01
2016-05-01
2016-09-01
2017-01-01
2017-05-01
2017-09-01
2018-01-01
2018-05-01
2018-09-01
Date

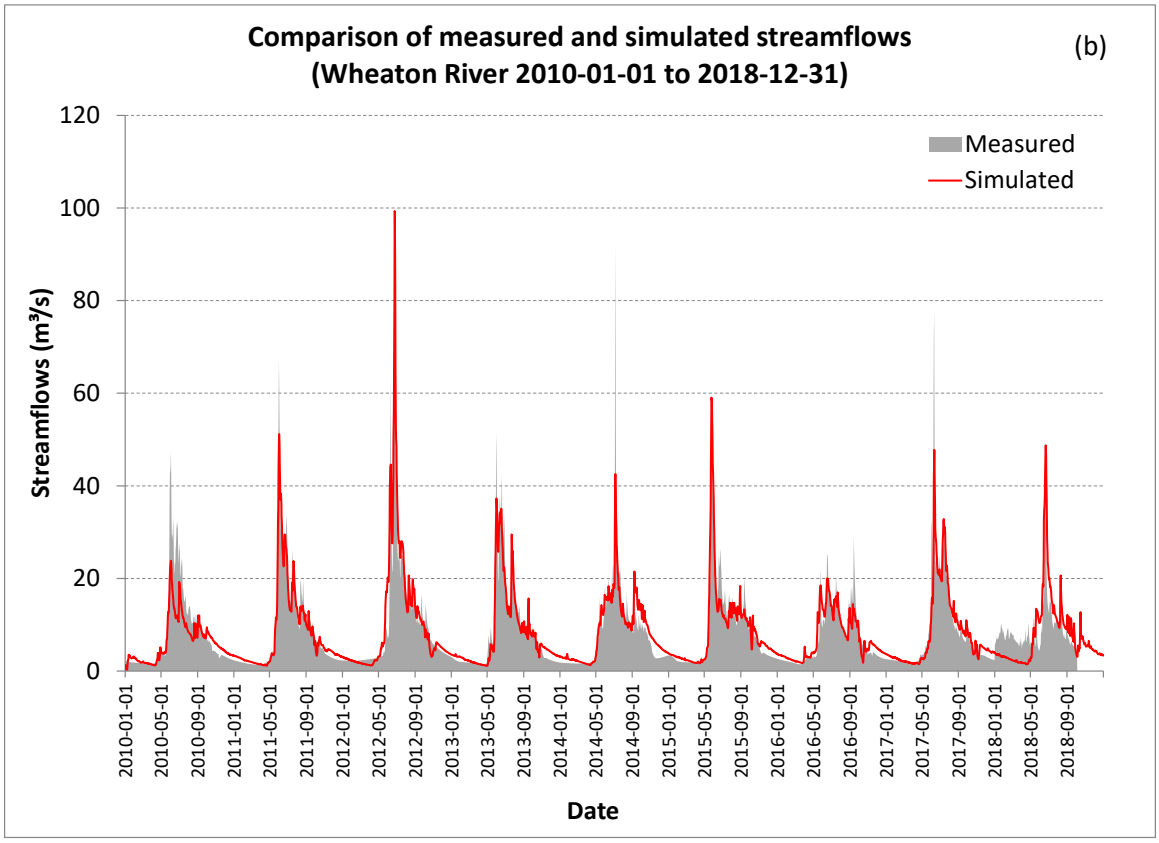
Comparison of measured and simulated streamflows
(Wheaton River 2010-01-01 to 2018-12-31)
(b)
Measured
Simulated
Streamflows (m³/s)
0
20
40
60
80
100
120
2010-01-01
2010-05-01
2010-09-01
2011-01-01
2011-05-01
2011-09-01
2012-01-01
2012-05-01
2012-09-01
2013-01-01
2013-05-01
2013-09-01
2014-01-01
2014-05-01
2014-09-01
2015-01-01
2015-05-01
2015-09-01
2016-01-01
2016-05-01
2016-09-01
2017-01-01
2017-05-01
2017-09-01
2018-01-01
2018-05-01
2018-09-01
Date

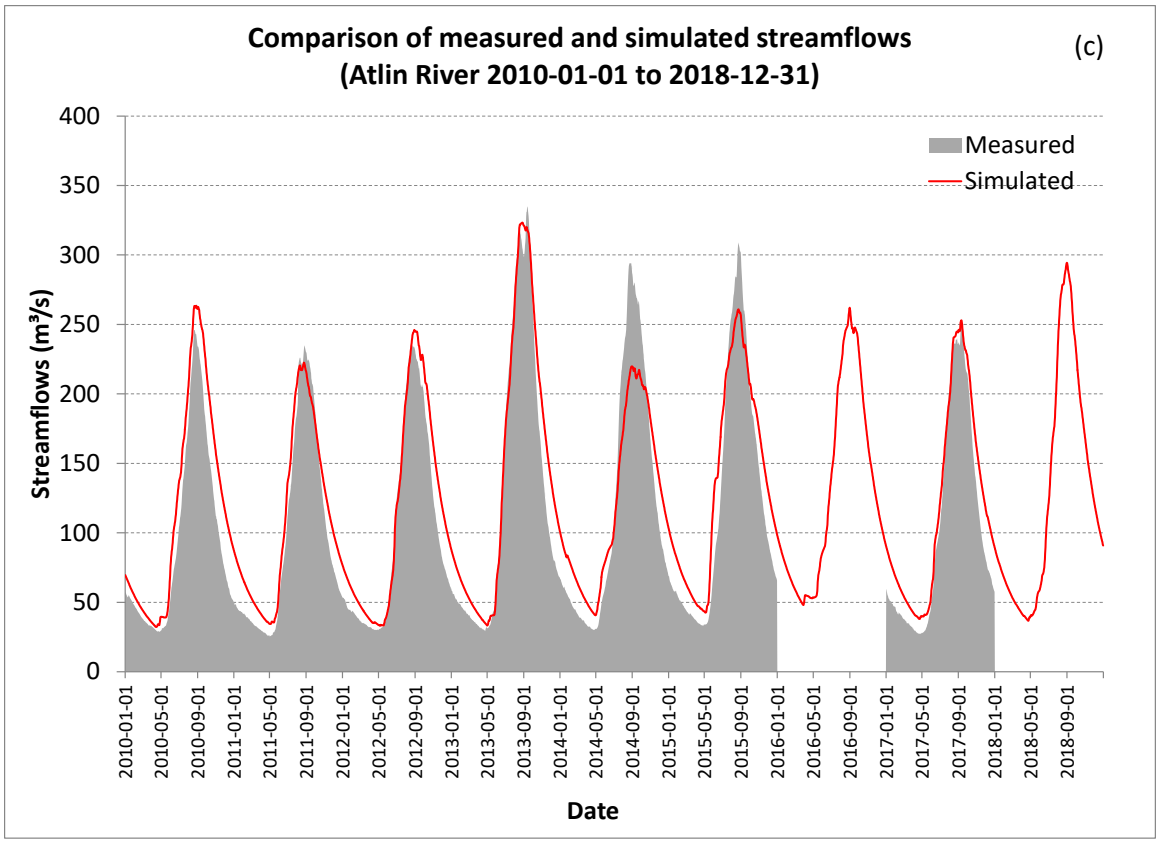
Comparison of measured and simulated streamflows
(Atlin River 2010-01-01 to 2018-12-31)
(c)
Measured
Simulated
Streamflows (m³/s)
0
50
100
150
200
250
300
350
400
2010-01-01
2010-05-01
2010-09-01
2011-01-01
2011-05-01
2011-09-01
2012-01-01
2012-05-01
2012-09-01
2013-01-01
2013-05-01
2013-09-01
2014-01-01
2014-05-01
2014-09-01
2015-01-01
2015-05-01
2015-09-01
2016-01-01
2016-05-01
2016-09-01
2017-01-01
2017-05-01
2017-09-01
2018-01-01
2018-05-01
2018-09-01
Date

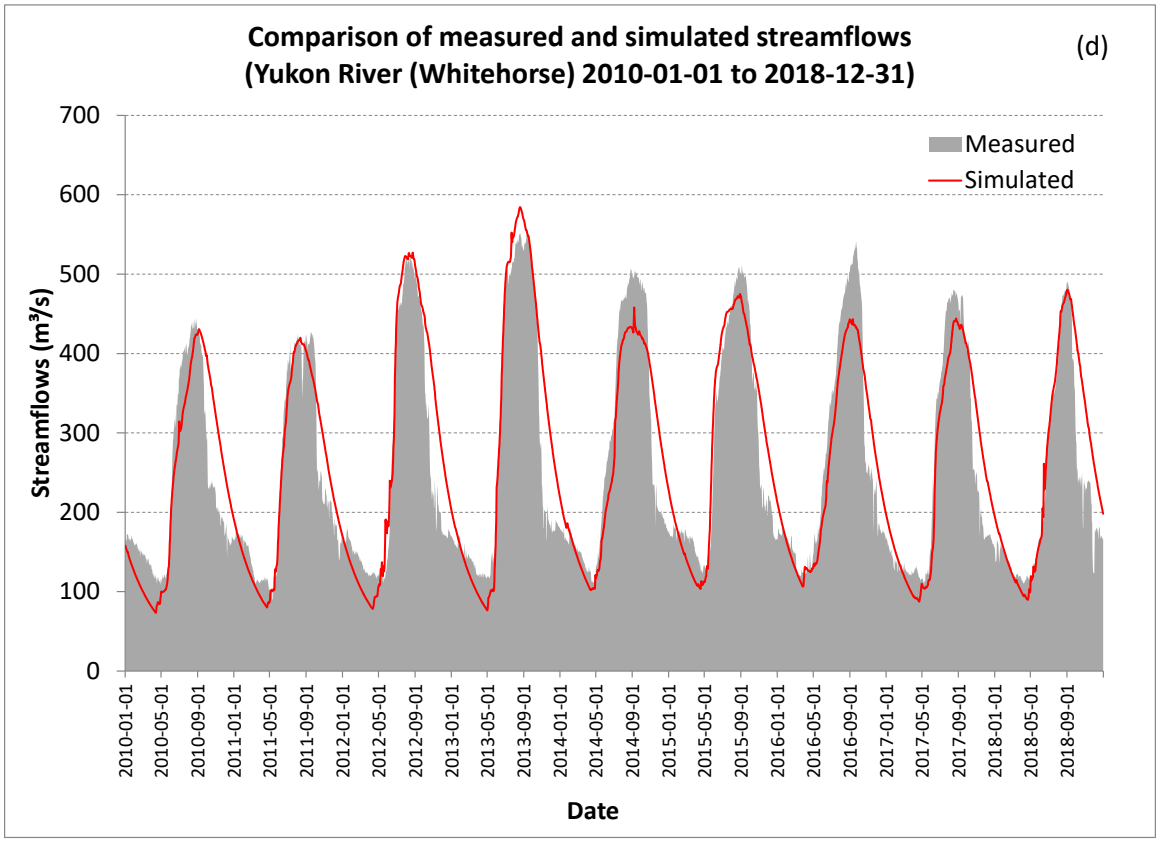
Comparison of measured and simulated streamflows
(Yukon River (Whitehorse) 2010-01-01 to 2018-12-31)
(d)
Measured
Simulated
Streamflows (m³/s)
0
100
200
300
400
500
600
700
2010-01-01
2010-05-01
2010-09-01
2011-01-01
2011-05-01
2011-09-01
2012-01-01
2012-05-01
2012-09-01
2013-01-01
2013-05-01
2013-09-01
2014-01-01
2014-05-01
2014-09-01
2015-01-01
2015-05-01
2015-09-01
2016-01-01
2016-05-01
2016-09-01
2017-01-01
2017-05-01
2017-09-01
2018-01-01
2018-05-01
2018-09-01
Date

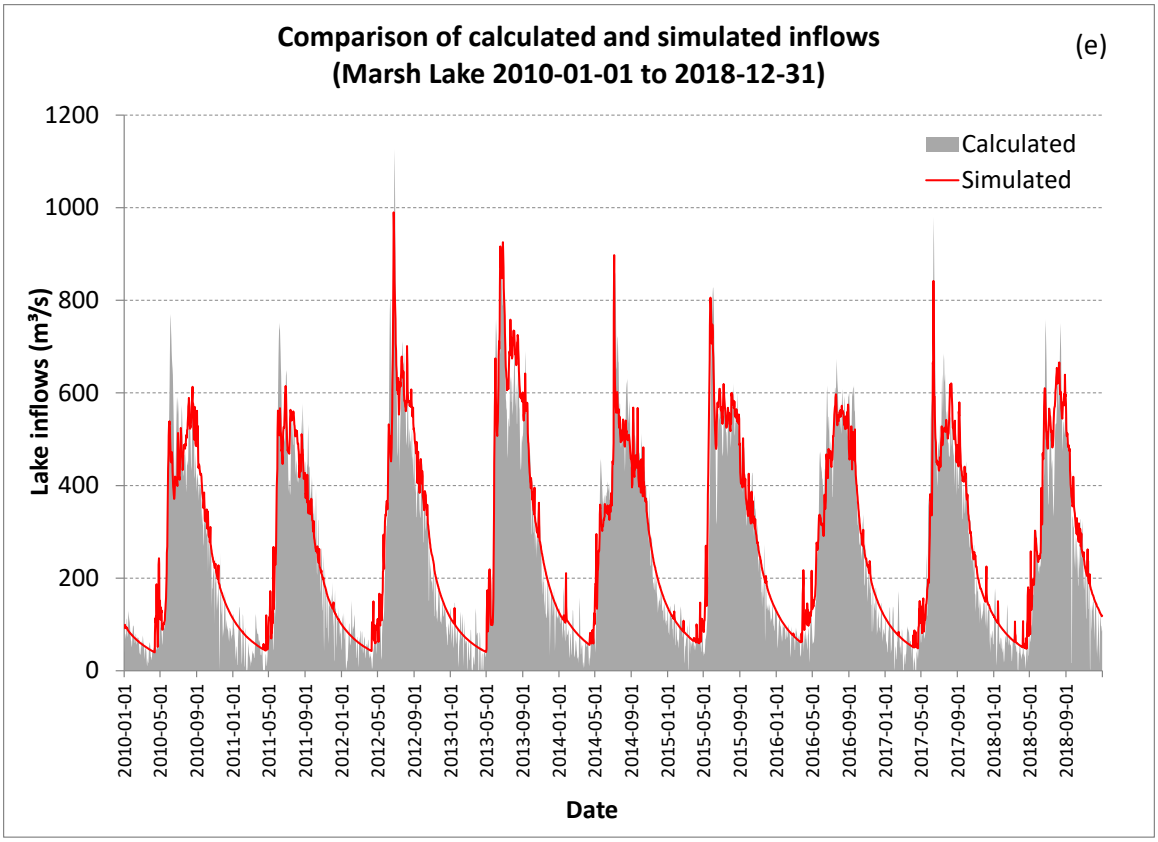

Figure 2.13 Graphical comparisons of measured flows or calculated inflows with simulated flows or inflows for: (a) Tutshi River, (b) Wheaton River, (c) Atlin River, (d) Yukon River (Whitehorse) and (e) Marsh Lake.

Table 2.10 Calibration performance in corroborating observed flows or reconstructed inflows (values in parentheses representing observed values) for each watershed or sub-watershed.

Watershed	Site	NS	$Runoff_{year}$ (mm)	$PBIAIS$ (%)	$RMSE$(m^3/s)	Comment*
Aishihik	Sekulmun River	0.87	172 (167)	3.57	2.36	Very Good
	Aishihik Lake	0.53	114 (118)	-2.96	7.99	Poor
Mayo	Mayo Lake	0.68	321 (325)	-1.12	10.14	Good
Upper Yukon	Tutshi River	0.92	482 (484)	-0.37	4.48	Very Good
	Wheaton River	0.82	304 (306)	-0.65	3.80	Very Good
	Atlin River	0.91	555 (493)	12.58	24.94	Very Good
	Yukon River (Whitehorse)	0.85	416 (407)	2.29	51.97	Very Good
	Marsh Lake	0.90	453 (429)	5.57	66.32	Very Good

* Based on the work of Moriasi et *al*. (2007)

Based on the results introduced in Figures 2.11, 2.12, 2.13 and Table 2.10, it can be observed that HYDROTEL performs better given observed natural or near natural flows, albeit with poor representation of those of Sekulmun River for years 2014 and 2016, with a slight overestimation of winter low flows for Atlin River and underestimation of winter low flows for the Yukon River at Whitehorse. Figure 2.13c shows a good representation of spring freshet for Atlin River except for years 2014 and 2015. This representation benefits from the addition of a simple glacier model (Mixed (degree-day) energy-budget method) distributed over different altitude bands. Also, for Atlin River, the flows of the spring and early summer freshets of years 2014 and 2015 are underestimated. In all likelihood, this is related to an underestimation of the snowpack accumulation process by HYDROTEL and perhaps a misrepresentation of glacier melt process in this specific watershed. For the inflows of Aishihik Lake and Marsh Lake, the model failed to capture important daily variations. However, the model captured well the general shape of the annual hydrograph. For Aishihik Lake, the early peaks of spring freshet for years 2014 and 2015 were underestimated by the model. For Marsh Lake, the early peak inflows of the spring freshet for years 2010 and 2011 were underestimated by the model. For Mayo Lake, again the model captured well the general shape of the annual hydrograph, but clearly underestimated summer and fall peak flows as indicated by the P-BIAS value. Moreover, the inflows of Mayo Lake show less daily variations than those of Aishihik Lake or Marsh Lake. Despite these discrepancies, it can be said that HYDROTEL successfully depicts the general shape of the annual hydrograph of each watershed.

It is noteworthy that the model is now more adapted to the Upper Yukon River. Indeed, the model now explicitly accounts for the presence of glaciers in the south-west mountainous part of the watershed. Glacier melt and mass balance are accounted for in the model and, thus, in all likelihood it provides a good representation of the associated runoff. Given the modelling of the glacier melt process, the model can be used to produce both daily forecast and seasonal forecast. That being mentioned, the glacier model remains simple and may result in inexact rates of glacier melt for long-term simulations as required for climate change studies. At this final stage of the project, the model is currently used in a forecasting mode on the Aishihik, Mayo, Upper Yukon River Watersheds and Marsh Lake Sub-watershed. Calibrated models for Aishihik and Mayo were shared with our colleagues at YU to develop the data assimilation (DA) scheme. Meanwhile, we implemented the scheme on the Upper Yukon River Watershed and Marsh Lake Sub-watershed and then integrated models into the forecasting system.

As a complement to Table 2.10, Table 2.11 includes observed and simulated annual runoff from 1981 to 2018. Meanwhile, Table 2.12 introduces the annual runoff over the scale of a hydrological year (October to September) from 1981 to 2018. Moreover, Figures 2.14, 2.15 and 2.16 provide comparison of monthly stream flows/inflows from 1981 to 2018 for all modelled watersheds and sub-watersheds. The quality of the information provided by these tables and figures indicates that the resulting models can be useful for long range forecast and climate change simulations.

Table 2.11 Observed and simulated annual runoff (mm/year) for the 1981-2018 periods for each watershed or sub-watershed.

	ANNUAL RUNOFF (mm/year)			
	SEKULMUN RIVER FLOWS		AISHIHIK LAKE INFLOWS	
YEAR	OBS.	SIM.	OBS.	SIM.
1981	110.29	162.51	81.67	107.98
1982	160.70	233.46	132.97	167.78
1983	163.59	231.96	97.73	170.37
1984	124.88	157.12	90.00	97.88
1985	124.53	204.69	98.25	128.04
1986	155.76	215.16	134.41	143.19
1987	114.88	171.66	94.81	99.17
1988	264.03	292.99	164.54	203.25
1989	87.92	112.95	93.57	121.74
1990	136.78	259.15	102.07	210.68
1991	223.09	273.71	180.44	215.74
1992	244.23	239.42	177.60	180.30
1993	132.67	171.07	101.38	133.16
1994	45.00	100.24	63.50	81.67
1995	106.24	144.60	68.34	86.73
1996	109.47	165.31	73.83	96.12
1997	191.16	189.79	107.23	106.97
1998	59.59	94.38	47.53	60.93
1999	154.32	108.11	96.60	67.80
2000	297.19	210.29	205.74	165.58
2001	162.99	152.71	118.65	106.07
2002	105.45	118.58	89.58	81.67
2003	87.48	118.98	67.19	65.60
2004	102.78	123.71	80.65	76.33
2005	131.10	172.28	92.87	98.94
2006	97.92	159.38	79.64	91.30
2007	220.95	194.97	126.33	112.52
2008	166.21	176.09	117.36	95.48
2009	133.33	206.89	99.08	121.18
2010	125.34	142.28	90.03	83.37
2011	265.98	244.53	180.52	169.49
2012	257.32	265.22	172.11	181.50
2013	219.15	258.68	141.46	184.79
2014	129.22	164.23	88.11	106.94
2015	123.58	114.28	89.42	71.90
2016	122.10	85.33	83.43	54.38
2017	168.50	178.79	135.65	116.39
2018	87.53	99.03	77.50	58.18

	ANNUAL RUNOFF (mm/year) MAYO LAKE INFLOWS	
YEAR	OBS.	SIM.
1981	211.50	243.65
1982	278.29	180.81
1983		
1984	254.13	211.20
1985	277.22	222.09
1986	304.57	285.66
1987	309.62	227.03
1988	328.87	272.66
1989	200.15	162.34
1990	231.34	310.41
1991	293.80	322.50
1992	334.27	348.49
1993	250.31	235.73
1994	197.29	214.08
1995	205.55	183.25
1996	199.18	240.54
1997	334.98	374.63
1998	147.29	166.98
1999	247.15	235.75
2000	349.73	409.93
2001	314.07	376.20
2002	254.58	290.60
2003	221.06	291.39
2004	211.92	237.83
2005	307.87	419.12
2006	267.28	277.07
2007	376.15	287.69
2008	407.53	397.50
2009	342.99	310.16
2010	201.85	222.99
2011	418.99	404.55
2012	354.51	313.32
2013	361.48	304.16
2014	351.92	349.85
2015	438.63	386.05
2016	380.22	338.48
2017	186.93	236.82
2018	226.20	332.08

	ANNUAL RUNOFF (mm/year)									
	TUTSHI RIVER FLOWS		WHEATON RIVER FLOWS		ATLIN RIVER FLOWS		YUKON RIVER FLOWS		MARSH LAKE INFLOWS	
YEAR	OBS.	SIM.	OBS.	SIM.	OBS.	SIM.	OBS.	SIM.	OBS.	SIM.
1981	651.78	198.65	449.62	181.08	554.66	422.67	496.90	256.78	524.22	307.43
1982	475.14	303.66	302.44	277.20	471.46	520.67	393.17	358.98	412.99	397.96
1983	444.92	246.02	216.15	222.09	392.85	492.58	351.45	317.74	363.64	359.21

1984	396.47	233.89	276.16	205.78	332.70	420.84	304.64	272.08	318.78	311.06
1985	482.09	217.17	220.64	194.33	347.16	424.10	322.64	276.24	340.92	311.70
1986	572.02	310.12	343.08	267.53	410.20	485.24	385.53	330.39	416.95	384.40
1987	523.65	319.72	319.47	279.31	444.64	512.30	383.06	357.94	400.05	386.75
1988	605.00	326.64	360.01	302.11	432.62	513.63	411.68	359.64	434.59	405.28
1989	522.71	416.90	336.43	380.23	564.70	711.01	457.09	494.77	482.08	554.22
1990	518.89	321.97	285.46	297.08	549.16	644.24	446.88	440.58	471.64	471.74
1991	516.87	310.80	274.36	279.20	489.01	510.39	414.17	348.44	438.99	389.68
1992	626.48	384.58	244.87	356.99	488.82	610.87	436.70	455.89	447.88	485.07
1993	615.09	313.21	330.17	290.85	549.45	605.75	457.24	397.63	493.12	453.73
1994	585.32	367.07	275.69	342.21	502.63	629.71	452.11	443.83	462.16	480.88
1995	349.43	258.79	242.70	236.97	480.88	614.38	385.02	388.38	399.72	433.65
1996	387.60	296.07	185.74	265.50	375.20	514.00	309.57	348.32	323.79	384.10
1997	442.29	289.45	201.60	204.86	466.56	587.20	395.58	357.55	404.67	426.39
1998			126.64	145.14			338.34	351.18	349.21	397.39
1999			283.91	87.29			332.92	309.72	354.82	354.01
2000			351.13	130.68			402.17	329.50	425.26	373.18
2001	524.91	211.33	322.06	30.50	423.52	495.96	368.63	280.26	384.60	325.09
2002	444.03	226.67	219.65	92.23	431.38	494.85	344.10	283.72	367.77	339.73
2003	392.25	300.51	212.84	189.16	422.66	538.63	334.45	337.15	345.54	385.78
2004	528.17	368.23	277.28	344.52	515.36	671.90	414.96	464.59	434.47	502.40
2005	482.00	248.10	287.84	180.03	477.72	549.00	413.24	323.36	444.78	386.38
2006	547.66	498.25	315.25	273.98	475.16	582.75	401.81	417.87	419.20	460.77
2007	603.76	640.91	417.32	430.96	568.02	635.26	482.24	501.89	504.13	539.57
2008	428.44	440.36	246.97	279.05	403.29	506.88	346.61	370.85	361.64	395.97
2009	502.90	558.80	278.51	314.90	521.90	625.63	403.55	460.75	426.14	501.24
2010	452.81	429.87	294.52	231.86	430.51	534.41	371.16	370.63	391.76	413.47
2011	443.93	465.66	313.30	305.66	431.40	491.32	373.35	374.06	391.18	401.42
2012	593.23	585.84	360.55	399.14	451.34	510.70	407.51	440.16	430.66	469.38
2013	529.91	576.07	305.46	295.53	584.04	646.66	450.31	482.33	479.40	524.80
2014	505.74	497.89	304.37	315.16	539.13	544.27	439.38	421.90	464.54	456.70
2015			305.94	317.07	549.17	617.48	441.72	458.07	462.16	498.09
2016	439.01	381.81	253.37	259.06			426.26	405.47	438.88	442.89
2017	477.30	467.55	301.34	302.15	463.63	538.43	392.12	391.40	414.96	427.89
2018	415.68	446.48	322.03	316.31			360.75	402.27	385.87	439.91

Table 2.12 Observed and simulated hydrological year (October to September) annual runoff (mm/year) for the 1981-2018 periods for each watershed or sub-watershed.

HYDROLOGICAL YEAR ANNUAL RUNOFF (mm/year)	
SEKULMUN RIVER FLOWS	AISHIHIK LAKE INFLOWS

YEAR	OBS.	SIM.	OBS.	SIM.
1981-1982	172.65	230.44	127.83	164.73
1982-1983	147.82	226.62	99.89	163.44
1983-1984	117.67	164.66	87.31	106.10
1984-1985	125.97	195.00	96.18	122.68
1985-1986	165.30	221.39	133.77	144.40
1986-1987	101.45	155.56	96.97	95.42
1987-1988	264.40	302.30	160.56	204.30
1988-1989	109.40	135.34	99.18	132.36
1989-1990	141.66	230.40	106.39	188.83
1990-1991	191.68	276.80	153.83	219.63
1991-1992	251.12	255.98	195.45	194.93
1992-1993	142.12	167.78	99.77	126.10
1993-1994	67.51	110.21	75.50	89.64
1994-1995	101.22	138.21	64.49	85.10
1995-1996	116.16	168.89	78.45	99.29
1996-1997	183.10	188.46	106.98	105.48
1997-1998	67.44	111.73	49.73	65.87
1998-1999	164.32	93.59	91.16	62.80
1999-2000	264.86	190.87	191.15	148.03
2000-2001	183.68	163.36	129.14	120.86
2001-2002	116.88	137.56	95.46	86.36
2002-2003	91.83	110.51	69.88	65.67
2003-2004	100.18	128.77	77.79	76.45
2004-2005	123.08	154.23	88.58	92.26
2005-2006	110.79	165.98	86.00	95.29
2006-2007	205.89	196.14	117.42	112.22
2007-2008	167.92	170.71	117.96	95.83
2008-2009	147.38	212.34	106.29	121.90
2009-2010	104.53	133.39	79.49	79.68
2010-2011	262.52	249.60	180.59	166.66
2011-2012	246.31	253.77	169.64	177.59
2012-2013	228.15	261.41	144.48	183.70
2013-2014	138.55	166.64	93.71	110.75
2014-2015	116.70	117.64	80.56	75.12
2015-2016	129.22	111.29	93.48	67.73
2016-2017	173.46	164.61	130.79	108.64
2017-2018	89.31	105.93	83.95	61.94
2018-2019	172.65	230.44	127.83	164.73

	HYDROLOGICAL YEAR ANNUAL RUNOFF (mm/year) MAYO LAKE INFLOWS	
YEAR	OBS.	SIM.
1981-1982	280.20	192.62
1982-1983	-	-

1983-1984	192.34	170.12
1984-1985	308.63	228.18
1985-1986	303.30	273.85
1986-1987	271.48	214.87
1987-1988	369.42	296.92
1988-1989	209.85	173.16
1989-1990	201.19	247.82
1990-1991	316.41	361.48
1991-1992	339.75	362.38
1992-1993	249.76	238.81
1993-1994	195.78	211.21
1994-1995	200.39	179.86
1995-1996	200.91	223.13
1996-1997	330.86	377.44
1997-1998	160.38	187.67
1998-1999	233.25	218.34
1999-2000	333.32	394.66
2000-2001	335.45	393.48
2001-2002	239.98	271.71
2002-2003	232.30	307.37
2003-2004	213.81	262.48
2004-2005	296.89	371.13
2005-2006	250.59	295.40
2006-2007	371.04	293.82
2007-2008	356.75	375.46
2008-2009	403.25	319.34
2009-2010	223.91	253.24
2010-2011	391.13	376.93
2011-2012	377.99	331.51
2012-2013	315.66	264.03
2013-2014	312.55	354.40
2014-2015	474.11	385.05
2015-2016	423.75	372.74
2016-2017	203.28	223.00
2017-2018	229.17	348.82
2018-2019	280.20	192.62

	HYDROLOGICAL YEAR ANNUAL RUNOFF (mm/year)									
	TUTSHI RIVER FLOWS		WHEATON RIVER FLOWS		ATLIN RIVER FLOWS		YUKON RIVER FLOWS		MARSH LAKE INFLOWS	
YEAR	OBS.	SIM.	OBS.	SIM.	OBS.	SIM.	OBS.	SIM.	OBS.	SIM.
1981-1982	502.86	325.08	320.58	284.69	496.92	502.86	436.56	346.29	434.84	398.36
1982-1983	457.85	245.39	228.58	226.91	424.19	505.36	360.38	328.26	384.19	365.68

1983-1984	394.43	226.19	268.36	199.67	339.20	435.96	307.60	280.67	319.80	315.13
1984-1985	494.62	243.88	234.67	209.09	346.80	417.11	322.30	278.29	346.71	314.33
1985-1986	532.13	252.61	315.75	230.68	375.13	451.27	364.04	296.00	383.43	343.48
1986-1987	520.68	352.05	323.06	294.73	441.64	525.85	381.01	370.02	399.60	408.89
1987-1988	609.82	332.47	368.21	306.61	441.60	511.88	410.42	359.73	434.36	405.88
1988-1989	534.00	395.72	330.38	365.15	535.70	650.74	447.45	450.57	477.21	521.56
1989-1990	524.09	360.54	295.52	324.42	551.47	681.01	446.55	473.06	478.11	504.14
1990-1991	500.94	277.51	279.71	258.98	490.83	533.78	411.44	355.91	423.99	386.09
1991-1992	653.27	417.83	252.14	375.36	532.42	613.20	466.54	458.98	485.86	499.83
1992-1993	580.07	287.29	315.19	281.35	492.62	574.91	426.69	383.55	455.04	432.02
1993-1994	571.44	353.83	268.52	327.78	523.37	623.37	452.85	428.63	465.34	474.53
1994-1995	419.70	298.86	261.78	264.66	490.49	626.23	404.86	411.06	427.20	450.00
1995-1996	380.75	292.08	192.21	260.47	407.99	545.05	321.93	363.06	339.11	398.35
1996-1997	436.91	277.07	189.29	212.28	435.69	554.22	364.82	352.78	386.99	412.43
1997-1998	240.52	269.59	130.75	146.77			354.99	353.31	355.50	404.35
1998-1999			281.58	113.73			334.29	314.43	351.19	357.03
1999-2000			340.35	135.53			389.27	323.03	410.26	367.45
2000-2001	617.23	204.35	326.55	32.87	439.22	501.89	385.83	290.65	404.34	333.22
2001-2002	425.88	214.97	223.96	62.79	424.70	495.60	339.85	279.35	357.88	328.96
2002-2003	395.28	289.85	200.96	179.81	422.28	527.36	330.65	325.82	348.52	382.08
2003-2004	528.60	389.52	291.98	343.26	514.99	666.30	410.30	453.21	431.01	508.43
2004-2005	492.59	246.86	283.43	187.51	480.53	551.73	422.38	335.52	444.16	384.09
2005-2006	528.93	480.58	314.25	261.33	460.96	578.60	389.44	407.63	413.61	453.32
2006-2007	619.62	639.28	413.27	435.40	575.15	621.26	468.33	484.18	507.68	537.90
2007-2008	422.46	453.71	250.79	272.60	409.91	548.94	361.43	405.30	368.89	412.50
2008-2009	499.65	532.12	272.28	307.84	501.81	589.36	390.85	430.42	419.69	482.24
2009-2010	459.79	435.12	297.93	241.61	457.37	557.34	389.31	392.12	399.00	425.88
2010-2011	444.31	471.11	314.17	314.21	428.31	515.98	368.82	387.20	390.33	413.37
2011-2012	585.02	570.47	342.74	392.19	439.48	482.26	402.23	413.64	424.65	450.48
2012-2013	528.89	591.30	323.79	299.64	560.63	616.58	436.02	472.45	469.82	519.24
2013-2014	490.72	461.28	292.95	293.06	528.23	557.93	427.65	426.25	444.94	445.84
2014-2015	383.56	476.67	307.27	327.33	569.67	625.22	454.44	466.99	474.41	508.89
2015-2016	491.84	394.57	259.56	270.31	559.74	689.11	425.04	409.84	456.90	453.68
2016-2017	477.63	479.29	302.80	300.65			405.72	395.11	415.40	426.77
2017-2018	383.17	409.40	279.45	284.72			369.20	399.53	389.19	440.86
2018-2019	502.86	325.08	320.58	284.69			436.56	346.29	434.84	398.36

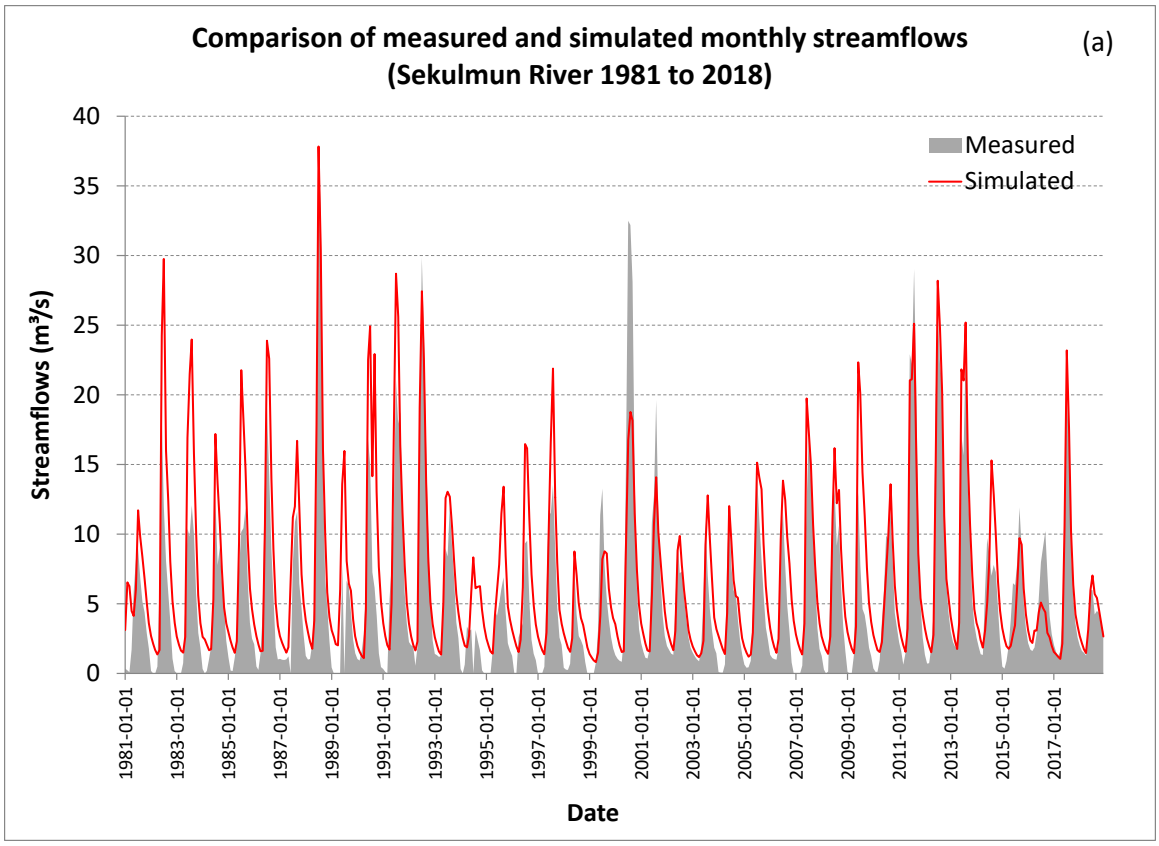
Comparison of measured and simulated monthly streamflows
(Sekulmun River 1981 to 2018)
(a)
Measured
Simulated
Streamflows (m³/s)
40
35
30
25
20
15
10
5
0
1981-01-01
1983-01-01
1985-01-01
1987-01-01
1989-01-01
1991-01-01
1993-01-01
1995-01-01
1997-01-01
1999-01-01
2001-01-01
2003-01-01
2005-01-01
2007-01-01
2009-01-01
2011-01-01
2013-01-01
2015-01-01
2017-01-01
Date

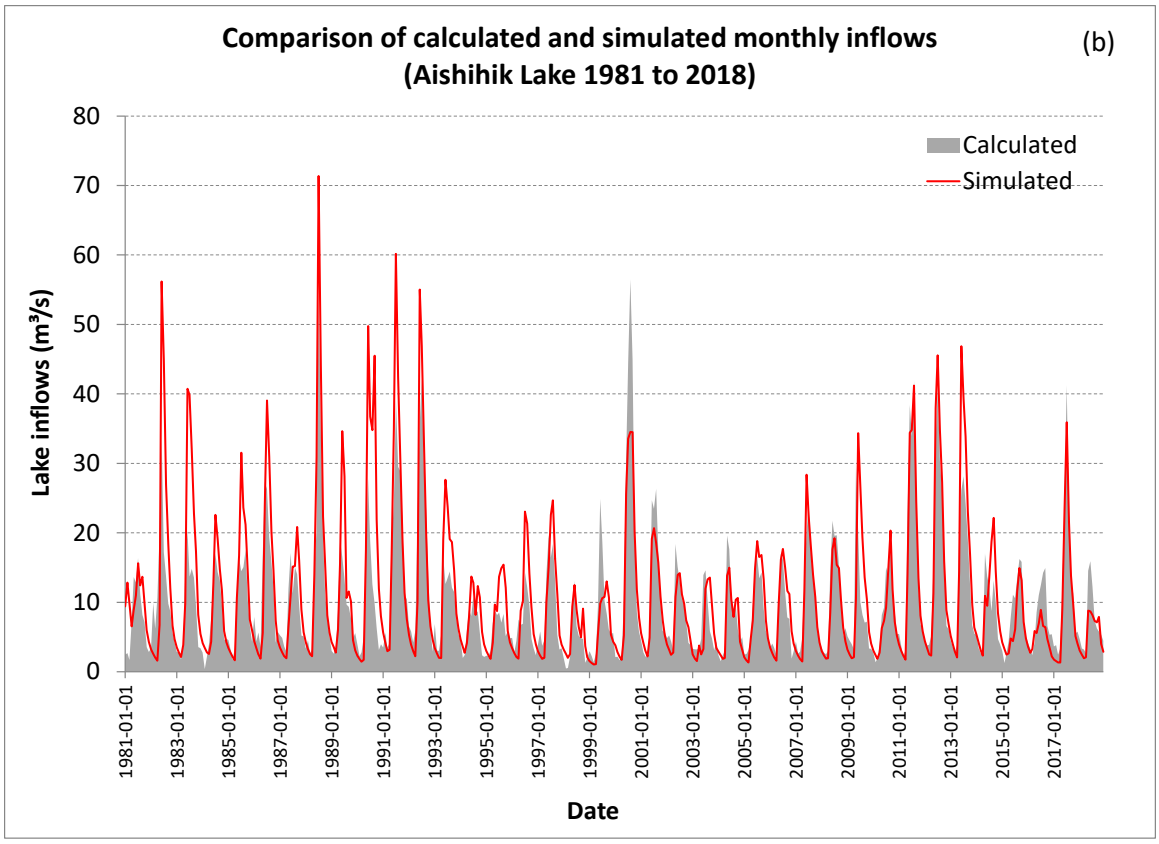

Figure 2.14 Graphical comparisons of monthly measured flows or calculated inflows with simulated flows or inflows for: (a) Sekulmun River, (b) Aishihik Lake.

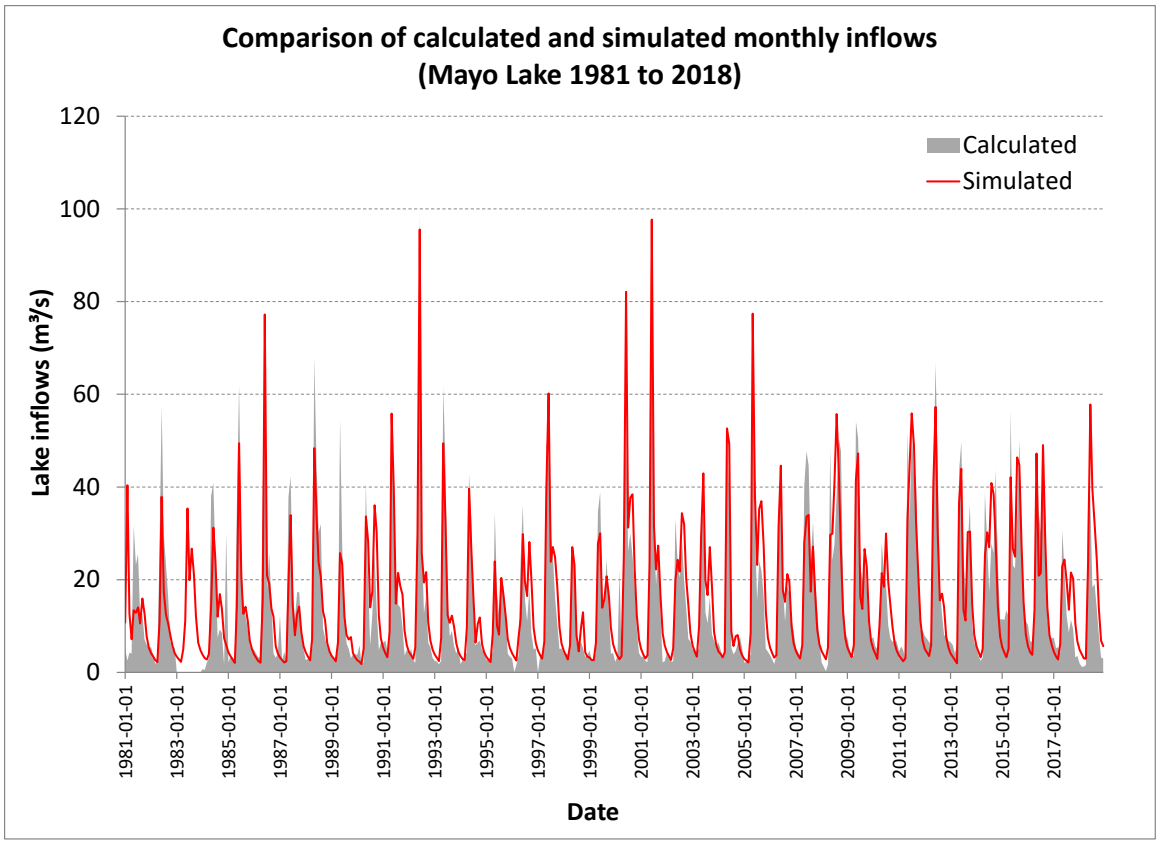

Figure 2.15 Graphical comparisons of monthly calculated inflows with simulated inflows for Mayo Lake.

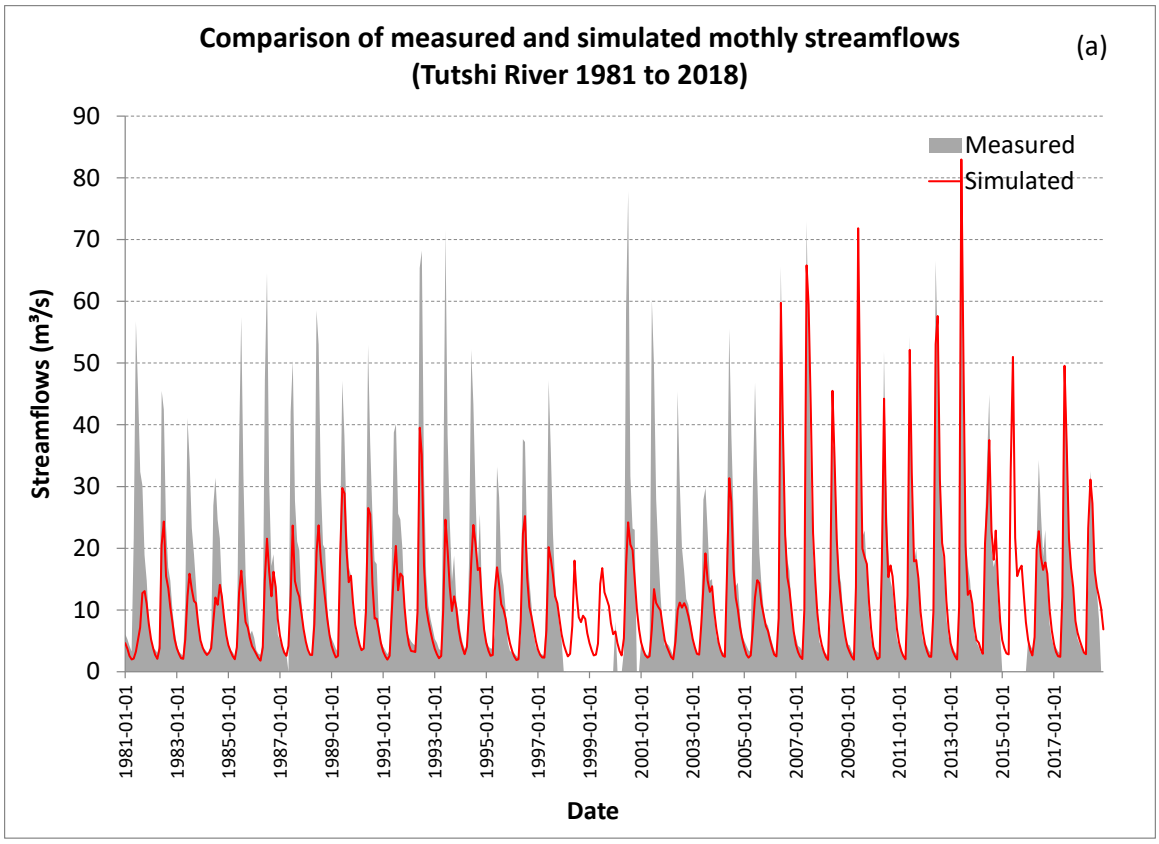
Comparison of measured and simulated mothly streamflows
(Tutshi River 1981 to 2018)
(a)
Measured
Simulated
Streamflows (m³/s)
0
10
20
30
40
50
60
70
80
90
1981-01-01
1983-01-01
1985-01-01
1987-01-01
1989-01-01
1991-01-01
1993-01-01
1995-01-01
1997-01-01
1999-01-01
2001-01-01
2003-01-01
2005-01-01
2007-01-01
2009-01-01
2011-01-01
2013-01-01
2015-01-01
2017-01-01
Date

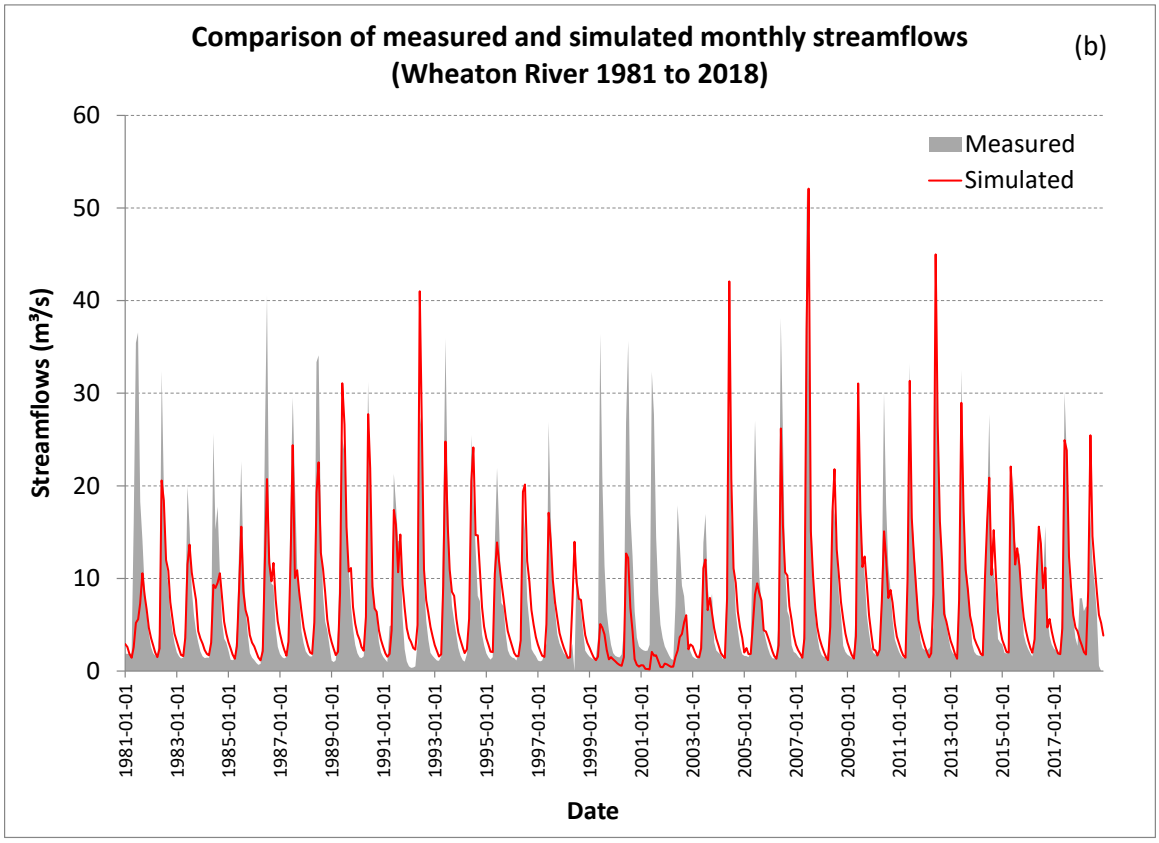
Comparison of measured and simulated monthly streamflows
(Wheaton River 1981 to 2018)
(b)
Measured
Simulated
Streamflows (m³/s)
0
10
20
30
40
50
60
1981-01-01
1983-01-01
1985-01-01
1987-01-01
1989-01-01
1991-01-01
1993-01-01
1995-01-01
1997-01-01
1999-01-01
2001-01-01
2003-01-01
2005-01-01
2007-01-01
2009-01-01
2011-01-01
2013-01-01
2015-01-01
2017-01-01
Date

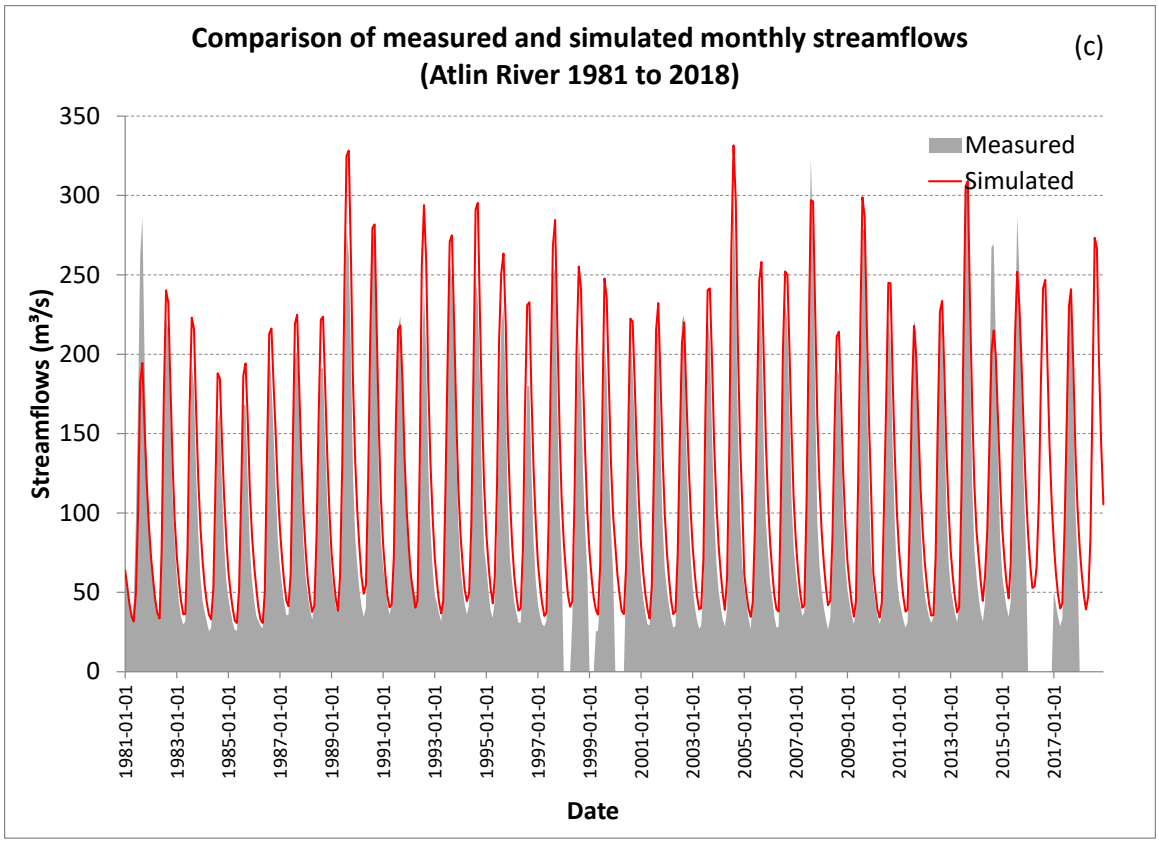
Comparison of measured and simulated monthly streamflows
(Atlin River 1981 to 2018)
(c)
Measured
Simulated
Streamflows (m³/s)
350
300
250
200
150
100
50
0
1981-01-01
1983-01-01
1985-01-01
1987-01-01
1989-01-01
1991-01-01
1993-01-01
1995-01-01
1997-01-01
1999-01-01
2001-01-01
2003-01-01
2005-01-01
2007-01-01
2009-01-01
2011-01-01
2013-01-01
2015-01-01
2017-01-01
Date

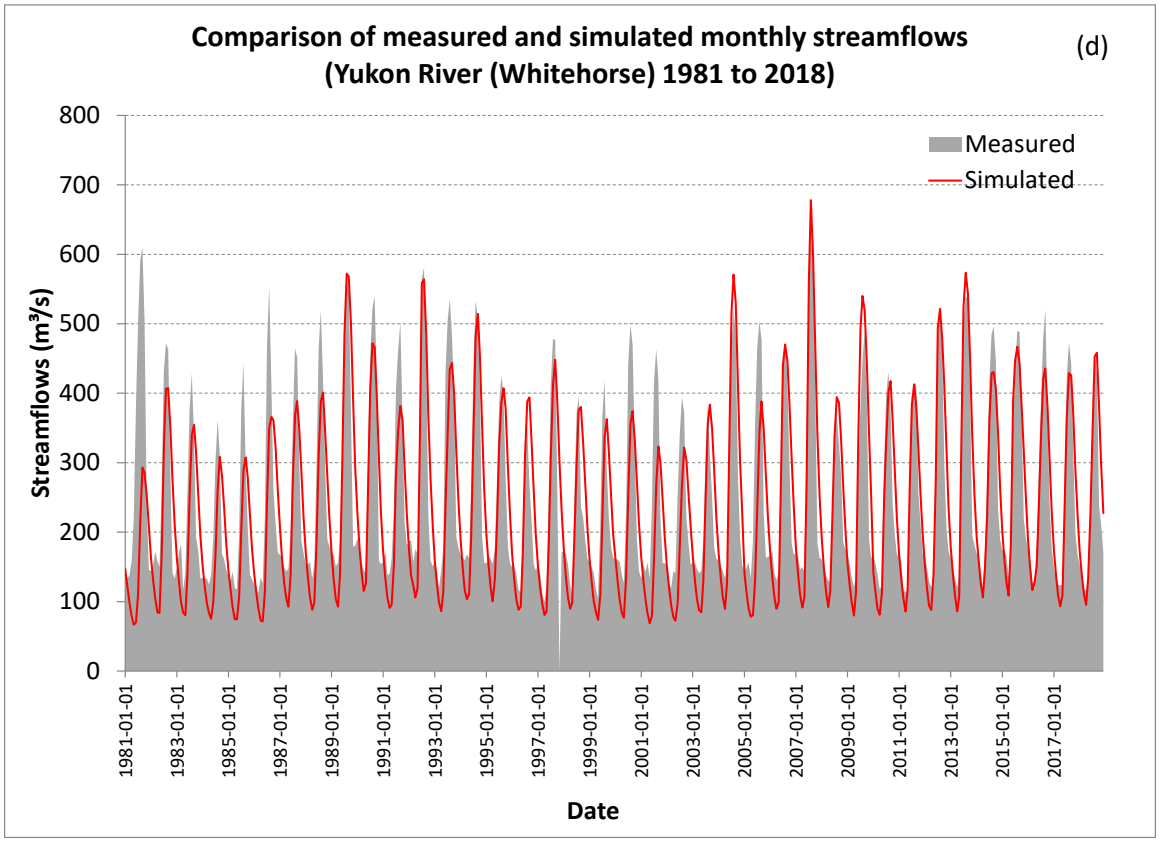
Comparison of measured and simulated monthly streamflows
(Yukon River (Whitehorse) 1981 to 2018)
(d)
Measured
Simulated
Streamflows (m³/s)
800
700
600
500
400
300
200
100
0
1981-01-01
1983-01-01
1985-01-01
1987-01-01
1989-01-01
1991-01-01
1993-01-01
1995-01-01
1997-01-01
1999-01-01
2001-01-01
2003-01-01
2005-01-01
2007-01-01
2009-01-01
2011-01-01
2013-01-01
2015-01-01
2017-01-01
Date

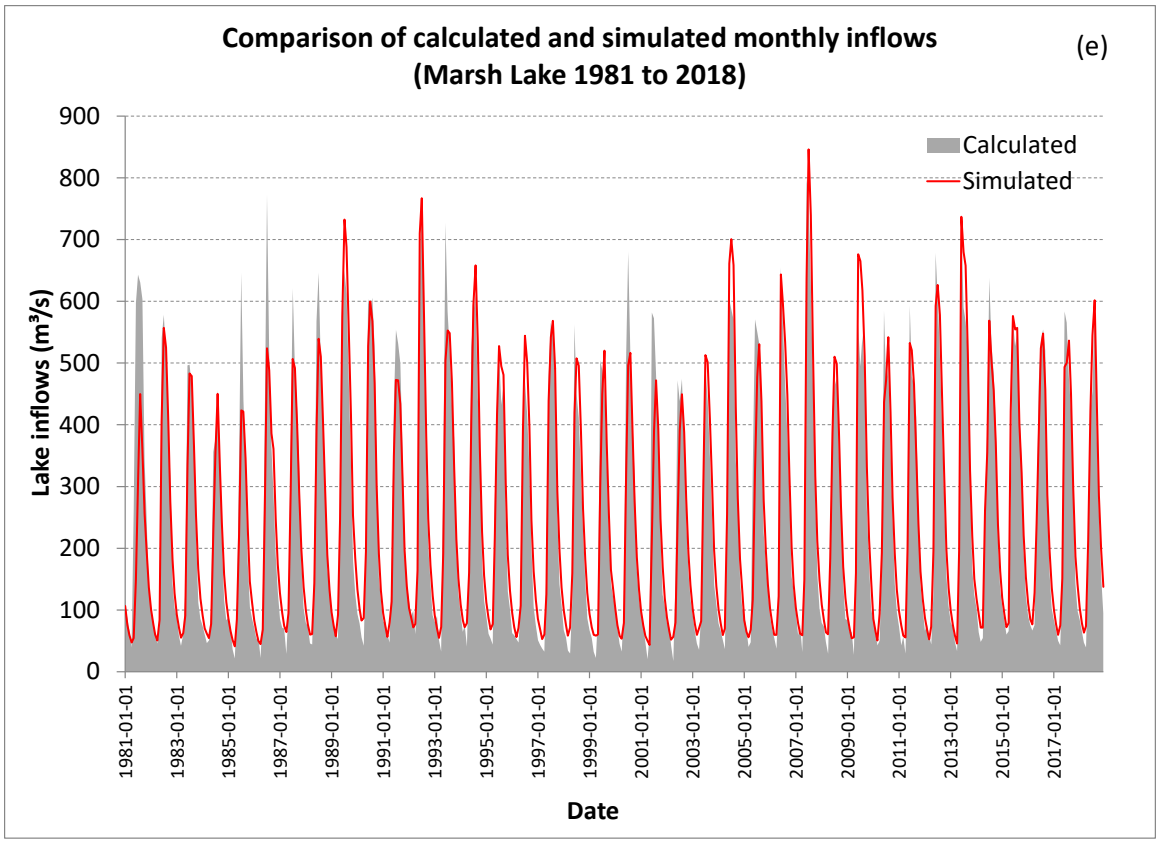

Figure 2.16 Graphical comparisons of monthly measured flows or calculated inflows with simulated flows or inflows for: (a) Tutshi River, (b) Wheaton River, (c) Atlin River, (d) Yukon River (Whitehorse) and (e) Marsh Lake.

It is noteworthy that results for the Upper Yukon River watershed do not include snow survey correction prior to 2006. Such limitation has a major impact on model performance especially for the Tutshi River watershed.

2.2.4. Data assimilation

Data Assimilation (DA) consists of correcting the values of the model state variables in order to reproduce either observed flows or calculated inflows. It works by reading, arranging and generating ensembles of errors of real-time observed flows (from Environment Canada website and YEC ftp sites) and meteorological data (from NAEFS and CanSIPS website). It then corrects and forces the Hydrotel model to simulate 1000 model states and forecasted inflows and updates the states of Hydrotel. Subsequently, the updated states are returned to the HYDROTEL model to be used for the next forecasts.

Three DA approaches were tested in this project: (type #1) Kalman filtering (EnKF) by simulating state estimation and assuming constant model parameters and (type #2) Kalman Filtering by simulating simultaneous state-parameter estimation, and (type #3) particle filtering (PF). The best DA approach was found to be types #1 and the worst DA approach was found to be type #3. As such, type #1 was used.

The method, developed for Aishihik and Mayo with 2016 hydrometeorological data, was adapted using the 2017 hydrometeorological data to the Upper Yukon watershed (including Marsh Lake sub-watershed). The procedure was developed and applied using a daily time step, correcting for each day the simulated hydrological state variables to improve the forecasted flows or inflows.

Figures 2.17, 2.18, 2.19, 2.20 and Table 2.13 illustrate the type of improvement that was achieved for the Sekulmun River flows, Aishihik Lake inflows, Mayo Lake inflows, Upper Yukon River (Whitehorse) flows and Marsh Lake inflows for the year 2018. For the Upper Yukon River watershed and Marsh Lake sub-watershed the system was built using the Mayo Lake DA scheme and tested for the current 2018 year.

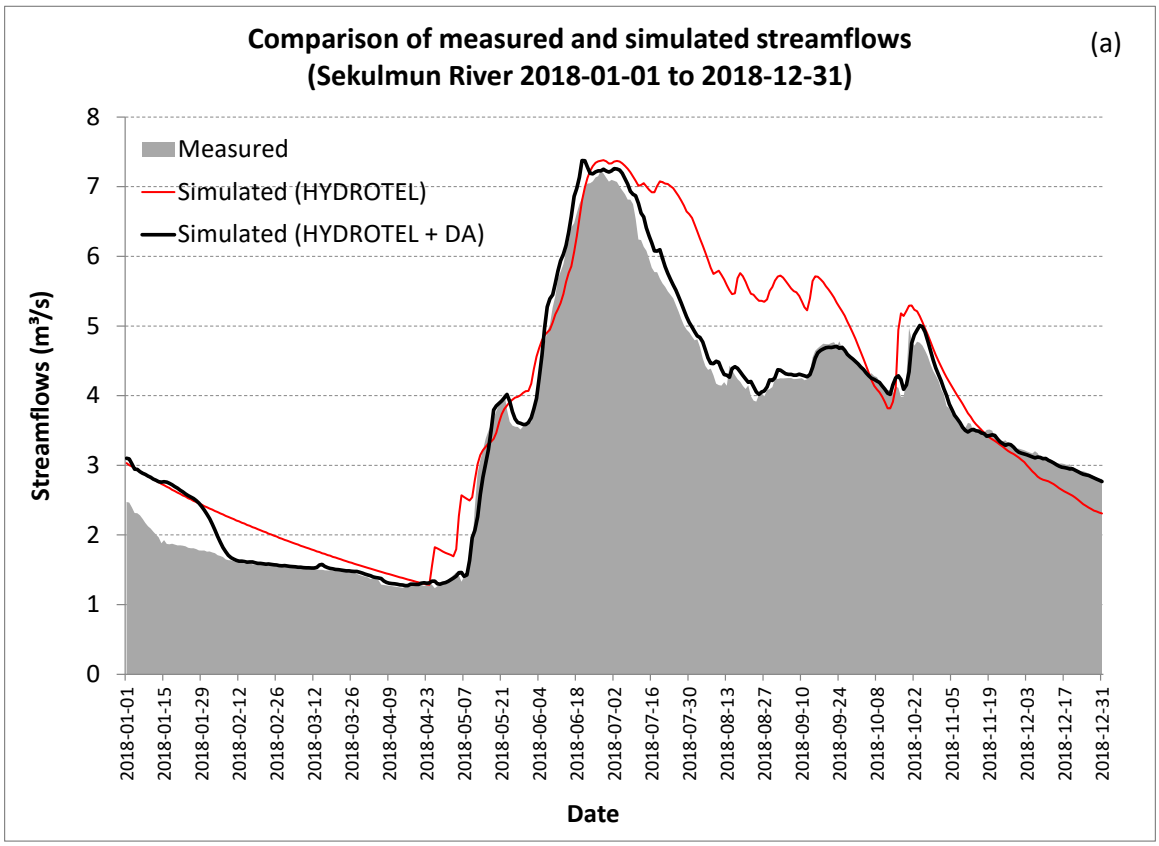

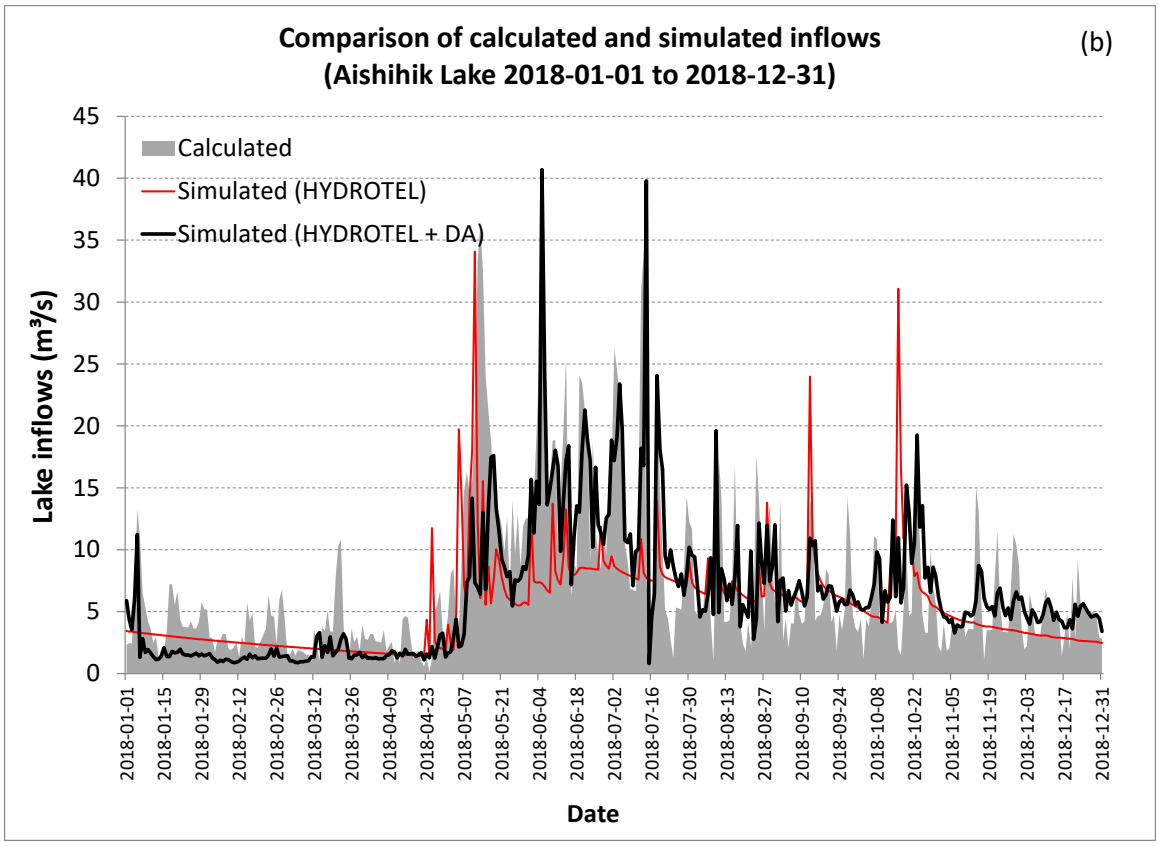

Figure 2.17 Graphical comparisons of measured flows or calculated inflows with simulated flows and inflows after the implementation of the DA scheme for: (a) Sekulmun River, (b) Aishihik Lake.

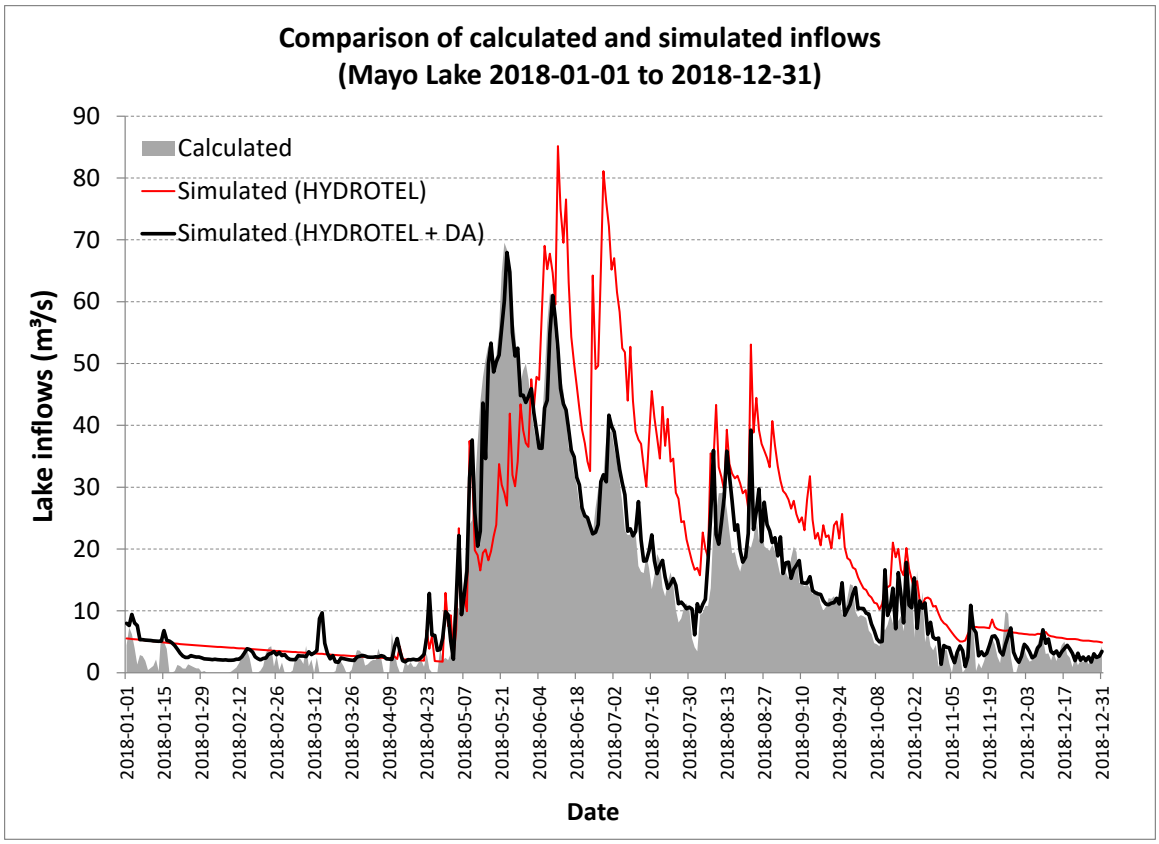

Figure 2.18 Graphical comparisons of calculated inflows with simulated inflows after the implementation of the DA scheme for Mayo Lake.

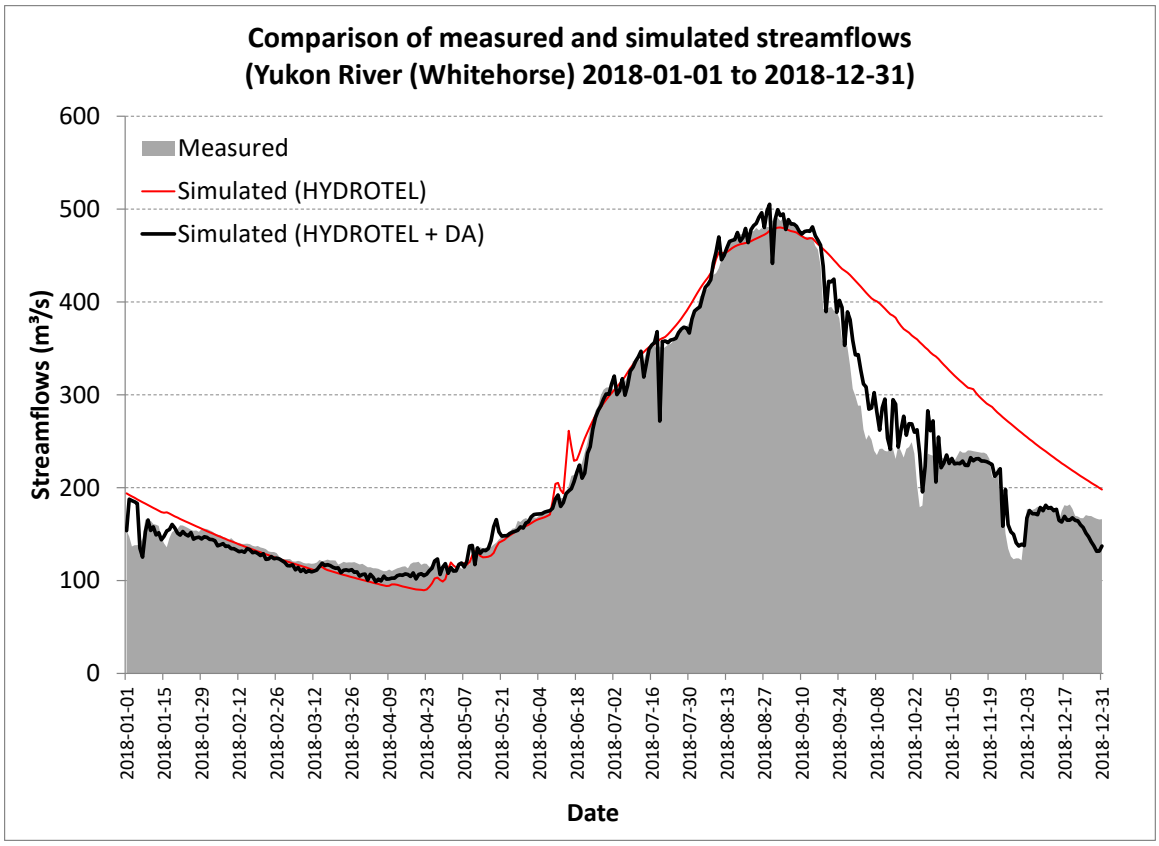

Figure 2.19 Graphical comparisons of measured flows with simulated flows the implementation of the DA scheme for the Upper Yukon River.

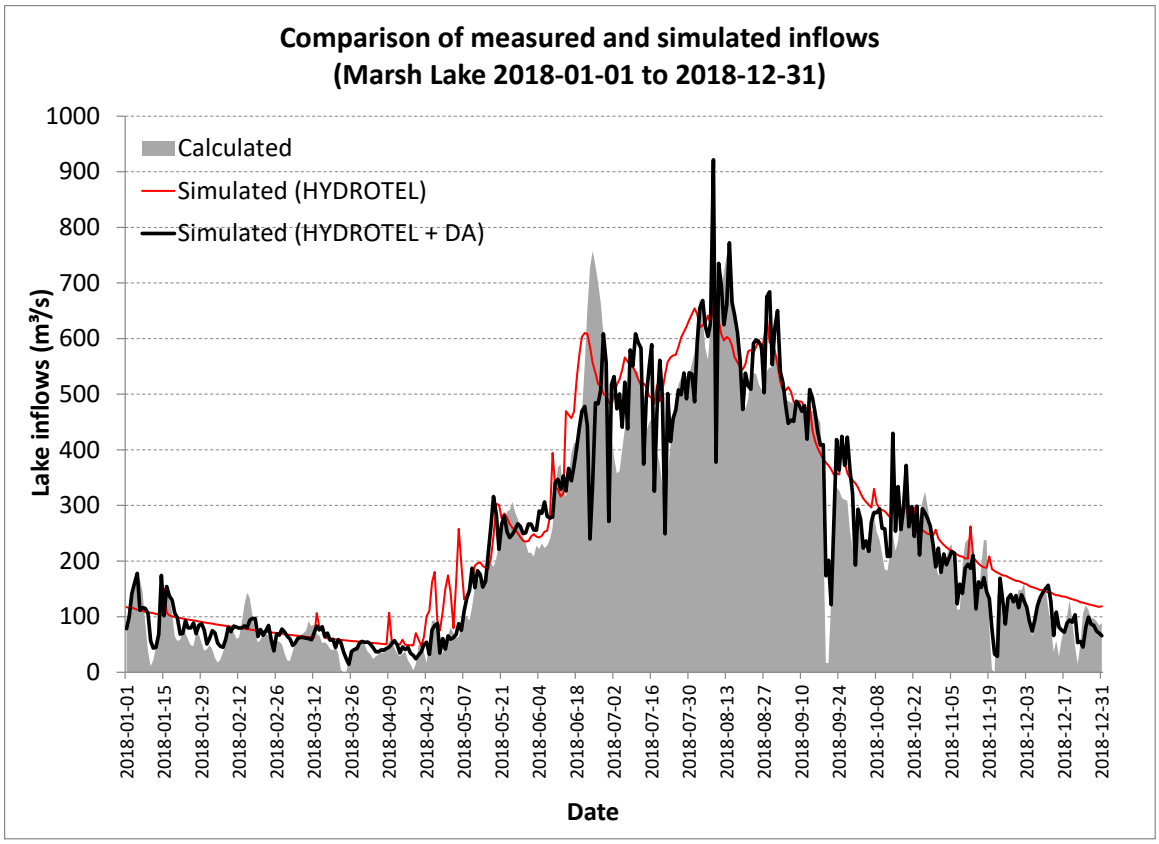

Figure 2.20 Graphical comparisons of calculated inflows with simulated inflows the implementation of the DA scheme for Marsh Lake.

Table 2.13 Model performance in representing observed flows or inflows (in parentheses) without (in red) and with data (in black) assimilation.

Watershed	Site	NS	$Runoff_{year}$ (mm)	$PBIAIS$ (%)	$RMSE$(m³/s)	Remarks
Aishihik	Sekulmun River (2018)	0.81	99 (88)	13.14	0.72	Very good
		0.98	91 (88)	3.43	0.26	Very good
	Aishihik Lake(2018)	0.13	58 (78)	-24.93	5.90	Unsatisfactory
		0.37	69 (78)	-11.37	5.02	Poor
Mayo	Mayo Lake (2018)	0.31	332 (226)	46.81	12.77	Poor
		0.93	247 (226)	9.27	4.09	Very good
Upper Yukon	Yukon River (Whitehorse) (2018)	0.78	402 (361)	11.51	55.54	Good
		0.98	363 (361)	0.51	17.89	Very good
Upper Yukon	Marsh Lake (2018)	0.87	440 (386)	14.01	70.44	Good
		0.89	400 (386)	3.63	66.32	Very good

As indicated, data assimilation provides a clear enhancement of the representation of the Sekulmun River flows, the Mayo Lake inflows, the Upper Yukon River flows (Whitehorse) and Marsh Lake inflows. For the Aishihik Lake inflows, data assimilation offers an interesting gain in model performance, but the combination of HYDROTEL and DA has yet to capture the daily variations of the calculated inflows. Similarly daily variations for Marsh Lake inflows are not all captured well by data assimilation. Nonetheless, these results are satisfying, thus they increase our confidence to deliver robust daily forecast flows for Sekulmun River flows, Mayo Lake inflows, Upper Yukon River flows and Marsh Lake inflows as well as produce relevant shapes of hydrographs for Aishihik Lake inflows.

2.2.5. Challenges and potential solutions

The first results show good performances in the representation of the flows for the Sekulmun River, inflows at Mayo Lake, flows for the Upper Yukon River (Whitehorse) and inflows for Marsh Lake, any future efforts should focus on improving the results for the inflows at Aishihik Lake. As mentioned before, calculation of inflows for the Aishihik Lake is associated with non-negligible uncertainties related to the measurements of numerous independent variables such as water levels; flows downstream of Aishihik Lake and flows of the Giltana Creek. Efforts should be made towards improving the robustness of the measurements prior to calculating inflows. Assessment of the flows at the outlet of Aishihik Lake (through the butterfly valve of the lake control unit) could represent a valuable first step and then the ensuing flows could directly be taking into account in the inflow calculation.

For both Aishihik and Mayo, operational meteorological stations on the outskirt or within the watershed boundaries are limited. Adding meteorological stations could certainly further improve the performance of the forecasting system for the coming years. Indeed, we recommended to YEC in a requested technical note (Strategic planning of meteorological and snow monitoring stations – Case of the Mayo watershed) produced by Rousseau and Savary (2017). And accordingly actions were taken to improve these limitations. First Geonor gauges were installed at the new GMON stations near the Mayo Lake outlet and Aishihik Village and they will directly contribute to have a better knowledge of what is actually falls as snow within the watershed boundary.

For the Upper Yukon River Watershed including Marsh Lake, future efforts should be directed towards the improvement of the glacier module added to HYDROTEL or updating the glacier map.

2.2.6. Reanalysis data

During the calibration of HYDROTEL, we investigated the use of reanalysis data for Aishihik and Mayo; that is CFSR (Saha et *al.*, 2010), ERA-Interim (Dee et al., 2011), MERRA2 (Rienecker et *al*., 2011], JRA55 (Kobayashi et *al*. 2015) data were considered. This investigation turned to be non-conclusive. Indeed, the meteorological conditions (precipitations) proposed by the diverse reanalysis datasets did not corroborate very well with the observed conditions (see Figure 2.21). Given this outcome, it would not have been consistent to calibrate HYDROTEL with any of the aforementioned reanalysis data.

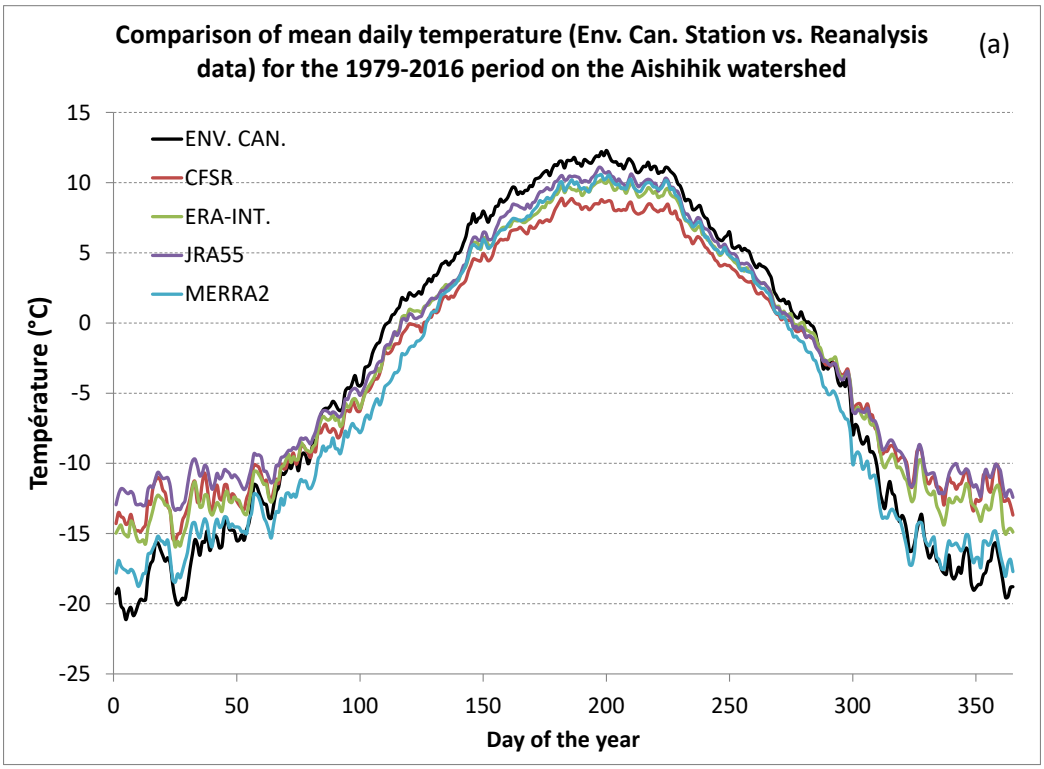

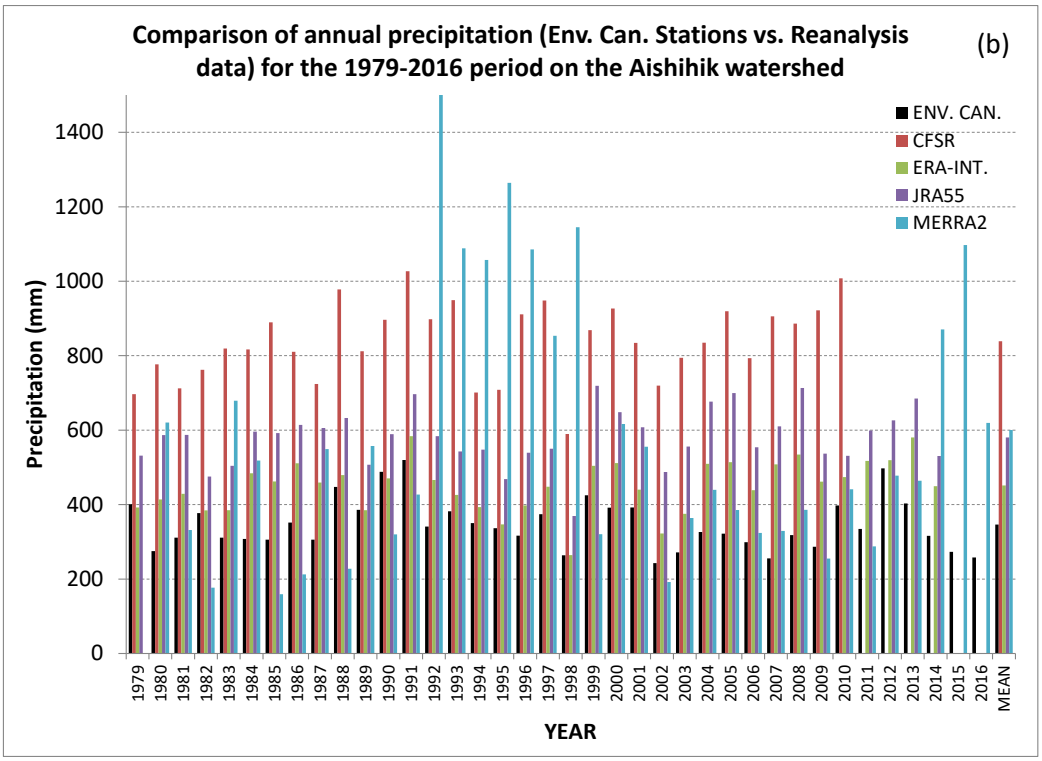
Comparison of annual precipitation (Env. Can. Stations vs. Reanalysis data) for the 1979-2016 period on the Aishihik watershed
(b)
ENV. CAN.
CFSR
ERA-INT.
JRA55
MERRA2
Precipitation (mm)
0
200
400
600
800
1000
1200
1400
1979
1980
1981
1982
1983
1984
1985
1986
1987
1988
1989
1990
1991
1992
1993
1994
1995
1996
1997
1998
1999
2000
2001
2002
2003
2004
2005
2006
2007
2008
2009
2010
2011
2012
2013
2014
2015
2016
MEAN
YEAR

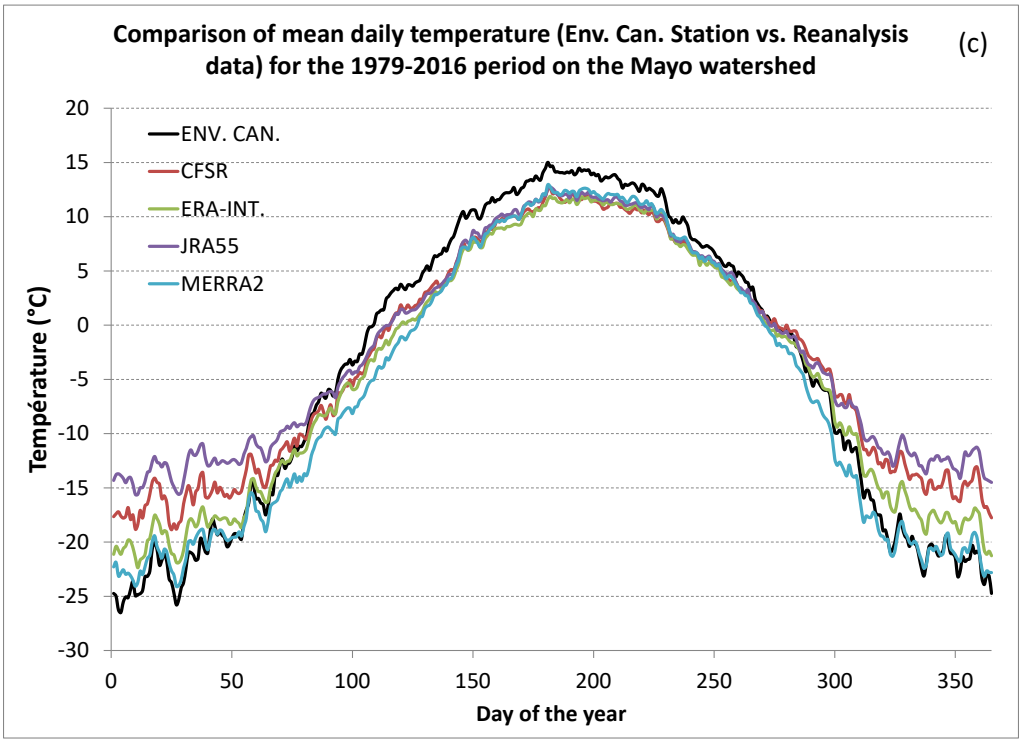
Comparison of mean daily temperature (Env. Can. Station vs. Reanalysis data) for the 1979-2016 period on the Mayo watershed
(c)
ENV. CAN.
CFSR
ERA-INT.
JRA55
MERRA2
Température (°C)
20
15
10
5
0
-5
-10
-15
-20
-25
-30
0
50
100
150
200
250
300
350
Day of the year

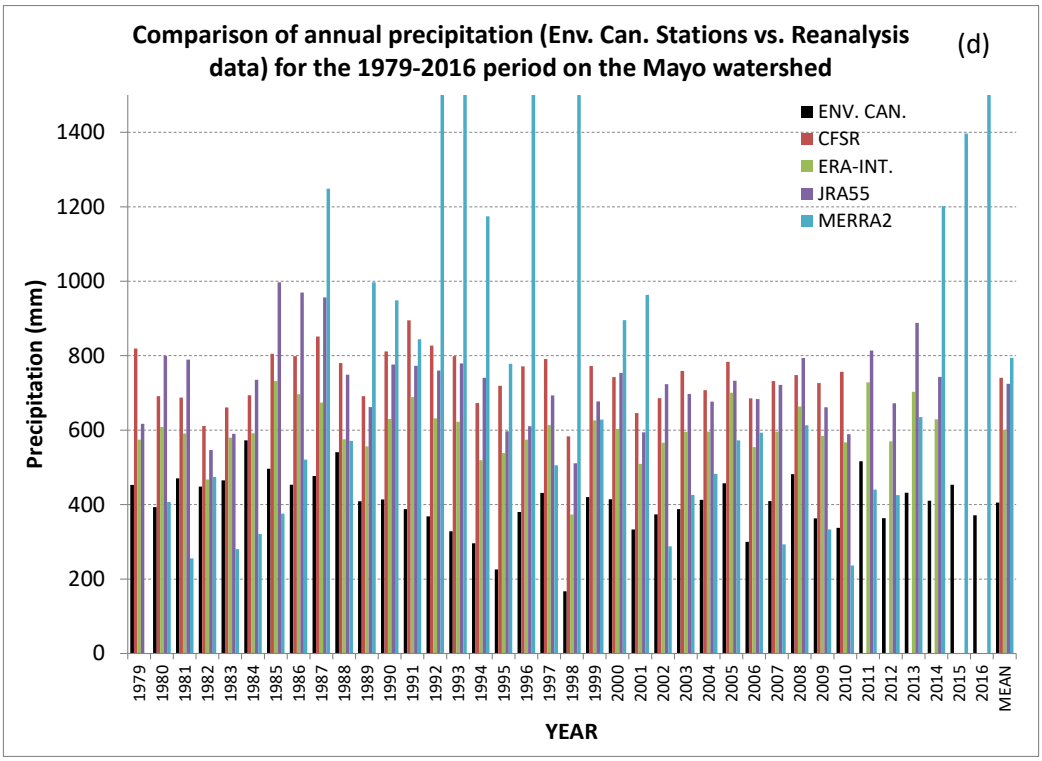

Figure 2.21 Comparison of observed (Environment Canada) and reanalysed (CFSR, ERA-INT, JRA55, MERRA2) mean daily temperature and total annual precipitation at the scale of the Aishihik (a, b) and Mayo (c, d).

Figure 2.18 illustrates clear tendencies that can be summarized as follows:

1. For both Aishihik and Mayo, summer temperatures from reanalysis data underestimate observed temperatures. On the opposite, winter temperatures from reanalysis data mainly overestimate those observed.

2. Total annual precipitations from CFSR, ERA-INT and JRA55 systematically overestimate those observed precipitations for both watersheds - except for year 1979, 1989 and 1990 for ERA-INT and in the case of the Aishihik Watershed. For Aishihik, the ratio of reanalysed over observed total annual precipitations for CFSR, ERA-INT, JR55 and MERRA2 are 2.5, 1.3, 1.7, 1.8 and for Mayo 1.9, 1.5, 1.8, 2.1. Moreover the correlations are very low for all series for both watersheds. For Aishihik, the coefficient of determination for CFSR, ERA-INT, JRA55 and MERRA-2 are 0.23, 0.21, 0.14, 0.01, respectively and for Mayo 0.11, 0.36, 0.24, 0.14.

Based on such observations, the reanalysis data could not be considered as reliable data for model calibration in the current context and further development of the forecasting system.

2.3. Forecasting system

At first it is important to mention that the development of the forecasting system is joint venture between INRS and YU. The forecasting system regroups four major components: (1) the data manager component; (2) the HYDROTEL model; (3) the DA scheme and (4) the graphical user interface (GUI). As part of the project, we put together a User's Manual which was delivered separately to Yukon Energy (Rousseau et al., 2020).

The system operates under two specific meteorological forecast ensembles: the North American Ensemble Forecast System (NAEFS) issued by the Meteorological Service of Canada (MSC) for the 1 to 14 days weather forecast and ECCC's seasonal forecasting system CanSIPS for longer lead times (*i.e.*, seasonal flows or inflow forecasts; 1 to 12 months).

Figure 2.22 provides an overview of the flow/inflow forecasting system including: (a) NAEFS and (b) CanSIPS meteorological ensemble forecast. Both flow charts where provided by NCE.

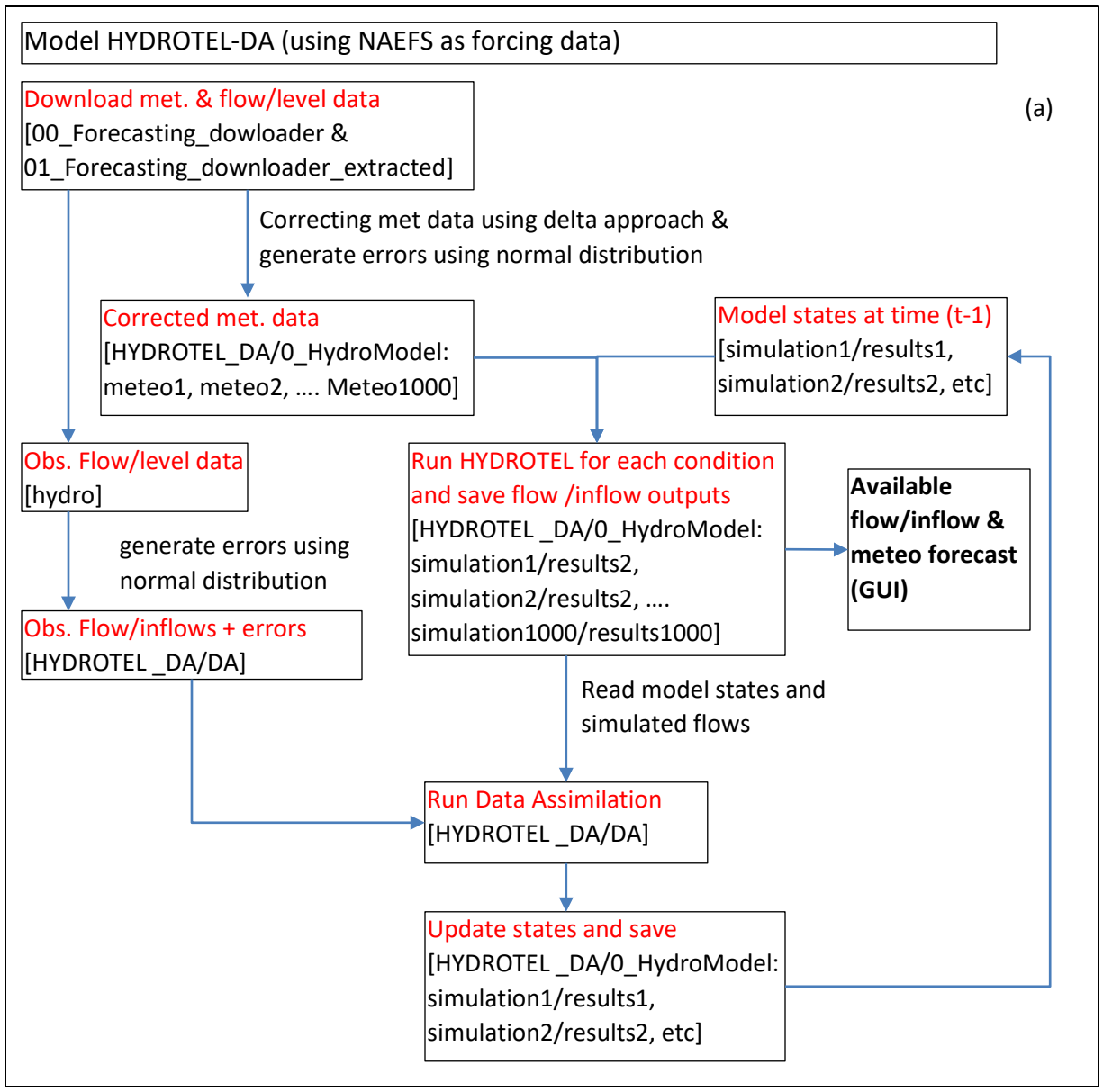
Model HYDROTEL-DA (using NAEFS as forcing data)
(a)
Download met. & flow/level data
[00_Forecasting_dowloader &
01_Forecasting_downloader_extracted]
Correcting met data using delta approach &
generate errors using normal distribution
Corrected met. data
[HYDROTEL_DA/0_HydroModel:
meteo1, meteo2, …. Meteo1000]
Model states at time (t-1)
[simulation1/results1,
simulation2/results2, etc]
Obs. Flow/level data
[hydro]
generate errors using
normal distribution
Obs. Flow/inflows + errors
[HYDROTEL _DA/DA]
Run HYDROTEL for each condition
and save flow /inflow outputs
[HYDROTEL _DA/0_HydroModel:
simulation1/results2,
simulation2/results2, ….
simulation1000/results1000]
Available
flow/inflow &
meteo forecast
(GUI)
Read model states and
simulated flows
Run Data Assimilation
[HYDROTEL _DA/DA]
Update states and save
[HYDROTEL _DA/0_HydroModel:
simulation1/results1,
simulation2/results2, etc]

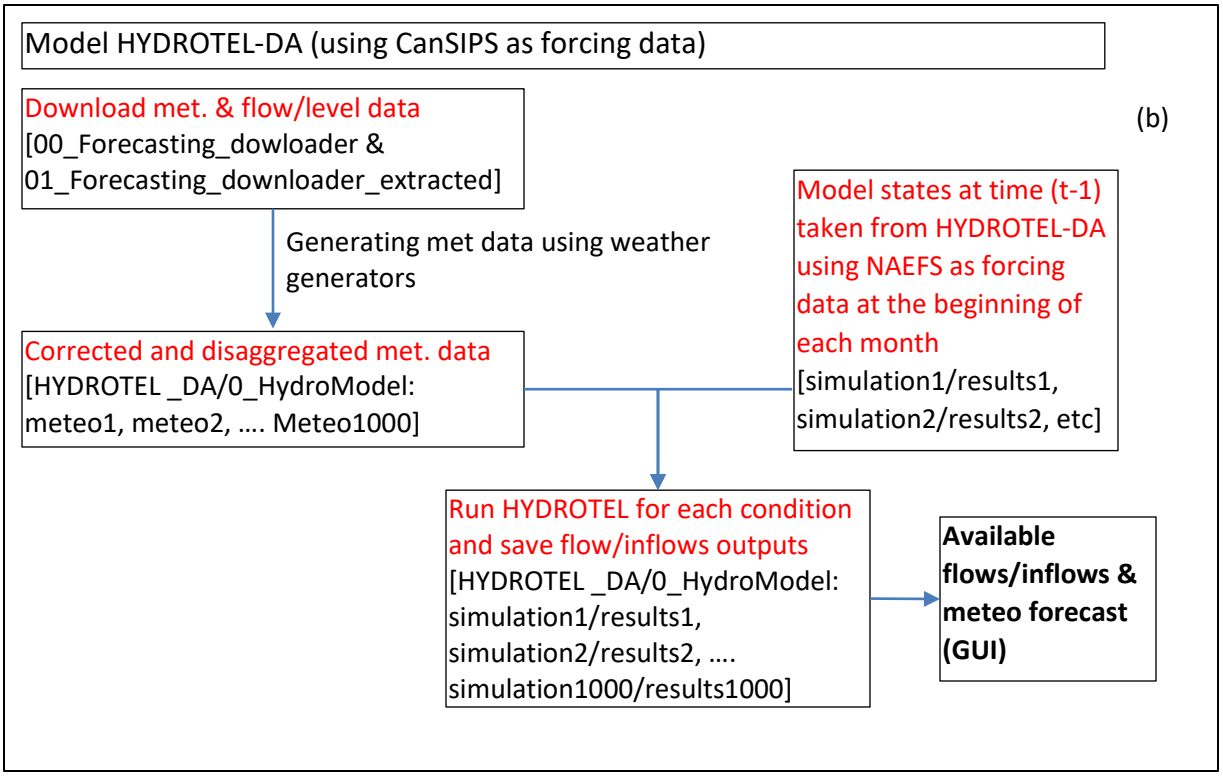

Figure 2.22 Forecasting system flow chart (including working directory) for both NAEFS (a) and CanSIPS (b) meteorological forecasting ensembles.

The forecasting system operates in a step-by-step fashion as follows:

1. Automatic download and correction of the NAEFS meteorological ensemble forecast and, if available, download correction and disaggregation of CanSIPS meteorological ensemble forecast. CanSIPS data are monthly values that need to be downscaled to daily value in order to be used with HYDROTEL. The time-downscaling procedure uses a weather generator developed by YU.

2. Automatic download and update of the hydro data recorded by the hydrometric stations; including flows and water levels. Also the user can update manually the required data; including snow course measurements;

3. Errors (white noise) are added to recorded hydrometric data and weather forecast data in order to produce multiple hydrological simulations and state variable values including simulated flows/inflows.

4. For NAEFS, the data assimilation is first applied on the previous-day simulated hydrological state variables. This procedure attempts to correct and update the previous-day simulated state variables to better represent the corresponding flows or calculated inflows. Updated and corrected previous-day hydrological state variables then act as initial conditions for the current day and following forecast.

5. Run HYDROTEL in a forecast mode using the initialized ensembles of hydrological state variables with the ensemble of meteorological forecast to get flow/inflow forecasts. For CanSIPS monthly forecast, the initial conditions correspond to the average of the previous month of the daily NAEFS corrected hydrological state variables conditions. Note that CanSIPS forecasts are updated at the beginning of each month (i.e., first day of the month).

6. The GUI displays historical results from the coupled HYDROTEL-Data assimilation procedure and measured flows or calculated inflows as well as forecasted inflows/ flows based on NAEFS or CanSIPS ensemble forecast.

Figure 2.23 presents a screenshot of the hydrological forecast system GUI with annotated numbers for further description.

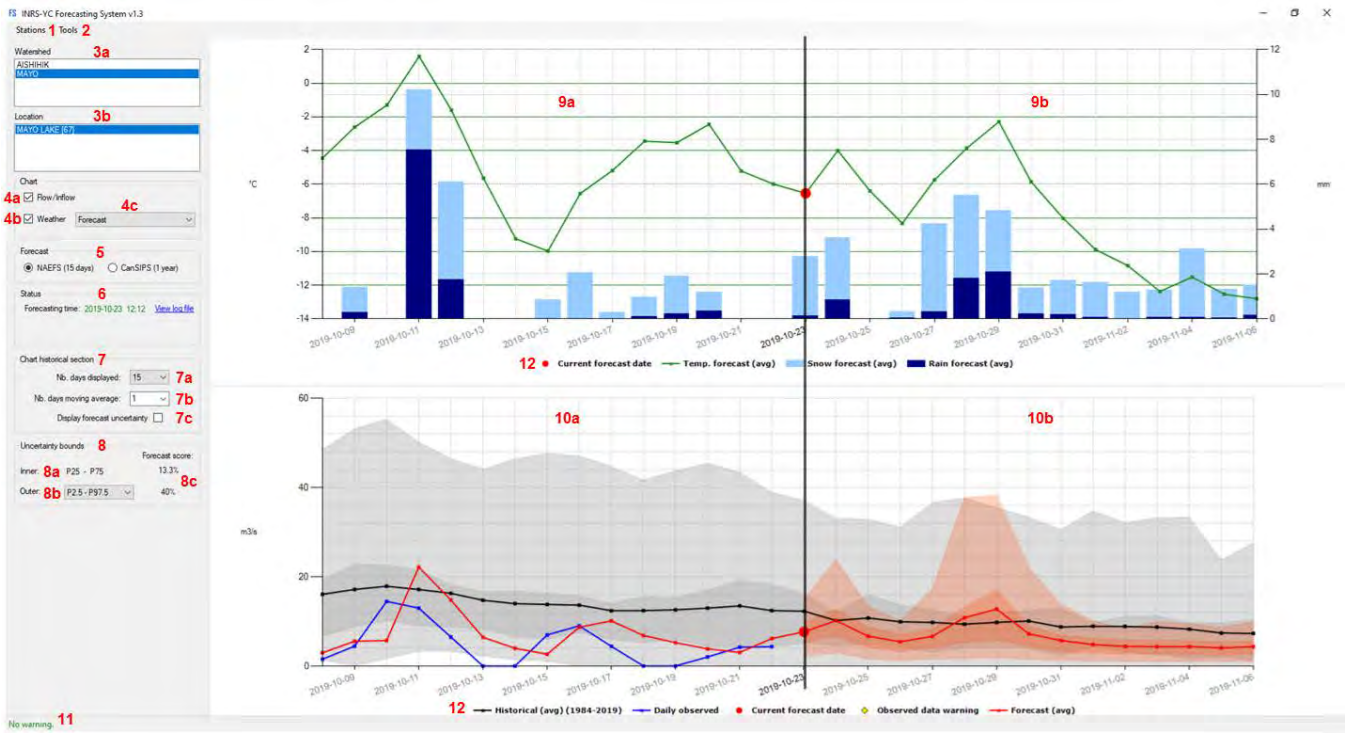

Figure 2.23 Screenshot of the hydrological forecast system GUI.

The following list describes the hydrological forecast system GUI using the annotated numbers (see Figure 2.23).

1. The Stations menu gives an access to all the data recorded at the meteorological stations, hydrometric stations (including inflows calculation) and snow survey sites. The user can have access to the stations list. By clicking on any station of the list, the user can then modify, and update manually observed records. Stations can also be added or removed from the list. Also note that the forecasting system cannot automatically update the snow data and the user must add them manually when they become available. Figure 2.24 gives an example of the user access to the stations.

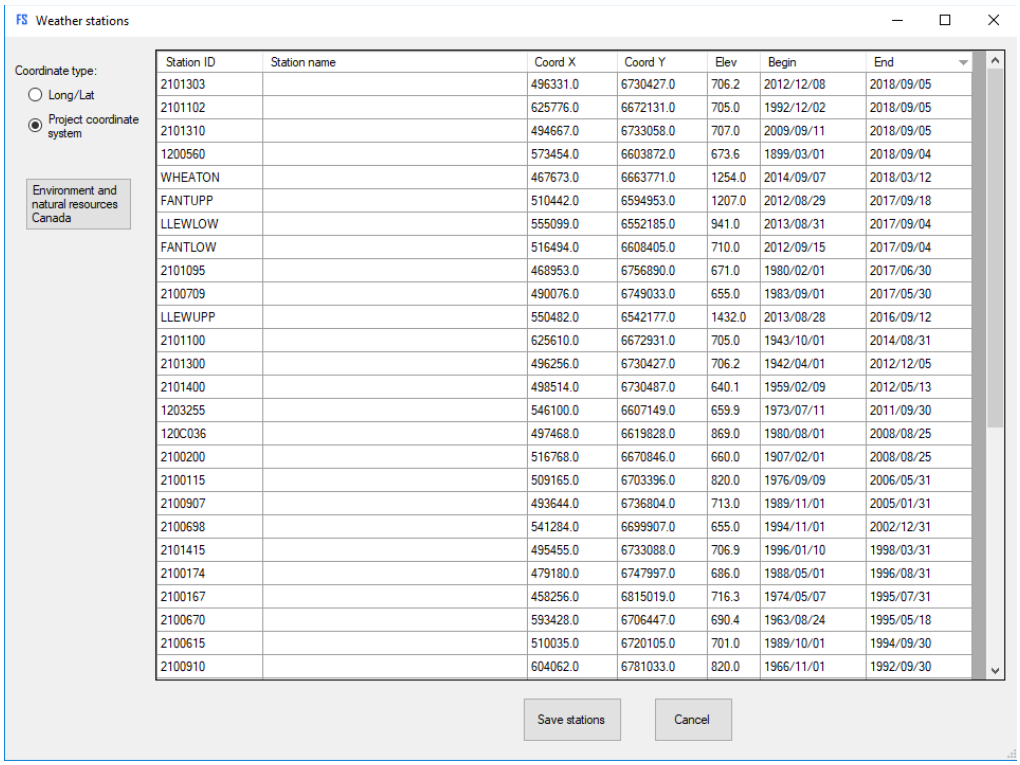

Station ID	Station name	Coord X	Coord Y	Elev	Begin	End
2101303		496331.0	6730427.0	706.2	2012/12/08	2018/09/05
2101102		625776.0	6672131.0	705.0	1992/12/02	2018/09/05
2101310		494667.0	6733058.0	707.0	2009/09/11	2018/09/05
1200560		573454.0	6603872.0	673.6	1899/03/01	2018/09/04
WHEATON		467673.0	6663771.0	1254.0	2014/09/07	2018/03/12
FANTUPP		510442.0	6594953.0	1207.0	2012/08/29	2017/09/18
LLEWLOW		555099.0	6552185.0	941.0	2013/08/31	2017/09/04
FANTLOW		516494.0	6608405.0	710.0	2012/09/15	2017/09/04
2101095		468953.0	6756890.0	671.0	1980/02/01	2017/06/30
2100709		490076.0	6749033.0	655.0	1983/09/01	2017/05/30
LLEWUPP		550482.0	6542177.0	1432.0	2013/08/28	2016/09/12
2101100		625610.0	6672931.0	705.0	1943/10/01	2014/08/31
2101300		496256.0	6730427.0	706.2	1942/04/01	2012/12/05
2101400		498514.0	6730487.0	640.1	1959/02/09	2012/05/13
1203255		546100.0	6607149.0	659.9	1973/07/11	2011/09/30
120C036		497468.0	6619828.0	869.0	1980/08/01	2008/08/25
2100200		516768.0	6670846.0	660.0	1907/02/01	2008/08/25
2100115		509165.0	6703396.0	820.0	1976/09/09	2006/05/31
2100907		493644.0	6736804.0	713.0	1989/11/01	2005/01/31
2100698		541284.0	6699907.0	655.0	1994/11/01	2002/12/31
2101415		495455.0	6733088.0	706.9	1996/01/10	1998/03/31
2100174		479180.0	6747997.0	686.0	1988/05/01	1996/08/31
2100167		458256.0	6815019.0	716.3	1974/05/07	1995/07/31
2100670		593428.0	6706447.0	690.4	1963/08/24	1995/05/18
2100615		510035.0	6720105.0	701.0	1989/10/01	1994/09/30
2100910		604062.0	6781033.0	820.0	1966/11/01	1992/09/30

Figure 2.24 User access to the stations (ex: Meteorological stations).

1a Hydrometric (a.k.a. hydrological) data section: this section regroups the available operations related to hydrometric data including calculated lake inflows.

The station button gives access to the list of hydrometric stations. By clicking on any station included in the list, the user can view the hydrometric records (flows, water levels, lake inflows). Stations can also be added or removed from the list.

1b Meteorological data section: this section regroups the available operations related to meteorological data including measured snow data.

The station button provides an access to the list of meteorological stations. By clicking on any station of the list, the user can then modify and update manually the meteorological records. Stations can also be added or removed from the list.

1c The snow station button provides access to the list of snow course stations. By clicking on any station of the list, the user can then modify and update manually the snow conditions. Note

that the forecast system cannot automatically update the snow data and the user must add new data manually when they become available.

2. The Tools, Settings menu gives a direct access to the existing projects available in the forecasting system and the time of day at which the system is updated (i.e. the time of the day at which the system starts the forecasts). Figure 2.25 shows the tools menu window.

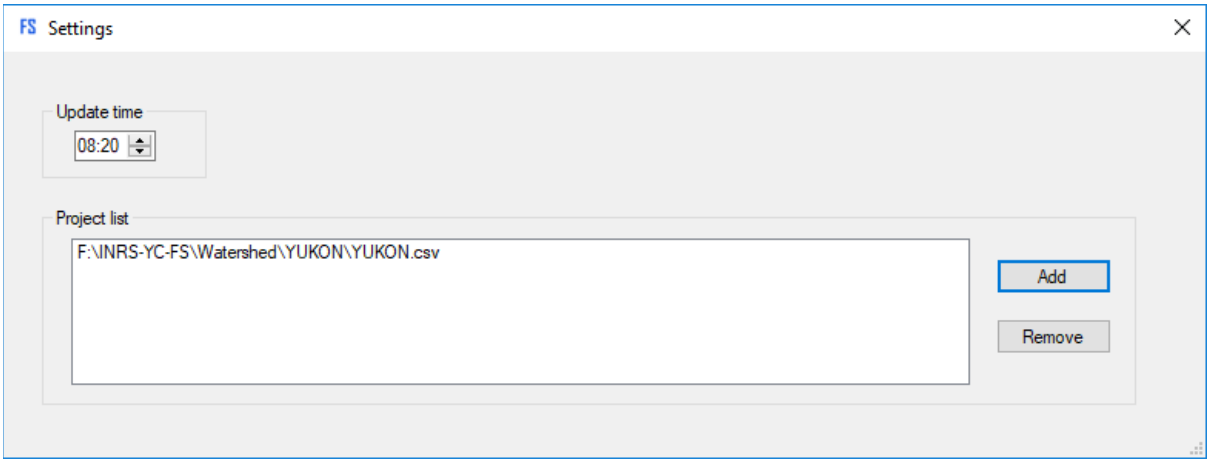

Figure 2.25 Tool menu window.

2a. The Tools, Export Data menu can be used to export the data that are saved in a local MS-SQL Server database if applicable. Note that this menu will be disabled in case there are no MS-SQL Server database configured in the FSsvc.ini file. Those data are the same that the one saved in the local file of the system (forecast_naefs_xxx.csv, forecast_cansips_xxx.csv, \ObservedFlowDA*.txt).

3. Watershed section: this section regroups the available watersheds and the available locations within the watershed.

3a. Watershed list: (Aishihik, Mayo, Upper Yukon or Marsh). Allows the user to change the current selected watershed. Each watershed managed by the system is displayed in the list.

3b. Location list: Allow the user to change the current selected location. The list displays the available locations for the current selected watershed. Each location corresponds to a river segment or lake in the hydrological model. The name and the identification number are

displayed. The chart area displays the data for the current selected watershed and location. The listed locations also correspond to the available forecasts for the current project (watershed) (ex: Sekulmun River, or Aishihik Lake inflows for the Aishihik Watershed).

4. Chart section: this section allows the user to select which chart will be displayed. It can be the weather chart, the flow/inflow forecast chart or both.

   4a. Displays or hides the flow/inflow forecast chart.

   4b. Displays or hides the weather chart.

   4c. Allows the user to select which type of weather chart to display. The weather chart displayed can be one of the following chart: Forecast, Historical avg. temp., Historical tot. prec. cumul., Historical rain cumul., Historical snow cumul.

   - Forecast: displays the forecast of the temperature and precipitation coming from the NAEFS or CanSIPS forecasts after being interpolated by the HYDROTEL simulations. The data displayed are average of the results from the 1000 HYDROTEL simulations.
   - Historical avg. temp.: this chart presents the historical observed temperature along with the temperature forecast.
   - Historical tot. prec. cumul.: Cumulative historical and forecasts of total precipitation.
   - Historical rain cumul.: Cumulative historical and forecasts of rain precipitations.
   - Historical snow cumul.: Cumulative historical and forecasts of snow precipitations.

   The start (reset) date of the cumulative data is October 1st.

5. Forecast section: this section regroups the available NAEFs (14 days) or CanSIPS (1 year) forecasts. The user can select the displayed information.

6. Status section: this section informs the user of the last forecasting date and time and gives an indication of whether there are warnings or not. The green color indicates that the system is up to date and that there are not any warnings, while the red color indicates the system is outdated or running in warning mode. Note that in the case of a long-term error of the system, a manual update of the NAEFS, CanSIPS or observed flows/inflows data files may be needed as the data may be no

longer available on the Environment and Climate Change Canada website. As a reminder the CanSIPS forecasts are only renewed at the beginning of each month. Thus, running the forecast past the beginning of the month would end up with results identical to those obtained at the beginning of the month except in the case of modification of snow data and snow assimilation process based on updated or newly available snow measurements.

Forecast warning can be one of the following:

- « *Warning: missing NAEFS forecast data*. »: The forecast was issued without the NAEFS data of the current day because they could not be downloaded. The data of the last downloaded files are used instead of those of the current day.
- « *Warning: missing hydrometric data*. »: The forecast was issued without the hydrometric data of the current day because they could not be downloaded. The last flow forecast is used instead of the measured data.
- « *Warning: missing NAEFS forecast and hydrometric data*. »: The forecast was issued without the NAEFS and the hydrometric data of the current day because they could not be downloaded.
- « *Warning: missing NAEFS forecast and/or hydrometric data for more than one day*. »: The forecast was issued without the up to date NAEFS and hydrometric data for more than one day.
- « F*orecast is out-of-date*. »: This message is shown when the date of the forecast is prior to the current day.

7. Historical charts section: this section regroups the different available functions linked to the generated historical charts section (see number 9a and 10a on Figure 2.23).

   7a. Number of historical days (prior to current forecast) displayed on the chart. Number of days for NAEFS (15, 30, 90, 180, 365, ALL) or months for CanSIPS (12, 24, ALL).

   7b. Numbers of consecutive days used in the calculation of the moving average of forecasted flows/inflows in the historical portion of the graph. Note that this number does not affect the number of days used for daily inflow calculation.

   7c. Checkbox to allow the user to display or not the forecast uncertainty bounds for the historical part of the chart.

8. Uncertainty bounds section: this section regroups the different available information and options linked to the generated chart section.

   8a Uncertainty inner bounds. The uncertainty inner bounds are fixed to value of 25-75%. The bounds are displayed in darker gray and red.

   8b. Selection box of the illustrated uncertainty outer bounds (None, Min – Max, 2.5-97.5%, 5-95%, 10-90%, 25-75%) displayed in light gray and light red.

   8c. Forecast score, that is the percentage of forecasted values within the the inner and outer uncertainty bounds.

9. This annotation only indicates the historical part (9a) and forecast portion (9b) of the chart for the weather data.

10. This annotation only indicates the historical part (10a) and forecast portion (10b) of the flows or calculated inflows and simulated/corrected flows or inflows with uncertainties.

11. Status bar displays the overall status of the system. Warning message will be displayed in case there is at least one effective warning for one of the watersheds managed by the system. If every watersheds forecast are in «OK» condition, the message «No warning» will be displayed. To get more detailed information of the system status and events, the contents of the log file can be viewed by clicking the link «View log file» in the «Status» section (6) of the interface.

12. Graph legend file: Black line with gray shade corresponds to the historical flows and they are computed using all of the observed data available. The average for each day is displayed as well as inner and outer bounds; Blue line corresponds to the daily or monthly observed flows / inflows values. Forecasting date corresponds to the first day of the current forecast. When the forecast is up to date, this is actually the current day or current month. Each forecast contains 14 days for NAEFS and 12 months for CanSIPS. Red line with red shade corresponds to the forecast results. The forecast are computed using the results of 1000 simulations. The average for each day is displayed as well as inner and outer bounds.

It is noteworthy that throughout the duration of the project great efforts were dedicated to increasing system robustness and portability according to autonomous working mode and development process.

3. Permafrost and multilayer snow modules

3.1. Permafrost module

3.1.1. General methodology and literature review

A warming climate can induce thawing of permafrost and activate deeper groundwater flow paths resulting in greater base flow and affecting the overall hydrological dynamics of a watershed (Slaughter *et al.*, 1995, Kurylyk *et al.*, 2014). For example, in near-arctic landscape and ecosystem, Karlsson *et al.* (2011) illustrated how climate change leads to a reduction of the permafrost areal extent as well as significant hydrological changes. Saito *et al.* (2007) concluded that by 2100, a significant proportion of permafrost will become a deeper active layer, highlighting the importance of simulating the thawing process in hydrological studies (see, for example, Wellmann *et al.*, 2013, Wright *et al.*, 2009). In the Wolf Creek watershed in southeastern Yukon, where discontinuous permafrost is present, Carey *et al.* (2013) explained that a considerable portion of the snowmelt discharge results from near-surface saturated soil melt. Indeed, in this watershed, Rasouli *et al.* (2014) found that permafrost degradation and ground thaw have been induced by an overall warming climate. Given the potential impacts of permafrost thaw on watershed hydrology, several authors have proposed various simulation models. Kurylyk *et al.* (2014) presented several mathematical theories and simulation tools, including analytical solutions for subsurface heat transport with freezing and thawing. Riseborough *et al.* (2008) summarized recent advances in permafrost modelling while focusing on the Stefan Model, which is a widely used analytical equation (*e.g.* Williams et *al.,* 2015). Hayashi *et al.* (2007) introduced a simple heat transfer model to simulate the thawing of the permafrost's active layer and provided a methodology that can be integrated into a hydrological model. Their results corroborated the field data from a wet, organic-covered watershed in a discontinuous permafrost region of northwestern Canada. There are also other models which are based on the complete energy balance (*e.g.* Lehning *et al.,* 2006). However, input data and intensive computational requirements are not well suited for hydrological forecasting systems relying on modest resources.

In general, current permafrost models are all composed of a soil thermal model and a soil moisture model. For instance, the Variable Infiltration Capacity (VIC) model, which is one of the most known hydrological models, has a permafrost component (Cherkauer and Lettenmaier, 1999). The snow module in VIC is based on soil thermal and moisture models operating at hourly time steps. The model has demonstrated a decent performance in the permafrost study areas for runoff simulation. However, it overestimates the runoff in a discontinuous permafrost region.

In Yukon, due to lack of information for permafrost depth, ice content, and soil temperature, it is necessary to look for other sources of information. This has not been a successful effort so far.

It is theoretically possible to build a permafrost module in HYDROTEL by coupling the soil thermal models, such as the Rankinen or Thorsen models, to the vertical water budget module (BV3C). In fact, when the soil layer has a negative temperature, infiltrated water can be considered as frozen, which means that it will not flow through the soil layer. The definition of permafrost implies that this stagnant water has to be frozen for two consecutive years.

While building a permafrost model with the tools already available in HYDROTEL is conceivable, the limiting factor is the availability of data for permafrost depth and soil temperature for model validation. Such information is required in order to compare the performance of HYDROTEL against those that has already been tested in the field (e.g. VIC). Therefore, given the fact that permafrost is not prevalent in either one of the studies watersheds, this research activity was not pursued in this project.

3.2. Snow module

3.2.1. General methodology and literature review

Hydrological models vary greatly in terms of their snow modules, from simple empirical degree-day models to complete thermodynamic models, explicitly simulating energy and mass exchange through the whole snowpack. The former group of snow models (*a.k.a.* one-layer models) have been shown to accurately simulate point-scale snow accumulations as well as snowmelt (*e.g.* SRM: Martinec, 1975; Abudu *et al.*, 2012). Meanwhile, thermodynamic snow models (e.g. SNTHERM: Jordan, 1991, CROCUS: Brun *et al.*, 1989, 1992, or SNOWPACK: Bartelt and Lehning, 2002, to name a few) simulate the

snowpack's stratigraphy and energy exchange between the snow layers. Langlois *et al.* (2009) recently showed that these multi-layer models could produce satisfactory snow water equivalent (SWE) estimates over boreal environments. However, they require extensive meteorological data and structural information on snow cover. Moreover, when simulating watershed discharge with SAC-SMA (Finnerty *et al.*, 1997; Burnash, 1995), Franz *et al*. (2008) illustrated that a more complicated model with several layers (e.g. SAST: Jin *et al*, 1999a,b) may not necessarily perform better than a simple monolayer model (e.g. SNOW17: NWS, 2004). Essery *et al.* (2013) compared several models and concluded that there is no "best" model, but rather a group of model configurations that can provide consistently satisfactory results.

The snow module, which is currently available in HYDROTEL, is a single-layer, mixed degree-day/energy balance (DD/EB) model (Fortin *et al.*, 2001; Turcotte *et al.*, 2003, 2007) requiring daily minimum and maximum air temperatures and precipitation as input data. The model simulates five snowpack state variables; namely SWE, snow depth, heat deficit, liquid water content, and surface albedo. The following processes are modelled based on empirical relationships: melt at the air/snow interface, melt at the ground/snow interface, compaction rate, time-dependent albedo, and liquid water retained by the snow cover. Using a 5-year ground-based gamma ray monitoring and flow measurement in a boreal watershed in northern Quebec, Oreiller *et al.* (2014) compared simulations of SWE and streamflow with two contrasting approaches. In the first approach, the current HYDROTEL module was calibrated, and a small number of inputs were required, while in the second approach, known as the CROCUS (Brun *et al*., 1989, 1992), a large number of inputs were used and no calibration was performed. Results indicated that after accounting for blowing snow sublimation and relocation based on a simple parameterisation (effective once a certain wind speed threshold is reached), CROCUS performed better than the current DD/EB model. In addition, streamflow simulations showed that the main peak flow was captured with CROCUS too. However, the second peak resulting from delayed snowmelt from forested areas was not reproduced due to the lack of sub-canopy radiation data. Results also highlighted the lack of thermal inertia associated with a single-layer model. More specifically, for a specific spring, a sudden and unexpected loss of one third of the simulated SWE was manifested by the DD/EB model due to seven days of warm weather conditions with daily maximum temperatures above 0°C and highs near 10°C. In such cases, CROCUS was shown to provide better results. In general, these results illustrate that there is

a potential trade-off between the simple single-layer model and the multi-layer model. For northern environments, such as the Yukon Territory, blowing snow and snowpack sublimation (*e.g.* Pomeroy *et al.* 2012, MacDonald *et al.* 2009, Musselman *et al.* 2015), besides other processes such as snow redistribution (*e.g.* MacDonald *et al*. 2009) can result in additional challenges too. Depending on the topography, climatic conditions, wind speed, and land cover, the impact of sublimation can vary greatly, while different types of sublimation (e.g. blowing snow sublimation, drifting snow sublimation, among others) can become more or less important.

Given the above details, the focus of this study was to assess and improve the DD/EB model in HYDROTEL given SWE data collected in Yukon and derive/adapt a two- or multi-layer snow module that can account for snow sublimation and redistribution. The MASiN model (Mas, 2016), the MISBA model of Islam and Gan (2015), and the Distributed Snow Model (DSM) of Musselman *et al.* (2015) provided the starting inspiration to modify the snow model in HYDROTEL, with an upper snow layer and a lower snow layer interacting with the atmosphere and the soil, respectively. Since snow tends to accumulate first and melt last in potholes, for snow redistribution purposes, a topography-based concept could be explored as well. Meanwhile, simulated SWE was assessed against snow surveys conducted by NCE and Yukon Government as well as ground-based gamma ray data monitored in the Upper Yukon River watershed by YEC.

The MASiN multi-layer snow model (Mas, 2016) applies the energy and mass balance rather than a DD equation. It has been applied to several study sites in Canada and Sweden. The model was compared against two empirical models: those of Farbrot and Hanssen-Bauer (2009) and Baraer *et al*. (2010), and the mixed DD/EB of HYDROTEL. The results showed that MASiN could achieve better performance on average than any of the aforementioned models.

Complexity varies significantly between the existing snow models and often requires a certain level of parameterization to account for snow cover dynamics. However, parameter values are not always known *a priori*; at best a range of values might be known, and thus, model calibration is required. Hence, snow models can have a different number of parameters to be calibrated. In this study, the conceptual CEMANEIGE model (Valéry, 2010) with a few calibration parameters was compared to HYDROTEL and MASiN, both of which have several calibration parameters. CEMANEIGE is a single-layer DD model. The

model requires the distribution of meteorological data into five different altitude classes of equal areas. However, given the computational structure of HYDROTEL, which is based on the average altitude of each RHHU, the five classes of altitude were considered into only one at the time we conducted this work package. It is noteworthy that the latest version of HYDROTEL implemented on the Upper Yukon River watershed, and used for the hydroclimatic impact assessment study presented in Chapter 6, was adapted to run using elevation bands.

The aforementioned models were calibrated with respect to SWE and observed stream flow data in order to understand the impact of selecting one objective function at the expense of the other, and vice versa. In other words, we wanted to know what would be the trade-off between having a snow model calibrated with respect to a discrete state variable such as SWE with the capacity of the model to reproduce the observed hydrograph. To achieve this objective, each snow model was coupled loosely to HYDROTEL (i.e. the input data of each model were supplied by HYDROTEL, either partially or in full, while their output were inserted back into HYDROTEL for runoff simulation).

Secondly, although MASiN is a multilayer snow model, where the maximum number of snow layers to simulate can be parametrized, only 70 layers were considered by the authors to optimize the estimation of energy and mass flux between each snow layer. Furthermore, given the fact that the model runs at hourly time steps, the parametrisation practice was investigated to define the optimal trade-off between computational budget and model performance with respect to SWE estimation. In fact, decreasing the maximum number of layers during the simulation can limit the interaction between different snow layers and thus reduce the computational effort. Armstrong (1980), Arndt and Paul (2018), Brun et al. (1992), and Monti et al. (2012) have provided an overview of the number of snow layers that can be naturally observed. Based on their findings, in this study, it was decided to consider a range of 1 to 20 snow layers in order to maintain the consistency with the aforementioned articles.

3.2.2. Research framework

Data sites

For the comparison of snow models, SWE and streamflow data were required. For SWE calibration, the study sites are located within the boundaries of the Upper Yukon River watershed, including Lower

Fantail (LF), Lower Llewellyn (LL), Upper Fantail (UF), Upper Llewellyn (UL) and Wheaton (WN), where data are available between 2013 and 2017. Due to quality concerns with SWE observations, data from Upper Fantail and Upper Llewellyn GMON stations were removed from the study. Furthermore, for the remaining three stations, since accurate precipitation measurements were not available, precipitation data were reconstructed based on the observed SWE. For streamflow calibration, hydrometric data measured at the location of the following hydrometric stations between 1994 and 1995 were considered for a warming period of calibration and between 1995 and 2005 for the estimation of the performance: 09AA006 (Atlin River), 09AA012 (Wheaton River), 09AA013 (Tutshi River), and 09AB001 (Yukon River at Whitehorse).

For the SWE simulation, meteorological data were obtained from nearby meteorological stations, and for runoff simulation, meteorological data were downscaled at the RHHU level based on the weighted average of the three closest stations (i.e., inverse distance weighting).

Automatic model calibration/ efficiency coefficient

- Typically, snow models require the adjustment of different parameter values for simulating SWE or streamflow. A number of automated model calibration algorithms were selected and compared to highlight their strengths and weaknesses in achieving an optimal set of parameter values, including:
    - ‘Shuffle Complex Evolution’ by University of Arizona (SCE-UA) (Duan *et al*., 1992), which is based on a combination of probabilistic and deterministic approaches, and a systematic evolution of a complex set of points spanning the space in the direction of global improvement and competitive evolution.
    - ‘Dynamically dimensioned search’ (DDS) (Tolson and Shoemaker, 2007), which is a stochastic and heuristic method based on a single solution.
    - ‘Pareto archived dynamically dimensioned search’ (PA-DDS) (Asadzadeh & Tolson, 2009, 2013), which is the multi-objective version of DDS allowing the calibration to be performed based on several objective functions. A trade-off between the objective functions can be defined by the

user by estimating the Pareto front between them. For example, in this research, a trade-off was established between the accuracy of SWE and runoff simulations.

Automatic model calibration needs an efficiency criterion to be defined in order to rank the model performances. In this study, the applied criterion was the Kling-Gupta Efficiency (KGE; Gupta *et al*., 2009), given as follows:

$$KGE = 1 - \sqrt{(1 - {\mu_s}/{\mu_o})^2 + (1 - {\sigma_s}/{\sigma_o})^2 + (1 - r)^2} \quad (3.1)$$

where μ is the average of the data, σ is the standard deviation of the data, and r is the linear correlation coefficient. The simulated and observed data are denoted by the s and o subscripts, respectively. The value of KGE ranges from $-\infty$ to 1 from the lowest to highest performance, respectively.

Snow models

In this study, three snow models were initially considered to be mutually compared, but only two were ultimately evaluated. Indeed, each snow model has distinct characteristics. HYDROTEL has a single-layer snow module, whereas MASiN has a multilayer configuration. The CEMANEIGE snow model is a DD model, while HYDROTEL is a mixed DD/EB model. CEMANEIGE was removed from the list, since although it provides proper SWE estimates, it does not provide the other required data (e.g. snow cover depth and albedo) that can be used in HYDROTEL for runoff simulation. In fact, adding more hypotheses and parameters to CEMANEIGE, to have it coupled with HYDROTEL, would increase its complexity when compared to that of HYDROTEL snow model, while it benefits from the limited number of parameters to calibrate.

To run MASiN, the user can set the maximum number of snow layers to simulate. If this limit is exceeded, MASiN will merge some of the layers along with their respective physical characteristics. To test the full extent of the model, the maximum number of layers was set to 70. The model, however, requires more input data than HYDROTEL (e.g. hourly relative humidity and wind speed). To investigate the impact of the number of snow layers on the model's performance for simulating SWE, MASiN was calibrated for each possibility between 1 and 20 layers, and the calibrations were compared to the full extent of MASiN, which was run with 70 layers.

The snow module of HYDROTEL has a monolayer configuration, where the internal energy flux of the snow layer varies based on different factors, such as melting at the atmosphere/snow interface and the soil/snow interface, convection loss, etc. Therefore, it is interesting to investigate how such an internal flux of energy would work if a two-layer configuration were considered instead. Several theories have been developed in this regard, where different phenomena participating in the evolution of the snow cover are attributed to each layer. For example, the impact of the atmospheric heat, based on the vegetation at the atmosphere/snow interface, like a coniferous forest, is attributed to the top layer, while the heat from the soil is attributed to the bottom layer. At each time step, when the top layer melts, the excess water is infiltrated into the bottom layer to contribute to its warming. This excess water has thus the final temperature of the top layer when it reached its final state.

The first theory is based on the estimation of the thickness of each layer, at every time step during the melting period, based on physical laws. By applying the first principle of thermodynamic to a system, composed of only one snow layer, the change in internal energy of the system can be linked to a temperature gradient. Thus, the snow cover is discretized into two systems, where:

- The top border of the top layer is the atmosphere/snow interface and the bottom border of the bottom layer is the soil/snow interface.
- The bottom border of the top layer and the top border of the bottom layer are identical.

The thickness of each snow layer depends on the location of the border between the layers. For determining the border's location, the temperature gradient caused by the different phenomenon in each layer has to equalize temperatures at the border/interface between both systems. However, this scenario is disadvantageous when water retention and melting condition associated with the calorific deficit are considered into the global equation for both layers. In fact, equations resulting from these conditions can have several solutions since there are different combinations of possible final calorific deficit and water amounts retained in each layer. Determining a hypothesis for choosing the best condition to respect is too costly for the global development of this two-layer configuration. Furthermore, the potential to develop such a bi-layer version for winter is limited, since the heat-loss equation depends on the thickness of the layer. Such an equation is implicit and should be determined

through iteration at each time step. Therefore, developing a model of this type has the potential to increase the computational budget at an unrealistic level for operational purposes.

Therefore, another theory was developed to limit the computational budget. The thickness of each layer was defined based on the ratio of the bottom layer thickness to the thickness of the total snow cover. Three different scenarios were tested here:

- V4.0 - This ratio is calibrated and constant at each time step during the melting period:

$$ratio = ratio_{calibration} \tag{3.2}$$

- V4.1 - The calibrated ratio of V4.0 is combined with another ratio, estimated between the height of the snow cover during the current time step and the maximum height observed during the current winter:

$$ratio = \text{ratio}_{calibration} * \frac{height_{tot}(j)}{\max(height_{tot}(j))} \tag{3.3}$$

where $height_{tot}(j)$ is the initial height of total snowpack at time step j, and $\max(height_{tot}(j))$ is the maximum height observed during the current winter up to time step j.

- V4.2 - This ratio is only based on the height of the snow pack during the current time step and the maximum height observed during the current winter.

$$ratio = \frac{height_{tot}(j)}{\max(height_{tot}(j))} \tag{3.4}$$

Based on Tolson & Shoemaker(2008), the parametrization of DDS is as follows:

- 30 to 33 trials of 100 evaluations for the HYDROTEL snow model (depending on if any additional parameter is considered or not, like in V4.0 and V4.1 bilayer snow model configurations)
- 33 trials of 100 evaluations for MASiN snow model.

3.2.3. Results

Comments on automated model calibration

The choice of an automated model calibration represents an important step towards the determination of the optimal sets of parameters. Since some snow models required more computational budget than expected at the beginning of the study (e.g. calibration of MASiN by SCE-UA), it was decided to calibrate all the snow models with DDS, thanks to its capacity to achieve an optimal set of parameter values at a faster rate than SCE-UA.

Comparison of SWE calibrations

Each model was calibrated at each GMON site. Table 3.1 shows the performance of the 10 best parameter sets obtained by DDS calibration for the monolayer snow model in HYDROTEL, the physically-based snow model in MASiN, and the three different scenarios of bilayer snow models in HYDROTEL.

Table 3.1 Performance of each snow model (*i.e.*, KGE on SWE calibration) using the 10 best sets of optimized parameter values for LF (Lower Fantail), LL (Lower Llewellyn), and W (Wheaton).

Calibration based on	HYDROTEL monolayer	MASiN	HYDROTEL bilayer V1	HYDROTEL bilayer V2	HYDROTEL bilayer V3
LF	[0.935-0.951]	[0.967-0.977]	[0.931-0.974]	[0.930-0.964]	[0.944-0.966]
LL	[0.874-0.906]	[0.707-0.805]	[0.884-0.918]	[0.855-0.901]	[0.846-0.917]
W	[0.944-0.970]	[0.975-0.983]	[0.961-0.979]	[0.955-0.972]	[0.944-0.964]

The measurement uncertainty bound is based on the uncertainty described by Campbell Scientific for a CS275 sensor: ±15mm of the observed SWE when less than 300 mm and ±15% of the observed data when greater than 300 mm. The following graphs illustrate the observed data in black, the measurement uncertainty bound in grey. The model simulations are introduced in the following order: Monolayer HYDROTEL, V4.0, V4.1, V4.2, and MASiN, and their 10 best calibrations by DDS, for the modelling uncertainty, in color. Results of the Lower Fantail station are shown in Figure 3.1 to Figure 3.5, those of the Lower Llewellyn station are demonstrated in Figure 3.6 to Figure 3.10, and those of the Wheaton station are displayed in Figure 3.11 to Figure 3.15.

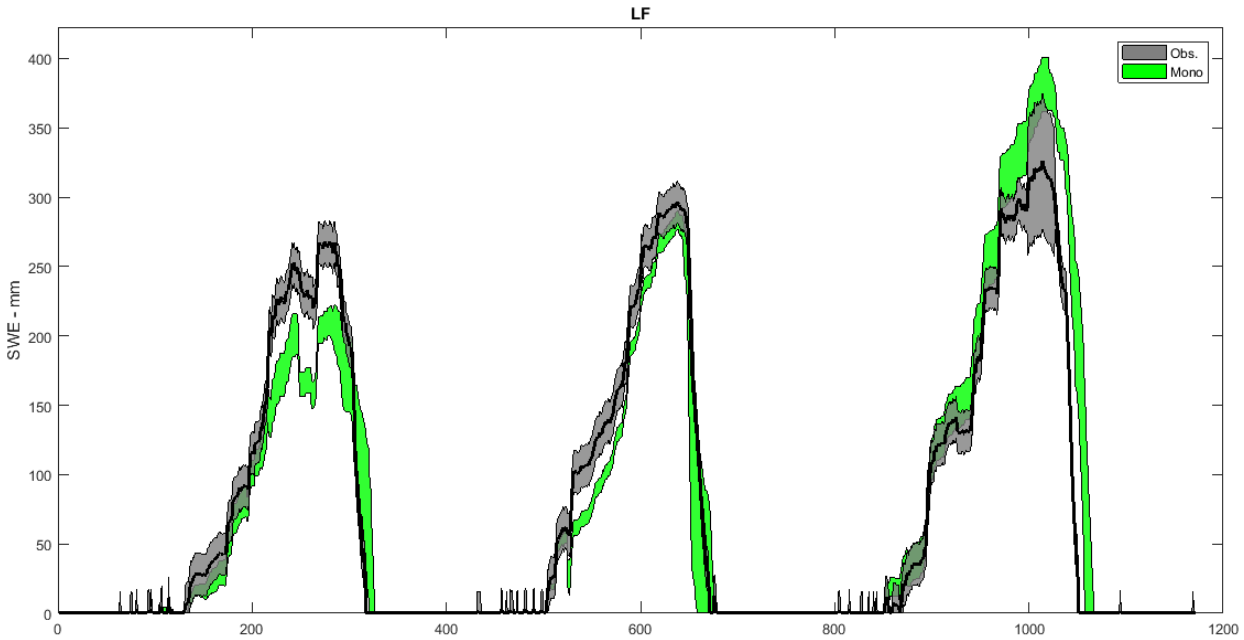

Figure 3.1 Simulations of monolayer model HYDROTEL at Lower Fantail station.

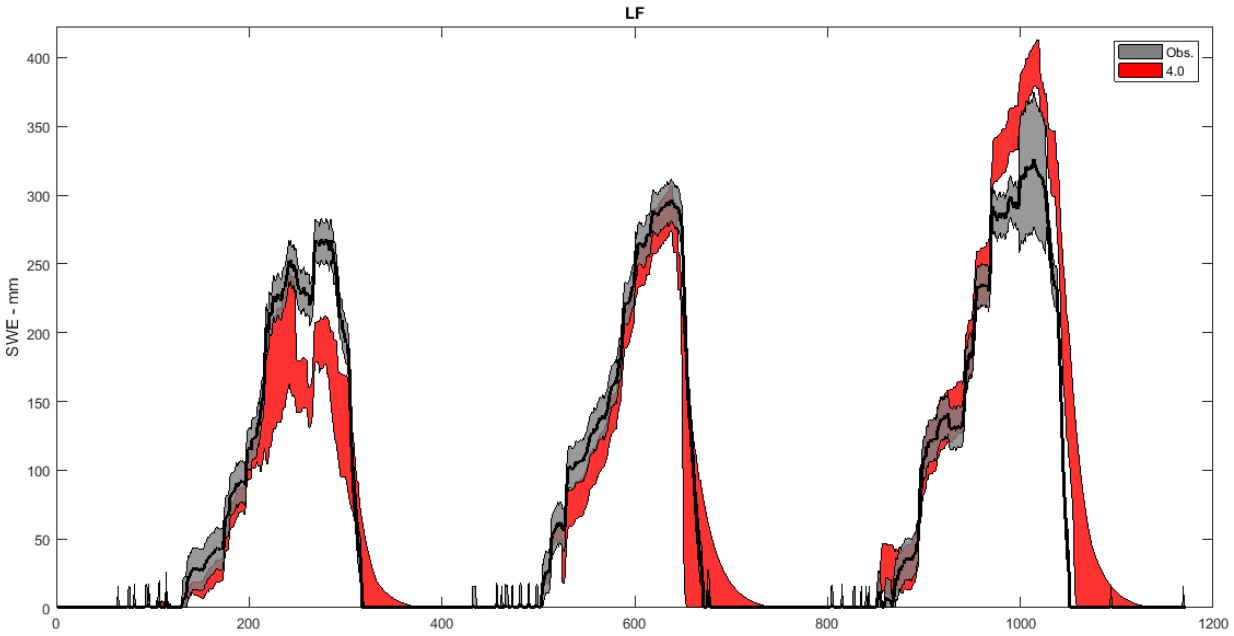

Figure 3.2 Simulations of V4.0 model at Lower Fantail station.

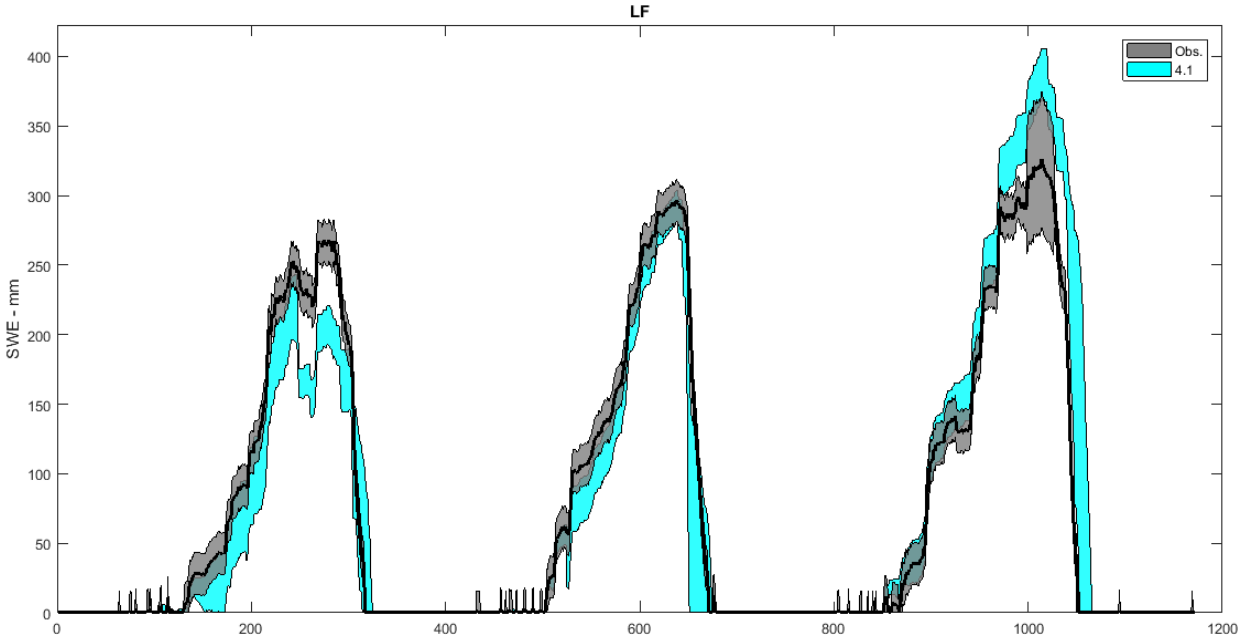

Figure 3.3 Simulations of V4.1 model at Lower Fantail station.

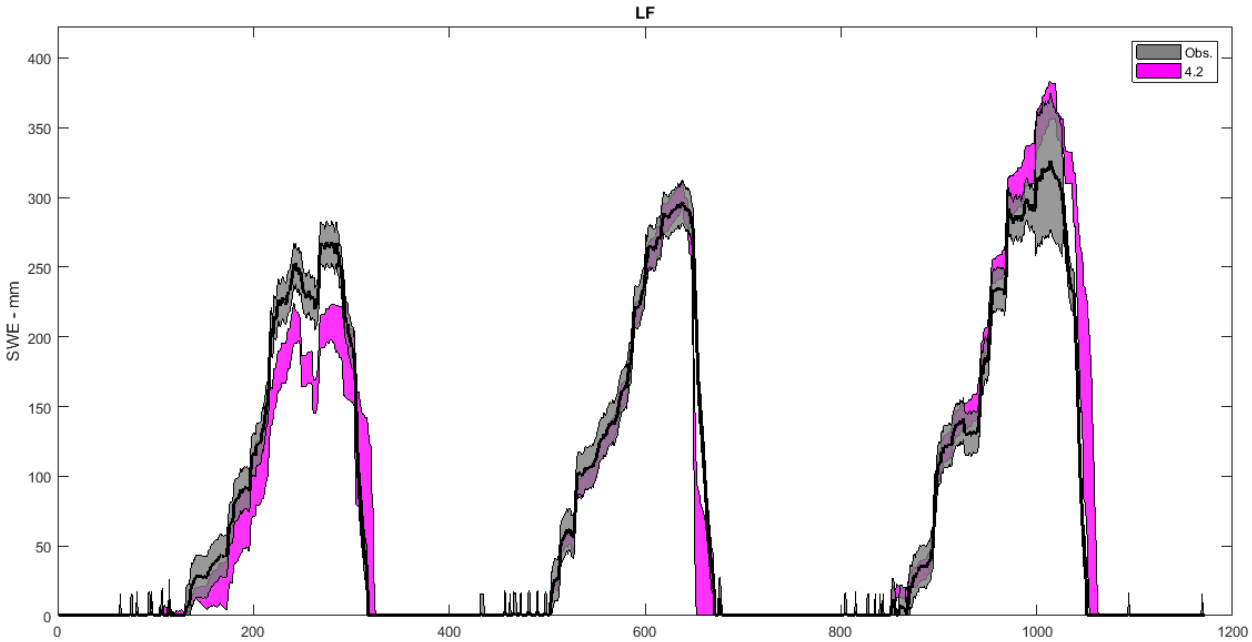

Figure 3.4 Simulations of 4.2 model at Lower Fantail station.

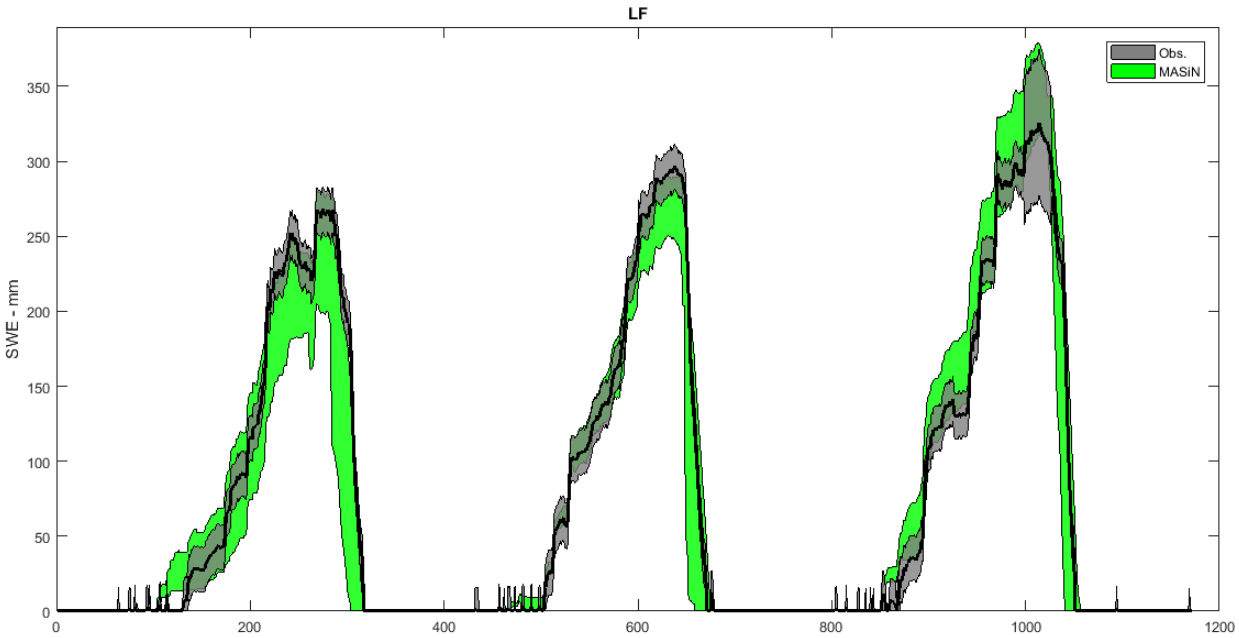

Figure 3.5 Simulations of MASiN model at Lower Fantail station.

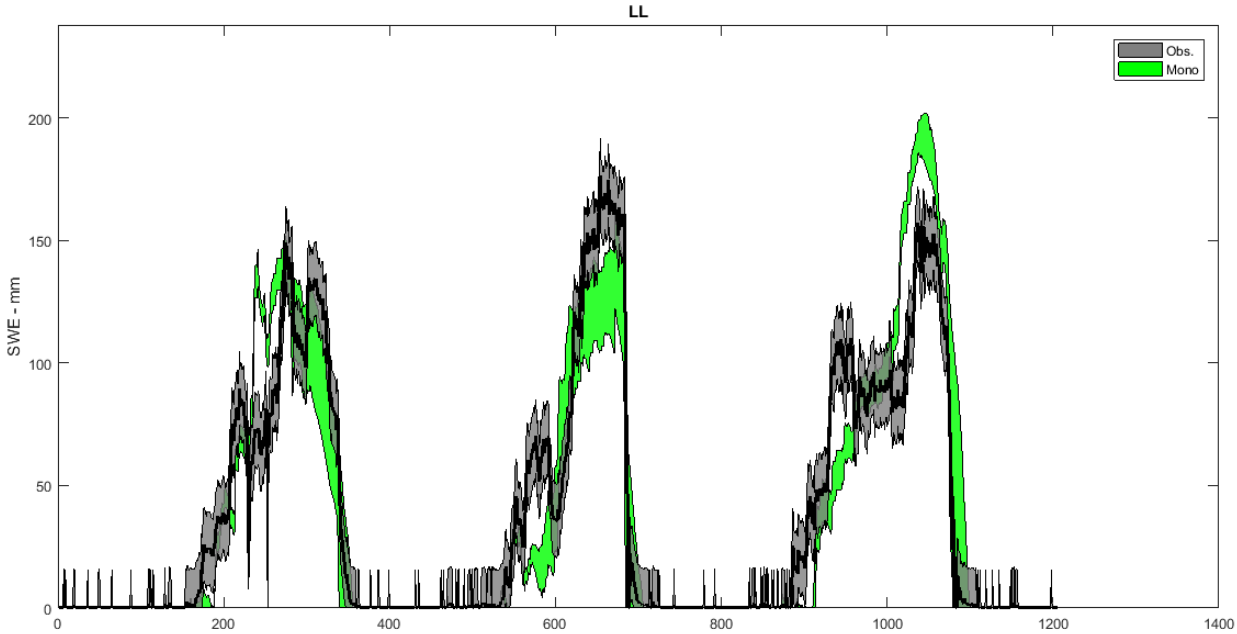

Figure 3.6 Simulations of monolayer model HYDROTEL at Lower Llewellyn station.

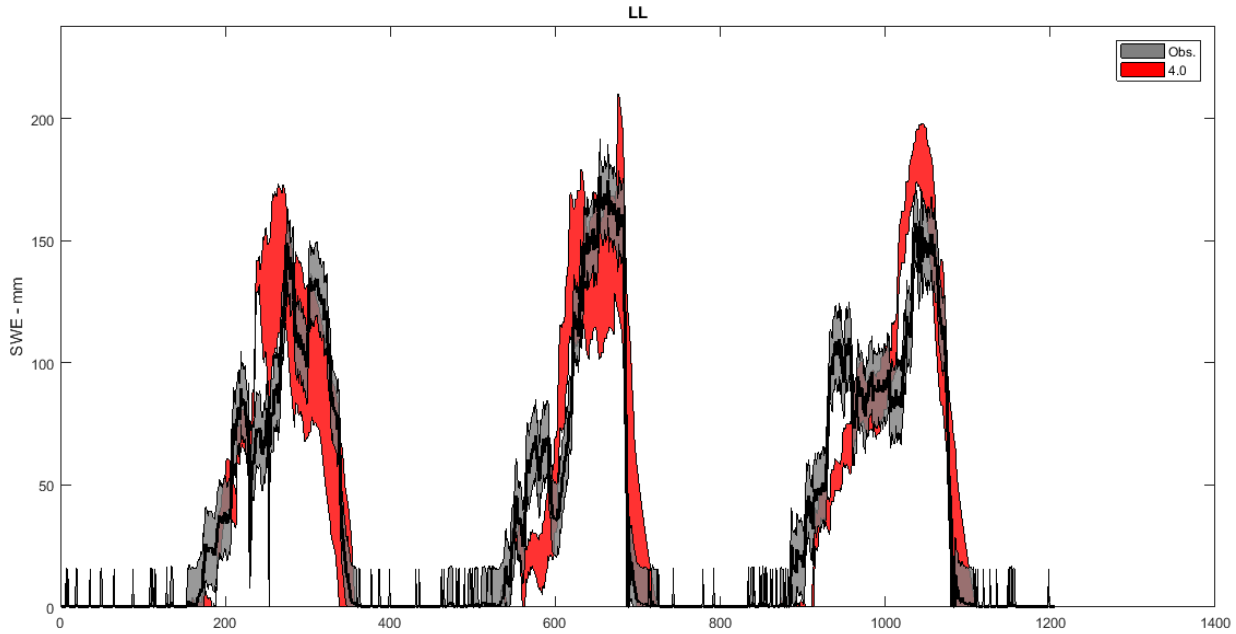

Figure 3.7 Simulations of V4.0 model at Lower Llewellyn station.

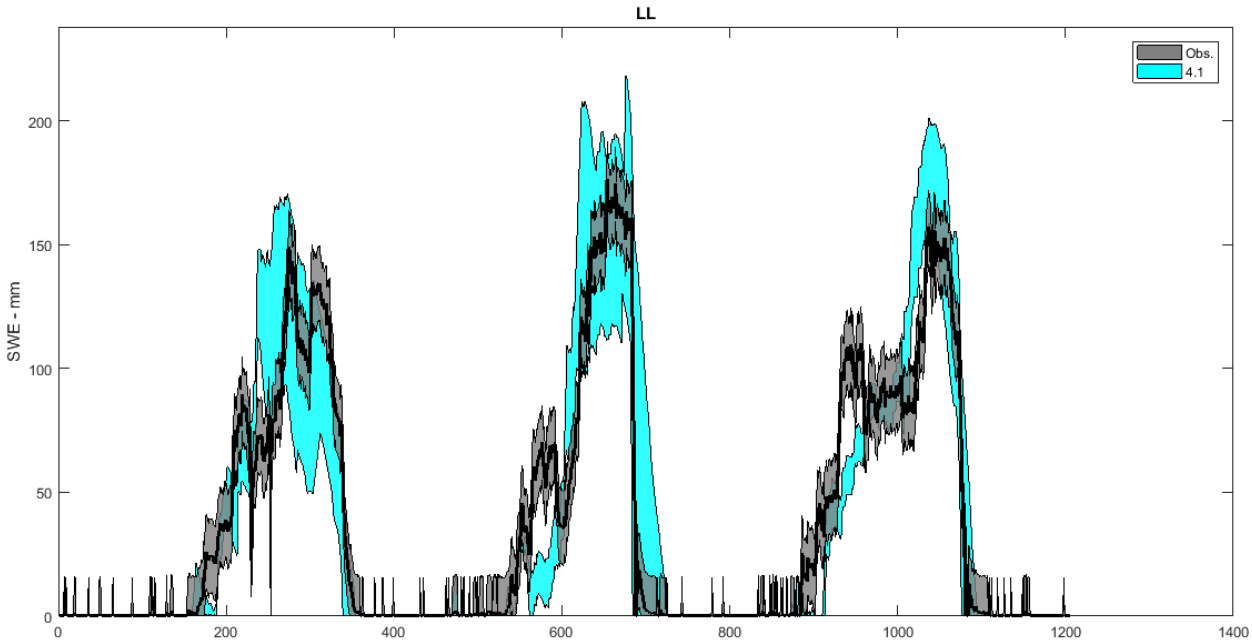

Figure 3.8 Simulations of V4.1 model at Lower Llewellyn station.

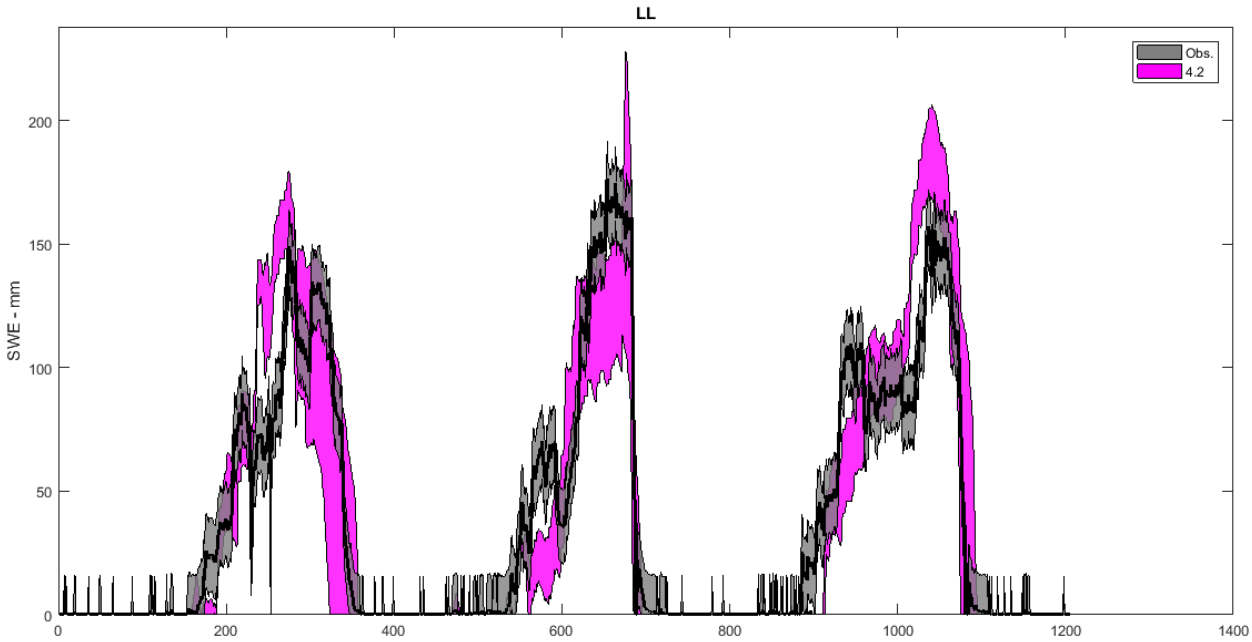

Figure 3.9 Simulations of V4.2 model at Lower Llewellyn station.

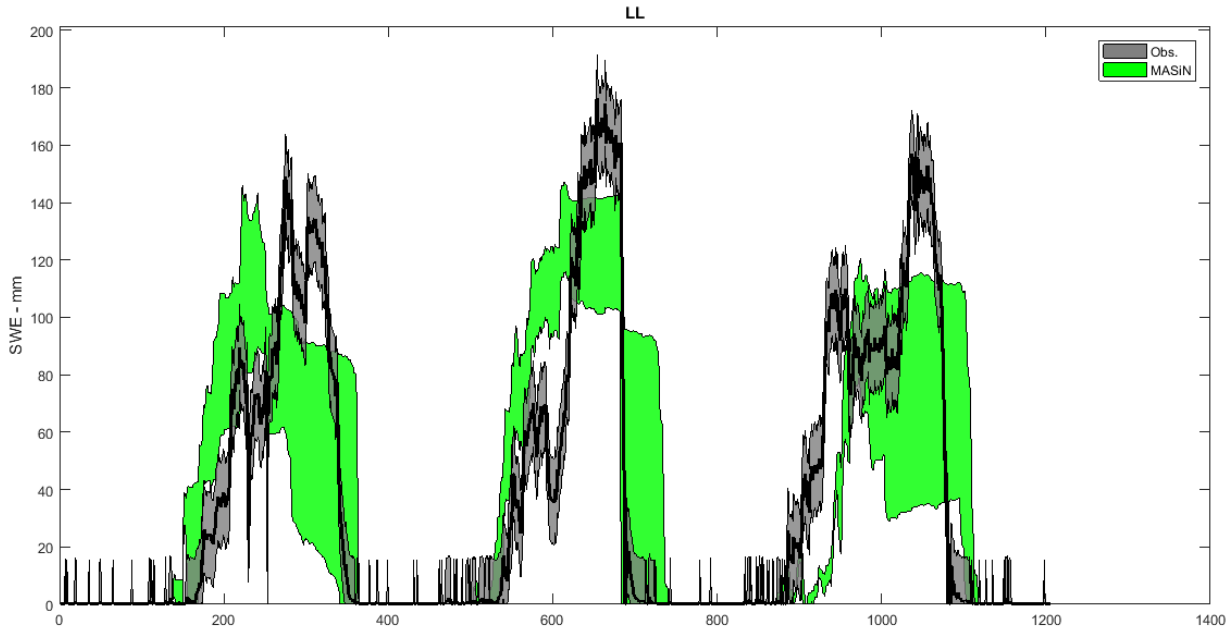

Figure 3.10 Simulations of MASiN model at Lower Llewellyn station.

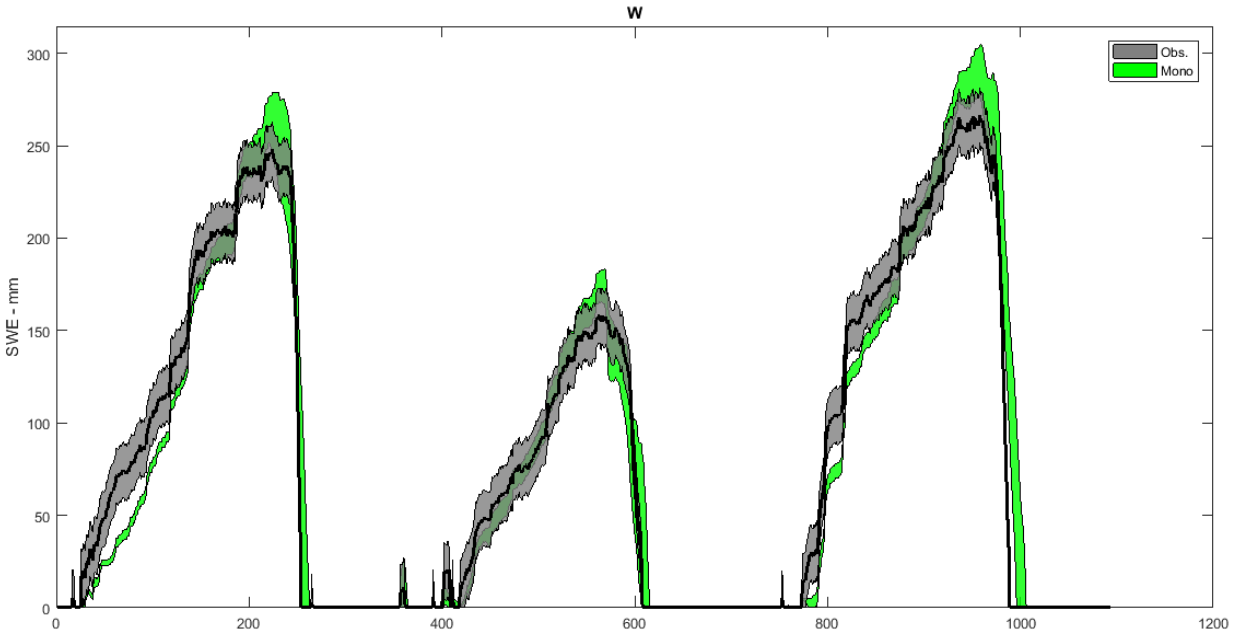

Figure 3.11 Simulations of monolayer model HYDROTEL at Wheaton station.

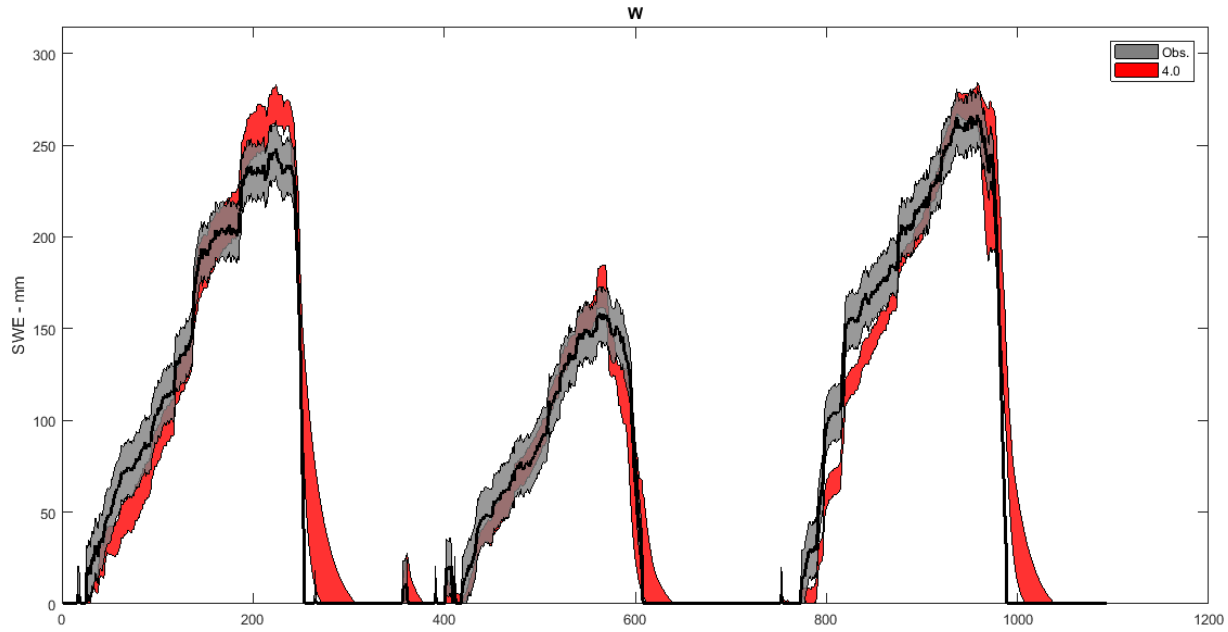

Figure 3.12 Simulations of V4.0 model at Wheaton station.

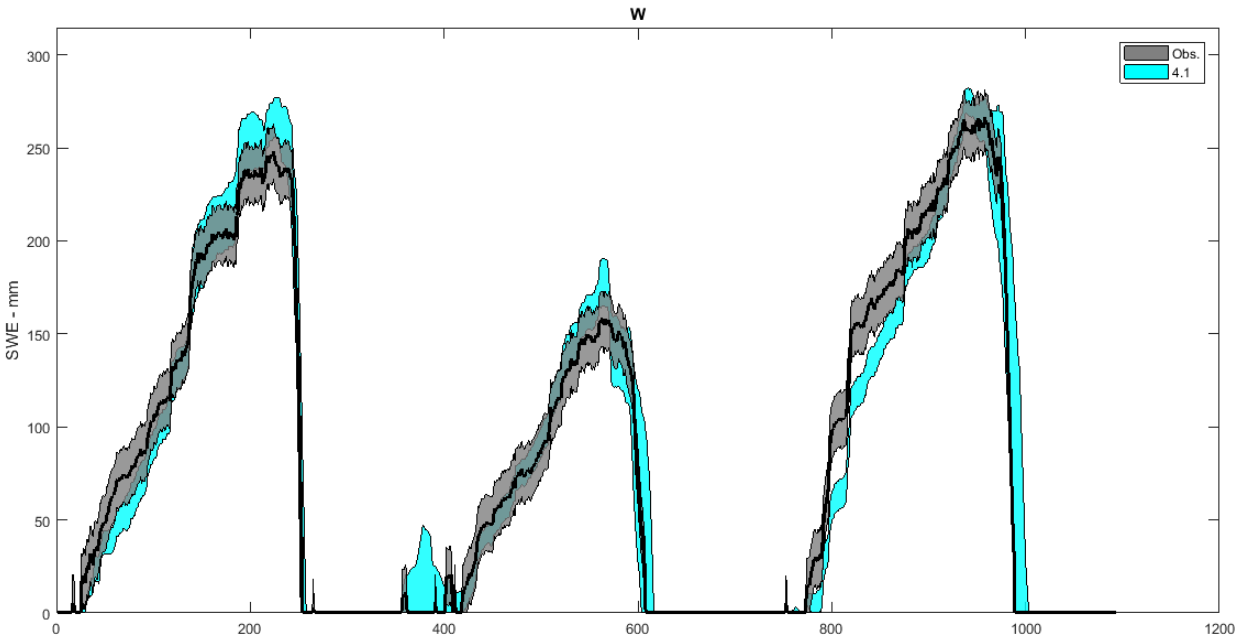

Figure 3.13 Simulations of V4.1 model at Wheaton station.

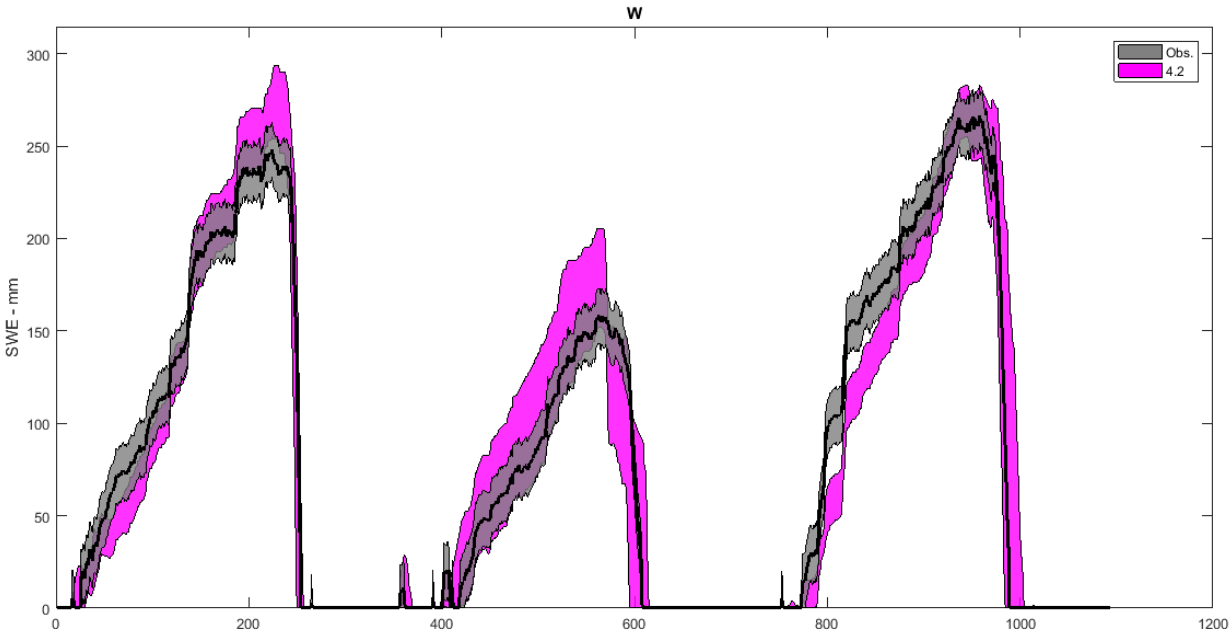

Figure 3.14 Simulations of V4.2 model at Wheaton station.

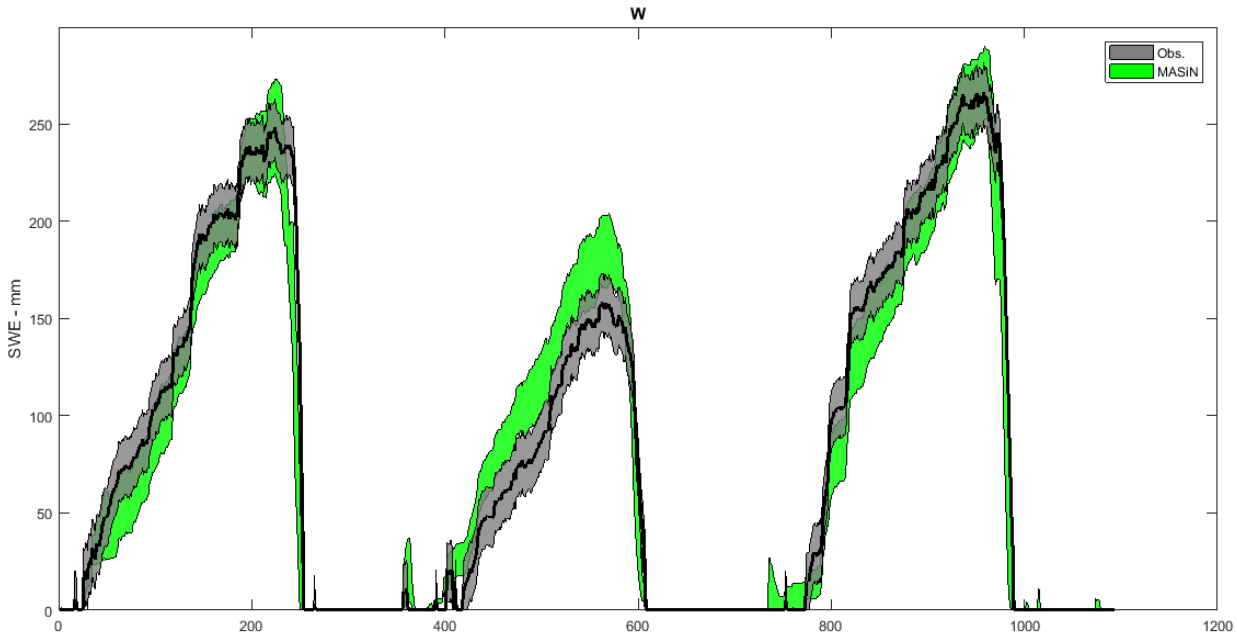

Figure 3.15 Simulations of MASiN model at Wheaton station.

In terms of performance, Table 3.1 shows that MASiN does not perform better than HYDROTEL's monolayer or its different bilayer versions, despite the fact that it is a physical model performing at hourly time steps. Therefore, given its computational budget, required data, and global performance with respect to snow modeling, MASiN does not seem to be the right choice for runoff modelling. The model is thus removed from the list of snow models to be further considered. However, MASiN was still conserved as a reference against which snow cover estimates were compared when the atmospheric temperature scenario will be considered later on in the presentation. Since MASiN simulates SWE during the third winter for the GMON station at Wheaton almost perfectly, it is used to observe the calibration performance of other models when temperature changes.

Three different scenarios were tested:

1. Increasing temperature by 2°C during accumulation phase, excluding precipitation days.
2. Increasing temperature by 2°C during peak phase, excluding precipitation days.
3. Increasing temperature by 2°C during melting phase, excluding precipitation days.

The results are shown respectively in Figure 3.16, Figure 3.17, and Figure 3.18.

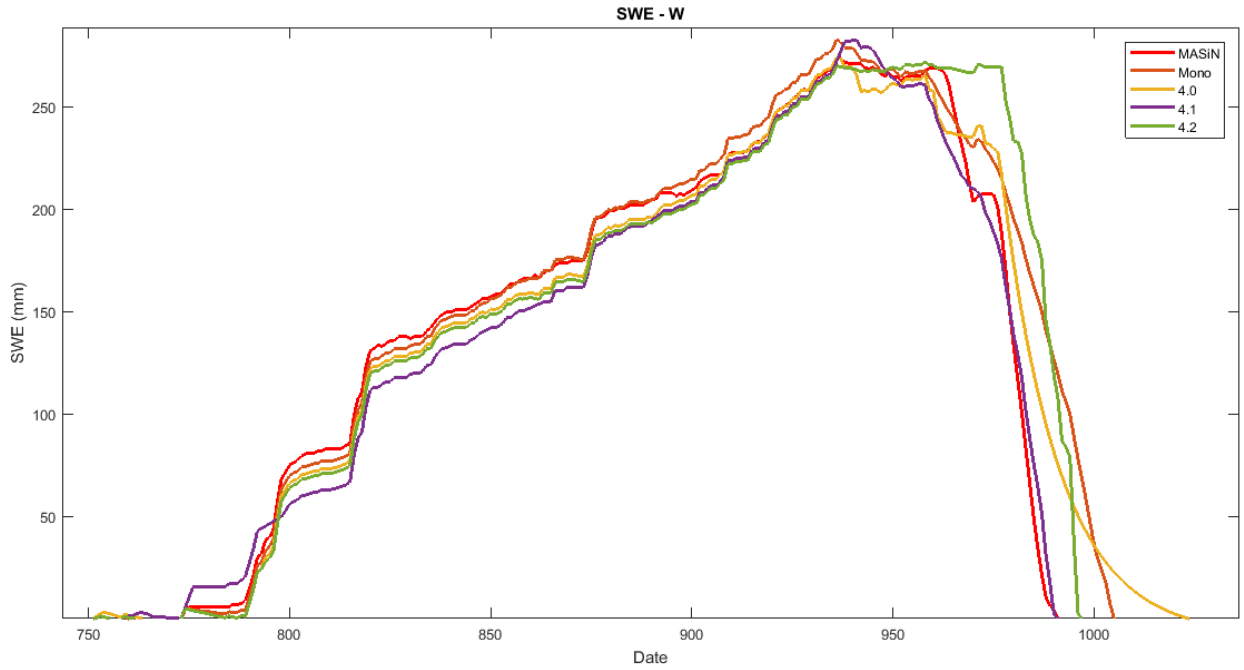

Figure 3.16 Scenario 1: Increasing temperature by 2°C during accumulation phase, excluding precipitation days.

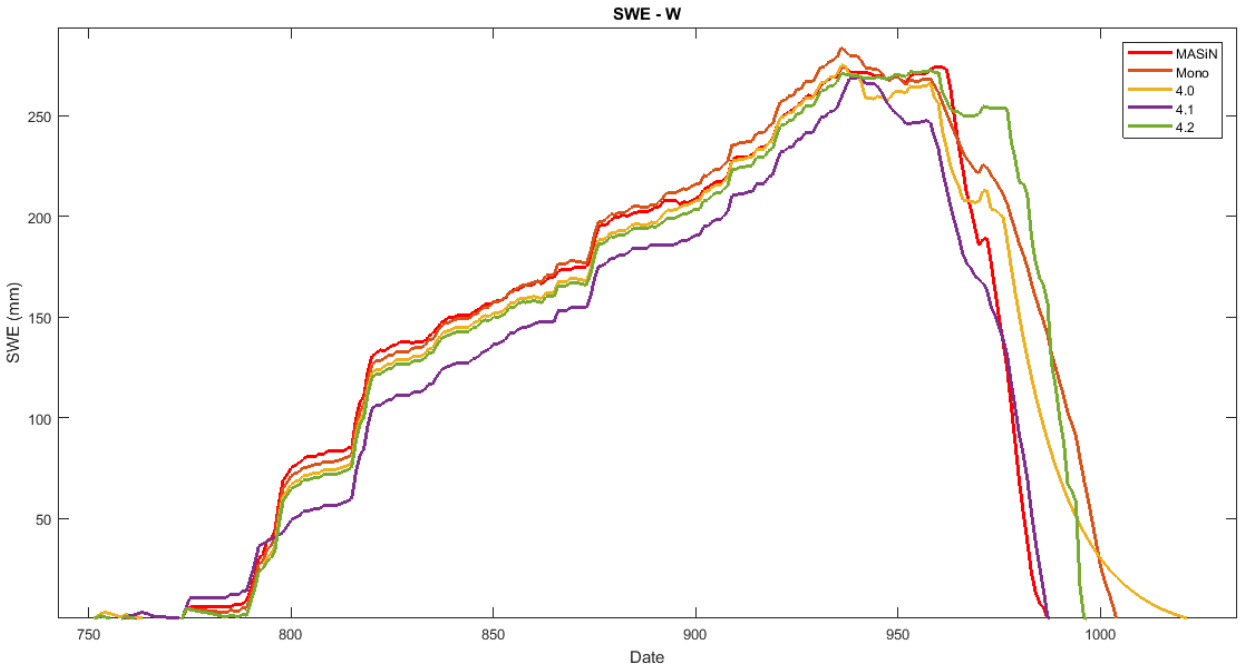

Figure 3.17 Scenario 2: Increasing temperature by 2°C during peak phase, excluding precipitation days.

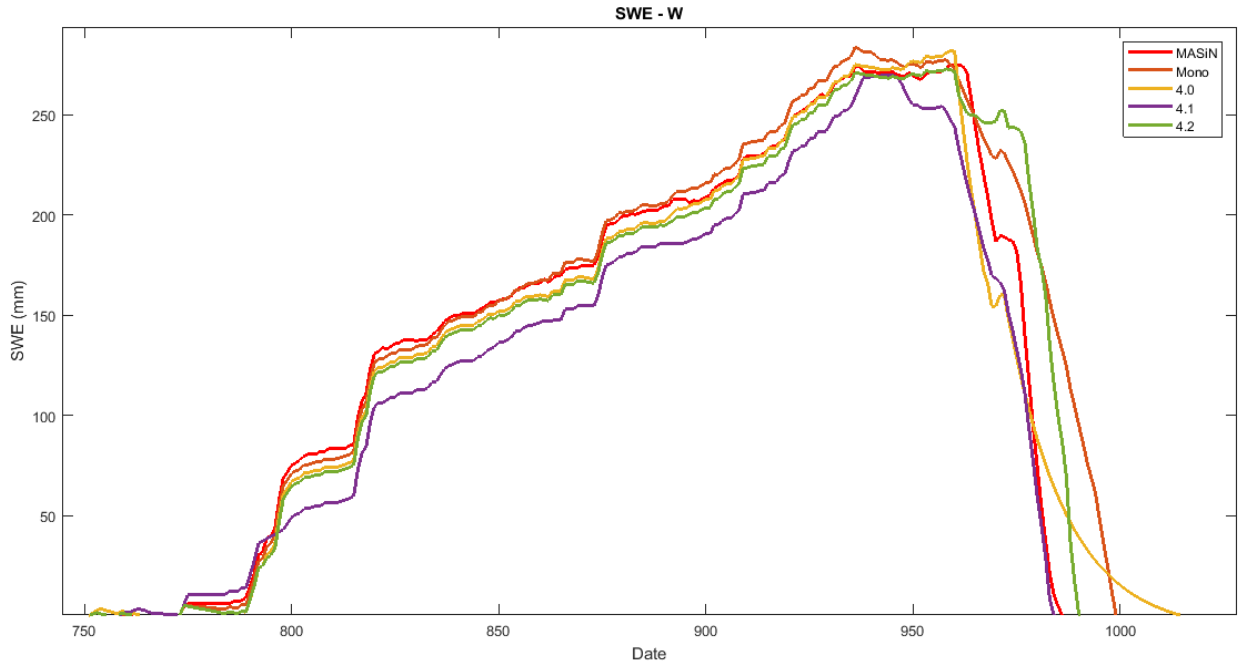

Figure 3.18 Scenario 3: Increasing temperature by 2°C during melting phase, excluding precipitation days.

Given the fact that MASiN was the best model for simulating SWE during the third winter at Wheaton, the performance of the different configurations of the HYDROTEL's snow model can be described through several metrics. These metrics were compared to the metrics belonging to MASiN simulations and included:

- The days on which snow cover appears and disappears,
- The day on which the simulated SWE reaches its maximum amount and the respective amount,
- The duration of the snow cover,
- The days on which an accumulation of 1 cm of SWE is reached for the first and last times,
- The average rate of accumulation, and
- The average melting rate.

These metrics are presented in Table 3.2 for the accumulation phase scenario, in Table 3.3 for the peak phase scenario, and in Table 3.4 for the melting phase scenario.

As Table 3.5 provides, the V4.0 bilayer snow model can be removed from the list, since, compared to V4.1 and V4.2, it does not perform realistically during the melting period. When comparing V4.1 and V4.2 snow model configurations, it can be seen that after calibration and test with modified temperature series, they display an almost identical performance. Knowing that the concept of the V4.1 model is a combination of those of V4.0 and V4.2 models, it is conceivable to conclude that the V4.2 snow model is suited for the task at hand, inheriting of the good performance seen from the V4.1 model while accounting for the influence of the components of the V4.0 model. Therefore, only the V4.2 model was compared to the monolayer snow model in HYDROTEL to investigate the performance of the runoff simulation.

Table 3.2 Metrics for accumulation phase scenario.

Models	1st Day snow appears (d)	Day of max SWE (d)	SWE max(mm)	Day snow cover ends (d)	Duration of snow cover (d)	Day Accumulation begins (>10mm) (d)	Day Accumulation ends (<10mm) (d)	Average accumulation rate (mm/d)	Average melting rate (mm/d)
MASiN	19-oct	31-mar	274.03	23-may	216	04-nov	21-may	1.86	5.37
Monolayer	19-oct	30-mar	282.92	06-jun	230	04-nov	05-jun	1.94	4.22
V4.0	19-oct	30-mar	274.33	25-jun	249	05-nov	14-jun	1.89	3.61
V4.1	19-oct	04-apr	282.63	23-may	216	20-oct	22-may	1.70	5.89
V4.2	19-oct	21-apr	271.76	29-may	222	05-nov	28-may	1.63	7.34

Table 3.3 Metrics for peak phase scenario.

Models	1st Day snow appears (d)	Day of max SWE (d)	SWE max (mm)	Day snow cover ends (d)	Duration of snow cover (d)	Day Accumulation begins (>10mm) (d)	Day Accumulation ends (<10mm) (d)	Average accumulation rate (mm/d)	Average melting rate (mm/d)
MASiN	19-oct	31-mar	274.25	19-may	212	04-nov	17-may	1.87	5.84
Monolayer	19-oct	30-mar	283.96	05-jun	229	04-nov	04-jun	1.94	4.30
V4.0	19-oct	30-mar	275.29	23-jun	247	05-nov	12-jun	1.90	3.72
V4.1	19-oct	04-apr	269.38	20-may	213	20-oct	19-may	1.62	5.99
V4.2	19-oct	21-apr	272.99	29-may	222	05-nov	28-may	1.63	7.38

Table 3.4 Metrics for melting phase scenario.

Models	1st Day snow appears (d)	Day of max SWE (d)	SWE max (mm)	Day snow cover ends (d)	Duration of snow cover (d)	Day Accumulation begins (>10mm) (d)	Day Accumulation ends (<10mm) (d)	Average accumulation rate (mm/d)	Average melting rate (mm/d)
MASiN	19-oct	22-apr	274.89	18-may	211	04-nov	17-may	1.63	11.00
Monolayer	19-oct	30-mar	283.96	31-may	224	04-nov	31-may	1.95	4.58
V4.0	19-oct	23-apr	282.08	16-jun	240	05-nov	05-jun	1.67	6.56
V4.1	19-oct	08-apr	270.01	17-may	210	20-oct	15-may	1.59	7.30
V4.2	19-oct	21-apr	273.09	23-may	216	05-nov	22-may	1.64	8.91

These performances are also compared between each configuration and summarized in Table 3.5.

Table 3.5 Summary performance for scenarii of increasing temperature

Differences with MASiN	Scenarios	1st Day snow appears (d)	Day of max SWE (d)	SWE max (mm)	Day snow cover ends (d)	Duration of snow cover (d)	Day Accumulation begins (>10mm) (d)	Day Accumulation ends (<10mm) (d)	Average accumulation rate (mm/d)	Average melting rate (mm/d)
Best	Constitution	All	4.0	Mono	4.2	4.2	All	Mono	4.0	4.0
	Peak	All	4.0	4.1	4.0	4.0	All	4.0	4.0	4.0
	Melting	All	All	All	4.1	4.1	All	Mono 4.1 4.2	All	4.2
Worst	Constitution	-	Mono 4.2	4.1	4.0	4.0	-	4.1	Mono 4.2	Mono
	Peak	-	Mono 4.2	4.0	4.2	4.2	-	4.2	Mono 4.2	Mono
	Melting	-	-	-	4.0	4.0	-	4.0	-	Mono

Streamflow/SWE Inter-comparison

Monolayer and V4.2 models were compared for the simultaneous simulation of runoff and snow. Both models were calibrated using the PA-DDS algorithm while taking into account the observed runoff from the 09AA012 hydrometric station at Wheaton and its associated delimitated sub-watershed (Wheaton River) along with the corresponding SWE observations taken from the local GMON station. To determine the runoff, more parameters, including the multiplicative coefficient for Penman-Monteith potential evapotranspiration, the thickness of each of the three soil layers, and the recession coefficient for the vertical water budget BV3C were added. Including these hydrological parameters, in addition to those from the snow model, was done in order to avoid favouring any snow model during the runoff calibration.

To compare these snow and runoff performances simultaneously, the PA-DDS algorithm was used to create a Pareto front. A Pareto front is composed of different parameter sets, which provides, for a given performance of an objective function, the best performance for the other objective function. This list of parameter sets can help the user to make the optimal trade-off between them. Figure 3.19 shows the Pareto front between SWE and runoff simulations based on observations at Wheaton GMON station and 09AA012 hydrometric station for the monolayer and V4.2 HYDROTEL models.

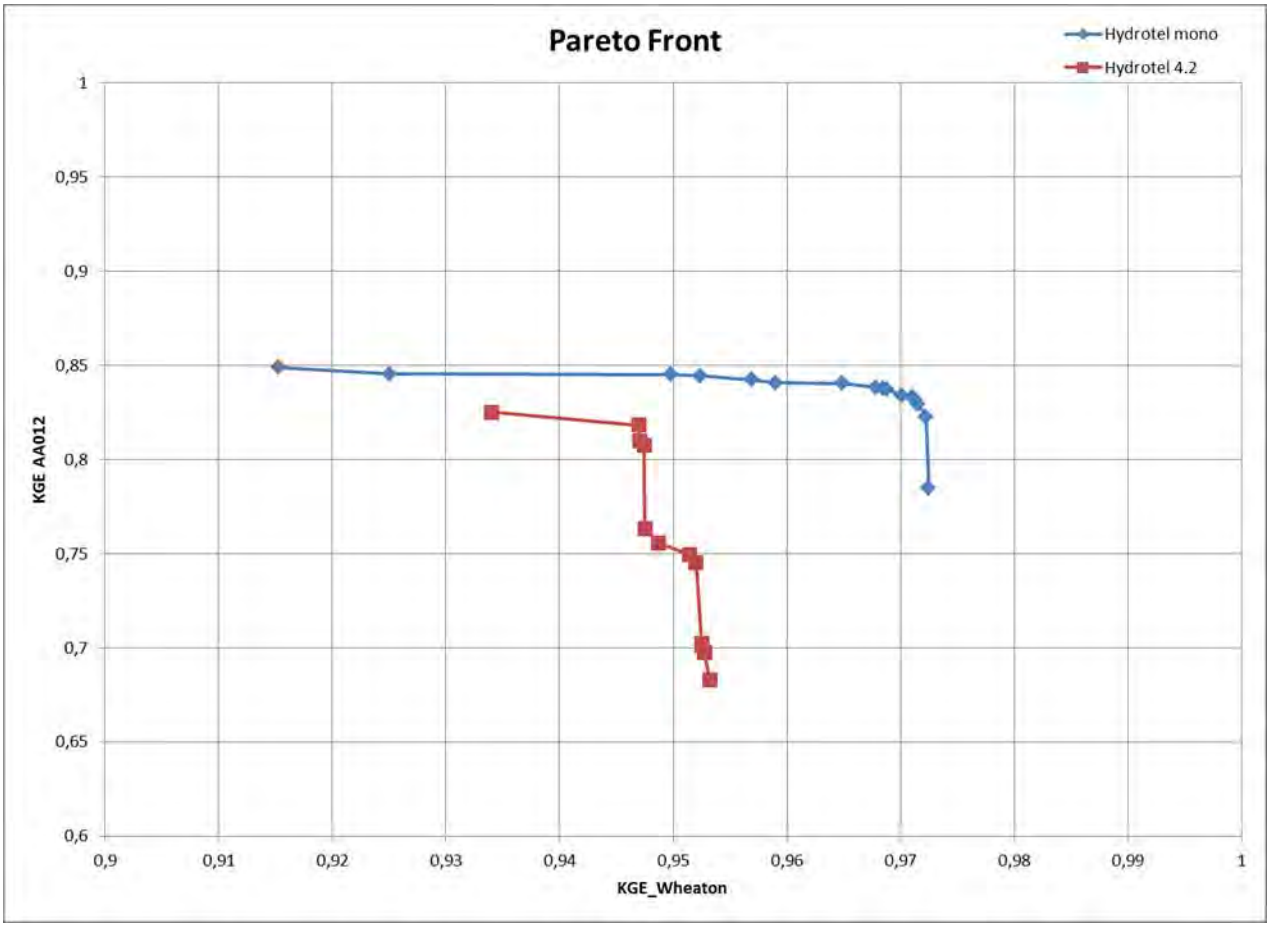

Figure 3.19 Pareto front between runoff and SWE simulation on Wheaton GMON station and 09AA012 hydrometric station.

The Pareto fronts show the trade-off between the KGE values for the objective functions defined in terms of the SWE and runoff simulations. Knowing that the ideal value of KGE is equal to 1, the closer are the values for both state to this optimal point, the better would be the calibration result. Based on the results of the multi-objective calibration, as shown in Figure 3.19, the best trade-off is obtained for the monolayer snow model in HYDROTEL. Figure 3.20 and Figure 3.21 show, respectively, the SWE simulation and the calibrated runoff for each model, based on the Pareto front.

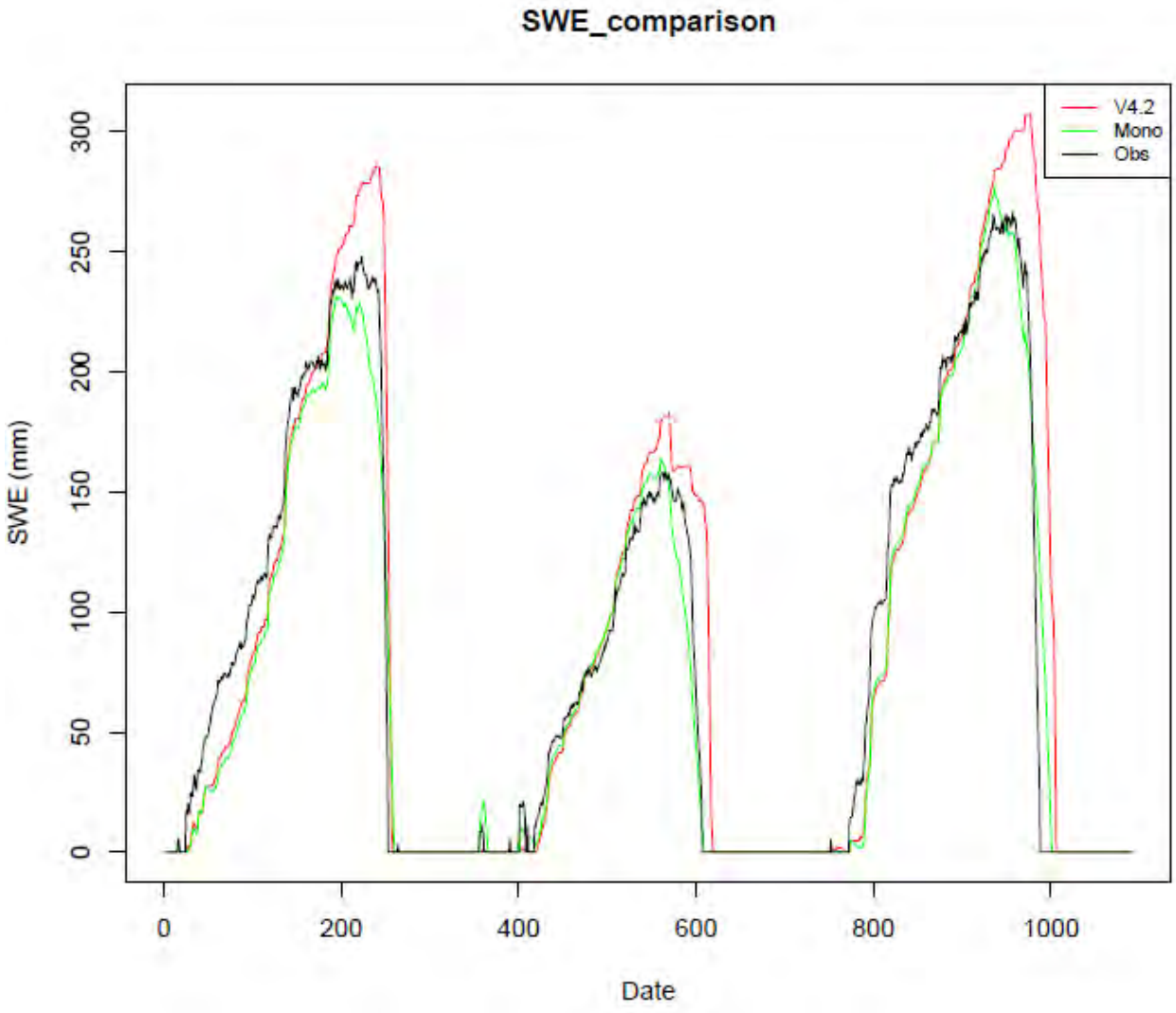

Figure 3.20 SWE simulations derived based on the PA-DDS optimization algorithm.

Figure 3.20 shows that the monolayer underestimates the accumulation phase of the snow cover more than the V4.2 snow model, while it captures the peak and melting phase more accurately (for monolayer model, KGE = 0.95 and for V4.2 model, KGE = 0.93).

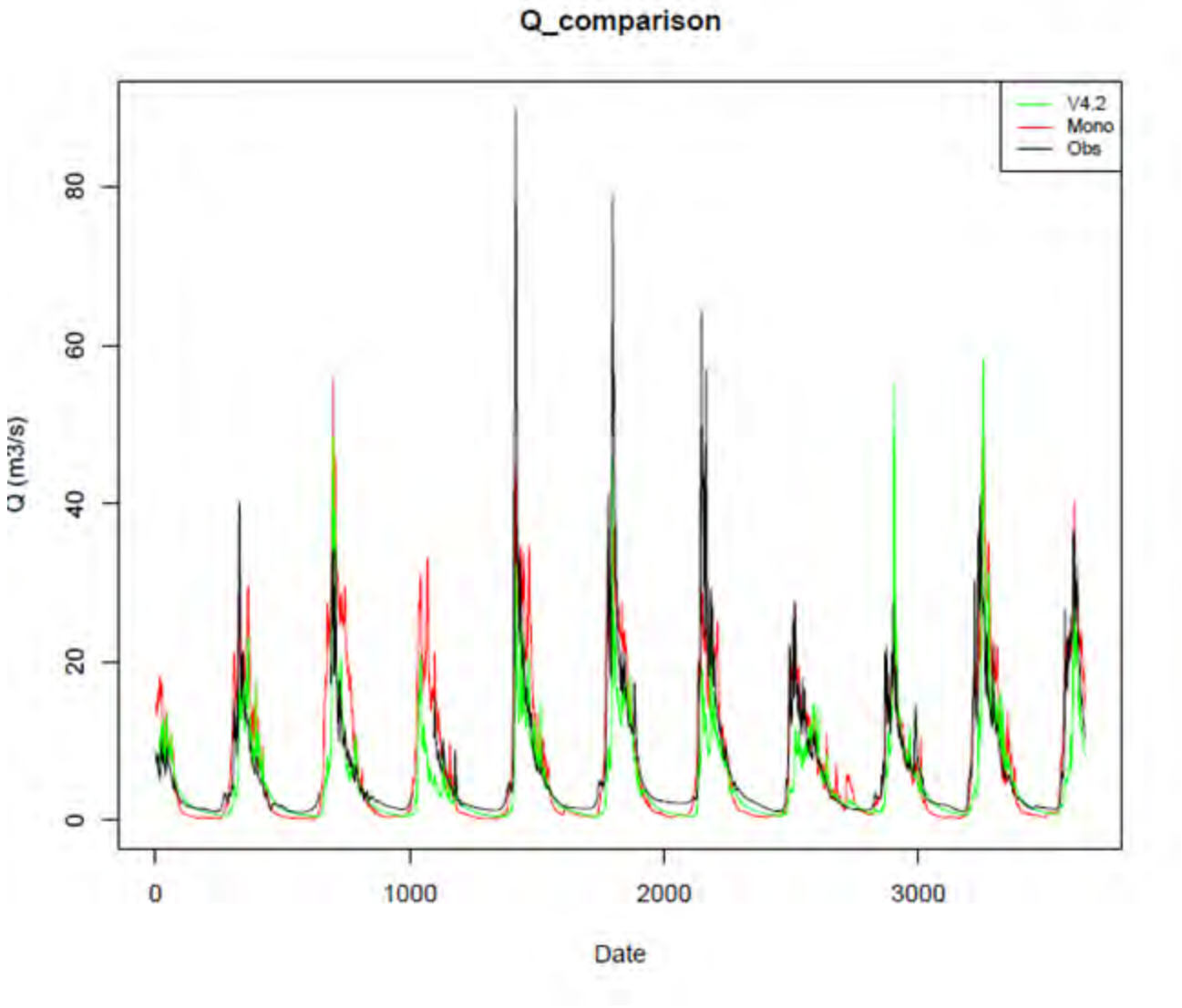

Figure 3.21 Flow simulations derived based on the PA-DDS optimization algorithm.

Figure 3.21 indicates that the monolayer model is more accurate than the V4.2 model because of a better representation of the peak flows and the melting phase (for monolayer model, KGE = 0.84 and for V4.2 model, KGE = 0.83). At this point, and since the peaks are properly captured, the performance of the model during the SWE accumulation phase is not considered as a priority.

Influence of the maximum number of layers to simulate in MASiN

The parametrization of the number of layers was done by taking into account values between 1 and 20 layers, while they were all compared to the 70-layer MASiN configuration.

Figure 3.22 to Figure 3.24 present the optimal performance at different GMON stations, depending on the maximum number of snow layers parametrized in the MASiN snow model.

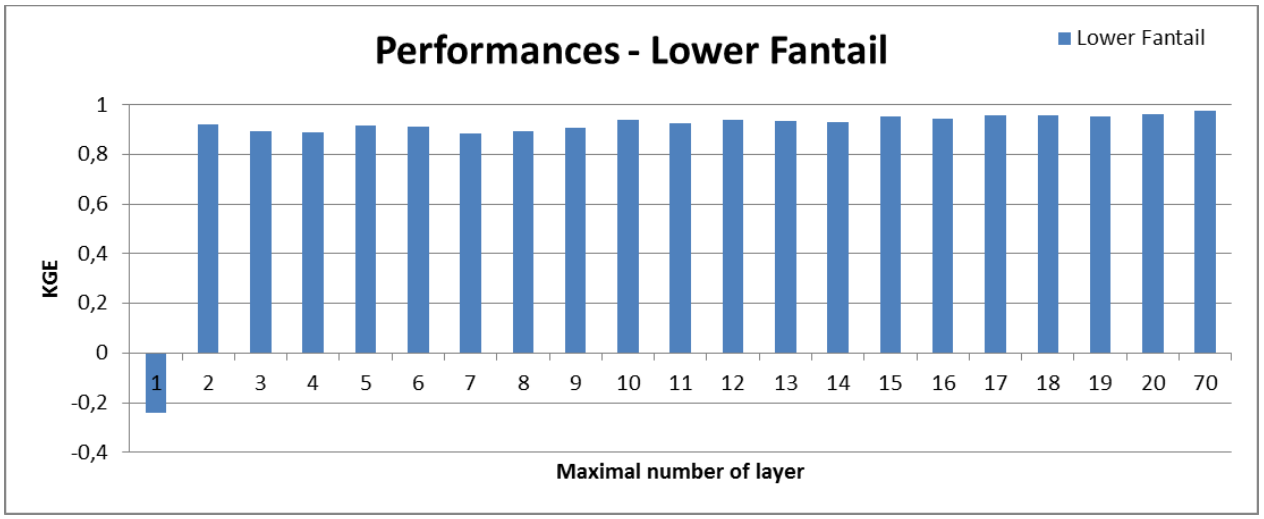

Figure 3.22 Optimal KGE vs. the maximal number of snow layers at Lower Fantail.

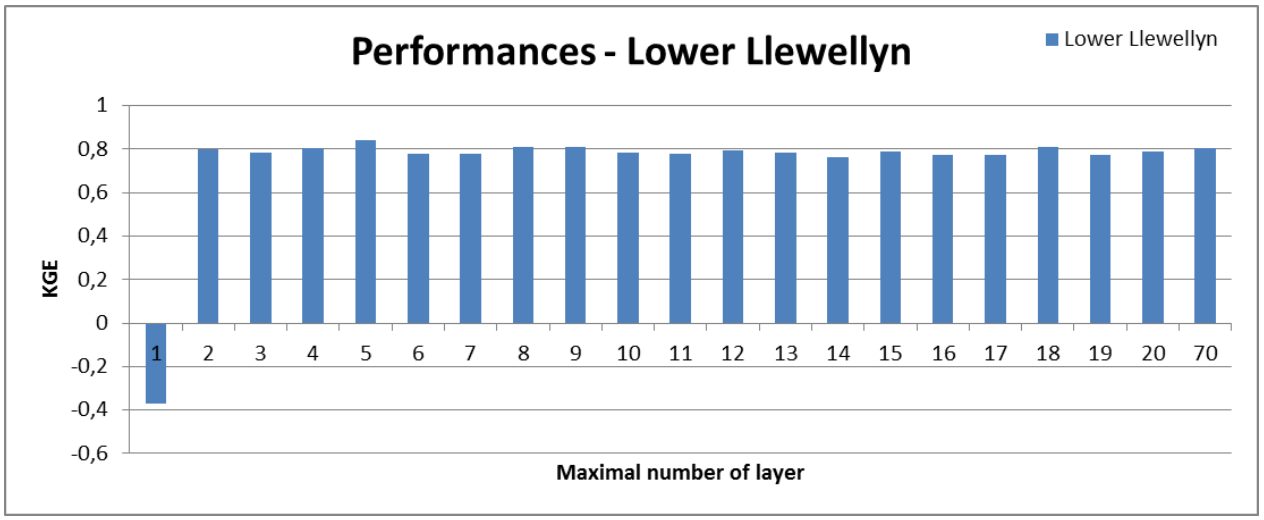

Figure 3.23 Optimal KGE vs. the maximal number of snow layers at Lower Llewellyn.

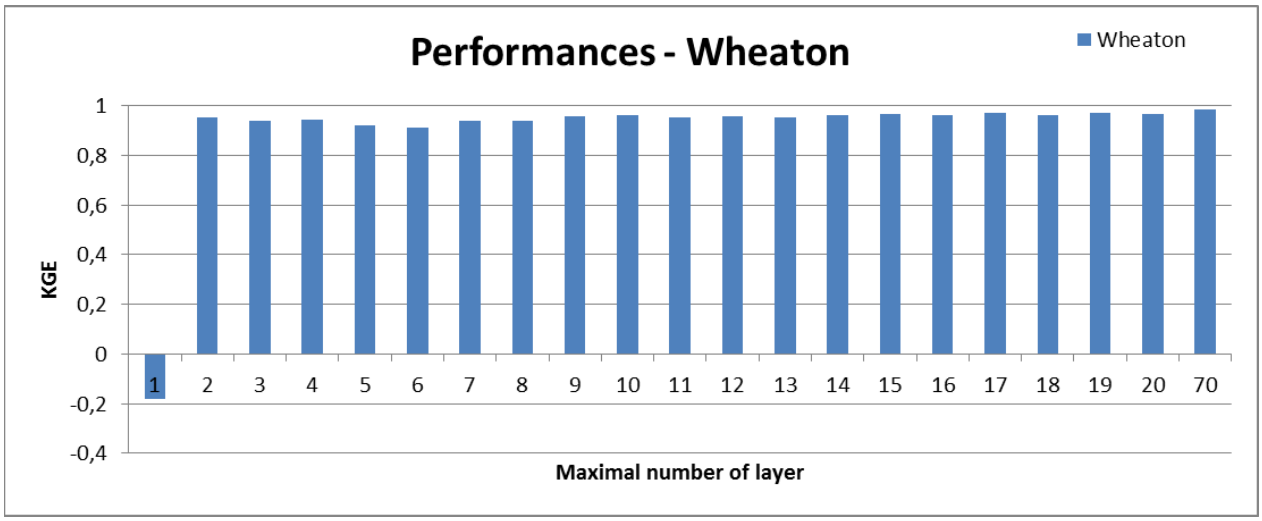

Figure 3.24 Optimal KGE vs. the maximal number of snow layers at Wheaton.

Based on the calibration, the 70-layer MASiN configuration does not outperform the other models. The only performance dropout was observed with the monolayer configuration.

To assess the potential of decreasing the number of layers to be parameterized for simulation, the best 10 out of 33 calibrated parameter sets were extracted, as well as their performances.

The violin graph shown in Figure 3.25 compares the KGE values at each GMON station for different number of layers.

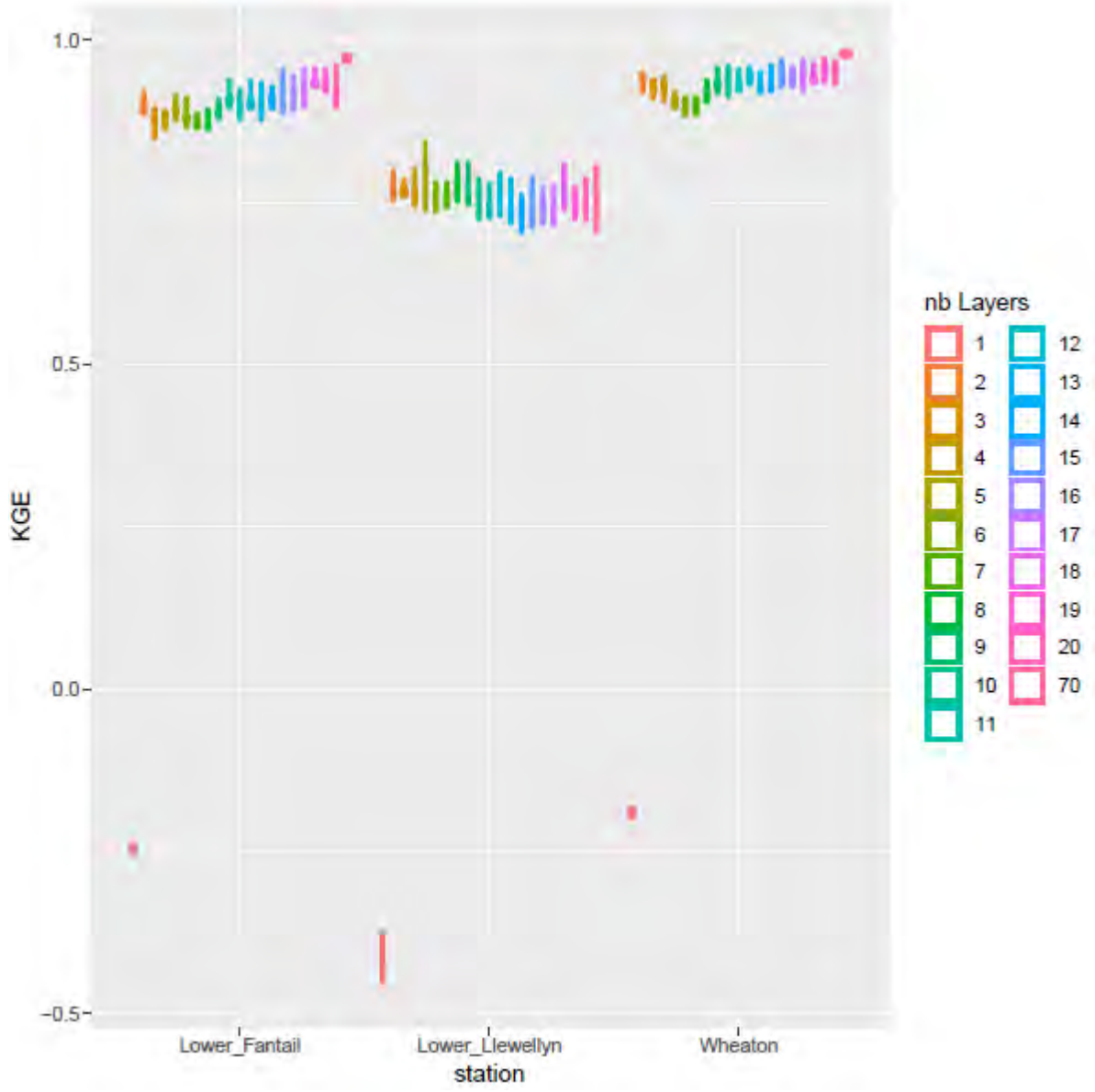

Figure 3.25 KGE at each GMON station.

First, the monolayer configuration has drastically lowered the performance of MASiN on SWE simulation, while for the other maximal numbers of layers, the performance levels are comparable to those of the full-extent configuration of MASiN. In Lower Llewellyn, the performance stayed at the same level, while for Lower Fantail and Wheaton, the performance decreased slightly by reducing the number of layers. At Wheaton, KGE reaches the lowest value for around seven layers. By continuing to calibrate the missing maximal number of layers, it is possible to define the existence of an important performance dropout.

Modifying the amount of interaction between the snow layers in MASiN can affect the parameterization performance. Accordingly, three categories of performance were observed. The first category is identified by no significant change, where the following parameters can be identified: the minimal snow density which triggers the metamorphism phenomenon (Figure 3.26), the temperature threshold associated with the minimum density of the snowfall (Figure 3.27), roughness (Figure 3.28), the turbulence reduction coefficient (Figure 3.29), and the maximum retention coefficient (Figure 3.30).

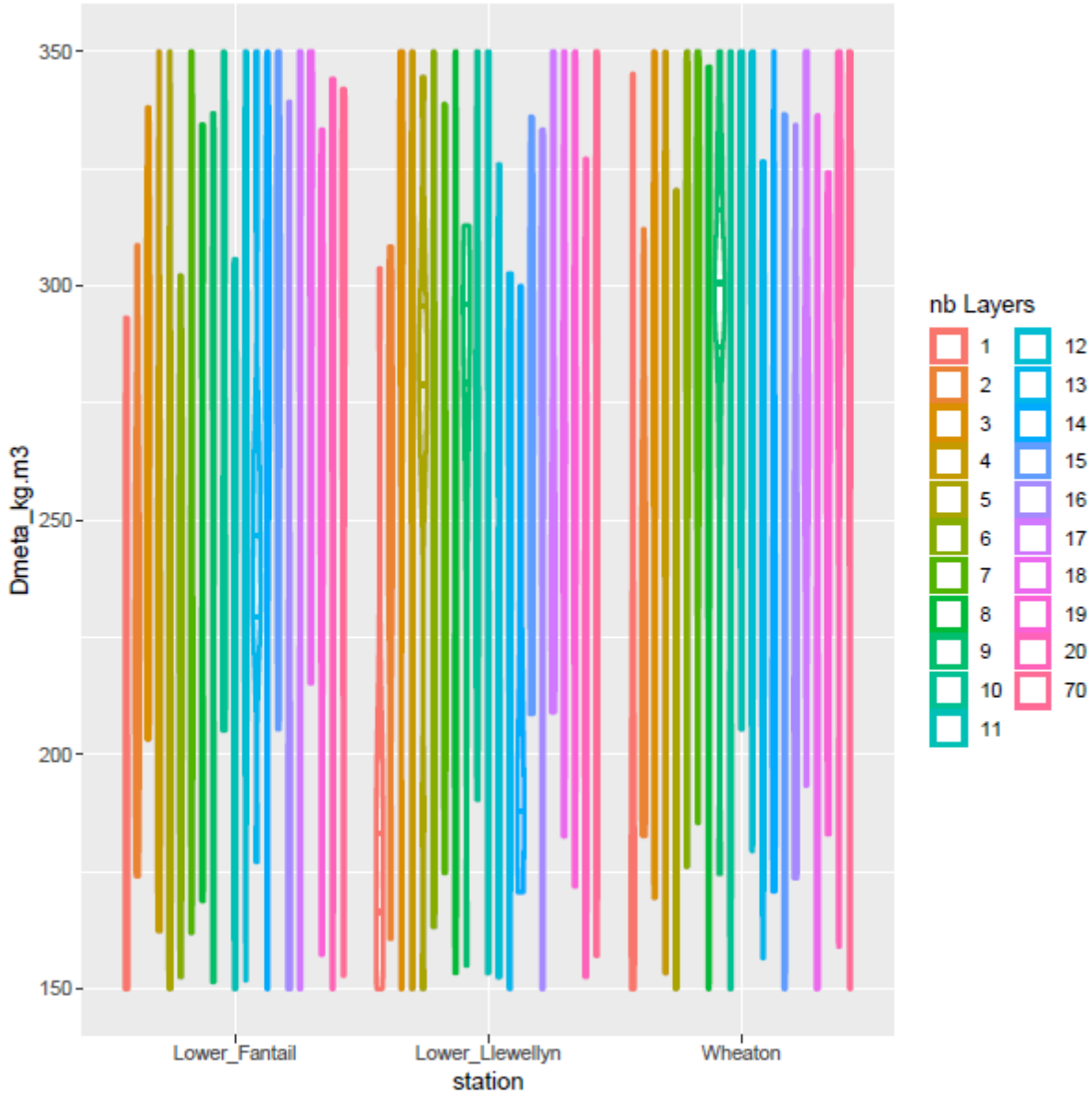

Figure 3.26 Minimal density of metamorphism at each GMON station.

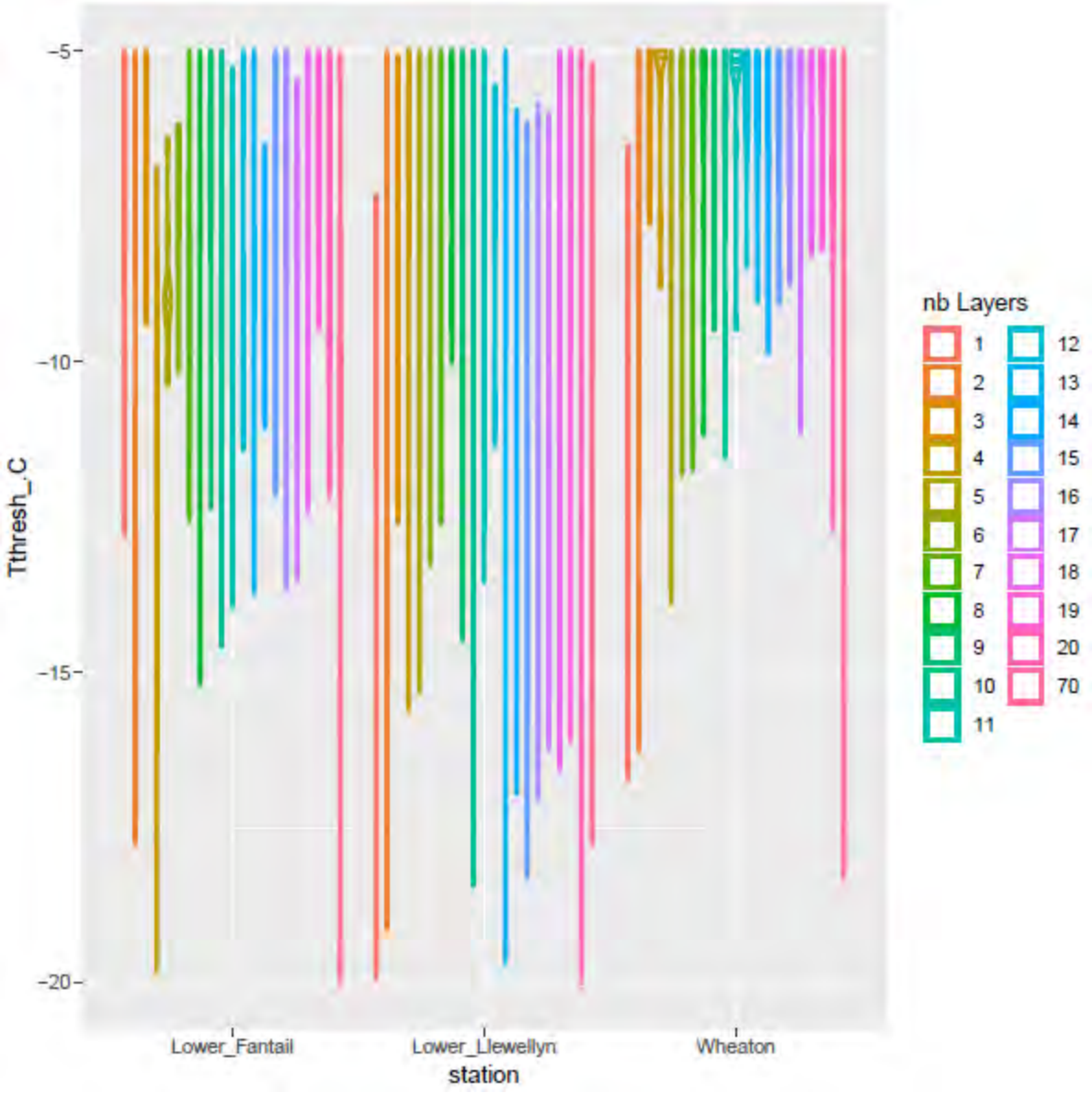

Figure 3.27 Minimum temperature threshold for snowfall at each GMON station.

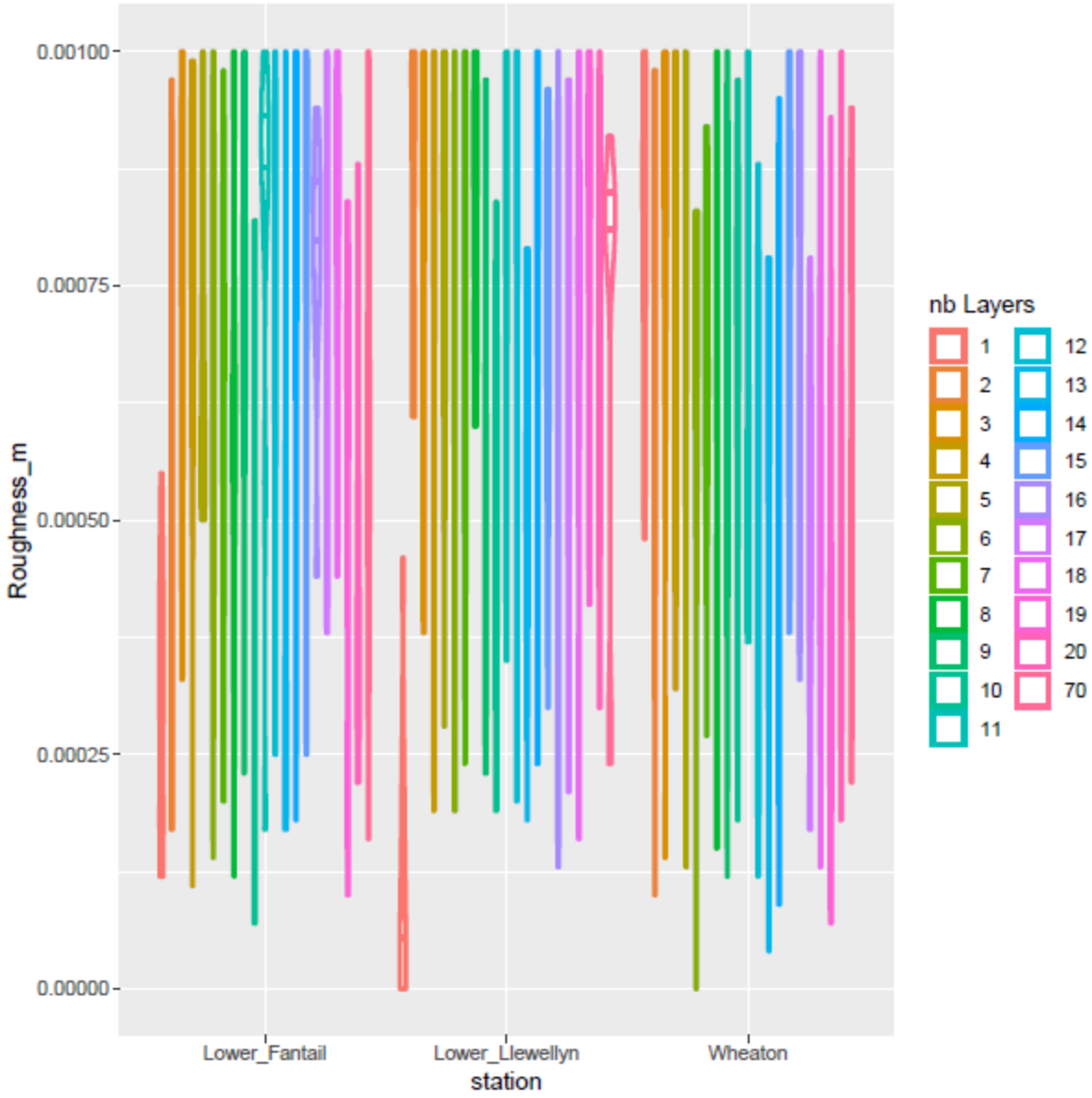

Figure 3.28 Roughness at each GMON station.

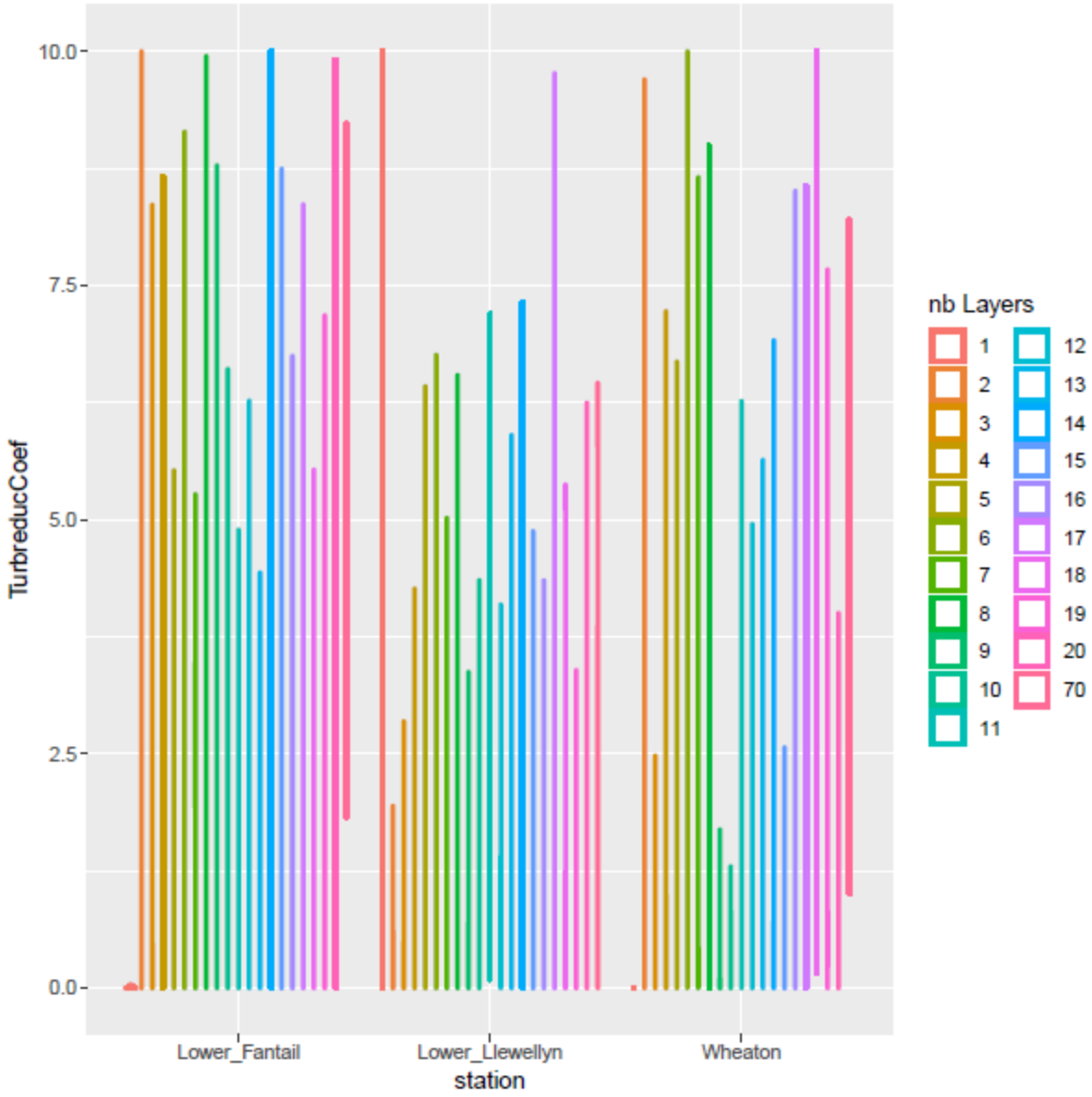

Figure 3.29 Turbulence reduction coefficient at each GMON station.

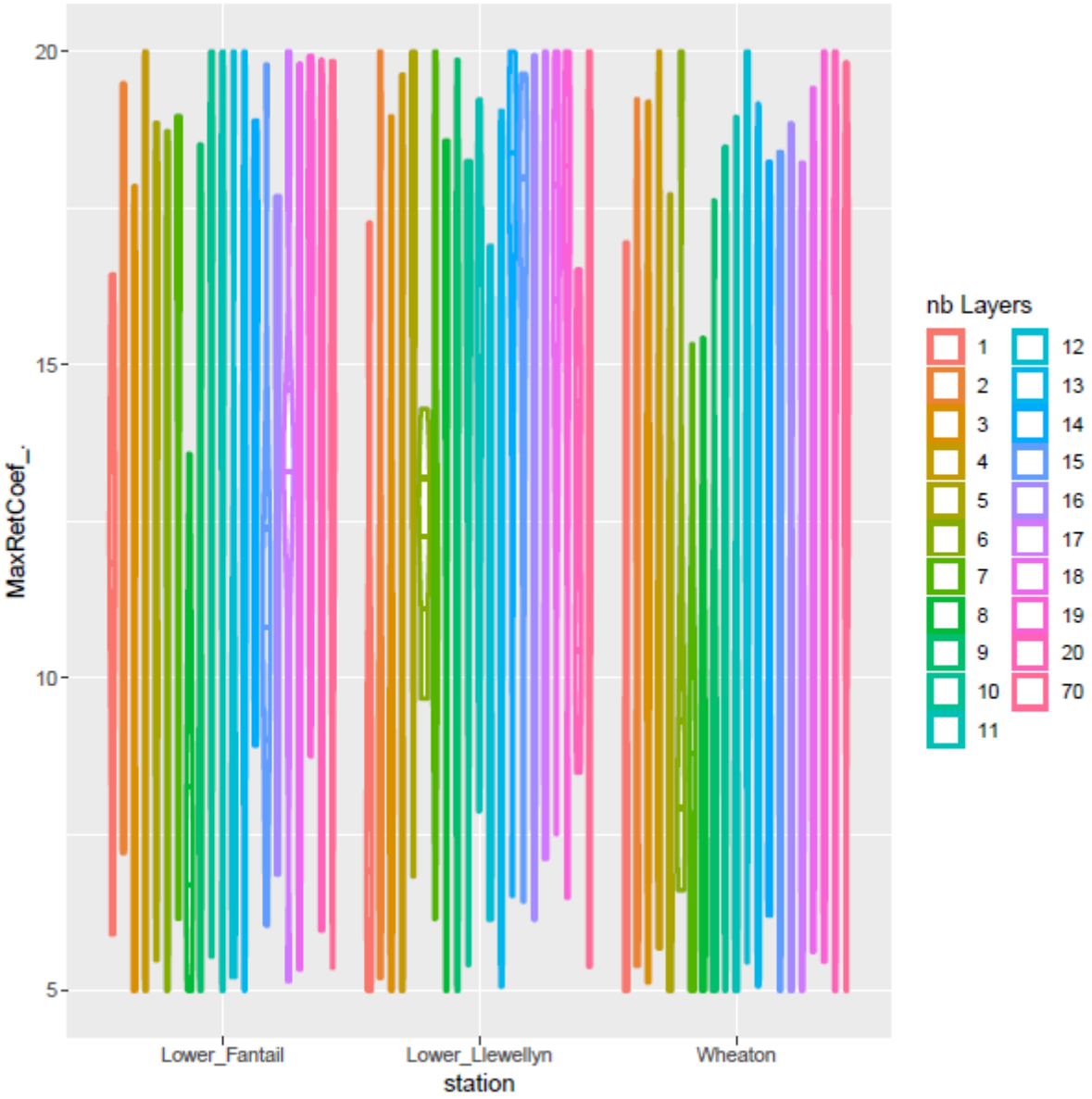

Figure 3.30 Maximal retention coefficient at each GMON station.

The second category is when the average value of the parameter values vary as can be visually inspected. The minimum density of fresh snowfall falls into this category; the average minimal density of fresh snowfall values decrease when the maximum number of snow layers and the heat flux from soil increase, as can be seen in Figure 3.31 and Figure 3.32, respectively.

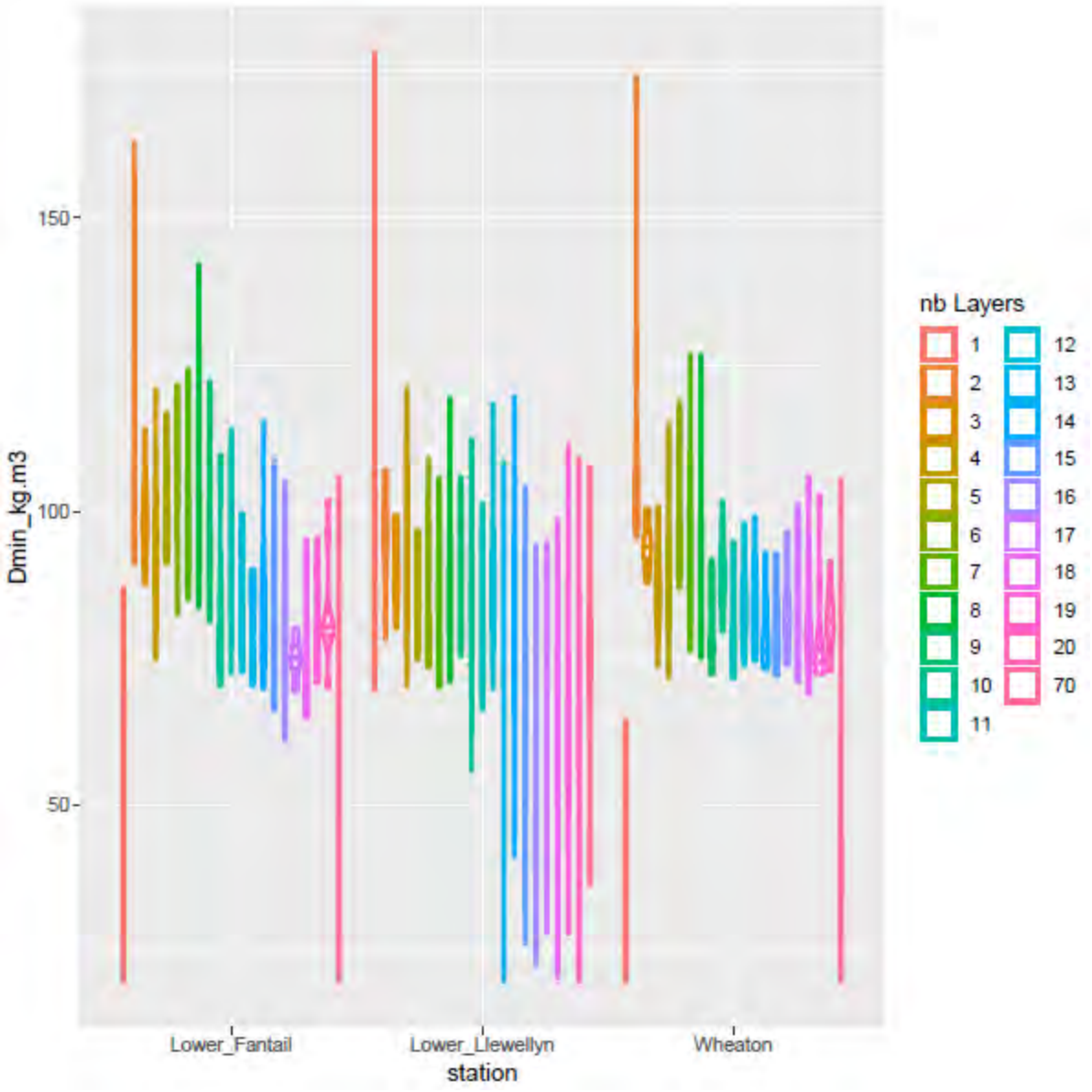

Figure 3.31 Minimal density of fresh snowfall at each GMON station.

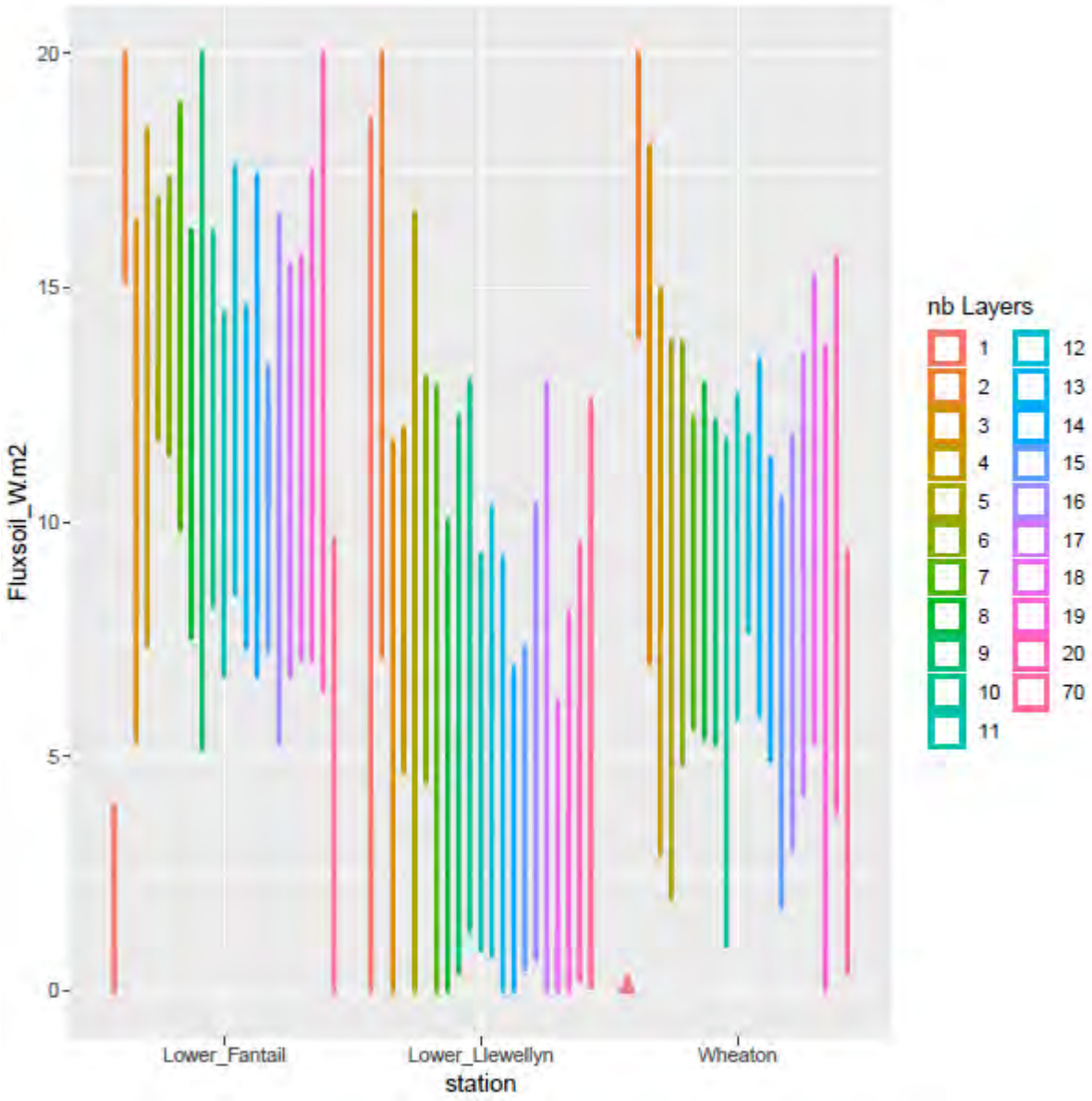

Figure 3.32 Heat flux from soil at each GMON station.

The last category is when a change in performance is observed on some GMON stations only. The settlement coefficient seems to increase for a maximum number of up to 12 snow layers for the Wheaton GMON station (Figure 3.33). Also, the minimal and maximal radiation coefficients decrease when the maximum number of layers increases at the Lower Llewellyn GMON station (Figure 3.34 and Figure 3.35, respectively) as well as the separation temperature of rainfall and snowfall at Lower Fantail station (Figure 3.36).

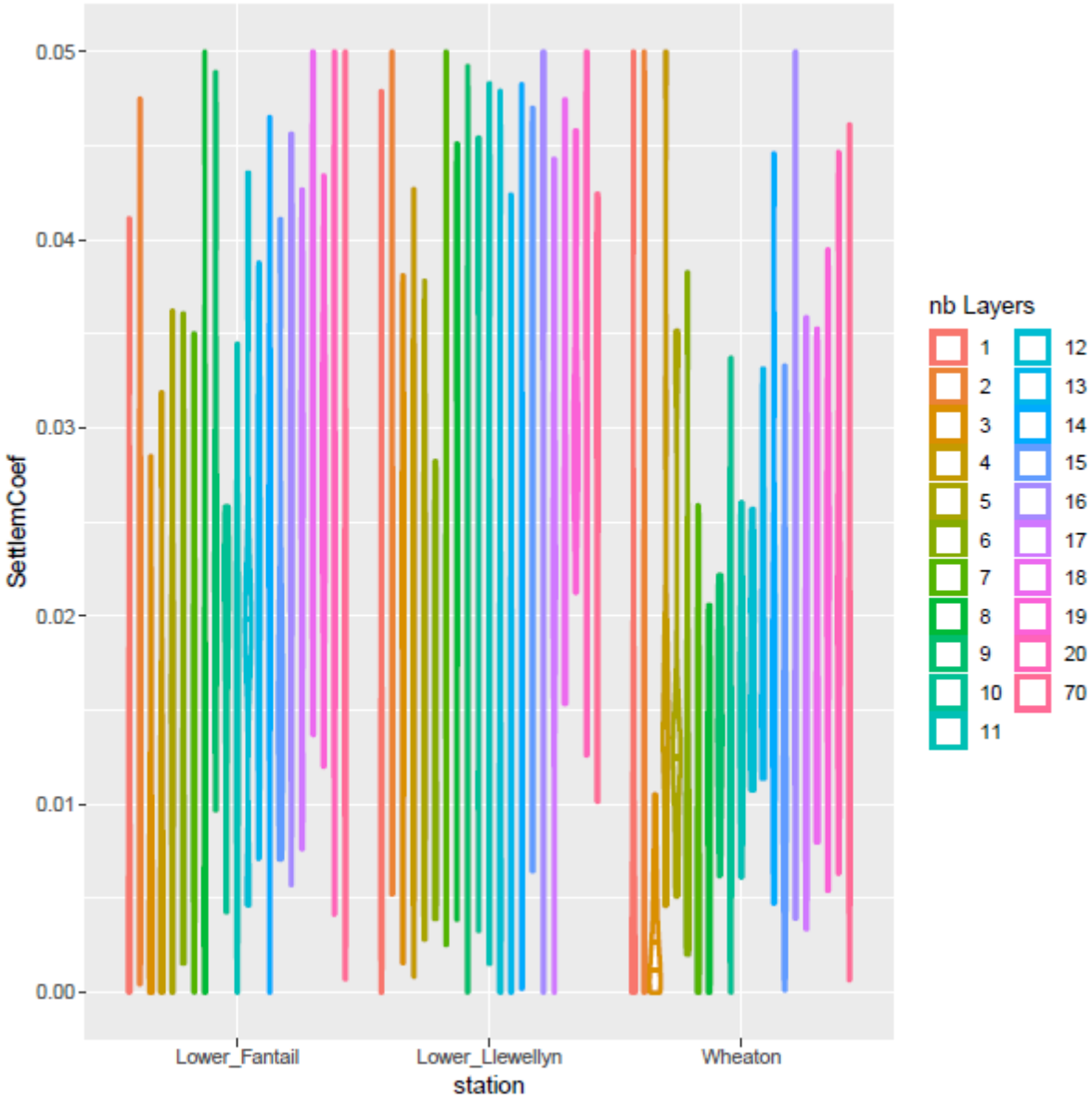

Figure 3.33 Settlement coefficient at each GMON station.

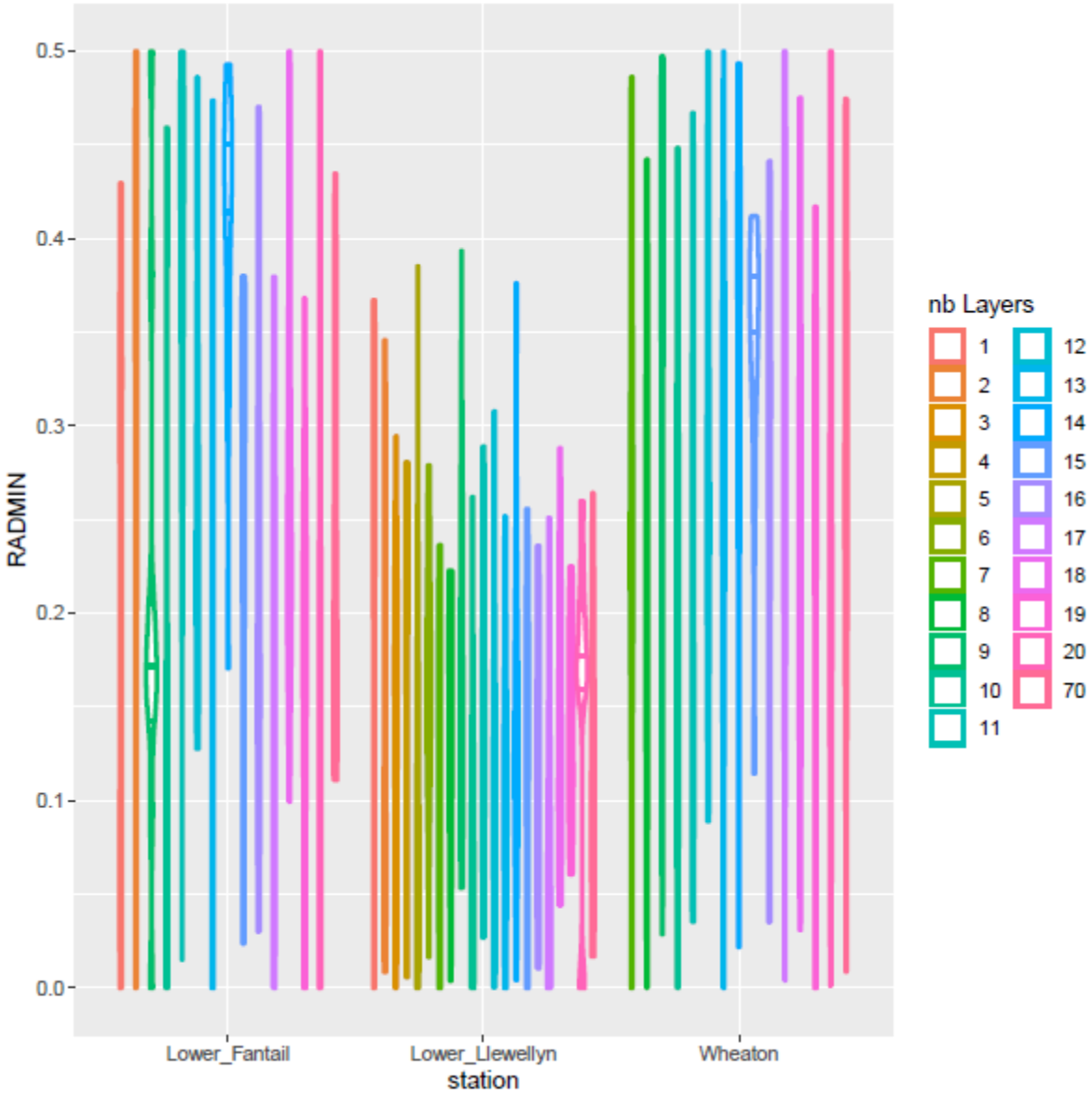

Figure 3.34 Minimal radiation coefficient at each GMON station.

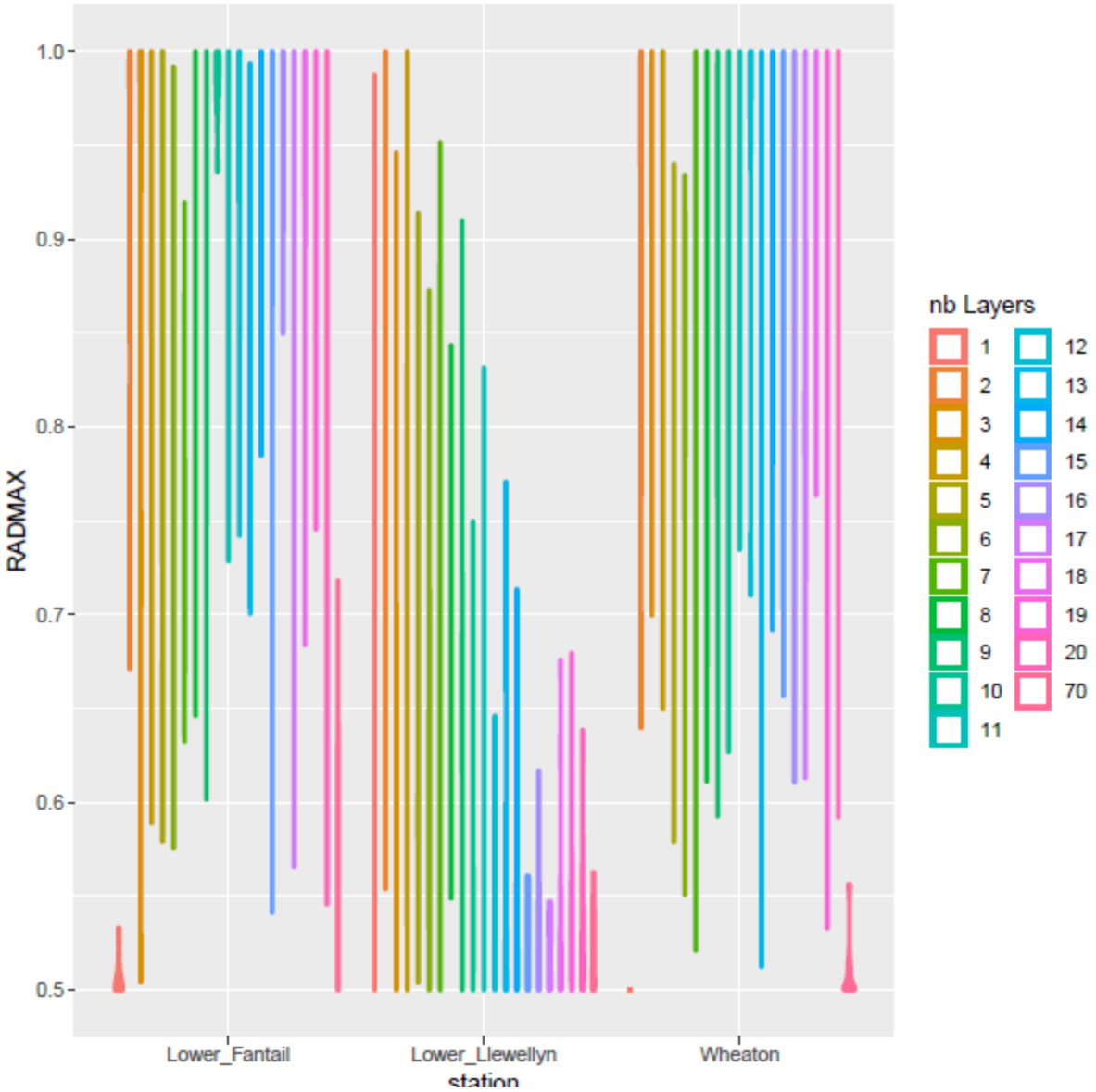

Figure 3.35 Maximal radiation coefficient at each GMON station.

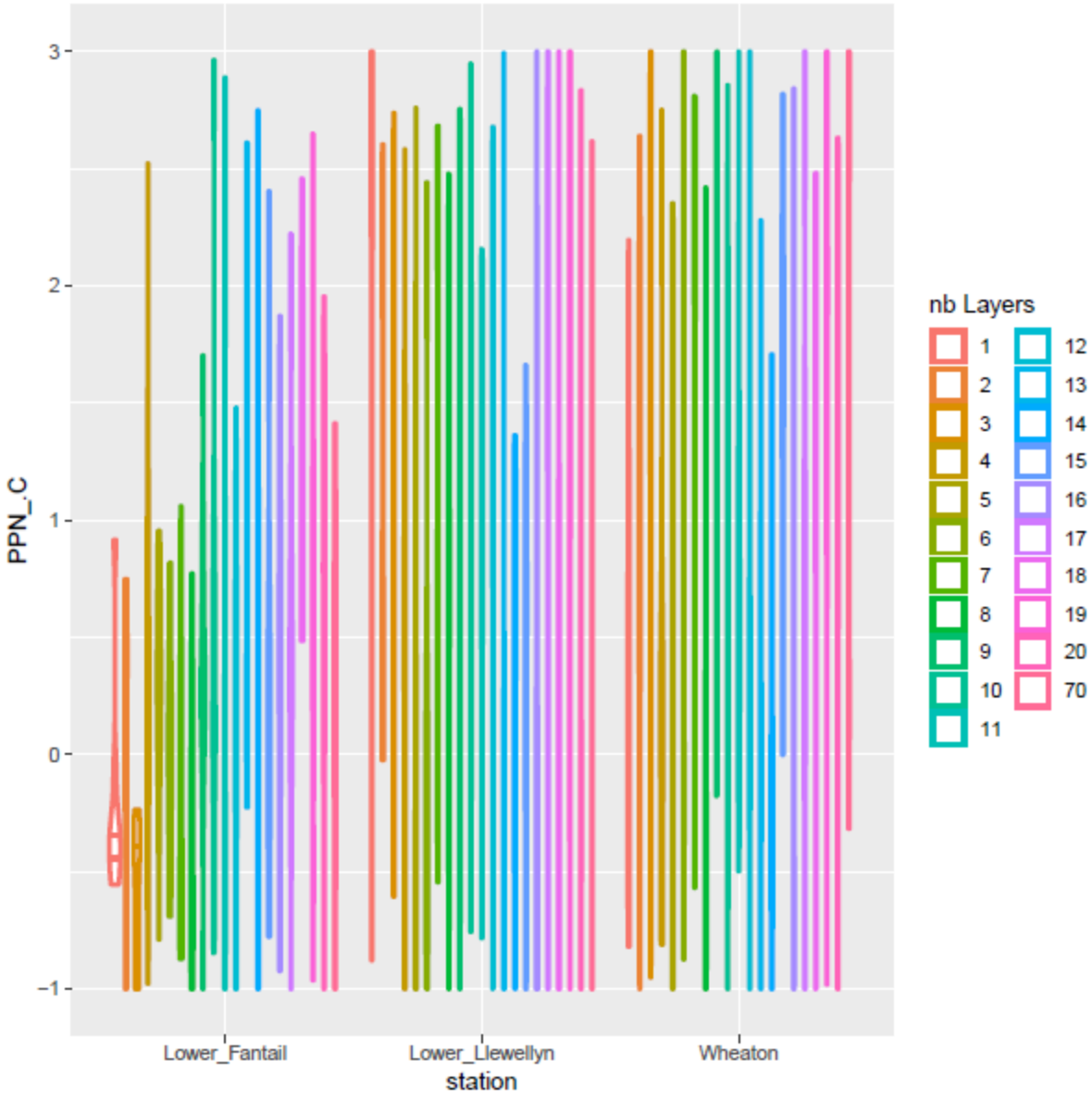

Figure 3.36 Separation temperature of rainfall and snowfall at each GMON station.

In summary, it is possible to conserve an acceptable level of performance by decreasing the number of snow layers in the model. However, an optimum number, or an optimum range of optimum numbers, has to be further investigated by calibrating the models at more GMON stations. Furthermore, some parameters are sensitive to this parametrization scheme, such as the minimum density of fresh snowfall, the heat flux from soil, the settlement coefficient, the minimal and maximal radiation coefficient, and the separation temperature of rainfall and snowfall.

3.2.4. Conclusion

A physically-based snow model, such as MASiN, can provide a good level of performance, similar to that of the monolayer snow module in HYDROTEL, for snow cover simulation. However, the main disadvantage of MASiN is its computational budget and the amount of required data for operational purposes.

HYDROTEL's snow module has an acceptable performance for SWE simulation, and given its flexibility for an operational purpose, a bilayer snow model version can be suggested to improve SWE and runoff simulations. In this study, it was shown that the performance improves slightly on SWE simulations by providing more degrees of freedom on the melting phase, which allows constraining the parameter sets slightly to better estimate the accumulation phase. However, this improvement was not observed in each winter for each GMON station and it does not improve the performance of the runoff simulation. This underperformance could be in part due to the formation of this bilayer snow model, which might be not the most adaptable version. Other conceptions of bilayer snow model have to be designed and tested in this regard.

Comparisons conducted here were based on raw models, where the snow assimilation feature, which is used in the operational model to update the simulations by including the observed snow measurements into the analysis, was disabled. It has also been suggested that the quality of precipitation data can be improved if CaPA data are used as input in the model (see Appendix II for a complete analysis).

For the MASiN model, in terms of the influence of the maximum number of snow layers to include for simulation, the computational budget can be reduced by decreasing the number of layers to simulate. However, a threshold below which the performance decreases below the acceptable limit cannot be clearly defined yet. Simultaneously, other parameters can be affected by parametrizing the number of snow layers. However, the reconstruction of the precipitations in this study may not constrain MASiN on the global mass balance, by providing a SWE inputs similar to the expected SWE outputs, which were used for the calibrations. As the mass balance were, by construction of the precipitation series, adapted to the SWE observations, MASiN was calibrated by estimating mainly the necessary global energy balance to maintain this SWE in the snowpack according to the SWE observations. Thus, it can be

assumed that MASiN did not require a snow system composed of a important number of snow layer for controlling the necessary energy of the snow melt, as the mass input was already accorded to the SWE observations. This assumption can explain why MASiN conserved a good SWE modelling performance with only a few number of snow layers. Accordingly, performing the calibration by incorporating more GMON, with independent precipitation series of the SWE observations, stations into the analysis could provide more information during this assessment of the model. Thuis latter comment does not apply to the Forecasting Sytem per say since were interested in different spatial scales.

4. Glacier module

During the course of the first year of the project, it was decided to include the Upper Yukon River Watershed into the forecasting system. Such decision required the development and implementation of a glacier module in HYDROTEL. Glacier dynamics become relevant to watershed hydrology during the recession limb of the annual hydrograph as summer flows are mostly made up of precipitation runoff, subsurface runoff and glacier melting processes.

4.1. Identification of Glacier module

In the literature, it is found there are different types of glacier models used throughout the world. MacDougall et al. (2011) listed two (2) major groups of distributed empirical models commonly used to characterize the melting of glaciers. There are the temperature index models and the physically-based models derived from energy balance. The first type of models assumes a strong correlation between air temperature and melting of glaciers through an empirical degree-day (DD) coefficient. In the second type, the melt is computed based on the energy fluxes components to and from the surface (i.e. net radiation, sensible heat flux, latent heat of fusion, ground heat flux, sensible heat flux supplied by rain and energy consumed by melt) (Hock, 2005).. For their study on the River Bridge Watershed in British Columbia, Stahl et al. (2008) used the first type of models to account for the impact of glacier melt on stream flow. The glacier mass balance was calculated by using the semi-distributed HBV-EC model. Hock (2003) confirmed that the DD approach represents a simple method to effectively determine the mass balance of a glacier. Similarly, Samuel et al. (2016) used the empirical DETIM model in their study in the Upper Yukon Watershed. They compared mass balance provided by DETIM with those derived from satellite imagery as well as that estimated by the distributed CRHM model which has been widely used in cold regions of Canada. In addition to daily flow, Gsell (2014) used the annual glacier mass balance to validate the hydrologic model used in a mountainous watershed and avoid uncertainties from the compensation effect.

In this study, to calibrate and validate our hydrological modelling results, we have decided to determine glacier volumes using two methods.

4.2. Determination of Surface – Volume equation in sub-arctic area

The volume of glaciers is widely determined by a volume-surface relationship. This is based on the fact that glacier surface can be determined by satellite data. Samuel *et al*. (2016) used a volume-surface relationship to determine the rate of change of glacier volume. Stahl *et al*. (2008) simulated the advance or withdrawal of glaciers using a mass balance determined through modelling. The relationship exploited in these two studies carried out in a subarctic zone, is that of Chen and Ohmura (1990). Bahr *et al*. (1997) confirmed the physical basis of this empirical equation based on the geometry of different types of glaciers (temperate, cold and polythermal) throughout the world (Stahl *et al*., 2008). The purpose of this literature review is to assess the consistency of the relationship for subarctic glaciers which are mainly polythermal. To achieve this goal, we analyzed two surface-volume methods used worldwide: (i) the empirical method estimated by Chen and Ohmura (1990); and (ii) the physical relationship determined by Bahr *et* al. (1997).

4.2.1. Thermal regimes of glaciers

According to Foutain and Walder (1998), there are three types of glaciers based on their thermal regime.

1. The temperature of temperate glaciers is equivalent to that at the onset of ice starting to melt under a specific pressure called the pressure melting point (Irvine-Fynn *et al*. 2011). Temperate glaciers made of water, ice and interstitial liquid are sensitive to small temperature change. They are found in different parts of the world (USGS, 2017).

2. The temperature of cold glaciers is below the pressure melting point. The interstitial liquid of these glaciers is non-significant.

3. Polythermal glaciers are made by temperate and cold ice. These glaciers are mainly located in the vicinity and within the polar area (Artic, Alaska, Antarctic and Greenland ice sheets) which has the most important masses of glaciers worldwide (Wilson *et al*. 2013). The temperate and cold ice distribution within polythermal glaciers varies from the base to the surface (Irvine-Fynn *et al*. 2011). This range of temperature depends on altitude, climate and time period. A delay is observed

between glacier temperature and actual climate. Thus, polythermal glaciers can be dominated by cold ice due to a long climatic record.

Difference between these three types of glaciers can lead to different volume estimates with the same the method. Thus, it is important to identify the equation fitting well with subarctic glaciers.

4.2.2. Surface-volume relationships used

Empirical equation

Chen and Ohmura (1990) developed the first surface-volume relationship (cf. Equation 4.1). Equation 4.2 was determined using 63 alpine glaciers worldwide. Thus, this equation, deemed valid for temperate, cold and polythermal glaciers, provides a global estimate.

$$V = c_0 S^{C_1} \quad (4.1)$$

V: volume; *S*: surface; c_0 and c_1: scaling constants

$$V = 28{,}5\ S^{1{,}357} \quad (4.2)$$

Other studies provide different types of relationships, but they are all based on Equation 4.1.

Integration of physical parameters in the surface-volume equation

Bahr *et al*. (1997) integrated four parameters in Equation (4.1) using 100 different glaciers located throughout the Alps and central Asia (Equation 4.3). These parameters which account for glacier width (*q*), slope (*r*), slide drag (*f*) and mass balance (*m*) were integrated as follows:

$$V = c_0 S^{1+\frac{1+m+n(f+r)}{(q+1)(n+2)}} \quad (4.3)$$

Where *V* represents the glacier volume (10^6 m^3); *S*, the glacier surface (km^2); c_0, a random variable; and *n*, a flow law parameter.

Parameters *q* and *m* were determined using 5,400 Alps and 24,000 Eurasian glaciers, respectively. Glen's flow law leads to take *n* equal to 3. Parameter *r* corresponds to 0 given the unpredictable topography of the glacier bed. Finally, *f* is 0.

Bahr (1997) determines c_0 by considering 144 different glaciers and c_1 in Equation (4.1).

$$V = 0{,}19S^{1{,}375} \quad (4.4)$$

Using data from 23 glaciers located in the Chugach Mountains, Arendt *et al*. (2006) proposed a c_1 of 1,375 (see Equation 4.5).

$$V = 0{,}28S^{1{,}375} \quad (4.5)$$

4.2.3. Application of surface-volume equation in subarctic area

Needless to mention that the accuracy of a good surface-volume relationship depends on the values taken by c_0 and c_1 (Equation 4.1). Different authors have shown that within the same geographical region, c_0 differs from one glacier to another according to flow regime, glacier properties (slope, aspect, elevation and area distribution according to elevation) and regional climate evolution (Bahr 1997; Arendt *et al*., 2006; Debeer and Sharp, 2007). These studies showed that small glaciers are more sensitive to local, seasonal and interannual variabilities (Bahr, 1997; Barrand and Sharp 2010). Thus, glacier-dependent c_0 can lead to important discrepancies in values obtained within the same area based on the size of the glaciers. Nonetheless if, average values can provide good results (Bahr, 1997; Arendt *et al*., 2006), important disparities in regional glacier size contribute to additional uncertainties in c_0 estimates. According to these findings, use of weighted average values accounting for glacier size could increase the accuracy in c_0 estimate for a specific area. Different classes of surface area can be defined for the average weighting. Chen and Ohmura (1990) determined five surface classes (10^6 m^2) to better characterize the underlying error in volume estimation. These classes are S< 0.5; 0.5 < S < 1.0; 1.0 < S < 5.0; 5.0 < S < 10.0 and 10< S < 20.0 km^2. The first two classes were defined to account for glacier surface dynamics. Then, they suggested to separate glaciers with surface area larger than 20 km^2 to reduce uncertainties. Debeer and Sharp (2007) defined three classes according to the difference in surface change: small (0.5 km^2), intermediate (1-10 km^2) and large (>20 km^2). Thus, in our study, we chose three classes of glacier size for determining c_0: small (<0.5 km^2), intermediate (0.5-20 km^2) and large (>20 km^2) (Equation 4.6).

$$C_{0w} = \frac{(c_{0s} * \%\mathrm{s}) + (c_{0i} * \%\mathrm{i}) + (c_{0l} * \%\mathrm{l})}{100} \quad (4.6)$$

Where C_{0w} could be an alternate calculation of c_0 as a weighted average based on c_{0s}, c_{0i}, and c_{0l}: for small, intermediate and large glaciers; %*s*, %*i* and %*l* : pourcentage of small, intermediate and large glaciers.

c_1 values from studies using different methods and different glacier data, are similar. Indeed, Bahr *et al*. (1997) obtained a value of 1.375 using physical arguments. Empirical values are more like 1.36 according to Eurasian and Alpine glaciers (Chen and Ohmura, 1990; Meier and Bahr, 1996). Many studies considered c_1 = 1.375 given the similarities (Arendt *et al*., 2006; Radi and Hock, 2010). Two studies conducted in the Upper Yukon watershed provided values for c_1. NCE (2014) obtained 1.38 according to two large glaciers. Samuel *et al*. (2016) derived a value of 1.31 based on four large glaciers. These studies, which considered just a few large glaciers, are in agreement with previous findings. Thus, c_1 = 1.375 can be taken to estimate the volume of regional glaciers based. Considering pertinent past works in the Upper Yukon River, the following equation presents one surface-volume relationship.

$$V = 37.1S^{1.31} \quad (4.7)$$

This relationship has some limitations. Arendt *et al*., (2006) showed that this equation fails to provide good results when there is a loss in volume unrelated to a change in surface area. Bahr (1997) indicated that c_1 is sensitive to important mass balance change. We must also take into account different types of glaciers according to their shape, location and origin (i.e., continental ice sheets and ice caps, valleys, outlet, piedmont and tidewater). Thus, alternative data is needed to improve Equation 4.7.

4.3. Glacier module

The glacier module implemented into HYDROTEL is an altitude/elevation band based model running at the RHHU (hillslope).

1. Calculation of the volume of ice for each RHHU (hillslopes) and elevation band using Equation 4.7. This framework considers the ice surface within each band and the ice thickness is proportional to the altitude (use of a thickness gradient);

2. Conversion of the volume of ice into a mass of ice using a density of 750 kg/m³;

3. Conversion of the mass of ice into a water height (mm) over each existing ice area of each hillslope;

4. Under snowpack free conditions, estimation of ice melting using mixed degree-day solar radiation equation for each RHHU (hillslopes):

$$F = C(T_a - T_m)\frac{R_s}{R_h}(1 - a) \quad (4.8)$$

Where:

F = Ice melt (mm);

C = Melting rate (mm/day/°C; ex: 7.5mm/day/°C);

T_a = Air temperature (°C);

T_m = Threshold melting temperature (°C; ex: 1.0°C);

$\frac{R_s}{R_h}$ = Ratio of theoretical solar radiation considering the slope of the RHHU (R_s) and the theoretical solar radiation on a horizontal surface (R_h);

a = Ice albedo (ex: 0.4)

5. Subtracting melted ice (express in water height (mm) from the mass of glacier (express in water height (mm) for each RHHU (hillslopes) elevation bands)).

This elevation-band based glacier model provides an opportunity to account directly for the effect of the temperature gradient on melting and a variable distribution of ice thickness (high altitude glaciers have thicker ice distribution).

4.4. High resolution estimations of glacier melt in Gulf of Alaska area using GRACE TWS data

GRACE mission provides, using inter-satellite measurements (*i.e.*, data) a monthly field of gravity over the world at the spatial scale of several hundreds of kilometers (Tapley *et al.*, 2004). The main objective

of our study is to downscale GRACE spatial data to better estimate glacier mass loss in the Upper Yukon watershed. Findings obtained can be used to validate the hydrological modelling of glacier-covered watersheds and to further developed the surface-volume relationship.

4.4.1. Introduction

Glaciers represent 68.9% of fresh water worldwide and are considered as significant water resources. In different regions of the world, people rely on glacier meltwater for agriculture, hydropower, industries and municipal water requirements (Chen and Ohmura, 1990; Blanchon and Boissière, 2009). However, over the last decades, glacier mass losses have raised concerns among the research communities. Indeed, glaciers have an important influence on sea level rise; threatening the living environment of costal dwellings. Jin and Feng (2016) estimated the contribution of glaciers melt to sea level change between 2003 and 2012 at 1.94±0.29 mm/yr. Impact of climate change on glaciers may lead important reductions in volume through time. From 120,000 glaciers available in the World Glacier Inventory, Radić and Hock (2011) estimated that the loss in volume could be as much as 21±6% by 2100, leading to a sea level rise contribution of 124±37 mm. Larsen *et al*. (2007) investigated glacier changes in southeast Alaska and northwest British Columbia over the 1948 to 1987 period and estimated ice volume loss to be around 16.7±4.4 km^3/yr.

In situ observations and other remote sensing data represent the two main sources of information to estimate accurately glacier mass loss. Spaceborne gravimetry consists in the measurement of the gravity field and inherent variation that have direct relationship with changes associated with the distribution of mass on the Earth. Gravimetric data can be obtained specifically *in situ*, using airborne or satellite sensors, but the problem of using these two techniques is that they are limited in spatial distribution and, thus, surface coverage (Neumeyer *et al*., 2009; Cai *et al*., 2013). Since 2002, the USA (NASA) and the German (DLR) space agencies have supported a satellite gravimetry mission called GRACE (Gravity Recovery and Climate Experiment). This mission assesses variations of the Earth's gravity with a temporal resolution of a few days to a month, with a spatial resolution of +/-400 km (Tapley *et al*., 2004; Baghdadi and Zribi, 2017). The variation in the Earth's mass distribution causes a change in the gravity field (Wahr *et al*., 1998). By mapping variations of the gravitational field, GRACE assesses the Earth's mass distributions. The mass redistribution obtained from GRACE data, contains terrestrial water storage

change (TWS), and oceanic mass change (Wahr *et al*., 1998; Chen *et al*., 2006). Yiradw *et al*. (2009) noted that GRACE mission estimates could be used to monitor the rate of change of TWS over large spatial scales. Baghdadi and Zribi (2017) further stressed that continental hydrology is one of the main applications of GRACE data. The change of TWS consists of changes of surface water, soil moisture, ground water, snow and ice. Thus, GRACE data can be used to determine the change in glacier mass. Jin and Zou (2015) used GRACE data to estimate with high precision glacier mass dynamics in Greenland. In the Golf of Alaska (GOA) region, GRACE data have been used in different studies to estimate glacier mass loss (see *e.g*. Tamisea *et al*., 2005; Chen *et al*., 2006; Arendt *et al*., 2008; Luthcke *et al*., 2008; Arendt *et al*., 2009; Baur *et al*., 2013; Arendt *et al*., 2013; Beamer *et al*., 2016; Wahr *et al*., 2016; Jin *et al*., 2017).

The main problem of using GRACE data to investigate hydrological fluxes such as glacier mass loss, lies in the low spatial resolution and inability to discriminate side-by-side mass changes. Because of this low resolution, Baghdadi and Zribi (2017) explained that GRACE data are plagued with errors over a small area. They reported a data accuracy of 7 mm and 3 mm of water equivalent for watersheds of 400,000 km^2 and 4,000,000 km^2, respectively. Longuevergne *et al*. (2010) showed the limit to interpret GRACE data on 200,000-km^2watershed. To overcome this problem, scientists started to combine GRACE data with other sources. The development of processing techniques and the combination of GRACE data have increased over the years since GRACE was launched. The possibility of separate spatial signals has increased and allows focusing the signal to local area. But use of GRACE data on small watersheds with spatial resolution less than hundreds of km or water resources management spatial scale remains the main problem to solve.

Studies on the GOA to estimate glacier mass loss have different surface coverage. Some of these surfaces are much larger than the spatial scale of water resources management. Nonetheless, an inversion method can be applied to improve the spatial resolution of GRACE data (Farinotti *et al*., 2015; Long *et al*., 2016; Castellazzi *et al*., 2018). Chen *et al*. (2015) used forward modelling to restore GRACE signal amplitude of Antarctic ice and glacier loss due to noise reduction. Long *et al*. (2016) showed that constrained forward modelling can spatially recover details of GRACE signal distribution. Farinotti *et al*. (2015) estimated glacier mass loss in the Tien Shan Mountains of China by subtracting non-glacier contributions from the total mass change. They used an inversion method with *a priori* information

about glacier spatial distribution in area subdivisions (*i.e*., mascons and sub-mascons). By improving GRACE spatial resolution, their results are comparable to altimetric method and glaciological modelling. Studying groundwater depletion in Central Mexico, Castellazzi *et al*. (2018) improved the GRACE spatial resolution using InSAR as *a priori* to constrain the data. They subtracted groundwater contributions from other components of TWS and delineated areas of interest. Their results were comparable to governmental groundwater budgets. As several authors injected ancillary data into GRACE post-processing to improve its resolution, comparisons with more simplistic approaches such as spatial averaging (*e.g.* over watersheds or glacierized regions) and estimates of the limits of such procedure are still lacking.

In this study, we use several GRACE solutions and apply a spatial constraint to focus the signal. The core objective of this study was to come up with a high-spatial resolution estimate of glacier mass loss in Yukon and Alaska.

4.4.2. Study area

During the last decade, different studies used GRACE data to estimate glacier mass loss in subarctic area and particularly on the GOA (Fig. 4.1). However, we have noted some discrepancies in results obtained (Table 4.1). Indeed, measured glacier mass loss varies from -47 to -110 Gt/yr and these differences can be explained by many factors.

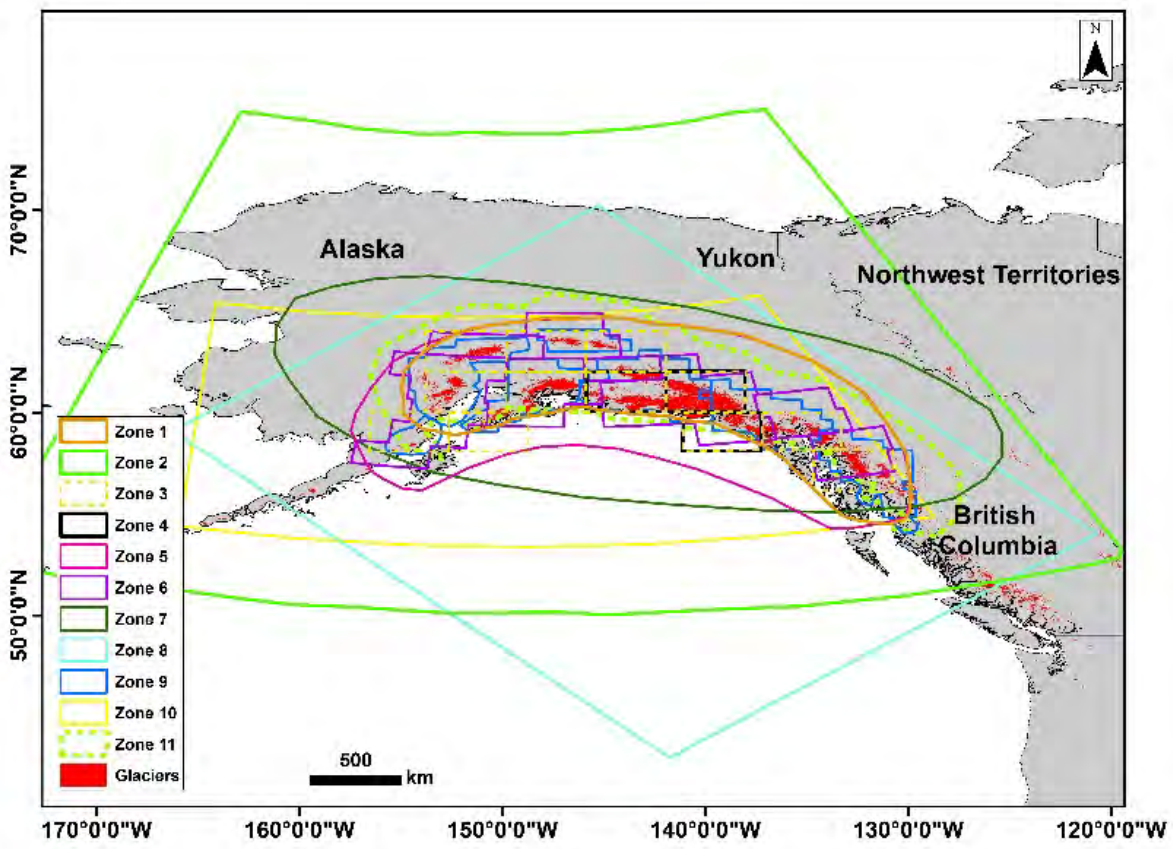

Figure 4.1 Glaciers of the GOA and footprints of the studies focusing on the use of GRACE data to assess glacier melt. The study area considered here is identified as Zone 11 (Doumbia et al., 2020).

First, size of the study area and data time period like those showed in Table 4.1 contributes to discrepancies of mass loss estimates in the GOA. Indeed, the total surface coverage considered by Tamisiea *et al*. (2005) and Beamer *et al*. (2016) is 701,000 km² and 420,300 km² respectively. The first three studies show high values of mass loss (Tamisiea *et al*. 2005; Chen *et al*. 2006; Luthcke *et al*. 2008). It is mainly due to the use of the earlier released of GRACE data plagued with some uncertainties. Thus, trend estimates over three or four years are not consistent.

Then different GRACE TWS data and interpretation processing methods were used. Two main types of GRACE solutions called Level-2 are used in hydrological applications. There are unconstrained solutions, relying on de-stripping and spherical harmonic truncature, and constrained solutions often relying on

regularization or stabilization. Among the later, mascon solutions (e.g. Save *et al*. 2016) have become particularly popular in the last years.

In our study area, different studies used unconstrained solutions from the Science Data Center (SDS) (Tamisea *et al*., 2005; Chen *et al*., 2006; Baur *et al*., 2013; Jin *et al*., 2017). Generally, unconstrained GRACE spherical harmonic solutions present errors at high spatial frequencies (*e.g*., N>60 or 300 km) and North-South stripes mainly due to gravitational model correction and instrument errors. Filtering methods are applied at these level-2 solutions to eliminate stripes (*e.g.*, de-striping) and to reduce high frequency errors (*e.g*., truncation, Gaussian smoothing). Tamisea *et al*. (2005) completed solutions used to Spherical Harmonics (SH) degree and order 70. While, others applied a truncation at degree and order 60 (Chen *et al*., 2006; Baur *et al*., 2013; Jin *et al*., 2017). The aforementioned studies have applied Gaussian filter with a radius of 500 km. Filtering techniques induce GRACE signal attenuation and leakage. Different strategies like scaling approach, additive approach, multiplicative approach and unconstrained or constrained forward modelling approaches permit to overcome this signal loss (Long *et al*., 2016). Meanwhile, Tamisea *et al*. (2005) used a scaling factor approach. Forward modelling approach can also be used (Baur *et al*., 2013; Jin *et al*., 2017). Save *et al*. (2016) proposed the use of mascon solution to mitigate GRACE signal attenuation. Spherical harmonic is up to a certain degree and order to relate mascon to the inter-satellite measurement. Many GOA glacier mass loss studies based on GRACE data, used mascons solutions at different spatial and temporal resolution (Luthcke *et al*., 2008, 2013; Arendt *et al*., 2008, 2009, 2013; Jacob *et al*. 2012; Bearmer *et al*., 2016; Wahr *et al*., 2016).

Different interpretation methods are used with GRACE data to improve spatial resolution and validate glacier mass loss measurement. Thus, remote sensing of ice surface elevation (*e.g*. ICESat NASA, airborne laser altimetry) is combined with GRACE data (Arendt *et al*., 2008, 2013; Jin *et al*., 2017). Meteorological models are also used with GRACE data (Arendt *et al*., 2009; Wahr *et al*., 2016). Some studies combined remote sensing and meteorological data to enrich and validate glacier mass loss estimates (Ardent et al., 2013; Luthcke *et al*., 2013). Beamer *et al*. (2016) developed hydrological models and compared their results with airborne altimetry and GRACE data.

Table 4.1 Estimates of glacier mass loss in the GOA according to different authors.

Study area (Zones on Fig. 1)	Authors (Year)	Data time period	Estimated mass loss (Gt/yr)	Data source	Glaciers area considered (km²)
1	Tamisiea et al.,2005	2002–2004	110	GRACE	87,000
2	Chen et al., 2006	2002–2005	101	GRACE	~90,957
3	Luthcke et al., 2008	2003–2006	102	GRACE	~82,505
		2003–2007	84		
4	Arendt et al., 2008	2003–2007	20,6	GRACE	32,900
5	Jacob et al., 2012	2003–2010	46	GRACE	~90,000
6	Arendt et al., 2013	2003–2009	61	GRACE	82,505
		2003–2010	65		
		2004–2010	71		
7	Baur et al., 2013	2002-2011	56	GRACE with geocenter correction	~80,000
			47	GRACEwithout geocenter correction	
8	Beamer et al., 2016	2004-2013	60,1	GRACE	72,302
9	Wahr et al., 2016	2002-2014	52	GRACE and Meteorological model	~72,600
10	Jin et al., 2017	2003-2009	57.5	ICESat altimetry and GRACE	86,715

4.4.3. Data and Methods

Glaciers data and mascon delineation

In this study, we used pre-delineated glacier area as *a priori*. The glacier distribution map used is constituted of outlines from the GLIMS Glacier Database released 27/10/2017 and available online (http://nsidc.org/glims/) (GLIMS and NSIDC, 2005, updated 2013). According to Raup *et al*. (2007), it is an extension of the World Glacier Inventory data and is constituted of different sources like imagery satellite data, historical information from maps, and aerial photography. Recently, GLIMS glacier Database was completed with Randolph Glacier Inventory (RGI) data. The latter is produced to support the fifth report of the Intergovernmental Panel on Climate Change (IPCC AR5) (Pfeffer *et al*., 2014). Therefore, GLIMS database can contain some errors like one glacier may be counted more than once. The total glacier cover in an enlarge study area (Gulf of Alsaka including southern Yukon River glacier) is

around 90,000 km^2 (Fig. 4.2) according to this database.[1] This compares well with glacier area of studies presented in Table 4.1.

Mass concentrations (mascon) technique is used in GRACE data inversion method to re-focus signal and estimate mass variations in a local area (Farinotti *et al*., 2015; Save *et al*., 2016). In this study, we tested three different spatial distributions of mascons with more or less uniform size (Table 4.2). Our purpose was to illustrate how a strongly dominated GRACE signal can be downscaled to higher resolution. We supposed a uniform distribution of ice loss in each mascon which contains glacier spatial distribution information. GLIMS outlines used as *a priori* were resampled to a 0.25° grid (~28km x ~14km).

[1] This is an area much larger than the area studied by Yukon University in their previous study on the glaicers of the Upper Yukon River watershed.

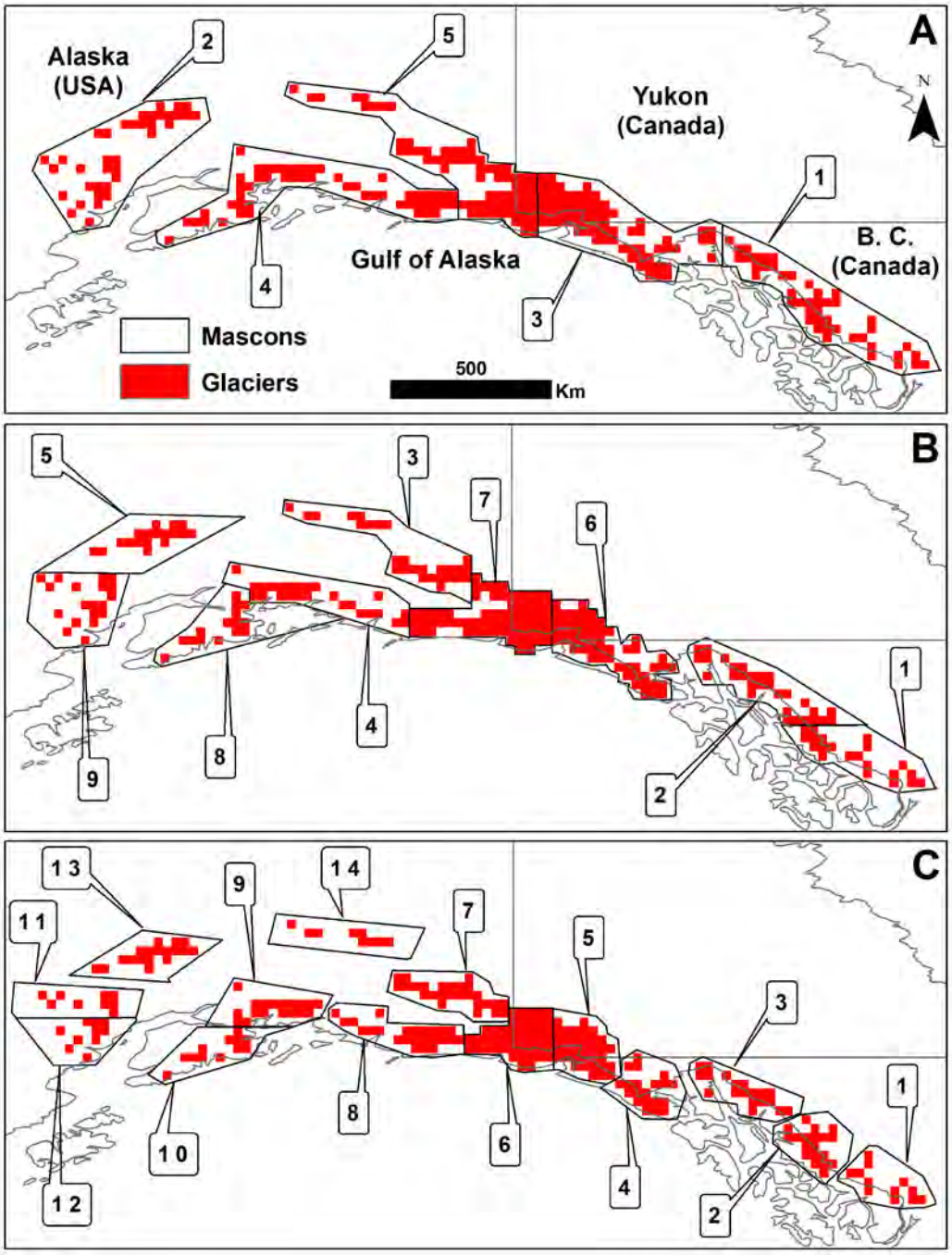

Figure 4.2 Glacier distribution map used to focus GRACE trend maps. Three mascon delineation scenarios are presented: (A) 5 mascons with an average area of ~55,000km^2, (B) 9 mascons with an average area of ~30,000km^2, and (C) 14 mascons with an average area of ~20,000km^2 (Doumbia et al., 2020)..

Table 4.2 Characteristics of the three mascons delineations

Mascon number	Total Surface (km²)	Average (km²)	Standard deviation (km²)
5	272,400	54,480	1,214
9	282,970	31,441	1,657
14	278,760	19,911	690

GRACE TWS data

Three versions (usually referred to as 'solutions') of Level-2 GRACE TWS (Total Water Storage) data are considered. The first is a typical unconstrained solution from the Center for Space Research (CSR RL06) complete up to Spherical Harmonics (SH) degree and order 96 and de-striped/filtered in a single step by applying the DDK8 filter (Kusche, 2007, 2009). Second, is the stabilized solution complete up to SH degree and order 90 from the Space Geodesy Research Group (GRGS RL04 - http://grgs.obs-mip.fr/grace). The CSR RL05 regularized Mascon solution from Save et al. (2016) as available at http://www2.csr.utexas.edu/grace/, is the third GRACE data used. All solutions were truncated at degree/order 90 to reduce errors in results due to the difference in resolution. The solutions are referred to as T96DDK8, GRGS, and CSR-MASC hereafter. They are derived from different processing strategies and follow different protocols and assumptions; hence we consider that their discrepancy represents a good estimation of the errors related to the choice of the processing strategy.

Generally, GRACE TWS signal is considered to be composed of different components or water storages (Ice Storage, Groundwater Storage, Surface Water Storage, Snow water Storage and Soil Moisture Storage). Glacial Isostatic Adjustment (GIA) is also one of the GRACE TWS signal components. CSR-MASC is already corrected of isostatic effects, based on the model of Geruo *et al*. (2013). We applied this model based on the ICE-5G data to subtract GIA contribution to GRGS and T96DDK8 variations in our study area. GOA signal shows a strong negative anomaly in all three solutions considered (Fig. 4.3). The masses loss observed are very similar. The anomaly from GRGS solution shows a slight spatial difference at the eastern tip due to the differences in the de-stripping strategy. Considering the important part of glaciers in the GOA area, we supposed that GRACE TWS signal is solely dominated by Ice Storage of glaciers.

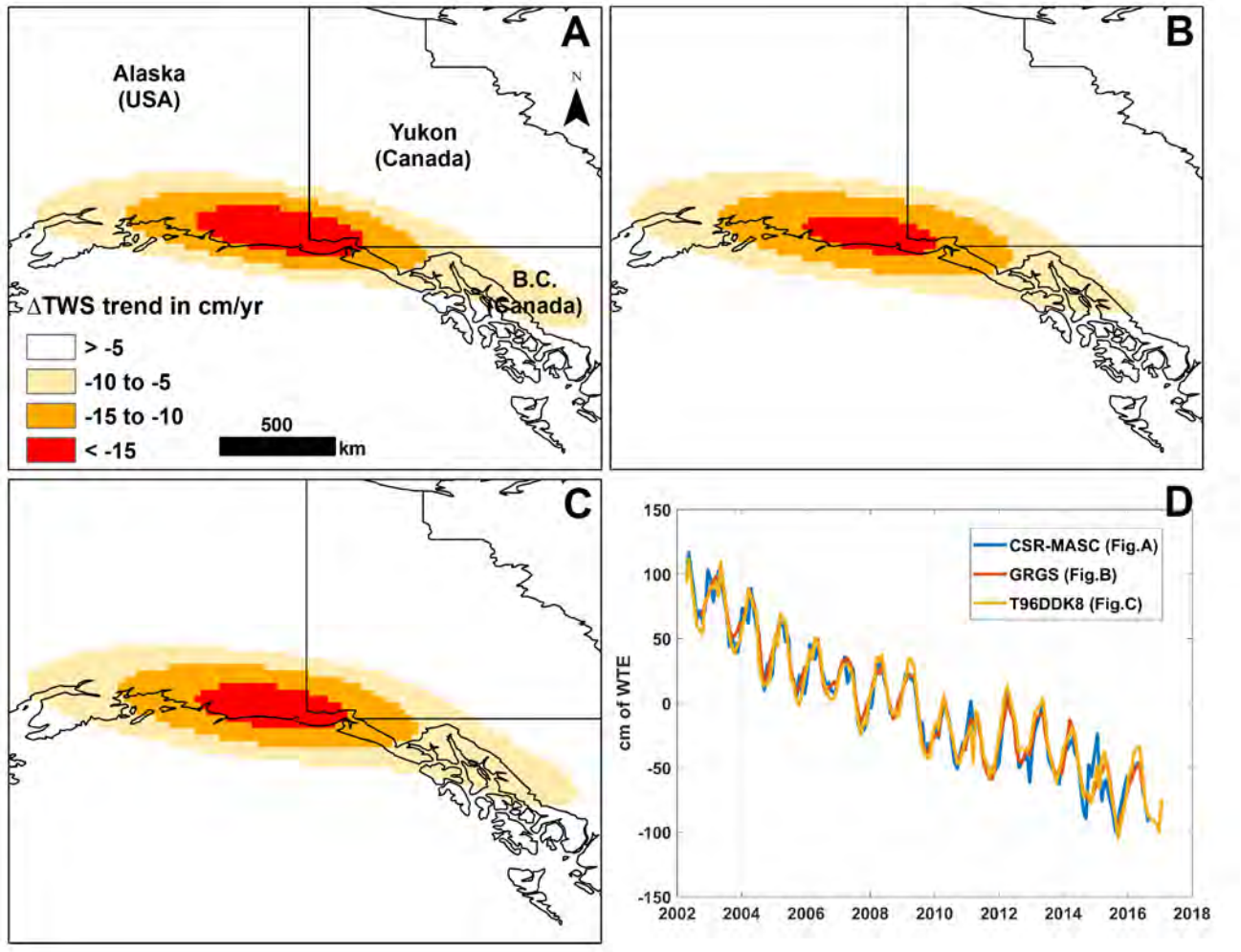

Figure 4.3 GRACE TWS signal trend over the study area from three GRACE solutions: (A) CSR MASC, (B) GRGS, (C) T96DDK8, and (D) signal trend of the middle of the anomaly (Doumbia et al., 2020).

In forward modelling, we used solely GRACE TWS solutions trend. Thus, three 2D trend maps were derived from the three solutions 3D data-cubes (Space x Space x Time). First, we subtracted a one-year period sine curve with an iteratively fitted amplitude. Second, we applied a 13-month moving average to smoothen the curve. Finally, a linear curve (ax + b) was fitted, where the slope represents the trend.

Inversion procedure

The focusing procedure consists in allocating masses to each mascon with an even distribution to each pixel of glacier and interchanging mass allocations until the model converges toward the real GRACE TWS signal. In other words, the inversion process minimizes the difference between a synthetic and

automatically generated mass distribution map and the real GRACE TWS map. We also performed a simulation with synthetic data to evaluate the effect of diffuse masses over the mass retrieval process and to validate the inversion procedure. The inversion procedure and the simulation with synthetic data applied in this study are well explained by (Doumbia et al., 2020).

We present ice mass loss results obtainedat GOA and Mascon-scale. We also analysed the residual maps from the focusing procedure. In this study, Absolute Error (AE) is the objective function used into the Pattern Search algorithm that aims to reduce the difference between the Forward Model (FM) and the GRACE trend map. The ice mass loss results obtained correspond to the minimum value of residual between the FM and the GRACE trend map.

4.4.4. Results and Discussion

Glaciers mass loss maps on GOA area

The total mass loss rates from the three solutions show a consistency (Table 4.3). The Coefficient of Variation (COV) has been used to evaluate the discrepancies between results. The COV from different solutions over the same spatial distribution and by using different distributions with the same solution are ~3.5% and ~2.1% respectively. These results confirm the similarity between solutions observed in Figure 4.3. These similarities show the stability of GRACE TWS solutions at these spatial resolutions in the GOA glacier mass loss assessment.

Table 4.3 Mass loss estimated according to the three solutions and mascon delineation considered at GOA scale.

Number of mascons / mean area	CSR-MASC	GRGS	T96DDK8	Mean (Gt/yr)	COV (stdev in % of mean)
5 / 55 000km2	41.86	39.31	41.28	40.82(1.34)	3.28
9 / 30 000km2	40.18	37.56	39.65	39.13(1.39)	3.55
14 / 19 000km2	41.41	38.59	40.78	40.26(1.48)	3.68
Mean (Gt/yr)	41.15(0.87)	38.48(0.88)	40.57(0.84)	-	-
COV (stdev in % of mean)	2.11	2.29	2.07	-	-

Comparison with other glacier mass loss estimates in the GOA

In our study, the three solutions considered provided similar results by using the three mascon delineation at the GOA scale (Table 4.3). Thus, we compare here the mean results with glacier mass loss estimated by different GRACE studies of GOA glaciers (Table 4.1). Our study focuses approximately on the same glaciers that these studies (Fig. 4.1/Zone 11). We note a good agreement between our results with rates obtained by Jacob *et al*. (2012) (-46 Gt/yr), Baur *et al*. (2013) (-47 Gt/yr) and Wahr *et al*. (2016) (-52 Gt/yr) (Fig. 4.4). Discrepancies with results obtained by Tamisiea *et al*. (2005), Chen *et al*. (2006) and Luthcke *et al*. (2008) are mainly due to the shorter data time span and inherent uncertainties associated with the earlier GRACE TWS data. Difference between our estimates and other published rates can be explained by different in GRACE TWS data and interpretation processing used (cf. 4.4.2).

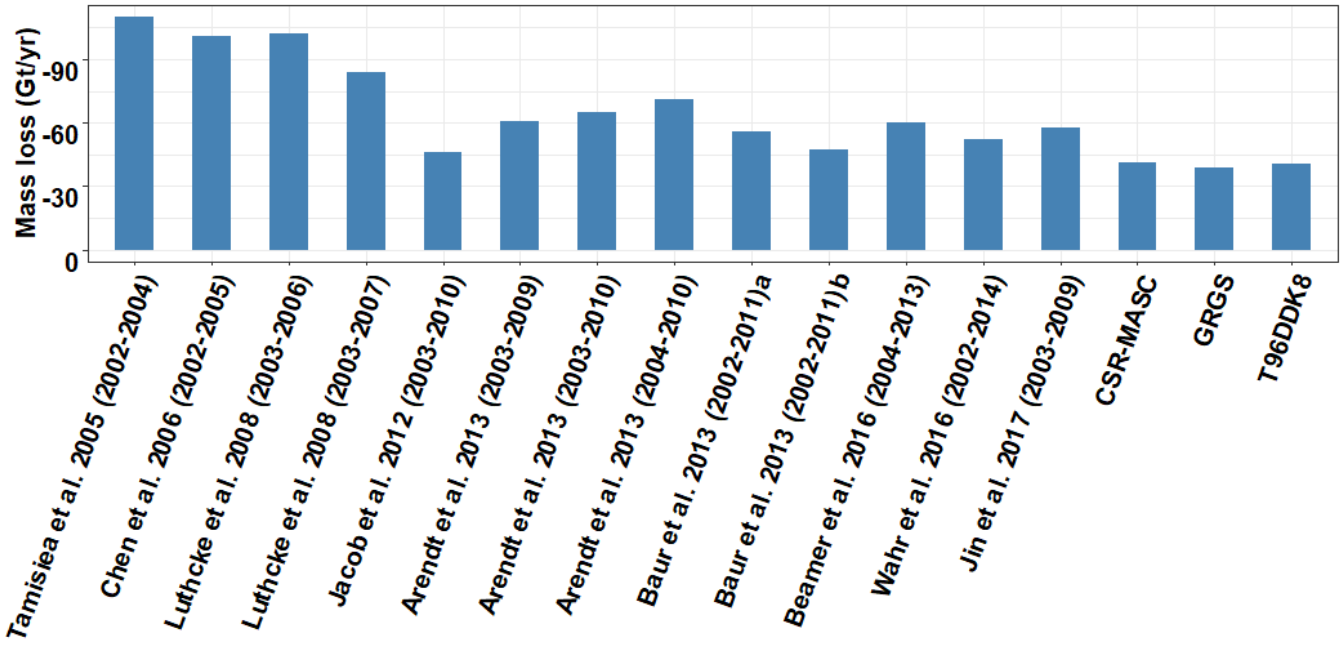

Figure 4.4 GOA glacier mass loss estimates from different studies (Doumbia et al., 2020).

Another difference may be attributed to the use of *a-priori* distribution; so potentially, we discriminate better the glacier signal from other contributors. The use of the same size of mascon area contribute also to have good results. Indeed, use of forward modelling based on an equivalent size of mascons with a uniform distribution of mass changes using *a-priori* information provides good glacier mass loss

estimates by reducing uncertainties (*e.g.* signal attenuation) due to GRACE data processing (Chen *et al*. 2015; Farinotti *et al*., 2015; Castellazzi *et al*. 2018).

Detection of high resolution limits and adequate GRACE TWS solutions

Analysis in this section are based on similarities between solutions. Indeed, we suppose that good agreement of solutions indicate good glacier mass loss estimates. Table 4.4 show the total mass loss obtained per mascon and the maps shown the spatial distribution of the mean and standard deviation value are presented in Figure 4.5. For each delineation we analysed similarity between the three solutions based COV results (Table 4.5).

Table 4.4 Mass loss measured (Gt/yr) for the three mascon delineations. Note that mascon numbers do not correspond between the different delineations (see Fig. 4.2) (Doumbia et al., 2020).

	1	**2**	**3**	**4**	**5**	**6**	**7**	**8**	**9**	**10**	**11**	**12**	**13**	**14**
5 Mascon – 55 000km² scale														
CSR-MASC	6.74	3.23	9.35	14.31	8.23	-	-	-	-	-	-	-	-	-
GRGS	5.28	4.02	9.14	14.32	6.55	-	-	-	-	-	-	-	-	-
T96DDK8	6.5	4.02	9.29	14.13	7.34	-	-	-	-	-	-	-	-	-
COV (%)	13	12	1	1	11									
9 Mascon – 30 000km² scale														
CSR-MASC	2.68	4.84	3.22	8.88	1.06	7.03	8.74	1.27	2.47	-	-	-	-	-
GRGS	2.31	3.73	2.88	8.72	1.71	7.06	7.25	1.41	2.50	-	-	-	-	-
T96DDK8	2.85	4.43	3.39	8.39	1.65	7.21	7.58	1.50	2.64	-	-	-	-	-
COV (%)	10	13	8	3	25	1	10	9	4					
14 Mascon – 20 000km² scale														
CSR-MASC	2.50	1.3	4.47	0.85	6.69	2.97	2.43	8.28	4.93	1.55	0.38	1.77	1.61	1.68
GRGS	1.72	1.69	2.91	1.58	6.69	1.45	2.57	7.84	4.74	1.84	0.65	1.5	2.11	1.3
T96DDK8	2.29	1.76	3.82	1.09	7	1.7	2.62	8.09	4.60	1.87	0.75	1.55	2.05	1.59
COV (%)	19	16	21	32	3	40	4	3	3	10	32	9	14	13

Figure 4.5 shows that variations increase over the East/West extremes with the number of mascons. This spatial difference between solutions are explained by the low signal observed Eastern/Western in the GRACE TWS trend maps (Figure 4.3). Thus, the spatial difference in low resolution data is propagate into the ice mass loss high resolution maps. We observed low values of COV observed over the middle part of the GOA where the signal is the strongest (Figure 4.3). These results over this part, containing the

Upper Yukon glaciers show the reliability of the ice mass loss estimates from our method in this location (Table 4.4 and Figure 4.5). This is confirmed by comparing our results with those of different studies and data aiming to estimate ice mass loss over the central part of GOA (Doumbia et al., 2020). The use of short GRACE data times-series (3-4 years from 2003) lead to an overestimation of ice mass loss by ~20% (Doumbia et al., 2020). Our results are more reliable because of the use of long GRACE data times-series (from 2002 to 2017).

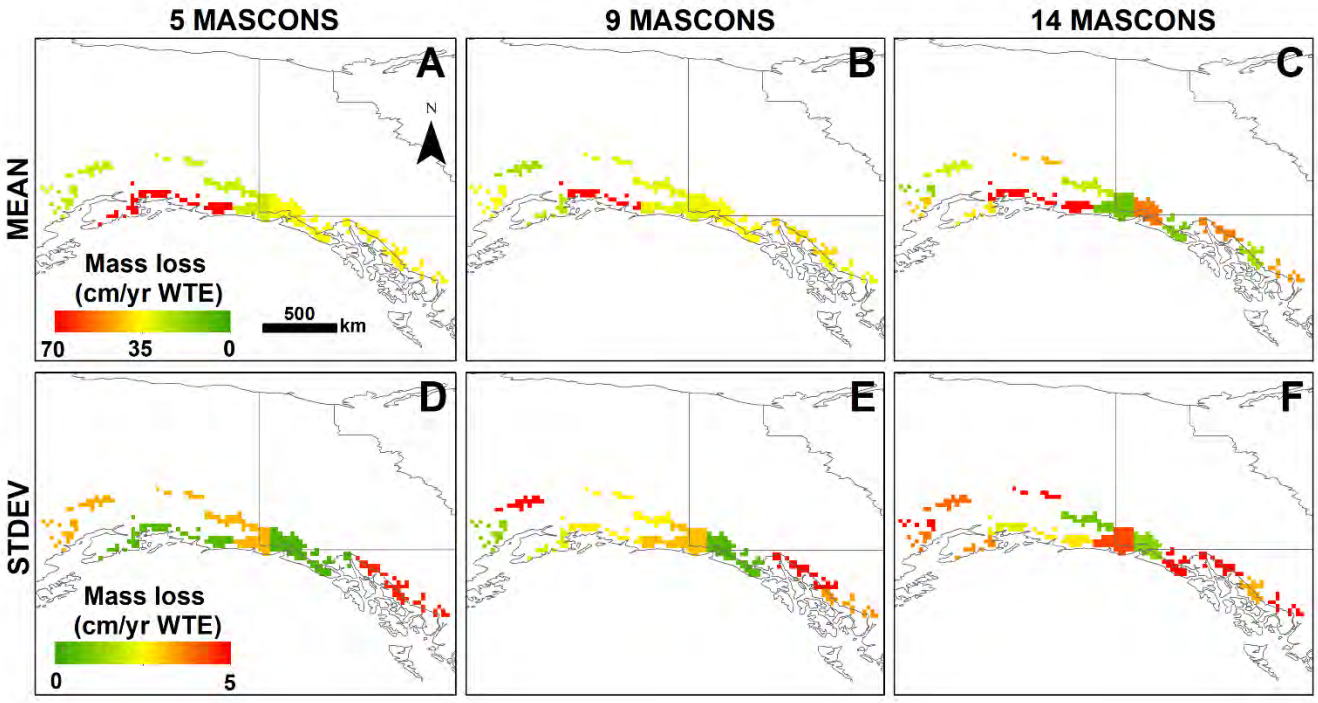

Figure 4.5 High resolution mapping (average and standard deviation values of annual water height losses) according to the delineation scenarios introduced in Figure 4.2. This mapping is derived from the forward modelling results based on the three solutions considered and each mascon delineation chosen (Doumbia et al., 2020).

Forward modelling residuals

The residuals maps are obtained by substracting the FM of the inversion from the GRACE TWS data shown in Figure 4.3. The use of a large number of mascon provide the lower amplitude of residuals (Figure 4.6). This indicates that a large number of mascon allows to retrieve ice mass loss by using the inversion procedure but this could induce important uncertainties (e.g 14-mascon delineation).

The residuals are low inland and CSR-MASC presents the less important residuals near to the ocean. The high residual value near to the ocean is probably due to the use of land mask. Thus, the land mask not totally covers the signal from coastal glaciers.

To validate our results, we compared the residuals values with the amplitude of the noise from GRACE data measurements and processing errors (Wahr et al., 2006). The noise level corresponds to the maximum GRACE signal over the Pacific Ocean at similar latitudes than GOA. We found the noise values ~1.4, 1.6 and 1.5 cm/year for CSR-MASC, GRGS and T96DDK8 respectively (Doumbia et al., 2020). Theses values compare well with the residuals values (from -2 to +2 cm/year). These results show that our method retrieve well the ice mass loss.

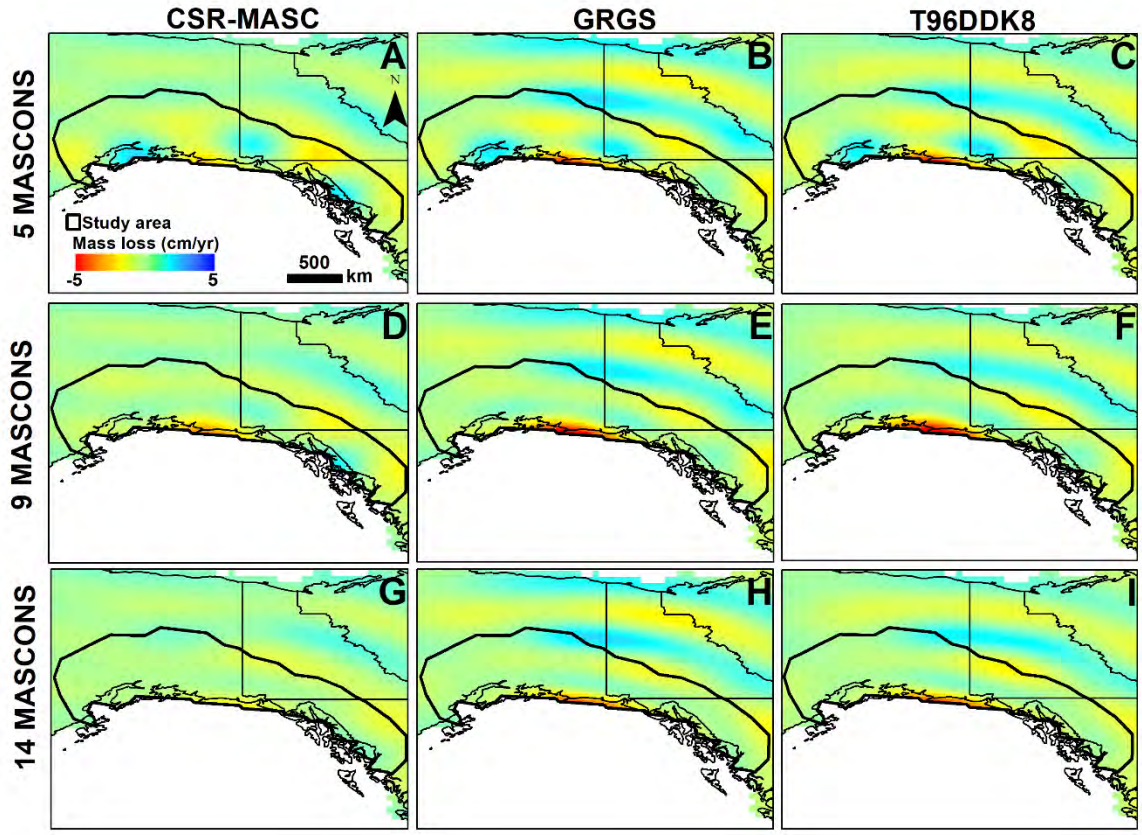

Figure 4.6 Residuals of the focusing procedure according to the three solutions considered and each mascon delineation chosen (Doumbia et al., 2020).

The results obtained (i.e. COV from Table 4.4; Standard deviation map from Figure 4.5 and the residuals results) show that an acceptable accuracy is provided by using mascon size up to 30,000 km^2. This is confirmed by the synthetic test realised by (Doumbia et al., 2020).

4.4.5. Conclusion

In this section, we downscaled three GRACE TWS data by using a forward modelling with uniform glacier area size and uniform spatial glacier mass loss in each mascont to estimate glacier mass loss within the GOA and at high spatial resolution.

The analyis of the three GRACE TWS data indicates that glacier melt dominates the GRACE TWS signal in the GOA. The residuals result show that the inversion procedure used retrieves well the ice mass loss.

At the GOA-scale, we obtained approximatively the same total ice mass loss value (~40 Gt/year) by using the three solutions with an uncertainty of 2-4%. We compared our results from the three solutions according to the three-glacial zones with estimated GOA glacier mass loss reported in other studies. We found ~-40 Gt/yr as the generally agreed value of global glacier mass loss. Discrepancies with other studies (Table 4.1) are due to data time span, use of a-priori distribution, interpretation strategies and the size of study area chosen (Fig. 4.1).

At mascon-scale, this study shows that the ice mass loss estimates are more accurate by using a delineation size of 30,000 km2 or larger. The spatial resolution of 14 mascons is too high to give consistent glacier mass loss estimates by the three solutions. The analyses of the comparison of our results with those from studies and data at the center of GOA, where the signal is the highest, show a good agreement. The ice mass loss from the latter area containing the Upper Yukon glacier is the most reliable by using our method.

To our knowledge this is the first study to use several GRACE solutions and apply a spatial constraint to focus the signal on GOA glaciers. It will be interesting to try different types of decorrelation filters on unconstrained solutions and to further investigate the difference in mass loss results on mascon 3 of the 9 mascon zoning. Comparison of our findings with results from other types of data could also prove to be helpful. The use of altimetry data as a-priori could provide a robust forward model. It could also be

interesting to use the average of the consistent solutions. Truncation at high degree and order SH of simulated CSR-MASC, should be investigated to reduce residual.

In parallel we did implement a full elevation band based glacier module into the HYDROTEL to more distribute spatially the melt and to explicitly assess the contribution of glaciers to Upper Yukon River hydrologic budget. For this implementation, we did benefit from the previous work conducted by Yukon University; that is we built the model using their development of : (i) a surface-volume relationship, (ii) glacier mass-loss tendencies, (iii) initial parameter values of ice melting rate and melting temperature threshold.

5. Watershed hydrology and large-scale circulation patterns

5.1. Literature review

In regions with snowmelt-driven runoff, spring freshet represents a major contribution to annual runoff. The possibility of oceanic-atmospheric circulation patterns inducing regime shifts could have significant implications for seasonal inflow and river forecasting. The El Niño Southern Oscillation (ENSO) index is the most dominant interannual signal of climate variability induced by such patterns; influencing precipitation, streamflow and flood-risk around the world (Ward et *al.*, 2014). For southern Yukon, the Pacific Decadal Oscillation (PDO) has a more dominating effect than ENSO (PDO response being modulated by ENSO) (Wang et *al.*, 2006). Investigating potential links between PDO and seasonal streamflow patterns in southeast Alaska, Neal et *al.* (2002) showed that annual discharge had not changed significantly; however, seasonal patterns did change significantly throughout the year. There was relatively high winter flow and low summer flow during warm PDO in non-glacier-fed watersheds. Analyzing the two most recent modes of PDO in the Yukon River Watershed, Brabets and Walvoord (2009) observed that during warm PDO, there was increased winter flow, likely resulting from groundwater input increased by permafrost thaw. Woo and Thorne (2008) found that rivers in Alaska, Yukon, Northwest Territories, British Columbia and Alberta have variable responses to PDO signals; non-climatic factors such as location, topography and storage modifying the responses.

Using self-organizing maps based on an Artificial Neural Network algorithm Cassano and Cassano (2010) found clear links between atmospheric circulation patterns and spatial distribution of summer and winter precipitations in the Yukon Territory. Kalra et *al.* (2013) applied a Support Vector Machine (SVM) technique (*i.e.*, statistical-learning model) to a snowmelt-driven watershed to forecast spring-summer flow from climate indices (PDO, ENSO, among others). Results revealed a strong association between coupled indices compared to their individual effects. Taschetto *et al.* (2014) analyzed ENSO representation in 34 CMIP5 (Coupled Model Intercomparison Project Phase 5) models produced by the Intergovernmental Panel on Climate Change (IPCC) (Taylor et *al.*, 2012) and found most of them realistically simulated observed intensity and location of maximum sea surface temperature (SST) anomalies during ENSO events. CMIP5 generation of global climate models are known to corroborate

key Pacific climate mode and their teleconnections to North American climates (Polade et *al.*, 2013). Sheffield et *al.* (2013) analyzed CMIP5 historical simulations, and found that frequency and mean amplitude of ENSO were generally well reproduced, although teleconnections with North American climate varied widely among models. Fuentes-Franco *et al.* (2015) analyzed ENSO and PDO in CMIP5 simulations and found the models reproduced well the constructive interference between these oscillations patterns when compared to observations (*i.e.*, positive ENSO and PDO or negative ENSO and PDO). The destructive interference was less accurately reproduced. For the 2nd half of the 21st century, overall strengthening of both ENSO and PDO signals could be found.

For this project, we are using climate models to highlight the structure of teleconnections between Pacific climate variability and the regional hydroclimate of the Yukon Territory delineated by a buffer region including parts of Alaska, British-Columbia, Alberta and Northwest Territories. The focus of the current work package is to investigate the transferability of the teleconnections and their use in an operational context.

Three indices of influence are considered to study teleconnections: the Artic Oscillation (AO), the Pacific Decadal Oscillation (PDO) and the Multivariate ENSO Index (MEI). The AO index is obtained by projecting the AO loading pattern to the daily 1000-millibar height anomaly field over 20°N-90°N latitude. The AO loading pattern has been chosen as the first mode of the empirical orthogonal function (EOF) analysis using monthly mean 1000-millibar height anomaly data over 20°N-90°N. The PDO is defined by the leading pattern (EOF) of sea surface temperature (SST) anomalies in the North Pacific basin (typically, polewards of 20°N). The MEI index is a multivariate index characterising ENSO with the six main observed variables over the tropical Pacific. These six variables are: sea-level pressure (P), zonal (U) and meridional (V) components of the surface wind, sea surface temperature (S), surface air temperature (A), and total cloudiness fraction of the sky (C). All these indices are compiled by the Earth System Research Laboratory of NOAA, the National Oceanic and Atmospheric Administration, and are available on-line (https://www.ncdc.noaa.gov/teleconnections/) for AO and PDO, and (https://www.esrl.noaa.gov/psd/enso/mei/) for MEI.

5.2. Transferability of teleconnections across different data sources and time periods

Spearman rank correlations are used between monthly index values and precipitation/temperature data over the region of interest. Multiple datasets have been downloaded for local information: two sets of local observations from stations, four large-scale reanalyses and two products from climate models available for both past and future time periods.

The first set of local information is retrieved from available stations using different quality criteria:

- Data should be available for at least 30 years;
- No more than 4 missing months missing over each 12-month period;
- Missing data should not account for more than 10% of all data over the entire time series.

All historical data from Environment and Climate Change Canada and from COOP and METAR stations in Alaska over 55°N-67°N and 124°O-146°O which met these criteria were selected. It consists in 33 stations including nine (9) stations in Alaska.

The second set of observations is the Adjusted and homogenized Canadian climate data available over the zone. They are homogenized time series, set up from the original observations of the first set. They are used to validate observations from the first set.

Observations from stations being sparse within the zone of interest, additional four large-scale reanalyses were considered. These reanalyses provide local information on a regular grid at a daily time step. Contrary to stations, there is no missing data across the period. Provided data is spatialized over a grid; comparison to point observations should be made with caution. The twentieth century reanalysis (20CR, Compo et *al*., 2011) by NOAA and ECMWF twentieth century reanalysis (ERA-20C, Poli et *al*., 2013) are the two reanalyses spanning the entire twentieth century. Both of them were produced with climate models and assimilation of surface pressure. As there is no assimilation of meteorological data and a low grid resolution (approx. 200 km for 20CR and 125 km for ERA-20C), these reanalyses are considered not accurate enough to provide local precipitation and temperature (it would require a downscaling step). However, as they are the only source of data spanning the entire twentieth century, they were kept in

the analysis. ERA-20C consists in a single member while 56 members are provided for 20CR. ERA-Interim by ECMWF (ERA-I, Dee, D. P., *et al.*, 2011) and JRA-55 by the Japan Meteorological Agency (Kobayashi, S., *et al.*, 2015) were also considered for this study. ERA-I is available from 1979 and assimilates numerous observations to provide a good estimation of precipitation and temperature over an 80-km grid. JRA-55 is available from 1958 and relies on the same principles than ERA-I, but over a 55-km grid (approx.). The latter reanalysis will only be used beyond the 1970s to avoid the bias associated with the use of different systems of observations in the data assimilation process (satellite observations became available after 1970).

The last two products used are the CMIP5 and CORDEX datasets, made available by the Ouranos consortium. They consist in realizations from multiple climate models over the past (1950-now) and the future (up to 2100) considering different representative concentration pathways. No assimilated data is used to derive these products. Thus, contrary to previous reanalyses, the correct weather sequences are not reconstructed in the past. This is suitable for our study as the aim is to evaluate the temporal stability of teleconnections. Ensembles from CMIP5 were derived from global models, and local variables were debiased by Ouranos. Ensembles from CORDEX are provided using multiple dynamical and statistical downscaling models with forcing climate models from the CMIP5 archive. Consequently, CORDEX is available at a higher resolution (generally around 50 km) than CMIP5.

Figures 5.1 and 5.2 provide the precipitation and temperature time series from aforementioned datasets for the WHITEHORSE A meteorological station at annual and seasonal time scales (spring = April-June, summer = July- September, winter = October-March). Absolute values of precipitation and temperature should not be compared to observations, since an observation is a local grid point whereas other products are spatialized over a grid point. ERA-I and JRA-55 reproduce precipitation variability for all seasons correctly, as well as ERA-20C at the annual time scale and in spring. Similarly, some CORDEX models are able to provide a coherent variability for precipitation. 20CR places too much variability on precipitation whereas CMIP5 shows very little variability. All reanalyses are able to capture the observed temperature variability, contrary to CMIP5 and CORDEX. For both precipitation and temperature, the 56 members of 20CR behave less consistently before the 1930s. Precipitation and temperature regimes

provided in Figure 5.3 show that CMIP5 captures a regime similar to observations. On the contrary, 20CR and CORDEX are not able to capture the regimes well.

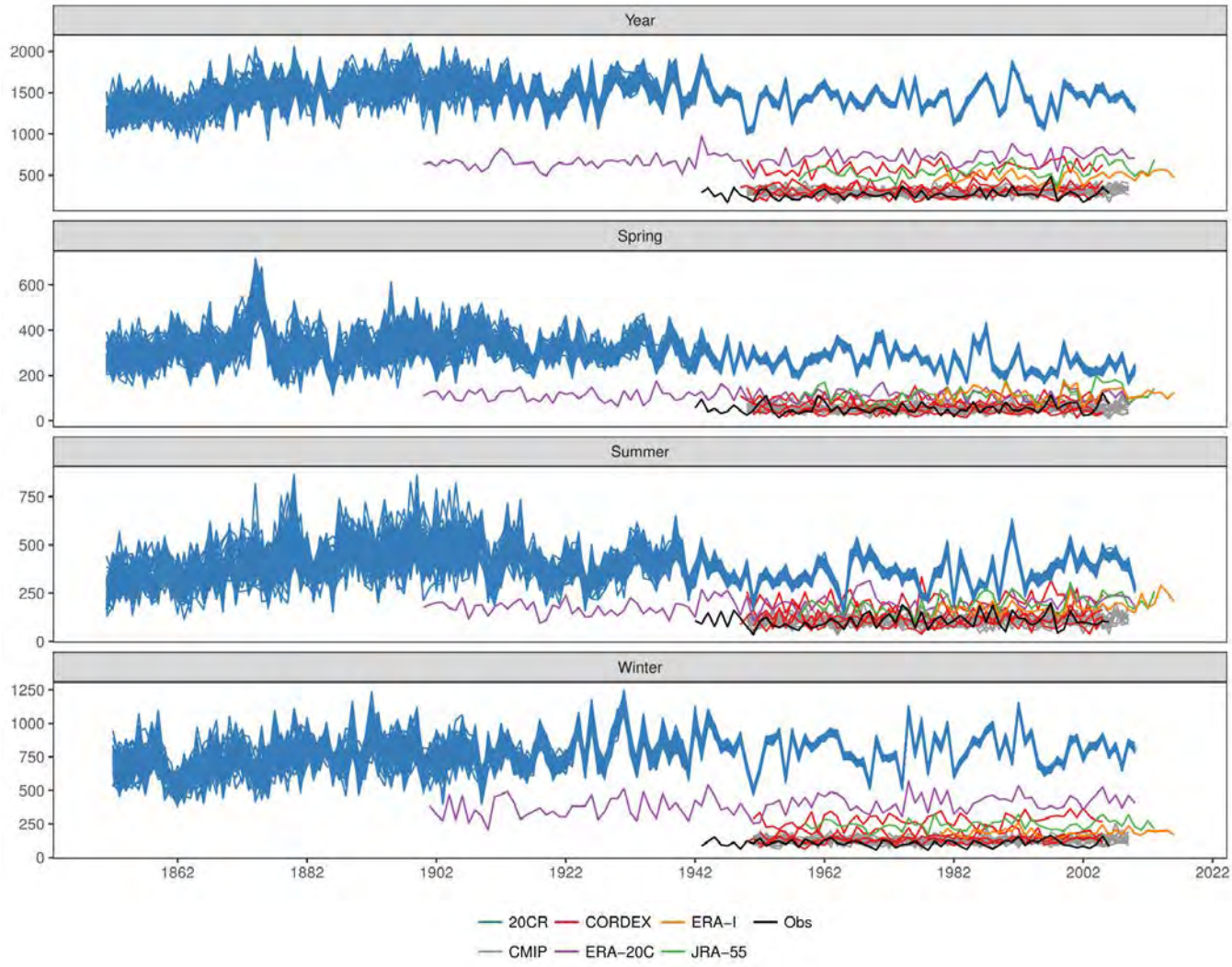

Figure 5.1 Annual and seasonal precipitation time series (mm) for the 56-members of 20CR (blue), ERA-20C (violet), CMIP5 (gray), CORDEX (red), ERA-I (orange), JRA-55 (green) and observations (black).

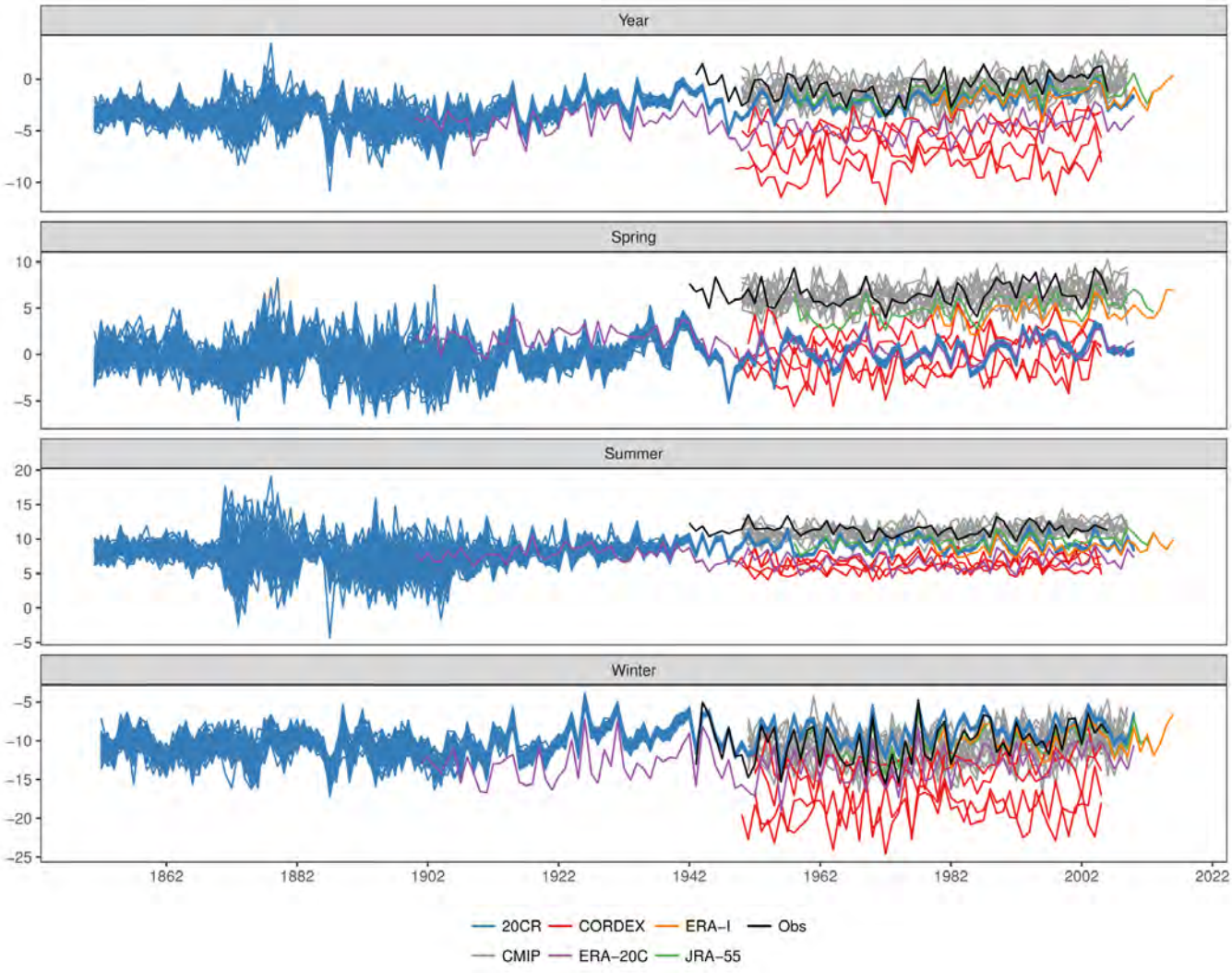

Figure 5.2 Annual and seasonal temperature time series (Celcius degree) for the 56-members of 20CR (blue), ERA-20C (violet), CMIP5 (gray), CORDEX (red), ERA-I (orange), JRA-55 (green) and observations (black).

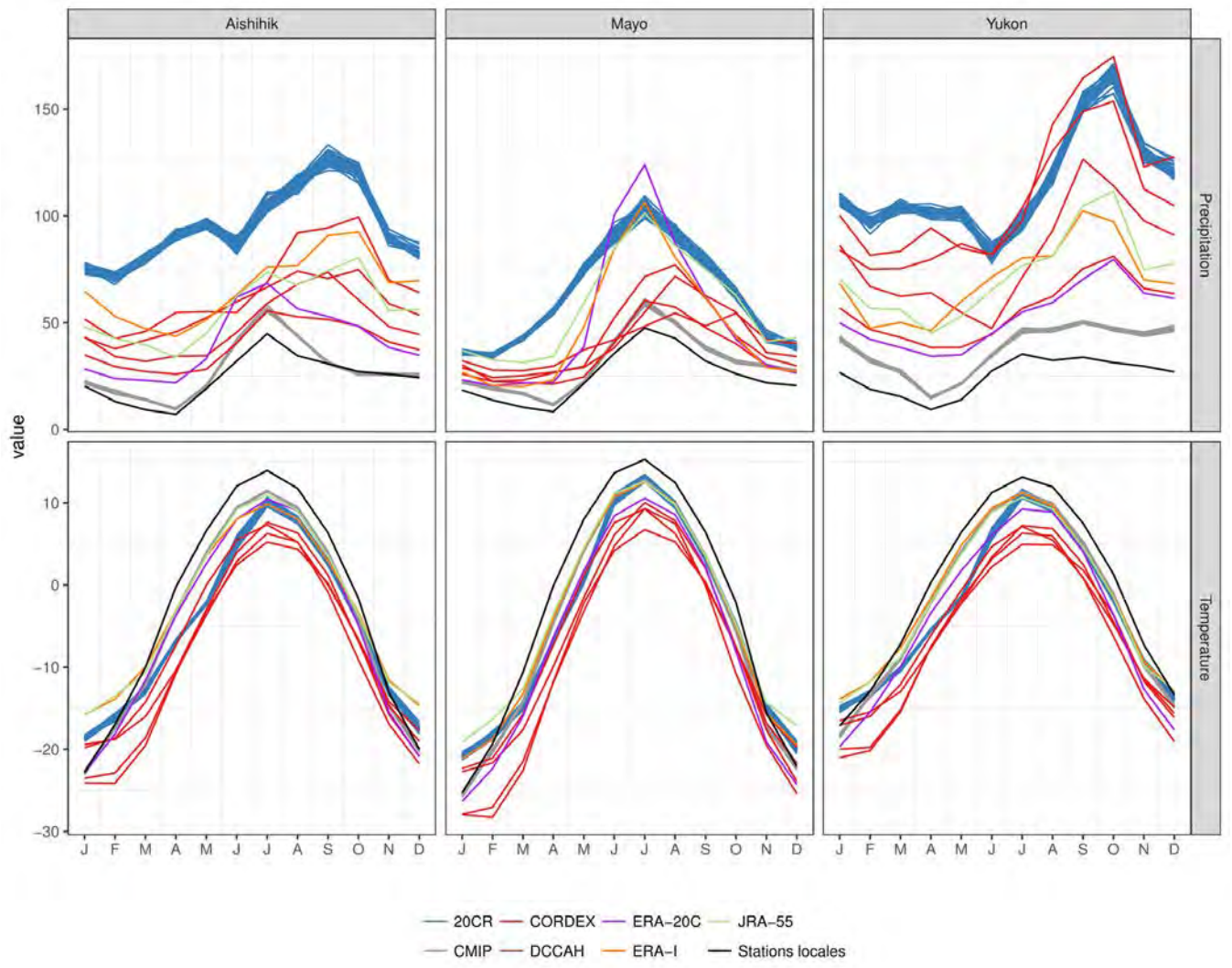

Figure 5.3 Inter-annual regimes (in mm and degree Celsius) for the 56-members of 20CR (blue), ERA-20C (violet), CMIP5 (gray), CORDEX (red), ERA-I (orange), JRA-55 (green) and spatialized observations (black) for all watersheds.

Spearman rank correlations are computed between all these datasets and climate indices at a seasonal time scale (spring, summer, winter). Only correlations significant at the 0.1 level are kept. Results for the winter season and the PDO index are provided in Figure 5.4 (left for precipitation, right for temperature). The median correlation is taken for 20CR. Only a few correlations are significant for precipitation, aside from some negative correlations in the observations for Aishihik, taking PDO from all previous seasons.

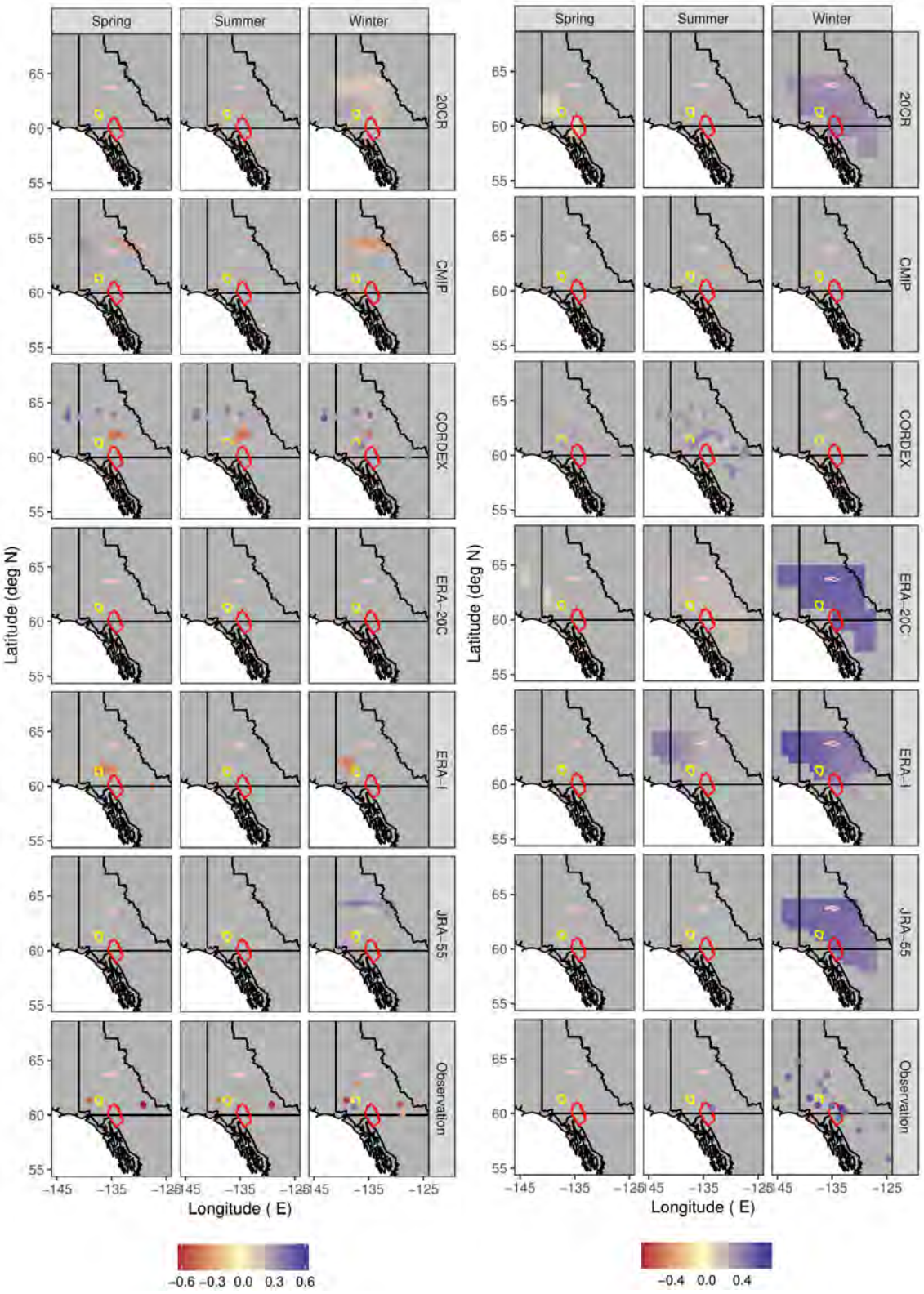

Figure 5.4 Significant spearman correlation (p<0.1) between PDO from previous spring, summer and current winter and winter precipitation (left) or temperature (right).

Correlations for temperature are stronger for all datasets. Positive correlations are found between winter temperature and winter PDO for all datasets except CMIP and CORDEX. CORDEX only shows weak correlation between winter temperature and summer PDO. CMIP5 does not show any correlations. The same pattern can be found for MEI (positive correlations for temperature, few correlations for precipitation) and AO (negative correlations for temperature, few for precipitation).

For the spring season (not shown), only temperature shows positive correlations with the MEI index, for all datasets except CMIP and CORDEX. No significant correlations are found in summer. At the annual time scale, only PDO shows some positive correlation with temperature. CMIP5 often shows different patterns than the reanalyses or the observations. For example, it is the only dataset showing correlations in summer for temperature.

Considering 20CR, correlations are not consistent within the 56 members. This shows that depending on the dataset, and even for the same dataset, the transferability of teleconnections remains uncertain. The transferability of these teleconnections in future periods using CMIP5 and CORDEX needs to be assessed. Nevertheless, very few correlations are found in the past using these datasets, further complicating the transferability study.

5.3. Using climate indices to improve seasonal forecasts

The other part of this working package consists in using climate indices (PDO, AO, MEI) to improve seasonal forecasts in an operational context. To this end, the work is divided in two parts:

1. Finding the most appropriate climate index for precipitation and temperature, for each watershed (for now, Mayo and Upper Yukon). The proposed methodology requires some degree of correlation between weather stations and climate indices (AO/MEI/PDO). It was assessed in the early stage of the project when applying the methodology that correlation was simply too low for Aishihik using the proposed indicices. Implementing the same methodology using other (more complex) indices is theoretically possible but poor correlations listed in the literature does not ensure getting higher correlations. It may prove rather difficult, or nigh impossible to find a fitting climate index. Hence, the methodology was not applied to the Aishihik watershed.
2. Using this index to provide an ensemble of seasonal forecasts for a chosen lead time.

5.3.1. Choosing the appropriate index

For the first point, Spearman rank correlations are considered. Monthly observed precipitation and temperature data used to compute correlations were obtained from two (2) meteorological stations for Mayo and from three (3) stations for Upper Yukon. Data were downloaded from the Environment and Climate Change Canada database. To select these stations, data from all stations localized at maximum 200 km from the watershed centers were first downloaded. Then, the final selection was formed by stations following these criteria: (i) at least 30 years of data; (ii) maximum 10% of missing data in the entire time series; and (iii) maximum 4 months missing for each 12-months period. Missing data were filled in using an inverse distance weighting interpolation of other available stations in each watershed. Finally, in order to be consistent in the choice of indices, only stations available on common periods for each watershed were used. The common period for Mayo is 1955-11-06 - 1995-05-02 and the common period for Upper Yukon is 1944-07-08 - 1980-03-05.

Spearman rank correlations were used to establish the link between monthly meteorological data and oscillation indices. Meteorological time series were created for a specific month (January, February, ..., December), using total precipitation or mean temperature over one (1) month (current month), and up to 12 future months (current year); this is symbolized in gray in Figure 5.5. The chosen period corresponds to the lead time required for the forecast (from 1 to 12 months). Correspondent climate index time series were created using the index value of the previous month, or an average of values between the previous month and up to 12 months before (previous year). This is symbolized in green in Figure 5.5. As there could be a lag in the influence of indices on local meteorology, a lag from 1 to maximum 6 months was considered to create time series. This is symbolized in orange in Figure 5.5.

As an example for the generic month N, correlations were computed between total precipitation or mean temperature over months [N], [N to N+1], [N to N+2], ..., [N to N+12] and indices (AO / PDO / MEI) averaged over months [N-1], [N-1 to N-2], ... [N-1 to N-12], [N-2], [N-2 to N-3], ... [N-2 to N-13], ..., [N-6], [N-6 to N-7], ..., [N-6 to N-18]. This is summed up by Figure 5.5; the gray area corresponding to the forecast period, the green area corresponding to the period where indices are averaged for the correlation and the orange corresponding to the potential lag between climate indices and local

meteorology. This configuration allows investigating the best period of influence of an index over a specific period for local meteorology.

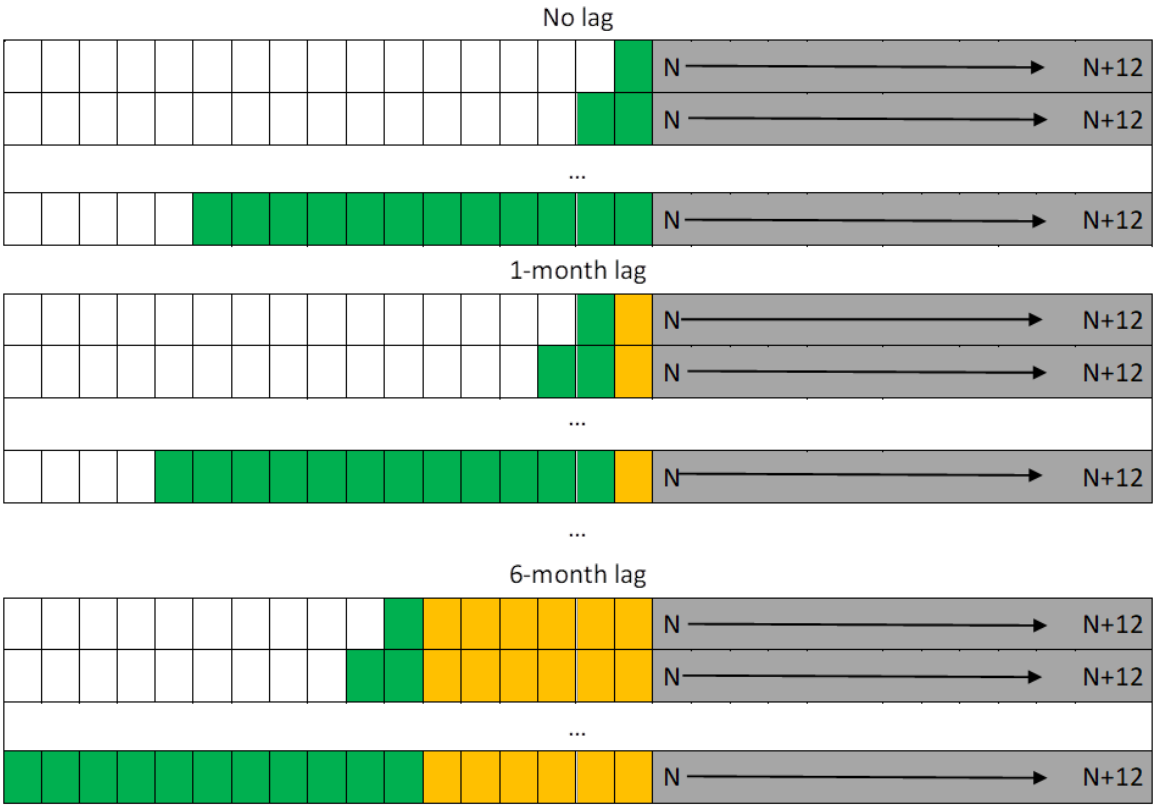

Figure 5.5 Computational scheme for correlations computed between averaged indices on the green period and total precipitation or mean temperature over the grey period for a generic month N (January, February, …)

At this point, multiple correlations have been computed. Only indices with significant correlations at the 0.1 level were kept. In order to get indices per watershed, mean correlations were computed using an inverse distance weighting of significant correlations for each studied index (relative to the watershed centroid). The number of stations detecting (having a significant correlation) the index was also kept. Optimal indices were selected considering a compromise between high averaged correlations and high number of stations in the watershed detecting this correlation. This led to the selection of a single index for each month (January to December), each variable (P, T), each forecast length (between 1 and 12) and each watershed (instead of stations).

5.3.2. Choosing the lead time

It is then up to the user to choose a specific lead time (or forecast length), considering the value of the correlation found. For example, results for the month of January for Upper Yukon are presented in Figure 5.6. An x-axis at 7 months for precipitation can be read as "Time series of total precipitation on January-July showed a significant correlation of approx. 0.5 at the 0.1 level with an AO index for 33% of the stations of the Upper Yukon watershed (1 out of 3)".

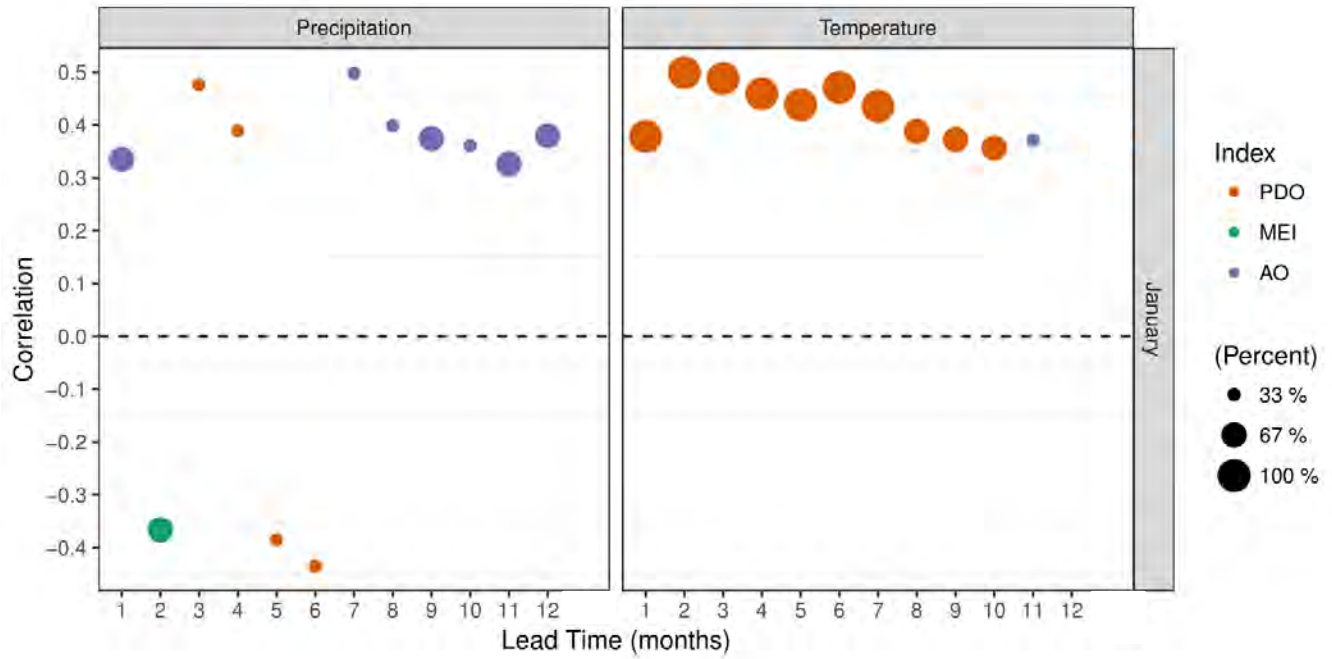

Figure 5.6 Final indices selected for January for both precipitation and temperature for the Upper Yukon watershed. x-axis represents lead times (between 1 and 12). y-axis represents corresponding correlations.

For this study, lead times were chosen as a compromise between high correlation (top or down circles in Figure 5.6, high number of stations detecting the correlation (biggest circles on Figure 5.6) and long lead time (circles furthest to the right on Figure 5.6), for both precipitation and temperature. For the month of January, indices for temperature are detected by all stations except for lead times of 12- (0 station), 11- (1 station), 10-, 9- and 8-months (2 stations). The lead time of 7 months is the longest having good correlations for both precipitation and temperature as well as a maximum number of stations detecting the index for temperature. For these reasons, it was chosen as the best compromise for the

month of January and for the Upper Yukon watershed. The same reasoning was applied to all months for both watersheds. The final lead times with the corresponding indices are provided in Table 5.1.

Table 5.1 Monthly function chosen indices and lead time for each watershed.

Watershed	Month	Lead Time	Index (P/T)	Corr (P/T)	First month (P/T)	Length (P/T)	% stations (P/T)
Yukon	January	7	AO/PDO	0.50/0.44	Sept/Dec	4/1	33%/100%
Yukon	February	7	AO/AO	0.44/0.50	Nov/Jan	9/6	33%/100%
Yukon	March	6	AO/AO	0.45/-0.41	Oct/Feb	8/3	33%/100%
Yukon	April	6	AO/AO	0.50/-0.43	Mar/Feb	1/8	33%/100%
Yukon	May	11	AO/PDO	-0.38/0.34	Dec/Nov	3/2	67%/100%
Yukon	June	12	AO/AO	-0.40/-0.49	Dec/May	4/1	67%/100%
Yukon	July	11	AO/AO	-0.41/-0.49	Jan/May	11/1	33%/100%
Yukon	August	11	AO/AO	-0.45/-0.46	Apr/May	1/1	67%/100%
Yukon	September	11	AO/AO	-0.42/-0.45	Apr/May	1/1	67%/100%
Yukon	October	10	AO/AO	-0.42/-0.44	Apr/May	1/1	67%/100%
Yukon	November	11	AO/PDO	0.44/0.41	Aug/Oct	1/1	33%/100%
Yukon	December	10	AO/PDO	0.37/0.48	Aug/Nov	1/1	67%/100%
Mayo	January	6	AO/MEI	0.38/0.54	Nov/Jul	12/2	100%/100%
Mayo	February	5	AO/MEI	0.46/0.56	Nov/Oct	4/6	50%/100%
Mayo	March	9	PDO/AO	0.39/0.44	Feb/Nov	2/1	50%/100%
Mayo	April	8	PDO/AO	0.41/0.43	Feb/Nov	1/1	50%/100%
Mayo	May	7	PDO/AO	0.43/0.46	Feb/Nov	1/1	50%/100%
Mayo	June	12	PDO/MEI	-0.41/0.39	May/May	1/1	50%/100%
Mayo	July	12	PDO/MEI	-0.51/0.47	Jun/Jun	2/2	50%/100%
Mayo	August	12	PDO/MEI	-0.45/0.45	Jul/Jul	2/2	50%/100%
Mayo	September	8	PDO/MEI	-0.40/0.44	Jul/Jul	3/2	100%/100%
Mayo	October	7	PDO/MEI	-0.43/0.47	Jul/Jun	1/2	100%/100%
Mayo	November	8	PDO/PDO	-0.41/0.67	Jul/Oct	3/1	100%/100%
Mayo	December	8	PDO/PDO	-0.37/0.58	Jul/Oct	2/1	100%/100%

Table 5.1 presents the watershed, month, chosen lead time, indices for precipitation and temperature, corresponding correlation, first month of the index, length (number of previous months before first month, including first month) and the percentage of stations detecting the significant correlation.

The first line of Table 5.1 can be read as "Total precipitation over January-July (7 months) has a significant correlation of 0.50 at the 0.1 level with AO averaged on previous September, August, July and June for 1 station out of 3 for Upper Yukon. Mean temperature over January-July (7 months) has a significant correlation of 0.44 at the 0.1 level with PDO from previous December for 3 out of 3 stations for Upper Yukon. The lead time of 7 months is the best compromise between high correlation, high lead time and high number of stations detecting the indices for both variables".

For both watersheds, the index selected for temperature was detected by all stations (Table 5.1). Only two combinations of indices are selected for Upper Yukon: AO / PDO (for precipitation / temperature) for 4 months (January, May, November, and December) and AO / AO for all other months. Some combinations are exactly the same for different months, such as the AO in April and the AO in May for precipitation and temperature from August-June, September-July and October-June. For the Mayo watershed, 4 combinations of indices are selected: AO / MEI for January and February, PDO / AO between March and May, PDO / MEI between June and October and PDO / PDO for November and December. For each combination except for AO / MEI, very similar patterns are found in terms of first month and length.

5.3.3. Creating seasonal forecasts

The use of climate information for forecasting purposes is achieved through Ensemble Streamflow Forecast (ESP) schemes. ESP is a well-known technique consisting in randomly selecting historical sequences of climate data at the time of the forecast to force a hydrological model, providing a plausible range of future meteorological scenarios. The integration of climate information is done using an analog approach, introduced by Lorenz in 1969, and regularly adopted in statistical downscaling techniques. This approach considers that similar large-scale situations could lead to similar local effects.

Three different methods have been developed to integrate oscillation indices in the choice of past meteorological scenarios. They are explained using the same example as above: a 7-month forecast from the month of January 2019 for Upper Yukon. The first step, common to all methods, is to retrieve the corresponding indices associated with this forecast. In this case, the best index for precipitation is AO averaged over the previous months of June, July, August and September. For temperature, the best index

is PDO over the previous month of December. These indices are then computed with 2018 values. The aim now is to find the year in an archive of observations with the closest configuration in terms of index values. This archive is made of all available stations from Environment and Climate Change Canada, following the same quality criteria than the previously selected observation, but without a length of 30 years.

The first method is called **Euclidean index**. For each year in the archive, the Euclidean distance between corresponding indices and current indices is computed. Then, the January-July (7-month lead time or forecast) precipitation and temperature data of the 20 closest years are selected to produce the ensemble meteorological scenarios of the January-July 2019 forecasts. The second method is called **Stepwise T-P**. For each year in the archive, the distance between corresponding index for temperature and current index for temperature is computed. The 40 years giving the smallest distance are kept. Then, for each of the 40 years, the distance between corresponding index for precipitation and current index for precipitation is computed. Finally, the January-July precipitation and temperature data of the 20 closest years are selected to produce the ensemble meteorological scenarios of the January-July 2019 forecasts. The third method is called **Stepwise P-T** and is the same method than Stepwise T-P, with precipitation for the first level of selection and temperature for the second.

Three methods are used as benchmark methods to evaluate the performance of the previously developed methods. The first method, is called **Traditional ESP**. Twenty years are randomly selected in the meteorological archive to produce the 20-member ensemble meteorological scenarios forcing the hydrological model. It does not take into account climate indices. The second method is called **Best index previous month**. For each month and each watershed, Spearman rank correlations are computed between monthly meteorological data and indices from previous months (for example, January precipitation with AO/PDO/MEI from previous December). Conversely to the above method, averages over several months and index lags are not considered. Then, only indices with a significant correlation at the 0.1 level are kept. It happens that some months, variable and watershed do not have any significant correlations. As for the Euclidean index method, the 20 most analog years in terms of Euclidean distance between indices are kept to constitute the ensemble meteorological scenarios. For a specific month and watershed, if precipitation or temperature is not associated with an index, the

distance is transformed in an absolute error, only using the index associated with the other variable. The third method is called **PDO previous month**. As PDO is the index having the most important influence in the zone of interest according to previous studies, this method selects for each variable and each watershed the 20 most analog years in terms of PDO from the previous month.

All six methods are applied to both watersheds for each month in the 2013-2016 period.

5.3.4. Results

First results are presented for a 12-month forecast from the month of June. All methods are applied to obtain 12-month forecasts from June 2013, June 2014, June 2015 and June 2016. They are all compared to the streamflow simulated by HYDROTEL using real observations over the period (called Obs). Daily time series are presented in Figure 5.7 for Mayo and Figure 5.8 for Upper Yukon. CanSIPS data, the usual dataset used for seasonal forecasts, is also presented for the Mayo watershed. Data assimilation developed by Yukon University was taken into account for CanSIPS only. Figure 5.7 shows that CanSIPS overestimates spring flows in 2014, 2015, 2016 as well as winter streamflows, especially for the 2015-2016 winter. All other methods present equivalent time series, with a good reproduction of flows, even if there is a slight overestimation of flows in summer. Observation generally fits in the ensemble member. Results for Upper Yukon (Figure 5.8) show that flows are well represented. There is still an underestimation of flows in summer. All methods show relatively equivalent forecasts.

Member 1 of each method are presented on Figure 5.9. For methods using climate indices, it corresponds to the member having the closest index to the original index in the archive, it is referred to as “the best analog”. Member 1 for CanSIPS (among 1000 members) and Traditional ESP are random members, equiprobable to all other members. CanSIPS is only available for Mayo. For Mayo, CanSIPS shows too flat a signal in comparison to observations. Other models show quite equivalent performances, except Traditionnal ESP often showing too high values in May. For Upper Yukon, the random member of Traditional ESP has less accuracy than the other methods, with an under estimation of flows in 2013, 2014 and 2015. Stepwise P-T also shows this underestimation, while Best index previous month shows an over estimation in 2013. For this case, best models are Euclidean index, Stepwise T-P and PDO previous month.

A closer look at specific scores is provided in the next figures. Figure 5.10 shows June forecasts rank histograms. Rank histograms (Hamill, 2001) present the rank of the observation in the forecast ensemble for each day. For example on Figure 5.10, the 1461 days in June 2013-May 2017 are divided in quantile categories. For Traditional ESP and Mayo, approximately 170 days out of the 1461 days have an observation equivalent to the median (0.5) of the 20 forecasts. A histogram associated with a perfect forecast would be flat (same data count for each quantile). Ensemble forecasts biases will be represented by a sloped rank histogram. A U shaped histogram reveals under dispersion (observations often fall outside the forecasts) and a V shaped histogram an over dispersion (over confidence). Figure 5.10 shows that CanSIPS presents a strong negative bias (increasing slope towards the right), meaning that the observations are underestimated. All other methods show a small negative bias, meaning that the general tendency is the underestimation of observations. Nevertheless, a large number of days shows observations around the median of the forecasts. The percentage of days with observations included in the ensemble (numbers in Figure 5.10) is equivalent for all methods. For Mayo, the methods using indices show a flatter rank histogram, construed as more reliable than Traditional ESP or CanSIPS. For Upper Yukon, all histograms seem equivalent.

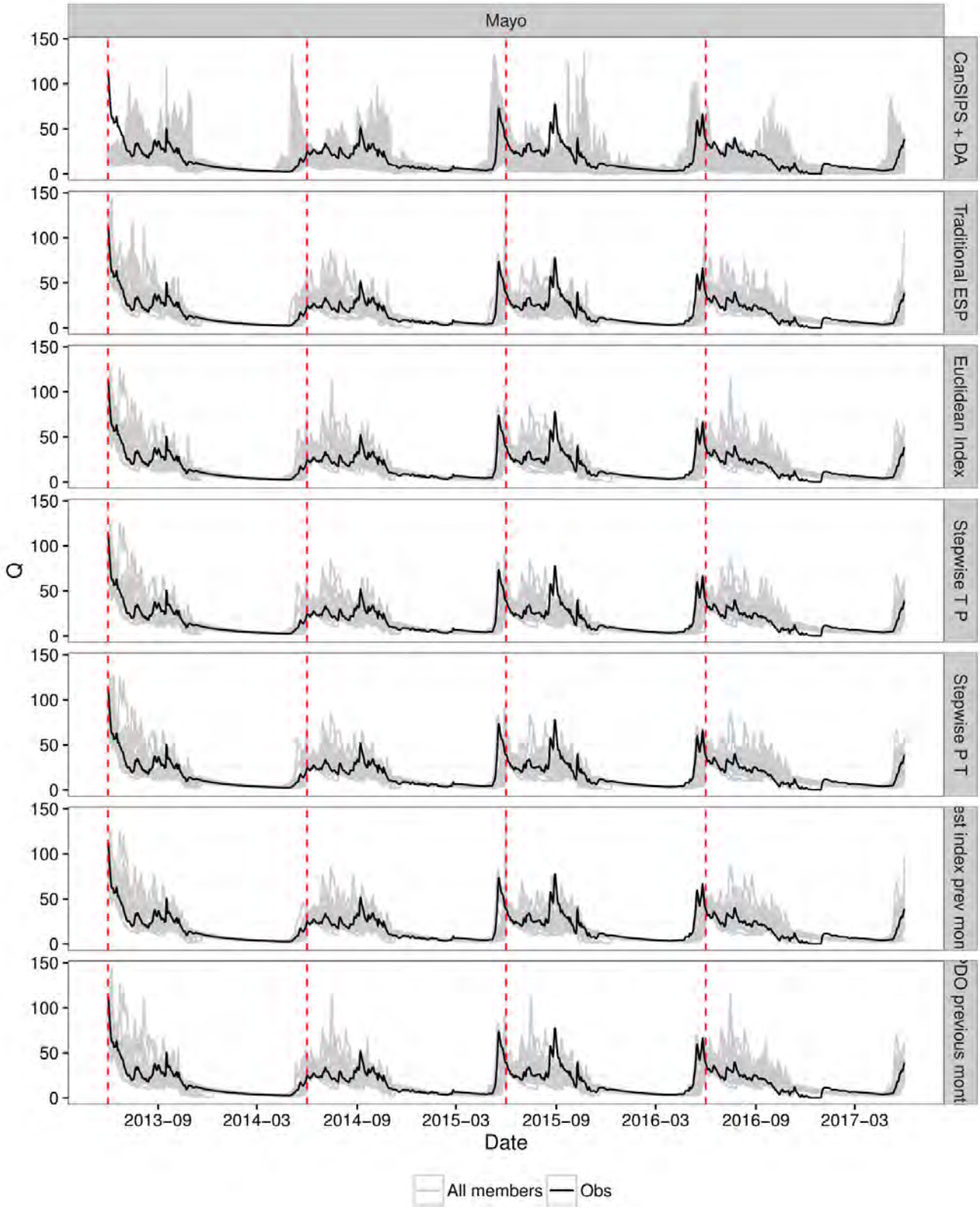

Figure 5.7 Streamflow time series for June forecasts for the Mayo watershed. Red dash lines represent the beginning of each forecast, and the discontinuities.

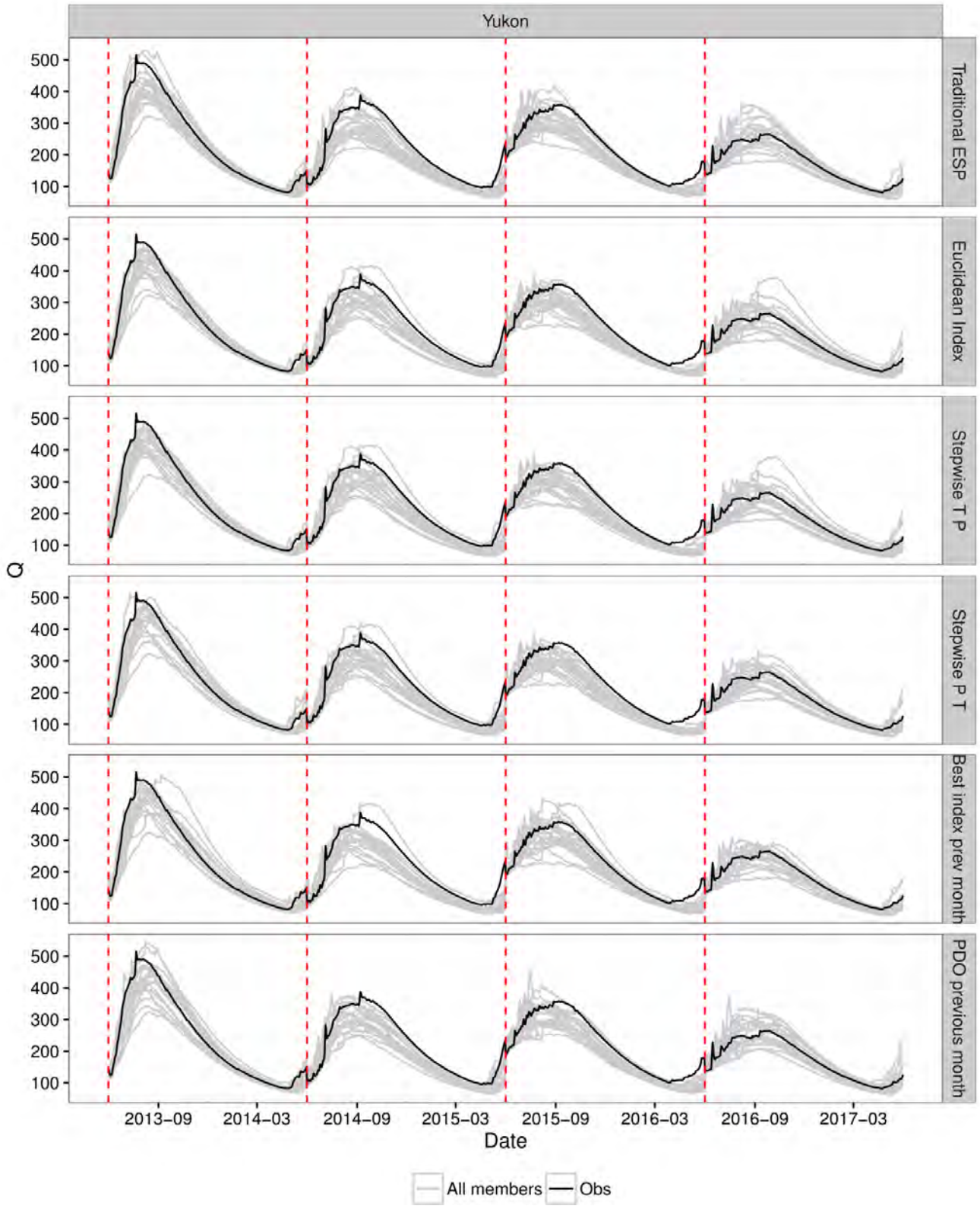

Figure 5.8 Streamflow time series for June forecasts for the Upper Yukon watershed. Red dash lines represent the beginning of each forecast, and the discontinuities.

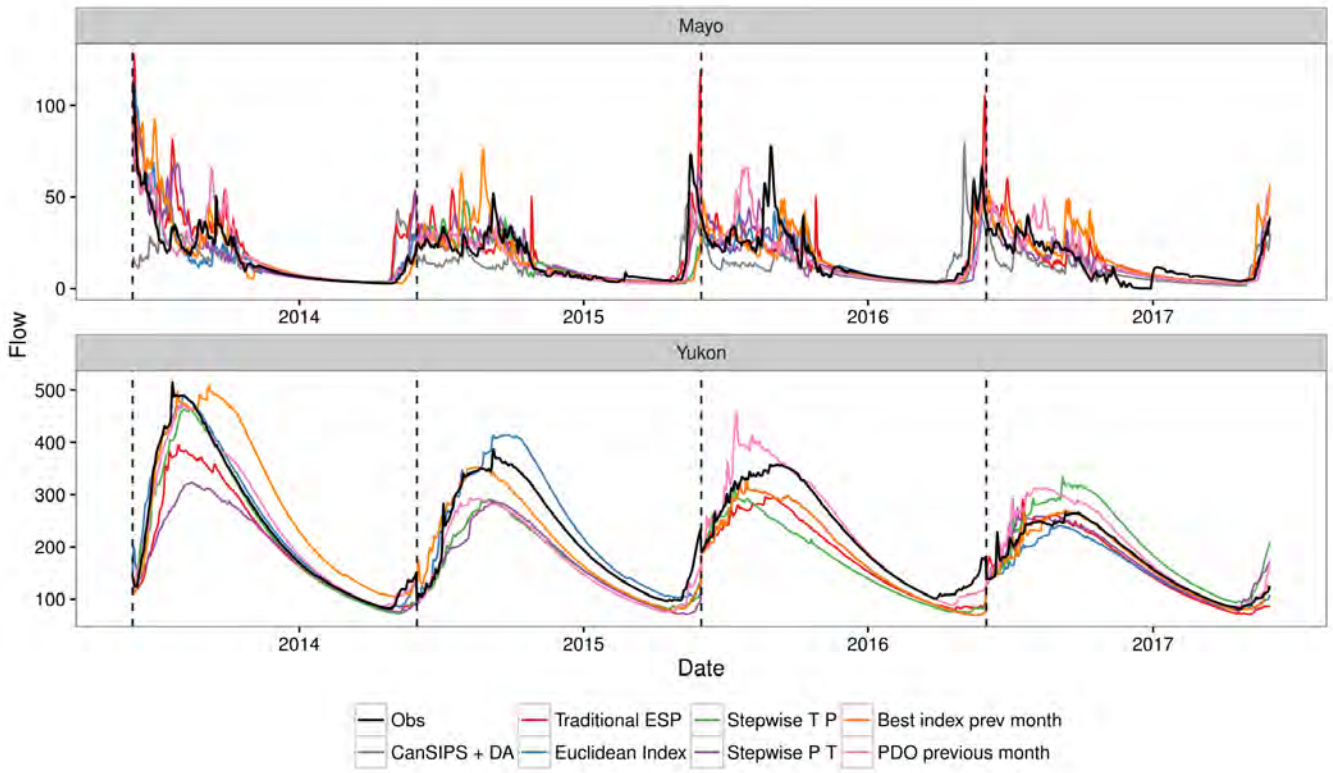

Figure 5.9 Streamflow time series for June forecasts with member 1 of each method for both watersheds. Black dash lines represent the beginning of each forecast, and the discontinuities.

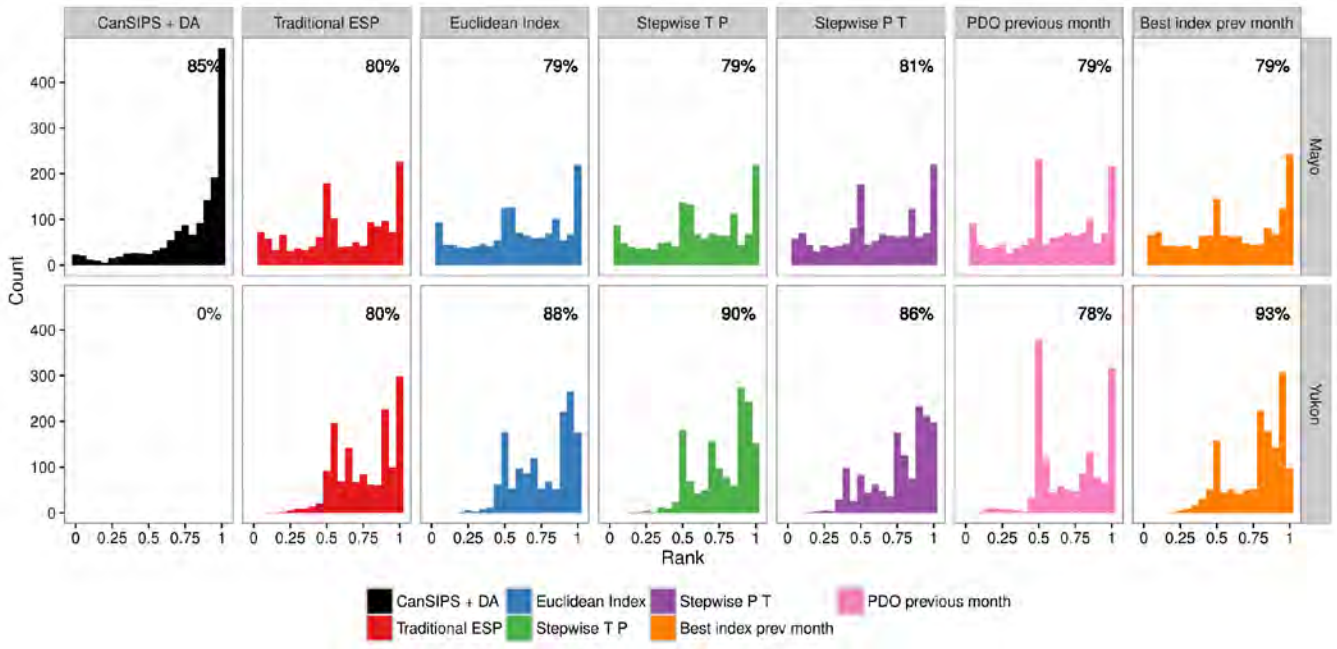

Figure 5.10 Rank histogram of daily June forecasts. The percentage of observed values within the forecasted ensemble is given for each panel.

The computation of scores for the June forecasts and both watersheds is provided in Figures 5.11 and 5.12. The Kling-Gupta Efficiency (KGE) at a daily and monthly time scale is provided for all methods in Figure 5.11, for member 1. They are computed for each year, and for intermediate lead time between 1 and 12. For example, the "2" panel at the monthly time scale provides the 4 KGE values computed on the June-July period for member 1 of each method and for each year (2013, 2014, 2015, 2016). At a monthly time scale, values should be treated with caution as few values are used to compute the score. All methods provide better KGE values than CanSIPS. Stepwise P-T and Euclidean Index respectively provide slightly better scores than other methods for Mayo and Upper Yukon. The longer the lead times, the longer the scores, probably because the snowmelt period (first lead time) is the most difficult period to represent in the forecasts.

Figure 5.12 shows, in an equivalent way, the CRPSS score (Hersbach, 2000). It is a probabilistic score taking into account all members. It corresponds to the Mean Absolute Error (MAE) for single-valued forecasts and uses a reference dataset to provide a comparison. Here, a value above translates into a higher CRPSS for the evaluated method than for the Traditional ESP (method of reference). Under 0, it means that the Traditional ESP provides a better score. This score can be divided in two parts, the

reliability part, closely connected to the rank histogram of the ensemble, and the resolution/uncertainty, related to the average spread within the ensemble and the behaviour of its outliers. CRPSS are quite equivalent for Mayo, with a slight improvement using Stepwise P-T or Best index previous month at a monthly time scale. For the Upper Yukon watershed, CRPSS are positive when using methods with indices. CRPSS for CanSIPS are far under the 0 value, meaning that this dataset is less suitable than random historical years to produce future forecasts.

All the above results were presented for forecasts beginning in June. The same work can be applied to study all months, using the forecasted lead time determined in the previous section. Figure 5.13 provides the CRPSS for all months. This figure relies on the same principle that Figure 5.12, except that only the last lead time is provided for each month (see Table 1). For example, for the month of June, it corresponds to the 12-month lead time, and the panel “12” in Figure 5.12. This figure shows that using climate indices to select forecasts provides better results than CanSIPS and a random selection of years, for months between June and December for Mayo. For other months, a selection with indices provide an equivalent score than the random selection, but is still better than using CanSIPS. The same results apply to the Upper Yukon watershed, and these results are particularly true for the months of May, June, November and December. However, using climate indices for August and the Yukon watershed provide a CRPSS less than zero.

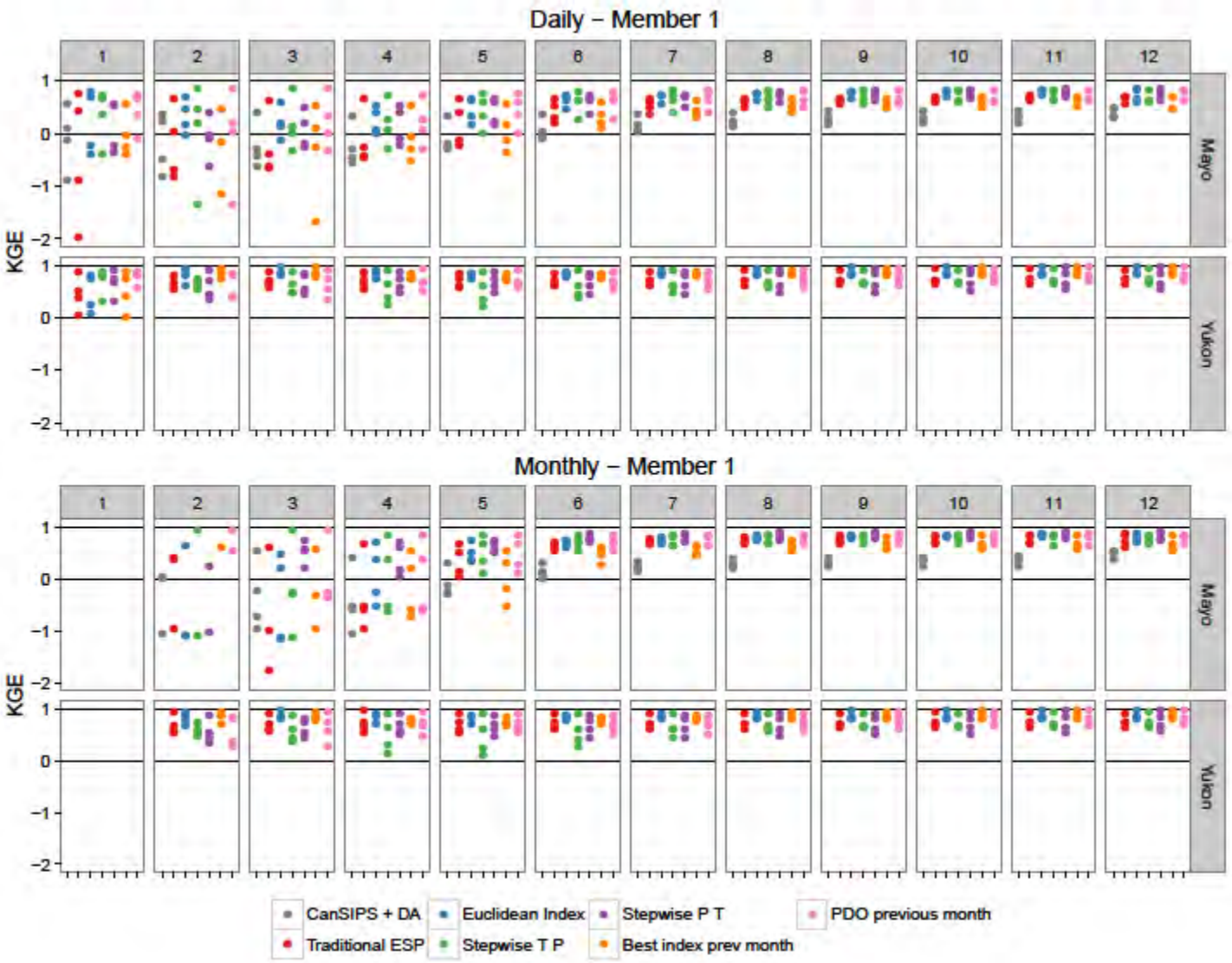

Figure 5.11 KGE values computed between forecasts from member 1 and observation for each year and each lead time between 1 and 12. A maximum of four points are represented for each x-axis tick, one point representing one year. Values under -2 are not shown.

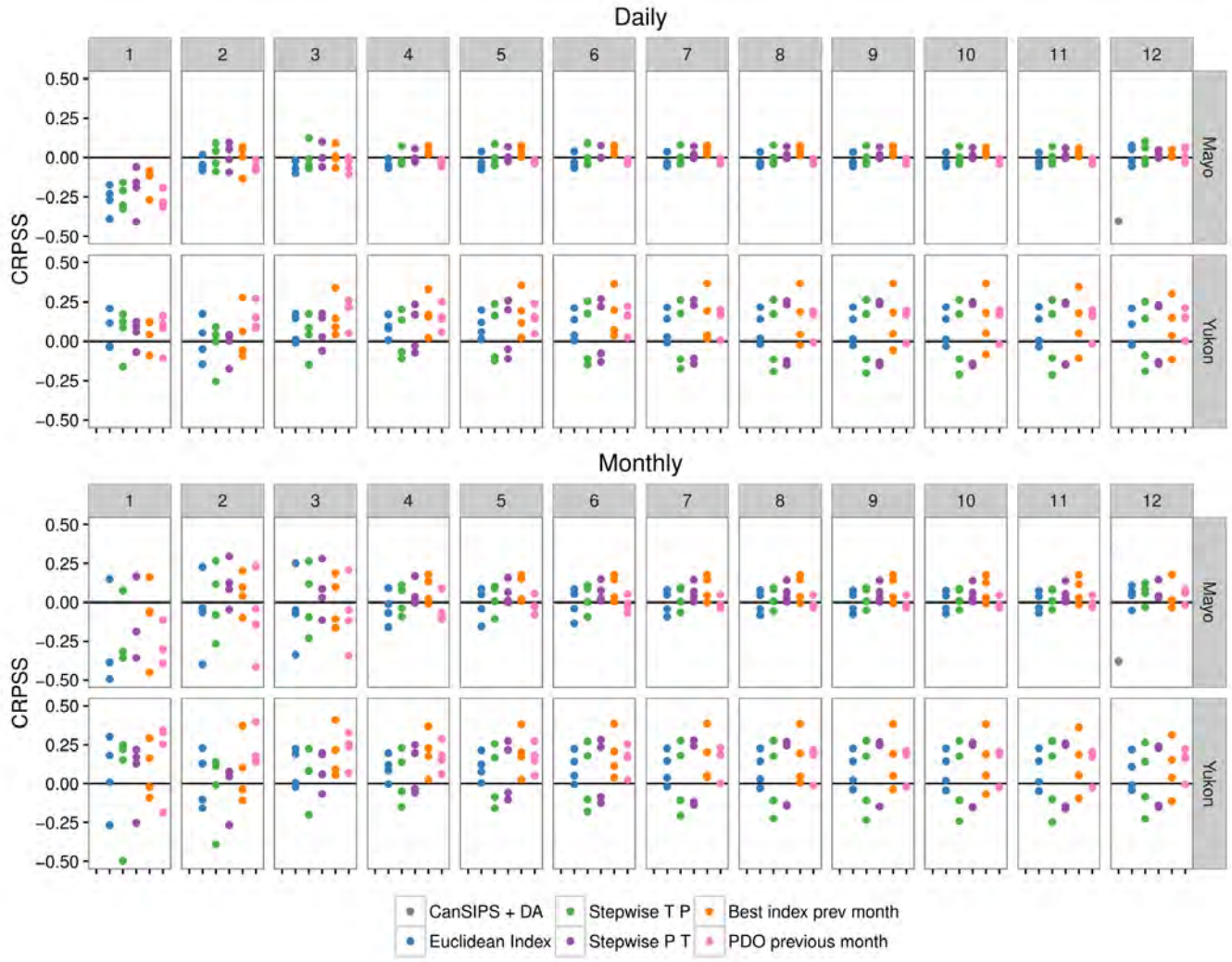

Figure 5.12 CRPSS values considering Traditional ESP as a reference for June forecasts. The score is computed for each year and each lead time between 1 and 12. A maximum of four points are represented for each x-axis tick, one point representing one year. Values under -0.5 are not shown.

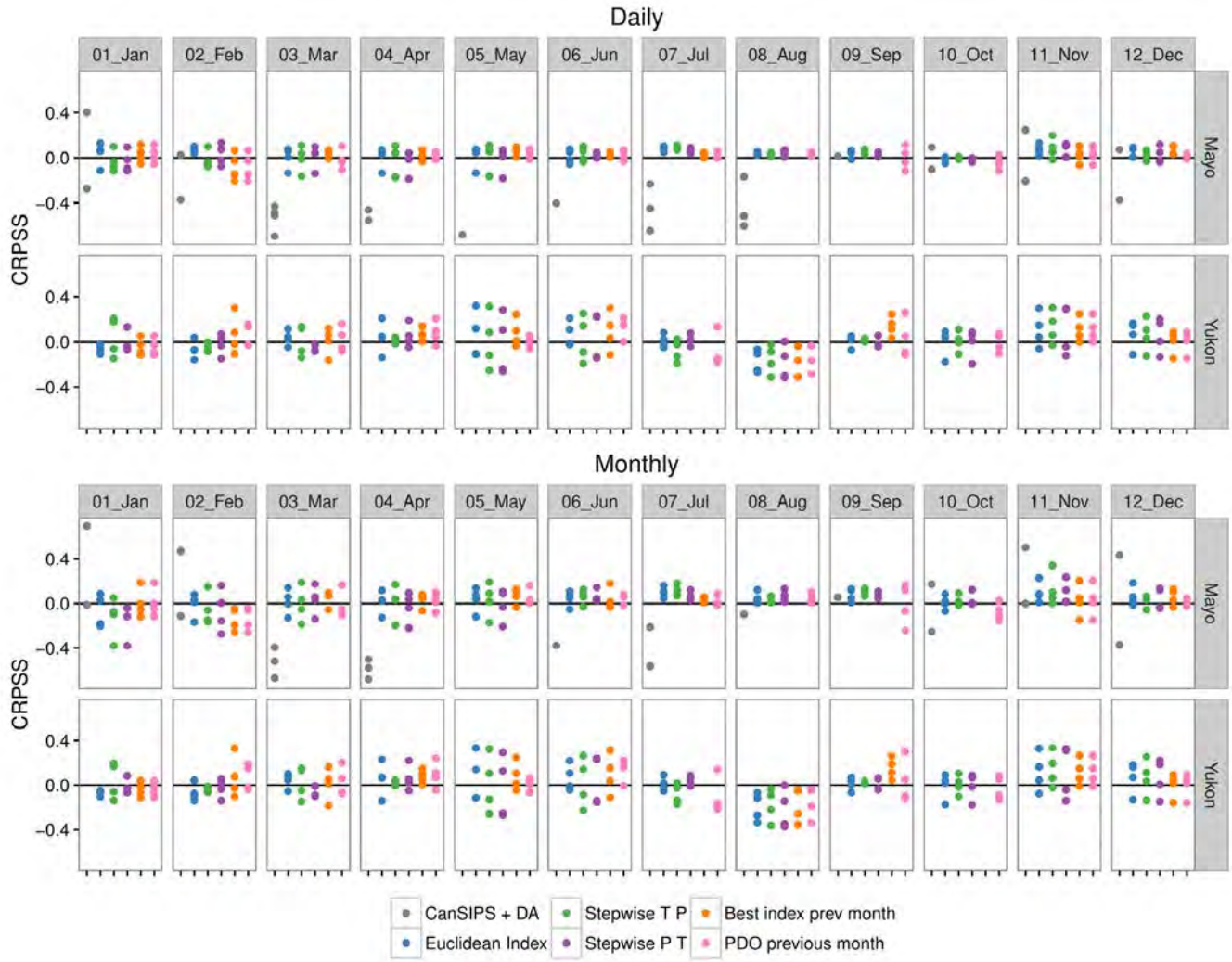

Figure 5.13 CRPSS values considering Traditional ESP as a reference for all month. The score is computed for each year. A maximum of four points are represented for each x-axis tick, one point representing one year. Values under -0.7 are not shown

5.3.5. Conclusions

Using climate indices to produce seasonal forecasts represents an interesting alternative to provide pertinent forecasts. Usual methods do not include climate information, but only random past observations. As our zone is influenced by close climatic indices, several methods have been tested to include these data in the selection of past historical years. Results show that using past observations instead of CanSIPS data can lead to an improvement of seasonal forecasts for both Mayo and Upper

Yukon. Using climatic information provides slightly better improvements compared to only using random historical data depending on the month. Improvements are better for Upper Yukon.

The development of these methods could continue, with the possibility of using other large-scale variables or other indices as predictors to increase forecasts reliability. These methods could eventually be tested under operational conditions as they are not too hard to implement and do not require extensive downloading of data. Moreover, depending on the index found during the correlation step, it is possible to begin the forecast several months before the forecasting date (if the index presents a lag), increasing again the forecast length.

6. Hydroclimatic assessment

6.1. General methodology and literature review

Hydroclimatic assessment is based on downscaled daily Canada-wide climate scenarios from the latest CMIP5 climate simulations (Taylor et *al.*, 2012) offered by the Pacific Climate Impacts Consortium (PCIC). Three scenarios of Representative Concentration Pathways (RCPs), namely RCP2.6 RCP4.5 and RCP8.5, were considered in this study; the former being viewed as optimistic, while the latter deemed pessimistic (Van Vuuren et *al.*, 2011). Combinations of 12 climate models and RCPs where selected and made available to this project by the Ouranos consortium. Table 6.1 presents the list of combinations used. The horizons of interest are 2010-2040 and 2041-2070; the 1980-2010 horizon representing the reference. The number of climate change scenarios available was thus 33 with bias correction. To provide a consistent picture of potential impacts of climate change on future inflows at Mayo Lake and Aishihik Lake, HYDROTEL was used as the basic hydrologic model and the scenarios where formatted accordingly. The final emphasis of this project topic is on identifying long-term trends in the average annual hydrograph and characterizing key elements such as annual runoff high and low flows.

Table 6.1 List of climate change scenarios

Model	Original Source	RCP		
		2.6	4.5	8.5
access1.0	Bureau's Research & Development Branch,UK Meteorological Office's Unified Model.		√	√
canesm2	Canadian Centre for Climate Modelling and Analysis.	√	√	√
ccsm4	National Science Foundation and the U.S. Department of Energy.	√	√	√
cnrm-cm5	Centre National de Recherches Météorologiques	√	√	√
csiro-mk3.6.0	Commonwealth Scientific and Industrial Research Organisation	√	√	√
gfdl-esm2g	Geophysical Fluid Dynamics Laboratory	√	√	√
hadgem2-cc	Met Office Hadley Centre		√	√
hadgem2-es	Met Office Hadley Centre	√	√	√
inmcm4	Russian Institute for Numerical Mathematics Climate Model		√	√
miroc5	The University of Tokyo Center for Climate System Research	√	√	√
mpi-esm-lr	Max-Planck-Institut für Meteorologie	√	√	√
mri-cgcm3	Meteorological Research Institute	√	√	√

6.2. Results

At first, using the meteorological data interpolation module of HYDROTEL, it was possible to determine temperature and precipitation changes at the watershed level, as well as determine the impact of climate change scenarios on flows/inflows at Aishihik Lake, Mayo Lake, Marsh Lake and Yukon River at Whitehorse, expressed as annual runoff. The methodology refers to simply perform continuous simulations using different scenarios and analyze the results in terms of potential impacts and tendencies. The period of simulation extended from 1950-01-01 to 2100-12-01. But the results mostly focussed on specific periods including recent climate (1981-01-01 to 2016-01-01); short-term horizon (2010-01-01 to 2040-12-31) and long term horizon (2041-01-01 to 2100-12-31). The simulations results were bias-corrected to better represent the observed mean of the recent climate period (1981-2016) and the same correction procedure was applied to all the results to ensure a certain level of confidence in future flows, which could be related to a misrepresentation of recent inflows. Figures 6.1 to 6.6 and Table 6.2 and 6.3 present the results for Aishihik Lake and Figures 6.7 to 6.12 and Table 6.4 and 6.5 those for Mayo Lake.

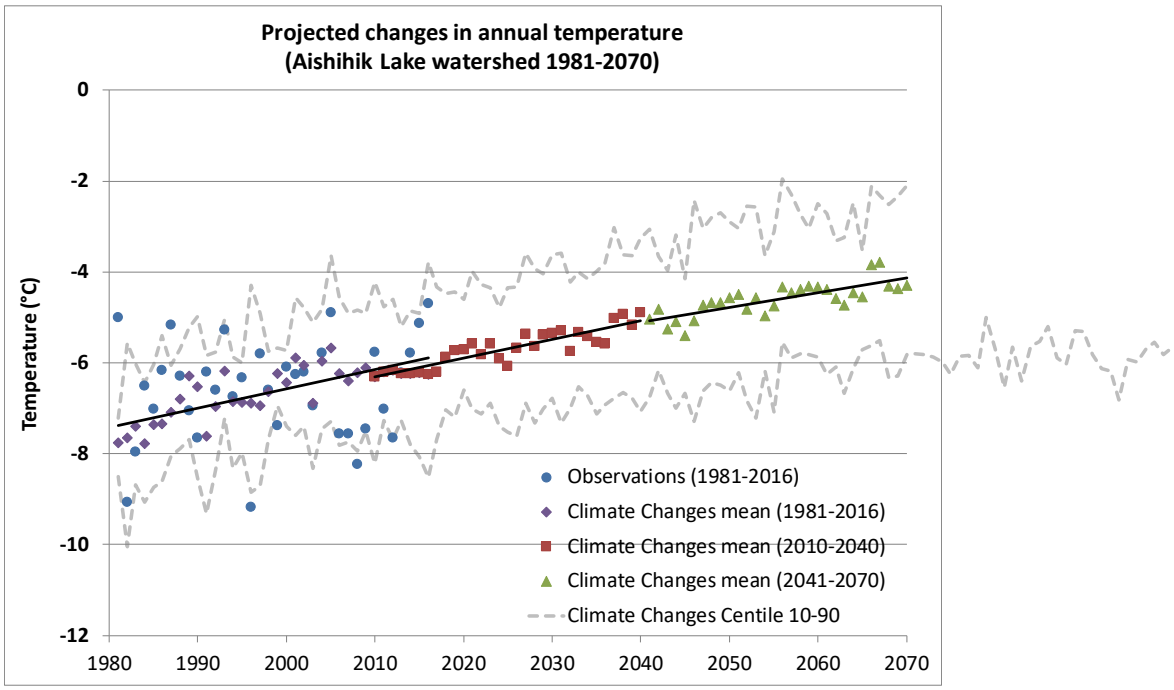

Figure 6.1 Projected changes in annual temperature for the Aishihik Lake watershed (1981-2070).

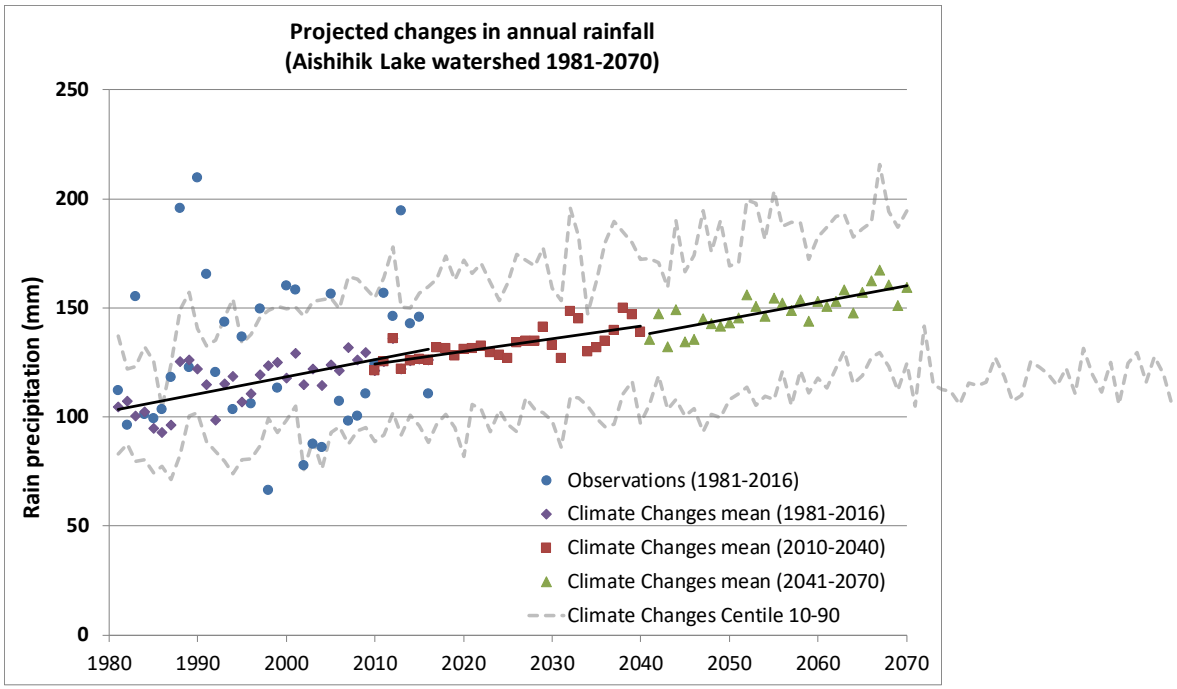

Figure 6.2 Projected changes in annual rainfall for the Aishihik Lake watershed (1981-2070).

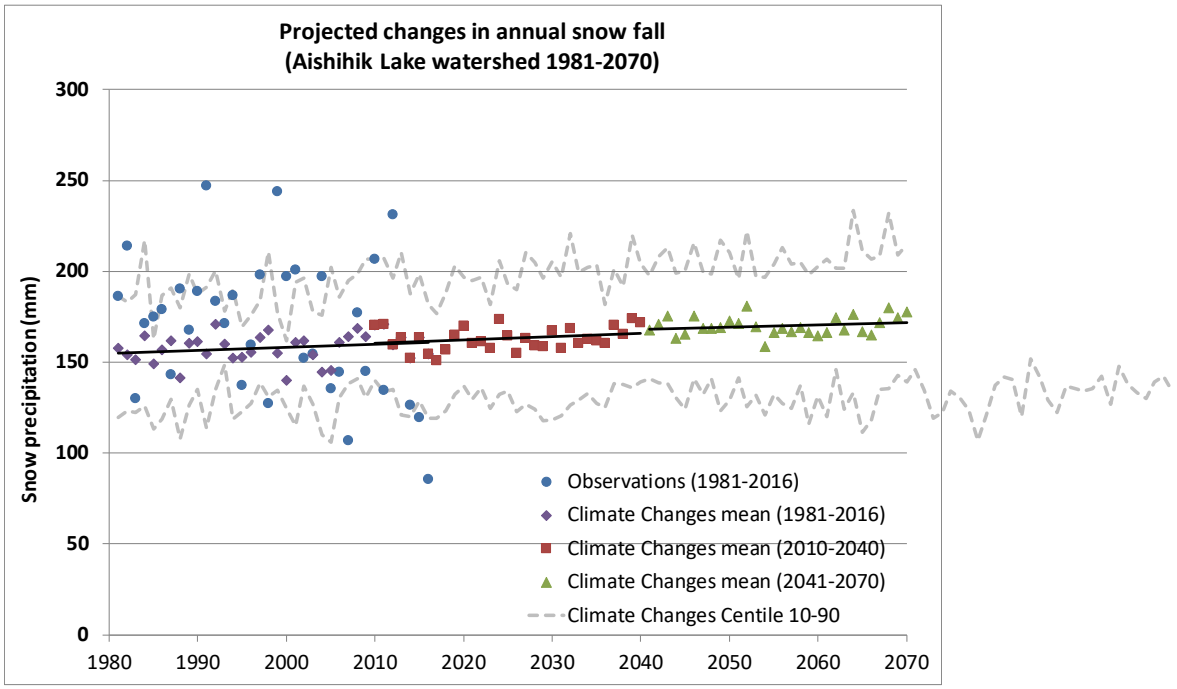

Figure 6.3 Projected changes in annual snow fall for the Aishihik Lake watershed (1981-2070).

Table 6.2 Projected changes in meteorological conditions for the Aishihik Lake watershed (horizon 2010-2040 and 2041-2070)

Variable	2010-2040		2041-2070	
	Average	(Centile 10th-90th)	Average	(Centile 10th-90th)
Temperature ΔT (°C)	0.94	(0.61 – 1.26)	2.03	(1.32 – 3.04)
Precipitations (Coefficient)				
Total Precipitation	1.08	(1.02 – 1.12)	1.16	(1.09 – 1.26)
Rain	1.14	(1.06 – 1.20)	1.28	(1.17 – 1.40)
Snow	1.03	(0.96 – 1.10)	1.08	(0.96 – 1.20)

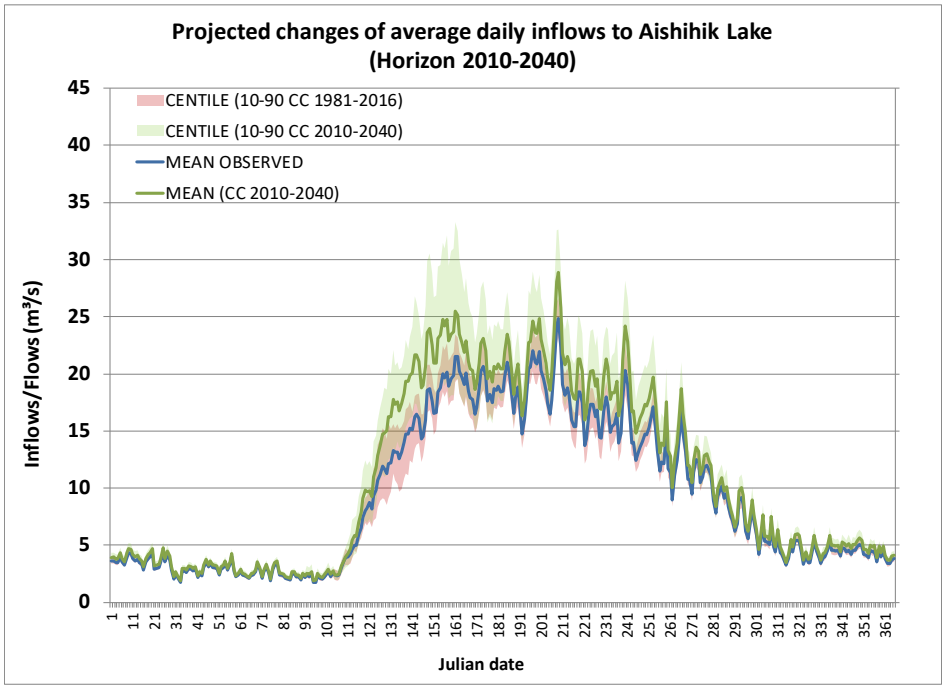

Figure 6.4 Projected changes of average daily inflows to Aishihik Lake (horizon 2010-2040).

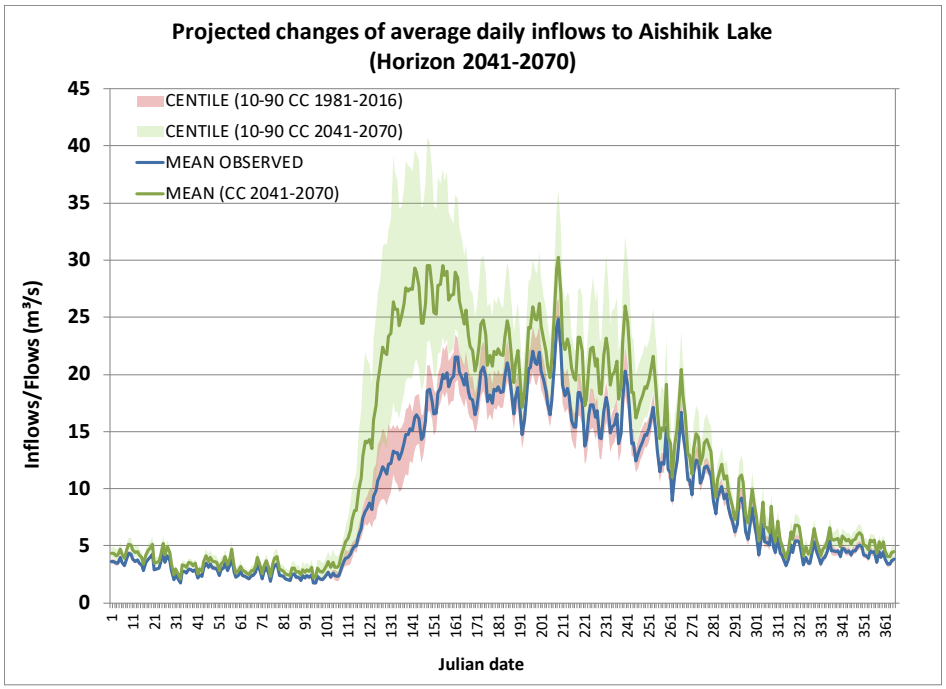

Figure 6.5 Projected changes of average daily inflows to Aishihik Lake (horizon 2041-2070).

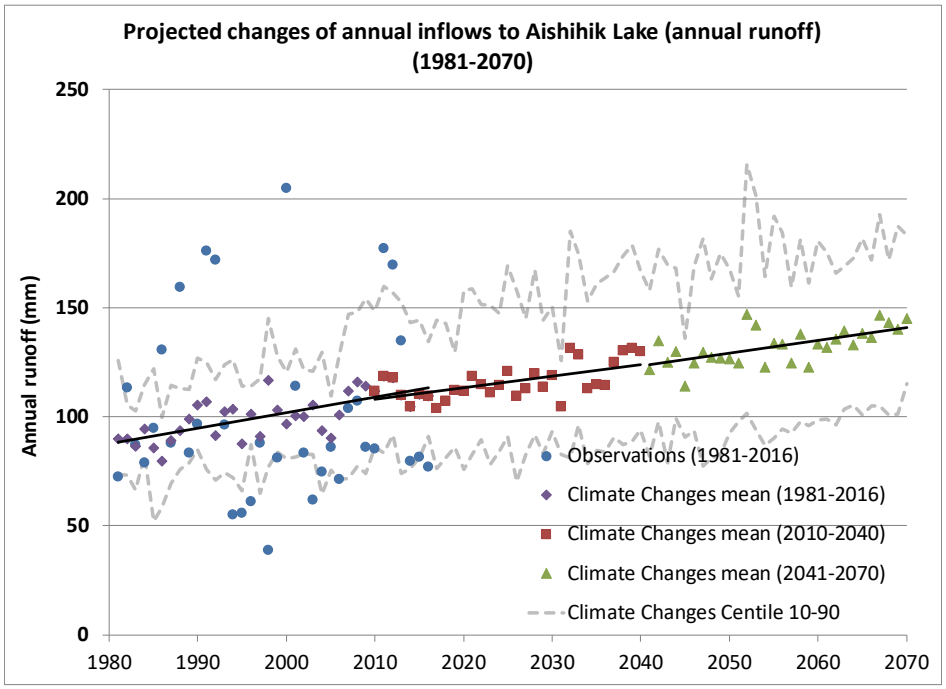

Figure 6.6 Projected changes of annual inflows to Aishihik Lake (in terms of annual runoff) (1981-2070).

Table 6.3 Comparison between observed and projected annual inflow characteristics (in terms of annual runoff) for Aishihik Lake. Note the percentages in parentheses are relative to the mean value of the reference (i.e., observed) period.

	1981-2016	2010-2040		2041-2070	
Annual runoff	Observed	Projected	Var. (%) vs. obs. (mean)	Projected	Var. (%) vs. obs. (mean)
Mean	100.74	115.97	15.1% (15.1%)	132.37	31.4% (31.4%)
Centile 10	61.48	82.79	34.7% (-17.8%)	92.01	49.7% (-8.7%)
Centile 90	170.85	158.37	-7.3% (57.2%)	180.24	5.5% (62.6%)

In terms of climate, Figures 6.1, 6.2 and 6.3 and Table 6.2 show distinct tendencies; that is while annual temperature and rain fall steadily increase, snow fall remains relatively stable. Meanwhile, the ranges of annual values (i.e., dashed lines illustrating the 10^{th} and 90^{th} centiles) remain relatively constant for all the climate change scenarios. According to climate change projections, Figures 6.4, 6.5, 6.6 and Table 6.3 indicate clear tendencies of increasing inflows or annual runoff based. Also for both future horizons, daily inflows and annual runoffs will in all likelihood increase when compared to the reference period. Predicted annual runoffs show less dispersion than observations. For the first and second future horizons, the projected 10^{th} centiles is greater than that of the reference period, but remains smaller than the mean of the reference period; illustrating wetter conditions. For the projected 90^{th} centiles, only the second future horizon has a value greater than the 90^{th} centile of the reference period. Moreover for both future horizons, the projected mean is greater than that of the reference period mean. Finally, both future horizons are characterized by consecutive wet years with runoff values greater than the mean of the reference period, although without never reaching the peaks of the years with the greatest observed values.

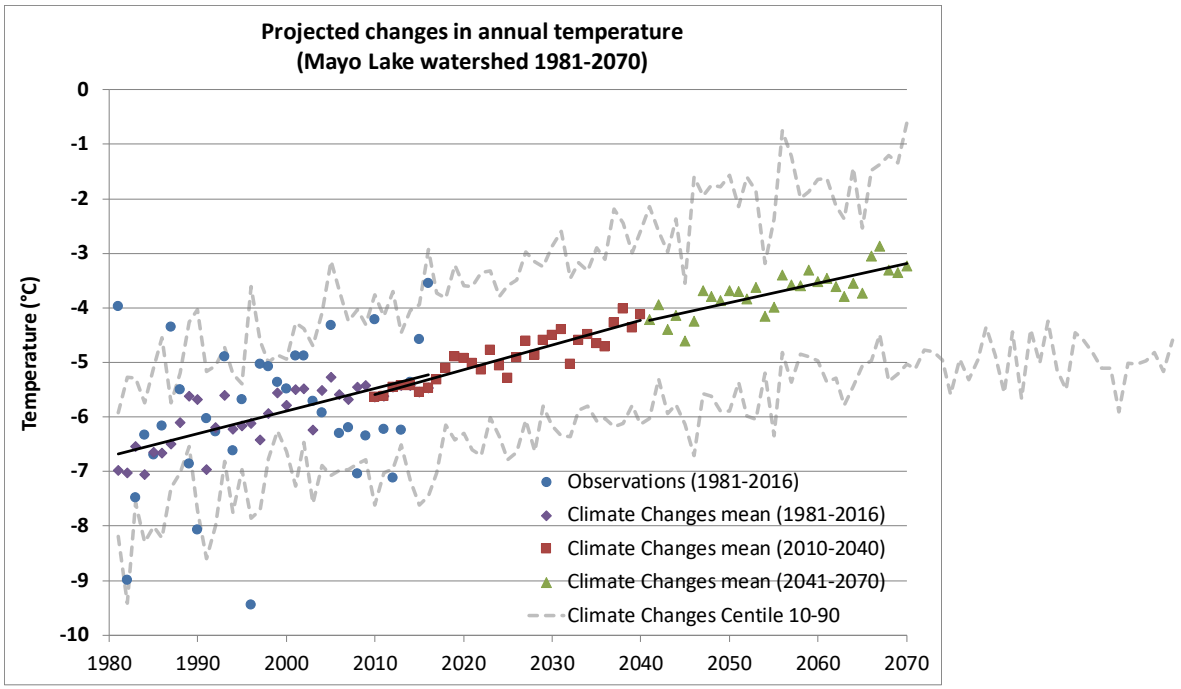

Figure 6.7 Projected changes in annual temperature for the Mayo Lake watershed (1981-2070).

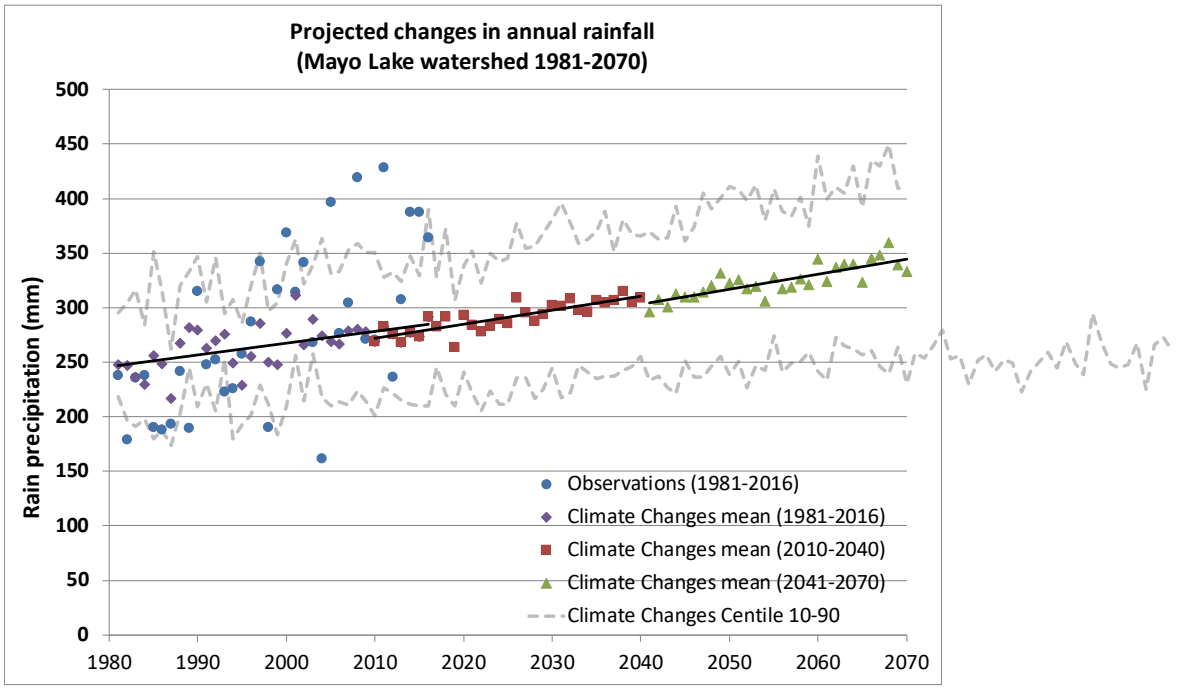

Figure 6.8 Projected changes in annual rainfall for the Mayo Lake watershed (1981-2070).

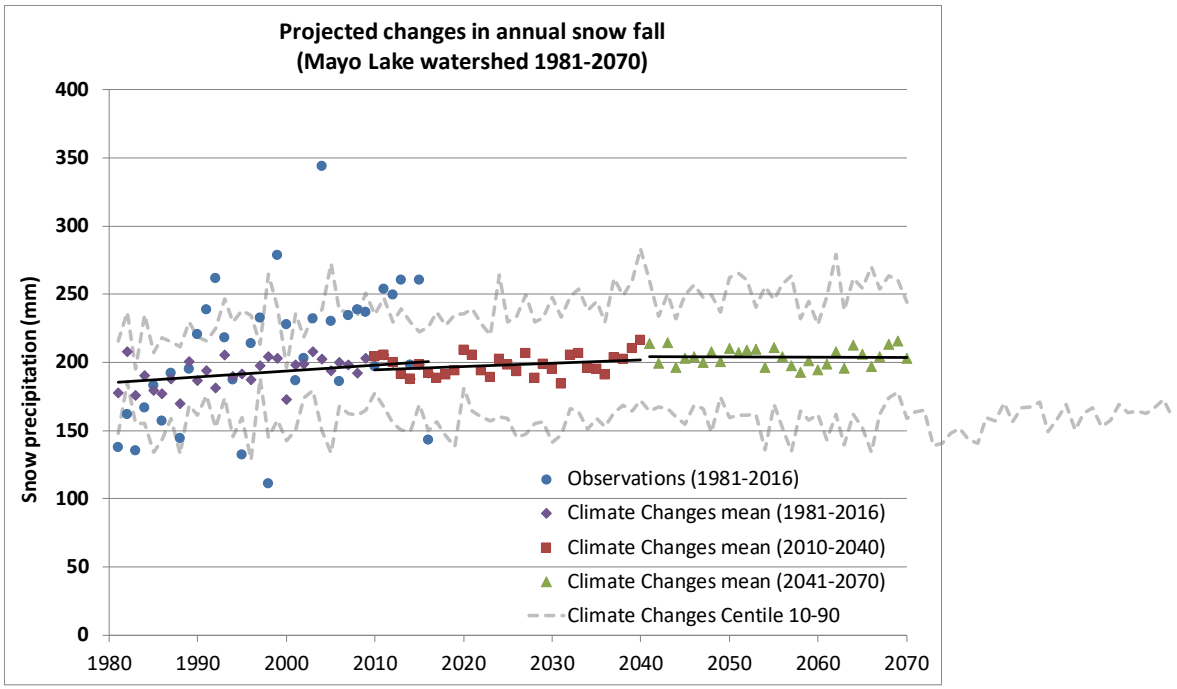

Figure 6.9 Projected changes in annual snow fall for the Mayo Lake watershed (1981-2070).

Table 6.4 Projected changes in meteorological conditions for the Mayo Lake watershed (horizon 2010-2040 and 2041-2070).

Variable	2010-2040		2041-2070	
	Average	(Centile 10th-90th)	Average	(Centile 10th-90th)
Temperature ΔT (°C)	1.05	(0.69 – 1.40)	2.25	(1.44 – 3.27)
Precipitations (Coefficient)				
Total Precipitation	1.07	(1.02 – 1.13)	1.15	(1.08 – 1.22)
Rain	1.10	(1.02 – 1.19)	1.22	(1.07 – 1.35)
Snow	1.03	(0.96 – 1.09)	1.06	(0.98 – 1.15)

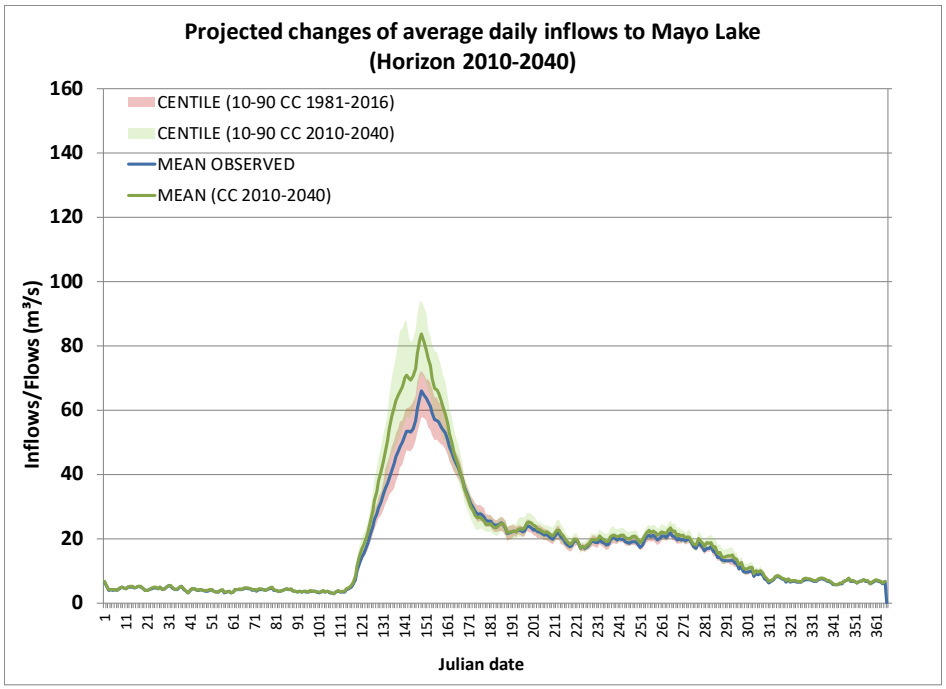

Figure 6.10 Projected changes of average daily inflows to Mayo Lake (horizon 2010-2040).

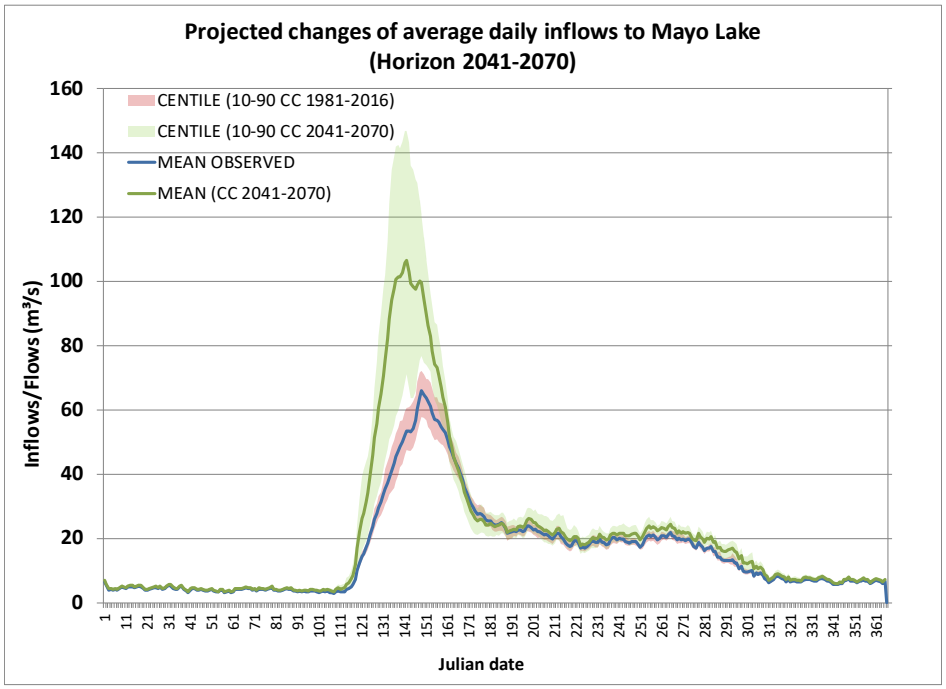

Figure 6.11 Projected changes of average daily inflows to Mayo Lake (horizon 2041-2070).

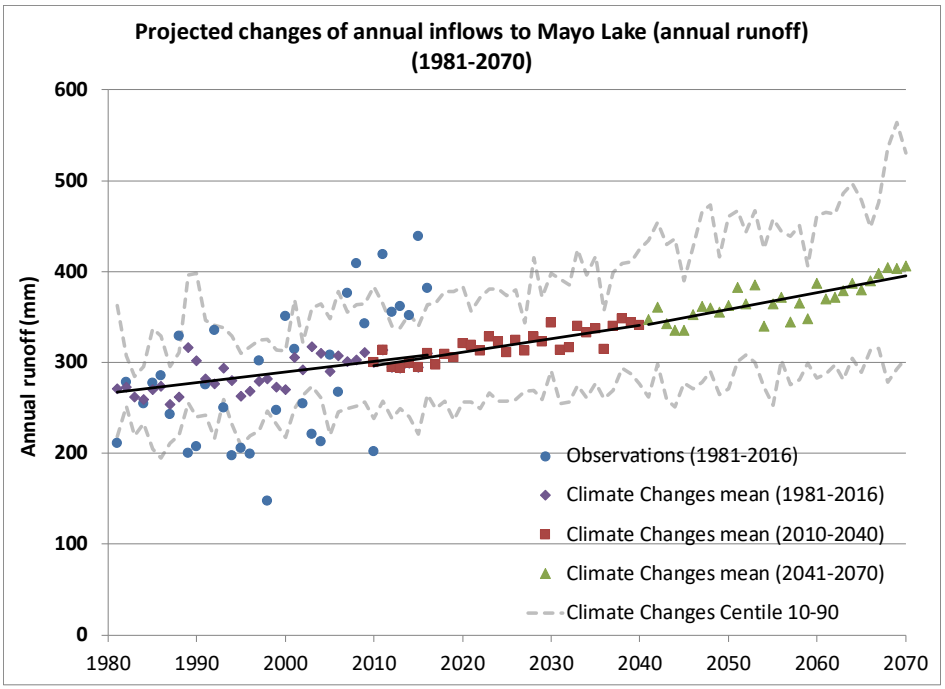

Figure 6.12 Projected changes of annual inflows to Mayo Lake (in terms of annual runoff) (1981-2070).

Table 6.5 Comparison between observed and projected annual inflow characteristics (in terms of annual runoff) for Mayo Lake. Note the percentages in parentheses are relative to the mean value of the reference (i.e., observed) period.

	1981-2016	2010-2040		2041-2070	
Annual runoff	Observed	Projected	Var. (%) vs. obs. (mean)	Projected	Var. (%) vs. obs. (mean)
Mean	286.05	318.99	11.5% (11.5%)	368.32	28.8% (28.8%)
Centile 10	200.83	253.13	26.0% (-11.5%)	277.22	38.0% (-3.7%)
Centile 90	379.22	387.13	2.1% (35.3%)	467.69	23.3% (63.5%)

For Mayo, Figure 6.7, 6.8 and 6.9 and Table 6.4 show distinct tendencies; that is while annual temperature and rainfall increase, snow fall remains relatively constant. Meanwhile, the ranges of annual values (i.e., dashed lines illustrating the 10^{th} and 90^{th} centiles) are relatively constant over the simulation period. Figures 6.10, 6.11, 6.12 and Table 6.5 indicate again clear tendencies of increasing inflows or annual runoff. Also for both future horizons, daily inflows and annual runoffs increase when

compared to those of the reference period (i.e., observed values). Projected annual runoffs show less dispersion than observations. For the first and second future horizons, the projected 10^{th} and 90^{th} centiles are greater than the corresponding values of the reference period, but the projected 10^{th} centiles remain smaller than the mean of the reference period. Moreover, for both future horizons, the projected means are greater than the mean of the reference period. Finally, both future horizons are characterized by consecutive wet years with runoff values greater than the mean of the reference period, although none of them have values greater than the peaks of the years with the largest observed values.

For both Aisihik Lake and Mayo Lake, the spring peak flows and freshet volumes show increasing tendencies while winter low flows remain similar. The magnitude of changes steadily increases with time and given climate projections, the direction of change is highly probable.

In early 2020, we conducted the hydroclimatic simulations for the Upper Yukon River watershed. With the addition of a simple glacier model accounting for different band elevations, long term simulations were performed. The glacier model accounts for both glacier melting and negative net budget; that is, ice melt from the glacier is not replaced by any ice formation processes and simply subtracted from the glacier mass. The remaining procedure is identical to the one described for Aishihik Lake and Mayo Lake. Also current climate period did not include glacier mass loss since glacier distribution of the land cover map is representative of the 2010 period while starting the simulation in 1981 including glacier mass loss would not have made any sense. The focus was on predicting the general impact of climate change scenarios on annual flows/inflows. Figures 6.13 to 6.18 and Tables 6.6 and 6.7 present the impact of climate change on meteorological conditions for both Upper Yukon (Whithehorse) and Marsh Lake watersheds while Figures 6.19, 6.20, 6.21 and Table 6.8 present the impact on flows at Whitehorse while accounting for net loss of glacier mass. Similarly, Figures 6.22, 6.23, 6.24 and Table 6.9 present results for Marsh Lake inflows.

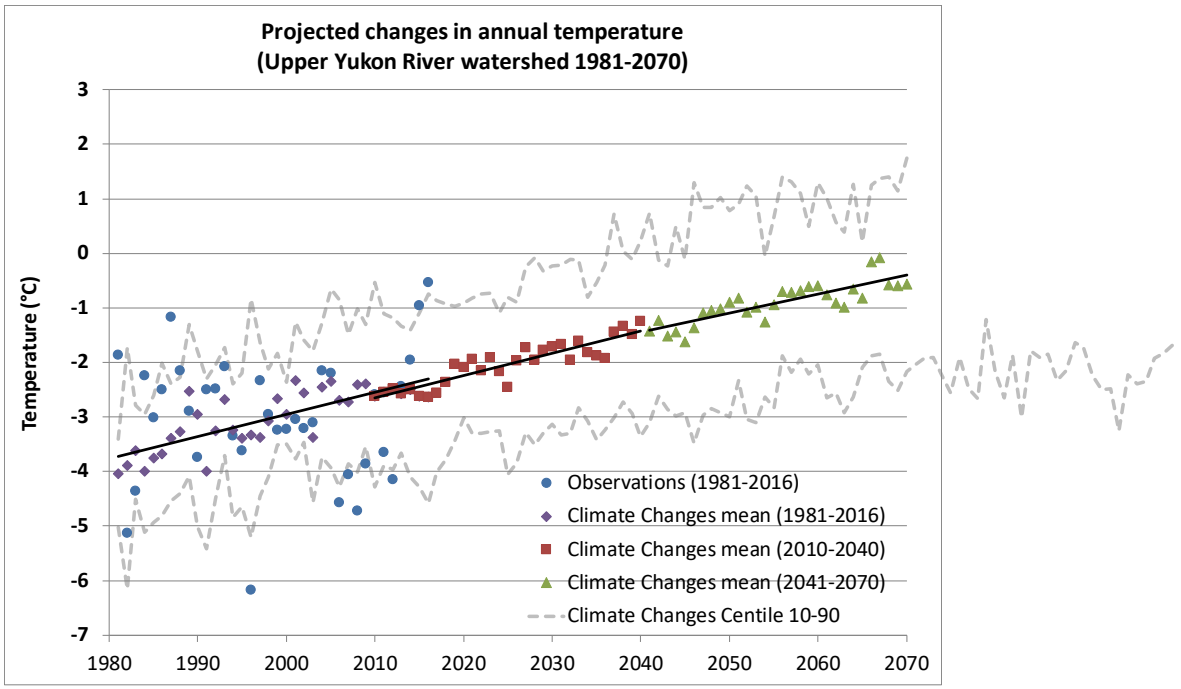

Figure 6.13 Projected changes in annual temperature for the Upper Yukon River watershed (1981-2070).

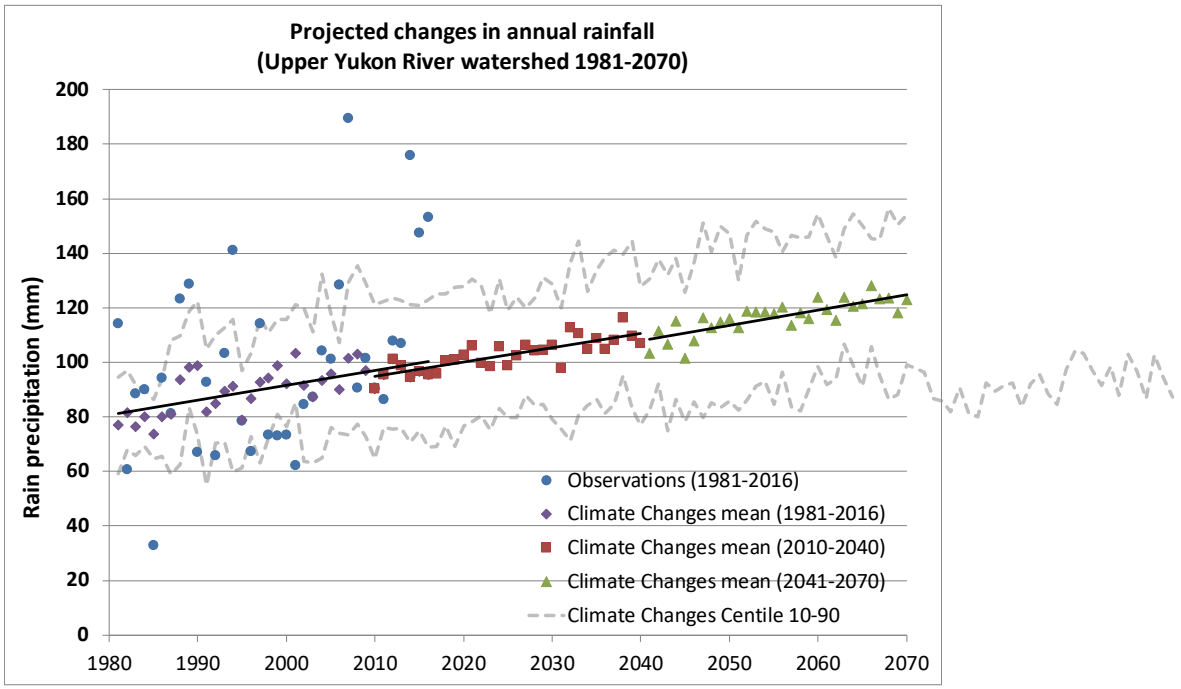

Figure 6.14 Projected changes in annual rainfall for the Upper Yukon River watershed (1981-2070).

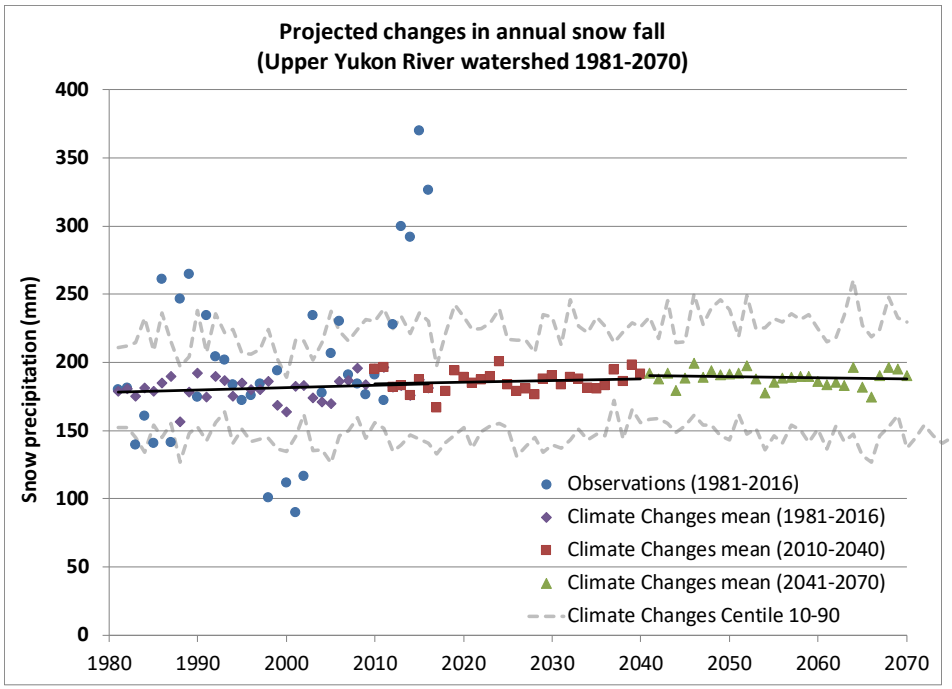

Figure 6.15 Projected changes in annual snow fall for the Upper Yukon River watershed (1981-2070).

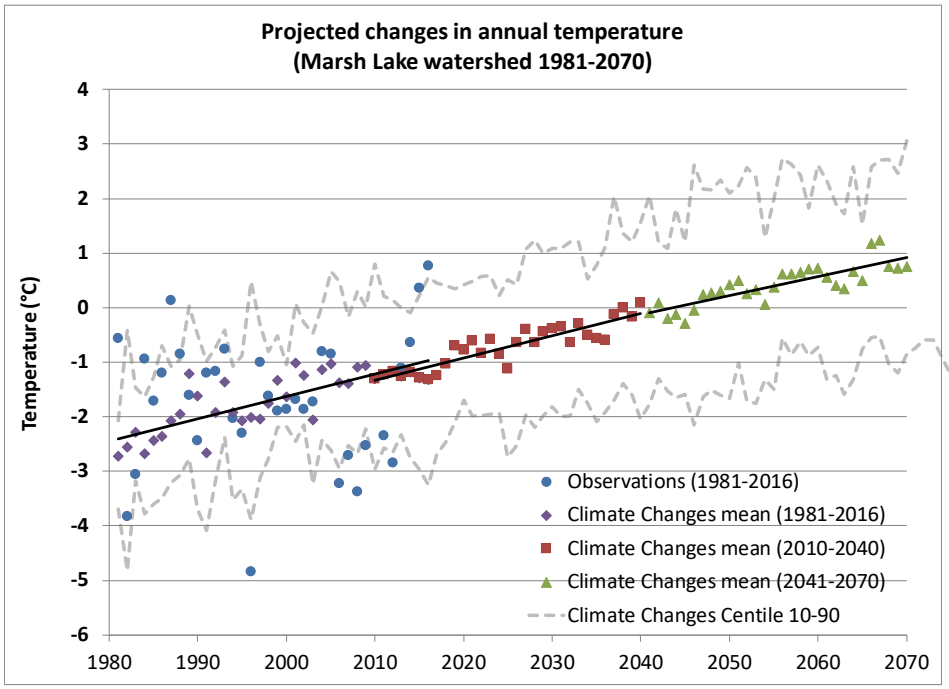

Figure 6.16 Projected changes in annual temperature for the Marsh Lake watershed (1981-2070).

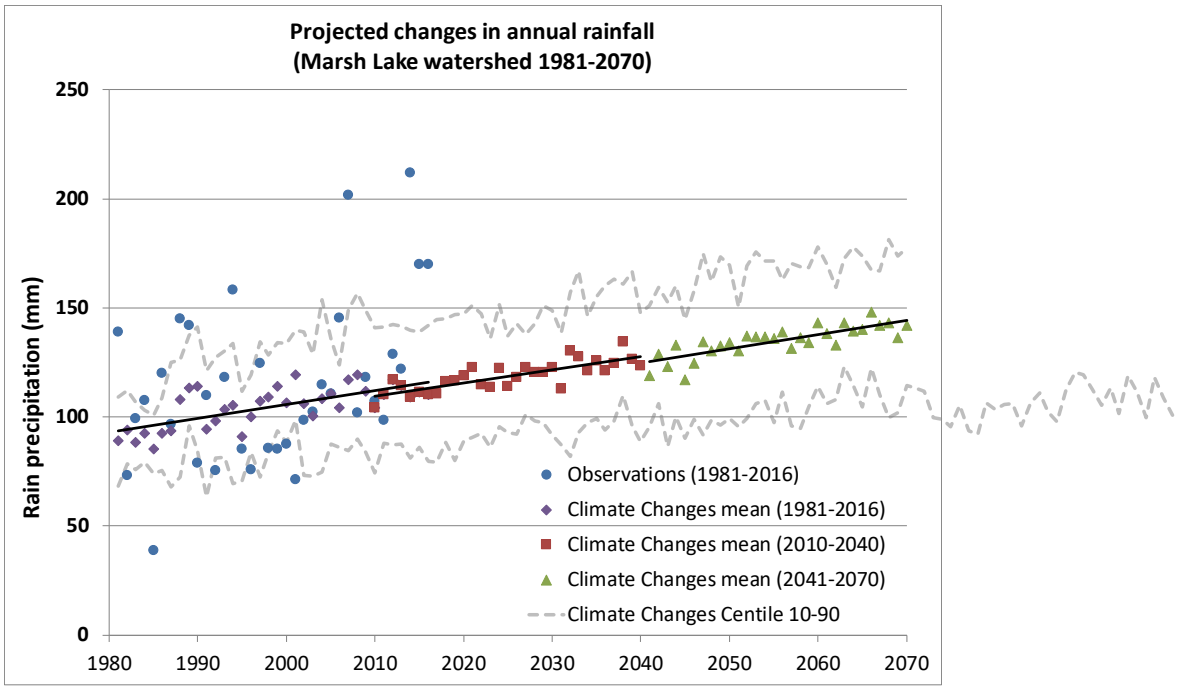

Figure 6.17 Projected changes in annual rainfall for the Marsh Lake watershed (1981-2070).

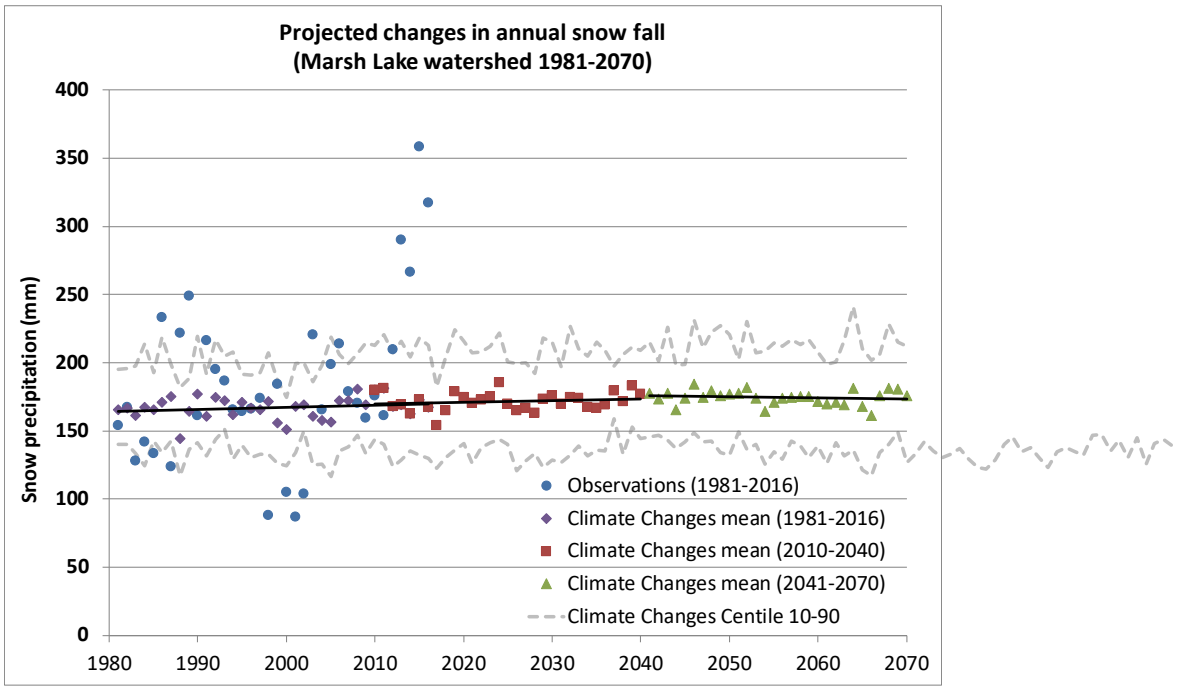

Figure 6.18 Projected changes in annual snow fall for the Marsh Lake watershed (1981-2070).

Table 6.6 Projected change in meteorological conditions for the Upper Yukon River watershed (horizon 2010-2040 and 2041-2070).

Variable	2010-2040		2041-2070	
	Average	(Centile 10th-90th)	Average	(Centile 10th-90th)
Temperature ΔT (°C)	0.97	(0.61 – 1.30)	2.10	(1.34 – 3.04)
Precipitations (Coefficient)				
Total Precipitation	1.06	(1.01 – 1.11)	1.12	(1.06 – 1.20)
Rain	1.13	(1.09 – 1.18)	1.29	(1.20 – 1.40)
Snow	1.03	(0.96 – 1.09)	1.04	(0.95 – 1.13)

Table 6.7 Projected change in meteorological conditions for the Marsh Lake watershed (horizon 2010-2040 and 2041-2070).

Variable	2010-2040		2041-2070	
	Average	(Centile 10th-90th)	Average	(Centile 10th-90th)
Temperature ΔT (°C)	0.97	(0.61 – 1.30)	2.11	(1.34 – 3.04)
Precipitations (Coefficient)				
Total Precipitation	1.07	(1.02 – 1.11)	1.14	(1.07 – 1.21)
Rain	1.13	(1.09 – 1.18)	1.29	(1.19 – 1.40)
Snow	1.03	(0.96 – 1.09)	1.04	(0.95 – 1.14)

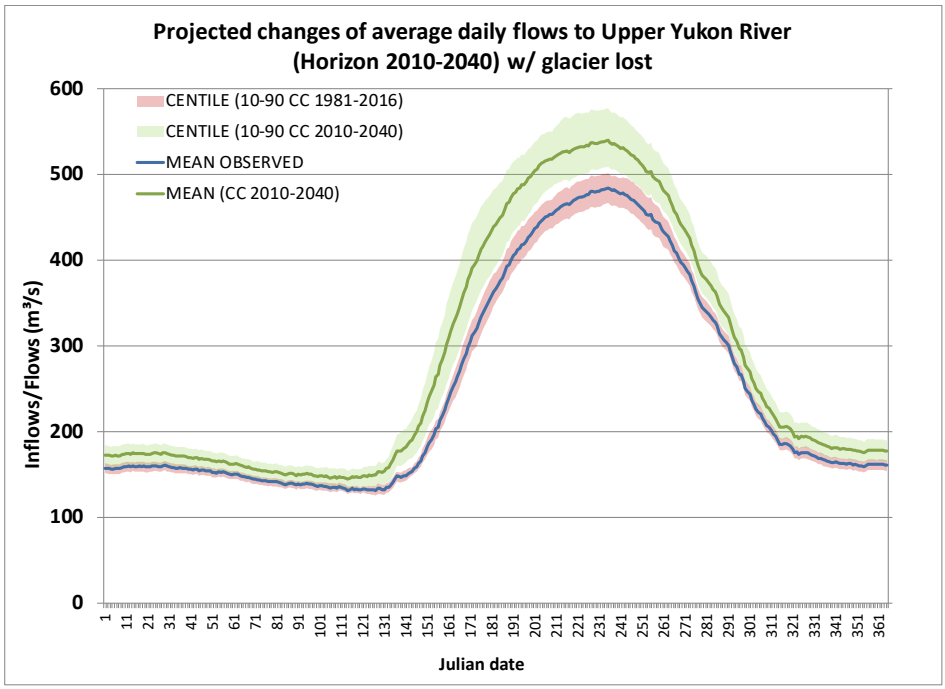

Figure 6.19 Projected changes of average daily flows to Upper Yukon River at Whitehorse (horizon 2010-2040 with glacier mass loss).

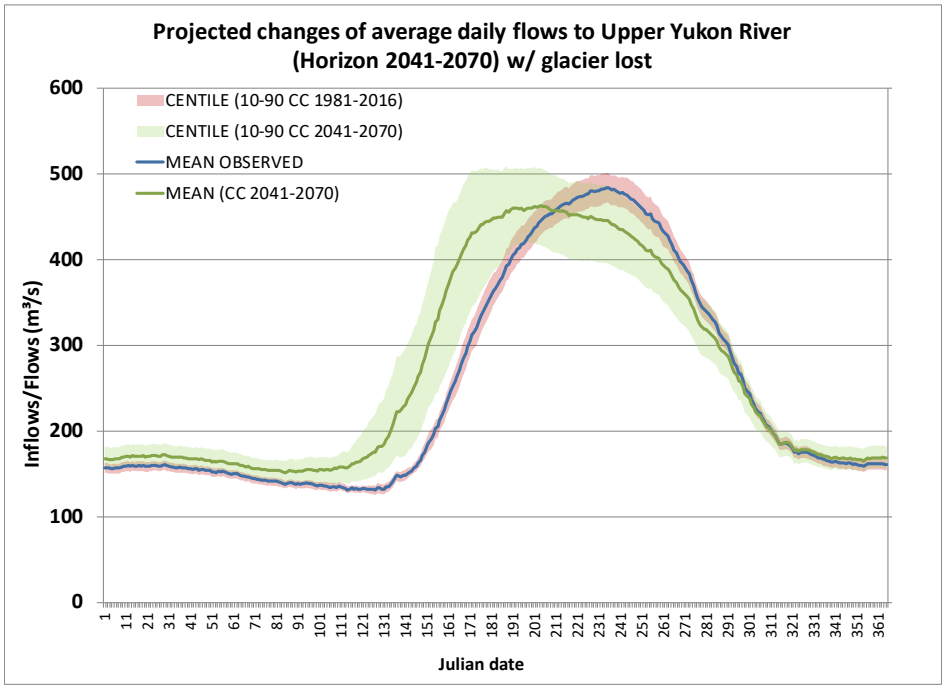

Figure 6.20 Projected changes of average daily flows to Upper Yukon River at Whitehorse (horizon 2041-2070 with glacier mass loss).

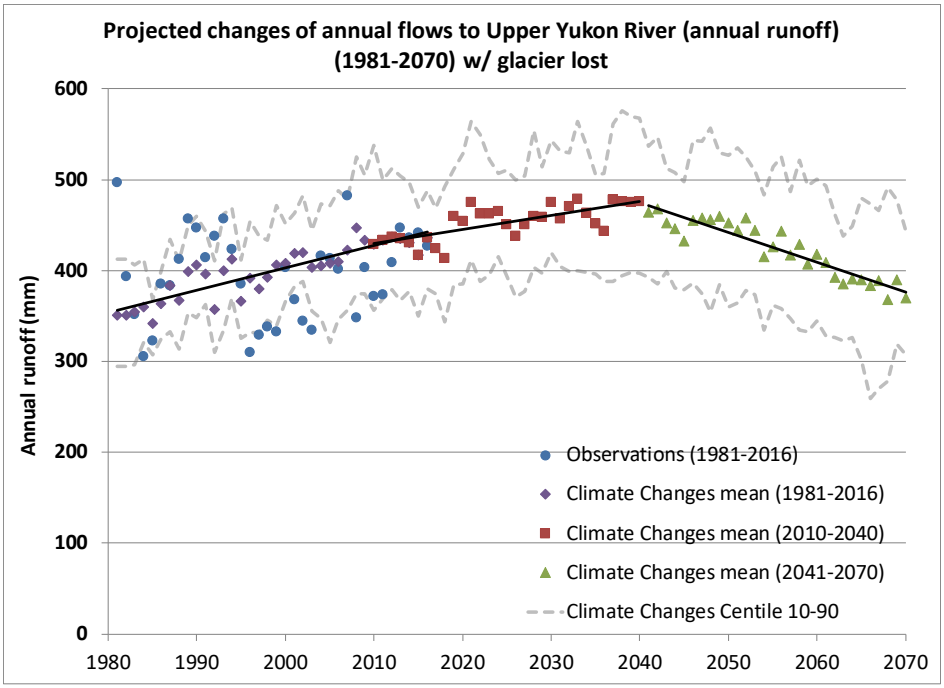

Figure 6.21 Projected change of annual flows to Upper Yukon River at Whitehorse (in terms of annual runoff) (1981-2070) with glacier mass loss.

Table 6.8 Comparison between observed and projected annual inflow characteristics (in terms of annual runoff) for the Upper Yukon River at Whitehorse. Note the percentages in parentheses are relative to the mean value of the reference (i.e., observed) period.

	1981-2016	2010-2040		2041-2070	
Annual runoff	Observed	Projected	Var. (%) vs. obs. (mean)	Projected	Var. (%) vs. obs. (mean)
Mean	394.55	452.79	14.8% (14.8%)	423.73	7.4% (7.4%)
Centile 10	331.19	381.01	15.0% (-3.4%)	334.69	1.1% (-15.2%)
Centile 90	452.07	531.44	17.6% (34.7%)	517.04	14.4% (31.0%)

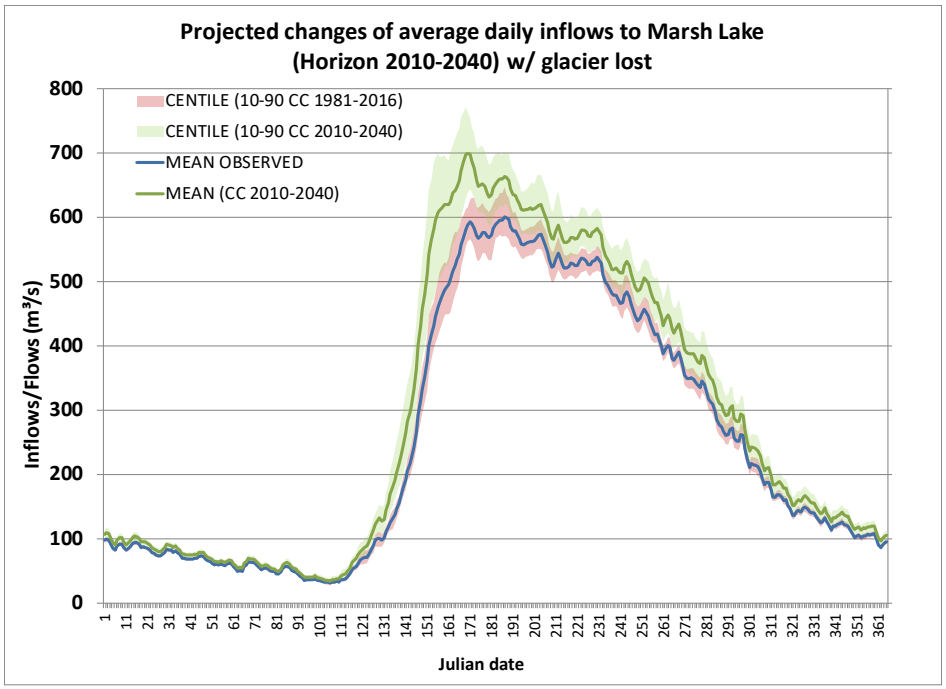

Figure 6.22 Projected changes of average daily inflows to Marsh Lake (horizon 2010-2040) with glacier mass loss.

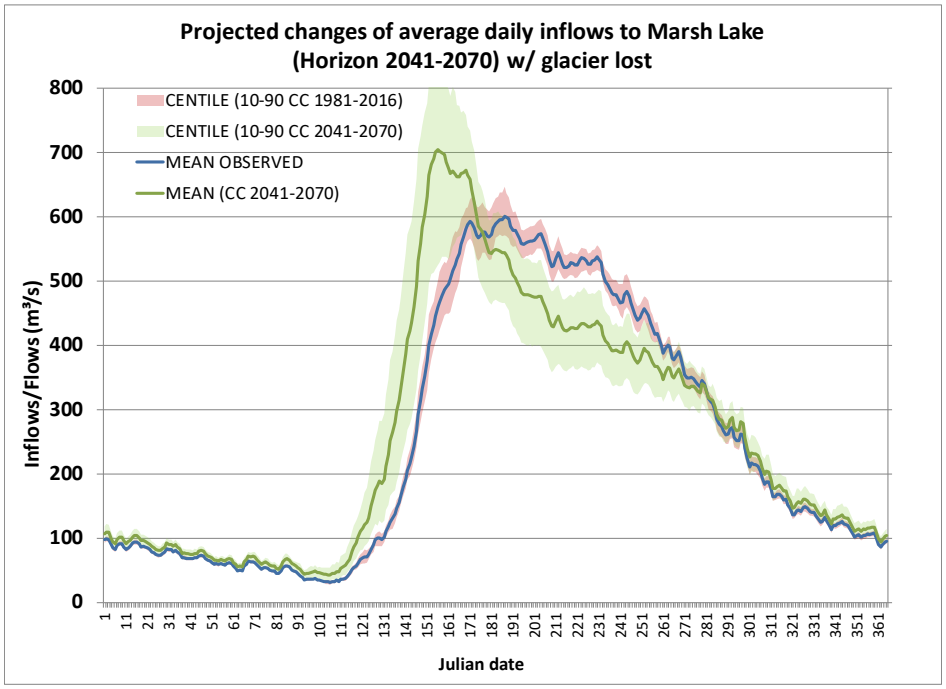

Figure 6.23 Projected changes of average daily inflows to Marsh Lake (horizon 2041-2070) with glacier mass loss.

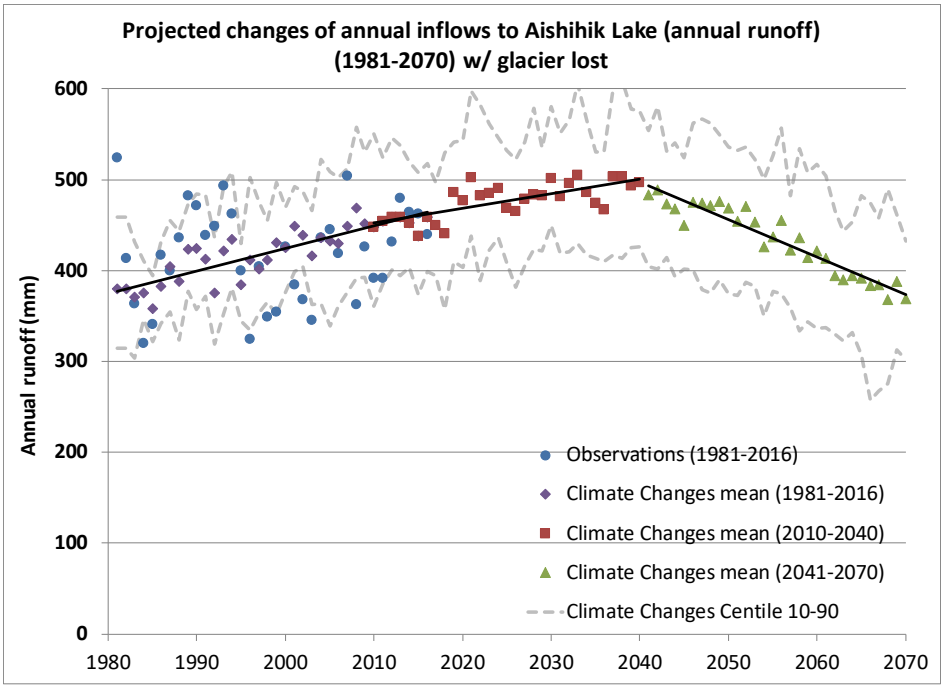

Figure 6.24 Projected changes of annual inflows to Marsh Lake (in terms of annual runoff) (1981-2070) with glacier mass loss.

Table 6.9 Comparison between observed and projected annual inflow characteristics (in terms of annual runoff) for the Upper Yukon River at Marsh Lake. Note the percentages in parentheses are relative to the mean value of the reference (i.e., observed) period.

	1981-2016	2010-2040		2041-2070	
Annual runoff	Observed	Projected	Var. (%) vs. obs. (mean)	Projected	Var. (%) vs. obs. (mean)
Mean	417.29	476.37	14.2% (14.2%)	433.14	3.8% (3.8%)
Centile 10	347.38	402.51	15.9% (-3.5%)	338.07	-2.7% (-19.0%)
Centile 90	480.74	561.59	16.8% (34.6%)	530.68	10.4% (27.2%)

For the Upper Yukon River at Whitehorse and Marsh Lake, Figures 6.13, 6.14, 6.15, 6.16, 6.17 and 6.18 and Table 6.6 and 6.7 show distinct tendencies; that is while temperature and rainfall increase snow fall remains relatively stable. Meanwhile, the ranges of annual values (i.e., dashed lines illustrating the 10th and 90th centiles) are relatively constant for all the climate change scenario. Performing hydroclimatic

projections for the Upper Yukon River watershed remains a challenging task. The results demonstrate important tendencies as the climate change scenarios lead to increases in flows/inflows (or annual runoffs) with maximum values occurring over the 2040 horizon followed by a decrease over the 2041-2070 period. When accounting for melting processes and loss of glacier mass, the 2010-2040 annual runoff benefits from the increased glacier melting impacts induced by the increasing temperature and precipitation projections. However, the diminishing mass of glacier will irreversibly lead to a diminution of the relative contribution of glacier melt to the annual runoff. Rate of glacier melt for the 2010-2040 period and the 2040-2071 period is such that by the end of the latter period the annual runoff is similar to that at the beginning of the 1981-2010 period. Results also indicates shift in spring freshet timing and amplitude for the 2041-2070 horizon with earlier freshet and similar amplitude for flows at Whitehorse and earlier and larger freshet for inflows at Marsh Lake. Inflows/Flows following 2041-2070 spring freshets have smaller values than those of the reference period. For the first and second future horizons the simulated 10^{th} and 90^{th} centiles at Whitehorse are generally greater than those of the reference period except for the Marsh Lake 2041-2070 10^{th} centile. Moreover, the simulated 10^{th} centile remains lower than the mean of the reference period for both the Upper Yukon River at Whitehorse and the inflows to Marsh Lake. It is noteworthy that for both future horizons the projected mean is greater than that of the reference period. From a global perspective, climate projections combined with glacier melting and loss will affect the hydrological regime of the Upper Yukon River watershed in terms of the amplitude if the inflows/flows and annual runoff.

7. INRS Project schedule

In the end, the project met the global planning; with all the packages (WPs) completed while a few of them had a late start, but not to the point of slowing down the project. Table 7.1 summarizes the project schedule which was updated after the second year of the project and includes the change to the working package (few months after the beginning of the project it was decided to substitute the reservoir management work package (old WP3) for the hydrological modelling of the Upper Yukon River Watershed (new WP3) and subsequent integration in the forecasting system). The following paragraphs summarize the state of each WP described in the previous chapters of this report with respect to the project schedule introduced in Table 7.1.

WP1 – Forecasting System

In November 2019, INRS updated the implementation of the forecasting system on the modelling server at YEC in Whitehorse (WP1). The system is now operational for Aishihik and Mayo and Upper Yukon River watershed (including Marsh Lake sub-watershed) - this is on schedule with respect to all watersheds regarding the implementation of the Ensemble Kalman Filter (EnKF) DA developed by NCE (see ARD progress report produced by YU). The DA developed by Yukon University was integrated in the forecasting system in October 2017. For the Upper Yukon River and the Marsh Lake sub-watershed, the DA scheme developed for Mayo was adapted for short lead time (14-day forecast based on NAEFS) and seasonal forecast and annual lead times (CanSIPs). Meanwhile, we also modified the structure of the DD/EB snow model so it can run on an elevation-band basis and integrated a DD elevation-band based glacier module to HYDROTEL (new WP3). A complete training session was provided to YEC in November 2019 and in March 2020 we proposed a service framework focusing on the maintenance of the forecasting system with respect to specific requests to come over the coming year. As a complement, the forecasting system will keep on running on a local computer at INRS. The forecasting system is currently used for hydrological forecasting (i.e., inflows and stream flows) with different lead times (e.g., 1-14 days) to assist hydroelectric operations as well as seasonal and long-term planning.

WP2 – Permafrost and Snow

The development and validation of the permafrost and multilayer snow modules are the thesis subjects of an INRS Ph.D. student who started in September 2017. The development of a multilayer snow model has led to interesting results, but the number of layers do not significantly improve the overall model performance. Thus, we decided to adapt the structure of the original HYDROTEL Degree-Day/Thermal Energy Balance snow model so it can run on an elevation-band basis and this proved to be well suited for forecasting purposes as well as for the hydroclimatic portion of the project (WP5). While building a permafrost model with the tools already available in HYDROTEL was conceivable, the limiting factor was the availability of data for permafrost depth and soil temperature for model validation. Such information is required in order to compare the performance of HYDROTEL against those that has already been tested in the field. Therefore, given the fact that permafrost is not prevalent in either one of the study watersheds, this research activity was not pursued in this project.

Simulated SWEs were assessed using historical snow surveys conducted by Yukon University and Yukon Government. Supplemental snow surveys on foot were done during winter/spring in Aishihik and Mayo by Yukon University as well as with historical data collected using GMON stations in the Upper Yukon River. A snow temperature profile sensor was installed in Aishihik by Yukon University. Despite a late start due to administrative constraints related to the issuing of a student visa - the PhD student actually arrived at INRS in September 2017 instead of June. That being mentioned, this WP delivered the main outcome since the adapted Degree-Day/Elevation-Band Thermal Energy Balance snow model allowed for the development of a robust forecasting system..

WP3 – Glacier

This WP focuses on the development and integration of a glacier module in HYDROTEL in order to explicitly account for the presence of glaciers in the Upper Yukon River Watershed. It is the thesis subject of an INRS PhD student. As reported in Chapter 4, a first version of a degree-day glacier module was integrated to HYDROTEL and an elevation-band based version was developed and implemented for the hydroclimatic assessment of the Upper Yukon River watershed. Furthermore, the Ph.D. student applied an iterative constraint modeling strategy over the Gulf Of Alaska (GOA) to improve the resolution of ice loss estimates derived from Gravity Recovery And Climate Experiment (GRACE). Three GRACE solutions from the most common processing strategies and three ice distribution maps of resolutions ranging from

55,000 to 20,000 km^2 were used. At this scale, all solutions and distribution maps agree, showing about 40 Gt/year of mean ice mass loss over the period 2002–2017. This is on target with respect to the project schedule and quite an accomplishment given the fact that the PhD student started in September 2017 due administrative constraints related to a student visa that took more time than expected to be issued.

WP4 – Ocean and atmosphere circulation and hydrology

This item is completed as it was originally planned to start in January 2018. Indeed, it started in September 2017, thanks to the successful recruitment of the postdoctoral fellow who accepted to start early her internship at INRS. This WP meets the topics of the scheduled works. Using climate indices, such as the Artic Oscillation (AO), the Pacific Decadal Oscillation (PDO) and the Multivariate ENSO Index (MEI), to produce seasonal forecasts provides an interesting alternative to usual methods which do not include climate information, but only random past observations. At this point, using climatic information provides slightly better improvements only for the Upper Yukon River compared to only using random historical data depending on the month. Nevertheless, our results show that using past observations as displayed in the current version of the Forecasting System is the recommended approach to provide a background comparison with annual forecasts using solely CanSIPS data. That being mentioned, the development of methods based on climate indices could continue, with the possibility of using other large-scale variables or other indices as predictors to increase forecasts reliability. Future work, as part of a new project, could focus on integrating the scheme developed to the forecasting system in order to provide complementary prediction to CanSIPS-based seasonal and long-term forecasts.

WP5 – Hydroclimatic Assessment

This item is completed for all three YEC watersheds; including the work conducted beyond the December 2019 deadline; that is the assessment of the Upper Yukon River and Marsh Lake watersheds. Hydroclimatic assessment is based on downscaled daily Canada-wide climate scenarios from the latest CMIP5 climate simulations offered by the Pacific Climate Impacts Consortium (PCIC). Three scenarios of Representative Concentration Pathways (RCPs), namely RCP2.6 RCP4.5 and RCP8.5, were considered in this study; the former being viewed as optimistic, while the latter deemed pessimistic. Combinations of 12 climate models and RCPs where selected and made available to this project by the Ouranos consortium. The horizons of interest were 2010-2040 and 2041-2070; the 1980-2010 horizon

representing the reference. The number of climate change scenarios available was 33 with bias correction. To provide a consistent picture of potential impacts of climate change on future inflows at Mayo Lake, Aishihik Lake, Yukon River at Whitehorse and Marsh Lake, HYDROTEL was used as the basic hydrologic model and the scenarios were formatted accordingly. The final emphasis of this project topic was on identifying long-term trends in the average annual hydrograph and characterizing key elements such as annual runoff as well as high and low flows. The results will provide strategic information to YEC for the assessment of potential energy projects to supply Yukon with enough electricity to meet projected demands. Understanding climate change and associated effects will be useful to other processes such as relicensing activities.

Meetings and Activities

During two first year of the project, regular conference calls, involving project managers at INRS, YEC and YU, were held to insure the project was on track.

In the second year of the project INRS team members travelled twice to Whitehorse for technical meetings (March and July) and a YU member travelled once to Quebec City to coordinate the integration of the DA in the forecasting system. The planned December 2017 visit to Whitehorse was postponed to January 2018 due to outstanding airfares. The January 2018 trip involved technical and technology transfer meetings between INRS, YEC and YU. INRS provided a first training and educative video conference held in May 2018, but technical issue occurred and limited the outcome of the training session. The INRS team travelled again to Whitehorse for technical meetings in September 2018.

Finally, the INRS-YU team shared preliminary findings of the project with the scientific community via a poster presentation at the Ouranos Symposium held in Montreal in November (Rousseau et al., 2017a) and two oral presentations at the Arctic Change 2017 conference held in Québec City in December (Rousseau et al., 2017b; Samuel et al., 2017). New results were shared with the scientific community at the 2018 AGU fall meeting held in Washington D.C (Caillouet et al., 2018; Doumbia et al., 2018, Augas et al., 2018); the 27th IUGG General Assembly - International Union of Geodesy and Geophysics 2019 summer meeting held in Montréal, Canada (Doumbia et al., 2019a; Foulon et al., 2019b;); the AQT/RHQ 2019 conference at Bishop's University held in Sherbrooke, Canada (Foulon et al. 2019b; Doumbia et al,

2019b); and the 2020 EGU annual conference held in Vienna, Austria (Abbasnezhadi and Rousseau, 2020a). In terms of scientific papers, the project has so far produced four papers (Samuel et al. 2019; Doumbia et al., 2019c, 2020; Abbasnezhadi and Rousseau, 2020b); additional papers will follow in the coming years as the two Ph.D. and two postdoctoral students complete their studies.

In the third year of the project, the INRS team members travelled twice to Whitehorse for technical meetings (January and November). The January 2019 trip involved technical and technology transfer meetings between INRS, YEC and YU. At the November 2019 meeting, INRS provided another training session to YEC staff.

Table 7.1 Project schedule

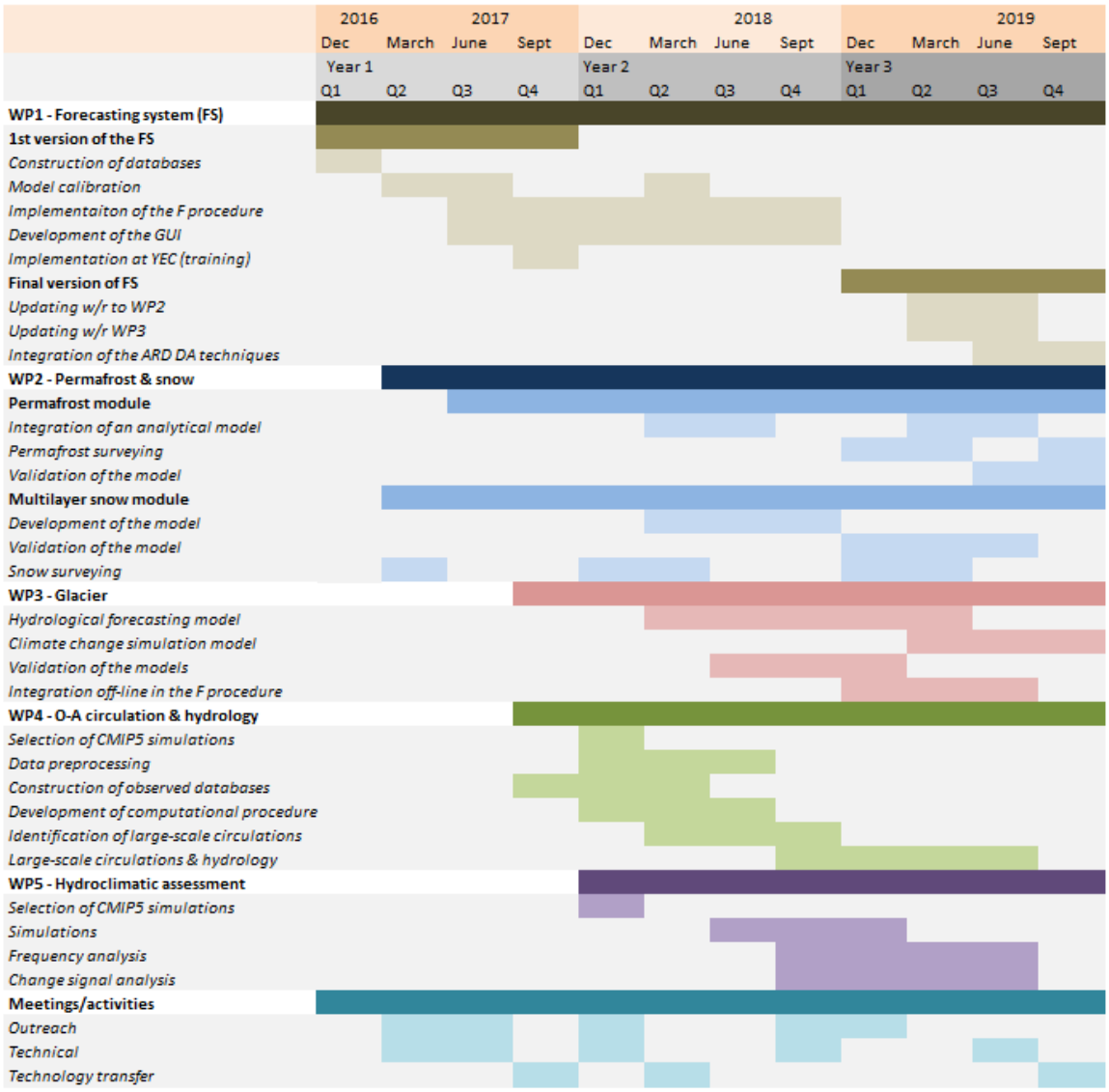

8. YU Project schedule

Summary

Yukon University is happy to state that the project has met the goals and outcomes of developing a hydrological modeling framework using a combination of field studies and cutting-edge data assimilation techniques. As can be seen in the table above (Yukon University Workplan, milestones and deliverables checklist), Work packages 1-4 were successfully completed. Details for each can be found below. Work package 5 was not completed (see below for reasoning); however, this did not impact the overall goals of developing an accurate forecasting system for YEC. Outreach activities have also not been complete as there are still some planned for the fall of 2020.

WP1 - Effects of large-scale climatic oscillations on climate

The main objective of WP1 is to investigate the statistical linkages and lags between various largescale climatic oscillations and observed precipitation and temperature (PT) in the Aishihik and Mayo basins. Investigations of large-scale climatic oscillations on climate (WP1 steps 1-3) revealed that there is a weak correlation between precipitation and climate oscillation for the entire Yukon, as well as Aishihik and Mayo basins. As such, a computer code to automatically generate forecasted climate data when large-scale oscillation indices are available (WP1 step 4) was not developed.

WP2 - Bias correction of forecasting meteorological data

The objectives of WP2 are to correct the bias of meteorological forecasting data (steps 1-3) and disaggregate them to spatial and temporal scales suitable for simulating and forcing the hydrologic model to forecast flows (step 4). All steps were successfully completed in this work package.

WP3 - Additional in-situ measurements

The main objective of this work package was to install automated meteorological stations and conduct In-situ measurements via snow surveys to generate high quality spatio-temporal meteorological data in the Aishihik and Mayo basins. One automated station and one Geonor (highly accurate automated precipitation measuring device) were successfully installed in both the Aishihik and Mayo basins. Additional Geonor stations have been purchased with the intention of also being installed in the Mayo and Aishihik basins to bolster the data; however, due to travel and field work restrictions from the COVID-19 pandemic, this work is delayed. This work is tentatively planned for the fall of 2020 but may be delayed again if travel and field work is still not possible.

Monthly snow surveys were conducted at three locations in the Aishihik basin by the YukonU research team from 2017-2020. Surveys commenced each year when snow was present (usually in October) and ended when snow was no longer present (usually April). In 2019, due to warm conditions in the spring, a survey was not completed in April due to lack of snow. Unfortunately, snow surveys in 2020 ended in February as travel and field work restrictions due to the COVID-19 pandemic meant travel was not possible starting March 16.

Monthly snow surveys did not occur in Mayo. The YukonU research team travelled to Mayo and trained staff members of First Nation of Na-Cho Nyak Dun (FNNND); however, changes to staff resulted in a loss of communication between YukonU and the FNNND. Fortunately the automated stations allowed for enough high quality spatio-temporal meteorological data in the Mayo area in order to fulfil the purpose of the work package.

WP 4 - DA model development, comparison and evaluation

The main objective of this work package was to apply and evaluate the robustness of various Data Assimilation (DA) approaches to meet YEC's operational purposes. Three DA approaches were tested in this project: 1) Kalman filtering (EnKF) by simulating state estimation and assuming constant model parameters; 2) Kalman Filtering by simulating simultaneous state-parameter estimation; and 3) particle

filtering (PF). It was found that the best DA approach suggested to use for the YEC's operational purpose is types #1 and the worst DA approach is type #3. A 4th type was originally planned to be investigated but as accuracy was decreasing with each subsequent approach tested, it was deemed that the 4th would be less accurate than the 1st and therefore not useful the project. As such, the 4th type was not investigated and the first approach (Kalman filtering (EnKF) was used in the forecasting system.

WP5 - Sensitivity analysis of the role of hydro-meteorological variables on flow forecasting

The objective of this work package is to improve our understanding of the role of individual and coupled hydrometeorological variables (precipitation, maximum and minimum air temperature) on flow forecasting accuracy. This study has not been completed. The reason being that a crucial staff member of the project team responsible for this task left the project. It was then agreed upon by project partners that the staff member hired in replacement, focus their efforts on other questions YEC wanted investigated, such as investigating the contribution of precipitation to streamflow in the Aishihik, Mayo and upper Yukon River basins as well as determining the optimal number of meteorological stations required to adequately represent each basin.

Outreach Activities

The following outreach activities were planned at the start of the project: Annual presentations to the public and local schools, telling the public about our work, etc. (fall) as well as providing presentations in the communities of Whitehorse, Mayo, and Haines Junction. While this plan was not followed directly, there was several outreach activities that were successfully completed. The project team presented to members of the technical community in Whitehorse in Fall and early winter 2019 to all interested stakeholders and First Nation governments were invited. YukonU had follow up calls with the Champagne and Aishihik First Nation and First Nation of the Nacho Nyak Dun and made plans to present

to their governments and citizens; however, due to COVID-19, these have been delayed. Efforts are being made to do online presentations with each community during the summer and fall of 2020.

External evaluation

In the last year of the project, YEC contracted an external examination of the project by D.I. Smith P.Eng. with an emphasis on reviewing the inflow forecasting modelling development. The external examiner went through all the material that we presented and exchanged at our meetings in early November 2019 and produced a report that raised a number of questions and comments. Overall, the content of the report was very positive and indeed D.I. Smith commended the quality of our work. Our responses to his questions and comments after three rounds of exchanges can be found in Appendix III.

9. References

Abbasnezhadi K, AN Rousseau (2020a) Can assimilating snow monitoring information offset the adverse effects of precipitation data scarcity in hydrological modelling applications? EGU2020-11428 | Displays | HS4.4. Fri, 08 May, 08:30–10:15 | D182

Abbasnezhadi, K, AN Rousseau (2020b) Verification of Regional Deterministic Precipitation Analysis products using snow data assimilation for application in meteorological network assessment in sparsely gauged Nordic basins (JHM-D-20-0106) submitted on 2020/04/23 to Journal of Hydrometeorology

Abudu S, C-L Cui, M Saydi, JP King (2012) Application of snowmelt runoff model (SRM) in mountainous watersheds: A review, Water Science and Engineering, 5(2): 123-136, DOI: 10.3882/j.issn.1674-2370.2012.02.001.

Ainslie B, PL Jackson (2010) Downscaling and Bias Correcting a Cold Season Precipitation Climatology over Coastal Southern British Columbia Using the Regional Atmospheric Modeling System (RAMS), Journal of Applied Meteorology and Climatology, 49 (5): 937-953, DOI: 10.1175/2010JAMC2315.1.

Ambach, W., Blumthaler, M. and Kirchlechner, P. (1981) 'Application of the gravity flow theory to the percolation of melt water through firn', Journal of Glaciology, 27(95), pp. 67–75. doi: 10.3189/s0022143000011230.

Anderson M, Z Chen, M Kavvas, A Feldman (2002) Coupling HEC-HMS with Atmospheric Models for Prediction of Watershed Runoff, Journal of Hydrological. Engineering, 10.1061/(ASCE)1084-0699(2002)7:4(312), 312-318.

Arendt, A. et al. (2006) 'Updated estimates of glacier volume changes in the western Chugach Mountains, Alaska, and a comparison of regional extrapolation methods', 111(F03019). doi: 10.1029/2005JF000436.

Arendt, A. A. et al. (2008) 'Validation of high-resolution GRACE mascon estimates of glacier mass changes in the St Elias Mountains, Alaska, USA, using aircraft laser altimetry', Journal of Glaciology, 54(188), pp. 778–787. doi: 10.3189/002214308787780067.

Arendt, A. A., Luthcke, S. B. and Hock, R. (2009) 'Glacier changes in Alaska: can mass-balance models explain GRACE mascon trends?', Annals of Glaciology, 50(50), pp. 148–154. doi: 10.3189/172756409787769753.

Arendt, A. et al. (2013) 'Analysis of a GRACE global mascon solution for Gulf of Alaska glaciers', Journal of Glaciology, 59(217), pp. 913–924. doi: 10.3189/2013JoG12J197.

Armstrong, R. L. (1980). An analysis of compressive strain in adjacent temperature- gradient and equi-temperature layers in a natural snow cover. Journal of Glaciology, 26(94), 283–289. https://doi.org/10.1017/S0022143000010820

Arndt, S., & Paul, S. (2018). Variability of Winter Snow Properties on Different Spatial Scales in the Weddell Sea. Journal of Geophysical Research: Oceans, 123(12), 8862–8876. https://doi.org/10.1029/2018JC014447

Asadzadeh, M., & Tolson, B. (2013). Pareto archived dynamically dimensioned search with hypervolume-based selection for multi-objective optimization. Engineering Optimization, 45(12), 1489–1509. https://doi.org/10.1080/0305215X.2012.748046

Asadzadeh, M., & Tolson, B. A. (2009). A new multi-objective algorithm, pareto archived DDS. In Proceedings of the 11th annual conference companion on Genetic and evolutionary computation conference - GECCO '09 (p. 1963). New York, New York, USA: ACM Press. https://doi.org/10.1145/1570256.1570259

Aschwanden, A. and Blatter, H. (2005) 'Meltwater production due to strain heating in Storglaciären, Sweden: MELTWATER PRODUCTION', Journal of Geophysical Research: Earth Surface, 110(F4), p. n/a-n/a. doi: 10.1029/2005JF000328.

Aschwanden, A. and Blatter, H. (2009) 'Mathematical modeling and numerical simulation of polythermal glaciers', Journal of Geophysical Research, 114(F1). doi: 10.1029/2008JF001028.

Augas J, AN Rousseau, S Savary, L Caillouet, M Baraer (2018) Comparison between a single-layer snow model and a multi-layer snow model for snow-water equivalent modeling. AGU Fall Meeting 2018,10-14 December in Washington, D.C.

Baghdadi, N. and Zribi, M. (2017) Observations des surfaces continentales par télédétection micro-onde: techniques et méthodes. Available at: http://proxy.bibliotheques.uqam.ca/login?url=http://ressources.bibliotheques.uqam.ca/re/mono_elect/157_Observation_des_surfaces_continentales_par_teledetection_micro-onde_UQAM.pdf (Accessed: 27 May 2018).

Bahr, D. B. (1997) 'Global distributions of glacier properties: A stochastic scaling paradigm', 33(7), pp. 1669–1679. doi: 10.1029/97WR00824.

Bahr, D. B., Meier, M. F. and Peckham, S. D. (1997) 'The physical basis of glacier volume-area scaling', 102(B9), pp. 20355–20362. doi: 10.1029/97JB01696.

Bahr, D. B., Pfeffer, W. T. and Kaser, G. (2015) 'A review of volume-area scaling of glaciers', 53(95–140). doi: 10.1002/2014RG000470.

Baraer, M. et al. (2012) 'Glacier recession and water resources in Peru's Cordillera Blanca', 58(207), pp. 134–150. doi: 10.3189/2012JoG11J186.

Baraer M, CA Madramootoo, BB Mehdi (2010) Evaluation of winter freeze damage risk to apple trees in global warming projections. Transaction of the ASABE, vol. 53, n◦ 5. p. 1387-1397.

Barrand, N. E. and Sharp, M. J. (2010) 'Sustained rapid shrinkage of Yukon glaciers since the 1957–1958 International Geophysical Year', 37(L07501). doi: 10.1029/2009GL042030.

Bartelt P, M Lehning (2002) A physical SNOWPACK model for the Swiss avalanche warning Part I: numerical model, Cold Regions Science and Technology, 35: 123-145, DOI: 10.1016/S0165-232X(02)00074-5.

Baur, O., Kuhn, M. and Featherstone, W. E. (2013) 'Continental mass change from GRACE over 2002–2011 and its impact on sea level', Journal of Geodesy, 87(2), pp. 117–125. doi: 10.1007/s00190-012-0583-2.

Beamer, J. P. et al. (2016) 'High-resolution modeling of coastal freshwater discharge and glacier mass balance in the Gulf of Alaska watershed: COASTAL FWD AND GVL IN GOA WATERSHED', Water Resources Research, 52(5), pp. 3888–3909. doi: 10.1002/2015WR018457.

Bisson JL, F Roberge (1983) Prévision des apports naturels: Expérience d'Hydro-Québec. Paper presented at the Workshop on Flow Predictions, November, Toronto, Canada.

Blanchon, D. and Boissière, A. (2009) 'Atlas mondial de l'eau: de l'eau pour tous'. Paris: Éditions Autrement.

Blatter, H. and Haeberli, W. (1984) 'Modelling temperature distribution in alpine glaciers', Annals of Glacialagy. (International Glaciological Society), 5.

Bonsal BR, TD Prowse, CR Duguay, MP Lacroix (2006) Impacts of large-scale teleconnections on freshwater-ice break/freeze-up dates over Canada, Journal of Hydrology 330:340–353.

Brabets TP, MA Walvoord (2009) Trends in streamflow in the Yukon River Basin from 1944 to 2005 and the influence of the pacific decadal oscillation, Journal of Hydrology, 371 (1-4): 108-119, DOI: 10.1016/j.jhydrol.2009.03.018.

Braithwaite, R. J. and Raper, S. C. B. (2009) 'Estimating equilibrium-line altitude (ELA) from glacier inventory data', Annals of Glaciology, 50(53), pp. 127–132. doi: 10.3189/172756410790595930.

Brun E, P David, M Sudul, G Brunot (1992) A numerical model to simulate snow-cover stratigraphy for operational avalanche forecasting, Journal of Glaciology, 38 (128).

Brun E., E Martin, V Simon, C Gendre, C Coléou (1989). An energy and mass model of snow cover suitable for operational avalanche forecasting. Journal of Glaciology, vol. 35, no. 121, p. 333- 342.

Burnash RJC (1995) The NWS River Forecast System - Catchment Model, Chapter 10, in Computer Models of Watershed Hydrology, Vijay P. Singh, editor, Water Resources Publications.

Cai, S., Zhang, K. and Wu, M. (2013) 'Improving airborne strapdown vector gravimetry using stabilized horizontal components', Journal of Applied Geophysics, 98, pp. 79–89. doi: 10.1016/j.jappgeo.2013.08.004.

Caillouet L, AN Rousseau, S Savary (2018) Improving operational ensemble streamflow forecasts by selecting past meteorological scenarios according to climate indices. AGU Fall Meeting 2018,10-14 December in Washington, D.C.

Cannon AJ, PH Whitfield (2002) Downscaling recent streamflow conditions in British Columbia, Canada using ensemble neural network models, Journal of Hydrology, 259 (1-4): 136-151, DOI: 10.1016/S0022-1694(01)00581-9.

Carey SK, JL Boucher, CM Duarte (2013) Inferring groundwater contributions and pathways to streamflow during snowmelt over multiple years in a discontinuous permafrost subarctic environment (Yukon, Canada), Hydrogeology Journal, 21: 67-77. DOI: 10.1007/s10040-012-0920-9.

Cassano EN, JJ Cassano (2010) Synoptic forcing of precipitation in the Mackenzie and Yukon River basins, International Journal of Climatology, 30: 658-674, DOI: 10.1002/joc.1926.

Castellazzi, P. et al. (2018) 'Quantitative mapping of groundwater depletion at the water management scale using a combined GRACE/InSAR approach', Remote Sensing of Environment, 205, pp. 408–418. doi: 10.1016/j.rse.2017.11.025.

CEHQ (2015) Hydroclimatic Atlas of Southern Québec. The Impact of Climate Change on High, Low and Mean Flow Regimes for the 2050 horizon, Rep., 81 pp, Québec.

Centre for Land and Biological Resources Research (1996) Soil Landscapes of Canada, v.2.2, Research Branch, Agriculture and Agri-Food Canada. Ottawa.

Chen, J. and Ohmura, A. (1990) 'Estimation of Alpine glacier water resources and their change since the 1870s', 193, (Symopsium at Lausanne, 1990 – Hydrology in Mountainous Regions I), pp. 127–135.

Chen, J. L., Tapley, B. D. and Wilson, C. R. (2006) 'Alaskan mountain glacial melting observed by satellite gravimetry', Earth and Planetary Science Letters, 248(1–2), pp. 368–378. doi: 10.1016/j.epsl.2006.05.039.

Chen, J. L. et al. (2015) 'Reducing leakage error in GRACE-observed long-term ice mass change: a case study in West Antarctica', Journal of Geodesy, 89(9), pp. 925–940. doi: 10.1007/s00190-015-0824-2.

Cherkauer, K. A., & Lettenmaier, D. P. (1999). Hydrologic effects of frozen soils in the upper Mississippi River basin. Journal of Geophysical Research Atmospheres, 104(D16), 19599–19610. https://doi.org/10.1029/1999JD900337

Compo, G. P., Whitaker, J. S., Sardeshmukh, P. D., Matsui, N. , Allan, R. J., Yin, X. , Gleason, B. E., Vose, R. S., Rutledge, G. , Bessemoulin, P. , Brönnimann, S. , Brunet, M. , Crouthamel, R. I., Grant, A. N., Groisman, P. Y., Jones, P. D., Kruk, M. C., Kruger, A. C., Marshall, G. J., Maugeri, M. , Mok, H. Y., Nordli, Ø. , Ross, T. F., Trigo, R. M., Wang, X. L., Woodruff, S. D. and Worley, S. J. (2011), The Twentieth Century Reanalysis Project. Q.J.R. Meteorol. Soc., 137: 1-28. doi:10.1002/qj.776

Debeer, C. M. and Sharp, M. J. (2007) 'Recent changes in glacier area and volume within the southern Canadian Cordillera', 46, pp. 215–221. doi: https://doi.org/10.3189/172756407782871710.

Dee DP, SM Uppala, AJ Simmons, P Berrisford, P Poli, S Kobayashi, U Andrae, MA Balmaseda, G Balsamo, P Bauer, P Bechtold, ACM Beljaars, L van de Berg, J Bidlot, N Bormann, C Delsol, R Dragani, M Fuentes, AJ Geer, L Haimberger, SB Healy, H Hersbach, EV H´olm, L Isaksen, P Kallberg, M Kohler, M Matricardi, AP McNally, BM Monge-Sanz, J-J Morcrette, BK Park, C Peubey, P de Rosnay, C Tavolato, J-N Thépaut, F Vitart (2011) The ERA-Interim reanalysis: configuration and performance of the dataassimilation system. Q. J. R. Meteorol. Soc. 137: 553– 597. DOI:10.1002/qj.828.

Dee, D. P., et al., 2011: The ERA-Interim reanalysis: configuration and performance of the data assimilation system, Quarterly Journal of the Royal Meteorological Society Volume 137, Issue 656, (DOI: 10.1002/qj.828)

Doumbia C, P Castellazzi, AN Rousseau, M Amaya (2020) Corrigendum: High Resolution Mapping of Ice Mass Loss in the Gulf of Alaska From Constrained Forward Modeling of GRACE Data. Front. Earth Sci. 8:57. doi: 10.3389/feart.2020.00057

Doumbia C, P Castellazzi, AN Rousseau, M Amaya (2019a) High Resolution Mapping of Glacier Mass Loss in Yukon and Alaska Derived from GRACE Data. 27th IUGG General Assembly -International Union of Geodesy and Geophysics, July 8-18 2019, Montréal, Canada.

Doumbia C, P Castellazzi, AN Rousseau, M Amaya (2019b) Cartographie à haute résolution de la perte de masse des glaciers au Yukon et en Alaska dérivée de données de GRACE. Colloque AQT /RHQ 2019 – La télédétection et l'eau dans tous leurs états. Campus de l'université Bishop's, Sherbrooke. L'Association québécoise de télédétection et La recherche en hydrologie au Québec. 15-17 mai 2019.

Doumbia C, P Castellazzi, AN Rousseau, M Amaya (2019c) High resolution mapping of ice mass loss in the Gulf of Alaska from constrained forward modelling of GRACE data. Frontiers in Earth Science 7:360. doi: 10.3389/feart.2019.00360

Doumbia C, P Castellazzi, AN Rousseau, M Amaya (2018) High resolution mapping of glacier mass loss in Yukon and Alaska derived from GRACE data. AGU Fall Meeting 2018,10-14 December in Washington, D.C.

Duan, Q., S. Sorooshian, and V. Gupta (1992), Effective and efficient global optimization for conceptual rainfall-runoff models, Water Resour. Res., 28(4), 1015–1031, doi:10.1029/91WR02985.

Dyurgerov, M., Meier, M. F. and Bahr, D. B. (2009) 'A new index of glacier area change: a tool for glacier monitoring', Journal of Glaciology, 55(192), pp. 710–716. doi: 10.3189/002214309789471030.

Essery R, S Morin, Y Lejeune, CB Ménard (2013) A comparison of 1701 snow models using observations from an alpine site, Advances in Water Resources, 55: 131-148, DOI: 10.1016/j.advwatres.2012.07.013.

Farbrot, H, I Hanssen-Bauer (2009) A simple station-based empirical model for local snow conditions. Oslo (Norvège) : The Norwegian Meteorological Institute. 19 p.

Farinotti, D., L. Longuevergne, G. Moholdt, D. Duethmann, T. Molg, T. Bolch, S. Vorogushyn, and A. Guntner (2015), Substantial glacier mass loss in the Tien Shan over the past 50 years, Nature Geoscience, 8(9), 716-+.

Farinotti, D. and Huss, M. (2013) 'An upper-bound estimate for the accuracy of glacier volume–area scaling', 7(1707–1720). doi: 10.5194/tc-7-1707-2013.

Finnerty BD, MB Smith, D Seo, VI Koren, GE Moglen (1997) Space-Time Scale Sensitivity of the Sacramento Model to Radar-Gage Precipitation Inputs, Journal of Hydrology, 203, 21-38.

Fortin J-P, R Turcotte, S Massicotte, R Moussa, J Fitzback, J-P Villeneuve. (2001) Distributed watershed model compatible with remote sensing and GIS data, part I: description of the model. Journal of Hydrologic Engineering 6(2): 91–99.

Fortin V (2000) Le modèle météo-apport HSAMI: Historique, théorie et application. Research report, Varennes, QC, Canada : Institut de recherche d'Hydro-Québec.

Fortin V, G Roy, N Donaldson (2014) Assimilation of radar QPE in the Canadian Precipitation Analysis (CaPA). 2014 ASCE International Symposium on Weather Radar and Hydrology, April 7th-10th, Washington.

Fortin V, G Roy, N Donaldson, A Mahidjiba (2015) Assimilation of radar quantitative precipitation estimations in the Canadian Precipitation Analysis (CaPA). Journal of Hydrology, 531(2): 296–307.

Fossey M, AN Rousseau, F Bensalma, S Savary, A Royer (2015) Integrating isolated and riparian wetland modules in the PHYSITEL/HYDROTEL modelling platform: model performance and diagnosis. Hydrological Processes 29, 4683–4702 (2015) doi: 10.1002/hyp.10534.

Foulon E, L Caillouet, AN Rousseau, S Savary. (2019a) Improving Streamflow and Inflow Forecasts to Assist Hydroelectric Operations. 27th IUGG General Assembly -International Union of Geodesy and Geophysics, July 8-18 2019, Montréal, Canada.

Foulon E, S Savary, L Caillouet, AN Rousseau, J Samuel (2019) Améliorer les prévisions de débits et les apports en soutien à la production hydroélectrique. Colloque AQT /RHQ 2019 – La télédétection et l'eau dans tous leurs états. Campus de l'université Bishop's, Sherbrooke. L'Association québécoise de télédétection et La recherche en hydrologie au Québec. 15-17 mai 2019.

Fountain, A. G. and Walder, J. S. (1998) 'Water flow through temperate glaciers', Reviews of Geophysics, 36(3), pp. 299–328. doi: 10.1029/97RG03579.

Franz KJ, TS Hogue, S Sorooshian (2008) Operational snow modeling: Addressing the challenges of an energy balance model for National Weather Service forecasts, Journal of Hydrology, 360: 48-66, DOI: 10.1016/j.jhydrol.2008.07.013.

Fuentes-Franco R, F Giorgi, E Coppola, F Kucharski (2015) The role of ENSO and PDO in variability of winter precipitation over North America from twenty first century CMIP5 projections, Climate Dynamics, Article in press, DOI: 10.1007/s00382-015-2767-y.

Gärtner-Roer, I. et al. (2014) 'A database of worldwide glacier thickness observations', 122, pp. 330–344. doi: http://dx.doi.org/10.1016/j.gloplacha.2014.09.003.

Geruo, A., Wahr, J. and Zhong, S. (2013) 'Computations of the viscoelastic response of a 3-D compressible Earth to surface loading: an application to Glacial Isostatic Adjustment in Antarctica and Canada', Geophysical Journal International, 192(2), pp. 557–572. doi: 10.1093/gji/ggs030.

Gignac C, E Crobeddu, L Rémillard (2014) Prévisions d'apports probabilistes à Hydro-Québec Production. From operational hydrological forecast to reservoir management optimization - Des prévisions hydrologiques opérationnelles vers une optimisation de la gestion des reservoirs. September 17-19, 2014, Québec, Québec, Canada.

GLIMS and NSIDC (2005, updated 2013) 'Global Land Ice Measurements from Space glacier database', Compiled and made available by the international GLIMS community and the National Snow and Ice Data Center, Boulder CO, U.S.A. doi: 10.7265/N5V98602.

Goldberg, D. E. (1989) Genetic algorithms in search, optimization, and machine learning. Addison-Wesley Longman Publishing Co., Inc. Boston, MA, USA.

Gsell P.-S. (2014). Apports et voies d'amélioration de la représentation des glaciers et de leur évolution au sein d'un modèle hydrologique. HAL Id: tel-01164802, https://tel.archives-ouvertes.fr/tel-01164802

Gupta, H.V., Kling, H., Yilmaz, K. and Martinez, G. (2009). Decomposition of the Mean Squared Error and NSE Performance Criteria: Implications for Improving Hydrological Modelling. Journal of Hydrology. 377. 80-91. DOI:10.1016/j.jhydrol.2009.08.003.

Haeberli, W. and Hoelzle, M. (1995) 'Application of inventory data for estimating characteristics of and regional climate-change effects on mountain glaciers: a pilot study with the European Alps', 21, pp. 206–212.

Hamill, T. M. 2001: Interpretation of Rank Histograms for Verifying Ensemble Forecasts, Monthly Weather Review, 129:550-560 (DOI: 10.1175/1520-0493(2001)129<0550:IORHFV>2.0.CO;2).

Hayashi M, N Goeller, WL Quinton, N Wright (2007) A simple heat-conduction method for simulating the frost-table depth in hydrological models, Hydrological Processes, 21: 2610-2622. DOI: 10.1002/hyp.6792.

Hersbach, H. 2000: Decomposition of the continuous ranked probability score for ensemble prediction systems, Weather Forecast., 15 (2000), pp. 559-570

Hock Regine (2003). Temperature index melt modelling in mountain areas. Journal of Hydrology, 282 (2003) 104–115, doi:10.1016/S0022-1694(03)00257-9.

Hock, R., Hutchings, J. K. and Lehning, M. (2017), Grand Challenges in Cryospheric Sciences: Toward Better Predictability of Glaciers, Snow and Sea Ice.

Holland, J. H. (1992) Adaptation in Natural and Artificial Systems: An Introductory Analysis with Applications to Biology, Control and Artificial Intelligence. MIT Press Cambridge, MA, USA.

Huss, M. and Farinotti, D. (2012) 'Distributed ice thickness and volume of all glaciers around the globe: GLOBAL GLACIER ICE THICKNESS AND VOLUME', Journal of Geophysical Research: Earth Surface, 117(F4), p. n/a-n/a. doi: 10.1029/2012JF002523.

Hutchinson MF, DW McKenney, K Lawrence, JH Pedlar, RF Hopkinson, E Milewska, P Papadopol (2009) Development and testing of Canada-wide interpolated spatial models of daily minimum-maximum temperature and precipitation for 1961-2003. Journal of Applied Meteorology and Climatoogy, 48, 725-741, doi: 10.1175/2008JAMC1979.1.

Irvine-Fynn, T. D. L. et al. (2011) 'Polythermal glacier hydrology : A review', Reviews of Geophysics, 49(4). doi: 10.1029/2010RG000350.

Islam Z and TY Gan (2015) Potential combined hydrologic impacts of climate change and El Niño Southern Oscillation to South Saskatchewan River Basin, Journal of Hydrology, 523: 34-48, DOI: 10.1016/j.jhydrol.2015.01.043.

Jacob, T. et al. (2012) 'Recent contributions of glaciers and ice caps to sea level rise', Nature, 482(7386), pp. 514–518. doi: 10.1038/nature10847.

Janke, J. R., Ng, S. and Bellisario, A. (2017) 'An inventory and estimate of water stored in firn fields, glaciers, debris-covered glaciers, and rock glaciers in the Aconcagua River Basin, Chile', Geomorphology, 296, pp. 142–152. doi: 10.1016/j.geomorph.2017.09.002.

Jarosch AH, AS Anslow, GKC Clarke (2012) High-resolution precipitation and temperature downscaling for glacier models, Climate Dynamics, 38: 391-409, DOI: 10.1007/s00382-010-0949-1.

Jin, S. and Zou, F. (2015) 'Re-estimation of glacier mass loss in Greenland from GRACE with correction of land–ocean leakage effects', Global and Planetary Change, 135, pp. 170–178. doi: 10.1016/j.gloplacha.2015.11.002.

Jin, S. and Feng, G. (2016) 'Uncertainty of grace-estimated land water and glaciers contributions to sea level change during 2003–2012', in. IEEE, pp. 6189–6192. doi: 10.1109/IGARSS.2016.7730617.

Jin, S., Zhang, T. Y. and Zou, F. (2017) 'Glacial density and GIA in Alaska estimated from ICESat, GPS and GRACE measurements: Glacial Density and GIA in Alaska', Journal of Geophysical Research: Earth Surface, 122(1), pp. 76–90. doi: 10.1002/2016JF003926.

Jin J, X Gao, S Sorooshian, Z-L Yang, R Bales, RE Dickinson, S-F Sun, G-X Wu (1999a) One-dimensional snow water and energy balance model for vegetated surfaces, Hydrological Processes, 13: 2467-2482, DOI: 10.1002/(SICI)1099-1085(199910)13:14/15<2467::AID-HYP861>3.0.CO;2-J.

Jin J, X Gao, Z-L Yang, RC Bales, S Sorooshian, RE Dickinson, SF Sun, GX Wu (1999b) Comparative Analyses of Physically Based Snowmelt Models for Climate Simulations, Journal of Climate, 12 (8): 2643–2657, DOI: http://dx.doi.org/10.1175/1520-0442(1999)012<2643:CAOPBS>2.0.CO;2.

Jordan R (1991) A one-dimensional temperature model for a snow cover. U.S. Army Cold Regions Research and Engineering Laboratory, Special Report 91-16, Hanover, NH, U.S.A.

Jutras S, AN Rousseau, C Clerc (2009). Implementation of a peatland-specific water budget algorithm in HYDROTEL. Canadian Water Resources Journal, 34(4): 349-361.

Kalnay E, M Kanamitsu, R Kistler, W Collins, D Deaven, L Gandin, M Iredell, S Saha, G White, J Woollen, Y Zhu, A Leetmaa, B Reynolds, M Chelliah, W Ebisuzaki, W Higgins, J Janowiak, KC Mo, C Ropelewski, J Wang, R Jenne, D Joseph (1996) The NCEP/NCAR 40-year reanalysis project, Bulletin of the American Meteorological Society, 77(3): 437-471.

Kalra A, S Ahmad, A Nayak (2013) Increasing streamflow forecast lead time for snowmelt-driven catchment based on large-scale climate patterns, Advances in Water Resources, 53: 150-162, DOI: http://dx.doi.org/10.1016/j.advwatres.2012.11.003.

Karlsson, JM, A Bring, GD Peterson, LJ Gordon, G Destouni (2011) Opportunities and limitations to detect climate-related regime shifts in inland Arctic ecosystems through eco-hydrological monitoring, Environmental Research Letters, 6: 014015. DOI: 10.1088/1748-9326/6/1/014015.

Kayastha N, J Ye, F Fenicia, V Kuzmin, DP Solomatine (2013) Fuzzy committees of specialized rainfall-runoff models: further enhancements and tests. Hydrology and Earth System Sciences, 17, 4441-4451.

Kerkhoven E, TY Gan (2011) Differences and sensitivities in potential hydrologic impact of climate change to regional-scale Athabasca and Fraser River basins of the leeward and windward sides of the Canadian Rocky Mountains respectively, Climatic Change, 106: 583–607, DOI: 10.1007/s10584-010-9958-7.

Kobayashi, S., Y. Ota, Y. Harada, A. Ebita, M. Moriya, H. Onoda, K. Onogi, H. Kamahori, C. Kobayashi, H. Endo, K. Miyaoka, and K. Takahashi, 2015: The JRA-55 Reanalysis: General Specifications and Basic Characteristics. J. Met. Soc. Jap., 93(1), 5-48 (DOI: 10.2151/jmsj.2015-001).

Koren V, S Reed, M Smith, Z Zhang, DJ Seo (2004) Hydrology Laboratory Research Modeling System (HL-RMS) of the U.S. National Weather Service, Journal of Hydrology, 291, 297–318.

Kouwen N, M Danard, A Bingeman, W Luo, FR Seglenieks, ED Soulis (2005) Case Study: Watershed Modeling with Distributed Weather Model Data, Journal of Hydrologic Engineering, 10(1): 23-38, DOI: 10.1061/(ASCE)1084-0699(2005)10:1(23).

Kurylyk BL, KTN MacQuarrie, JM McKenzie (2014) Climate change impacts on groundwater and soil temperatures in cold and temperate regions: Implications, mathematical theory, and emerging simulation tools, Earth-Science Reviews, 138: 313-334, DOI: 10.1016/j.earscirev.2014.06.006.

Kusche, J. (2007) 'Approximate decorrelation and non-isotropic smoothing of time-variable GRACE-type gravity field models', Journal of Geodesy, 81(11), pp. 733–749. doi: 10.1007/s00190-007-0143-3.

Kusche, J. et al. (2009) 'Decorrelated GRACE time-variable gravity solutions by GFZ, and their validation using a hydrological model', Journal of Geodesy, 83(10), pp. 903–913. doi: 10.1007/s00190-009-0308-3.

Langlois A, J Kohn, A Royer, P Cliche, L Brucker, G Picard, M Fily, C Derksen, J Willemet (2009) Simulation of snow water equivalent (SWE) using thermodynamic snow models in Québec, Canada. Journal of Hydrometeorology 10: 1447–1463.

Larouche B, J Paquin, M Latraverse, P Côté (2014) Dealing with uncertainties in water management systems: from theoretical to practical framework. From operational hydrological forecast to reservoir management optimization - Des prévisions hydrologiques opérationnelles vers une optimisation de la gestion des reservoirs. September 17-19, 2014, Québec, Québec, Canada.

Larsen, C. F. et al. (2007) 'Glacier changes in southeast Alaska and northwest British Columbia and contribution to sea level rise', Journal of Geophysical Research, 112(F1). doi: 10.1029/2006JF000586.

Lehning M, I Völksch, D Gustafsson, TA Nguyen, M Stähli, M Zappa (2006) ALPINE3D: a detailed model of mountain surface processes and its application to snow hydrology, Hydrological Processes, 20: 2111-2128. DOI: 10.1002/hyp.6204.

Lindström G, B Johansson, M Persson, M Gardelin, S Bergström (1997) Development and test of the distributed HBV-96 hydrological model, Journal of Hydrology, 201: 272-288, DOI: 10.1016/S0022-1694(97)00041-3.

Long, D. et al. (2016) 'Have GRACE satellites overestimated groundwater depletion in the Northwest India Aquifer?', Scientific Reports, 6(1). doi: 10.1038/srep24398.

Longuevergne, L., Scanlon, B. R. and Wilson, C. R. (2010) 'GRACE Hydrological estimates for small basins: Evaluating processing approaches on the High Plains Aquifer, USA: GRACE HYDROLOGICAL ESTIMATES FOR SMALL B', Water Resources Research, 46(11). doi: 10.1029/2009WR008564.

Lorenz, E. N.: Atmospheric Predictability as Revealed by Naturally Occurring Analogues, Journal of Atmospheric Sciences, 26, 636–646, 1969

Luthcke, S. B. et al. (2008) 'Recent glacier mass changes in the Gulf of Alaska region from GRACE mascon solutions', Journal of Glaciology, 54(188), pp. 767–777. doi: 10.3189/002214308787779933.

Luthcke, S. B. et al. (2013) 'Antarctica, Greenland and Gulf of Alaska land-ice evolution from an iterated GRACE global mascon solution', Journal of Glaciology, 59(216), pp. 613–631. doi: 10.3189/2013JoG12J147.

MacDonald M, JW Pomeroy, A Pietroniro (2009) Parameterizing redistribution and sublimation of blowing snow for hydrological models: tests in a mountainous subarctic catchment, Hydrological Processes, 23: 2570-2583, DOI: 10.1002/hyp.7356.

MacDougall, A. H., Wheler, B. A., Flowers, G. E. (2011). A preliminary assessment of glacier melt-model parameter sensitivity and transferability in a dry subarctic environment. The Cryosphere. 5, 1011–1028, doi:10.5194/tc-5-1011-2011.

Martin A, P Côté, R Leconte (2014) Utilisation des prévisions d'ensemble pour améliorer les règles de gestion du réservoir de la rivière Nechako, C.-B., établies à l'aide de la programmation dynamique stochastique. From operational hydrological forecast to reservoir management optimization - Des prévisions hydrologiques opérationnelles vers une optimisation de la gestion des reservoirs. September 17-19, 2014, Québec, Québec, Canada.

Martinec J. (1975) Snowmelt runoff model for stream flow forecasts, Nordic Hydrology, 6(3): 145-154, DOI: doi:10.2166/nh.1975.010.

Mas A. (2016) Développement d'un modèle numérique d'évolution du couvert nival adapté à la modélisation hydrologique. Mémoire présenté à l'École de Technologie Supérieur (ÉTS), Université du Québec, Montréal, Qc, Canada

Merryfield WJ, B Denis, J-S Fontecilla, S Kharin, J Hodgson, B Archambault (2011) The Canadian Seasonal to Interannual Prediction System (CanSIPS), Environment Canada, Development and Operations

divisions at CMC and Climate Research division, Version 1.6, November 24, 2011, link: https://weather.gc.ca/grib/grib2_cansips_e.html (consulted on December 16, 2015).

Moeys J. (2009) The Soil Texture Wizard : R functions for plotting, classifying and transforming soil texture data. 99p.

Monti, F., Cagnati, A., Valt, M., & Schweizer, J. (2012). A new method for visualizing snow stability profiles. Cold Regions Science and Technology, 78, 64–72. https://doi.org/10.1016/j.coldregions.2012.02.005

Moriasi DN, JG Arnold, MW Van Liew, RL Bingner, RD Harmel, TL Veith (2007) Model evaluation guidelines for systematic quantification of accuracy in watershed simulations. Trans. ASABE 50(3):885-900.

Müller, F. (1962) 'Zonation in the accumulation area of the glaciers of Axel Heiberg Island, NWT, Canada', 4, pp. 302–311.

Musselman KN, JW Pomeroy, RLH Essery, N Leroux (2015) Impact of windflow calculations on simulations of alpine snow accumulation, redistribution and ablation, Hydrological Processes, 29: 3983-3999, DOI: 10.1002/hyp.10595.

National Academies of Sciences, Engineering, and Medicine (2016) Next Generation Earth System Prediction: Strategies for Subseasonal to Seasonal Forecasts. Washington, DC: The National Academies Press. doi: 10.17226/21873.

National Weather Service (NWS) (2004) National Weather Service River Forecast System—User's manual, Silver Spring, Md.

Navarro, F. J., Macheret, Y. Y. and Benjumea, B. (2005) 'Application of radar and seismic methods for the investigation of temperate glaciers', Journal of Applied Geophysics, 57(3), pp. 193–211. doi: 10.1016/j.jappgeo.2004.11.002.

Neal EG, MT Walter, C Coffeen (2002) Linking the pacific decadal oscillation to seasonal stream discharge patterns in Southeast Alaska, Journal of Hydrology, 263: 188-197, DOI: 10.1016/S0022-1694(02)00058-6.

Neumeyer, J. et al. (2009) 'Derivation of gravity anomalies from airborne gravimeter and IMU recordings—Validation with regional analytic models using ground and satellite gravity data', Journal of Geodynamics, 47(4), pp. 191–200. doi: 10.1016/j.jog.2008.08.001.

Northern Climate ExChange (2014) Projected Future Changes in Glaciers and their Contribution to Discharge of the Yukon River at Whitehorse. Whitehorse, YT: Northern Climate ExChange, Yukon Research Centre, Yukon College, p. 44.

Oreiller M, DF Nadeau, M Minville, AN Rousseau (2014) Modelling snow water equivalent and spring runoff in a boreal watershed, James Bay, Canada, Hydrological Processes, 28 : 5991-6005, DOI : 10.1002/hyp.10091.

Orlandini S, G Moretti, M Franchini (2003) Path-based methods for the determination of non-dispersive drainage directions in grid-based digital elevation models. Water Resources Research, 39(6), 1114.

Oudin L, V Andreassian, T Mathevet, C Perrin, C Michel (2006) Dynamic averaging of rainfall-runoff model simulations from complementary model parameterizations, Water Resources Research, 42(7), W07410, doi:10.1029/2005WR004636.

Perreault L, B Bobée, R Roy, L Mathier (1995) La combinaison de modèles appliquée à la validation en temps réel des apports naturels aux réservoirs hydriques Revue canadienne de génie civil, 22(5): 934-944, doi.org/10.1139/l95-110.

Pfeffer, W. T. et al. (2014) 'The Randolph Glacier Inventory: a globally complete inventory of glaciers', Journal of Glaciology, 60(221), pp. 537–552. doi: 10.3189/2014JoG13J176.

Pinard, J-P, R Benoit, JD Wilson (2009) Mesoscale Wind Climate Modelling in Steep Mountains, Ocean Atmosphere, 47(1): 63-78, DOI: 10.3137/AO922.2009.

Poitras V, S Sushama, F Seglenieks, MN Khaliq, E Soulis (2011) Projected Changes to Streamflow Characteristics over Western Canada as Simulated by the Canadian RCM, Journal of Hydrometeorology, 12 (6): 1395-1413, DOI: 10.1175/JHM-D-10-05002.1.

Polade SD, A gershunov, DR Cayan, MD Dettinger, DW Pierce (2013) Natural climate variability and teleconnections to precipitation over the Pacific-North American region in CMIP3 and CMIP5 models, Geophysical Research Letters, 40 (10): 2296-2301, DOI: 10.1002/grl.50491.

Poli P, H Hersbach, DP Dee, P Berrisford, AJ Simmons, F Vitart, P Laloyaux, DG Tan, C Peubey, J Thépaut, Y Trémolet, EV Hólm, M Bonavita, L Isaksen, and M Fisher (2016) ERA-20C: An Atmospheric Reanalysis of the Twentieth Century, Journal of Climate 29:11, 4083-4097, DOI : 10.1175/JCLI-D-15-0556.1.

Pomeroy J, X Fang, C Ellis (2012) Sensitivity of snowmelt hydrology in Marmot Creek, Alberta, to forest cover disturbance, Hydrological Processes, 26: 1891-1904, DOI : 10.1002/hyp.9248.

Quick MC (1995) The UBC watershed model. In Computer Models of Watershed Hydrology (Ed. Singh VP) Water Resources Publications, Highlands Ranch, CO.

Radić, V., Hock, R. and Oerlemans, J. (2007) 'Volume–area scaling vs flowline modelling in glacier volume projections', Annals of Glaciology, 46, pp. 234–240. doi: 10.3189/172756407782871288.

Radić, V. and Hock, R. (2010) 'Regional and global volumes of glaciers derived from statistical upscaling of glacier inventory data', 115(F01010). doi: 10.1029/2009JF001373.

Radic, V. and Hock, R. (2011) 'Regionally differentiated contribution of mountain glaciers and ice caps to future sea-level rise', 4, pp. 91–94. doi: 10.1038/ngeo1052.

Rankinen K, T Karvonen, D Butterfield (2004) A simple model for predicting soil temperature in snow-covered and seasonally frozen soil: model description and testing, Hydrology and Earth System Sciences, 8, 706-716, doi:10.5194/hess-8-706-2004.

Rasouli K, JW Pomeroy, JR Janowicz, SK Carey, TJ Williams (2014) Hydrological sensitivity of a northern mountain basin to climate change, Hydrological Processes, 28: 4191-4208. DOI: 10.1002/hyp.10244.

Raup, B. et al. (2007) 'The GLIMS geospatial glacier database: A new tool for studying glacier change', Global and Planetary Change, 56(1–2), pp. 101–110. doi: 10.1016/j.gloplacha.2006.07.018.

Rawls WJ, DL Brakensiek (1989) Estimation of soil water retention and hydraulic properties. In Unsaturated Flow in Hydrologic Modeling: Theory and Practice, Morel-Seytoux HJ (ed), NATO ASI series. Series C: Mathematical and Physical Sciences 275. Kluwer Academic: Boston; 275–300.

Rawlins MA, S Frolking, RB Lammers, CJ Vörösmarty (2006) Effects of Uncertainty in Climate Inputs on Simulated Evapotranspiration and Runoff in the Western Arctic, Earth Interactions, 10 (18).

Rienecker MM, MJ Suarez, R Gelaro, R Todling, J Bacmeister, E Liu, MG Bosilovich, SD Schubert, L Takacs, G-K Kim, S Bloom, J Chen, D Collins, A Conaty, A da Silva, W Gu, J Joiner, RD Koster, R Lucchesi, A Molod, T Owens, S Pawson, P Pegion, CR Redder, R Reichle, FR Robertson, AG Ruddick, M Sienkiewicz, J Woollen (2011) MERRA—NASA's Modern-Era Retrospective Analysis for Research and Applications. J. Climate, DOI: 10.1175/JCLI-D-11-00015.1.

Riseborough D, N Shiklomanov, B Etzelmüller, S Gruber, S Marchenko (2008) Recent Advances in Permafrost Modelling, Permafrost and Periglacial Processes, 19: 137-156, DOI: 10.1002/ppp.615.

Rousseau, AN, S Savary, S Tremblay (2020) The INRS-YC Forecasting System - User's Manual and System Description. (INRS Centre Eau Terre Environnement, Documents scientifiques et techniques; R1931)

Rousseau AN, S Savary (2017) Strategic planning of meteorological and snow monitoring stations - Case of the Mayo watershed. Technical Note. Institut national de la recherche scientifique Centre - Eau Terre Environnement; 4 pages. (INRS Centre Eau Terre Environnement, Documents scientifiques et techniques; R1769).

Rousseau AN, S Savary, J Samuel, B Horton, C Doumbia, J Augas, L Caillouet (2017a) Development of a Forecasting System to support Hydroelectric Production in Yukon - Challenges and Opportunities Associated with Calibration of a Physically-Based Distributed Hydrological Model. ECO10 - III. Climate Change Impacts on Arctic Freshwater Systems Session Date and Time: Wednesday, December 13, 15:30 - 17:00, Arctic Change 2017 Conference, December 11-15, 2017 in Québec City, Canada

Rousseau AN, B Horton, J Samuel, S Mallory, G Sreckovic, MA Lavigne, S Savary, S Tremblay, L Caillouet, J Augas, C Doumbia, D Chaumont (2017b) Prévisions des apports aux barrages hydroélectriques du Yukon sous des conditions de climats actuel et futur. 7e Symposium d'Ouranos)- Gestion et évolution du risque hydrologique. Plaza Centre-Ville, Montréal, 15 au 17 novembre, 2017.

Rousseau AN, J-P Fortin, R Turcotte, A Royer, S Savary, F Quévy, P Noël, C Paniconi (2011) PHYSITEL, a specialized GIS for supporting the implementation of distributed hydrological models. Water News - Official Magazine of the Canadian Water Resources Association, 31(1): 18-20.

Rousseau AN, IM Klein, D Freudiger, P Gagnon, A Frigon, C Ratté-Fortin (2014) Development of a methodology to evaluate probable maximum precipitation (PMP) under changing climate conditions: Application to southern Quebec, Canada. Journal of Hydrology (2014) http://dx.doi.org/10.1016/j.jhydrol.2014.10.053.

Royer A, AN Rousseau, J-P Fortin, R Turcotte (2006) PHYSITEL, un SIG pour la mise en place de modèles hydrologiques. Poster presented at « Deuxième Symposium Scientifique d'Ouranos sur la Climatologie et adaptation à l'échelle régionale », 2-3 November 2006, Montreal, QC, Canada.

Saha S, S Moorthi, H-L Pan, X Wu, J Wang, S Nadiga, P Tripp, R Kistler, J Woollen, D Behringer, H Liu, D Stokes, R Grumbine, G Gayno, Y-T Hou, H-Y Chuang, H-MH Juang, J Sela, M Iredell, R Treadon, D Kleist, P van Delst, D Keyser, J Derber, M Ek, J Meng, H Wei, R Yang, S Lord, H van den Dool, A Kumar, W Wang, C Long, M Chelliah, Y Xue, B Huang, J-K Schemm, W Ebisuzaki, R Lin, P Xie, M Chen, S Zhou, W Higgins, C-Z Zou, Q Liu, Y Chen, Y Han, L Cucurull, RW Reynolds, G Rutledge, M Goldberg (2010) The NCEP Climate Forecast System Reanalysis. Bull. Amer. Meteorol. Soc. 91: 1015–1057. doi: 10.1175/2010BAMS3001.1.

Saito K, M Kimoto, T Zhang, K Takata, S Emori (2007) Evaluating a high-resolution climate model: Simulated hydrothermal regimes in frozen ground regions and their change under the global warming scenario, Journal of Geophusical Research, 112: F02S11. DOI: 10.1029/2006JF000577.

Samuel, J. AN Rousseau, K Abbasnezhadi, S Savary (2019) Development and evaluation of a hydrologic data-assimilation scheme for short-range flow and inflow forecasts in a data-sparse high-latitude region using a distributed model and ensemble Kalman filtering. Advances in Water Resources doi.org/10.1016/j.advwatres.2019.06.004

Samuel J, Rousseau AN, S Savary (2017) Evaluation of Hydrologic Data Assimilation and Real-time Meteorological Data to Improve Flow Forecasts. ECO10 - III. Climate Change Impacts on Arctic Freshwater Systems Session Date and Time: Wednesday, December 13, 15:30 - 17:00, Arctic Change 2017 Conference, December 11-15, 2017 in Québec City, Canada

Samuel J, Kavanaugh B, Benkert B, Samolczyck M, Samolczyck S, Evans R, Saal S, Gonet J, Horton B, Clague J, Harmer Z, Kinnear L, (2016) Evaluating climate change impacts on the upper Yukon River basin: Projecting future conditions using glacier, climate and hydrological models. Whitehorse, Yukon: Northern Climate ExChange, Yukon Research Centre.

Save, H., Bettadpur, S. and Tapley, B. D. (2016) 'High-resolution CSR GRACE RL05 mascons: HIGH-RESOLUTION CSR GRACE RL05 MASCONS', Journal of Geophysical Research: Solid Earth, 121(10), pp. 7547–7569. doi: 10.1002/2016JB013007.

Stahl, K. et al. (2008) 'Coupled modelling of glacier and streamflow response to future climate scenarios', 44(W02422). doi: 10.1029/2007WR005956.

Stevens, I. T. et al. (2018) 'Near-surface hydraulic conductivity of northern hemisphere glaciers', Hydrological Processes, 32(7), pp. 850–865. doi: 10.1002/hyp.11439.

Schaffer J, Z Shawwash (2014) Performance of Sampling Stochastic Dynamic Programming Algorithm with Various Inflow Scenario Generation Methods. From operational hydrological forecast to reservoir management optimization - Des prévisions hydrologiques opérationnelles vers une optimisation de la gestion des reservoirs. September 17-19, 2014, Québec, Québec, Canada.

Seiller G, F Anctil, C Perrin (2012) Multimodel evaluation of twenty lumped hydrological models under contrasted climate conditions. Hydrology and Earth System Sciences, 16(4), 1171-1189, doi:1110.5194/hess-1116-1171-2012, 2012.

Sene K (2010) Hydrometeorology – Forecasting and Application, Springer Dordrecht Heidelberg New York.

Semmens KA, J Ramage, A Bartsch, EG Liston (2013) Early snowmelt events: detection, distribution, and significance in a major sub-arctic watershed, Environmental Research Letters, 8 (1): 014020, DOI: 10.1088/1748-9326/8/1/014020.

Sheffield J, SJ Camargo, R Fu, Q Hu, X Jiang, N Johnson, KB Karnauskas, ST Kim, J Kinter, S Kumar, B Langenbrunner, E Maloney, A Mariotti, JE Meyerson, JD Neelin, S Nigam, Z Pan, A Ruiz-Barradas, R Seager, YL Serra, DZ Sun, C Wang, SP Xie, JY Yu, T Zhang, M Zhao (2013) North American climate in CMIP5 experiments. Part II: Evaluation of historical simulations of intraseasonal to decadal variability, Journal of Climate, 26(23), 9247-9290, DOI: 10.1175/JCLI-D-12-00593.1.

Slaughter CW, VYE Glotov, LA Viereck, VM Mikhailov (1995) Boreal Forest Catchments: Research sites for Global Change at High Latitudes, Water, Air and Soil Pollution, 82: 351-361.

Smith TM, RW Reynolds, TC Peterson, J Lawrimore (2008) Improvements to NOAA's historical merged land-ocean surface temperature analysis (1880–2006), Journal of Climate, 21, 2283–2296.

Sorman AA, A Sensoy, AE Tekeli, AÜ Sorman, Z Akyürek (2009) Modelling and forecasting snowmelt runoff process using the HBV model in the eastern part of Turkey, Hydrological Processes, 23: 1031-1040, DOI: 10.1002/hyp.7204.

Stahl K., Shea J. M., Hutchinson D., Cannon A. J. (2008). Coupled modelling of glacier and streamflow response to future climate scenarios. Water Resources Research, vol. 44, W02422, doi:10.1029/2007WR005956,

Su M, WJ Stolte, G van der Kamp (2000) Modelling Canadian prairie wetland hydrology using a semi-distributed streamflow model, Hydrological Processes, 14: 2405-2422, DOI: 10.1002/1099-1085(20001015)14:14<2405::AID-HYP92>3.0.CO;2-B.

Szeto KK, T Motchalova, P Vivier (Updated by M. Law) (2000) (update 2008) On the preparation of a 1-km resolution gridded soil texture dataset - A CRB internal report. Environment Canada, Downview, Ontario.

Tamisiea, M. E. (2005) 'Constraining hydrological and cryospheric mass flux in southeastern Alaska using space-based gravity measurements', Geophysical Research Letters, 32(20). doi: 10.1029/2005GL023961.

Tapley, B. D. (2004) 'GRACE Measurements of Mass Variability in the Earth System', Science, 305(5683), pp. 503–505. doi: 10.1126/science.1099192.

Taschetto AS, AS Gupta, NC Jourdain, A Santoso, CC Ummenhofer, MH England (2014) Cold Tongue and Warm Pool ENSO Events in CMIP5: Mean State and Future Projections, Journal of Climate, 28 (8): 2861-2885, DOI: 10.1175/JCLI-D-13-00437.1.

Taylor KE, RJ Stouffer, GA Meehl (2012) An Overview of CMIP5 and the experiment design. Bulletin of the American Meteorological Society, 93, 485–498, doi:10.1175/BAMS-D-11-00094.1.

Thirel G, F Rousset-Regimbeau, E Martin, F Habets (2008) On the Impact of Short-Range Meteorological Forecasts for Ensemble Streamflow Predictions, Journal of HydroMeteorology, 9, 1301–1317, 2008.

Thorsen SM, A-G Roer, M van Oijen (2010) Modelling the dynamics of snow cover, soil frost and surface ice in Norwegian grasslands, Polar Research, 29, 110–126.

Tolson, B. A., & Shoemaker, C. A. (2008). Efficient prediction uncertainty approximation in the calibration of environmental simulation models. Water Resources Research, 44(4), 1–19. https://doi.org/10.1029/2007WR005869

Tolson, B. and Shoemaker, C. (2007). Dynamically Dimensioned Search Algorithm for Computationally Efficient Watershed Model Calibration. Water Resources Research - WATER RESOUR RES. 43. DOI:10.1029/2005WR004723.

Turcotte R, J-P Fortin, AN Rousseau, S Massicotte, J-P Villeneuve (2001). Determination of the drainage structure of a watershed using a digital elevation model and a digital river and lake network. Journal of Hydrology 240(3–4): 225–242.

Turcotte R, AN Rousseau, J-P Fortin, J-P Villeneuve (2003). A process-oriented multiple objective calibration strategy accounting for model structure. In Calibration of Watershed Models, Duan Q, Gupta VK, Sorooshian S, Rousseau AN, Turcotte R (eds). American Geophysical Union: Washington; 153–163.

Turcotte R, P Lacombe, C Dimnik, J-P Villeneuve (2004). Distributed hydrological prediction for the management of Quebec's public dams/Prevision hydrologique distribuée pour la gestion des barrages publics du Quebec, Canadian Journal of Civil Engineering, 31(2), 308–320.

Turcotte R, LG Fortin, J-P Fortin, V Fortin, J-P Villeneuve (2007) Operational analysis of the spatial distribution and the temporal evolution of the snowpack water equivalent in southern Quebec, Canada. Nordic Hydrology 38(3): 211–234.

Turcotte R, J Lafleur (2014) État d'avancement des activités de prévision hydrologique en support à la gestion des barrages publics du Québec. From operational hydrological forecast to reservoir management optimization - Des prévisions hydrologiques opérationnelles vers une optimisation de la gestion des reservoirs. September 17-19, 2014, Québec, Québec, Canada.

Uppala SM et al. (2005) The ERA-40 re-analysis, Quarterly Journal of the Royal Meteorological Society, 131 (612): 2961-3012, DOI: 10.1256/qj.04.176.

USGS (2017) Where on Earth are temperate glaciers located?, USGS. Available at: https://www.usgs.gov/faqs/where-earth-are-temperate-glaciers-located?qt-news_science_products=0#qt-news_science_products.

Valery A., (2010) Modélisation précipitations-débit sous influence nivale. Elaboration d'un module neige et évaluation sur 380 bassins versants, Thèse de doctorat d'AgroParisTech.

Van Vuuren DP, E Stehfest, MGJ Den Elzen, S Deetman, A Hof, M Isaac, K Klein Goldewijk, T Kram, A Mendoza Beltran, R Oostenrijk et al (2011) RCP2.6: Exploring the possibility to keep global mean temperature change below 2°C. Climatic Change. doi: 10.1007/s10584-011-0152-3.

Wahr, J., Swenson, S., Velicogna, I., 2006. Accuracy of GRACE mass estimates. Geophys. Res. Lett. 33, L06401. https://doi.org/10.1029/2005GL025305

Wahr, J., Molenaar, M. and Bryan, F. (1998) 'Time variability of the Earth's gravity field: Hydrological and oceanic effects and their possible detection using GRACE', Journal of Geophysical Research: Solid Earth, 103(B12), pp. 30205–30229. doi: 10.1029/98JB02844.

Wahr, J., Burgess, E. and Swenson, S. (2016) 'Using GRACE and climate model simulations to predict mass loss of Alaskan glaciers through 2100', Journal of Glaciology, 62(234), pp. 623–639. doi: 10.1017/jog.2016.49.

Wang JY, PH Whitfield, AJ Cannon (2006) Influence of Pacific Climate Patterns on Low-Flows in British Columbia and Yukon, Canada, Canadian Water Resources Journal, 31 (1):155-164, DOI: 10.4296/cwrj3101025.

Ward PJ, B Jongman, M Kummu, MD Dettinger, FC Sperna Weiland, HC Winsemius (2014) Strong influence of El Niño Southern Oscillation on flood risk around the world, PNAS, 111 (44): 15659–15664, DOI: 10.1073/pnas.1409822111.

Wellmann TP, CI Voss, MA Walvoord (2013) Impacts of climate, lake size, and supra- and sub-permafrost groundwater flow on lake-talik evolution, Yukon Flats, Alaska (USA), Hydrogeology Journal, 21: 281-298. DOI: 10.1007/s10040-012-0941-4.

Williams TJ, JW Pomeroy, JR Janowicz, SK Carey, K Rasouli, WL Quinton (2015) A radiative–conductive–convective approach to calculate thaw season ground surface temperatures for modelling frost table dynamics, Hydrological Processes, 29: 3954–3965. DOI: 10.1002/hyp.10573.

Wilson, N. J., Flowers, G. E. and Mingo, L. (2013) 'Comparison of thermal structure and evolution between neighboring subarctic glaciers: THERMAL STRUCTURE OF TWO GLACIERS', Journal of Geophysical Research: Earth Surface, 118(3), pp. 1443–1459. doi: 10.1002/jgrf.20096.

Woo M-K, R Thorne (2008) Analysis of cold season streamflow response to variability of climate in north-western North America, Hydrology Research, 39 (4): 257-265, DOI: 10.2166/nh.2008.102.

Wright N, M Hayashi, W L Quinton (2009) Spatial and temporal variations in active layer thawing and their implication on runoff generation in peat-covered permafrost terrain, Water Resources Research, 45: W05414, DOI:10.1029/2008WR006880.

Yirdaw, S. Z. et al. (2009) 'Assessment of the WATCLASS hydrological model result of the Mackenzie River basin using the GRACE satellite total water storage measurement', Hydrological Processes, 23(23), pp. 3391–3400. doi: 10.1002/hyp.7450.

Appendix I Estimating the contribution of snow to simulated annual runoff for Aishihik Lake and Mayo Lake.

Using HYDROTEL it is possible to estimate the specific contribution of snow precipitation and melting to simulated annual runoff for both Aishihik Lake and Mayo Lake. The methodology consisted of comparing two separate simulations: the first included liquid and solid precipitation and snowpack update based on snow surveys while the second only considered liquid precipitation. Comparison between the two simulations allows estimating snow contribution to simulated annual runoff. The period of simulation was from 1981-01-01 to 2016-12-01 using year 1981 as a warming period for the model. This warming period is mostly required to ensure a certain stability in the water amount in the river and lake network as the model start with an estimate of the water amount as initial conditions. Figures AI.1, AI.2, AI.3 and Table AI.1 present the results for Aishihik Lake and Figures AI.3, AI.4 and Table AI.2 those for Mayo Lake.

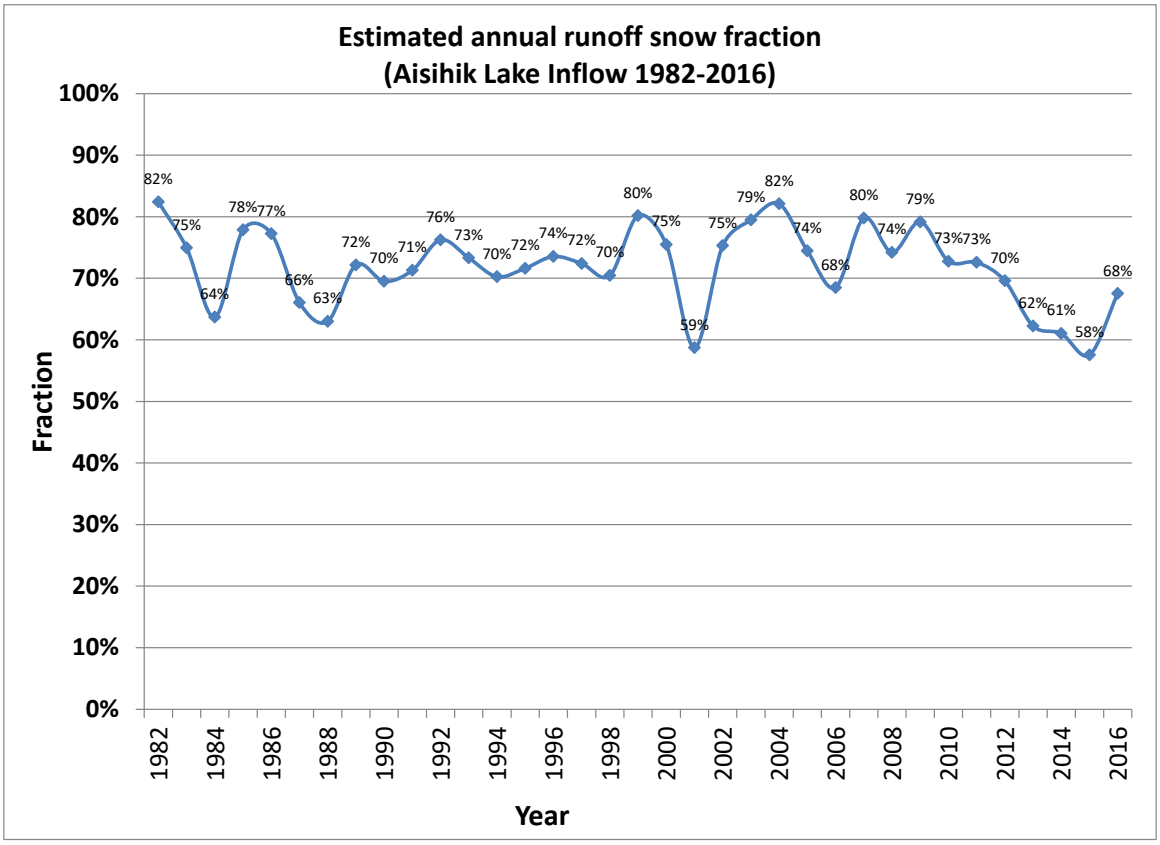

Figure AI.1 Estimated snow contribution to simulated annual runoff for Aishihik Lake inflows.

To illustrate the tendencies in inter-annual trend, Figure AI.2 presents the moving average of estimated snow contribution to simulated annual runoff for Aishihik Lake inflow. Moving averages allow to express tendencies over time without inter-annual variations amplitude.

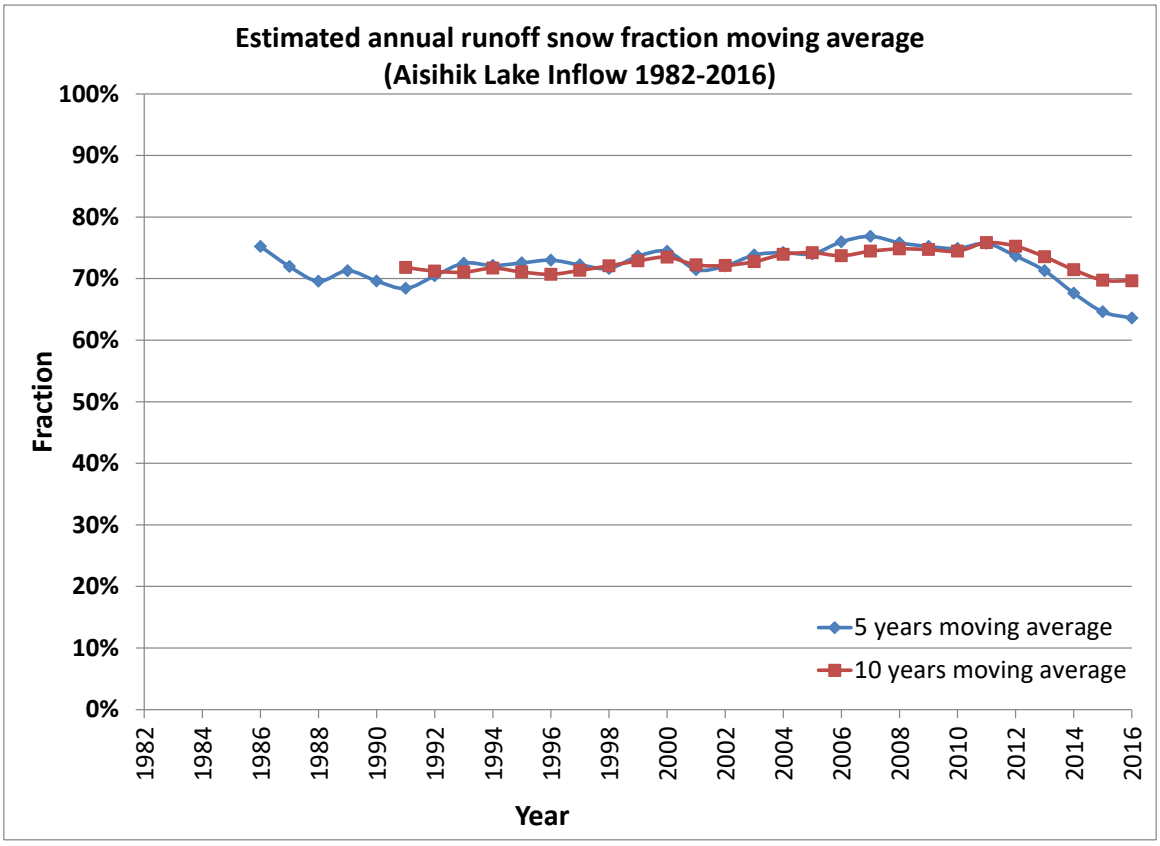

Figure AI.2 Moving average of estimated snow contribution to simulated annual runoff for Aishihik Lake inflow.

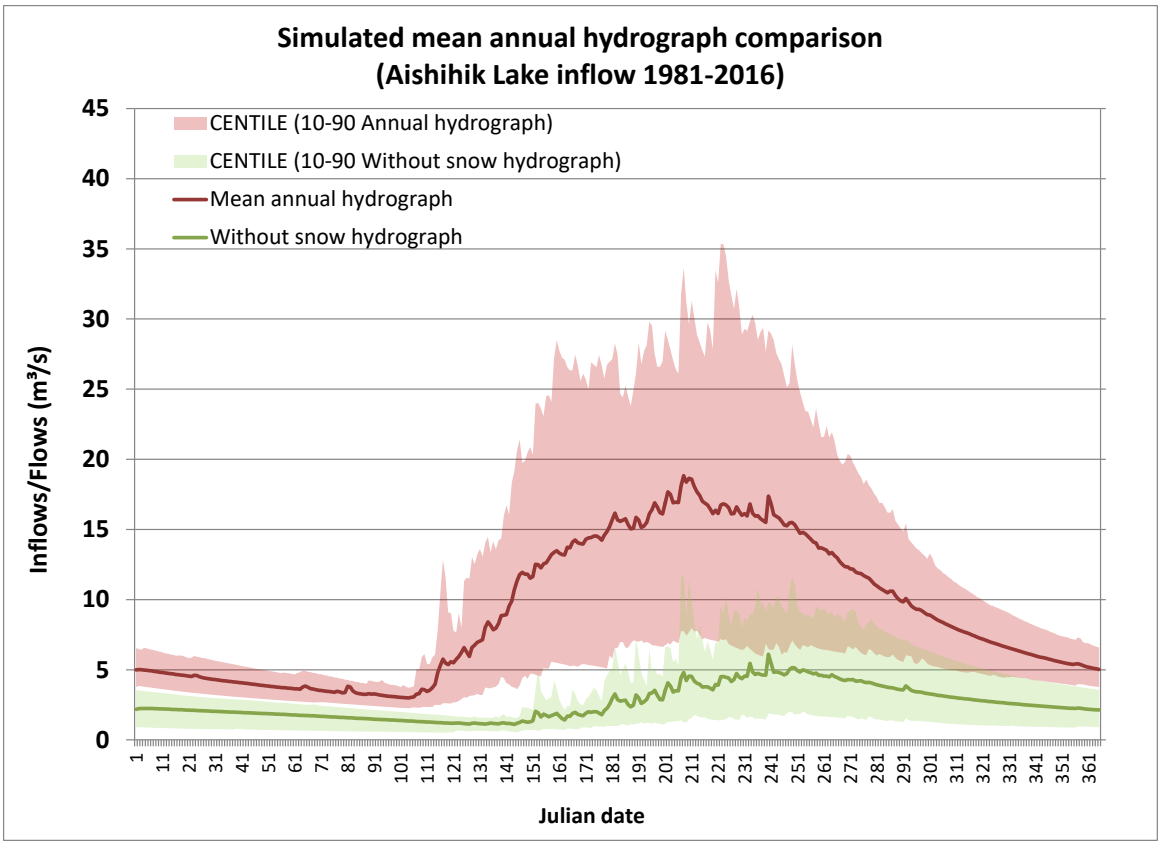

Figure AI.3 Simulated with and without snow mean annual hydrograph comparison for Aishihik Lake inflow.

Table AI.1 Estimated snow contribution to simulated annual runoff for Aishihik Lake inflow.

Statistics	1982-2016	2000-2016	2010-2016
Mean	71.91%	71.21%	66.19%
Median	72.58%	72.77%	67.52%
Min	57.57%	57.57%	57.57%
Max	82.40%	82.10%	72.77%

Figures AI.1, AI.2, AI.3 and Table AI.1 demonstrate the major contribution of snow to simulated annual runoff with values varying between 60% and 80%. Nevertheless, the recent years (2010-2016) have been characterized with lower contribution values; as indicated in the statistical results and tendencies.

As a complement Figures AI.4 and AI.5 present the simulated distributed mean annual precipitation and the simulated distributed mean annual snow fractions excluding snowpack update based on snow survey of the total precipitation over the entire Aishihik River watershed.

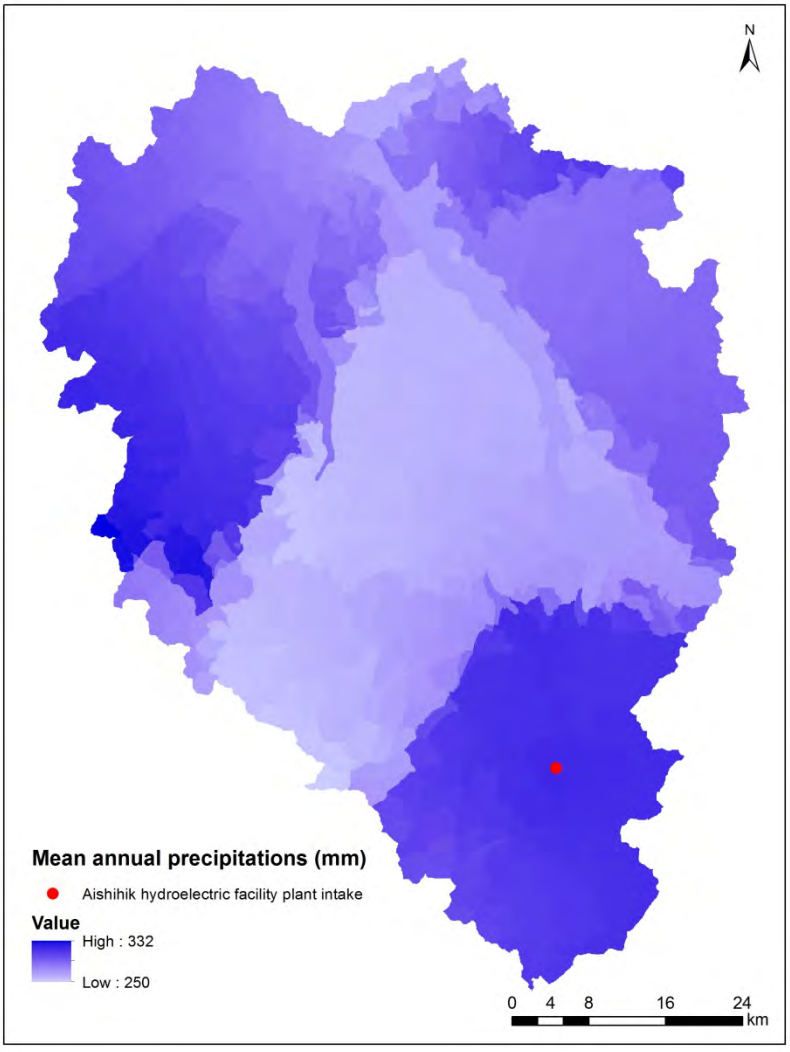

Figure AI.4 Simulated distributed mean annual total precipitations within the Aishihik River watershed.

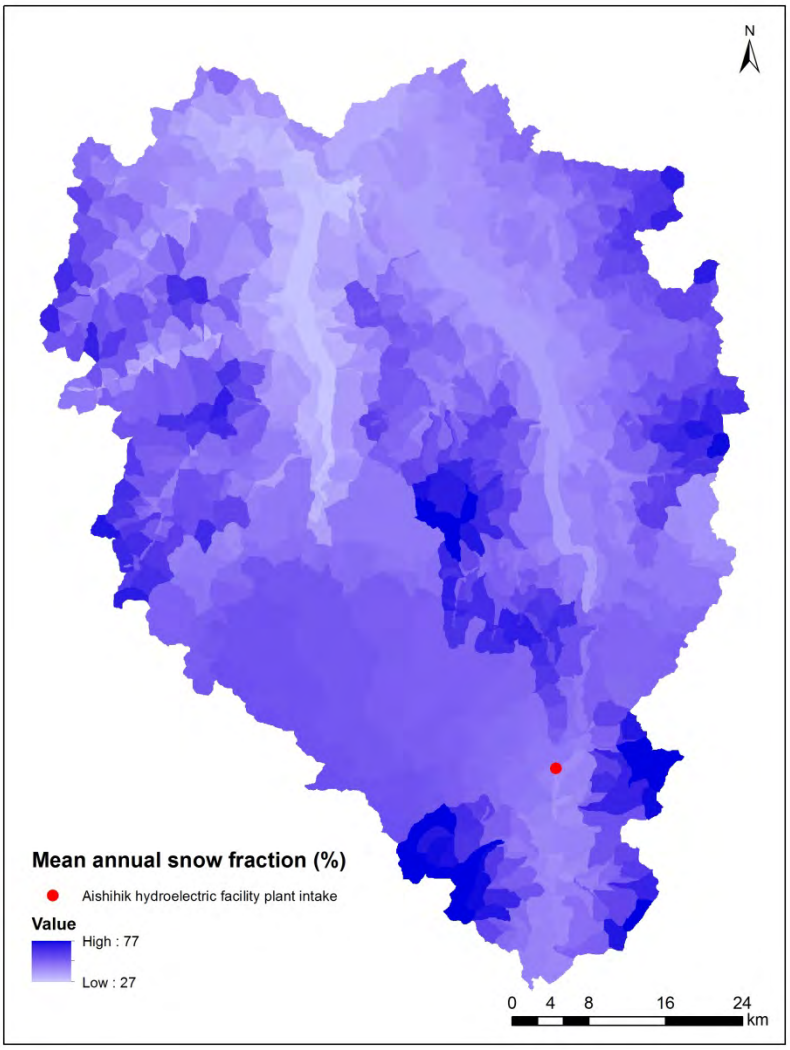

Figure AI.5 Simulated distributed mean annual snow fraction of total precipitations within the Aishihik River watershed.

Both Figures AI.4 and AI.5 show non uniform simulated distribution of mean annual total precipitation and snow fraction. The values of simulated mean annual snow fraction are somewhat lower than the estimated snow contribution to annual runoff displayed in Figures AI.1 and AI.2; illustrating the importance of considering during model calibration *in situ* snow water equivalent (SWE) values obtained during snow surveys to perform snow assimilation. This highlights pertinence to conduct snow surveys throughout the winter and spring seasons.

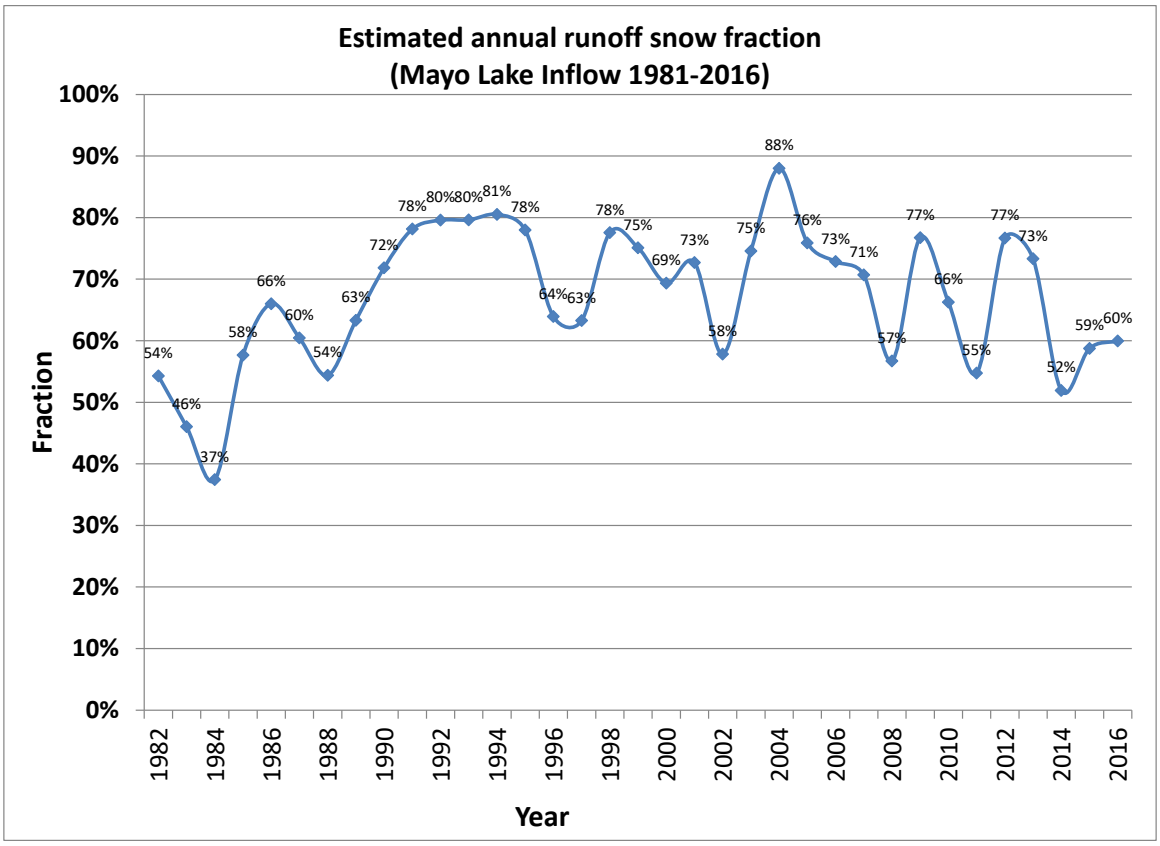

Figure AI.6 Estimated snow contribution on simulated annual runoff for Mayo Lake inflow.

Similarly, to illustrate tendencies in inter-annual trend, Figure AI.7 presents the moving average of the estimated snow contribution to simulated annual runoff for Mayo Lake inflow. As mentioned before moving averages allow to express tendencies over time without inter-annual variations amplitude.

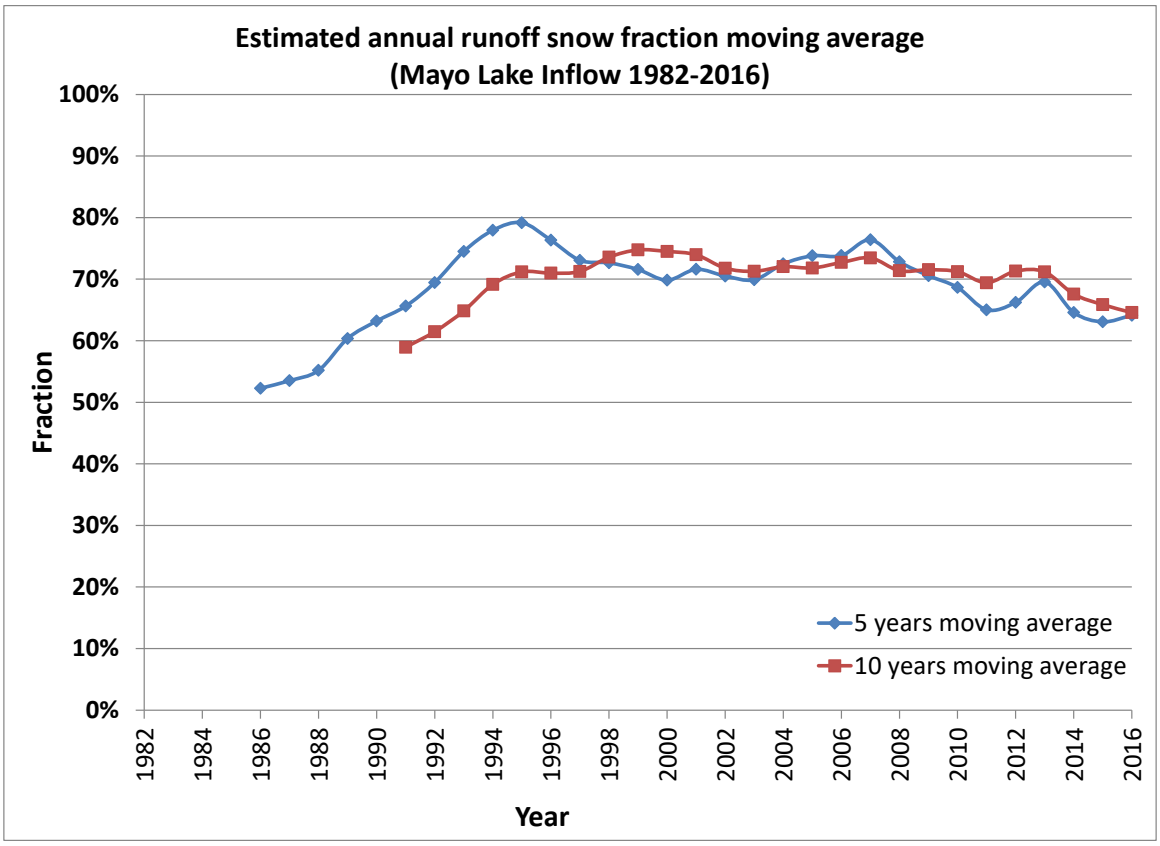

Figure AI.7 Moving average of estimated snow contribution to simulated annual runoff for Mayo Lake inflow.

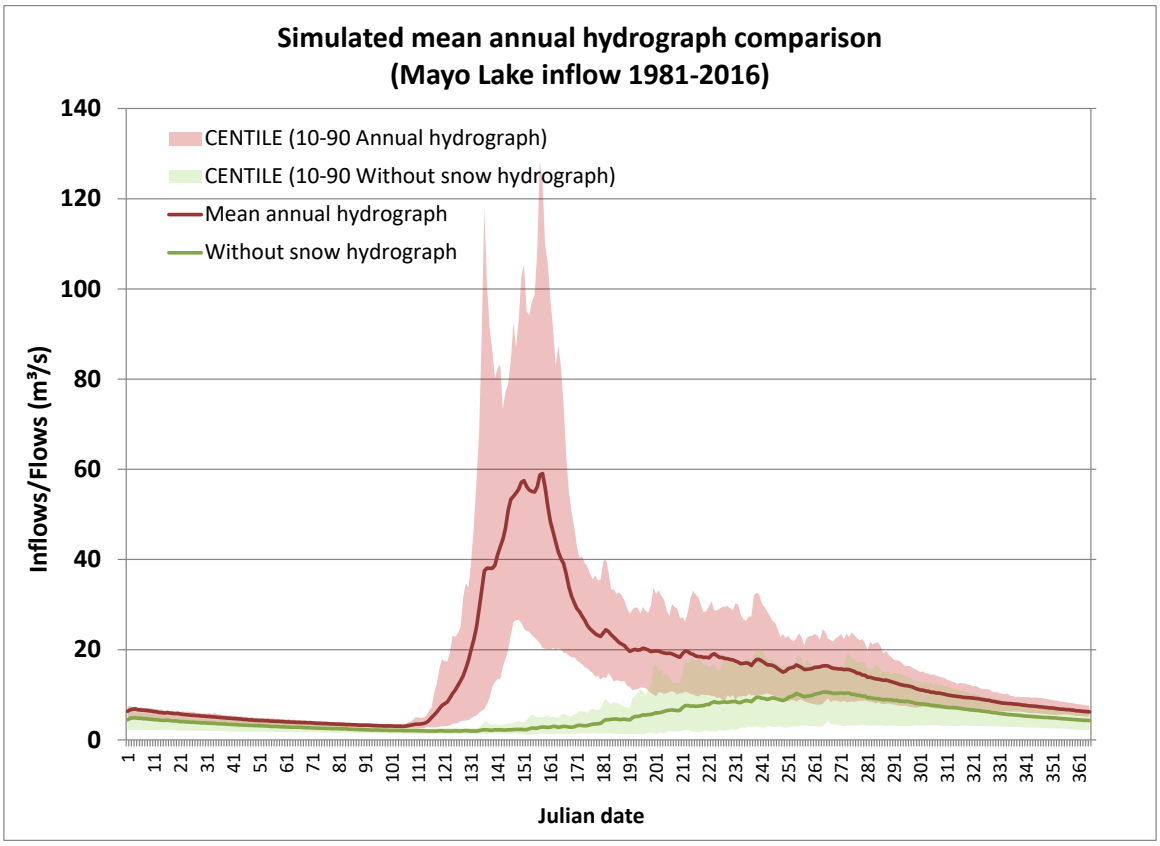

Figure AI.8 Simulated with and without snow mean annual hydrograph comparison for Mayo Lake inflow.

Table AI.2 Estimated snow contribution to simulated annual runoff for Mayo Lake inflow.

Statistics	1982-2016	2000-2016	2010-2016
Mean	66.97%	68.05%	63.09%
Median	69.35%	70.69%	59.96%
Min	37.42%	51.92%	51.92%
Max	87.99%	87.99%	76.65%

Figures AI.6, AI.7, AI.8 and Table AI.2 illustrate again the estimated major contribution of snow to simulated annual runoff with values mostly included within the 50%-80% interval. Earlier years show smaller contributions compared to recent years, although decreasing tendencies are seen in the later years for Mayo Lake.

As a complement, figures AI.9 and AI.10 introduce the simulated distributed mean annual precipitations and the simulated distributed mean annual snow fraction of total precipitation over the Mayo River watershed.

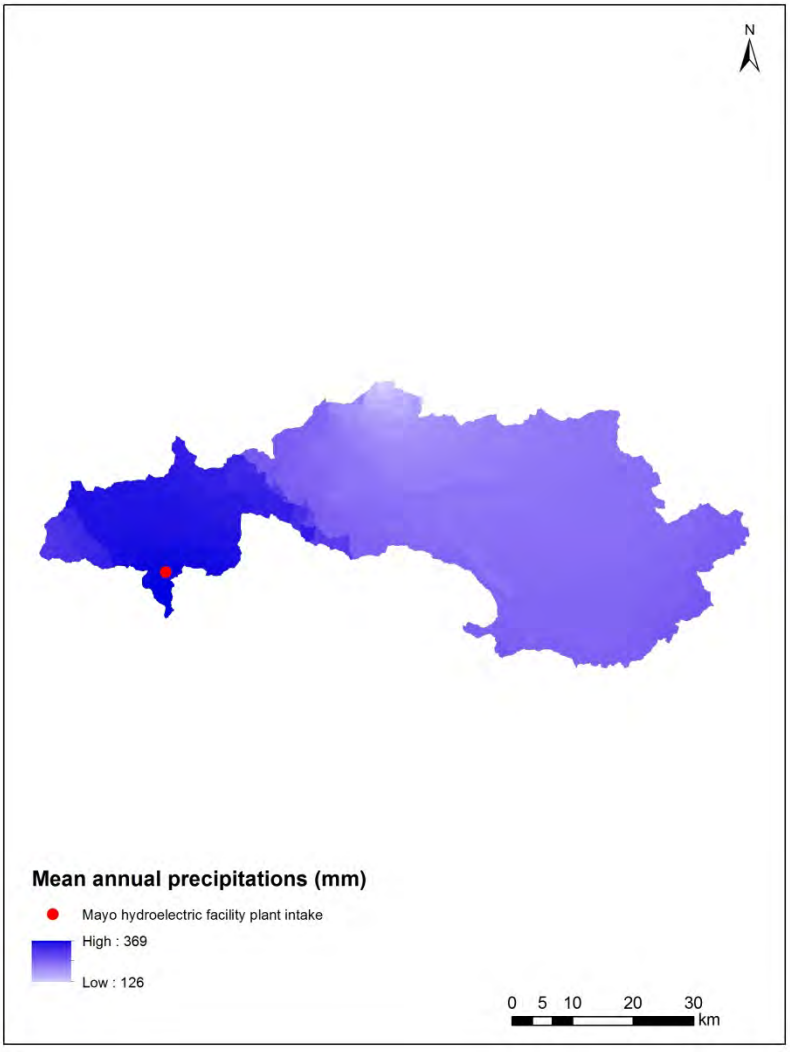

Figure AI.9 Simulated distributed mean annual total precipitation within the boundary of the Mayo River watershed.

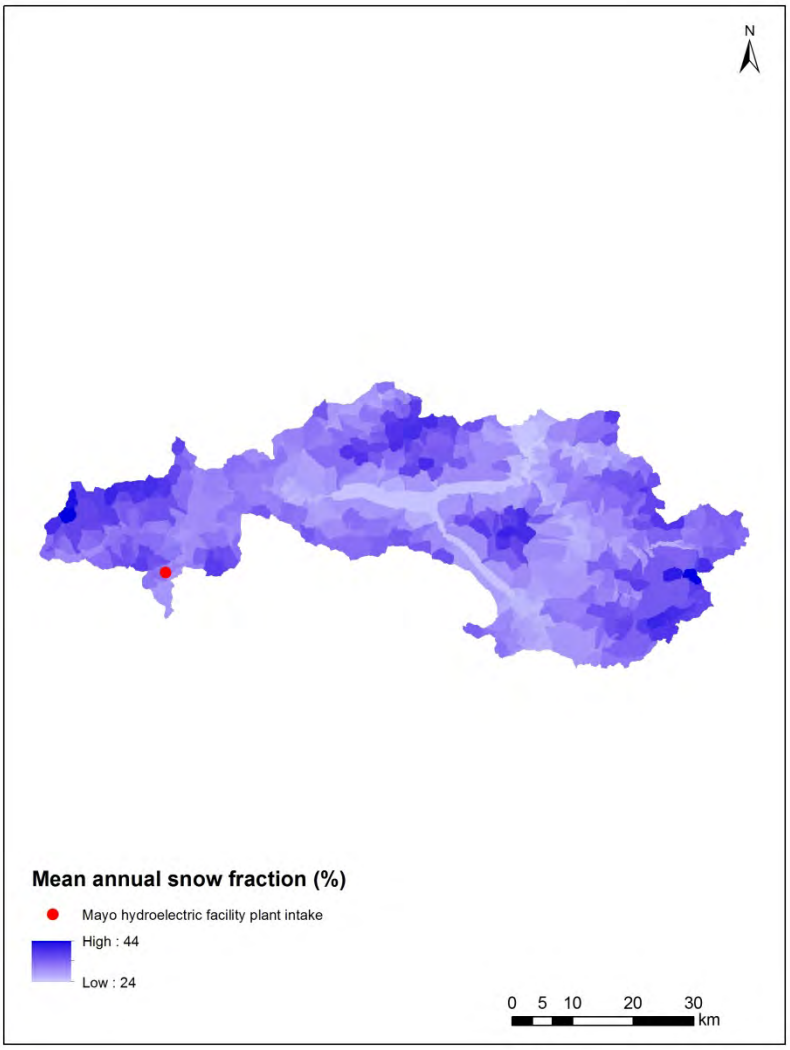

Figure AI.10 Simulated distributed mean annual snow fraction of total precipitation within the boundary of the Mayo River watershed.

Similarly to Aishihik results, Figures AI.9 and AI.10 show non-uniform simulated distribution of mean annual total precipitation and snow fraction. Again the values of simulated mean annual snow fraction are somewhat lower than the estimated snow contribution to annual runoff displayed in Figures AI.6 and AI.7; illustrating the importance of integrating during model calibration *in situ* snow water equivalent (SWE) values obtained during snow surveys. This highlights the need to conduct snow surveys throughout the winter and spring seasons.

Appendix II Meteorological Network Assessment in Sparsely Gauged Nordic Basins

Verification of Regional Deterministic Precipitation Analysis Products Using Snow Data Assimilation

Application in Meteorological Network Assessment in Sparsely Gauged Nordic Basins

Institut National de la Recherche Scientifique
Centre Eau Terre Environnement

INRS-ETE Technical Report R1928

Prepared by

Kian Abbasnezhadi, PhD, E.I.T.

Alain N. Rousseau, PhD, P.Eng.

April 15, 2020

Executive Summary

The northern and mid-cordilleran alpine, sub-alpine, and boreal watersheds in Yukon, Canada, are prime examples of Nordic regions where any hydrological modelling application is challenging due to lack of accurate distributed precipitation information. In the course of the past few years, proper advancements were tailored to resolve the challenges involved with flow estimation accuracy in Yukon, and a forecasting system was designed at the operational level for short-term to seasonal flow and inflow forecasting in major watersheds of interest to Yukon Energy. This forecasting system merges the precipitation products from the North American Ensemble forecasting System (NAEFS) and recorded flows or reconstructed reservoir inflows into HYDROTEL, a distributed hydrological model, using the Ensemble Kalman Filtering (EnKF) data assimilation technique. In order to alleviate the adverse effects of scarce precipitation information, the forecasting system also includes a snow data assimilation routine in which simulated snowpack water content is updated through a distributed snow correction scheme. Together, both data assimilation schemes offer the system with a framework to accurately estimate flow magnitudes. This robust system not only alleviates the adverse effects of meteorological data constrains in Yukon, but also offers an opportunity to investigate the hydrological footprint of the Regional Deterministic Precipitation Analysis products from the Canadian Precipitation Analysis system (CaPA-RDPA), which is exactly the motivation behind this study. Our overall goal, however, is more comprehensive as we are trying to elucidate whether assimilating snow monitoring information in a distributed hydrological model could meet the flow estimation accuracy in a sparsely gauged basin to the same extent that would be achieved through either: (i) the application of precipitation analysis products, or (ii) expanding the meteorological network. A proper answer to this question would provide us with valuable information with respect to the robustness of the snow data assimilation routine in HYDROTEL and the intrinsic added-value of using CaPA-RDPA products in sparsely gauged basins of Yukon.

Table of Contents

List of Figures

List of Tables

1. Introduction

The spatio-temporal representativeness of liquid and solid precipitation data is among the most crucial factors in every flow simulation practice. There are currently a few monitoring stations providing sparsely distributed observed precipitation information in major watersheds of interest in northern Canada. In Yukon, a territory located in northwestern Canada, these watersheds provide considerable inflow to large hydroelectric facilities in the territory, including those at the Whitehorse, Aishihik (/eyzhak/), and Mayo, operated by Yukon Energy (YE). For the corporation to efficiently sustain its hydroelectric operations in each watershed and gain a proper insight into short-term, seasonal, and long-term operations, an operational hydrologic forecasting system based on hydrologic model combine with Ensemble Kalman Filtering (EnKF) has been designed (Samuel et al., 2019). This forecasting system is operating over the modelling platform offered by the physically based semi-distributed HYDROTEL model (Fortin et al., 2001b; Turcotte et al., 2003; Turcotte et al., 2007a; Bouda et al., 2012; Bouda et al., 2014).

In the course of the last few years of development of the current forecasting system in Yukon, a number of challenges have been identified. These challenges have been investigated, and proper advancements were tailored to resolve them in order to alleviate the uncertainty involved with the predictions. The remaining issues of concern mainly consist of: (a) fine-tuning the model parameters in HYDROTEL by incorporating new calibration strategies and optimization methods (e.g. automated calibration, multi-criteria algorithms), and (b) including more in-situ information into the modelling framework.

The first issue is commonly observed in every rainfall-runoff modelling practice. It is often not a straightforward task to perform a model calibration due to a large number of parameters, the multi-modal nature of the objective function's response surface, and the computational requirements (Feyen et al., 2000). Commonly, model calibration is performed manually and through a trial-and-error approach, starting by identifying a range of possible values within specific lower and upper bounds for each parameter. Previous studies and the present experience in Yukon have shown that initial manual calibration is a suitable approach for parameter estimation (Bouda et al., 2012). However, with initial parameter values in hand, they can be fine-tuned through the application of automated calibration procedures and multi-criteria optimization algorithms. A major shortcoming of the manual approach is that the hydrologist may end up with a single set of parameters that may not necessarily be the best fit (Foulon and Rousseau, 2019). Conversely, automated calibration procedures apply algorithms for the numerical optimization of the goodness-of-fit criteria which yields best-fit parameter estimates along with a variety of statistics that characterize the parameters' uncertainty (Duan et al., 2003). In addition, the application of automated calibration techniques makes the calibration process less time consuming and less dependent on the expert's knowledge.

The second issue is specifically concerned with data constraints in Nordic watersheds in Canada, which have resulted in uncertainties with meteorological forcing in many hydrological modelling practices. Such constraints can adversely affect the performance of various modules in the modelling system. For instance, the accuracy of the current snow module in HYDROTEL, which is a single-layer, mixed degree-day/energy balance model (Fortin et al., 2001; Turcotte et al., 2003; Turcotte et al., 2007), majorly depends on the existence of accurate precipitation and air temperature input data. Therefore, it is obvious that augmenting the precipitation observation network in each watershed can greatly reduce the uncertainty involved with meteorological forcing.

There are other sources of information, which can reduce the input data uncertainty. For instance, the numerical weather prediction datasets produced by Environment and Climate Change Canada (ECCC), which are adjusted through an assimilation technique known as statistical interpolation (SI) represents a prime example of such atmospheric analysis gridded precipitation products. Currently, these adjusted products are created by the Canadian Precipitation Analysis (CaPA) system (Mahfouf et al., 2007; Fortin et al., 2015), the product of which is known as the Regional Deterministic Precipitation Analysis (RDPA). The CaPA-RDPA products are currently available in grib2 format on a polar-stereographic grid with a 10-km resolution (true at 60°N) at two temporal resolutions (6 hourly and 24 hourly). A high-resolution version of the system, known as High Resolution Deterministic Precipitation Analysis System (CaPA-HRDPA) is also in operation since 2018 and takes the HRDPS 2.5-km resolution field as the trial.

The CaPA system has gained considerable momentum in recent years, and the suitability of its precipitation products for application in hydrological modelling studies in Nordic watersheds in Canada have been the subject of a number of studies (e.g. Deacu et al., 2012; Zhao, 2013; Eum et al., 2014; Haghnegahdar et al., 2014; Gbambie et al., 2016; Hanes et al., 2016; Wong et al., 2017). Boluwade et al. (2018) compared the performance of CaPA-RDPA data against precipitation observations in the Lake Winnipeg basin which entails many of the hydro-climatological characteristics associated with the northern Great Plains and concluded that CaPA-RDPA data is a reliable precipitation product in sparsely gauged basin. Xu et al. (2019) evaluated daily total precipitation data derived from CaPA-RDPA, ERA-Interim, ERA5, JRA-55, MERRA-2, and NLDAS-2 over the Assiniboine River Basin, and concluded that in general, except for convective rainfalls in summer, CaPA-RDPA products demonstrated the best performance among all.

Currently, the adverse effects of scarce precipitation datasets in Yukon are alleviated through a combination of two independent data assimilation (DA) routines in HYDROTEL. These DA tasks are performed to update: (i) flow states, including soil temperature, soil moisture, overland flow routing, and river flow routing, based on in-situ discharge measurements, and (ii) snow states, including snow depth, snow water equivalent (SWE), snowpack thermal deficit, snowpack liquid water content, and surface albedo, based on snow survey data. The first DA routine was implemented by Samuel et al. (2019) where the North American Ensemble Forecasting System (NAEFS) precipitation products are merged into the operational flow forecasting platform in HYDROTEL through EnKF. This system is currently implemented at the operational level to forecast short-range flows and inflows in Upper Yukon, Aishihik, and Mayo watersheds. The snow DA routine, on the other hand, is fulfilled by performing a distributed snow correction of the simulated snowpack. When snow surveys are available, the simulated state variables including SWE and snow depth can be corrected based on sites measurements. The correction can be performed using either interpolation from the three nearest measurement sites or the Thiessen polygon interpolation approach (Turcotte et al., 2007).

The application of the snow DA routine in HYDROTEL is in line with the same practice followed in a number of other forecasting centers (see, e.g., Brasnett, 1999; Barrett, 2003; Drusch et al., 2004). In fact, in many countries around the globe, assimilation of in situ and remotely sensed measurements of snowpack state variables has become increasingly important for freshwater management (Helmert et al., 2018). Consequently, SWE reinitialization through various DA approaches has proven to be an effective approach to improve the degree of agreement between the simulated and observed discharge values when accurate meteorological forcing datasets are not readily available (see, e.g., Andreadis et al., 2006; Clark et al., 2006; Leisenring and Moradkhani, 2011; Nagler et al., 2008; De Lannoy et al., 2012; Liu et al., 2013; Saloranta, 2016). Several DA techniques are available for updating snow state variables, including

direct insertion (Liston et al., 1999), Cressman interpolation (Drusch et al., 2004), optimal interpolation (Brasnett, 1999), nudging (Boni et al., 2010), particle filtering (Arulampalam et al., 2002), and various types of Kalman filtering approaches with different levels of complexity (Gelb, 1974; Miller et al., 1994; Moradkhani, 2008; Evensen, 1994). Among these approaches, Kalman filtering and its nonlinear version, the EnKF approach, have been widely applied in different hydrological modelling studies (see, e.g., De Lannoy et al., 2012; Slater and Clark, 2006; Andreadis et al., 2006; Clark et al., 2006; Huang et al., 2017; Piazzi et al., 2018; Durand and Margulis, 2008; Magnusson et al., 2014; Su et al., 2008).

Li et al. (2019) have recently shown that in snow dominated basins, where the meteorological uncertainty during the forecast period is significant, which is the case for sparsely gauged networks, reinitializing the model based on observed SWE information can significantly improve streamflow forecasts. Similarly, in the absence of a high-density precipitation observation network in Yukon, the snow DA routine in HYDROTEL provides the possibility to handle different sources of uncertainty by merging the value of observed information into the model in order to correct the effects of model errors and improve forecasting capabilities (Turcotte et al., 2010). It is therefore possible to claim or at least expect that the current SWE correction performed in HYDROTEL can result in such streamflow estimates against which the hydrological footprint of CaPA-RDPA data can be compared. In other words, this study is trying to answer one simple question taken out of the technical debate: How much would be the benefit of using the CaPA-RDPA data compared to the existing snow DA performed in HYDROTEL? A proper answer to this question would provide us with valuable information with respect to the robustness of the snow DA routine in HYDROTEL and the accuracy, or the intrinsic added-value of using the CaPA-RDPA products in sparsely gauged regions of Yukon. This assessment would also support decision makers in their quest to elucidate whether assimilating snow survey data in hydrologic models could satisfy the flow estimation accuracy in sparsely gauged basins to the same extent that would be achieved by expanding the meteorological networks. The result of this assessment could also be used to investigate whether CaPA-RDPA data can be used to address an observation network assessment in key watersheds of interest to YE in Yukon. This study addressed all of the above questions.

The remainder of the report is organized as follows. In Section 2, the study area is described and specific details with respect to the hydrometeorological data used in the study are provided. Section 3 describes the HYDROTEL model and outlines the approaches carried out to: (a) perform HYDROTEL parameter sensitivity analysis and optimization, (b) validate the CaPA-RDPA products through the application of the snow data assimilation routine in the model, and (c) undertake the network assessment. Thereafter, results are presented and discussed in Section 4, and conclusions are drawn in Section 5.

2. Study area and data characteristics

2.1 Study basins

Fig. 1 illustrates the location of the three study watersheds, including the Mayo River basin, Aishihik River basin, and Upper Yukon River basin in Yukon, Canada. These watersheds are located in northern and mid-cordilleran alpine, sub-alpine, and boreal ecoclimatic regions (Strong, 2013) of central and southern Yukon. The Mayo basin covers a drainage area of roughly 2670 km^2. The mean annual precipitation and mean daily 2-m temperature are 316 mm and −2.6°C, respectively (true for 1976-2006). The flow volume varies on a seasonal basis, peaking in summer between June and July and dropping during winter in January and December. There are two control structures in Mayo: Mayo A, which is a 5-

MW station regulating Wareham Lake, and Mayo B, which is a 10-MW station 3.7 km downstream from Mayo A. The Aishihik basin covers a larger drainage area in the order of 4550 km^2 and is housing the Aishihik Facility, which is a 37-MW generating station. The mean annual precipitation is around 273 mm, and the mean daily annual 2-m temperature is in the order of –2°C (true for 1976-2006). The streamflow peaks in June, and the flow volume is relatively higher between May and October (Brabets and Walvoord, 2009). The Upper Yukon River basin is the largest of the three watersheds and covers a drainage area of around 19600 km^2. The basin is mountainous and is largely covered by sporadic permafrost. Runoff in the Upper Yukon is derived primarily from snowmelt and rainfall. The mean annual precipitation is around 299 mm, and the mean daily annual 2-m temperature is in the order of –3°C (true for 1981-2018). The streamflow peaks in August and is low between November and May. There is a 40-MW generating station in Whitehorse and one control structure on Marsh Lake.

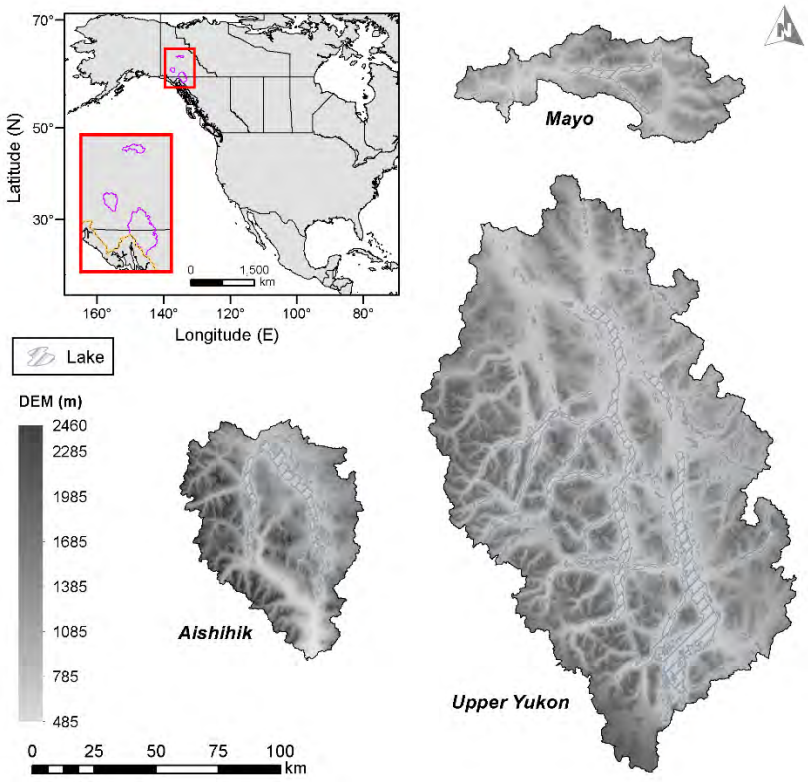

Fig. 1. The location of Mayo, Aishihik, and Upper Yukon River basins in central and southern Yukon. The southern half of the Upper Yukon basin is located within northern British Columbia.

2.2 Meteorological data

2.2.1 Ground observations

Table 1 provides a list of the meteorological stations located within and in the vicinity of the boundaries of each basin. Except for station #2100840 which is operated by YE, the other stations are operated by the Meteorological Survey of Canada (MSC).

Table 1. MSC meteorological networks in Mayo, Aishihik, and Upper Yukon (see Fig. 2).

Basin	Station Name	Station No.	Period	Time Step	Type
Mayo	ELSA	2100500	1948-1989	Daily	Manual
	Mayo A	2100700	1924-2013	Hourly & Daily	Auto
	Mayo A	2100701	2013-Present	Hourly & Daily	Auto
	Steward Crossing	2101030	1953-2008	Daily	Manual
	MAYOMET	MAYOMET	2018-Present	Hourly & Daily	Auto
Aishihik	Aishihik A	2100100	1943-1966	Hourly & Daily	Manual
	Blanchard River	2100163	1986-2012	Daily	Auto
	Burwash A	2100181	2011-Present	Hourly & Daily	Auto
	Burwash A	2100182	1966-2015	Hourly & Daily	Auto
	Burwash Airport BC	2100184	2013-Present	Hourly & Daily	Auto
	Carmacks CS	2100301	1999-Present	Hourly & Daily	Auto
	Haines Junction	2100630	1944-Present	Hourly & Daily	Auto
	Pelly Ranch	2100880	1898-2015	Daily	Manual
	Takhini River Ranch	2101095	1980-2015	Daily	Manual
	Otter Falls NCPC	2100840	1980-2015	Daily	Manual
	AISHMET	AISHMET	2018-Present	Hourly & Daily	Auto
Upper Yukon	Atlin	1200560	1899-Present	Daily	Manual
	Teslin	2101102	1944-Present	Hourly & Daily	Auto
	Whitehorse A	2101303	2012-Present	Hourly & Daily	Auto
	Whitehorse Auto	2101310	2009-Present	Hourly & Daily	Auto
	Fantail Lower	FANTLOW	2012-Present	Hourly	Auto
	Fantail Upper	FANTUPP	2012-Present	Hourly	Auto
	Llewellyn Lower	LLEWLOW	2013-Present	Hourly	Auto
	Llewellyn Upper	LLEWUPP	2013-2016	Hourly	Auto
	Wheaton	WHEATON	2014-Present	Hourly	Auto

Fig. 2 shows the distribution of the meteorological stations within and in the vicinity of the study basins. In Mayo, the precipitation gauge at the Mayo airport (Mayo A), which is located just beyond and very close to the watershed boundary, is the only active weather station in the basin with close to 100 years of available record. The MAYOMET station located near the outlet of Mayo Lake was installed in late 2018 and is the only active station within the basin. In Aishihik, the majority of the stations (17 out of 27) have less than 25 years of available data. There are three active MSC stations within a 75-km distance from the basin, including Carmacks CS (recording since 1999), Haines Junction (recording since 1944), and the one at Burwash airport, which is 50 km east of Aishihik, providing more than 50 years of historical precipitation data in conjunction with its nearby stations (Burwash & Burwash A). Within the basin boundaries, however, there are only two weather stations available (AISHMET & Otter falls NCPC), of which Otter falls NCPC has not been recording since 2015, and AISHMET is the one which was activated in late 2018. In Upper Yukon, more than 65% of the stations have less than 20 years of record, the majority of which have been installed in the past 10 years. The MSC station at Atlin is the only active station with more than 120 years of recorded precipitation amounts.

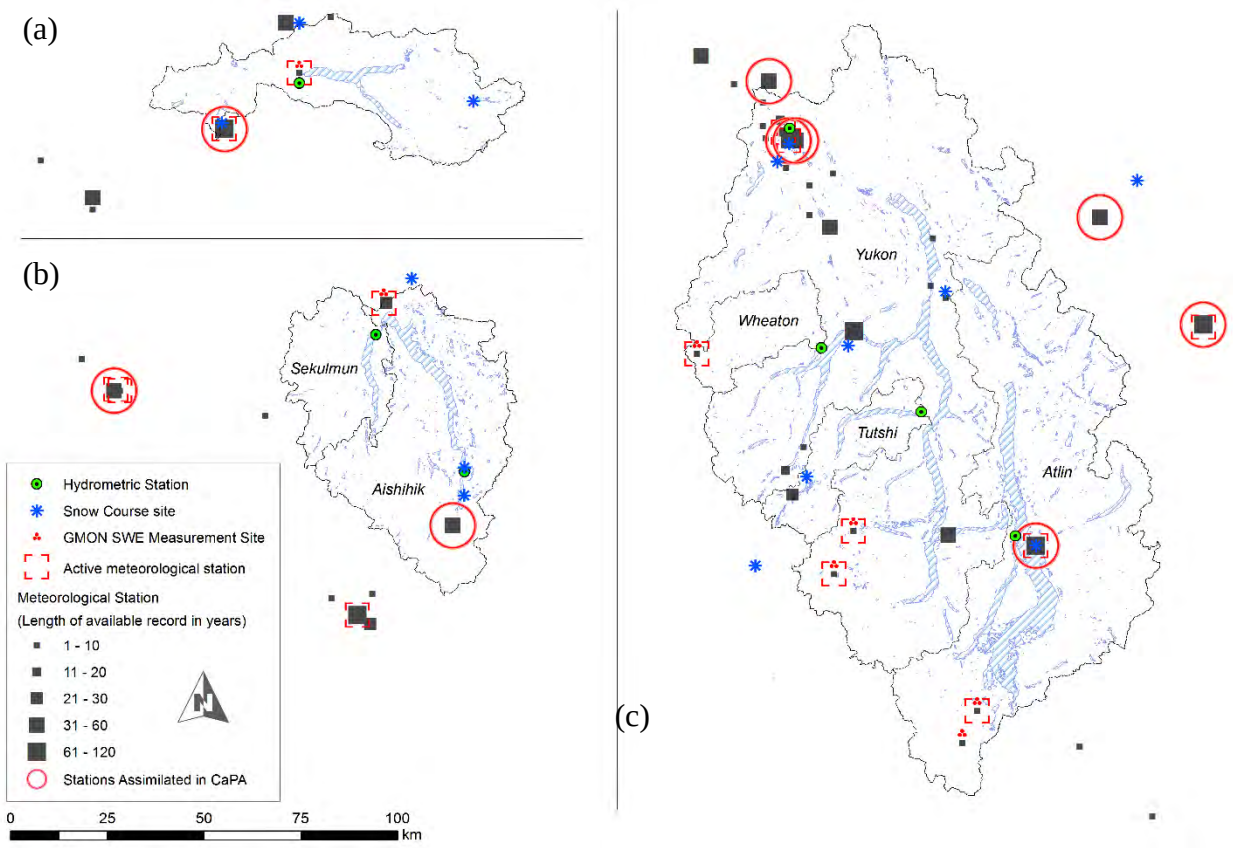

Fig. 2. The distribution of meteorological (solid black squares), hydrometric (co-centric green circles), snow course sites (blue asterisks), and GMON stations (solid red three-dot triangles) within and in the vicinity of the study basins: (a) Mayo, (b) Aishihik, and (c) Upper Yukon. Meteorological stations are graduated based on the number of years of available record. Active meteorological stations (hollow red squares with dashed perimeter) and the synoptic weather stations currently assimilated in CaPA (hollow red circles) are identified.

2.2.2 CaPA-RDPA data

The grib2 CaPA-RDPA v3.0.0 data from 2010-2018 at daily time steps were downloaded from ECCC ftp repository and decoded using NOAA/National Weather Service wgrib2 program. The decoded data sets were then converted from the polar-stereographic grid onto a rectangular grid covering each basin's drainage area with a spatial resolution of 0.10° in latitude and 0.15° in longitude (roughly 10 km in both directions at 60°N).

2.3 Hydrometric data

Table 2 provides a list of available hydrometric stations at which streamflow measurements are taken in each basin (see Fig. 2 for the specific location of the hydrometric stations). The inflows to Aishihik Lake and Mayo Lake do not represent naturally observed discharge values and were reconstructed based on recorded water levels (see Samuel et al. (2019) for a detailed description of the construction

methodology). For Mayo Lake, water level data obtained from the 09DC005 station and streamflow observed at the YECMAYO station were used for reconstructing inflows. Similarly, water levels recorded at station 08AA005 and streamflow recorded at 08AA008, 08AA009, and 08AA010 stations were used to reconstruct the inflows to Aishihik Lake. All flows and water levels were provided by the Water Survey of Canada (WSC), except for those at stations #0000003, ##0000003, and YECMAYO, which are recorded by YE.

Table 2. WSC and YE hydrometric networks in Mayo, Aishihik, and Upper Yukon basins. The gauges used for the HYDROTEL model calibration are in bold (see Fig. 2).

Basin	Station Name	Station No.	Period	Type
Mayo	Mayo Lake near the Outlet	09DC005	1979-Present	Water Level
	Mayo Lake at the Outlet	YECMAYO	1979-Present	Flow
	Inflow to Mayo Lake	**##0000003**	**1979-Present**	**Flow**
Aishihik	Aishihik Lake near Whitehorse	08AA005	1972-Present	Water Level
	Sekulmun River at Outlet of Sekulmun Lake	**08AA008**	**1981-Present**	**Flow & Water level**
	Giltana Creek near The Mouth	08AA009	1980-Present	Flow & Water level
	Aishihik River below Aishihik Lake	08AA010	1980-Present	Flow & Water level
	Aishihik Lake near Aishihik	08AA012	1995-2015	Water Level
	Inflow to Aishihik Lake	**#0000003**	**1980-Present**	**Flow**
Upper Yukon	**Atlin River near Atlin**	**09AA006**	**1950-Present**	**Flow**
	Wheaton River near Wheaton	**09AA012**	**1955-Present**	**Flow**
	Tutshi River near outlet of Tutshi Lake	**09AA013**	**1956-Present**	**Flow**
	Yukon River at Whitehorse	**09AB001**	**1902-Present**	**Flow**

2.4 Snow data

Table 3 provides the metadata of the snow depth and SWE monitoring networks managed by the Water Resources Branch (WRB) of Environment Yukon as well as the Gamma Monitoring (GMON) automatic snowpack sensor readings provided by YE. The GMON (a.k.a. Campbell Scientific CS725) sensor measures SWE by detecting the attenuation of naturally occurring electromagnetic energy from the ground. This contactless approach can offer highly reliable and accurate SWE measurements with an uncertainty level that does not exceed ±5% at maximum snow depth. Traditional SWE measurement approaches, such as the application of snow pillows, by which the snowpack weight is directly measured, are prone to higher uncertainty levels since snowpack properties (e.g. radiation characteristics) can be altered during the measurement. The GMON gauge, which monitors snowpack properties in a contactless mode, does not suffer from the same disadvantages. During the past few years, a number of GMON gauges were installed at those locations identified in Table 3 and Fig. 2 (5 stations were initially installed in Upper Yukon, but 2 were removed and relocated; 1 in Mayo; 1 in Aishihik). Once monitored, the collected information is transmitted via satellite connection and goes through quality control.

Table 3. WRB and YE snow course and GMON networks in Mayo, Aishihik, and Upper Yukon (see Fig. 2).

Basin	Station Name	Station No.	Period	Type	Sources*
Mayo	Calumet	09DD-SC01	1975-Present	Depth/SWE	WRB
	Edwards Lake	09DD-SC02	1987-Present	Depth/SWE	WRB
	Mayo Airport A	09DC-SC01A	1968-Present	Depth/SWE	WRB
	Mayo Airport B	09DC-SC01B	1987-Present	Depth/SWE	WRB
	MAYOMET	MAYOMET	2017-Present	GMON	YE
Aishihik	Canyon Lake	08AA-SC01	1975-Present	Depth/SWE	WRB
	Macintosh	09CA-SC02	1976-Present	Depth/SWE	WRB
	Aishihik Lake	08AA-SC03	1944-Present	Depth/SWE	WRB
	AISHMET	AISHMET	2017-Present	GMON	YE
Upper Yukon	Tagish	09AA-SC1	2006-Present	Depth/SWE	WRB
	Montana Mountain	09AA-SC2	2006-Present	Depth/SWE	WRB
	Log Cabin (BC)	09AA-SC3	2006-Present	Depth/SWE	WRB
	Atlin (BC)	09AA-SC4	2006-Present	Depth/SWE	WRB
	Mt. McIntyre	09AB-SC1B	2006-Present	Depth/SWE	WRB
	Whitehorse Airport	09AB-SC2	2006-Present	Depth/SWE	WRB
	Meadow Creek	09AD-SC1	2006-Present	Depth/SWE	WRB
	Moore Creek Bridge (AL)	0034K02	2006-Present	Depth/SWE	USDA-NRCS
	Eaglecrest (AL)	0034J03	2006-Present	Depth/SWE	USDA-NRCS
	Fantail Lower	FANTLOW	2012-2017	GMON	YE
	Fantail Upper	FANTUPP	2012-2017	GMON	YE
	Llewellyn Lower	LLEWLOW	2013-Present	GMON	YE
	Llewellyn Upper	LLEWUPP	2013-2016	GMON	YE
	Wheaton	WHEATON	2014-Present	GMON	YE

* WRB: Water Resources Branch, Environment Yukon; YE: Yukon Energy Corporation; USDA-NRCS: United States Department of Agriculture, Natural Resources Conservation Service

3. Models and methodology

3.1 HYDROTEL: Sensitivity analysis and model calibration

The semi-distributed physically based HYDROTEL model can simulate a variety of hydrological processes. These processes and the physically-based approaches used to simulate each one along with a list of parameters associated with each process used in the version of HYDROTEL utilized in this study are listed in Table 4. In HYDROTEL, the vertical water budget is computed over a computational unit called the Relatively Homogeneous Hydrological Unit (RHHU), which represents either a hillslope or elementary sub-watershed and are derived based on a digital elevation model and a digital network of lakes and river sections using PHYSITEL, a specialized GIS for distributed hydrological models (Turcotte et al., 2001; Rousseau et al., 2011; Noël et al., 2014), both of which overlaid by a multi-layer soil model. The soil column of a RHHU is stratified into three layers. The first soil layer (Z1) governs infiltration, and the other two layers (Z2 and Z3) control interflow and baseflow. The interpolation of meteorological variables process is based on the weighted mean of the nearest three stations to resolve the amount of total precipitation, which is then partitioned into rain and snow according to a threshold temperature and a simple weighted scheme based on daily minimum and maximum temperatures, on each RHHU. The accumulation and melt of snowpack process determine the timing and peak of the spring freshet. In the soil temperature and soil frost process, the only associated parameter (soil freezing temperature threshold) is not distributed over the entire RHHUs, and therefore, is not recommended to be modified. The next process is designed to identify the potential evapotranspiration which is dominantly going to impact the

total annual runoff and baseflow in summer. The sub-watershed flow process simulates the water flux towards the river network using a hydrogeomorphological unit hydrograph (a.k.a., HGM).

Table 4. HYDROTEL parameter sets associated with each hydrological process. Parameters that were calibrated in OSTRICH are identified by the importance level of 1 (see Section 3.1 for further discussion). The lower and upper bounds shown in the table are used in parameter optimization.

Process/Parameter	Unit	Lower Bound	Upper Bound	Importance Level	OSTRICH Code
Vertical water budget: *BV3C*					
Thickness of the first soil layer	m	0.05	0.60	1	Z1
Thickness of the second soil layer	m	0.05	0.60	1	Z2
Thickness of the third soil layer	m	0.05	0.80	1	Z3
Initial humidity of the first soil layer	--	0.90	0.90	0	--
Initial humidity of the second soil layer	--	0.90	0.90	0	--
Initial humidity of the third soil layer	--	0.90	0.90	0	--
Extinctive coefficient	--	0.3	0.9	2	--
Recession coefficient	m/h	0.0000001	0.00001	1	CR
Drying coefficient	--	0.5	1.0	2	--
Maximal variation of relative humidity of soil layer	--	0.2	0.4	2	--
Interpolation of meteorological variables: *Weighted mean of nearest three stations*					
Temperature gradient	°C/100 m	−1.5	0.0	1	GT
Precipitation gradient	mm/100 m	0.0	1.5	1	GP
Phase change temperature threshold	°C	−3.5	3.5	1	PPN
Snow accumulation and melt: *Mixed degree-day energy-budget approach*					
Melting rate (soil/snow)	mm/day	0.5	0.5	0	--
Maximal snow density	Kg/m^3	466	466	0	--
Compaction constant	--	0.01	0.01	0	--
Evergreen forest melting temperature threshold	°C	−3.5	3.5	1	SFC
Deciduous forest melting temperature threshold	°C	−3.5	3.5	1	SFF
Open area melting temperature threshold	°C	−3.5	3.5	1	SFD
Evergreen forest melting rate	mm/day °C	1	20	1	TFC
Deciduous forest melting rate	mm/day °C	1	20	1	TFF
Open area melting rate	mm/day °C	1	20	1	TFD
Albedo threshold	--	1	1	0	--
Soil temperature and soil frost: *Rankinen*					
Soil freezing temperature threshold	°C	−1	1	3	--
Potential evapotranspiration: *Penman-Monteith*					
Standard height for wind measurement	m	2	2	0	--
Standard height for humidity measurement	m	2	2	0	--
Wind speed at the Z elevation	m/s	2	2	0	--
Surface reference vegetation height	m	0.12	0.12	0	--
Stomatal resistance for reference surface	s/m	80	120	2	--
Multiplicative coefficient	--	0.25	1.30	1	FETP
Flow on sub-watersheds towards river network: *Kinematic wave*					
Manning coefficient for forest land cover classes	--	0.15	0.3	3	--
Manning coefficient for water land cover classes	--	0.015	0.03	3	--
Manning coefficient for other land cover classes	--	0.04	0.1	3	--
Channel flow: *Kinematic wave*					
Roughness optimization	--	1	1	0	--
Stream width optimization	--	1	1	0	--

While other studies have performed different types of sensitivity analyses of HYDROTEL on other basins (e.g., Bouda et al., 2013; Turcotte et al., 2003), a global sensitivity analysis was performed using the Variogram Analysis of Response Surfaces (VARS) toolbox (Razavi et al., 2019). The toolbox allows

the user to identify the parameters by the importance level (i.e., model sensitivity to changing parameter conditions) through a multi-method approach that unifies different theories and strategies. With sensitive parameters in hand, the model calibration becomes a less challenging task. However, since the HYDROTEL model calibration, in essence, is a multi-objective optimization problem (due to the number of flow gauges reporting flow in the basin for which several error criteria might be assessed), defining what makes the model calibrated is not an easy task. Moreover, other factors affecting the quality of the calibration result include error due to lake/reservoir inflow reconstruction and the quality of precipitation or temperature forcing data (elaborating on these concerns is beyond the scope of the current study). To properly respond to these challenges, model calibration was completed in OSTRICH (Optimization Software Toolkit for Research Involving Computational Heuristics), which is a model-independent and multi-algorithm optimization tool (Matott, 2017). The toolkit, which supports both single- and multi-criteria optimization options, can be used for the weighted non-linear least-squares calibration of the model parameters or for constrained optimization of a set of design variables according to pre-defined cost functions. OSTRICH can incorporate different algorithms to search for the optimal value of the objective functions and to identify the parameter set associated with such optima. There are several optimization algorithms available, which can be classified as either deterministic local or heuristic global search methods incorporating elements of structured randomness. For multi-criteria optimization, the Pareto Archive Dynamically Dimensioned Search (PA-DDS; Asadzadeh and Tolson, 2009, 2013) and the simple multi-objective optimization heuristic algorithms are available, while for uncertainty-based calibration, several sampling-based algorithms (i.e. Generalized Likelihood Uncertainty Estimation and Metropolis-Hastings Markov Chain Monte Carlo) are available. In addition, the asynchronous parallel processing architecture provided by OSTRICH, which is based on the industry standard Message Passing Interface (MPI), provides the means to speed up the calibration procedure.

The model was calibrated for the period of 2010-2018 using PA-DDS by maximizing the Kling-Gupta Efficiency (KGE; Gupta et al., 2009) and minimizing the root mean squared errors (RMSE) values. HYDROTEL was forced with CaPA-RDPA and meteorological data, including daily precipitation and maximum and minimum temperatures time series described in Table 1, as well as snow course observations provided in Table 3. Daily historical discharge data measured at the location of available hydrometric stations or daily reconstructed inflows described in Table 2 and identified in Fig. 2 were obtained from the Water Survey of Canada (WSC) and were used for model calibration.

3.2 Impact of snow data assimilation and CaPA-RDPA forcing

In order to investigate the impact of SWE assimilation on model performance, and also to understand how robust the accuracy of CaPA-RDPA products were over the three study basins for hydrologic application purposes, two separate sets of modelling experiments were designed. In the first set (experiment Set 1), the model was trained with forcing CaPA-RDPA, while in the second set (experiment Set 2), MSC meteorological data were used as input. Depending on whether the GMON and snow course monitoring information are assimilated during the calibration and the ‘stand-alone’ run (i.e. when the model runs once the calibration is completed), two separate runs can be considered for each set (see Table 5). In Exp. 1.2, the model is calibrated while assimilating SWE measurements. The assimilation was then switched off and the model was forced with CaPA-RDPA once again (Exp. 1.2). This experiment was designed to indicate the extent by which the model would be able to preserve the flow estimation accuracy with forcing precipitation analysis products. The second set of experiments (Exp. 2.1, Exp. 2.2) are similar to the first set except that CaPA-RDPA are replaced with observed meteorological forcing.

Table 5. Application of snow assimilation during the experiments.
× : snow assimilation was performed during the calibration/stand-alone run,
✓: snow assimilation was not performed during the calibration/stand-alone run.

Exp.		Meteorological Forcing	Snow Assimilation ✓: active / ×: inactive	
Set	Run		Calibration	Stand-alone Run
1	1.1	CaPA-RDPA	✓	✓
	1.2		✓	×
2	2.1	MSC Meteorology	✓	✓
	2.2		✓	×

3.3 Network assessment

Depending on whether the former assessment of the CaPA-RDPA forcing in HYDROTEL may suggest if the gridded analysis products can be adequately used for streamflow simulation in Mayo, Aishihik, and Upper Yukon, a simple network sensitivity analysis based on CaPA gridded products was proposed for flow simulation in HYDROTEL. Such an assessment was designed to guide future network assessment procedures. Following Abbasnezhadi (2017), a meteorological network assessment problem may belong to any of the following two main categories: Type I (a.k.a. network rationalization), in which a dense network is reduced while maintaining the same overall precision, and Type II (a.k.a. network extension) in which a sparse network with less than optimal station density is explored for possible augmentation. Type II problems can further be categorized into two subgroups: Type IIa, in which the locations of more observation sites in the expanded network are proposed, and Type IIb, where the best sites among a set of potential candidates (derived from a Type IIa assessment) are designated. Obviously, in case of the current network condition in Yukon, a Type IIa assessment is required to determine the most optimal network density (Type IIb assessment to identify the location of the monitoring stations among the pool of candidates, derived from the Type IIa assessment, is beyond the scope of the current study). A Type IIa network assessment methodology was proposed by Abbasnezhadi et al. (2019), where a stochastic network assessment scheme was applied to find the optimal density of the observation network in the Churchill River basin in northern Manitoba and Saskatchewan in Canada. The network assessment was undertaken with the objective to maximize the accuracy of precipitation products for hydrologic modelling applications. The stochastic network assessment methodology simulates a DA technique known as Statistical Interpolation (SI), which is the algorithm used in the CaPA system for updating trial field. Given the fact that at least two basins (Mayo and Aishihik) in the study consist of relatively small drainage areas, it is expected that expanding the network within each basin, even by heuristic approaches, can greatly reduce the uncertainty associated with precipitation information. Therefore, a network assessment procedure similar to that of Abbasnezhadi et al. (2019) was followed here, except that the assessment did not include artificially generated reference and error fields. Rather, a subset of grid points was extracted to shape network scenarios of different resolutions from the RDPA domain over each basin, while the respective precipitation analysis was directly used during the assessment. However, such an uncontrolled framework could be specifically useful for the case of this study only if the SWE DA-CaPA coupling could prove to output such streamflow estimation that could closely match flow observations. Sampling grids pertaining to each study basin are shown in Fig. 3 (to see individual scenarios for each basin, see the Appendix).

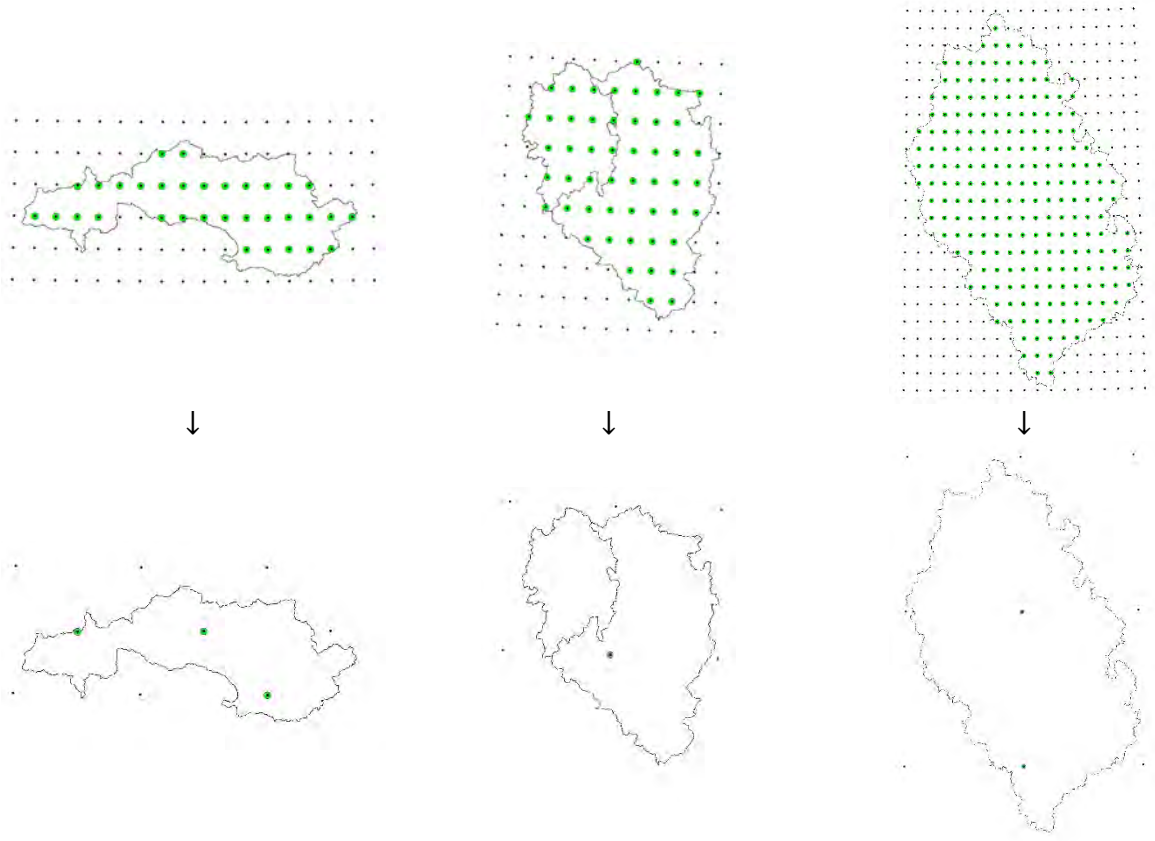

$\Theta^{\nu} \mid \nu \in [0.10^{\circ}, \ldots, 0.35^{\circ}]$ $\Theta^{\nu} \mid \nu \in [0.1^{\circ}, \ldots, 0.5^{\circ}]$ $\Theta^{\nu} \mid \nu \in [0.1^{\circ}, \ldots, 0.8^{\circ}]$

(a) Mayo (b) Aishihik (c) Upper Yukon

Fig. 3. Network scenarios, defined in term of the network resolution (ν) in decimal degrees, extracted from the CaPA grid. See the individual scenarios in the Appendix.

4. Results and Discussion

4.1 Sensitivity analysis and model calibration

The sensitivity analysis results provided by VARS indicated that among the parameters used to regulate the vertical water budget, the second soil layer thickness (Z2), which affects flow peaks, is a sensitive parameter. The third soil layer thickness (Z3), which mostly affects baseflow, was identified to be a less sensitive parameter in this group. Also, the recession coefficient, which affects summer baseflow and works with Z3, was found to be a relatively sensitive parameter. Among the parameters used for calculating the weighted mean of the nearest three stations, VARS indicated that the third parameter in this group (PPN) has more impact on the results, and the first two (GT and GP) are almost equal in sensitivity. Also, the snow process melting temperature thresholds and rates for all three land classes in this group (SFC, SFF, SFD, TFC, TFF, TFD) were shown to have equal sensitivity levels. The multiplicative coefficient (FETP) applied to the Penman-Monteith equation was found to be the only sensitive evapotranspiration parameter. None of the parameters in the sub-watershed flow process was found to be sensitive, while any modification to these parameters would force the model to recalculate the

HGM file which would be time-consuming. The parameters associated with the channel flow process, computed using the kinematic wave equation, were also not found to be sensitive.

With sensitive parameters in hand, comprising of a set of 14 parameters indicated in Table 4 by those with the importance level of 1, the model was calibrated in OSTRICH. The standard upper and lower bound values used for each parameter in OSTRICH are provided in Table 4, while the initial estimates for each parameter were based on those derived in previous calibration efforts. Those past efforts were based on the adjustments made manually to each parameter in order to achieve a desired hydrological performance. The following set of constraints were included when calibrating the parameters pertaining to the snow accumulation and melt, and the vertical water budget processes: $SFC \geq SFF \geq SFD$, $TFC \leq TFF \leq TFD$, and $Z1 \leq Z2 \leq Z3$. The toolbox utilized 8 computational cores for asynchronous parallel processing at the budget of 2-18 hours (depending on the basin's drainage area) for 1000 iterations.

In Mayo, the model calibration was completed in OSTRICH based on the inflow time-series into Mayo Lake associated to YE gauge ##0000003 (see Fig. 2). In Aishihik, the model calibration was completed in two stages. In the first stage, the model was calibrated for Sekulmun River streamflow time-series at the outlet of Sekulmun Lake observed at WSC Gauge 08AA008 (see Fig. 2). The Sekulmun portion of the Aishihik model was isolated and separated in HYDROTEL GUI (graphical user interface) to decrease the model run time. In the second stage, the model was setup to simulate the reconstructed inflow time series to Aishihik Lake associated with YE gauge #0000003. The original reconstructed inflow data display high-intensity fluctuations and were not deemed suitable for the calibration. Instead, they were first treated by using a 7-day moving average window (windows of longer durations were also tested and did not enhance the calibration results). In Upper Yukon, the model calibration was also performed in two stages. In the first stage, the model was calibrated separately for three gauged sub-basins, including Atlin River (WSC gauge 09AA006), Tutshi River (WSC gauge 09AA013), and Wheaton River (WSC gauge 09AA012) (See Fig. 2). In the second stage, the model was then setup to simulate the flow time series in Yukon River at Whitehorse observed at WSC gauge 09AB001.

Fig. 4 shows the flow duration curves for Mayo, Aishihik (including the Sekulmun sub-basin), and Upper Yukon (including the Atlin, Tutshi, and Wheaton sub-basins). In Mayo, the simulation has fully preserved the exceedance probability of observed flows. In Aishihik and Sekulmun, other than some overestimation of winter low flows, the remainder has been well captured by the model. In Upper Yukon, in general, the exceedance probabilities of the simulated flows closely resemble the observed one although the low flows are underestimated in sub-basins with small drainage areas (Tutshi and Wheaton), which has similarly impacted the low flows in Yukon too. In Atlin, the exceedance probability of the observed high flows (corresponding to the flow peaks) are marginally underestimated.

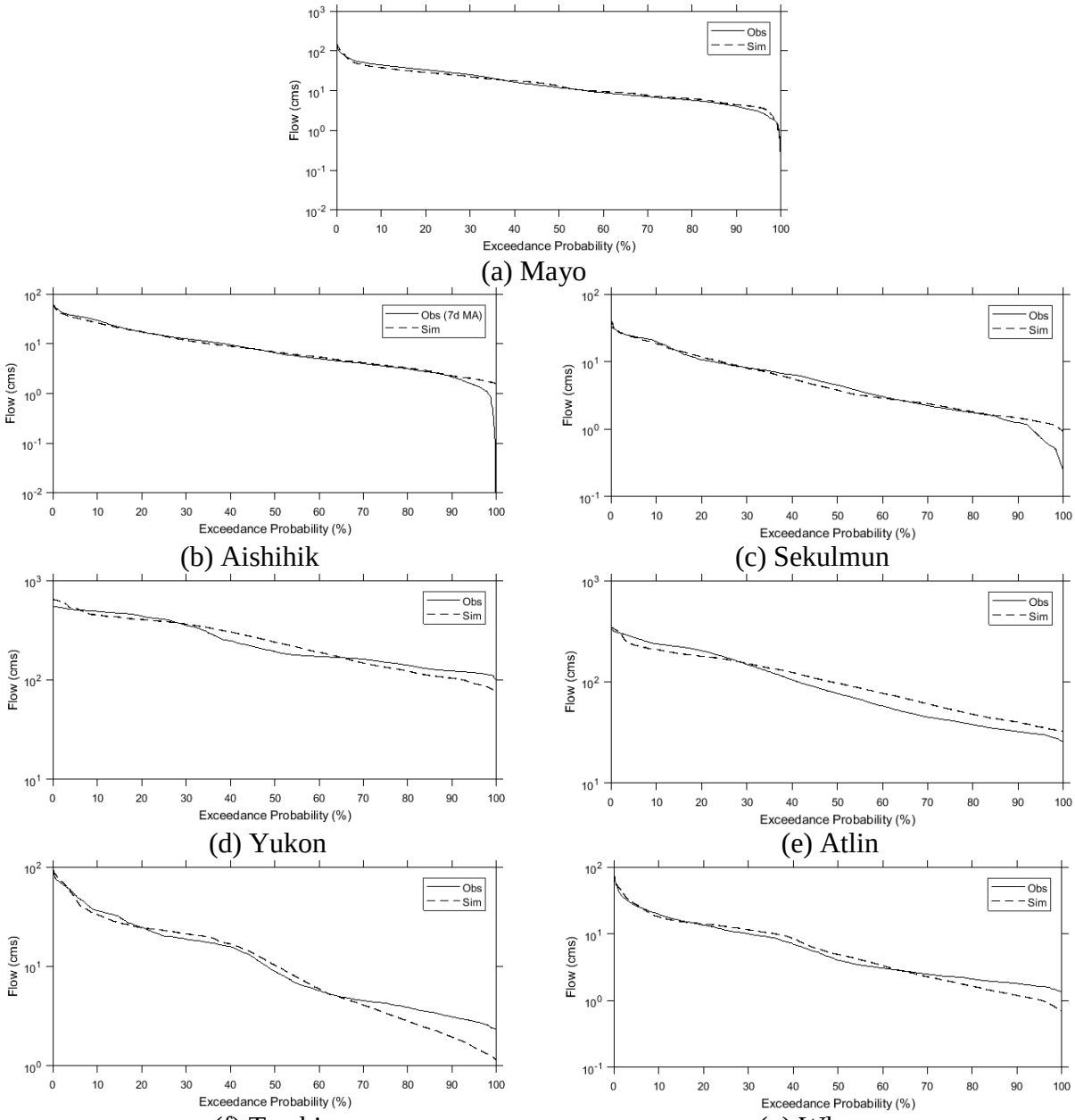

(a) Mayo

(b) Aishihik

(c) Sekulmun

(d) Yukon

(e) Atlin

(f) Tutshi

(g) Wheaton

Fig. 4. Calibration flow duration curves for different hydrometric stations. Observations are shown as solid lines and simulations are dashed.

4.2 Proxy validation of CaPA-RDPA

The impact of the snow DA routine in HYDROTEL and CaPA-RDPA forcing data on modelling results were assessed based on the set of experiments discussed in Section 3.2. Fig. 5 compares the metrics in Mayo for the first and the second sets of experiments (for the full description of the metrics used in the figures of this section, see the Appendix). The metrics reported by the experiments indicate that the calibration results for the case when CaPA-RDPA are used as input (Exp. 1.1 and Exp. 1.2) surpass, in both cases, those derived by station observations (Exp. 2.1 and Exp. 2.2). In addition, the best outcome is obtained with Exp. 1.1 when the model calibration is performed with CaPA-RDPA forcing and the snow DA routine in active mode. Exp. 1.2 (CaPA-RDPA forcing and no snow DA), on the other hand, indicates that the model's performance is not undermined if the snow DA routine is turned off in HYDROTEL (when the model has already been calibrated with the snow DA routine in active mode). In other words, the assimilation of snow monitoring data has no impact on the flow estimation accuracy if CaPA-RDPA data is used as input. In contrast, the metrics obtained from the second set of experiments indicate that when the model is calibrated using MSC meteorological data as input and with the snow DA routine in active model (Exp. 2.1), the metrics are on the ballpark of an acceptable level, while still falling short of those obtained with CaPA-RDPA. However, as Exp. 2.2 indicates, if the snow DA routine is turned off, the flow estimation accuracy declines significantly. This illustrates that for the second set of experiments with sparsely gauged meteorological input data, the snow DA routine has a compensating impact on the flow estimation accuracy.

Although the new GMON stations do not provide a long record of measurements yet, the snow course sites in all three watersheds provide enough and continuous records of snow depth and SWE measurements. Results from the second set of experiments shown in Fig. 5 indicate that, in Mayo, these snow course measurements provide valuable snow measurements by which the SWE measurements provided by the meteorological network can be corrected through the snow assimilation routine in HYDROTEL. In other words, the flow estimation accuracy in Mayo is highly dependent on the external information from the snow course sites. On the other hand, the proxy validation of the CaPA-RDPA in Mayo based on the reconstructed inflow associated with gauge ##0000003 shows that the analysis is accurate enough to the extent that would not call for any correction through snow measurements. To this point, these results indicate that in Mayo: (a) CaPA-RDPA products can be used for flow estimation, (b) given the fact that very few precipitation stations are currently assimilated in CaPA, if the current network is extended, the modelling accuracy will improve, and (c) in the absence of a precipitation observation network with an optimal density, the snow assimilation routine plays a significant role to compensate for proper precipitation information.

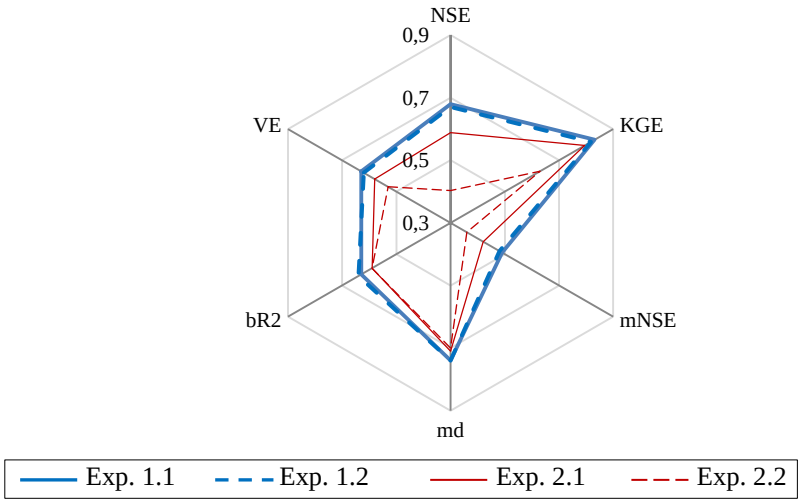

Fig. 5. Radial diagram for the performance of the model in response to the set of experiments completed in Mayo. NSE, VE, bR2, md, mNSE, and KGE stand for Nash-Sutcliffe Efficiency, Volumetric Efficiency, Modified Coefficient of Determination, Modified Index of Agreement Modified Nash-Sutcliffe Efficiency, and Kling-Gupta Efficiency, respectively.

Fig. 6a compares the metrics in Aishihik for the first and the second sets of experiments, while the performance of the model in response to the set of experiments completed in Sekulmun are shown in Fig. 6b. The results reported for both Aishihik and Sekulmun are not identical to those of Mayo and the experiments rather exhibit a contrasting outcome. While in Mayo, deactivating the snow assimilation routine in HYDROTEL when forcing the model with CaPA-RDPA (Exp. 1.2) would marginally impact the metrics compared to the case when the snow assimilation routine was active (Exp. 1.1), in Aishihik (including the Sekulmun sub-basin), deactivating the snow assimilation routine led the model performance to decay significantly. This suggests that the RDPA gridded products do not encompass the required accuracy over Aishihik, necessitating the assimilation of snow readings an essential component for accurate flow estimation. The inadequacy of the RDPA estimates over Aishihik is an indication of the detrimental impact of the sparse precipitation network on CaPA products over the basin. In Sekulmun, Exp. 2.2 provides marginally better results than Exp. 2.1, demonstrating that the measurements taken at the MSC meteorological stations better represent the ground SWE accumulation than the one recorded at the snow course sites. Nevertheless, in Sekulmun, when using CaPA-RDPA data as the input, the combined effect of incorporating the value of information from both the external assimilation of precipitation data in CaPA and the internal assimilation of snow readings in HYDROTEL has obviously improved the flow estimation accuracy (see Fig. 6b). In Aishihik, however, Exp. 2.1 displays a declined performance relative to Exp. 1.1, while Exp. 2.1 and Exp. 2.2 are relatively identical. These results, in total, revealed that in Aishihik and Sekulmun, the snow data are essential for accurate flow estimation if the model is forced with CaPA-RDPA, while the MSC precipitation input data seems to deliver sufficient accuracy (indicating the accuracy of the snow measurements taken as MSC stations which necessitates minimal correction by the data taken at the snow course sites). This, once again, indicates that the value of precipitation information from the MSC precipitation gauges is superior to those of CaPA-RDPA which illustrates the low accuracy of CaPA data over the basin.

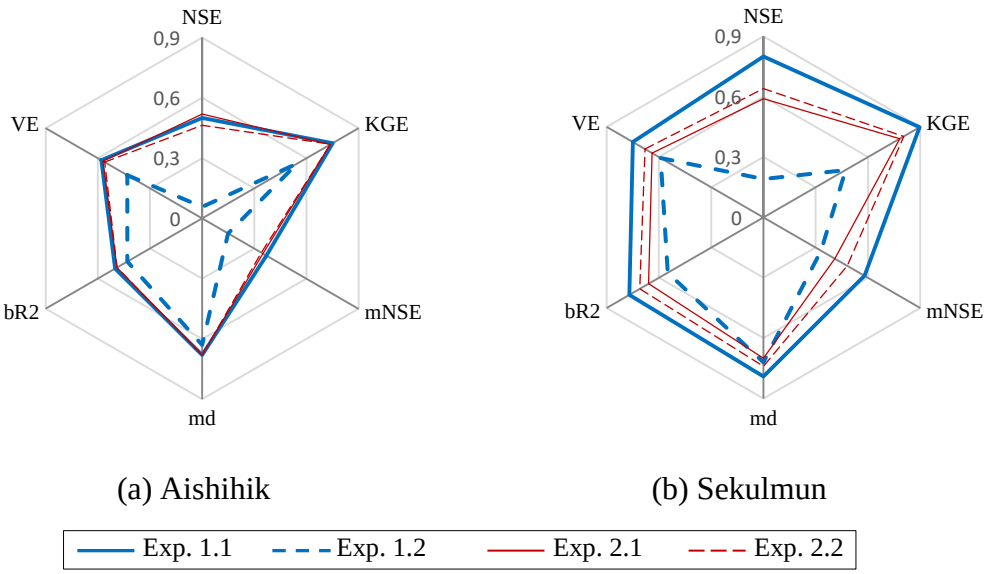

Fig. 6. Radial diagrams for the performance of the model in response to the set of experiments completed in Aishihik.

Fig. 7 compares the metrics in Upper Yukon, including those for Atlin, Tutshi, and Wheaton for the first and the second sets of experiments. In Atlin (Fig. 7a), there are marginal differences between the results derived from all four experiments. This agreement could be the outcome of several factors, including: (a) co-location of the snow course site and the MSC gauge in Atlin, (b) existence of a MSC gauge which is assimilated in CaPA (see Fig. 2); forcing the respective RDPA over the basin to become more or less identical to that of gauge reading, (c) the impact of the nearby MSC gauges on the northeast side of the basin (just beyond the basin boundary) on the accuracy of precipitation estimate over the basin. In Tutshi and Wheaton, however, a different outcome is evident. The impact of drainage area on the flow estimation accuracy for the given activity state of the snow assimilation routine seems to be a factor of importance. For instance, for a sub-basin such as Tutshi (Fig. 7b) with a small drainage area, the impact of the only snow course site in the basin (site #09AA-SC3) on the flow accuracy can be comprehended by the fact that deactivating the snow assimilation in Exp. 2.2 has significantly decayed the flow accuracy by almost half. On the other hand, in Wheaton (Fig. 7c), a sub-basin with a comparable drainage area to that of Tutshi, in the absence of any snow course site, Exp. 2.2 has apparently yielded about the same metrics obtained from Exp. 2.1. In general, the results of the experiments performed in Upper Yukon indicate that since the basin generally enjoys a higher number of weather stations (including those assimilated in CaPA and snow course sites), the results demonstrate better metric values.

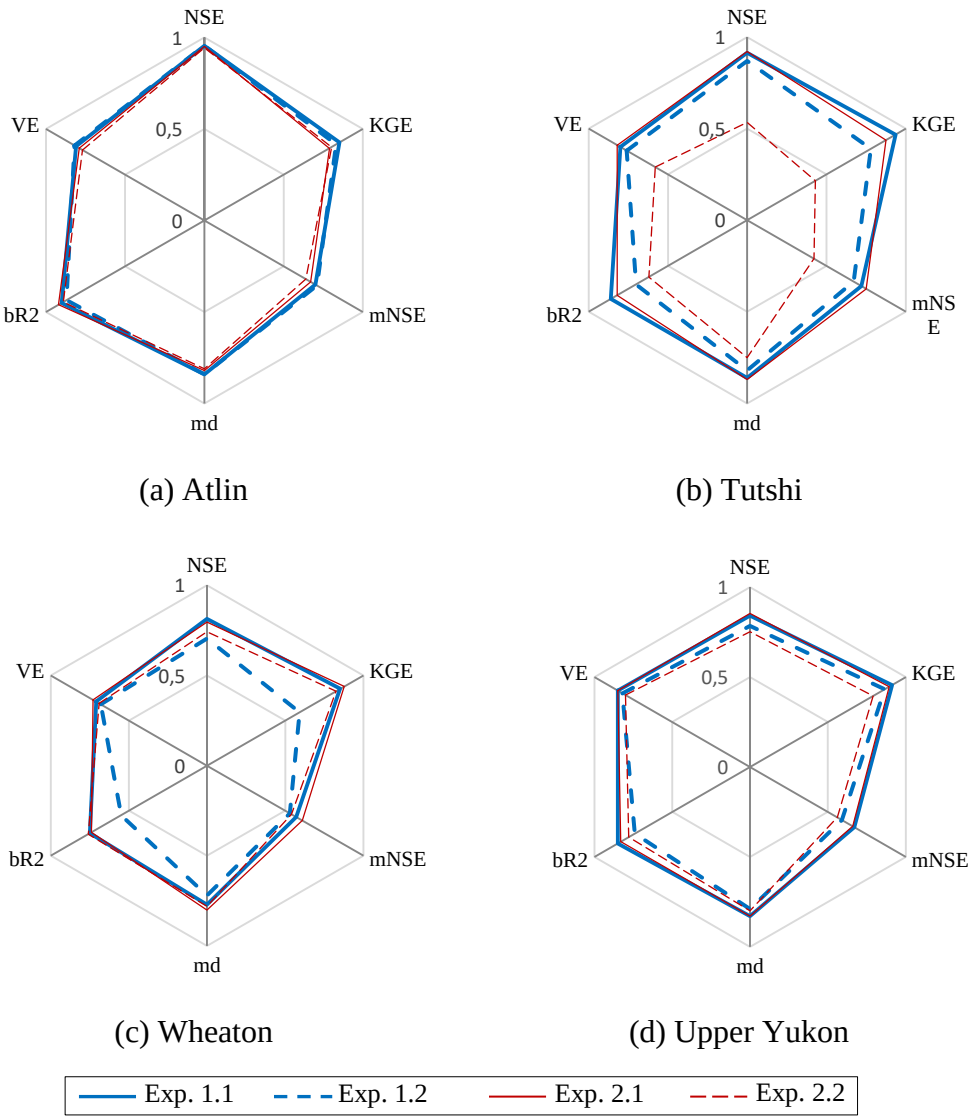

Fig. 7. Radial diagrams for the performance of the model in response to the set of experiments completed in Upper Yukon.

Table 6 summarizes the significance of the snow assimilation routine for each basin for the given meteorological forcing. In short, activating the snow assimilation routine would leave a significant impact on the flow estimation only in Mayo when forcing HYDROTEL with the MSC meteorology and in Aishihik when forcing the model with CaPA-RDPA data. In Yukon, it was shown that the model does not necessarily need the assimilation of snow products when the model is forced with either gauged or analysis precipitation products. Where snow assimilation significantly improves the results, it can be concluded that the corresponding meteorological forcing does not have the expected accuracy for hydrologic modelling purposes, including the assessment of the meteorological network density which is the subject of the next analysis in this study.

Table 6. Significance of the snow assimilation routine in HYDROTEL given the meteorological forcing for each study basin. Basin denominations are in bold, sub-basins are not.

Basin	CaPA-RDPA	MSC meteorology
	✓: Significant / ×: not significant	
Mayo	×	✓
Aishihik	✓	×
Sekulmun	✓	×
Upper Yukon	×	×
Atlin	×	×
Tutshi	×	✓
Wheaton	✓	×

4.3 Network sensitivity analysis

The information gained from the validation stage were used to decide whether the assessments should be undertaken with/without the assimilation of snow course data. The proxy validations indicated that at least in Aishihik, CaPA data do not have the required accuracy, while the validations in the other two basins (Mayo and UY) were promising. Therefore, in Aishihik, the network assessment was carried out while assimilating the snow course measurements. In Mayo and Upper Yukon, no snow assimilation was performed when evaluating the impact of different network scenarios.

Fig. 8 shows the variation of the NSE, KGE, and absolute PBias scores in Mayo with the changing resolution of the pseudo-network scenarios (for a description of the PBias (Percent Bias) score, see the Appendix). As the network resolution decreases (and so does the network density) from 0.10° to 0.35°, the scores go through two distinct areas of variation. First, decreasing the network resolution from 0.10° to 0.30° results in only marginal drop in all three performance scores. In comparison, the performance of the CaPA precipitation products for a network with a given resolution of 0.30° or higher is better than that of the existing meteorological precipitation network. The fluctuations and the unexpected drops in performance scores in this range is an artifact of the spatial variability of precipitation that has not been fully resolved by certain grid points. This phenomenon which is known as singularity has been reported previously by Abbasnezhadi et al. (2019) and Dong et al. (2005). Decreasing the network density below 0.30°, results in substantial performance deterioration to an extent well below the current sparse MSC network. This indicates that the limit at which the CaPA gridded data can outperform the existing network in Mayo is limited to a network with a density of at least 0.30°.

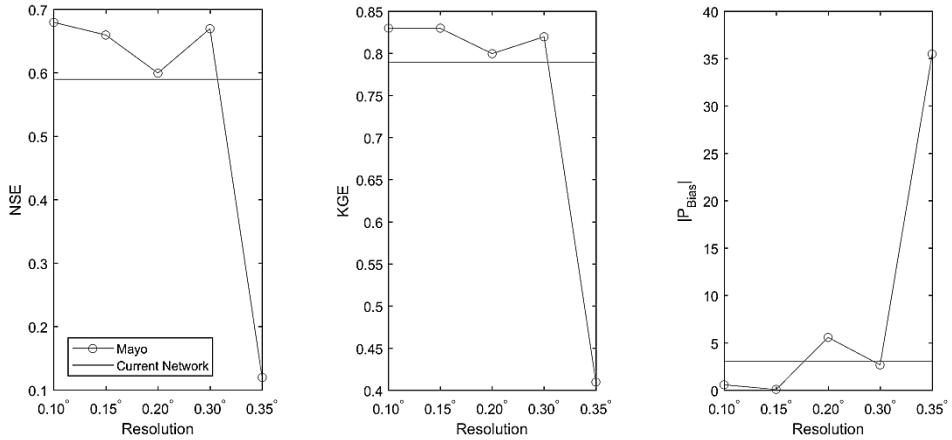

Fig. 8. Variation of the NSE, KGE, and absolute PBias in Mayo with changing network resolution. The existing meteorological precipitation network's performance is also shown.

Fig. 9 displays the variation of the NSE, KGE, and absolute PBias in Aishihik with changing network resolution and compares the performance of the pseudo-network scenarios constructed based on the CaPA grid definition with the existing MSC network in the basin. The same overall trend of variation previously observed in Mayo (Fig. 8) is evident here too where the scores drop (although less abruptly) after negligible changes before the threshold network density. The less sudden drop is an expected attenuation consequence a larger drainage area which is more evidently manifested by the NSE scores which is known to be a sensitive parameter to pick discharge values (see Abbasnezhadi et al., 2019 for the same performance outcome). In Aishihik, the network resolution of 0.4° can be viewed as the network resolution threshold below which the accuracy of the flow simulations degrades significantly. Any higher-density network would cause the scores to level off and little would be gained by further increasing the network density. The threshold network density of 0.4° derived for Aishihik, as shown in Fig. 9, closely resembles the performance established by the existing MSC meteorological network in the basin. Moreover, this threshold value is also slightly higher than the one determined for Mayo. This was an anticipated outcome as in basins with a larger drainage area, representativeness errors are averaged which makes missing a storm event less impactful on the overall network precision. In contrast, in smaller basins (as in Mayo), mesoscale precipitation systems are essentially significant for capturing proper flow statistics. Accordingly, a higher network threshold value can already be anticipated for Upper Yukon which takes an even higher drainage area than that of Aishihik.

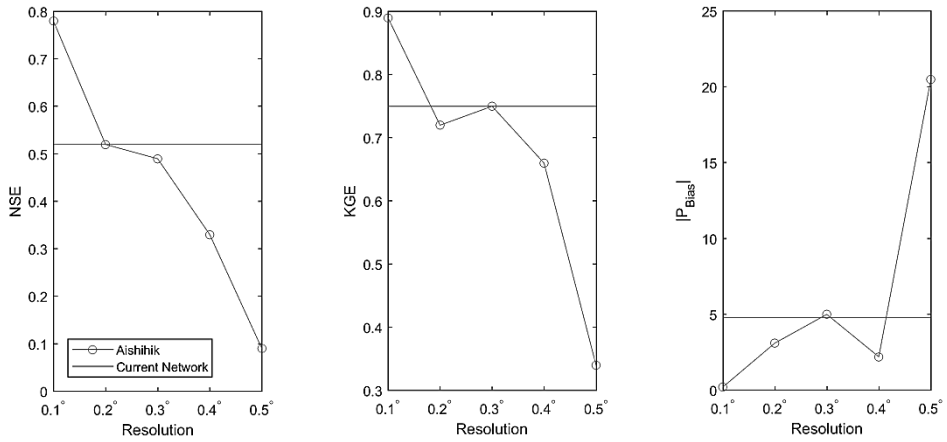

Fig. 9. Variation of the NSE, KGE, and absolute PBias in Aishihik with changing network resolution. The current network's performance is also shown.

As shown in Fig. 10, in the Upper Yukon, the same features previously observed in Fig. 8 and Fig. 9 are apparent while as it was discussed, a higher network threshold value (0.7°) has been resolved. In Upper Yukon, the existing MSC network maintains an accuracy which is comparable in performance to the highest network density of the original CaPA network. A pseudo-network with a density of the threshold value of 0.7° would as such provides a lower performance score.

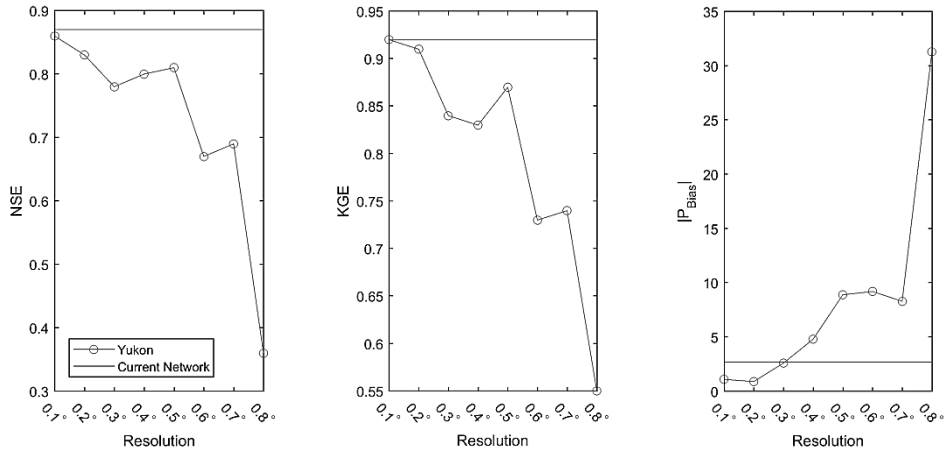

Fig. 10. Variation of the NSE, KGE, and absolute PBias in Upper Yukon with changing network resolution. The current network's performance is also shown.

The network assessment indicates that a number of additional stations can be installed in each basin to increase the accuracy for streamflow forecasting. The locations of these additional stations are shown in Fig. 11. There are already a few active stations operating throughout the region, some located very close to the locations of the proposed extended network; one station in western Mayo, one in southern Aishihik, and two stations in lower-central Upper Yukon. This decreases the number of stations to be added, and a

total of 7 more stations are recommended to be installed in all three watersheds (4 stations in Mayo, 2 in Aishihik, and 1 in Upper Yukon).

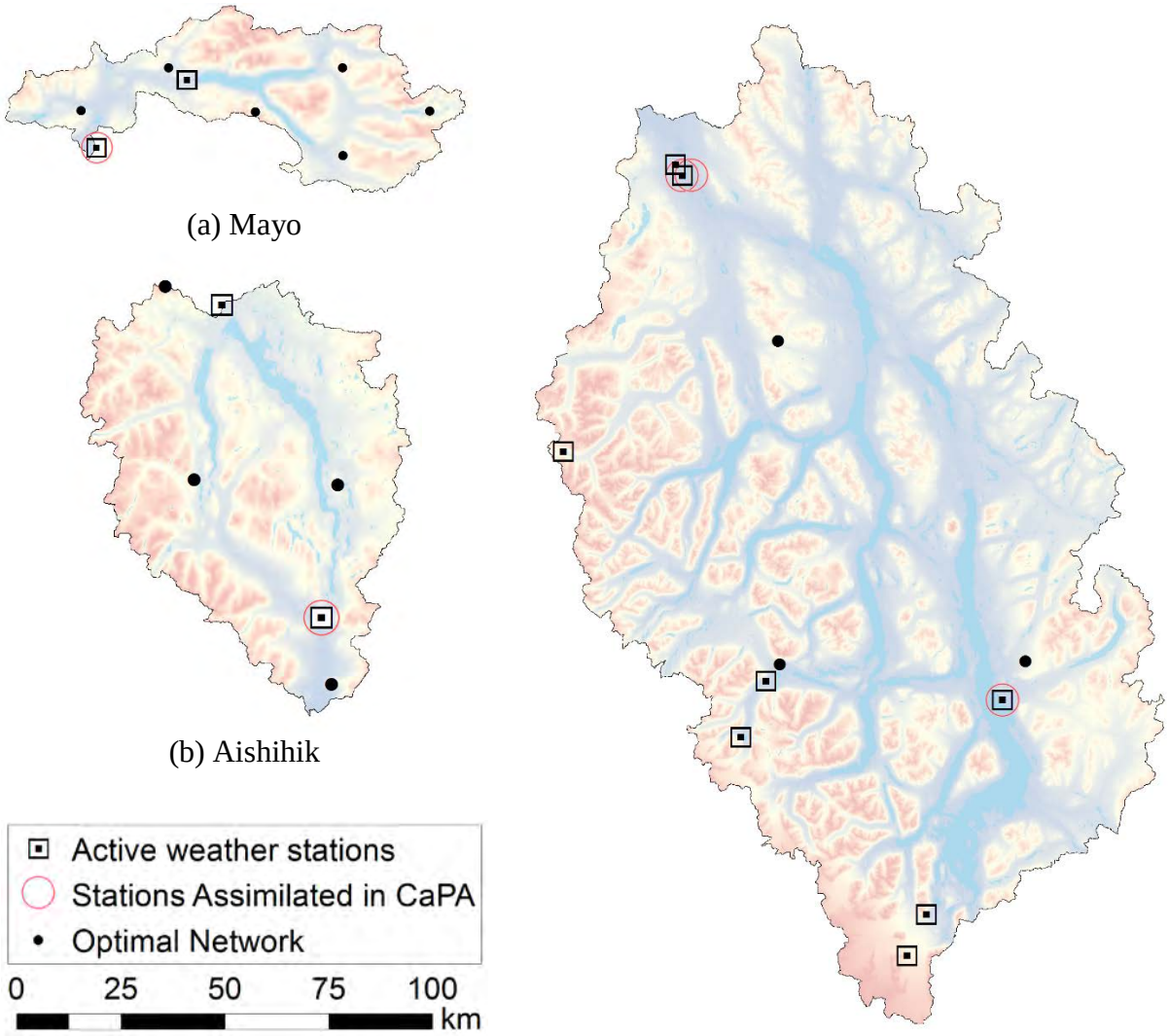

Fig. 11. Optimal network in different sub-basins in Yukon.

5. Conclusions

The physically based semi-distributed HYDROTEL model's snow data assimilation (DA) routine provides the opportunity to investigate the added value of using the CaPA-RDPA data for various applications in major basins of interest to Yukon Energy. The RDPA gridded data were mainly studied for their application in model calibration and meteorological network assessment. With recent upgrades and new developments in the quality of the CaPA products, it was recognized that the past model

calibrations for the major basins in Yukon, including Mayo, Aishihik, and Upper Yukon could be enhanced or confirmed. For this, the HYDROTEL model was calibrated with the CaPA-RDPA used as the precipitation forcing through the application of various toolkits, including VARS and OSTRICH. The opportunity to link HYDROTEL with OSTRICH for the case of this specific study was proved to be highly beneficial for calibrating other basins in Yukon too (e.g. Marsh Lake inflows in the Upper Yukon).

The hydrologic footprint of CaPA-RDPA data and MSC ground observations were validated against hydrometric observations. This validation was performed to examine if assimilating snow monitoring information in HYDROTEL can offset the adverse effects of precipitation data scarcity in Yukon. When snow assimilation could significantly improve the flow simulation outcomes, it was concluded that the corresponding meteorological forcing could not exclusively provide the required accuracy for hydrologic modelling purposes. The proxy validation of the CaPA-RDPA data indicated that the gridded analysis products enjoys the level of accuracy required for accurate flow simulation in Mayo and Upper Yukon which does not entail the application of snow assimilation in HYDROTEL. In Aishihik, however, the validations demonstrated that the regional precipitation analysis does not have the required accuracy, and therefore, assimilation of observed snow course information would have a significant impact on the flow estimation accuracy. Based on the results of these experiments, it can be concluded that although these basins are all located within similar ecoclimatic zones in southern Yukon and in the proximity of each other, the distribution of snow course sites and precipitation gauges have left a substantial impact on the accuracy of precipitation and snow assimilation procedures which directly affect the accuracy of flow simulations. These results indicate the importance of the snow assimilation routine in HYDROTEL.

With the experiments in hand, a network augmentation assessment was carried out subsequently by incorporating the value of data and products available from the CaPA assimilation system. Even though any proposed additional station would probably be equipped with various measuring apparatus for different meteorological variables, the network augmentation assessment was carried out with the objective that the network would be mainly measuring precipitation. This is mainly due to the fact that precipitation demonstrates a lot more spatial variability than other meteorological variables (e.g. temperature, wind).

The assessment indicated that a number of additional stations can be installed in each basin to increase the accuracy for streamflow simulation. It is worth reiterating that the analysis was performed based on CaPA-RDPA data and having real measurements on the ground could prove to require less stations, especially for Aishihik and Mayo. Although based on the analysis, adding more stations to all three basins would result in a better spatial representation of the precipitation fields in the region, it might not be economically conceivable to install them entirely. In this case, the following factors might be considered to direct the investment to install new gauges in the region:

- Combined importance of the basin for flow forecasting and forecasting challenge: In all three basins, adding more stations on the ground could provide pertinent information. However, any basin which is particularly challenging for flow forecasting should be given a higher network augmentation and investment priority. Through the development of the forecasting system, a certain appreciation of the different basin modelling challenges and the importance of the ground measurements were achieved. More specifically, Aishihik and Mayo remain the most challenging basins to forecast while they have a limited number of ground monitoring sites. In Aishihik, there are two stations within the watershed limits; station 2100840 OTTER FALLS NCPC, and the newly added YEC AISHMET station located near Aishihik Village north of Aishihik Lake. In Mayo, there is one station close to the watershed

limits (station 2100701 MAYO AIRPORT) as well as the newly added YEC MAYOMET station located near the outlet of Mayo Lake. In the Upper Yukon, there are fewer challenges in terms of forecasting and it has been revealed that the central portions of the watershed mainly suffer from the lack of ground measurements. It should be mentioned that once a few years of measurements are acquired from the newly added stations, they should be taken into the system for short-term and seasonal flow forecasting.

- Different types of gauging error (e.g. instrumentation error, representativeness error): The network analysis was performed based on an uncontrolled assessment where no observation error was added during the analysis to simulate the impact of such errors (including those related to solid precipitation in winter and convective storms during summer). Instead, CaPA-RDPA data were used directly into the assessment. This rationale was taken since ECCC does all sorts of quality control (QC) with station observations before assimilating them in CaPA, and the RDPA products can be assumed to be relatively error-free. However, the implication of such an assumption is that, the optimal number of gauges derived for each basin is valid when those stations would satisfy CaPA quality control procedures too. In other words, if the quality of measurements available from the proposed extended network can satisfy CaPA QC, they could benefit ECCC CaPA generation procedure too. The main concern would be with snow QC in the sense that solid precipitation is generally underestimated due to wind effects. More specifically, all automated stations are systematically removed in CaPA when temperature reading is below 0°C, while manned stations are rejected only if the 2-m wind speed is above a threshold that depends on the type of shield used with the gauge. For this, the snow QC in CaPA typically leads to rejection of many stations in winter. This ultimately means that adding new stations and augmenting the network may not prove to completely resolve the true distribution of precipitation during winter. It is ultimately beneficial if any additional station which can be directly used for flow forecasting in HYDROTEL may also be used (for the similar purpose) indirectly through the products of the CaPA's assimilation system. It should be reminded that adding new stations would not automatically improve flow or inflow forecasts. However, there is certainly a shortage of ground measurements in parts of each basin and adding new stations can benefit ground measurements and eventually flow/inflow forecasts.

- Pragmatic considerations: Other factors such as accessibility to the location of new gauges are factors of importance in high latitudes.

References

Abbasnezhadi, K. 2017. *Influence of meteorological network density on hydrological modeling using input from the Canadian Precipitation Analysis (CaPA).* PhD Thesis, Winnipeg, Manitoba, Canada: University of Manitoba. http://hdl.handle.net/1993/32177.

Abbasnezhadi, K., A. N. Rousseau, K. A. Koenig, Z. Zahmatkesh, and A. M. Wruth. 2019. "Hydrological assessment of meteorological network density through dataassimilation simulation." *Journal of Hydrology* 569: 844-858. https://doi.org/10.1016/j.jhydrol.2018.12.027.

Andreadis, K. M., and D. P. Lettenmaier. 2006. "Assimilating remotely sensed snow observations into a macroscale hydrology model." *Advances in Water Resources* 29: 872-886. https://doi.org/10.1016/j.advwatres.2005.08.004.

Arulampalam, M. S., S. Maskell, N. Gordon, and T. Clapp. 2002. "A tutorial on particle filters for on-line nonlinear/non-Gausssian Bayesin tracking." *IEEE Transactions on Signal Processing* 50: 174-188. https://doi.org/10.1109/78.978374.

Asadzadeh, M., and B. Tolson. 2009. "A New Multi-objective Algorithm, Pareto Archived DDS." Edited by G. et al. Raidl. *11th Annual Conference on Genetic and Evolutionary Computation Conference (GECCO 2009).* New York, NY: Association for Computing Machinery. 1963-1966. https://doi.org/10.1145/1570256.1570259.

Asadzadeh, M., and B. Tolson. 2013. "Pareto archived dynamically dimensioned search with hypervolume-based selection for multi-objective optimization." *Engineering Optimization* 45 (12): 1489-1509. https://doi.org/10.1080/0305215X.2012.748046.

Barrett, A. P. 2003. *National operational hydrologic remote sensing center snow data assimilation system (SNODAS) products at NSIDC.* Special Rep. 11, Boulder, CO, USA: NSIDC, 19. Accessed December 14, 2018. https://nsidc.org/pubs/documents/special/nsidc_special_report_11.pdf.

Boluwade, A., K.-Y. Zhao, T. Stadnyk, and P. Rasmussen. 2018. "Towards validation of the Canadian Precipitation Analysis (CaPA) for hydrologic modeling applications in the Canadian Prairies." *Journal of Hydrology* 556: 1244-1255. https://doi.org/10.1016/j.jhydrol.2017.05.059.

Boni, G., F. Castelli, S. Gabellani, G. Machiavello, and R. Rudari. 2010. "Assimilation of MODIS snow cover and real time snow depth point data in a snow dynamic model." *Geoscience and Remote Sensing Symposium* (Geoscience and Remote Sensing Symposium) 1788-1791. https://doi.org/10.1109/IGARSS.2010.5648989.

Bouda, M., A. N. Rousseau, B. Konan, P. Gagnon, and S. J. Gumiere. 2012. "Bayesian Uncertainty Analysis of the Distributed Hydrological Model HYDROTEL." *Journal of Hydrologic Engineering* 17 (9): 1021-1032. https://doi.org/10.1061/(ASCE)HE.1943-5584.0000550.

Bouda, M., A. N. Rousseau, S. J. Gumiere, P. Gagnon, B. Konan, and R. Moussa. 2013. "Implementation of an automatic calibration procedure for HYDROTEL based on prior OAT sensitivity and complementary identifiability analysis." *Hydrological Processes* 28 (12): 3947-3961. https://doi.org/10.1002/hyp.9882.

Brabets, T. P., and M. A. Walvoord. 2009. "Trends in streamflow in the Yukon River Basin from 1944 to 2005 and the influence of the pacific decadal oscillation." *Journal of Hydrology* 371 (1-4): 108-119. https://doi.org/10.1016/j.jhydrol.2009.03.018.

Brasnett, B. 1999. "A global analysis of snow depth for numerical weather prediction." *Journal of applied meteorology* 38 (6): 726-740. https://doi.org/10.1175/1520-0450(1999)038<0726:AGAOSD>2.0.CO;2.

Clark, M. P., A. G. Slater, A. P. Barrett, L. E. Hay, G. J. Mccabe, B. Rajagopalan, and G. H. Leavesley. 2006. "Assimilation of snow covered area information into hydrologic and land-surface models and land-surface models." *Advances in Water Resources* 29: 1209-1221. https://doi.org/10.1016/j.advwatres.2005.10.001.

De Lannoy, G. J. M., R. H. Reichle, K. R. Arsenault, P. R. Houser, S. Kumar, N. E. C. Verhoest, and V. R. N. Pauwels. 2012. "Multiscale assimilation of Advanced Microwave Scanning Radiometer-EOS snow water equivalent and Moderate Resolution Imaging Spectroradiometer snow cover fraction observations in northern Colorado." *Water Resources Research* 48: W01522. https://doi.org/10.1029/2011WR010588.

Deacu, D., V. Fortin, E. Klyszejko, C. Spence, and P. Blanken. 2012. "Predicting the net basin supply to the Great Lakes with a hydrometeorological model." *Journal of Hydrometeorology* 13 (6): 1739-1759. https://doi.org/10.1175/JHM-D-11-0151.1.

Dong, X., C. M. Dohmen-Janssen, and M. J. Booij. 2005. "Appropriate spatial sampling of rainfall or flow simulation." *Hydrological Sciences Journal* 50 (2): 279-298. https://doi.org/10.1623/hysj.50.2.279.61801.

Drusch, M., D. Vasiljevic, and P. Viterbo. 2004. "ECMWF's global snow analysis: Assessment and revision based on satellite observations." *Journal of Applied Meteorology* 43: 1282-1294. https://doi.org/10.1175/1520-0450(2004)043%3C1282:EGSAAA%3E2.0.CO;2.

Duan, Q., Gupta, H. V., S. Sorooshian, A. N. Rousseau, and R. Turcotte. 2003. *Advances in calibration of watershed models.* Water Science and Application. Vol. 6. Washigton, D.C.: American Geophysical Union. https://doi.org/10.1029/WS006.

Durand, M., and S. A. Margulis. 2008. "Effects of uncertainty magnitude and accuracy on assimilation of multi-scale measurements for snowpack characterization." *Journal of Geophysical Research Atmosphere* 113 (D2): D02105. https://doi.org/10.1029/2007JD008662.

Eum, H., D. Yonas, and T. Prowse. 2014. "Uncertainty in modelling the hydrologic responses of a large watershed: a case study of the Athabasca River basin, Canada." *Hydrological Processes* 28 (14): 4272-4293. https://doi.org/10.1002/hyp.10230.

Evensen, G. 1994. "Sequential data assimilation with a nonlinear quasi-geostrophic model using Monte Carlo methods to forecast error statistics." *Journal of Geophysical Research* 99: 10143-10162. https://doi.org/10.1029/94JC00572.

Feyen, L., R. Vázquez, K. Christiaens, O. Sels, and J. Feyen. 2000. "Application of a distributed physically-based hydrological model to a medium size catchment." *Hydrology and Earth System Sciences* 4 (1): 47-63. https://doi.org/10.5194/hess-4-47-2000.

Fortin, J. P., R. Turcotte, S. Massicotte, R. Moussa, J. Fitzback, and J. P. Villeneuve. 2001. "A distributed watershed model compatible with remote sensing and GIS data, part 1: description of the model." *Journal of Hydrological Engineering* 6 (2): 91-99. https://doi.org/10.1061/(ASCE)1084-0699(2001)6:2(91).

Fortin, V., G. Roy, N. Donaldson, and A. Mahidjiba. 2015. "Assimilation of radar quantitative precipitation estimations in the Canadian Precipitation Analysis (CaPA)." *Journal of Hydrology* 531: 296-307. https://doi.org/10.1016/j.jhydrol.2015.08.003.

Foulon, É., and A. N. Rousseau. 2018. "Equifinality and automatic calibration: What is the impact of hypothesizing an optimal parameter set on modelled hydrological processes?" *Canadian Water Resources Journal* 43 (1): 47-67. https://doi.org/10.1080/07011784.2018.1430620.

Gbambie, A. B., Poulin A., M. A. Boucher, and R. Arsenault. 2016. "Added value of alternative information in interpolated precipitation datasets for hydrology." *Journal of Hydrometeorology* 18 (1): 247-264. https://doi.org/10.1175/JHM-D-16-0032.1.

Gelb, A. 1974. "Optimal linear filtering." In *Applied Optimal Estimation*, 102-155. Cambridge, MA, USA: MIT Press.

Gupta, H. V., Kling, H., K. K. Yilmaz, and G. F. Martinez. 2009. "Decomposition of the mean squared error and NSE performance criteria: Implications for improving hydrological modelling." *Journal of Hydrology* 377 (1-2): 80-91. https://doi.org/10.1016/j.jhydrol.2009.08.003.

Haghnegahdar, A., B. A. Tolson, B. Davison, F. R. Seglenieks, E. Klyszejko, and E. D. Soulis. 2014. "Calibrating Environment Canada's MESH modelling system over the Great Lakes basin." *Atmosphere-Ocean* 52 (4): 281-293. https://doi.org/10.1080/07055900.2014.939131.

Hanes, C. C., P. Jain, M. Flannigan, and G. Roy. 2016. "Evaluation of the Canadian Precipitation Analysis (CaPA) to improve forest fire danger rating." *International Journal of Wildland Fire* 26 (6): 509-522. https://doi.org/10.1071/WF16170.

Helmert, J., Şorman A. Ş., R. A. Montero, C. De Michele, P. De Rosnay, M. Dumont, D. C. Finger, et al. 2018. "Review of Snow Data Assimilation Methods for Hydrological, Land Surface, Meteorological and Climate Models: Results from a COST HarmoSnow Survey." *Geosciences* 8 (12): 489. https://doi.org/10.3390/geosciences8120489.

Huang, C., A. J. Newman, M. P. Clark, A. W. Wood, and X. Zheng. 2017. "Evaluation of snow data assimilation using the ensemble Kalman filter for seasonal streamflow prediction in the western United States." *Hydrology and Earth System Sciences* 21: 635-650. https://doi.org/10.5194/hess-21-635-2017.

Leisenring, M., and H. Moradkhani. 2011. "Snow water equivalent prediction using Bayesian data assimilation methods." *Stochastic Environmental Research and Risk Assessment* 25: 253-270. https://doi.org/10.1007/s00477-010-0445-5.

Li, D., D. P. Lettenmaier, S. A. Margulis, and K. Andreadis. 2019. "The value of accurate high-resolution and spatially continuous snow information to streamflow forecasts." *Journal of Hydrometeorology* 20: 731-749. https://doi.org/10.1175/JHM-D-18-0210.1.

Liston, G. E., R. A., Sr. Pielke, and E. M. Greene. 1999. "Improving first-order snow-related deficiencies in a regional climate model." *Journal of Geophysical Research* 104: 19559-51567. https://doi.org/10.1029/1999JD900055.

Liu, Y., C. D. Peters-Lidard, S. Kumar, J. L. Foster, M. Shaw, Y. Tian, and G. M. Fall. 2013. "Assimilating satellite-based snow depth and snow cover products for improving snow predictions in Alaska." *Advances in Water Resources* 54: 208-227. https://doi.org/10.1016/j.advwatres.2013.02.005.

Magnusson, J., D. Gustafsson, F. Hüsler, and T. Jonas. 2014. "Assimilation of point SWE data into a distributed snow cover model comparing two contrasting methods." *Water Resources Research* 50 (10): 7816-7835. https://doi.org/10.1002/2014WR015302.

Mahfouf, J. F., B. Brasnett, and S. Gagnon. 2007. "A Canadian precipitation analysis (CaPA) project: Description and preliminary results." *Atmosphere-Ocean* 45 (1): 1-17. https://doi.org/10.3137/ao.v450101.

Matott, L. S. 2017. "OSTRICH: an Optimization Software Tool." Buffalo, NY: University at Buffalo Center for Computational Research. 79. www.eng.buffalo.edu/~lsmatott/Ostrich/OstrichMain.html.

Miller, R. N., M. Ghil, and F. Gauthiez. 1994. "Advanced data assimilation in strongly nonlinear dynamical systems." *Journal of the Atmospheric Sciences* 51 (8): 1037-1056. https://doi.org/10.1175/1520-0469(1994)051%3C1037:ADAISN%3E2.0.CO;2.

Moradkhani, H. 2008. "Hydrologic remote sensing and land surface data assimilation." *Sensors* 8 (5): 2986-3004. https://doi.org/10.3390/s8052986.

Nagler, T., H. Rott, P. Malcher, and F. Müller. 2008. "Assimilation of meteorological and remote sensing data for snowmelt runoff forecasting." *Remote Sensing of Environment* 112: 1408-1420. https://doi.org/10.1016/j.rse.2007.07.006.

Noël, P., A. N. Rousseau, C. Paniconi, and D. F. Nadeau. 2014. "An algorithm for delineating and extracting hillslopes and hillslope width functions from gridded elevation data." *Journal of Hydrologic Engineering* 19 (2): 366-374. http://dx.doi.org/10.1061/(ASCE)HE.1943-5584.0000783.

Piazzi, G., G. Thirel, L. Campo, and S. Gabellani. 2018. "A particle filter scheme for multivariate data assimilation into a point-scale snowpack model in an Alpine environment." *Cryosphere* 12 (7): 2287-2306. https://doi.org/10.5194/tc-12-2287-2018.

Razavi, S., R. Sheikholeslami, H. V. Gupta, and A. Haghnegahdar. 2019. "VARS-TOOL: A toolbox for comprehensive, efficient, and robust sensitivity and uncertainty analysis." *Environmental Modelling & Software* 112: 95-107. https://doi.org/10.1016/j.envsoft.2018.10.005.

Rousseau, A. N., J.-P. Fortin, R. Turcotte, A. Royer, S. Savary, F. Quévy, P. Noël, and C. Paniconi. 2011. "PHYSITEL, a specialized GIS for supporting the implementation of distributed hydrological models." *Water News-Official Magazine of the Canadian Water Resources Association* 31 (1): 18-20.

Saloranta, T. M. 2016. "Operational snow mapping with simplified data assimilation using the seNorge snow model." *Journal of Hydrology* 538: 314-325. https://doi.org/10.1016/j.jhydrol.2016.03.061.

Samuel, J., A. N. Rousseau, K. Abbasnezhadi, and S. Savary. 2019. "Development and evaluation of a hydrologic data-assimilation scheme for short-range flow and inflow forecasts in a data-sparse high-latitude region using a distributed model and ensemble Kalman filtering." *Advances in Water Resources* 130: 198-220. https://doi.org/10.1016/j.advwatres.2019.06.004.

Slater, A. G., and M. P. Clark. 2006. "Snow data assimilation via an ensemble Kalman filter." *Journal of Hydrometeorology* 7: 478-493. https://doi.org/10.1175/JHM505.1.

Strong, W. L. 2013. "Ecoclimatic Zonation of Yukon (Canada) and Ecoclinal Variation in Vegetation." *Arctic* 66 (1): 52-67. https://doi.org/10.14430/arctic4266.

Su, H., Z. L. Yang, G. Y. Niu, and R. E. Dickinson. 2008. "Enhancing the estimation of continental-scale snow water equivalent by assimilating MODIS snow cover with the ensemble Kalman filter." *Journal of Geophysical Research Atmospheres* 113 (D8): D08120. https://doi.org/10.1029/2007JD009232.

Tolson, B. A., and C. A. Shoemaker. 2007. "Dynamically Dimensioned Search Algorithm for Computationally Efficient Watershed Model Calibration." *Water Resources Research* (Water Resources Research) 43 (1). https://doi.org/10.1029/2005WR004723.

Turcotte, R., A. N. Rousseau, J.-P. Fortin, and J.-P. Villeneuve. 2003. "A process-oriented, multiple-objective calibration strategy accounting for model structure." In *Advances in calibration of watershed models*, edited by Q. Duan, H. V. Gupta, S. Sorooshian, A. N. Rousseau and R. Turcotte, 153-163. Washington, D.C.: American Geophysical Union. https://doi.org/10.1029/WS006p0153.

Turcotte, R., J.-P. Fortin, A. N. Rousseau, S. Massicotte, and J.-P. Villeneuve. 2001. "Determination of the drainage structure of a watershed using adigital elevation model and a digital river and lake network." *Journal of Hydrology* 240 (3-4): 225-242. https://doi.org/10.1016/S0022-1694(00)00342-5.

Turcotte, R., L. G. Fortin, V. Fortin, J.-P. Fortin, and J.-P. Villeneuve. 2007. "Operational analysis of the spatial distribution and the temporal evolution of the snowpack water equivalent in southern Québec, Canada." *Nordic Hydrology* 38 (3): 211-234. https://doi.org/10.2166/nh.2007.009.

Turcotte, R., T.-C. F. Filion, P. Lacombe, V. Fortin, A. Roy, and A. Royer. 2010. "Simulation hydrologique des derniers jours de la crue de printemps: le problème de la neige manquante." *Hydrological Sciences Journal* 55 (6): 872-882. http://dx.doi.org/10.1080/02626667.2010.503933.

Wong, J. S., S. Razavi, B. R. Bonsal, H. S. Wheater, and Z. E. Asong. 2017. "Inter-comparison of daily precipitation products for large-scale hydro-climatic applications over Canada." *Hydrology and Earth System Sciences* 21 (4): 2163-2185. https://doi.org/10.5194/hess-21-2163-2017.

Xu, X., S. K. Frey, A. Boluwade, A. R. Erler, O. Khader, D. R. Lapen, and E. Sudicky. 2019. "Evaluation of variability among different precipitation products in the Northern Great Plains." *Journal of Hydrology: Regional Studies* 24: 100608. https://doi.org/10.1016/j.ejrh.2019.100608.

Zhao, K.-Y. 2013. *Validation of the Canadian Precipitation Analysis (CaPA) for hydrological modelling in the Canadian Prairies.* Master's thesis, Winnipeg, Manitoba: University of Manitoba.

APPENDIX

1. Goodness-of-fit Metrics

Below is a list of metrics used for the set of experimentations performed in Sections 4.2 and 4.3.

- **md:** Modified Index of Agreement

The Index of Agreement (d) developed by Willmott (1981) is a standardized measure of the degree of model prediction error, and is given as follows:

$$\mathrm{md} = 1 - \frac{\sum_{i=1}^{N} |O_i - S_i|^j}{\sum_{i=1}^{N} |S_i - \bar{O}| + |O_i - \bar{O}|^j} \tag{1}$$

where, O_i is the observation at time step i, S_i is the simulation at time step i, $\bar{O}$ is the mean observation, j is the exponent used in the computation of the modified index of agreement where the default value of j is 1, and N is the total number of time steps.

md varies between 0 and 1. A value of 1 indicates a perfect match, and 0 indicates no agreement at all. The index of agreement can detect additive and proportional differences in the observed and simulated means and variances. However, it is overly sensitive to extreme values due to the squared differences (Legates and McCabe, 1999).

- **bR2:** Modified Coefficient of Determination

A model that systematically over or under-predicts all the time will still result in good Coefficient of determination (R^2 close to 1), even if all predictions were wrong (Krause et al., 2005). To alleviate this shortfall, the bR2 coefficient allows accounting for the discrepancy in the magnitude of two signals (depicted by b which is the slope of the regression line) as well as their dynamics (depicted by $R2$). The formulation is given as follows:

$$\mathrm{bR2} = \begin{cases} |b| R2 & \text{if} \quad |b| \leq 1 \\ \dfrac{R2}{|b|} & \text{if} \quad |b| > 1 \end{cases} \tag{2}$$

- **NSE:** Nash-Sutcliffe Efficiency

The Nash-Sutcliffe efficiency (NSE) is a normalized statistic that determines the relative magnitude of the residual variance compared to the measured data variance (Nash and Sutcliffe, 1970), and is given as follows:

$$\mathrm{NSE} = 1 - \frac{\sum_{i=1}^{N} [S_i - O_i]^2}{\sum_{i=1}^{N} [O_i - \bar{O}]^2} \tag{3}$$

NSE range from -Inf to 1 and indicates how well the plot of observed versus simulated data fits the 1:1 line. Essentially, the closer to 1, the more accurate the model is.

- **mNSE:** Modified Nash-Sutcliffe Efficiency

The modified NSE is not inflated by the squared values of the differences, because the squares are replaced by absolute values. The default value of j is 1.

$$\text{mNSE} = 1 - \frac{\sum_{i=1}^{N}|S_i - O_i|^j}{\sum_{i=1}^{N}|O_i - \bar{O}|^j} \tag{4}$$

- **VE:** Volumetric Efficiency

Volumetric efficiency was proposed by Criss and Winston (2008) in order to circumvent some problems associated to the Nash-Sutcliffe efficiency. VE ranges from 0 to 1 and represents the fraction of water delivered at the proper time. The formulation is provided as follows:

$$\text{VE} = 1 - \frac{\sum_{i=1}^{N}|S_i - O_i|}{\sum_{i=1}^{N} O_i} \tag{5}$$

- **KGE:** Kling-Gupta Efficiency

This goodness-of-fit measure was developed by Gupta et al. (2009) to provide a diagnostically interesting decomposition of the Nash-Sutcliffe efficiency (and hence MSE), which facilitates the analysis of the relative importance of its different components (correlation, bias and variability) in the context of hydrological modelling. KGE ranges from -Inf to 1, and is given as follows:

$$\text{KGE} = 1 - \text{ED} \tag{6}$$

Where, ED is the Euclidean distance of α, β, and r from the optimal point of unity in a three-dimensional space, as follows:

$$\text{ED} = \sqrt{(\alpha - 1)^2 + (\beta - 1)^2 + (r - 1)^2} \tag{7}$$

in which,

- α: the ratio between the standard deviation of the simulated values and the standard deviation of the observed ones.
- β: the ratio between the mean of the simulated values and the mean of the observed ones.
- r: the Pearson product-moment correlation coefficient.

- **Pbias**: Percent Bias

Pbias values are the Percent Bias between simulation and observations. It is a measure for the average tendency of the simulated values to be larger or smaller than the observed ones. The optimal value of Pbias is zero (i.e. small values of the Pbias indicate accurate model simulation). The formulation is given as:

$$\text{Pbias} = 100 \times \frac{\sum_{i=1}^{N}(S_i - O_i)}{\sum_{i=1}^{N}(O_i)}$$

Positive values indicate overestimation bias and negative values indicate underestimation. The absolute value of Pbias is zero, however, the absolute value of Pbias only demonstrates the percentage of bias in either direction.

References

Criss, R. E., and W. E. Winston. 2008. "Do Nash values have value? Discussion and alternate proposals." *Hydrological Processes*, 22: 2723-2725. https://doi.org/10.1002/hyp.7072

Gupta, H. V., H. Kling, K. K. Yilmaz, and G. F. Martinez. 2005. "Decomposition of the mean squared error and NSE performance criteria: Implications for improving hydrological modelling." *Journal of Hydrology* 377 (1-2): 80-91. https://doi.org/10.1016/j.jhydrol.2009.08.003

Krause, P., D. P. Boyle, and F. Base. 2005. "Comparison of different efficiency criteria for hydrological model assessment." *Advances in Geosciences* 5: 89-97. https://doi.org/10.5194/adgeo-5-89-2005

Legates, D. R., and G. J. McCabe Jr. 1999. "Evaluating the Use of Goodness-of-Fit Measures in Hydrologic and Hydroclimatic Model Validation." *Water Resources Research* 35(1): 233-241. https://doi.org/10.1029/1998WR900018

Nash, J. E., and J. V. Sutcliffe. 1970. "River flow forecasting through conceptual models, Part I -A discussion of principles." *Journal of Hydrology* 10 (3): 282-290. https://doi.org/10.1016/0022-1694(70)90255-6

Willmott, C. J. 1981. "On the validation of models." *Physical Geography* 2: 184-194. https://doi.org/10.1080/02723646.1981.10642213

2. Network Assessment Scenarios

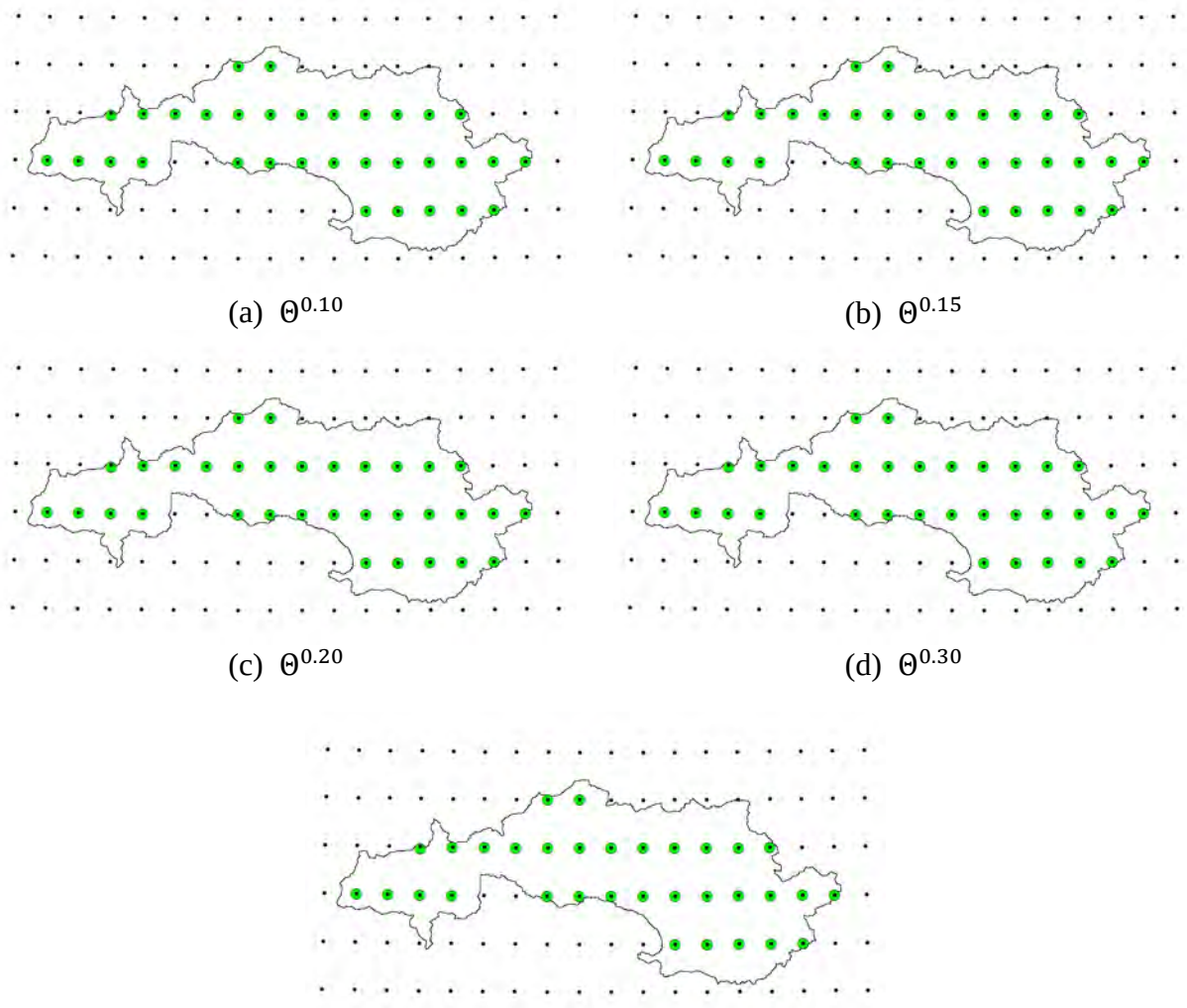

(a) $\Theta^{0.10}$ (b) $\Theta^{0.15}$

(c) $\Theta^{0.20}$ (d) $\Theta^{0.30}$

(e) $\Theta^{0.35}$

Figure 1. CaPA grid points (small black dots) overlaid by the network assessment scenarios (large green dots) in Mayo.

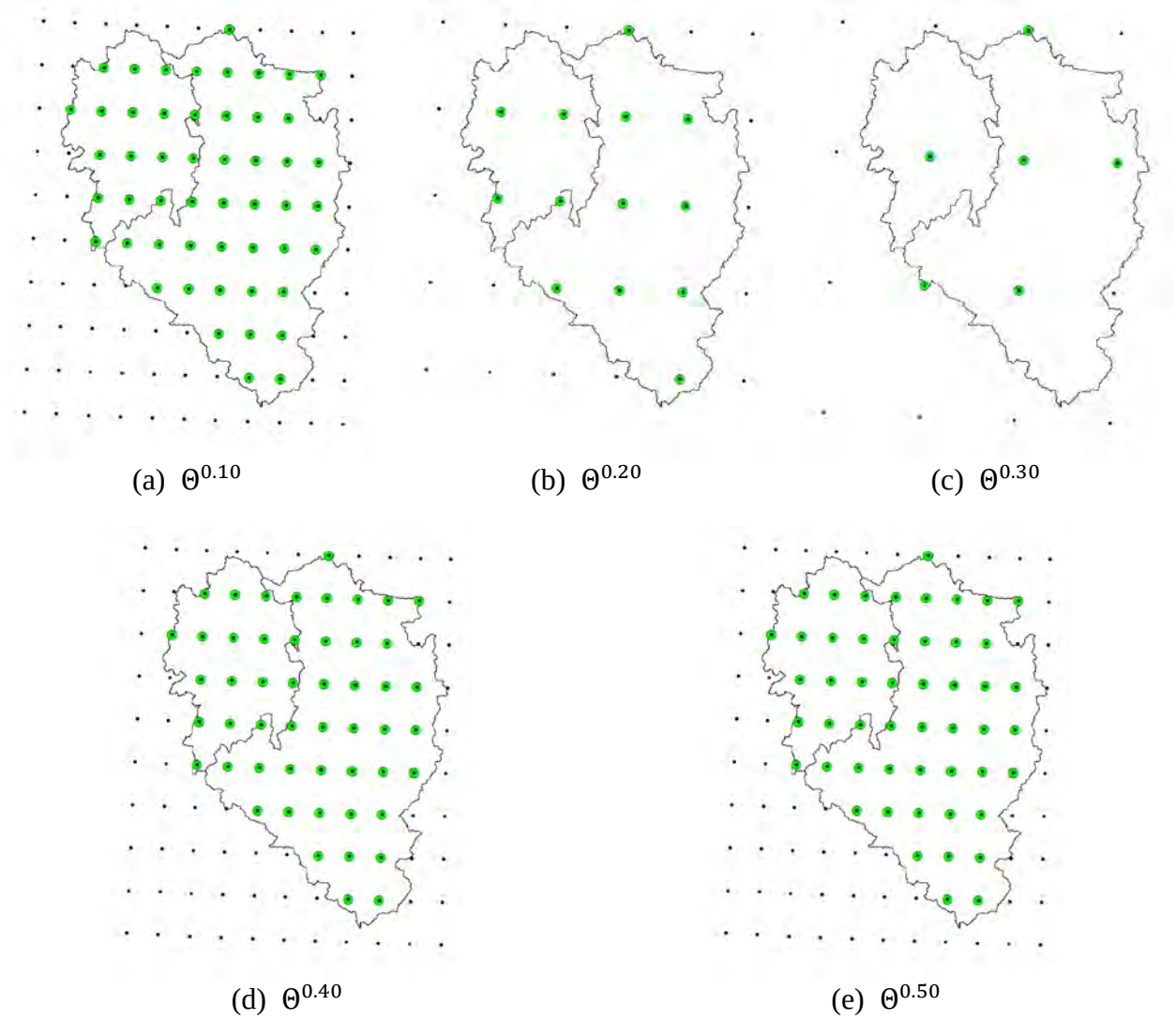

(a) $\Theta^{0.10}$ (b) $\Theta^{0.20}$ (c) $\Theta^{0.30}$

(d) $\Theta^{0.40}$ (e) $\Theta^{0.50}$

Fig. 2. CaPA grid points (small black dots) overlaid by the network assessment scenarios (large green dots) in Aishihik.

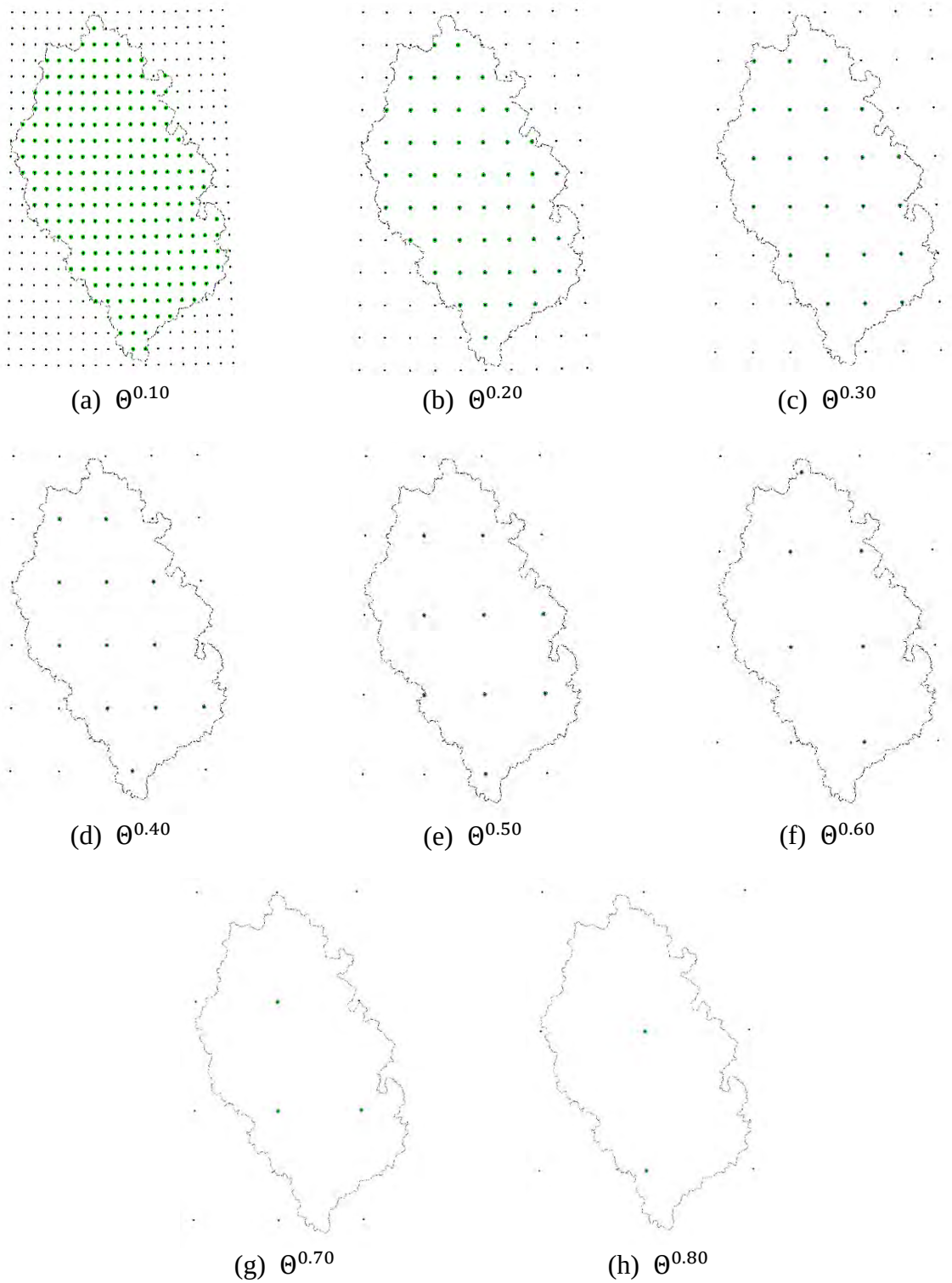

(a) $\Theta^{0.10}$ (b) $\Theta^{0.20}$ (c) $\Theta^{0.30}$

(d) $\Theta^{0.40}$ (e) $\Theta^{0.50}$ (f) $\Theta^{0.60}$

(g) $\Theta^{0.70}$ (h) $\Theta^{0.80}$

Fig. 3. CaPA grid points (small black dots) overlaid by the network assessment scenarios (large green dots) in Upper Yukon.

Appendix III External Evaluation

Discussion Thread for External Review - Comments and Questions

1) Long Term Annual Inflow

Comment or Question - D. Smith	Response – A. Rousseau
1.1) Long range forecasts are for long range energy planning which is all about developing strategies for reliable delivery of adequate volume of energy to meet future annual system load. The essential performance measure of interest in planning studies is annual volume of energy. And the annual volume of energy delivered by a hydro system is directly dependent on the annual volume of runoff. Therefore, the most appropriate measure for long term forecasting skill is the annual volume of runoff. The timing of the inflow within the year is of secondary interest, especially for hydro systems with sizable storage. 1.2) Model calibration for long term forecast must emphasize replicating annual runoff volumes in the calibration and verification periods. The better the hind casts of annual runoff volume, the higher the confidence in long range forecast for energy budgeting purposes. A comparison of the annual depth of runoff for each year of actual and hind cast runoff for all watersheds would be valuable. (See $Runoff_{year}$ (mm) in Table 2.10 for 2010-2018 and Table 2.11 for 2016 only, (R1831). 1.3) I would like to see comparisons of forecast and observed runoff expressed as (mm/yr) for each year of in the period of record for calibration, verification and reporting in long term simulations.	In the final version of the project report which will be submitted to YEC later on this spring, Table 2.10 introduces average observed and simulated annual runoff heights for the calibration period of 2010-2018.

Comment or Question - D. Smith	Response – A. Rousseau
1.4) In Table 2.10 for Sekulmun River, Aishihik Lake, and Mayo Lake I was able to replicate the statistical measures NS, Runoff (MM)/year, PBIAIS except for NS for Aishihik Lake. I got NS = 0.66 as oppose to your value of 0.53. This 0.66 would put Aishihik Lake into the "Good" ranks.	*Did you use the values of Table 2.11 to compute the NS coefficient? If so that is why results do not match. NS was computed using daily discharges as follows:* $$NS = 1 - \frac{\sum_{i=1}^{n}(Q_{obs} - Q_{sim})^2}{\sum_{i=1}^{n}\left(Q_{obs} - Q_{obs,mean}\right)^2}$$ *Where Q_{obs} represents the observed flow or reconstructed inflow, Q_{sim} the simulated flow or inflow, $Q_{obs,mean}$ the mean observed flow or reconstructed inflow from day 1 to (n) number of days (daily time step).* *In Table 2.10 all the results are based on daily flows/inflows comparison. We are not using the annual runoff of Table 2.11 to produce the statistical indicators.*
1.5) That is correct. I was using data from Table 2.11 as my sample. I was using Table 2.10 to check that my calculations of averages were consistent with yours. I also calculated NS and PBIAS on the 2.11 sample and noticed that these performance measures were all very close to your 2.10 values for NS and PBIAS except for Aishihik which was "better" as noted above. I was not expecting such close agreement.	*Table 2.12 now emphasizes the impact of data assimilation on year 2018; we point out that it would not be possible to perform data assimilation for long term Hindcast period. In addition, Table 2.11 presents observed and simulated annual runoff heights for the 1981-2018 period. As mentioned before such table would benefit to seasonal forecast. All the aforementioned tables can be found at the end of this Appendix.*
1.6) I understand that data assimilation is not relevant to hindcasting. The observed and simulation data in Table 2.11 is what I asked for. However, in retrospect I should have asked for water year (October to September) totals instead of calendar year total depths. Monthly values would be acceptable if those would be easier to generate.	*In Yukon, water year or calendar year give similar results, but here we have produced the corresponding results (seeTable 2.12 in this document). A table with monthly value from 1981 to 2018 would be very long and not very helpful, but we have built graph with monthly streamflow/inflow values (see Figures 2.14, 2.15 and 2.16 in this document) for the 1981-2018 period.*

1.7) These additional tables and figures are exactly what I was looking for. Thanks.	
1.8) Note, that watersheds in Table 2.11 which have missing data for some calendar years, have incorrect volumes for the corresponding hydrologic years in Table 2.12. See missing records for: Mayo 1983 Tutshi 1995 – 2000, 2015 Atlin 2016, 2018	Tables 2.11 and 2.12 are now up to date and corrected.

2) Calculated Inflows into Lake Storage.

Comment or Question - D. Smith	Response – A. Rousseau
2.1) Calibration hydrographs of inflow into Sekulmun, Aishihik and Mayo lakes reservoirs all show high short term volatility. These inflows are derived from reservoir levels and the calculated inflows inherit similar high volatility of the water level data. Small errors in reservoir levels produce large errors in runoff inflow into reservoirs. This high level of noise in the streamflow level data is due in part to the limited resolution of level measuring equipment which is probably in the order of +/- 2 mm under ideal conditions. Stage-storage curves for reservoirs are typically very flat i.e. small change in level produces a large change in inflow/outflow. Error of +/- 2 mm over the area of these large lakes represents a large volume of water. Wind induced waves and surges also aggravates accurate level measurements. 2.2) Note, that WSC water level data is recorded with 4 significant digits while discharge data is reported in 3 significant digits. This creates more systematic noise as the calculated inflows are subjected to round off or not. 2.3) Aishihik Lake is impacted by these noise sources on both its calculated inflows from	*As part of the project timeframe we have not been made aware of any gauge (reservoir or stream level) quality control review. For inflow calculations, stream gauge measurements especially impact Aishihik Lake. We suggested to YEC to use the Aishihik Lake outflow that goes through the butterfly valve measurements for inflow calculation. As this would require to recalibrate the valve rating curve, this suggestion has not been followed up so far by YEC. We have stressed this would be the easiest solution to ensure as accurate as possible inflow calculations. We tested using Aishihik Lake outflow measurements as is, but results remained similar (as much inter-daily variability).*

upstream at Sekulmun Lake as well as its calculated outflows. 2.4) Was there a quality review of WSC stream gauge performance in this project? If so did it include the history of rating curve evolution for each gauge? Changes in stream morphology can change the calibration accuracy of the rating table for the gauge. Frequent rating table revisions implies more gauge error.	
2.5) Thanks, this is good background information for me. I do not have schematics of any of these facilities. Using a valve for flow measurements is a good idea. How often is this valve operated?	*We actually do not know how YEC operates the valve at the outlet of Aishihik Lake. We would assume that it could be mimicked if we knew the electric demand since YEC has always mentioned to us that the Aishihik hydroelectric plant acts as a swing plant.*
2.6) In R1831, pp 43, you briefly describe a 3-day moving average procedure for computing reservoir inflows from gauge levels using Eq 2.1 through Eq 2.6. How was the average level calculated for each day? These level gauges record continuously. Standard on-line Water Survey of Canada downloadable records are reported at 5 minute clock intervals. How were these records integrated to get the average for the day? How effective is this moving average procedure at reducing spurious variability in levels and inflows?	*To cover the 1981-2018, YEC provided us with daily water level averages for both Aishihik Lake and Mayo Lake. Based on these daily averages (no intra-daily variability) daily volume variations were computed. Since the inter-daily variability was too high, we based our computation on a 3-day moving average of daily water level. This method reduced the inter-daily variability of inflows as well as the number of occurrences of negative inflows.*
2.7) This is clearer but inconsistent with explanations in R1831 which says you "adopted a calculation procedure based on the three-day *water level* average." You used average levels provided by YEC and you don't know how these "average daily levels" were calculated. These reservoir levels were converted to storage volume and then daily change in volume was used to calculate inflow for each day. A three day moving average of these inflows to filter out much of the inter-day volatility.	*What is the question exactly? Anyhow, our understanding is based on the fact that the data used to compute the daily volumes are the daily water level and to our knowledge YEC computes a geometric mean to obtain a daily water level. The method of computation being the lake stage-storage curve.*
2.8) Conceptually I understand the process for computing lake inflows and that it is based on average daily lake levels that are provided by YEC. What is not clear is	

exactly how these data are sampled, measured, and averaged over the day. This is a question for YEC.	
2.9) As an alternative, I would suggest that the next calibration update use a more explicit method of filtering the noise in these records of reservoir levels. Fourier analysis has the ability to remove the high frequency waves from a time series of level records and leave the low frequency (slow changing) harmonics that are better estimates the real storage inflows/outflows. This should be reasonably easy to implement but will likely require custom tuning for each time series.	*For the historical period of 1981-2018, daily water level or flow averages were provided. Averaging already filters out intra-daily variability, but it is true that other filtering techniques could be used. Nonetheless, inter-daily inflow variability is not due to intra-daily water level variability, but rather to day-to-day volume changes. As such using a different filtering techniques would not automatically result in a reduction of inter-daily inflow variability.* *To go further, the following Table 1 introduces the RMSE and correlation coefficient R between daily inflows and daily inflows computed from averaged daily volumes over two (2) to seven (7) days. Since the idea of using the average is to reduce variability while staying as close as possible to true values, we considered using either the 2- or 3-day moving average. Since the calibration of the hydrological model (on discharges/flows) for Aishihik Lake worked well with a 3-day moving average only, the 3-day moving average was chosen. Tables 2 and 3 below show that the averaging of daily water levels does not have the same impact in terms of loss of information for Marsh Lake and Mayo Lake. Indeed correlation coefficients remain high, RMSE remain well below half a standard deviation, and PBias is close to null.*
2.10) The r values in this Table 1 are not as good as those for Marsh and Mayo Lakes as you have noted. I would expect Aishihik to have higher r value than the other 2 just because it is larger than both of them. Larger lake, more inertia, higher serial correlation.	*You are right in principle, but your rationale does not account for the real problem being the location of the sensor monitoring the water level which measures those insane 5 min variations (due to either wind/waves or simple mechanical oscillation of the lake system). On the other hand, we assume that if the major source of inflow to a Lake comes from an upstream river that drains a large basin like Marsh Lake, there should be less inter-daily variation of the inflow when compared to the drainage area of Aishihik Lake or Mayo Lake. In other words, it is not the size of the lake as much as the*

	drainage area that induce inertia. Food for thoughts.

Table 1: Inflow computation from averaged-daily volumes at Aishihik Lake

	Inflows	2-day average	3-day average	4-day average	5-day average	6-day average	7-day average
RMSE		8.0	9.4	9.9	10.2	10.3	10.4
R		0.81	0.73	0.70	0.69	0.68	0.67
Pbias		-10.3	-15.8	-19.1	-20.9	-21.9	-22.7
Std	13.5						

Table 2: Inflow computation from averaged daily volumes at Marsh Lake

	Inflows	2-day average	3-day average	4-day average	5-day average	6-day average	7-day average
RMSE		35.2	47.0	52.7	56.7	60.1	63.2
R		0.99	0.98	0.97	0.97	0.96	0.96
Pbias		-0.2	-0.3	-0.3	-0.4	-0.4	0.4
std	215						

Table 3: Inflow computation from averaged daily volumes at Mayo Lake

	Inflows	2-day average	3-day average	4-day average	5-day average	6-day average	7-day average
RMSE		4.2	5.4	6.1	6.7	7.2	7.7
R		0.97	0.96	0.95	0.93	0.92	0.91
Pbias		-1.4	-2.0	-2.2	-2.4	-2.4	-2.4
std	18.5						

	Also, we should keep in mind that the forecasting system requires daily data only.
2.11) Fourier Analysis: A test of Fourier analysis was done on a small sample of reservoir level data (the first 2 days of 5 min data in January 2019 for 08AA008 Outlet of Sekulmun Lake extracted from WSC). Figure 1 shows the sample filter results. The variance is reduced by a factor of 10 in this sample. Sekulmun Lake is the least noisy of the three so I would expect even better variance reduction for these other three.	
2.12) For Figure 1 below, 5 minute level data was used as a demo to test the Fourier analysis method using Excel. I was aiming for filtered start of day levels as the key output. I got	*We agree that a Fourier analysis of reservoir level data would be one of the solution to filter out unwanted variability (due to wind, waves, mechanical high frequency resonance). However, as*

bogged down in programing and left it as is in Figure 1. 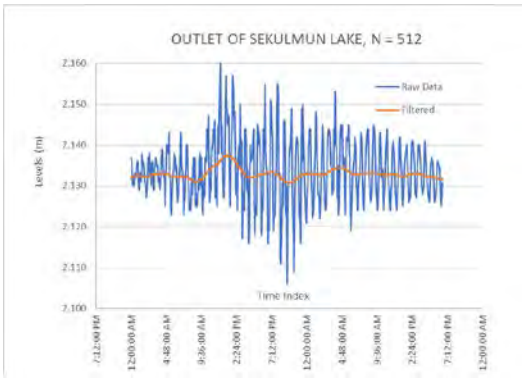 Figure 1: Sample Fourier Analysis for Sekulmun Lake Outlet 5 min level data.	*Perreault et al. (1995) demonstrated, this is a method designed to compute and validate natural inflows to a lake. Since our objective was to calibrate a hydrological model and use data assimilation to correct inflow or stream flow modeling, we did not implement a method based on Fourier analysis. Besides, this would be, in our opinion, another way to approach the problem entirely and would require substantial research work.* *Perreault L., Roy R., Mathier L., and Bobée B. (1995) La combinaison de modèles appliquée à la validation en temps réel des apports naturels aux réservoirs hydriques. Can J. Civ. Eng.* ***22****: 934 – 94*
I didn't intend for you to launch a recalibration of you model. I think your model forecast results are excellent. It's the observed flows for #0000003 that are puzzling. They are so noisy. I suggested using Fourier analysis too explicitly filter these observed flow records to get rid of the extraneous noise. I like this method because I can relate to the physics of what really needs to be filtered out. The moving average method basically adds more data to estimation and spreads the uncertainty over time. I'll find out how YEC did their averaging.	*This figure proves our point, average computed over the filtered or raw data would basically be about the same and would not reduce day-to-day volume changes.*
	We have to be very cautious here because we are not talking about lake outflows that could have a more inertia. Lake inflow should have on the other hand a daily variation due to precipitation or melting. Obviously, here we have too much variations (i.e., spikes), but we are starting to believe that inflows should have inter-daily variation and should not look as filtered as presented… Again, we can smooth daily water levels, but we will still have high inter-daily variation in term of inflows…

3) **Clarification on Eq A.3, Aishihik Lake Stage-Storage Curve** [2]	
3.1) For Aishihik Lake stage-storage curve, I expected these two polynomial equations for L < 915 and L>= 915 m in Eq A.3 to give the same volume at L = 915 m but got a large difference instead. I also noticed that there is no order 1 (one) term in the polynomial for the L< 915 m case. The highlighted text below is my estimated revision to correct for the disagreement between these two polynomials at L = 915 m. I suspect this is a reporting error in Ref 2 and does not affect the model results. Please confirm that this is so.	*We verified the whole procedure that was established for Inflow calculation for Aishihik Lake and we did see a small difference (0.011%) at the 915 level. Based on how the equation was established, it is perfectly normal to see a different result for L = 915 m. The first polynomial equation (6th order without intercept) was determined with 16 points (level / incremental volume couples) from levels 912 m to 915 m, however it is not valid for L=915 as stated by the condition (L <). The second polynomial equation (4th order with intercept) was determined with 6 points (level / incremental volume couple) from level 915 m to 916 m. Both polynomial equations where determined by YEC using the least-squares method independently. Consequently it is normal to see slight differences for a specific level. We could include a continuity condition at the expense of a better fit, therefore we did not recommend it.*

Figure 3: Equation A.3 – Stage Storage Curve for Aishihik Lake

When L < 915

$$V = -38{,}627.31\,L^6 + 678{,}170.61\,L^5 - 3{,}270{,}008.00\,L^4 + 6{,}352{,}008.56\,L^3 - 3{,}111{,}511.38\,L^2 + 134{,}383{,}853.50\,L^1 + 7{,}657{,}633.28$$

When L >= 915

$$V = -50{,}827{,}494.83\,L^4 + 731{,}085{,}628.63\,L^3 - 3{,}932{,}429{,}415.76\,L^2 + 9{,}545{,}583{,}654.41\,L - 8{,}448{,}705{,}648.59$$

There are actually two different versions of this equation in the material you provided:

Version 1: Page 25 in file "Training November 2019 INRS_YEC_YC_2019_11_05.pptx"

Version 2: Page 42 Eq 2.3 in file "IINRS_2nd_Year_Progress_Report_R1831_v2.pdf"
Page 218 Eq A.3, in Ref 2, file "Samuel_et_al_2019_ADWR.pdf"
Page 41, Eq 3, in "R1768"

We are sorry for the confusion here, there is an error in version 2… There is a L term missing

Here's what they look like. Which one is used in your process?	*after the coefficient 134,383,853.50…see part of the above equation highlighted in yellow. Our final report which will be delivered to YEC at the end of April presents the right equation.*

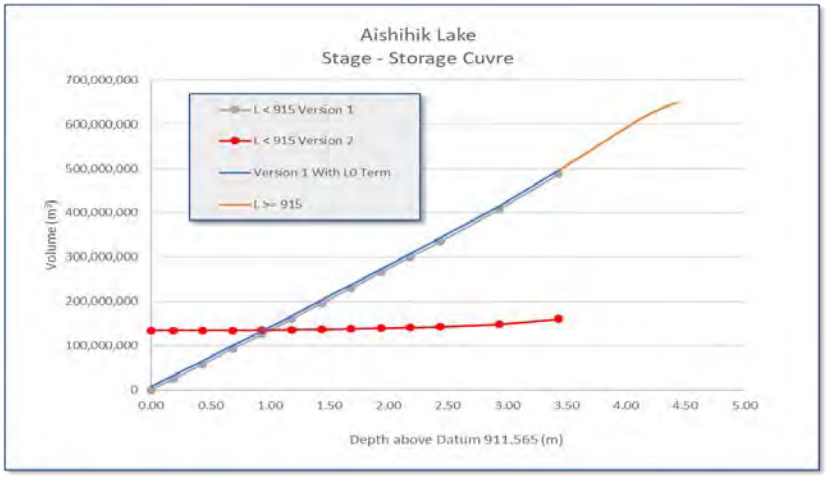

4) Climate Change versus Observed Lake Inflows

Comment or Question - D. Smith	Response – A. Rousseau
4.1) Figure 3 Climate change impact on the annual runoff [mm] at Aishihik Lake from 1981 to 2070 and Figure 6 for Mayo Lake (not shown) from *Technical note Climate Changes Impacts;* these figures show higher volatility for historical observations versus climate change model results. You explained this in our meeting in November but I did not capture it in my notes. Why are these so different?	*We have replaced this figure in the preliminary version of our Final Project Report that will be submitted later on this spring. To display uncertainty, it was replaced with the following figure, which now includes a band of climate change centiles (10-90th).* *Climate change scenarios capture part of the observed variability at the exclusion of "extreme values". Our understanding is that climate change scenarios capture average current climate conditions, but tend to fail to reproduce the local patterns inducing the extremes. One can also note that climate change scenarios are not meant to reproduce specific or individual year conditions, but rather larger period tendencies (30-50 yr-time spans) Moreover, climate change scenarios data do not account for observation errors that can very well be in the order of 10%.*

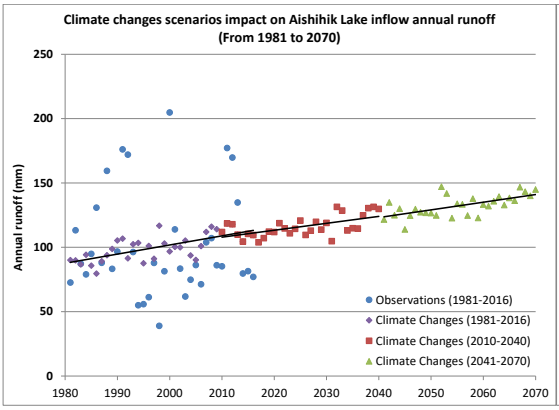

Figure 6.3 from R1831.

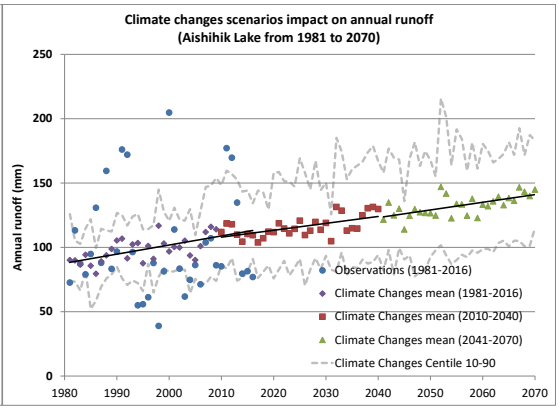

Figure 6.6 Replacement

Comment or Question - D. Smith	Response – A. Rousseau
5) Giltana Creek Near the Mouth WSC Station 08AA009 5.1) Was this station used in the calibration process? It is unregulated and is within the Aishihik watershed and looks like it has good clean data. I'd like to see some comparisons of observed versus modelled flows for this station. This station could be a good indicator of runoff response for the watershed as a whole. Due to its relatively small drainage area, it will respond quicker to changing weather conditions. It will also be indicative of the performance of all similar ungauged areas throughout Aishihik.	*AR This station was not used for the calibration process, because it has no impact on the inflows to Aishihik Lake. It is only used for the inflow calculation process.* *Similarly, the Sekulmun River station (Station 08AA008) has no impact on lake inflows. We tested the calibration over this upstream sub-watershed and got calibration objective function values above 0.9.* *Calibration results for Giltana Creek Near the mouth (WSC Station 08AA009) are expected to be as good, but we deemed this exercise unnecessary as it would neither have an impact on Aishihik Lake inflow calibration nor on the forecasting system.*
5.2) I understand that you didn't use Giltana gauge for calibrating the Aishihik model because it is not in Aishihik Lake watershed. But I still would like to see forecasted flows at this gauge. This creek contributes YEC's hydro system downstream so sooner or later it will be included in an operational inflow forecast model covering all of YEC's watersheds. How much effort is required to setup new reporting nodes in this HYDROTEL model? Kevin and I could do this as a training exercise.	*AR At this stage of the project and how the system is set up, it is not possible to forecast flows for Giltana Creek, This creek has a drainage area of 192 km² and an average flow of 0.62 m³/s which is one order of magnitude smaller than Aishihik River below Aishihik Lake which has a drainage area of 3315 km² and an average flow of 9.1 m³/s. But it is true that Giltana creek contributes to Aishihik Plant. Considering the current architecture of the forecasting system, it is impossible to add a third component for a watershed. Moreover, Giltana Creek would need to be an independent watershed.*

	Building/adapting the forecasting system to include this watershed would require about 2 months-worth of work including weekly guidance from INRS and the budget that would need to come along.
5.3) Note, WSC has the gross drainage area for Aishihik River below Aishihik Creek at 3,000 km². I assume your drainage areas are based on better mapping then what WSC may have. What is the gross drainage area of #0000003? And what is the gross drainage area to Canyon Lake outlet?	*AR We have remapped the entire Aishihik watershed based on a 30-m DEM using our in-house Hydrological GIS PHYSITEL which is used to set up HYDROTEL. Thus, for the #0000003 gauge station, that is the outlet of Aishihik Lake, we have a drainage area of 2922 km² while the drainage area at the outlet of Canyon Lake is 3170 km².*
5.4) What is an "independent watershed"? Is Sekulmun River (08AA008) an independent watershed?	*AR Independent not from a hydrological point of view, but given the architecture of the forecasting system program, Giltana creek would need to be represented as a specific watershed, thus the use of the "independent" adjective.*
5.5) Why was the outlet of Aishihik Lake selected for forecasted flows instead of Canyon Lake outlet?	*The system predicts inflows to Aishihik Lake, not the flows going out of Aishihik Lake. Flows that goes out of it. This common engineering practice as the Lake does not discharge freely, it is controlled by the demand for electricity – it is a hydroelectric reservoir, thus a managed reservoir.*

6) HYDROTEL Model Calibration 6.1) I agree with your assessment of HYDROTEL calibration. These results indicated that at sites #08AA008 (Sekulmun River, Aishihik), ##0000003 (Mayo), and #0000003 (Aishihik Lake), the performance of the forecasting system shows a high, medium, and low degrees of accuracy, respectively. This is based on a calibration sequence from 2010 to 2016. Now there is another 3 years of historical record which should be used to improve the estimates of performance measures. I think if the high frequency noise can be removed from the lake inflow/outflow calculations there will be a significant improvement in the performance metrics.	*AR For the latest calibration of HYDROTEL performed in late 2019, we used 2010-2018 data. Regarding Aishihik or Mayo Lake inflows, variability is related to inter-daily variation of the lakes water volumes as inflow calculations include daily comparison of lake water volumes.* *We would like to take the opportunity here to remind that in our opinion, the best option would be to make outflow measurement at the outlet of Aishihik Lake using the butterfly valve.*

6.2) I haven't seen any of the hydraulic components at the Lake's outlet but using a valve for measuring outflows seems reasonable.	
6.3) Calibration results for all basins have improved substantially with longer calibration period to end of 2018. Was there any other changes to the calibration that contributed to these improvements?	*For the Upper Yukon River watershed, the addition of the elevation-band based glacier module also provided an opportunity to improve calibration of HYDROTEL.*
Comment or Question - D. Smith	Response – A. Rousseau
7) Data Assimilation and Kalman Filtering	
7.1) You have shown that both of these concepts are viable in improving forecast skill. I didn't dig into these methodologies in great detail but understand what's going on. The Kalman Filtering is a significant accomplishment in my view.	
8) Forecast System (FS)	
8.1) The GUI for the FS controls daily schedule of model update and HYDROTEL execution. The main output is a display of the inflow forecast for the current day. It shows the meteorological input data and the corresponding inflow with the probabilistic bands around expected inflow for the 14 day forecast. There are various control options to change the graph window and probability bands for the forecast. There are controls for exporting some of the input data. This GUI is clean, robust and easy to use. Documentation is detailed and complete.	
8.2) What's missing? There are no outputs of state variables other than flows at #0000003 points. These are fundamental components of the DA process and should have high visibility. I appreciate that there is a high dimensionality to these datasets but without visibility you have a black box. Have you tried using Power BI or Tableau to build dashboard's for your large datasets?	*This is an interesting comment, but the rationale here was to build a GUI as simple as possible without overloading it with data that would not necessarily be of interst the forecaster. Now, we agree that it could be valuable to the forecaster to view the values of state variables, but YEC did not request any other information that what is currently displayed on the Forcasting System GUI. Adding the possibility of viewing other state*

	variables would have required a fair amount of programing time, which was not originally included in the budget of the project.
8.3) How do you generate outputs like those in Figure 2.11, 2.18, 3.16 or 3.20?	*We used HYDROTEL as a stand alone application which allowed us to produce historial streamflows for each watershed. We have a mirror version of HYDROTEL, (stand alone version) which allows us to produce streamflows quickly.*
8.4) What's in YEC's SQL server database and how is it used?	*The Forecasting System requires observed flow values mostly available and extracted from the YEC SQL server namely: the Mayo Lake outflows (m^3/s) and the Whitehorse facility flows (m^3/s). The first value is used to compute the Mayo Lake inflow and the second for comparison purposes and computation of the Marsh Lake inflows.*

References

1) *A Distributed Hydrological Modelling System to Support Hydroelectric Production in Northern Environments under Current and Changing Climate Conditions,* Progress Report presented to Yukon Energy Corporation, Alain N. Rousseau, P.Eng., Ph.D. , Report No-R1831, December 2018

2) *Development and evaluation of a hydrologic data-assimilation scheme for short-range flow and inflow forecasts in a data-sparse high-latitude region using a distributed model and ensemble Kalman filtering*, Jos Samuel, Alain N. Rousseau, Kian Abbasnezhadi, Stéphane Savary, Advances in Water Resources 130 (2019) 198–220. (Jos Samuel, (2019))

3) Progress Report R1768 (R1768) for *A Distributed Hydrological Modelling System to Support Hydroelectric Production in Northern Environments under Current and Changing Climate Conditions* by Alain N. Rousseau, et al. December 2017.